ACTA PHYSICA

ACADEMIAE SCIENTIARUM HUNGARICAE

REDIGIT

I. KOVÁCS

TOMUS XLVI FASCICULUS 1

AKADÉMIAI KIADÓ, BUDAPEST

1979

ACTA PHYS. HUNG. APAHAQ 46 (1) 1–54 (1979)

ACTA PHYSICA

ACADEMIAE SCIENTIARUM HUNGARICAE

SZERKESZTI

KOVÁCS ISTVÁN

Az *Acta Physica* angol, német, francia vagy orosz nyelven közöl értekezéseket. Évente két kötetben, kötetenként 4—4 füzetben jelenik meg. Kéziratok a szerkesztőség címére (1521 Budapest XI., Budafoki út 8.) küldendők.

Megrendelhető a belföld számára az Akadémiai Kiadónál (1363 Budapest Pf. 24. Bankszámla 215-11488), a külföld számára pedig a „Kultura" Külkereskedelmi Vállalatnál (1389 Budapest 62, P.O.B. 149. Bankszámla 217-10990), vagy annak külföldi képviseleteinél.

The *Acta Physica* publish papers on physics in English, German, French or Russian, in issues making up two volumes per year. Subscription: $ 36.00 per volume. Distributor: "Kultura" Foreign Trading Company (1389 Budapest 62, P.O. Box 149) or its representatives abroad.

Die *Acta Physica* veröffentlichen Abhandlungen aus dem Bereich der Physik in deutscher, englischer, französischer oder russischer Sprache, in Heften, die jährlich zwei Bände bilden.

Abonnementspreis pro Band: $ 36.00. Bestellbar bei »Kultura« Außenhandelsunternehmen (1389 Budapest 62, Postfach 149) oder seinen Auslandsvertretungen.

Les *Acta Physica* publient des travaux du domaine de la physique en français, anglais, allemand ou russe, en fascicules qui forment deux volumes par an.

Prix de l'abonnement: $ 36.00 par volume. On peut s'abonner à l'Entreprise du Commerce Extérieur «Kultura» (1389 Budapest 62, P.O.B. 149) ou chez représentants à l'étranger.

«*Acta Physica*» публикуют трактаты из области физических наук на русском, немецком, английском и французском языках.

«*Acta Physica*» выходят отдельными выпусками, составляющими два тома в год.

Подписная цена — $ 36.00 за том. Заказы принимает предприятие по внешней орговле «Kultura» (1389 Budapest 62, P.O.B. 149) или его заграничные представительства.

ACTA PHYSICA

ACADEMIAE SCIENTIARUM HUNGARICAE

TOMUS XLVI

AKADÉMIAI KIADÓ, BUDAPEST
1979

INDEX

Tomus 46

ACTA PHYSICA

ACADEMIAE SCIENTIARUM HUNGARICAE

TOMUS XLVI FASCICULUS 1

AKADÉMIAI KIADÓ, BUDAPEST
1979

ACTA PHYS. HUNG.

INDEX

Acta Physica Academiae Scientiarum Hungaricae, Tomus 46 (1), pp. 3—11 (1979)

ÜBER DAS TSEE-ADSORPTIONSMAXIMUM LITHIUM-DOTIERTER BeO-KERAMIKEN

Von

V. SIEGEL,[1] L. BOROS[2] und H.-H. KIRCHNER[1]

[1] PHYSIKALISCH-TECHNISCHE BUNDESANSTALT BRAUNSCHWEIG, BRD

[2] RADIOLOGISCHE KLINIK DER SEMMELWEIS UNIVERSITÄT FÜR MEDIZINISCHE WISSENSCHAFTEN BUDAPEST, UNGARN

(Eingegangen: 3. XII. 1978)

Vergleichende Untersuchungen an undotierten und Li-dotierten BeO-Keramiken zeigen, dass in den letzteren das TSEE-Maximum bei etwa 275 °C irreversiblen Änderungen unterworfen ist. Während sich dieses Emissionsmaximum für die undotierten Proben nach einer speziellen Vorbehandlung und einem H-Ionenbeschuss nach anschliessender γ-Strahlenanregung beliebig oft aufbauen lässt, ist dies für die Li-dotierten Proben nur in den ersten Messzyklen der Fall, wenn die BeO-Probe bei 500 °C in feuchter Luft getempert und gelagert wird. Nach wiederholten thermischen Behandlungen an feuchter Luft und Auswertungen wird das adsorptionsinduzierte TSEE-Maximum auch nach einem intensiven H-Ionenbeschuss kaum sichtbar. Das heisst aber, dass die oberflächlichen Lithium-Atome ihre aktive Rolle als Adsorptionszentren verloren haben, sei es durch eine chemische Umwandlung oder durch den Verlust von Li-Atomen durch Abdampfen.

Einführung

Der Einsatz von BeO-Keramiken als Exoelektronen-Dosimeter hat gezeigt, dass die Exoelektronen-Ausbeute bei mehrfachen Bestrahlungen mit der gleichen Energiedosis von γ-Strahlen grossen Streuungen unterworfen ist [1]. Diese Streuungen können nicht mit der Auswertemethode erklärt werden, sondern sind mit den Adsorptionseigenschaften des BeO verbunden. So konnte in [2—7] gezeigt werden, dass adsorbierte Oberflächenschichten auf verschiedenen Oxiden die thermisch stimulierte Exoelektronenemission (TSEE) stark beeinflussen. Untersuchungen des Verhaltens der beiden TSEE-Maxima bei etwa 270 °C und 324 °C an BeO-Keramiken haben ergeben, dass insbesondere das Maximum bei 270 °C von adsorbierten OH-Gruppen und Wasserdampf beeinflusst wird [8].

Dotierung der BeO-Proben mit Lithium

Für die Dotierung der BeO-Keramiken mit einer Reinheit von 99,25% wurde in Vaseline dispergiertes metallisches Lithium verwendet, das möglichst gleichmässig und mit der gleichen Masse auf die Oberfläche der scheibenförmigen Proben aufgetragen wurde. Danach wurden die Proben 1 Stunde lang

bei 1000 °C in trockener Luft getempert und rasch abgekühlt. Wegen der grossen Streuung der Messwerte für die frisch dotierten BeO-Keramiken wurden sie anschliessend einer mehrmaligen Bestrahlung mit γ-Strahlen und Temperung bis 800 °C unterzogen [9]. Eine ähnliche Vorbehandlung der undotierten BeO-Proben stellte sicher, dass die Ergebnisse der weiteren Untersuchungen an beiden Probenarten verglichen werden konnten.

Vorbehandlung der Proben und Messmethode

Ausgehend von den durch Messungen der Infrarotspektren festgestellten Desorptionsprozesse auf keramischen BeO-Proben [10, 11] wurden sowohl die nicht dotierten [12] als auch die mit Li dotierten BeO-Keramiken einer speziellen Vorbehandlung unterzogen. Sie bestand darin, dass die scheibenförmigen Proben innerhalb des Zählers in einer trockenen Methan-Atmosphäre auf 400 °C aufgeheizt wurden, um den physikalisch adsorbierten Wasserdampf zu desorbieren. Nach einer Abkühlung auf 20 °C wurde die Probe innerhalb des Zählers einem Beschuss durch Wasserstoffionen unterworfen. Zu diesem Zweck wurde an den Zähldraht des Proportionalzählers eine so grosse positive Hochspannung angelegt, dass die Gasverstärkung in Methan einsetzen konnte, wenn die BeO-Probe von aussen mit γ-Strahlen eines radioaktiven Präparates bestrahlt wurde. In diesem Falle werden in den Metallwänden des Zählers Compton- und Photo-Elektronen erzeugt, die in der Methan-Atmosphäre positive Ionen infolge der Dissoziation des Methans und Elektronen erzeugen. Diese negative Ladungsträger gelangen in unmittelbarer Nähe des positiven Zähldrahts in eine kritische Feldstärke, in der sie durch Stossionisation Elektronenlawinen auslösen, die am Ausgang des Zählers als Impulse nachgewiesen werden.

Auf der anderen Seite entstehen durch die Dissoziation des Methans positive Ionen, von denen die leichtesten H^+ und H_2^+ unter anderem in Richtung zur Probe wandern und dort auf der Oberfläche teilweise adsorbiert werden können. Wenn man annimmt, dass die Gasverstärkung während der Ionen Bedeckung konstant ist, dann ist die Anzahl der gezählten Elektronenlawinen (Impulse) ein Mass für die Anzahl der adsorbierten H-Atome.

Diese Vorbehandlung der Proben und anschliessende Auswertung wurde in einem mit Methan gespülten fensterlosen Proportionalzähler [13] ausgeführt. Während der Messung der thermisch stimulierten Exoelektronenemission wurde die Probe linear mit einer Rate von etwa 1,4 $K \cdot s^{-1}$ aufgeheizt. Vor jeder Messung wurden die Proben im Zähler, um den Einfluss von Wasserdampf zu vermeiden, mit einer γ-Strahlenquelle (^{137}Cs oder ^{60}Co) angeregt.

Messergebnisse

a) *Undotierte BeO-Proben*

Ohne die oben beschriebene spezielle Vorbehandlung der undotierten BeO-Keramiken beobachtet man nach der Anregung mit γ-Strahlen nur das thermisch stimulierte Exoelektronen-Maximum bei etwa 325 °C (Bild 1a). Erst wenn der Wasserdampf desorbiert und H-Ionen adsorbiert wurden, erscheint nach der Anregung mit γ-Strahlen das neue TSEE-Maximum bei etwa 270 °C (Bild 1b) und c). Die Impulsanzahl N_{EE} dieses Maximums hängt von der Anzahl der registrierten Exoelektronenlawinen (Impulse) während des Ionenbeschusses bei eingeschalteter Hochspannung am Zähldraht ab. Wie man in Bild 2 erkennt, wird bereits bei etwa 3000 Impulsen eine Adsorp-

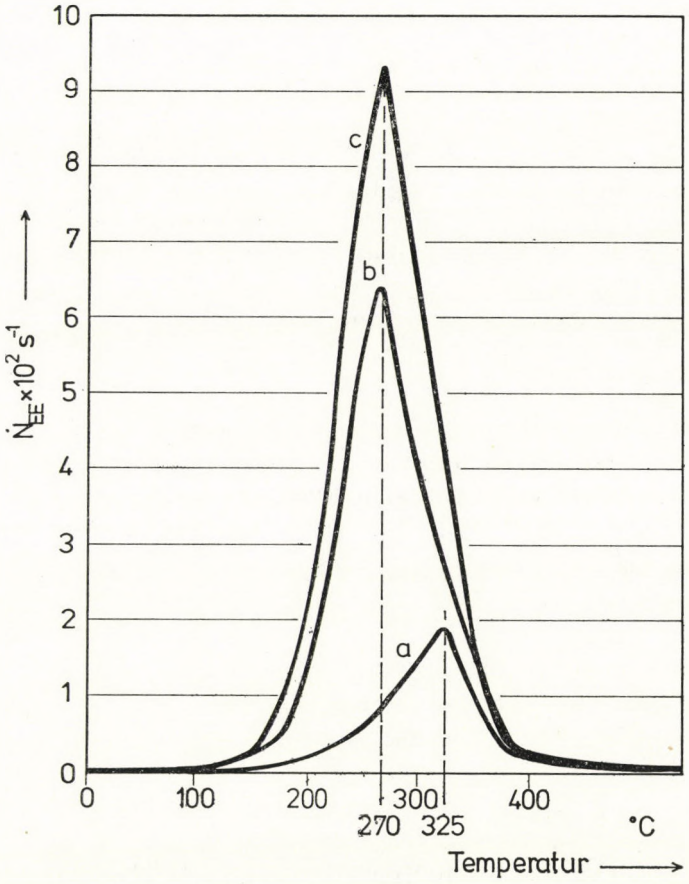

Bild 1. Änderung der TSEE-Maxima bei 270 °C und 325 °C in Abhängigkeit von der Vorbehandlung der undotierten BeO-Probe bei konstanter γ-Strahlenanregung. a — ohne Vorbehandlung, b — mit H-Ionenbeschuss (200 Impulse); c — (770 Impulse). $\dot{N}_{EE}$ — Impulsanzahl je Sekunde

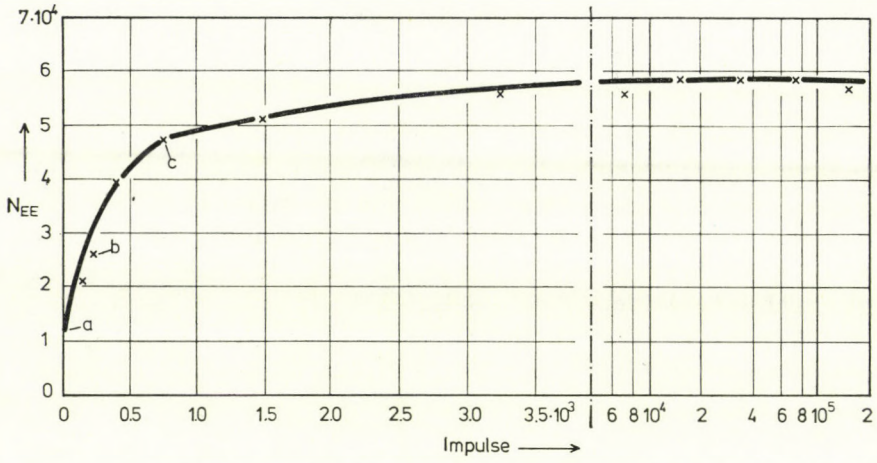

Bild 2. Änderung der Impulsanzahl N_{EE} für die undotierten BeO-Proben in Abhängigkeit von der Anzahl der erzeugten H-Ionen Impulse bei konstanter γ-Strahlenanregung. In Bild 1 sind die TSEE-Maxima für die Punkte a, b und c dargestellt

tionssättigung erreicht, da ein weiterer Ionenbeschuss keinen Anstieg der Exoelektronen-Ausbeute bei Anregung mit einer konstanten Energiedosis der γ-Strahlen zur Folge hat. Dieses neue TSEE-Maximum verschwindet wieder, wenn die speziell vorbehandelte BeO-Probe vor der γ-Strahlen-Anregung an feuchte Luft gebracht wird [9, 12].

b) *Li-dotierte BeO-Proben*

Dieselben Behandlungsmethoden und Messungen wie an den undotierten BeO-Keramiken wurden auch an den mit Lithium dotierten ausgeführt. Auch hier zeigen die nicht speziell vorbehandelten Proben nur das TSEE-Maximum bei 325 °C (Bild 3a). Auffällig ist hier aber, dass die Exoelektronen-Ausbeute N_{EE} bei gleicher Energiedosis der γ-Strahlen um den Faktor 10 bis 15 grösser ist als bei den undotierten BeO-Proben, d.h. die Li-dotierten BeO-Keramiken sind sehr viel empfindlicher [14]. Nach dem Ionenbeschuss innerhalb der Methan-Atmosphäre des Zählers erscheint wie im Falle der undotierten BeO-Keramiken nach der γ-Strahlen-Angerung das neue TSEE-Maximum bei etwa 275 °C (Bild 3b—d). Im Gegensatz zu den undotierten Proben liegt die Adsorptionssättigung für die Li-dotierten Proben bei der doppelten Anzahl von registrierten Elektronenlawinen (etwa 6000) während des Ionenbeschusses. Bei gleicher Energiedosis der anschliessenden γ-Bestrahlung liegt die Exoelektronen-Ausbeute im Bereich der Sättigung für die undotierte Probe bei $N_{EE} = 5{,}8 \cdot 10^4$, für die Li-dotierte BeO-Probe bei $N_{EE} = 8{,}6 \cdot 10^5$. Offenbar ist die Anzahl der besetzbaren Adsorptionsplätze auf Grund der Dotierung mit Lithium stark angestiegen.

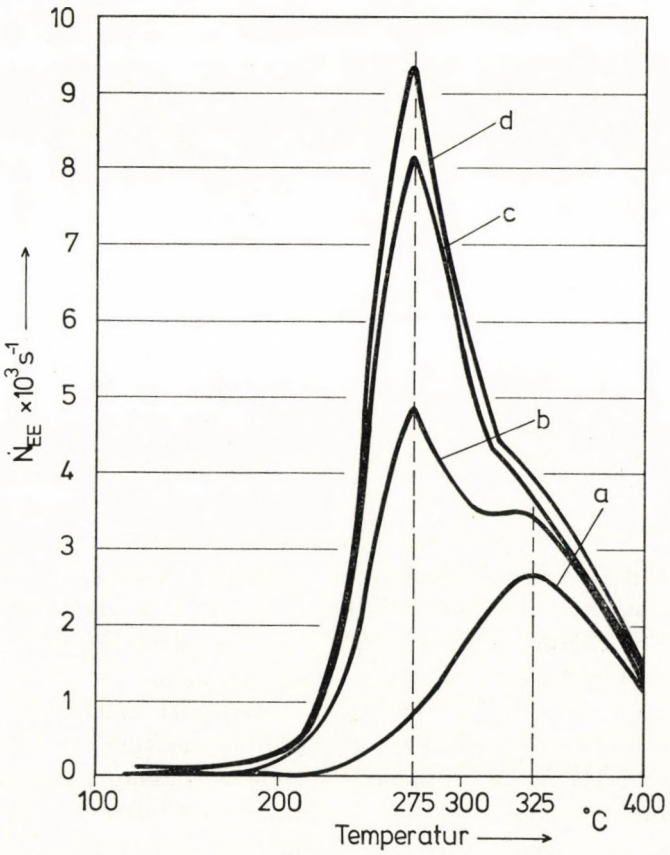

Bild 3. Änderung der TSEE-Maxima bei 275 °C und 325 °C in Abhängigkeit von der Vorbehandlung der Li-dotierten BeO-Proben bei konstanter γ-Strahlenanregung. a — ohne Vorbehandlung, b bis d mit H-Ionenbeschuss (b — 500, c — 1000, d — 5000 Impulse)

Wie im Falle der undotierten BeO-Proben wurden auch die dotierten vor jeder Messung bei 500 °C an feuchter Luft getempert, abgekühlt und gelagert. Dabei zeigte sich nach mehrfacher Verwendung derselben Proben ein neuer Effekt. Nach der eingangs beschriebenen speziellen Vorbehandlung und anschliessenden γ-Strahlenanregung sollte man wieder das neue TSEE-Maximum bei 275 °C erwarten. Wie Bild 4 aber zeigt, erscheint es bei einer registrierten Anzahl von 1000 Elektronenlawinen überhaupt nicht (Bild 4a) im Gegensatz zu Bild 3c, wo ebenfalls 1000 Elektronenlawinen an der frischen Probe gezählt wurden. Nach diesem Messzyklus wurde dieselbe BeO-Probe vor der speziellen Vorbehandlung mehrere Male bei 500 °C an Luft getempert. Die anschliessenden Messungen, ausgeführt wie zuvor, ergaben erneut, dass sich das TSEE-Maximum bei 275 °C nicht mehr aufbauen liess. Erst bei einer Anzahl registrierter Elektronenlawinen von 8000 (Kurve b) und 17 000

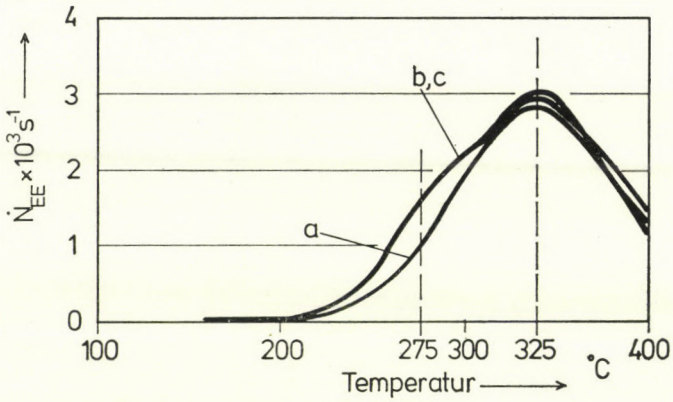

Bild 4. Änderung der TSEE-Maxima bei 275 °C und 325 °C in Abhängigkeit von der Vorbehandlung für eine mehrfach getemperte Li-dotierte BeO-Probe bei konstanter γ-Strahlenanregung. a bis c mit H-Ionenbeschuss (a — 3000, b — 8000, c — 17 000 Impulse)

(Kurve c) zeigt sich eine Andeutung des Maximums bei 275 °C. Nur an einer frischen Li-dotierten BeO-Keramik-Probe beobachtet man den wachsenden Anstieg des TSEE-Maximums bei 275 °C mit ansteigender Anzahl der registrierten Elektronenlawinen, wie er in Bild 3 dargestellt ist.

Dieses abweichende Verhalten der Li-dotierten BeO-Proben gegenüber dem H-Ionenbeschuss legt die Vermutung nahe, dass sich das Lithium auf der BeO-Oberfläche chemisch verändert hat oder abgedampft ist. Für einen Verlust an Lithium spricht eine Massenbestimmung des Li an einer unbehandelten und der hier mehrfach verwendeten BeO-Probe. Die unbehandelte Probe enthielt 210 μg Li, die mehrfach verwendete dagegen nur 60 μg Li. Diese Schlussfolgerung gilt aber nur für den Fall, dass beide Proben im Anfangszustand die gleiche Masse an Lithium enthielten, was nicht mehr kontrollierbar ist.

Aus [15] ist bekannt, dass sich bei der Einwirkung von H^+-Ionen oder H_2-Molekülen auf das Li schon bei 20 °C die sehr beständige Verbindung LiH bildet. Dieses LiH wird aber bei höheren Temperaturen durch das Einwirken des Luft-Stickstoffes im Beisein von Wasserdampf zum grösseren Teil in die Verbindung $LiNH_2$, Li_2NH und Li_3N und zum kleineren Teil in Li_2O umgewandelt.

Die oben beschriebenen Messungen an den Li-dotierten BeO-Keramiken wurden in Unkenntnis der eben genannten chemischen Umwandlungen nach dem Tempern und Lagern der Proben an feuchter Luft ausgeführt.

Im folgenden wurden die BeO-Keramiken um diese chemischen Umwandlungen zu vermeiden, vor jeder Messung

a) bei 1000 °C in trockener Luft oder Argon getempert und abgekühlt und anschliessend in einer trockenen Atmosphäre im Exsikkator gelagert,

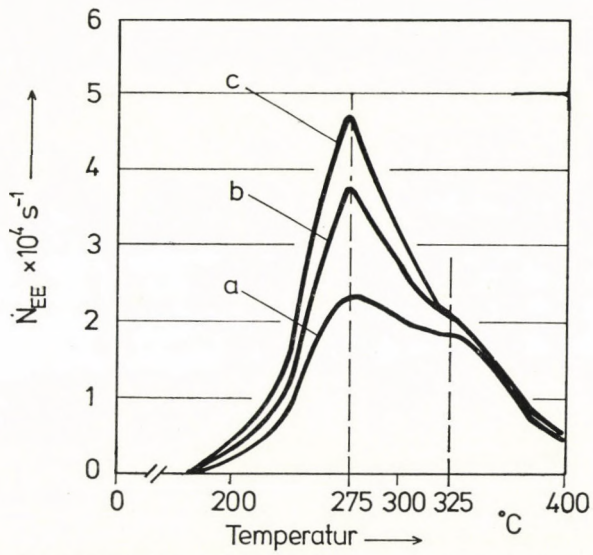

Bild 5. Änderung der TSEE-Maxima bei 275 °C und 325 °C einer Li-dotierten BeO-Probe nach dem Tempern und Lagern in trockener Luft und anschliessender konstanter γ-Strahlenanregung. H-Ionenbeschuss, a — 500, b — 1000, c — 5000 Impulse

b) bei 1000 °C in Argon getempert und anschliessend in feuchter Luft abgekühlt und gelagert.

Die Ergebnisse der Messreihe a) zeigen an einem Beispiel Bild 5 und der Messreihe b) Bild 6.

Nach dem Tempern in trockener Luft und der Lagerung im Exsikkator bleibt das TSEE-Adsorptionsmaximum bei 275 °C nach der gleichen Anzahl von gezählten Elektronenlawinen (Impulsen) und nach der Anregung mit der gleichen Energiedosis der γ-Quanten auch nach der 12. Messung über einen Zeitraum von 3 Wochen praktisch konstant. Wie Bild 5a—c zeigt, hängt die Impulsanzahl N_{EE} des TSEE-Maximums bei 275 °C wie bei einer frischen Probe von der Anzahl der gezählten Impulse beim Ionenbeschuss ab. Da das TSEE-Maximum bei 325 °C unbeeinflusst bleibt, bedeutet dies, dass die Empfindlichkeit der BeO-Probe über längere Zeit konstant bleibt.

Anders verhält es sich mit den Proben, die in Argon getempert und anschliessend an feuchter Luft gelagert wurden. Wie die Bilder 6 A und B zeigen, lässt sich zwar durch den H^+-Ionenbeschuss das TSEE-Maximum bei 275 °C erzeugen, aber die Impulsanzahl N_{EE} fällt von 100% bei der 1. bis 4. Messung (Bild 6 A) auf 50% bei der 18. Messung (Bild 6 B) ab. Dagegen sinkt die Impulsanzahl N_{EE} für das TSEE-Maximum bei 325 °C in derselben Messreihe nur um 25% vom ursprünglichen Wert ab. Beim Tempern der Proben bei 1000 °C in trockener Luft oder Argon werden die Lithiumnitride offenbar wieder reduziert, bilden sich aber erneut langsam beim Abkühlen und Lagern in feuchter Luft. Wie die Messreihe b) zeigt, überwiegt

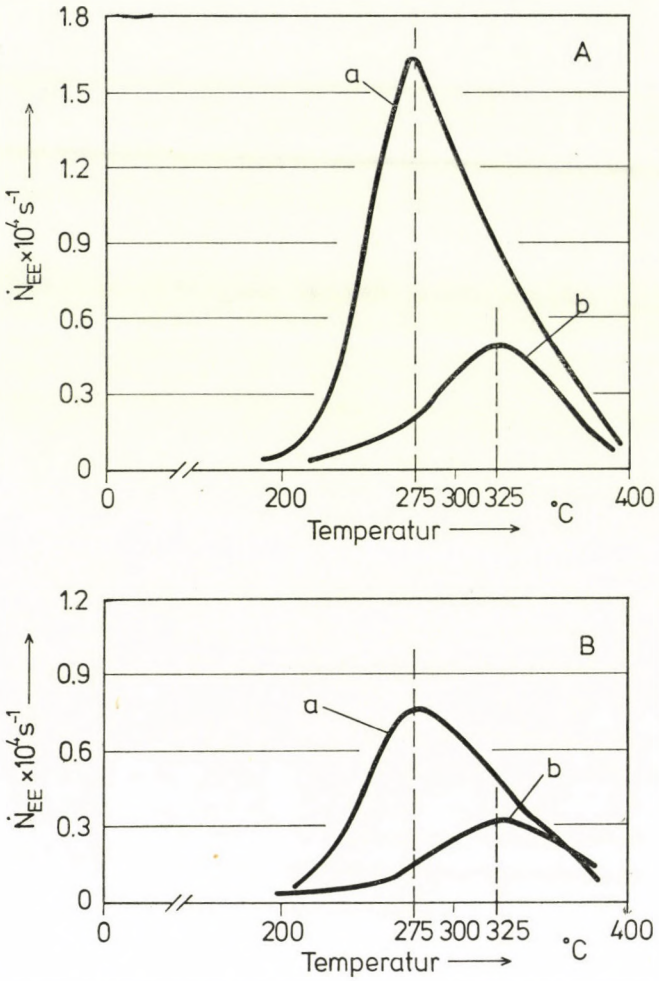

Bild 6. Änderung der TSEE-Maxima bei 275 °C und 325 °C einer Li-dotierten BeO-Probe nach Tempern in Argon und Lagern in feuchter Luft. a — Ionenbeschuss etwa 5000 Impulse, b — ohne H-Ionenbeschuss. A — 4. Messung; B — 18. Messung

jedoch die Bildung der Nitride, da die Impulsanzahl $N_{\Sigma E}$ des TSEE-Adsorptionsmaximums unter gleichen Vorbehandlungs- und Anregungsbedingungen im Verlauf der Messreihe stetig abnimmt.

Diskussion

In [14] wurde gezeigt, dass die Empfindlichkeit der Li-dotierten BeO-Keramiken konstant bleibt bei einer Lagerung in einer Argon-Atmosphäre, während die Reproduzierbarkeit der Messwerte in anderen Gasen (Sauerstoff,

Stickstoff, Luft) schlechter war. Betrachtet man das Verhalten der beiden TSEE-Maxima in feuchter Luft, so ändert sich bei gleichen Anregungsbedingungen insbesondere das adsorptionsinduzierte TSEE-Maximum bei 275 °C. Für das Lithium ist bekannt, dass es im adsorbierten Zustand als Donator-Zentrum wirkt, auch wenn es als Li_2O oder LiOH auf der Oberfläche eines Oxids vorliegt [18]. Beide Verbindungen reagieren aber bei höheren Temperaturen, ebenso wie LiH, im Beisein von Wasserdampf mit dem Luft-Stickstoff unter Bildung von $LiNH_2$, Li_2NH und Li_3N. Von diesen Verbindungen weiss man, dass sie in adsorbierter Form als Akzeptor Zentren wirken.

Offenbar wird durch diese Verbindungen beim Ionenbeschuss die Adsorption von H^+ und H_2^+ verhindert, die auf dem BeO OH-Gruppen bilden, welche bei der assoziativen Desorption Elektronen freisetzen, die als Exoelektronen nachgewiesen werden [9, 12]. Die drei Verbindungen Li_2NH, $LiNH_2$ und Li_3N zeigen denselben Vergiftungseffekt für die aktiven Oberflächenzentren der Exoelektronenemission wie adsorbierte Alkohole [16, 17], mit dem Unterschied, dass sie selektiv nur die Adsorptionsplätze für das TSEE-Maximum bei 275 °C blockieren.

Wenn man die hohe Empfindlichkeit der Li-dotierten BeO-Keramiken gegenüber ionisierenden Strahlen konstant halten will, muss man den Einfluss feuchter Luft vermeiden, um die sensibilisierende Wirkung des Lithiums auf der BeO-Oberfläche nicht durch chemische Umwandlungen zu gefährden.

LITERATUR

1. V. Siegel and W. Rasp, Actes du VIII^e Congrès International de la Société Francaise de Radioprotection, Saclay, 1977, p. 380.
2. I. V. Krylova, phys. stat. solidi (a), **7,** 359, 1971.
3. N. I. Konyushkina und I. V. Krylova, Fiz. Tverd. Tela, **15,** 1925, 1973.
4. I. V. Krylova, Proc. 4th Intern. Symp. on Exoelectron Emission and Dosimetry, Liblice/CSSR, 1973, p. 145.
5. M. Euler, W. Kriegseis und A. Scharmann, phys. stat. solidi (a), **15,** 431, 1973.
6. W. Kriegseis und A. Scharmann, phys. stat. solidi (a), **29,** 407, 1975.
7. M. Euler und A. Scharmann, phys. stat. solidi (a), **34,** 297, 1976.
8. V. Siegel, W. Rasp und H.-H. Kirchner, phys. stat. solidi (a), **42,** K 147, 1977.
9. L. Boros, Acta Phys. Hung., **34,** 255, 1973.
10. S. E. Ermatov und T. S. Kosherov, Izv. Akad. Nauk Kazak SSR, Ser. Fiz.-Mat., **12,** 29, 34, 1974.
11. S. E. Ermatov, Zh. Prikl. Spektrosk., **23,** 14, 1975.
12. V. Siegel, W. Rasp und H.-H. Kirchner, wird veröffentlicht.
13. H.-J. Kriks und W. Schaare, PTB-Mitt., **81,** 10, 1971.
14. D. F. Regulla, G. Drexler und L. Boros, Proc. Third Intern. Conf. on Luminescence Dosimetry, Riso/Denmark, Rep. No. 249, 1971, p. 601.
15. Gmelins Handbuch der anorganischen Chemie, Ser.-Nr. 20, Li, 8. Auflage, 1960, Verlag Chemie GmbH Weinheim/Bergstr.
16. V. Siegel, W. Rasp und H.-H. Kirchner, phys. stat. solidi (a), **34,** K 203, 1976.
17. V. Siegel, W. Rasp und H.-H. Kirchner, Proc. 5th Intern. Symp. on Exoelectron Emission and Dosimetry. Zvikov/CSSR, 1976, p. 58.
18. D. G. Thomas, J. Phys. Chem. Solids, **9,** 31, 1958.

Acta Physica Academiae Scientiarum Hungaricae, Tomus 46 (1), pp. 13—18 (1979)

ON A PLANE MAGNETOGASDYNAMIC SHOCK WAVE OF VARIABLE STRENGTH

By

B. G. VERMA and J. P. VISHWAKARMA

DEPARTMENT OF MATHEMATICS, UNIVERSITY OF GORAKHPUR, GORAKHPUR 273001, U. P., INDIA

(Received 5. XII. 1978)

A particular solution of the equations of one dimensional anisentropic flow of a polytropic gas is linked by a magnetogasdynamic shock to gas at rest in which the density is non-uniform and magnetic field is constant. The approach is inverse in the sense that the density distribution is derived from the position of the shock and the prescribed flow behind it. The velocity and strength of the shock each vary with time.

1. Introduction

COPSON [1], MACKIE and WEIR [2] and many other authors have discussed the problem of shock waves of constant strength moving with variable velocity. In these problems, there occurs a jump in the entropy across the shock, but the entropy remains uniform (at different levels) on both sides of the shock. More general situations are that in which a shock leaves a non-uniform distribution of entropy behind. SMITH [3] has discussed a problem of such a flow in ordinary gasdynamics. The present paper extends the discussion of SMITH's problem to a perfectly conducting gas in the presence of a transverse magnetic field. We have started from a known anisentropic flow and linked it through a shock wave to gas at rest. The state of the stationary gas is not known until the shock path has been determined. It is shown that the velocity and strength of the shock each vary with time.

For the anisentropic flow behind the shock, we have used the family of exact solutions obtained by WEIR [4].

2. Weir's solution

With viscosity and heat conduction neglected, the relevant equations for one-dimensional anisentropic flow are,

$$\frac{\partial \varrho}{\partial t} + u\frac{\partial \varrho}{\partial x} + \varrho\frac{\partial u}{\partial x} = 0, \tag{2.1}$$

$$\frac{\partial u}{\partial t} + u\frac{\partial u}{\partial x} + \frac{1}{\varrho}\frac{\partial p}{\partial x} + \frac{\mu h}{\varrho}\frac{\partial h}{\partial x} = 0, \tag{2.2}$$

$$\frac{\partial S}{\partial t} + u\frac{\partial S}{\partial x} = 0, \tag{2.3}$$

where p, ϱ, h, S, u and μ are respectively pressure, density, magnetic field, specific entropy, fluid velocity and magnetic permeability. For a polytropic gas the equation of state is

$$p = K\varrho^{\gamma} \exp\left(\frac{S}{C_v}\right), \tag{2.4}$$

where γ is the constant adiabatic index, C_v the specific heat at constant volume and K is the dimensional constant.

It can be verified that Eqs. (2.1) to (2.4) possess a solution (c.f. WEIR's solution [4])

$$u_{02} = 2\alpha t + \delta, \tag{2.5}$$

$$p^*_{02} = f(X), \tag{2.6}$$

$$\varrho_{02} = \frac{1}{2\alpha}\frac{df}{dX}, \tag{2.7}$$

where

$$p^*_{02} = p_{02} + \frac{1}{2}\mu h^2_{02}, \quad p_{02} = \beta p^*_{02}, \quad (0 < \beta < 1)$$

and particle paths are given by

$$X = x - \alpha t^2 - \delta t, \tag{2.8}$$

X being the material variable and the suffix 02 is introduced to distinguish between the WEIR's solution and the state of the gas behind the shock. The pressure and density are constant along the particle paths which are coaxial parabolas in the (x, t) — plane.

3. The shock path

We shall now link the solution given in Section 2 to a state of rest through magnetogasdynamic shock relations for a polytropic gas, namely:

$$\varrho_2 v_2 = \varrho_1 v_1, \tag{3.1}$$

$$h_2 v_2 = h_1 v_1, \tag{3.2}$$

$$p_2 + \frac{1}{2}\mu h_2^2 + \varrho_2 v_2^2 = p_1 + \frac{1}{2}\mu h_1^2 + \varrho_1 v_1^2, \tag{3.3}$$

$$\frac{\gamma}{\gamma - 1}\frac{p_2}{\varrho_2} + \frac{\mu h_2^2}{\varrho_2} + \frac{1}{2}v_2^2 = \frac{\gamma}{\gamma - 1}\frac{p_1}{\varrho_1} + \frac{\mu h_1^2}{\varrho_1} + \frac{1}{2}v_1^2, \tag{3.4}$$

where v is the velocity of the gas relative to the velocity of the shock and suffixes 2 and 1 are attached to the states immediately behind and in front (the stationary gas) of the shock, respectively.

These shock relations must be satisfied at the shock whose displacement is taken as $\xi = \xi(t')$, where the prime has been added to the time t since we shall subsequently use it as a parameter. From (2.8)

$$X = \xi(t') - \alpha t'^2 - \delta t' \tag{3.5}$$

on the shock. It then follows from (2.5), (2.6) and (2.7) that

$$u_2 = 2\alpha t' + \delta, \tag{3.6}$$

$$p_2^* = g(t'), \tag{3.7}$$

$$\varrho_2 = -\frac{\dot{g}(t')}{2\alpha[\dot{\xi}(t') - 2\alpha t' - \delta]}, \tag{3.8}$$

where

$$g(t') = f\{\xi(t') - \alpha t'^2 - \delta t'\}$$

and

$$p_2 = \beta p_2^*, \quad p_2^* = p_2 + \frac{1}{2}\mu h_2^2, \quad (0 < \beta < 1).$$

Furthermore,

$$v_2 = 2\alpha t' + \delta - \xi(t').$$

In front of the shock, we take the gas to be at rest so that $u_1 = 0$ and $v_1 = -\dot{\xi}(t')$. Further, $p_1^* = p_1 + \mu h_1^2/2 = k$, a constant, since h_1 is taken to be constant and by equation (2.2) the pressure gradient must be zero.

The elimination of the unknown ϱ_1 between equations (3.1) and (3.3) yields

$$p_2^* - p_1^* = \varrho_2 v_2 (v_1 - v_2). \tag{3.9}$$

Similarly from Eqs. (3.1), (3.2) and (3.4) we get

$$\left[v_1\left\{\frac{\gamma\beta}{\gamma - 1} - 2(1 - \beta)\right\} - v_2\frac{(\gamma - 2)(1 - \beta)}{(\gamma - 1)}\right]p_2^* v_2 - \frac{\gamma}{\gamma - 1}p_1^* v_1^2$$

$$= \frac{1}{2}\varrho_2 v_2 v_1 (v_1^2 - v_2^2). \tag{3.10}$$

Direct substitution in (3.9) and (3.10) of the flow quantities given previously yields

$$(2\alpha t' + \delta)\dot{g} + 2\alpha g - 2\alpha k = 0, \tag{3.11}$$

$$2\alpha\gamma(g - k)\dot{\xi}^2 - (\gamma - 1)(2\alpha t' + \delta)[(2\alpha t' + \delta)/2 - \dot{\xi}]\dot{g}\dot{\xi}$$
$$- 2\alpha(2\alpha t' + \delta)[\gamma^*\dot{\xi} + (\gamma - 2)(1 - \beta)(2\alpha t' + \delta)]g = 0, \tag{3.12}$$

where

$$\gamma^* = \gamma\beta + 2(1 - \beta).$$

Solving the differential equation (3.11), we have

$$g = \frac{2\alpha k t' + A}{2\alpha t' + \delta}, \quad t' \neq -\delta/2\alpha, \tag{3.13}$$

where A is a constant. The elimination of g between (3.12) and (3.13) yields the shock velocity as

$$\dot{\xi} = \frac{1}{2}(2\alpha t' + \delta)\left\{b + \left[b^2 + 4(\gamma - 2)(1 - \beta)\left(\frac{2\alpha t' + \delta}{\gamma} B + 1\right)\right]^{\frac{1}{2}}\right\}, \tag{3.14}$$

where

$$b = (2\alpha t' + \delta)\frac{B\gamma^*}{\gamma} + \left(\gamma^* - \frac{\gamma - 1}{2}\right),$$

and

$$B = \frac{k\gamma}{A - k\delta}.$$

Integrating the Eq. (3.14), we get the shock path as

$$\xi = \frac{\gamma^* B}{12\gamma\alpha}(2\alpha t' + \delta)^3 + \frac{1}{8\alpha}\left(\gamma^* - \frac{\gamma - 1}{2}\right)(2\alpha t' + \delta)^2 + C$$
$$+ \frac{1}{12N}(2\alpha t' + \delta)^2\left[b^2 + 4(\gamma - 2)(1 - \beta)\left(\frac{2\alpha t' + \delta}{\gamma} B + 1\right)\right], \tag{3.15}$$

where

$$N = b\left[\frac{2\alpha\gamma^* B}{\gamma}(2\alpha t' + \delta) + \alpha\left(\gamma^* - \frac{\gamma - 1}{2}\right)\right] +$$
$$+ 2\alpha(\gamma - 2)(1 - \beta)\left[\frac{3B}{\gamma}(2\alpha t' + \delta) + 2\right]$$

and C is a constant. Thus the shock relations determine the shock path and fix the flow quantities on both sides of the shock. In terms of the spatial variables, the total pressure and density behind the shock are given parametrically by

$$p_2^* = \frac{2\alpha k t' + A}{2\alpha t' + \delta}, \tag{3.16}$$

$$\varrho_2 = \frac{2(A - k\delta)}{(2\alpha t' + \delta)^3 (b - 2 + L)}, \tag{3.17}$$

$$x - \alpha t^2 - \delta t = \xi(t') - \alpha t'^2 - \delta t', \tag{3.18}$$

where

$$L = \left[b^2 + 4(\gamma - 2)(1 - \beta) \left(\frac{2\alpha t' + \delta}{\gamma} B + 1 \right) \right]^{\frac{1}{2}}.$$

The Eqs (3.16) and (3.17) follow from (3.7) and (3.8), and (3.18) is obtained by eliminating X between (2.8) and (3.5).

For the stationary gas in front of the shock, the density is given parametrically by

$$\varrho_1 = \frac{2(A - k\delta)}{(2\alpha t' + \delta)^3 (b + L)}, \tag{3.19}$$

$$x = \xi(t'). \tag{3.20}$$

Eq. (3.19), the density distribution as a function of time of the shock path, is obtained by calculating ϱ_1 from (3.1). To obtain the density as a function of x, we eliminate t' between (3.19) and the Eq. (3.20) of the shock path. Finally, the entropy of the stationary gas can then be derived from the equation of state (2.4) as a function of x.

4. Results and discussion

We have found a family of solutions whose members depend on the choice of values for the various constants. We assume $\alpha > 0$, $\delta > 0$ and $t \geq 0$. The shock must be compressive, that is, $0 < p_1^* < p_2^*$, or $0 < k < (2\alpha k t' + A)/(2\alpha t' + \delta)$. Thus $A - k\delta > 0$ and all pressures are positive. Inspection of (3.17) and (3.19) indicates that densities are positive if $\gamma > 1$.

Taking $\sigma = p_2/p_1$ as a measure of strength of the shock wave, we have maximum value of σ at $t = 0$ and $\sigma \to 1$ as $t' \to \infty$. Hence the strength of shock wave decreases with time. Also from (3.14), the shock velocity $\dot{\xi} \to \infty$ as $t' \to \infty$.

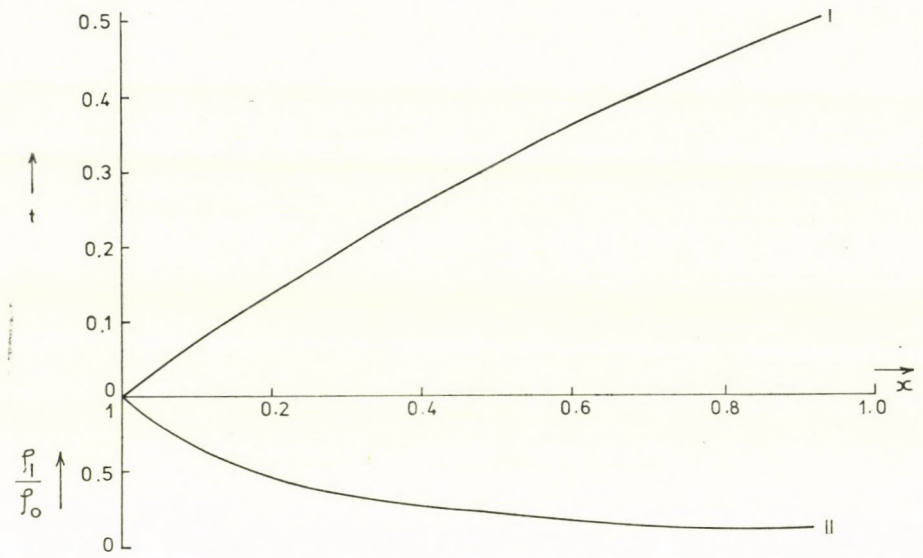

Fig. 1. Shock path in (x, y) plane (I). Variation of density with distance in the gas ahead of the shock (II)

Fig. 1. shows a typical configuration of the shock path in the (x, t) plane. The lower part of the Figure gives the density ratio in the gas upstream of the shock; ϱ_0 is the density at $x = 0$, $t = 0$. The value chosen for the various constants are as follows:

$$\alpha = \delta = 1;\ B = \frac{1}{2}(\gamma - 1);\ C = -\frac{5\gamma + 4}{40};\ \beta = \frac{2}{5};\ \gamma = \frac{7}{5}.$$

If $\alpha > 0$, the particle trajectories behind the shock are a family of straight lines with fluid velocity $u = \delta$. The gas ahead of the shock is at rest with constant density. The shock velocity is also constant and is given by

$$\dot{\xi} = \frac{\delta}{2}\left\{B\frac{\delta\gamma^*}{\gamma} + \left(\gamma^* - \frac{\gamma - 1}{2}\right) + \left[\left(\frac{B\delta\gamma^*}{\gamma} + \gamma^* - \frac{\gamma - 1}{2}\right)^2 + \right.\right.$$
$$\left.\left. + 4(\gamma - 2)(1 - \beta)\left(\frac{\delta B}{\gamma} + 1\right)\right]^{\frac{1}{2}}\right\}.$$

REFERENCES

1. E. T. Copson, Proc. Roy. Soc., A **222,** 254, 1954.
2. A. G. Mackie and D. G. Weir, Proc. Camb. Phil. Soc., **56,** 64, 1960.
3. P. Smith, Proc. Edinburgh Math. Soc., **13,** 297, 1963.
4. D. G. Weir, Proc. Camb. Phil. Soc., **57,** 890, 1961.

Acta Physica Academiae Scientiarum Hungaricae, Tomus 46 (1), pp. 19—26 (1979)

LIGTH EFFECT ON AMORPHOUS CRYSTAL TRANSITION IN $SSe_{22.5}$

By

M. F. KOTKATA, M. K. EL-MOUSLY and F. M. AYAD

PHYSICS DEPARTMENT, FACULTY OF SCIENCE, AIN-SHAMS UNIVERSITY, CAIRO, EGYPT

(Received in revised form 10. XII. 1978)

Isothermal phase transformation of massive $SSe_{22.5}$ in the presence and absence of light illumination has been carried out in the temperature range of 98—144 °C using the electric conductivity method. Illumination affects the nucleation process through "photo-nucleation". Kinetic studies have not, to date, been presented so as to identify separately the light effects on the crystallization processes of materials of Se-like structure. The obtained conductivity data are presented as power and logarithmic functions to study the crystallization kinetics in the light of the present concepts of crystallization in organic polymers.

Introduction

Studies of the morphology of crystalline selenium indicate that it crystallizes from the bulk amorphous phase by chain folding [1—3]. Selenium forms extended-chain crystals by a thickening mechanism similar to that found in organic polymers [3]. Spherulites in bulk polymers grow outward from a nucleation centre that is frequently of a heterogeneous character. The radial growth of a spherulite is commonly the result of the formation of stacks of bladelike lamellas that grow outward from the nucleation centre. In addition, the crystallization of amorphous selenium involves both the crystallization of polymeric Se_n chains and the polymerization of Se_8 rings [4].

The addition of an isoelectronic element as sulphur does not cause a great disturbance in the short-range order of the atomic distribution of selenium [5]. But, 3—5 at % sulphur doped in selenium results in minimizing the rate of crystallization [6, 7]. Light, on the other hand, can produce a marked enhancement on the crystallization kinetics over that obtained from purely thermal effects [8—11]. This effect has been used to write holograms [12] and discrete images [10] with lasers.

In this paper, quantitative data on percent crystallization in the absence and presence of photo illumination for S-doped Se amorphous sample, namely $SSe_{22.5}$, are estimated from recording the electric conductivity changes continuously during isothermal transformation processes. A kinetic study is presented using AVRAMI's theory.

Experimental

Bulk $SSe_{22.5}$ samples have been prepared in the amorphous phase through heating the constituents at 280 °C for 2 hrs and quenching in air at 18—20 °C inside evacuated [10^{-4} mm Hg] pyrex cells having parallel faces ($\sim$2 mm apart) and provided with two tungsten electrodes.

Crystallization has been carried out in preheated ovens (0.2 °C max. fluctuations) under dark and illuminated conditions. Illumination was achieved by a 250 W ultra high pressure Hg-quartz lamp. The IR part of the emitted spectrum was filtered out to reduce sample heating.

The crystallization was monitored by measuring the electronic conduction periodically (1/2 min interval) during several isothermal transformations in the range 98—144 °C using an electrometer with an error less than 2%. The remarkable increase of the electric conductivity accompanying the amorphous to crystalline phase change (in the absence or presence of light) implies that the measured conductivity σ at any time t is the result of two conductivities σ_a and σ_c corresponding to a double phase system, amorphous and crystalline.

Results and discussion

The use of conductivity-structure characterization for a proper description of the volume fraction which has crystallized depends on the specific regimes of percent transformation. Therefore, the time-dependence of the electronic conduction of $SSe_{22.5}$ is represented as power and logarithmic dependence and is given in Fig. 1 for some isotherms.

During the transformation process, whether purely thermal or with the photon effect, there appear to be at least three regimes of σ versus percent transformation: The conductivity remains at first approximately constant, but after a certain time depending on annealing temperatures it increases abruptly by several orders to attain a certain maximum value. Such a strong increase of σ is due mainly to the transformation of the very low conductivity amorphous into a continuous path of rather better conducting crystalline $SSe_{22.5}$. The constancy of the maximum conductivity attained at a given temperature indicates the stability of the transformed products. Such maximum value varies with temperature and so it may not always correspond to the same degree of structural perfection but may rather refer to the degree of crystallization [13].

In Fig. 1, the minimum to apparent maximum of log σ proceeds in a smooth stage *ad* for the non-illuminated and in two distinguishable stages *ab* and *cd* for illuminated samples. The decrease in log σ in the period *bc* is ascribed to photo effects. Such effects are more pronounced in the range 108

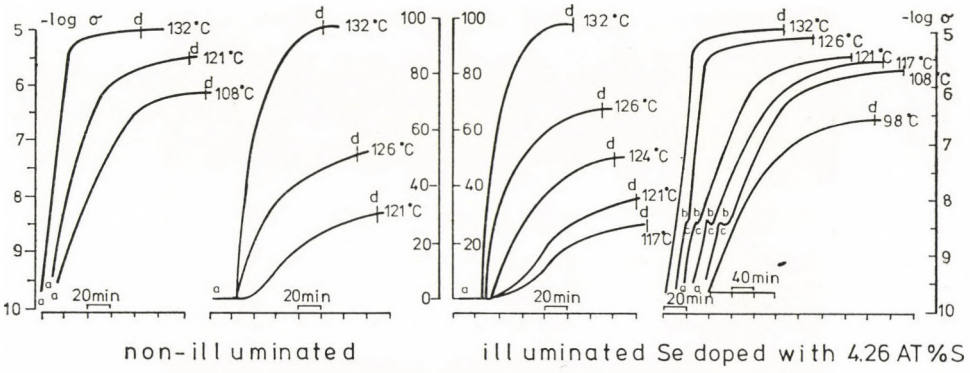

Fig. 1. Time-dependence of the electronic conduction represented as σ and log σ for Se doped with 4.26 at % S annealed under: (a) dark and (b) photo illumination for a variety of isotherms

to 126 °C when the isothermal time-dependence of the electronic conduction is represented as log σ_t rather than σ_t. Table I summarizes the effect of temperature on time and log σ associated with the individual stages together with the total change of log σ due to the crystallization of $SSe_{22.5}$ under photo illumintaion. The total time of crystallization shows a decrease with increasing temperature but it is longer for the samples annealed under photo illumination.

Table I

Conductivity-temperature dependence of photo-illuminated $SSe_{22.5}$ samples annealed at different isotherms

Annealing temp., °C	$-\log \sigma\ (\Omega\ \mathrm{cm})^{-1}$		Total change		First stage (ab)		Second stage (cd)	
	Initial	Final	$\Delta \log \sigma$	Δt, min	$\Delta \log \sigma_1$	Δt_1	$\Delta \log \sigma_2$	Δt_2
98	9.69	6.60	3.09	285	One stage process			
108	9.26	6.21	3.05	210	0.45	15	2.56	192
117	9.47	5.55	3.92	175	1.16	14	2.82	149
121	9.55	5.47	4.08	160	1.09	13	2.93	144
126	9.69	5.18	4.51	120	1.27	9	3.26	110
132	9.87	5.01	4.86	100	One stage process			
144	9.80	5.34	4.46	53	One stage process			

Plate 1 is a typical reflection micrograph pattern (X450) taken for $SSe_{22.5}$ thin film isothermally annealed at 100 °C for 2 hrs with 2.13 eV incident photons. This value is greater than the known value of dissociation energy of Se—Se bond, 1.8 eV [14]—1.9 eV [15]. Plate 2 is for an identical $SSe_{22.5}$ film annealed at 100 °C in the dark. The plates show that the growth is faster in the dark and leads to a more ordered crystalline network. The absorbed quanta of light produce, however, an increase in the number of dispersed centres. Also, the difference in the grain size due to illumination is clear in Plates 1 and 2.

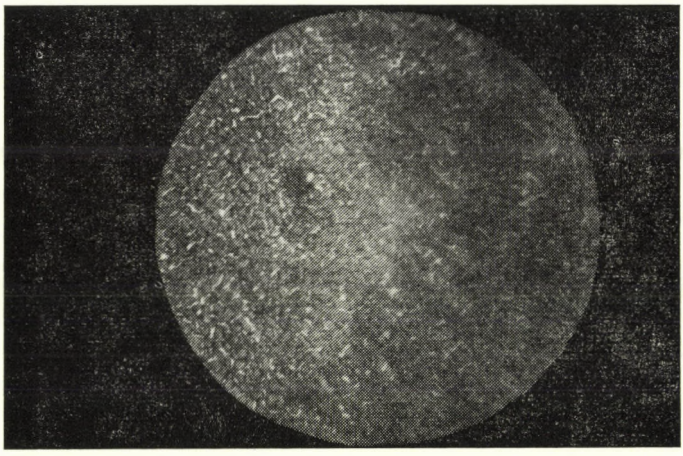

1

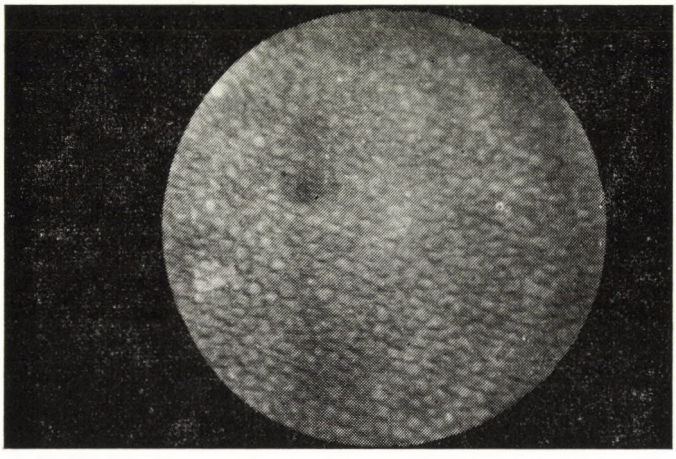

2

Plates 1 and 2: Typical micrograph patterns for Se doped with 4.26 at % S films annealed isothermally at 100 °C for 2 hrs in the presence (Plate 1) and absence (Plate 2) of photo illumination

Changing the energy of the incident photons in the range of 1.91—3.04 eV has no significant effect on the nature and total duration of the transformation process in the studied temperature range.

Crystallization kinetics

To study the kinetics of transformation the experimental data should be expressed in terms of the transformed fraction at different crystallization times. In the present work, $X(t)$ is evaluated for the S-doped Se sample by using the relative increase of the electric conductivity during the growth. This, however, may be realized by considering a power or logarithmic conductivity dependence according to ODELEVSKY [16] and LANDAUER [17], respectively.

For low crystallite volumes, a general power formula is written:

$$\sigma^k = \theta_1 \sigma_1^k + \theta_2 \sigma_2^k,$$

where θ_1 is the fraction left uncrystallized and θ_2 is the corresponding crystallized fraction. For $k = 1$, the conductivity at a time t is

$$\sigma_t = \theta_t \sigma_a + (1 - \theta_t)\sigma_c,$$

i.e.
$$\theta_t(\sigma) = (\sigma_c - \sigma_t)/(\sigma_c - \sigma_a). \tag{1}$$

On the other hand, when $\log \sigma$ is considered to represent the sensitive parameter characterizing the conductivity-content dependence, an empirical popular formula may be written as:

$$\log \sigma = \theta_1 \log \sigma_1 + \theta_2 \log \sigma_2,$$

i.e.
$$\theta_t(\log \sigma) = (\log \sigma_c - \log \sigma_t)/(\log \sigma_c - \log \sigma_a). \tag{2}$$

The subscripts a and c refer to values at the begining and at end of the process. These correspond to points a and d on the curves of Fig. 1.

The extent of crystallization X_t as a function of the annealing time is computed on the basis of Eqs. (1) and (2), and Fig. 2 shows some of these results. The crystallization curves appear to shift toward lower time scales with increasing temperature as one might expect from the decrease in viscosity with increasing temperature.

The crystalllization of organic polymers has been described by the AVRAMI [18] formula

$$X_t = 1 - \exp(-Kt^n), \tag{3}$$

where K is the temperature-dependent rate constant and n is a parameter depending on nucleation and growth mode [19].

To fit AVRAMI's equation, a plot of $\ln[-\ln(1 - X_t)]$ versus $\ln(t)$ must yield a straight line whose slope is n and whose intercept on the ordinate

at ln $(t) = 0$ is ln (K). Figs. 3 show just such plots for $SSe_{22.5}$ under the effect of photo illumination. At some temperatures, the plot takes on two distinct slopes during the isothermal crystallization which, therefore, can be described by two different values for both n and K in the rate equation. A change in the exponent n indicates a change in growth mechanism during crystallization, a phenomenon quite well known for polymer systems in which a secondary crystallization occurs after the primary crystallization event [20]. The results for n and K calculated on the basis of the ODELEVSKY approach (Eq. (1)) as well as the LANDAUER approach (Eq. (2)) are summarized in Table II.

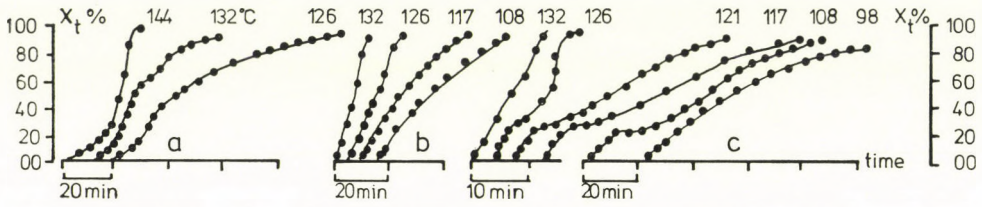

Fig. 2. Crystallinity percent vs annealing time for Se doped with 4.26 at % S derived from d.c. conductivity measurements: (a) and (b) under purely thermal effect, and (c) with photon effect (2.13 eV) on basis of: (a) σ, and (b) and (c) log σ. Here, $X_t = 1 - \theta_t$

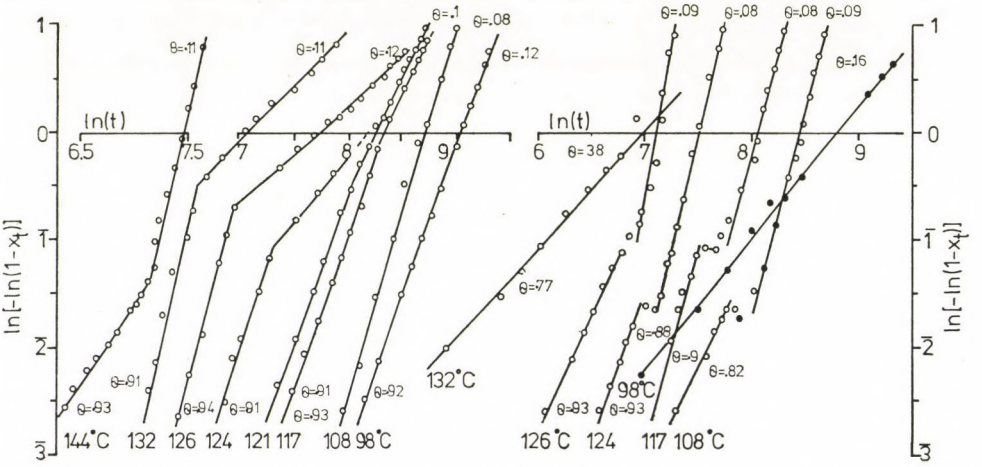

Fig. 3. ln $[-\ln (1 - X_t)]$ vs ln (t) plots for crystallization kinetics of photo-illuminated Se doped with 4.26 at % S on the basis of: (a) σ and (b) log σ

The kinetic calculations on the basis of log σ indicate that the crystallization growth under purely thermal effects proceeds by one process as characterized by a single value for n or K. The value of n decreases monotonically with temperature in the range 98—132 °C, while the crystallization rate constant K increases by 30% with temperature from 98 to 132 °C. In Table II, on the other hand, the values of n estimated on basis of σ show that the transforma-

tion clearly consists of two stages at temperatures above 120 °C which account for the presence of secondary crystallization. For the first stage, with θ up to 0.6—0.7, $n_1 > 2$ while for the second $n_2 \simeq 1$ which leads to the conclusion that in this latter stage crystallization is restricted to one-dimensional growth, the driving force is constant, and no new nuclei are formed. The considerably higher values of K_2 than K_1 indicate that the secondary crystallization is a faster process. But, at a relatively high temperature as 144 °C, $n_2 > n_1$ and $K_2 \ll K_1$ which may be ascribed to the limitation of the applicability of the σ-crystallinity correlation (ODELEVSKY approach). While the kinetic calculations on the basis of $\log \sigma$ (LANDAUER approach) indicate that $n_1 = 3.75$ and $n_2 = 1.26$ are consistent with the considered mechanism.

Table II

AVRAMI constants calculated on basis of σ and $\log \sigma$ as conductivity-structure characterization functions for both illuminated and non-illuminated $SSe_{22.5}$

Cryst. temp., °C	Crystallization under photo illumination							
	On basis of σ				On basis of $\log \sigma$			
	n_1	K_1	n_2	K_2	n_1	K_1	n_2	K_2
98	2.76	1.20×10^{-11}	—	—	1.12	7.55×10^{-5}	—	—
108	2.24	1.05×10^{-8}	—	—	1.27	8.30×10^{-5}	1.52	5.25×10^{-6}
117	2.70	1.30×10^{-10}	2.00	4.75×10^{-8}	1.48	1.90×10^{-5}	1.60	2.35×10^{-6}
121	2.75	1.66×10^{-10}	1.9	1.54×10^{-7}	0.92	7.30×10^{-4}	1.68	1.60×10^{-6}
124	3.20	5.05×10^{-11}	1.72	1.10×10^{-6}	0.88	9.60×10^{-4}	1.80	1.30×10^{-6}
126	3.80	1.10×10^{-11}	0.98	1.75×10^{-3}	0.86	1.45×10^{-3}	2.48	2.55×10^{-8}
132	4.20	5.30×10^{-13}	1.04	6.30×10^{-4}	1.24	1.60×10^{-4}	—	—
144	1.56	3.60×10^{-6}	4.10	5.00×10^{-14}	2.64	1.90×10^{-8}	0.94	1.69×10^{-3}

Cryst. temp., °C	Crystallization in the dark							
	On basis of σ				On basis of $\log \sigma$			
	n_1	K_1	n_2	K_2	n_1	K_1	n_2	K_2
98	3.20	1.45×10^{-13}	—	—	1.24	1.65×10^{-5}	—	—
108	2.20	1.05×10^{-8}	—	—	1.15	7.90×10^{-5}	—	—
117	1.50	6.35×10^{-6}	—	—	1.14	1.25×10^{-4}	—	—
121	1.80	4.78×10^{-7}	—	—	1.13	1.70×10^{-4}	—	—
124	2.40	1.50×10^{-8}	1.14	1.25×10^{-4}	1.12	2.10×10^{-4}	—	—
126	2.42	2.20×10^{-8}	1.12	1.65×10^{-4}	1.10	2.70×10^{-4}	—	—
132	2.48	3.50×10^{-8}	1.16	2.35×10^{-4}	1.08	5.28×10^{-4}	—	—
144	2.14	8.30×10^{-8}	6.50	1.55×10^{-21}	3.75	1.00×10^{-11}	1.26	1.66×10^{-4}

Subscripts 1 and 2 refer to the presence of primary and secondary modes.

Evidently, there is correspondence between the present kinetics for $SSe_{22.5}$ computed on the basis of σ and that of CRYSTAL [2] for pure Se computed from densitometric data. Doping of S leads to generating the secondary crystallization at a temperature about 124 °C instead of at 100 °C for Se [2, 21]. The big difference between the rate constant K for $SSe_{22.5}$ and that

of Se identifies the effect of addition of 4.26 at % S in inhibiting the crystallization process of Se.

The photo effect on the kinetics of $SSe_{22.5}$ as obtained on the basis of log σ shows two AVRAMI exponents referring to two growth stages defining the crystallization process in the range 108—126 °C (Fig. 3b). The observed kink between the two kinetic lines lies in the region of pronounced photo effect and corresponds to $\theta \simeq 0.7$. However, these results for n_1 (Table II), refer to one-dimensional nucleation growth which seems to be unrealistic.

Apart from this, AVRAMI's values of n_1 as reflected by σ changes (Fig. 3a), are 2.24 to 4.2 in the range 98—132 °C and those of n_2 fall in the range 1—2 which confirms the expected one-dimensional growth of binding the terminals of the formed individual crystallites as they come close to each other. A secondary crystallization has started at 117 °C which represents a lower temperature than that in dark, 124 °C. Moreover, nucleation of $SSe_{22.5}$ observed in the optical microscope is definitely heterogeneous in the entire temperature range studied. Heterogeneous nucleation has been found in liquid-crystalline transformation for pure Se and S-doped Se samples too [21].

However, the dramatic variation of the kinetic parameter n may be attributed to the complex nature of the crystallization of materials of Se-like structure compared with most polymers and other materials first described by AVRAMI theory.

A more detailed investigation of the effect of light on the process of crystallization is under way; the results will be published in the near future.

REFERENCES

1. B. FITTON and C. H. GRIFFITHS, J. Appl. Physics, **39,** 3663, 1968.
2. R. C. CRYSTAL, J. Polym. Sci., *A*-2, **8,** 1755, 1970.
3. M. C. COUGHLIN and B. WUNDERLICH, Kolloid Z. Z. Polym., **250,** 482, 1972.
4. M. C. COUGHLIN and B. WUNDERLICH, J. Polym. Sci., **11,** 1735, 1973.
5. J. SCHOTTMILLER, M. TABAK, G. LUCOVSKY and A. WARD, J. Non-Cryst. Solids, **4,** 80, 1970.
6. M. K. EL-MOUSLY, J. Neorg. Mat. (USSR), **13,** 801, 1977.
7. M. K. EL-MOUSLY and M. F. KOTKATA, Acta Phys. Hung., **43,** 117, 1977.
8. J. DRESNER and G. B. STRINGFELLOW, J. Phys. Chem. Solids, **29,** 303, 1968.
9. I. A. PARIBOK-ALEXANDROVICH, Soviet Phys.-Solid State, **11,** 1631, 1970.
10. J. FEINLEIB, J. DE-NEUFVILLE, S. C. Moss and S. R. OVSHINSKY, Appl. Phys. Lett., **18,** 254, 1971.
11. A. D. PEARSON and B. G. BAGLEY, Mat. Res. Bull., **6,** 1041, 1971.
12. R. G. BRANDES, F. B. LAMING and A. D. PEARSON, Appl. Optics, **9,** 1712, 1970.
13. K. P. MAMEDOV and Z. D. NURIEVA, Soviet Phys. Cryst., **12,** 605, 1968.
14. T. L. COTTROLL, "The Strength of Chemical Bonds", 2nd Ed., Butterworths, London, 1958, p. 258.
15. L. PAULING, "The Nature of the Chemical Bond", 3rd Ed., Cornell University Press, Ithaca, 1960, p. 85.
16. V. I. ODELEVSKY, J. Technical Physics (USSR), **21,** 673, 1951.
17. R. LANDAUER, J. Appl. Phys., **23,** 7, 77, 1952.
18. M. AVRAMI, J. Chem. Phys., **7,** 1103, 1939; ibid., **8,** 212, 1940; ibid., **9,** 117, 1941.
19. L. MANDELKORN, "Crystallization of Polymers", McGraw-Hill, New York, 1964.
20. F. RYBNIKAR, J. Polym. Sci., 44, 517, 1960.
21. M. K. EL-MOUSLY, M. F. KOTKATA and S. A. SALAM, J. Physics C, **11,** 1077, 1978.

Acta Physica Academiae Scientiarum Hungaricae, Tomus 46 (1), pp. 27—30 (1979)

DEBYE-WALLER FACTORS OF PLATINUM AND LEAD

By

K. N. MEHROTRA and J. P. DIXIT

DEPARTMENT OF PHYSICS, D.A.V. COLLEGE, KANPUR 208001, INDIA

(Received in revised form 10. XII. 1978)

The Debye—Waller factor temperature parameters at different temperatures for platinum and lead have been calculated by using a modified Sharma and Joshi model. The calculations were carried out according to previous results [1]. Comparison of theoretical results with available experimental data, as presented in the vibration spectrum dependent Debye—Waller factor temperature parameter (Y) versus temperature diagrams, reveals reasonably satisfactory agreement.

I. Introduction

In a previous paper [1] we have used the modified Sharma and Joshi model for the theoretical investigation of the temperature dependence of Debye—Waller factors of five FCC metals: copper, silver, gold, nickel and aluminium. The purpose of the present paper is to report on similar studies carried out with FCC platinum and lead. Theory and the method of the calculation were described in [1], to which the interested reader is referred for details. In this paper, similarly to paragraph IV in [1], we only wish to present and discuss results obtained with Pt and Pb. The various constants needed in the calculations are listed in Table I.

Table I

Constants and the parameters used in the calculation

Metal	Atomic mass in a.m.u.	Elastic constants (10^{11} dyn/cm^2)			Ref.	Temp.* (K)	Lattice parameter (Å)	Phonon frequencies (THz)			Ref.
		C_{11}	C_{12}	C_{44}				$\nu_L(100)$	$\nu_T(100)$	$\nu_L\left(\frac{1}{2}\frac{1}{2}\frac{1}{2}\right)$	
Platinum	195.09	34.67	25.07	7.65	a	300	3.924	5.789	3.750	5.650	c
Lead	207.19	4.953	4.229	1.49	b	300	4.9504	1.910	0.955	2.212	d

* Temperature at which the elastic constants are measured.

a. R. E. MACFARLANE, J. A. RAYNE and C. K. JONES, Phys. Lett., **18,** 91, 1965.
b. D. L. WALDORF and G. A. ALERS, J. Appl. Phys., **33,** 3266, 1962.
c. R. OHRLICH and W. DREXEL, Inelastic Scattering of Neutrons in Solids and Liquids, Vol. 1, International Atomic Energy Agency, Vienna, 1968 p. 203.
d. R. STEDMAN, L. ALMQVIST, G. NILSSON and G. RAUNIO, Phys. Rev., **162,** 545, 1967.

II. Results and discussion

1. *Platinum*

ALEXOPOULOS et al [2] have studied the temperature dependence of the Debye characteristic temperature for platinum by measuring the temperature variation of the integrated X-ray intensity of the (331), (420), (422) and (531) reflections from flat powder samples in the range of 100—700 °K. The values of the Debye—Waller factor temperature parameter Y obtained from these authors together with our calculated results are shown in Fig. 1 with the reference temperature $T_0 = 293$ °K. The agreement of the calculated Y values with experiment is satisfactory.

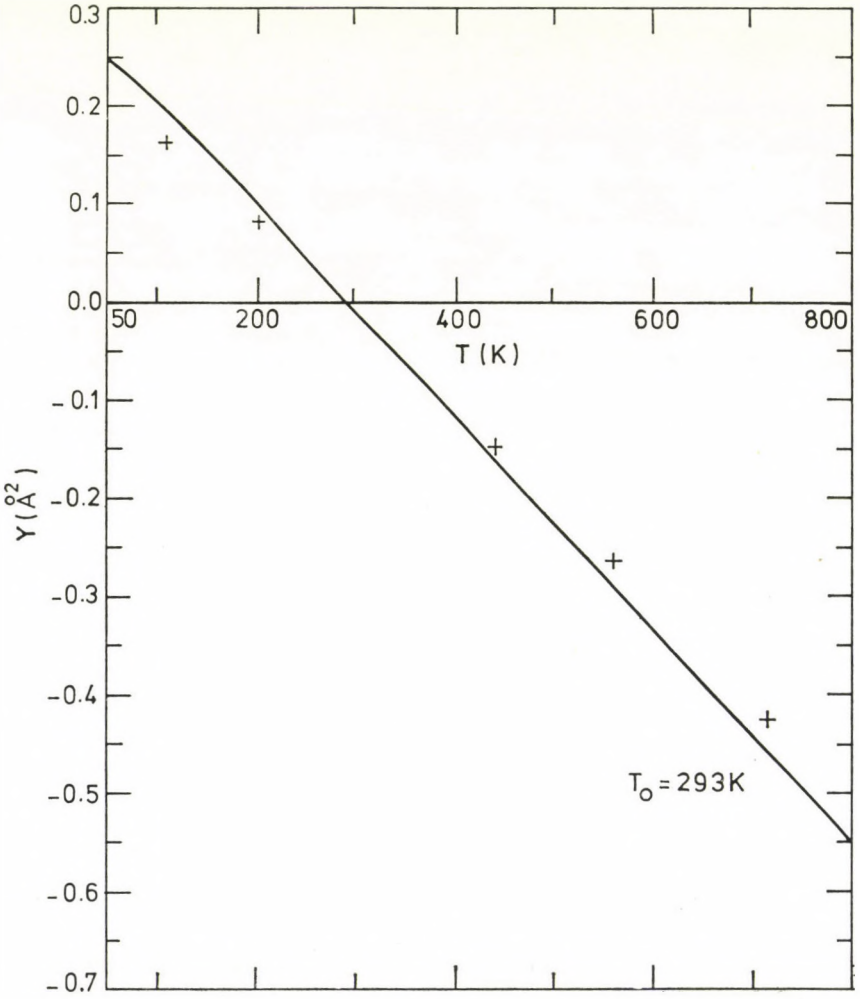

Fig. 1. Variation of Y for platinum. Solid line shows the present calculation. Experimental points: + ALEXOPOULOS et al.

2. *Lead*

The temperature dependence of the intensity of the X-ray reflections from lead has been studied by CARTZ [3], CHIPMAN and PASKIN [4], MOTHERSOLE and OWEN [5], CHIPMAN [6], and ALEXOPOULOS et al [2]. CARTZ has obtained the temperature variation of the Debye characteristic temperature for lead by measuring the intensity of the diffuse scattering of X-rays from single crystals at temperatures ranging from 150 to 600 °K. He also made correction for Compton scattering. CHIPMAN nad PASKIN carried out measurements on lead powder at room and liquid nitrogen temperatures. MOTHERSOLE and OWEN investigated in the temperature range 293—577 °K on fine grade

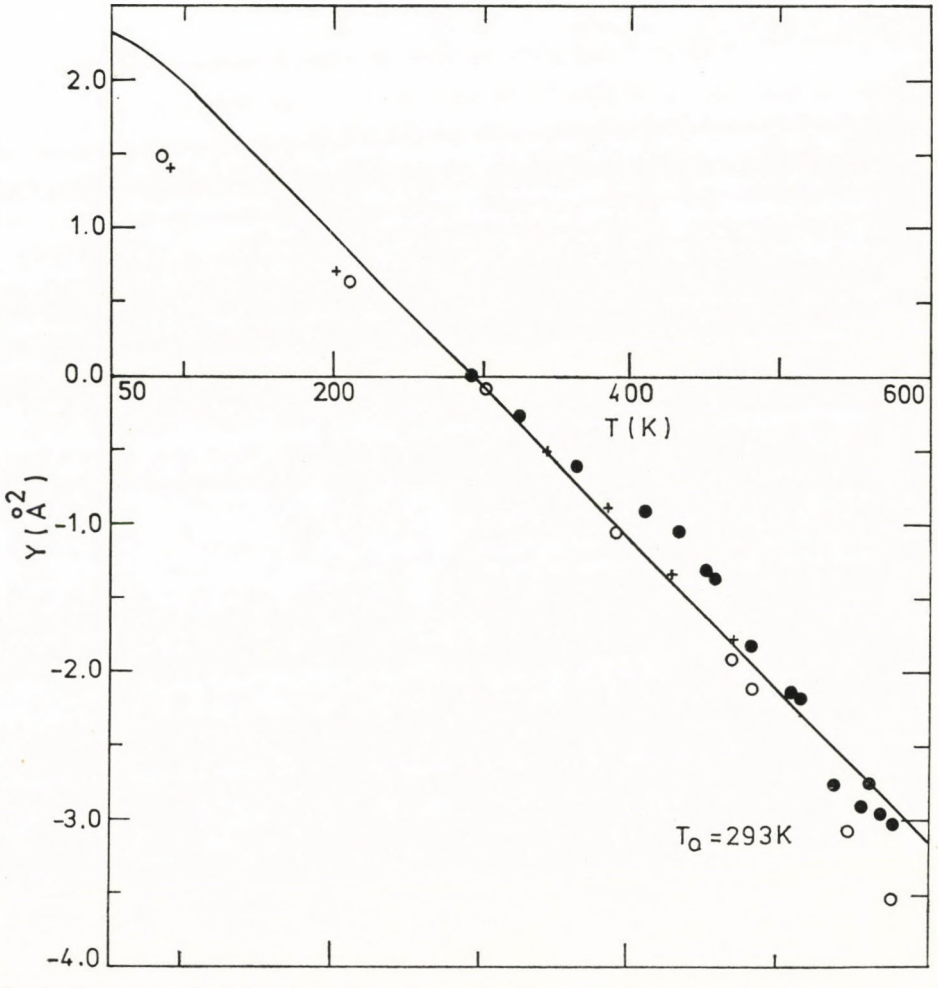

Fig. 2. Variation of Y for lead. Experimental points: ○ CHIPMAN; ● MOTHERSOLE and OWEN; + ALEXOPOULOS et al.

powder specimens. The Table summarising the results of these authors contains the values of Y at selected temperatures. CHIPMAN obtained the temperature variation of the Debye characteristic temperature by measuring the integrated intensity of a high angle X-ray diffraction peak between 85—576 °K correcting also for the thermal diffuse scattering (TDS). ALEXOPOULOS et al used flat powder samples in the temperature range of 100—500 °K for the reflections (331), (420), (422), (511)—(533), (531), (600)—(442). For the present comparison the data of MOTHERSOLE and OWEN, CHIPMAN, and ALEXOPOULOS et al were selected. The results are presented in Fig. 2 with $T_0 = 293$ °K. The theoretical results agree reasonably well with the experimental values.

The actual discrepancies between theory and experiment could be attributed to various causes discussed already in [1]. Nevertheless one may conclude that our attempt to explain the observed temperature variation of the Debye—Waller factors for platinum and lead on the basis of the modified Sharma and Joshi model appears to be successful.

Acknowledgement

One of the authors (J.P.D.) wishes to thank the University Grants Commission, New Delhi, for financial assistance.

REFERENCES

1. J. P. DIXIT and K. N. MEHROTRA, Acta Phys. Hung., **42,** 127, 1977.
2. K. ALEXOPOULOS, J. BOSKOVITS, S. MOURIKIS and M. ROILOS, Acta Cryst., **19,** 349, 1965.
3. L. CARTZ, Proc. Phys. Soc., **B68,** 951, 1955.
4. D. R. CHIPMAN and A. PASKIN, J. Appl. Phys., **30,** 1992, 1959.
5. N. MOTHERSOLE and E. A. OWEN, Brit. J. Appl. Phys., **16,** 1113, 1965.
6. D. R. CHIPMAN, J. Appl. Phys., **31,** 2012, 1960.

Acta Physica Academiae Scientiarum Hungaricae, Tomus 46 (1), pp. 31—37 (1979)

NON-LINEAR HYDROMAGNETIC WAVES IN TWO-ELECTRON TEMPERATURE PLASMA

By

M. L. MITTAL and D. GOVINDA THIRTHA

DEPARTMENT OF MATHEMATICS, INDIAN INSTITUTE OF TECHNOLOGY, BOMBAY 400 076, INDIA

(Received 12. XII. 1978)

The non-linear hydromagnetic waves for two-electron temperature plasma are shown to be governed by a Korteweg—de Vries—Burgers equation. Collisional effects have also been taken into account. Due to the magnetic field the amplitude of the solitary wave decreases while the width of the soliton and the speed of the shock wave increase.

1. Introduction

Following the work of JONES et al [1] on two-electron temperature plasma, there is a wide range of interest in the study of such plasmas due to its application in many physical problems. GOSWAMI and BUTI [2] considered the ion acoustic solitary waves in such a plasma with one of the species of the electrons as cold and obtained the condition for the existence of solitary waves. SHUKLA and TAGARE [3] included the effects of collisions by considering fluid equations with ion viscosity and ion thermal conductivity. They have shown that shock-like structures evolve when the temperature difference between the two components of electrons is fairly large.

In the present note the effects of uniform magnetic field on non-linear hydromagnetic waves in two-electron temperature plasma are investigated. The magnetic field is considered in the $x-z$ plane making an angle θ with the x-axis. Using the perturbation scheme given by DAVIDSON [4], a Korteweg—de Vries—Burgers equation governing the hydromagnetic waves is derived. Both collisional and collisonless plasmas are considered and solitary wave and shock wave solutions are obtained.

2. Analysis

Following SHUKLA and TAGARE [3], the governing wave equations in the presence of a magnetic field can be written as

$$\frac{\partial n_i}{\partial t} + \frac{\partial}{\partial x}(n_i u_{ix}) = 0, \tag{1}$$

$$\frac{\partial u_{ix}}{\partial t} + u_{ix}\frac{\partial u_{ix}}{\partial x} + \frac{1}{n_i}\frac{\partial}{\partial x}(n_i T_i) = E_x + R_i(u_{iy}B_z - u_{iz}B_y) + \frac{4}{3}\eta_i \frac{\partial^2 u_{ix}}{\partial x^2}, \quad (2)$$

$$\frac{\partial u_{iy}}{\partial t} + u_{ix}\frac{\partial u_{iy}}{\partial x} = E_y + R_i(u_{iz}B_x - u_{ix}B_z) + \frac{4}{3}\eta_i \frac{\partial^2 u_{iy}}{\partial x^2}, \quad (3)$$

$$\frac{\partial u_{iz}}{\partial t} + u_{ix}\frac{\partial u_{iz}}{\partial x} = E_z + R_i(u_{ix}B_y - u_{iy}B_x) + \frac{4}{3}\eta_i \frac{\partial^2 u_{iz}}{\partial x^2}, \quad (4)$$

$$\frac{3}{2}\left(\frac{\partial T_i}{\partial t} + u_{ix}\frac{\partial T_i}{\partial x}\right) + T_i \frac{\partial u_{ix}}{\partial x}$$

$$= k_i \frac{\partial^2 T_i}{\partial x^2} - \frac{1}{A^2 R_i}\left(\frac{\partial B_z}{\partial x}E_y - \frac{\partial B_y}{\partial x}E_z\right) + \frac{3}{4}\eta_i\left(\frac{\partial u_{ix}}{\partial x}\right)^2, \quad (5)$$

$$\frac{T_{ef}}{T_{el}} n_{el} E_x + \frac{\partial n_{el}}{\partial x} = 0, \quad (6)$$

$$\frac{T_{ef}}{T_{eh}} n_{eh} E_x + \frac{\partial n_{eh}}{\partial x} = 0, \quad (7)$$

$$-M\frac{\partial E_x}{\partial x} = n_{eh} + n_{el} - n_i, \quad (8)$$

$$A^2 R_i n_i u_{iy} = -\frac{\partial B_z}{\partial x}, \quad (9)$$

$$A^2 R_i n_i u_{iz} = \frac{\partial B_y}{\partial x}, \quad (10)$$

$$\frac{\partial E_z}{\partial x} = R_i \frac{\partial B_y}{\partial t}, \quad (11)$$

$$\frac{\partial E_y}{\partial x} = -R_i \frac{\partial B_z}{\partial z}. \quad (12)$$

In Eqs, (1) to (12), the ion density n_i, ion flow velocity u_i, ion temperature T_i, electric field E, magnetic field B and variables x and t are the non-dimensionalised with respect to N_0, C_{sf}, T_{ef}, T_{ef}/eL, B_0, L and L/C_{sf} respectively, where

$$C_{sf} = \left[\frac{T_{ef}}{m_i}\right]^{1/2}, \quad T_{ef} = \frac{T_{eh}\,T_{el}}{N_{eh}\,T_{el} + N_{el}\,T_{eh}},$$

$$R_i = \frac{\omega_i}{\omega_0}, \quad A = \frac{C_{sf}}{V_A}, \quad M = \left[\frac{\lambda_{Df}}{L}\right]^2.$$

N_0 is total electron density, ω_0 characteristic frequency, λ_{Df} Debye length, L characteristic scale length. Subscript i is used for ions and the subscripts

eh and *el* are used for high temperature and low temperature components of isothermal electrons.

Introducing the stretched variables $\xi = \varepsilon^{1/2}(x - V_P t)$ and $\tau = \varepsilon^{3/2} t$ ($\varepsilon^{1/2}$ is a small parameter proportional to the wave number and V_P is the non-dimensional phase velocity of the wave) and assuming E_x, E_z, B_y, u_{iy}, η_i and k_i to be of the order of $\varepsilon^{1/2}$ all the dependent variables are expanded as series of ε around the uniform state as follows:

$$g = g_0 + \sum_{j=1}^{\infty} \varepsilon^j g^{(j)}, \tag{13}$$

where g stands for dependent variables and g_0 represents the equilibrium state so that

$$g_0 = \begin{cases} 1,\ N_{e1},\ N_{eh} & \text{for the densities of ions, low and high-temperature electrons, respectively;} \\ 0 & \text{for all components of velocity and electric field;} \\ \cos\theta,\ 0,\ \sin\theta & \text{for the three components of the magnetic field;} \\ T_{i0} & \text{for the ion temperature.} \end{cases}$$

Substituting Eq. (13) in Eqs. (1) to (12) and equating the coefficients of ε, one has

$$V_p = \left[1 + \frac{5}{3} T_{i0} + \frac{\sin^2\theta}{A^2}\right]^{1/2}. \tag{14}$$

The phase velocity V_p in Eq. (14) is the same as the velocity of propagation of hydromagnetic waves which one can obtain for the same plasma system in the linear approximation.

Equating the coefficients of ε^2 in Eqs. (1) to (12) and eliminating the second order dependent variables, a Korteweg—de Vries—Burgers equation is obtained for $n_i^{(1)}$ as given below:

$$\frac{\partial n_1^{(i)}}{\partial \tau} + \frac{1}{2V_P}\left[(3 - \Delta) + \frac{40 T_{i0}}{9} + \frac{2\sin^2\theta}{A^2}\right] n_i^{(1)} \frac{\partial n_i^{(1)}}{\partial \xi} + \frac{1}{2V_P}\left[M + \frac{\sin^2\theta}{A^4 R_i^2}\left(1 - \frac{\cos^2\theta}{A^2 V_P^2}\right)\right] \frac{\partial^3 n_i^{(1)}}{\partial \xi^3} - 2\left[\frac{\eta_0}{3} + \frac{k_0 T_{i0} V_P^{-2}}{9}\right] \frac{\partial^2 n_i^{(1)}}{\partial \xi^2} = 0. \tag{15}$$

Here $\Delta = [N_{eh} T_{eh}^{-2} + N_{el} T_{e1}^{-2}] T_{ef}^2$, $\eta_i = \varepsilon^{1/2} \eta_0$, $k_i = \varepsilon^{1/2} k_0$.

In Eq. (15), the coefficient of third term describes the effect of dispersion.

For further discussion, Eq. (15) is written as

$$P_1^{-1}\frac{\partial f}{\partial \tau}+f\frac{\partial f}{\partial \varepsilon}+\beta_1\frac{\partial^3 f}{\partial \varepsilon^3}-\mu_1\frac{\partial^2 f}{\partial \varepsilon^2}=0 \tag{16}$$

which resembles the Korteweg—de Vries—Burgers equation obtained by SHUKLA and TAGARE [3]. But here

$$P_1=\left[(3-\Delta)+\frac{40T_{i0}}{9}+\frac{2\sin^2\theta}{A^2}\right]\Big/2V_p;$$

$$\beta_1=\frac{M+\dfrac{\sin^2\theta}{A^4R_i^2}\left(1-\dfrac{\cos^2\theta}{A^2V_p^2}\right)}{(3-\Delta)+\dfrac{40T_{i0}}{9}+\dfrac{2\sin^2\theta}{A^2}}$$

and

$$\mu_1=\frac{2}{P_1}\left(\frac{\eta_0}{3}+\frac{k_0\,T_{i0}\,V_p^{-2}}{9}\right).$$

For stationary solution. Eq. (16) yields

$$\beta_1\frac{d^2f}{d\chi^2}-\mu_1\frac{df}{d\chi}+\frac{1}{2}f^2-\left(\frac{U}{P_1}\right)f=0, \tag{17}$$

where $\chi=\xi-U\tau$ and $U=v_0/C_{sf}$.

The solitary wave solution of Eq. (17) in the limit $\mu_1/\beta_1\to 0$ will be

$$f=3U\left(\frac{1}{P_1}\right)\operatorname{sech}^2\left[\left(\frac{U}{4P_1\beta_1}\right)^{1/2}(\xi-U\tau)\right]. \tag{18}$$

In the finite limit of μ_1/β_1, Eq. (17) describes a shock wave [5] and the effective potential well is given by

$$V(f)=\frac{f^3}{6}-\frac{U}{2P_1}f^2. \tag{19}$$

The speed of the shock wave in the rest frame is

$$v_0=C_{sf}\left(1+\frac{P_1\bar{f}}{2}\right), \tag{20}$$

where $\bar{f}=f(-\infty)-f(\infty)$ and $f(\infty)=0$.

Following the method of KARPMAN [5], one can show that Eq. (17) has a monotonic shock wave solution when $\mu_1 > \mu_{1cr}$ and an oscillatory shock wave solution when $\mu_1 < \mu_{1cr}$ where

$$\mu_{1cr} = (2\beta_1 \bar{f})^{1/2}. \tag{21}$$

If $\mu_1 \ll \mu_{1cr}$, then the stationary solution is given by

$$f = \bar{f} + \text{const. exp}\left(\frac{\mu_1}{2\beta_1}\chi\right) \cos\left[\left(\frac{\bar{f}}{2\beta_1}\right)^{1/2}\chi\right]. \tag{22}$$

3. Numerical calculations and conclusions

Eq. (18) shows that due to the presence of magnetic field and the ion temperature, the range of Δ for which the solitary wave exists is increased. The solitary wave exists for $\Delta < 3 + \frac{5T_{i0}}{3} + \frac{2\sin^2\theta}{A^2}$. But an additional condition must be satisfied, i.e.

$$\frac{\lambda_D^2}{L^2} = M \geq \frac{\sin^2\theta}{A^4 R_i^2}\left(1 - \frac{\cos^2\theta}{A^2 V_P^2}\right). \tag{23}$$

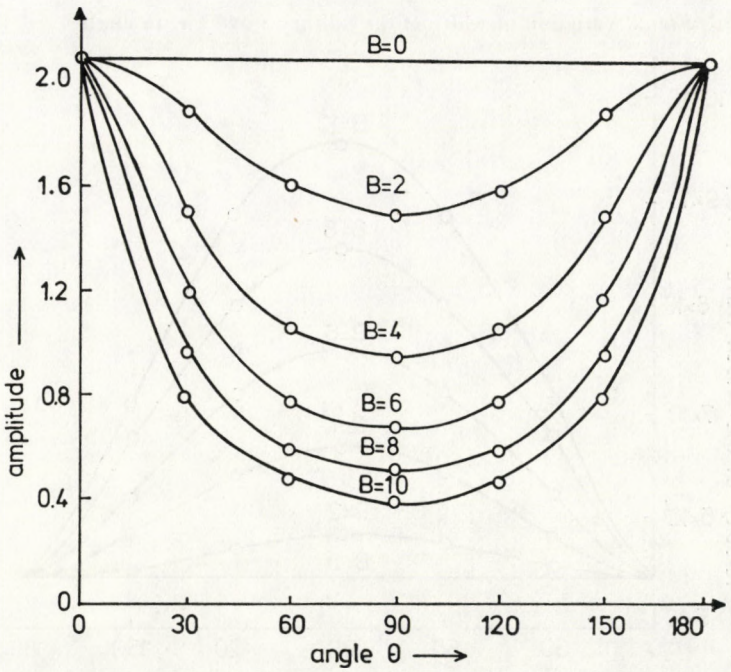

Fig. 1. Variation of the amplitude of the solitary wave w.r. to angle θ

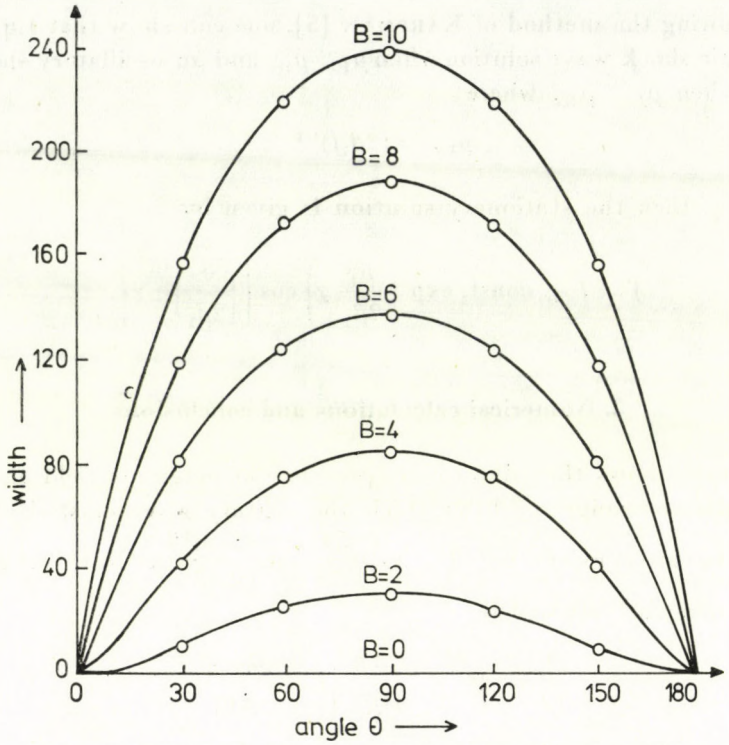

Fig. 2. Variation of width of the solitary wave w.r. to angle θ

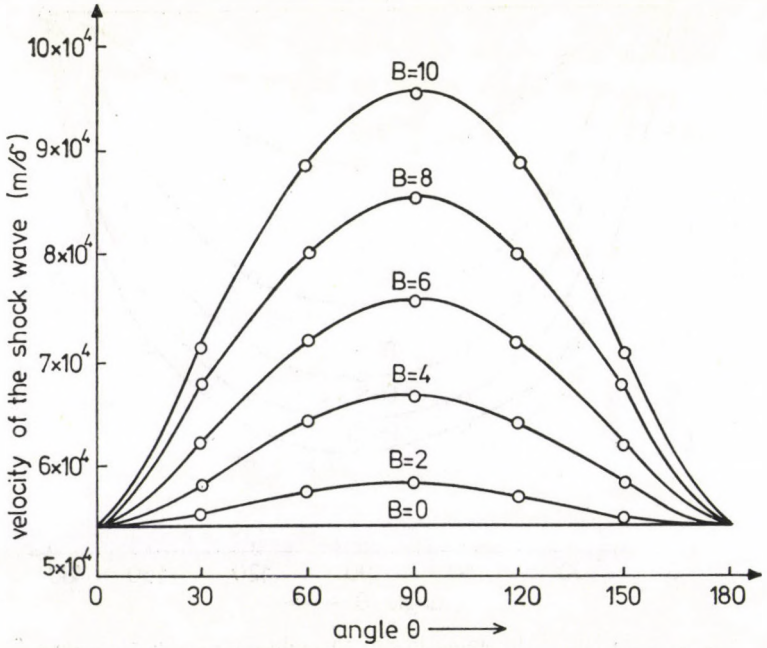

Fig. 3. Variation of the velocity of the shock wave w.r. to angle θ

compared to the obvious condition $M \geq 0$ in the absence of applied magnetic field. Some sample calculations have been made to show the effect of magnetic field explicitly on the amplitude and width of the solitons and the speed of the shock wave for a plasma with the following parameters:

$$T_i = 10^4\ ^\circ\mathrm{K}, \qquad N_0 = 10^{24}\ m^{-3}, \qquad L = 0.1\ \mathrm{m},$$
$$T_{e1} = 2 \times 10^5\ ^\circ\mathrm{K}, \qquad N_{e1} = N_{eh} = 0.5 \times 10^{24}\ \mathrm{m}^{-3}, \qquad U = \bar{f} = 1,$$
$$T_{eh} = 3 \times 10^5\ ^\circ\mathrm{K}, \qquad B = 2 \text{ to } 10 \text{ Tesla}, \qquad \eta_0 = k_0 = 1.$$

The amplitude and the width of the solitary wave are plotted in Figs. 1 and 2 for various values of the magnitude and direction of the magnetic field. The amplitude of the solitary wave decreases whereas its width increases as the magnitude of the magnetic field increases. The effect of the magnetic field is strongest for perpendicular propagation where it tends to flatten the soliton. Fig. 3 gives the speed of the shock wave and it is seen that it increases with the magnetic field.

REFERENCES

1. W. D. Jones, A Lee, S. M. Cleman and H. J. Doucet, Phys. Rev. Lett., **35**, 1349, 1975.
2. B. N. Goswami and B. Buti, Phys. Lett., **57A**, 149, 1976.
3. P. K. Shukla and S. G. Tagare, Phys. Lett., **59A**, 38, 1976.
4. R. C. Davidson, Methods in Nonlinear Plasma Theory, Academic Press, New York, Chap. 2, 1972.
5. V. I. Karpman, Nonlinear Waves in Dispersive Media, Pergamon Press, Oxford, 1975.

Acta Physica Academiae Scientiarum Hungaricae, Tomus 46 (1), pp. 39—43 (1979)

SIMILARITY SOLUTIONS FOR PLANE RELATIVISTIC FLOW IN A HOMOGENEOUS MEDIUM

By

G. DEB RAY

DEPARTMENT OF MATHEMATICS, ST. XAVIER'S COLLEGE, CALCUTTA-16, INDIA

(Received 27. XII. 1978)

Similarity solutions in closed forms for propagation of plane shock waves in a relativistic gas of uniform number density are obtained. The shock moves with constant speed.

Introduction

Similarity solutions for one-dimensional flow of a relativistic fluid headed by a shock front in a cold gas are studied by ELTGROTH [2], by assuming the velocity of the fluid as the similarity variable.

In the present paper similarity solutions in closed forms are obtained when the plane shock front moves through a homogeneous medium of uniform nucleon number density.

The origin of the (x, t) inertial co-ordinate frame is taken at a plane where an initial disturbance is given.

We find that such a flow for the similarity parameter $\xi = x^a t^b$, a and b being suitable constants, exists only when the shock moves with a constant velocity. The solutions given in this paper are applicable only to a medium of uniform pressure or a cold gas.

Equations of motion and boundary conditions

$$\frac{\partial}{\partial x}\left\{\frac{p+\beta^2 E}{1-\beta^2}\right\}+\frac{\partial}{\partial\, ct}\left\{\frac{\beta(p+E)}{1-\beta^2}\right\}=0, \tag{1}$$

$$\frac{\partial}{\partial x}\left\{\frac{\beta(p+E)}{1-\beta^2}\right\}+\frac{\partial}{\partial ct}\left\{\frac{E+\beta^2 p}{1-\beta^2}\right\}=0, \tag{2}$$

$$\frac{\partial}{\partial x}\left\{\frac{n\beta}{\sqrt{1-\beta^2}}\right\}+\frac{\partial}{\partial ct}\left\{\frac{n}{\sqrt{1-\beta^2}}\right\}=0, \tag{3}$$

where p is the pressure and E the proper energy density, both measured in the rest frame of the fluid; $c\beta$ is the fluid velocity in the (x, t) inertial frame, c being the speed of light and n is the nucleon number density.

The shock conditions are

$$\left[\frac{p+\beta^2 E}{1-\beta^2}\right]=\frac{dX}{dct}\left[\frac{\beta(p+E)}{1-\beta^2}\right], \tag{4}$$

$$\left[\frac{\beta(p+E)}{1-\beta^2}\right]=\frac{dX}{dct}\left[\frac{E+\beta^2 p}{1-\beta^2}\right], \tag{5}$$

$$\left[\frac{n\beta}{(1-\beta^2)^{1/2}}\right]=\frac{dX}{dct}\left[\frac{n}{(1-\beta^2)^{1/2}}\right]. \tag{6}$$

Here [ ] signifies the discontinuity sign and $\mathrm{d}X/\mathrm{d}t$ is the velocity of the shock, X being the distance of the shock plane from the origin.

The nucleon density of the pre-shock stage is given by

$$n_0 = \text{constant}. \tag{7}$$

Solutions of the equations

We next introduce the following similarity transformations as done by COURANT and FRIEDRICHS [1] for non-relativistic motions of gases:

$$c\beta = \frac{x}{t}\,U(\xi),$$

$$p = x^{k+2}\,t^{\lambda-2}\,P(\xi),$$

$$E = x^{k+2}\,t^{\lambda-2}\,Z(\xi),$$

$$n = x^{k}\,t^{\lambda}\,\Omega(\xi),$$

where

$$\xi = x^a t^b.$$

Here λ, k, a and b are constants to be determined from the problem.

By their direct substitutions in Eqs. (1)—(3) and boundary conditions (4)—(6), we find that these forms are compatible only when we choose $a/b = -1$ and $\lambda + k = 0$. Without any loss we take $a = 1$ and $b = -1$, $\lambda = 0$ and $k = 0$.

For our subsequent work we choose the similarity parameter in dimensionless form as

$$\eta = \frac{x}{ct}. \tag{8}$$

At the shock front $\eta = \eta_0$ and is taken as constant. So,

$$\eta_0 = \frac{X}{ct} = \frac{V}{c}, \tag{9}$$

V being the constant velocity of the shock front.

The boundary conditions at the shock front may be re-written as

$$\frac{p_1}{p_0} = \frac{\beta_1 \eta_0 N + 1}{1 - \beta_1 \eta_0}, \tag{10}$$

$$\frac{E_1}{E_0} = \frac{\eta_0 N + \beta_1}{N(\eta_0 - \beta_1)}, \tag{11}$$

$$\frac{n_1}{n_0} = \eta_0 \frac{(1 - \beta_1^2)^{1/2}}{\eta_0 - \beta_1}, \tag{12}$$

where $N = E_0/p_0$and the subscripts 1 and 0 stand respectively for quantities just behind the shock and just in front of it.

We find that unlike its non-relativistic analogue, there are two characteristic parameters, instead of one, namely, $\eta_0 = V/c$ and N, depending on the equation of state of matter in its pre-shock condition.

In the region behind the shock plane we take the equation of state,

$$p = \frac{1}{3} E. \tag{13}$$

Eqs. (1)—(3) are now transformed as

$$\frac{d}{d\eta}\left[\frac{E(1/3 + \beta^2)}{1 - \beta^2}\right] = \eta \frac{d}{d\eta}\left[\frac{4/3\, \beta E}{1 - \beta^2}\right], \tag{14}$$

$$\frac{d}{d\eta}\left[\frac{4/3\, \beta E}{1 - \beta^2}\right] = \eta \frac{d}{d\eta}\left[\frac{E(1 + \beta^2/3)}{1 - \beta^2}\right], \tag{15}$$

$$\frac{d}{d\eta}\left[\frac{n\beta}{\sqrt{1 - \beta^2}}\right] = \eta \frac{d}{d\eta}\left[\frac{n}{\sqrt{1 - \beta^2}}\right]. \tag{16}$$

Combining (1) and (2) we also find as ELTGROTH [2]

$$\frac{1}{E}\frac{dE}{d\eta} = \pm \frac{4}{\sqrt{3}} \cdot \frac{1}{(1 - \beta^2)} \frac{d\beta}{d\eta}. \tag{17}$$

Eqs. (1) and (2) are next re-arranged as

$$\frac{1}{E}\frac{dE}{d\eta} = \frac{d\beta}{d\eta} \cdot \frac{4}{(1 - \beta^2)} \cdot \frac{(\beta^2 \eta + \eta - 2\beta)}{(1 + 3\beta^2 - 4\beta\eta)} \tag{18}$$

and

$$\frac{1}{E}\frac{dE}{d\eta} = \frac{d\beta}{d\eta} \cdot \frac{4}{(1-\beta^2)} \cdot \frac{(2\beta\eta - 1 - \beta^2)}{(4\beta - 3\eta - \eta\beta^2)}, \tag{19}$$

Comparing (18) and (19) with (17) when $d\beta/d\eta \neq 0$, we get,

$$\frac{\beta^2\eta + \eta - 2\beta}{1 + 3\beta^2 - 4\beta\eta} = \frac{2\beta\eta - 1 - \beta^2}{4\beta - 3\eta - \eta\beta^2} = l, \tag{20}$$

where

$$l = \frac{1}{\sqrt{3}} \text{ or } -\frac{1}{\sqrt{3}}.$$

The trial $l = \frac{1}{\sqrt{3}}$ yields as a solution

$$\beta = \frac{\sqrt{3}\,\eta - 1}{\sqrt{3} - \eta} \tag{21}$$

and $l = -\frac{1}{\sqrt{3}}$, represents the solution

$$\beta = \frac{\sqrt{3}\,\eta + 1}{\sqrt{3} + \eta}. \tag{22}$$

Case I

We next investigate the existence of solutions for the case $N = 3$, which is appropriate for an ultra-relativistic initial state.

For the choice $n_0 = \text{const.}$ (Eq. (7)), we easily find from the shock conditions that in this case both E_0 and p_0 are constants.

Eqs. (10) and (11) now give

$$\beta_1 = \frac{3\eta_0^2 - 1}{2\eta_0}, \quad 0 < \eta_0 < 1 \text{ and } |\beta_1| \leq 1. \tag{23}$$

Besides, the solution (21) is consistent with (23) only when $\eta_0 = \frac{1}{\sqrt{3}}$ and $\eta_0 = 1$. Both these values of η_0 are not tenable, as $\eta_0 = \frac{1}{\sqrt{3}}$ in this case implies the shock speed as equivalent to the speed of sound and $\eta_0 = 1$, the shock speed attaining the photonic speed. The solution (22) is also inconsistent with the requirement (23).

So, for the medium considered here, we should take the other alternative in Eqs. (18) and (19), namely, $d\beta/d\eta = 0$

Hence,

$$\beta = \beta_1 \tag{24}$$

$$E = E_1 \tag{25}$$

and

$$n = n_1, \tag{26}$$

which are all constants.

Case II

Next we seek solutions for the other possibility $p_0 = 0$, appropriate for a cold gas. The modified shock conditions yield

$$\beta_1 = \frac{2\eta_0 \pm \sqrt{4\eta_0^2 - 3}}{3} . \tag{27}$$

Solution (21) is consistent with (27), only when $\eta_0 = \frac{\sqrt{3}}{2}$ and so $\beta_1 = \frac{1}{\sqrt{3}}$. Besides, it is found that solution (22) is unfavourable and extraneous.

For the value of β as given by (21), and from (18) and (16), respectively, we find that

$$\log \frac{E}{E_1} = \frac{2}{\sqrt{3}} \left[\log \frac{1+\eta}{1-\eta} + 2 \log (2 - \sqrt{3}) \right], \tag{28}$$

$$\log \frac{n}{n_1} = \frac{\sqrt{3}}{2} \left[\log \frac{1+\eta}{1-\eta} + 2 \log (2 - \sqrt{3}) \right]. \tag{29}$$

In this case if the gas is pushed instantaneously and thereby set into motion, there is a possible backflow as clearly indicated by our solutions. As $\eta \to -1$, both the energy density and number density tend to zero, thereby showing that a portion of matter moves backward and the edge of vacuum is at $\eta = -1$. At this boundary we find that the relativistic material moves with the speed of light into the vacuous region.

REFERENCES

1. R. COURANT and K. O. FRIEDRICHS, Supersonic Flow and Shock Waves, Inter Sc., New York, 1948.
2. P. G. ELTGROTH, Phys. Fluids, **14**, 2631, 1971.

Acta Physica Academiae Scientiarum Hungaricae, Tomus 46 (1), pp. 45—51 (1979)

EXCITATION PROCESSES IN A HOLLOW-CATHODE He—Zn DISCHARGE*

By

E. Lőrincz, P. Richter and I. Péczeli

D EPARTMENT OF ATOMIC PHYSICS, TECHNICAL UNIVERSITY, 1521 BUDAPEST

(Received 30. I. 1979)

Spectroscopic and electronic parameters of a hollow-cathode discharge in the mixture of He and Zn vapour were measured. The excitation processes important for the operation of metal vapour lasers are discussed under different conditions of the discharge.

1. Introduction

Research has been carried out for a long time on noble gas — metal vapour lasers. CW operation and excitation mechanisms of a He—Zn ion laser as a function of different parameters (current and pressure dependence of the output power) are described in [1]. Possible excitations of Zn II levels were examined using flowing afterglow technique in [2, 3] and [4].

In the present experiments the excitation processes of the He—Zn system were examined in a hollow cathode discharge tube by measuring spectroscopic (spontaneous line intensities) and electronic (discharge current and voltage) parameters. The results give information on the processes in the hollow cathode discharge and the excitation of the 4912 Å Zn II laser line.

2. Experimental details

The geometry of the hollow cathode discharge tube used in the experiments is shown in Fig. 1. The required Zn concentration in the tube was maintained by two ovens at equal temperatures. The discharge tube was evacuated by a small vacuum system that consisted of a mechanical and an oil diffusion pump and could be filled by high purity (>99.999%) He gas. The tube was excited by half-wave rectified current. The light from the discharge was imaged to the entrance slit of a Zeiss PGS-2 2 m spectrograph, used as a monochromator. The line intensities selected were measured by a photo-

* The present work has been carried out under a contract with the Central Research Institute for Physies of the Hungarian Academy of Sciences.

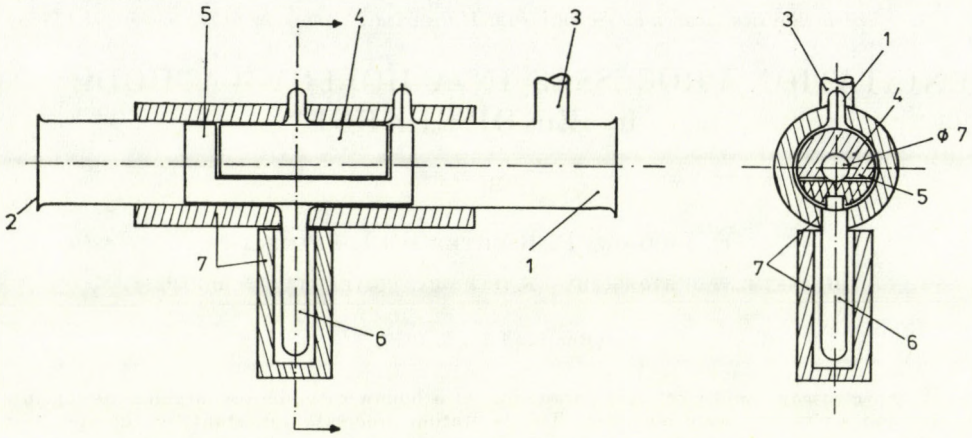

Fig. 1. The hollow cathode discharge tube 1. pyrex tube, 2. end window, 3. connection to the vacuum system, 4. cathode, 5. anode, 6. Zn metal, 7. ovens

multiplier IP28. The output of the multiplier or the discharge voltage was measured with an oscilloscope as a function of discharge current using the horizontal input of the oscilloscope for the latter.

3. Experimental results

Variation of the discharge voltage with the pressure is shown in Fig. 2 at $T = 20$ °C for three values of current. In order to be able to interpret these curves the line intensity of He II at 4685 Å was measured under the same conditions (Fig. 3). Above 6 torr a close correlation can be observed between the two sets of curves.

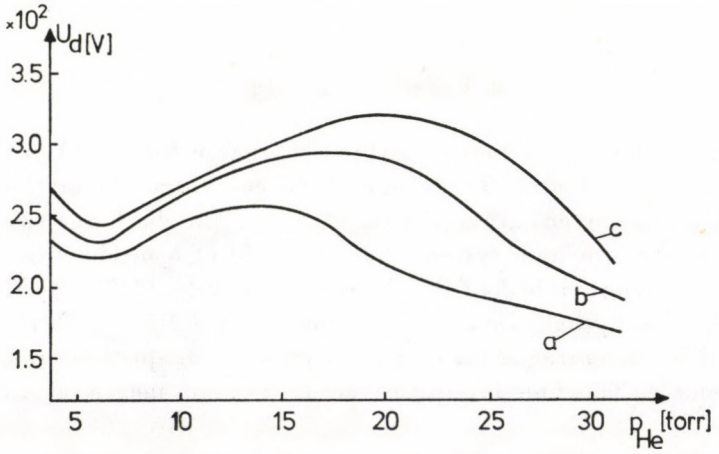

Fig. 2. The variation of discharge voltage with He pressure for different currents a. $I = 126$ mA; b. $I = 252$ mA; c. $I = 378$ mA

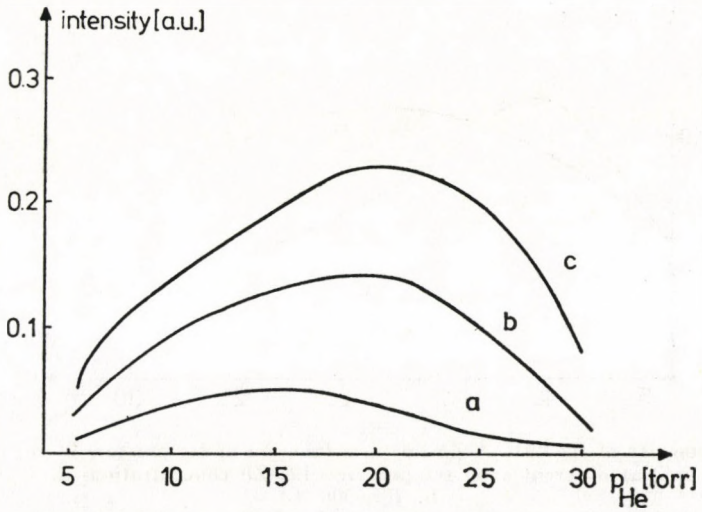

Fig. 3. The intensity of the 4685 Å He II line as a function of the pressure at $T = 20$ °C
a. $I = 126$ mA; b. $I = 252$ mA; c. $I = 378$ mA

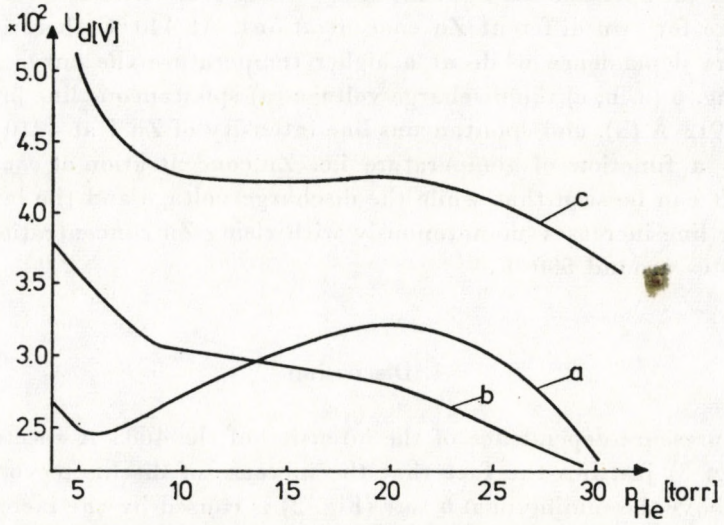

Fig. 4. The dependence of the discharge voltage on He pressure at constant current ($I = 378$ mA) for different oven temperatures (Zn concentration)
a. $T = 20$ °C; b. $T = 440$ °C; c. $T = 500$ °C

Next the voltage dependence on the pressure was measured for different Zn concentrations that were set by keeping the temperatures of the two ovens at determined and equal values. Fig. 4. shows that a low Zn concentration (the melting point of Z 1 is 419.6 °C) changes the original curve significantly and increasing Zn concentration raises the discharge voltage. Fig. 5 shows the

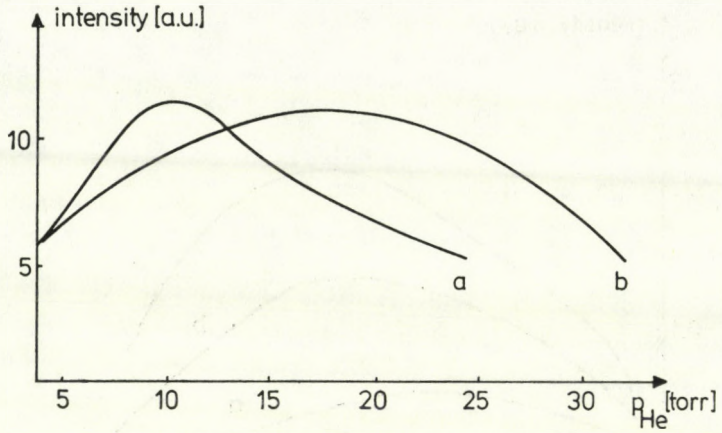

Fig. 5. The intensity of the 4912 Å Zn line as a function of He pressure at constant current ($I = 378$ mA) at different oven temperatures i.e. Zn concentrations a. $T = 440$ °C, b. $T = 500$ °C

variation of the spontaneous light intensity of the 4912 Å Zn II laser line with He pressure for two different Zn concentrations. At 440 °C there is a sharp He pressure dependence while at a higher temperature the curve broadens.

In Fig. 6 (a, b, c) the discharge voltage (a) spontaneous line intensity of Zn II at 4912 Å (b), and spontaneous line intensity of Zn I at 4810 Å (c) are plotted as a function of temperature i.e. Zn concentration at constant He pressure. It can be seen that while the discharge voltage and the intensity of the atomic line increases monotonously with rising Zn concentration the ion line saturates around 500 °C.

4. Discussion

The pressure dependence of the intensity of the 4685 Å spectral line of He II (Fig. 3) justifies the fact that the increase of discharge voltage with pressure above the minimum at 6 torr (Fig. 2) is caused by the increase of He ionization rate. The ionization potential of He is very large (about 25 eV) that means significant electron energy is lost in the course of an elementary ionization process, thus in order to maintain the constant current larger voltage is required. The drop of the discharge voltage at high pressure is probably in connection with the fact that the current is partly displaced from the hollow into the gap between the anode and the cathode in rate this pressure region. It was not possible to measure He ionization rate in the presence of Zn because the upper level for the 4685 Å He II line is of very high energy (about 51 eV) and therefore this level is not populated in the presence of a

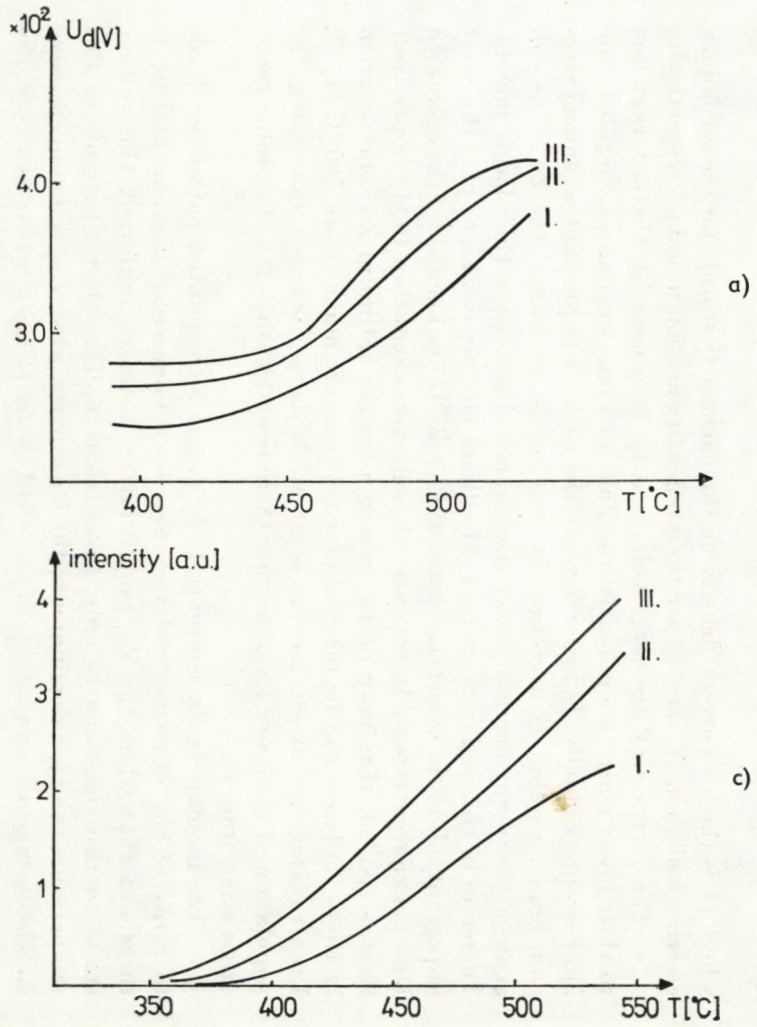

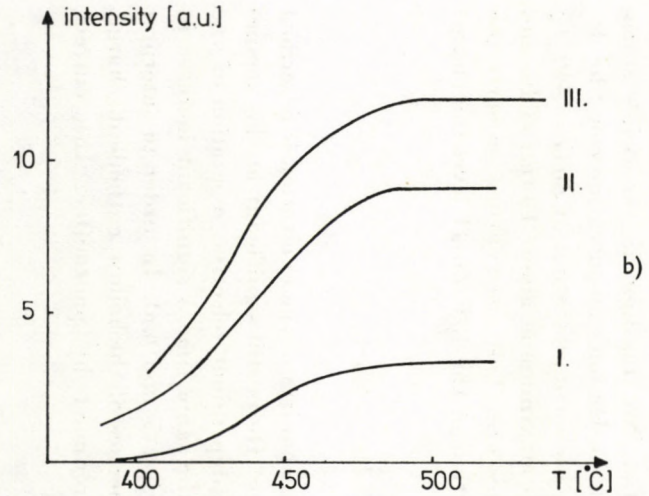

Fig. 6. The discharge voltage (6a), the intensity of the 4912 Å Zn II line (6b), and the intensity of the 4810 Å Zn I line (6c) as a function of oven temperatures, i.e. Zn concentration. He pressure = 10 torr, current I: 126 mA, II: 252 mA, III: 378 mA

component with low ionization potential. No transition in the visible starts from a lower energy level of He II. Still the He ion concentration could be deduced indirectly from Figs. 4 and 5. At a low concentration of Zn ($T = 440$ °C) the intensity of the 4912 Å Zn II line is maximum at about 10 torr of He and shows a strong dependence on He pressure. This observation supports the assumption that in the selective excitation of the $4f^2F$ Zn II level the charge transfer (Duffendach) collisions

$$He^+ + Zn \rightarrow He + Zn^{+*}$$

play an important role. The detailed mechanism of the excitation is described in [3]. This means that the ionization of He is still significant at this temperature. At $T = 500$ °C the He pressure dependent selective excitation of the 4912 Å Zn II line washes out and at the same time a significant increase in discharge voltage can be observed (Figs. 5 and 6/a). In order to interpret this effect one has to consider the properties of the hollow cathode discharge. Neglecting the effect of electrons produced by photoeffect the current density is [5]

$$j = j_c^+(1 + \gamma) = eN_c^+v_c^+(1 + \gamma),$$

where j_c^+ is the ion current density on the cathode, γ stands for the secondary electron emission, N_c^+ and v_c^+ are the ion density and ion mobility, respectively.

The increase of discharge voltage may be caused by the fact that due to their lower ionization potential the Zn^+ ions take over the main role in the ion current gradually. In order to reach the cathode to produce secondary electron emissions that is necessary for the stable discharge, the Zn^+ ions can achieve the energy necessary only at a higher voltage due to their larger masses. Therefore in this region most probably direct electron collisions play the most important role in the excitation of the 4912 Å Zn II line because of the decreased He^+ ion concentration. In this way the selective excitation to the upper laser level is spoiled, that may be the reason why the optimum Zn concentration in He — Zn lasers can be reached at a temperature much below 500 °C [1, 6]. Unfortunately no direct measurement could be carried out concerning the population of the lower level because there is no transition in the visible range originating from it.

The increase in Zn concentration, as has been pointed out above, leads to a rise of the discharge voltage (Fig. 6/a). Comparing Figs. 6a and 6c it turns out that while the Zn concentration increases uniformly the voltage starts to rise significantly only around 450 °C. This shows that under this temperature the He^+ dominates in the ion current while Zn^+ takes over above it. The spontaneous intensity of the 4912 Å Zn II laser line increases in the

temperature range 400—450 °C (range of selective excitation) more than above it and is saturated around 500 °C. The constant current and pressure limits the ionization in spite of the increasing Zn concentration.

5. Conclusion

It was shown that in the He—Zn hollow cathode discharge variation of He and Zn concentrations leads to changes in the discharge parameters through changing the ionization processes in the discharge. These have important effects on the excitation of the 4912 Å Zn II laser transition, namely at low Zn concentration the selective excitation to the upper level of this line dominate through resonant charge transfer collisions with He^+, while at higher Zn concentration direct electron excitation takes over and the selectivity disappears.

Further measurements will be carried out in the case when the Zn is introduced in the form of a volatile molecule to the same discharge. In this case the sufficient Zn concentration can be reached at a lower temperature and at the same time the presence of the electronegative component may cause changes in the discharge.

Acknowledgements

Thanks are due to Prof. I. Kovács for his help and support and to Drs L. Csillag, M. Jánossy and K. Rózsa for valuable discussions.

REFERENCES

1. J. A. Piper and P. Gill, J. Phys. D8, 127, 1975.
2. A. R. Turner-Smith, J. M. Green and C. E. Webb, J. Phys., **B6**, 114, 1973.
3. J. M. Green, G. J. Collins and C. E. Webb, J. Phys., **B6**, 1545, 1973.
4. G. J. Collins, J. Appl. Phys., **44**, 4633, 1973.
5. G. Francis in Encyclopedia of Physics, ed. Flügge, Vol XXII. Springer, Berlin—Göttingen, Heidelberg, 1956, p. 108.
6. J. A. Piper and C. E. Webb, J. Phys., **D6**, 400, 1973.

RECENSIONES

Inelastic Electron Tunneling Spectroscopy

Proceedings of the International Conference and Symposium on Electron Tunneling, University of Missouri—Columbia, USA, May 25—27, 1977. Springer Verlag, Berlin—Heidelberg—New York, 1978.

During the last decades several new material-testing methods have appeared and became generally accepted. A greater part of them is concerned with the investigation of solid surfaces. Let us mention the different electron and ion-irradiating methods (EMP, IMXA), secondary ion mass-spectrometry (SIMS) or the varieties of charged particles activation analysis with nuclear accelerators.

These methods include a separate but substantial group, formed by the different types of electron spectroscopies, by the help of which the spectra of electrons produced by different methods from the surface of solids are investigated, producing qualitative or quantitative or trace- and structure-analytical information. In this respect X-ray and ultra-violet induced photo-electron spectroscopy (XPS alias ESCA and UPS), Auger electron spectroscopy (AES) as well as ion-induced electron spectroscopy (INS) or characteristic energy-loss electron spectroscopy (ELS) should be mentioned.

In spite of its name inelastic electron tunneling spectroscopy (IETS) does not belong to the latter group in the strict sense. Under certain circumstances electrons may penetrate the insulating layer between two metal surfaces (mostly aluminium oxide on Al-surface with Pb evaporated on it) as the result of a quantummechanical tunneling effect. The probability of this penetration depends on the atoms and molecules present at the transition surface and their vibration states, respectively. These appear in the form of a regular spectrum if the second derivative of the current-voltage characteristic of the junction has been taken into consideration. It should be noted here that such investigations are carried out at the temperature of liquid He (4.2 °K) and with modulation techniques. Molecules to be observed e.g. cyclic compounds and materials interesting from the biological point of view should be deposited on the surface of the Al-oxide, in some way. Electron tunneling spectroscopy gives information similar to Raman- and infrared spectroscopy, we may say that it makes them complete.

The book which appeared in one of the Springer series (Series in Solid State Sciences) contains the lectures of an international scientific meeting the aim of which was not only to present and discuss recent scientific results in connection with the method, but also to present the method itself to the wide community of representatives of different fields of application. Thus the book is extremely useful and suitable also for beginners in this field.

The first chapter is devoted to the treatment of the method, the second one to the fields of application, while the third deals with theoretical aspects. Separate chapters are devoted to the description of up-to-date applications, as well as to molecular adsorption on non-metallic surfaces and finally to the application of the so-called elastic tunneling effect.

It is doubtless that IETS seems to possess unique features (e.g. in sensitivity) and to have several possible fields of applications in surface chemistry, biochemistry as well as in the investigation of greasing and adhesion phenomena etc., that is in every field, where the adsorption of complex molecules on metallic oxides have an important role.

Nowadays, however, we may talk about the wide-range possibilities of the method rather than about its justified applications. This fact is pointed out in the contributions by two surface-research scientists and a biologist (Chapter IV, Discussions and Comments). From this point of view tunneling spectroscopy has not achieved yet the maturity so far achieved by electron spectroscopy in the strict sense (XPS, UPS or APS).

D. BERÉNYI

A Perspective of Physics

Volume 2. Selections from 1977 Comments on Modern Physics. Introduced and put into perspective by Sir Rudolf Peierls.

Gordon and Breach Science Publishers, London—New York—Paris, 1978.

It is good to see the second volume of this highly promising series that gives a very useful insight into different fields of physics both by the ingeniously written introduction by Sir RUDOLF PEIERLS and by his careful selection of papers from Comments on Modern Physics by distinguished researchers of their fields.

Rereading the introduction of Vol. 1 one can clearly see the trends in the different branches of physics from the comparison with Vol. 2. The selected papers give a short and clear view of the field they represent. In this way a coherent picture is received by the reader from a very wide subject.

At the same time the individual papers represent most recent research thus giving a useful reference for the specialists as well.

The main chapters are: Nuclear and Particle Physics, Solid State Physics, Astrophysics, Atomic and Molecular Physics, Plasma Physics and Controlled Fusion.

P. RICHTER

E. W. WILLIAMS and R. HALL:

Luminescence and the Light Emitting Diode

International Series on Science of the Solid State. General Editor: B. R. Pamplin, Pergamon Press, Oxford, New York, Toronto, Sidney, Paris, Frankfurt 1978.

This book offers the readers a comprehensive survey of the physics and technology of the light emitting devices (LED's) and p-n junction lasers. The book begins with a good introduction to crystal structures and growth, and the optical and electrical properties of LED materials.

In Chapter 3 the authors summarize the different single crystal growth methods used generally in LED production. A short discussion of the fabrication of the devices together with a useful data collection regarding diffusion processes are included in Chapter 4. A simplified theory of the radiative and nonradiative recombination processes, the luminescent efficiency and the solid-state lasers made from LED materials are discussed in Chapters 5 and 6.

The most important characterization measurement methods such as the photoluminescence, the cathodluminescence, capacity measurements, diode emission evaluation techniques (flux, intensity and colour measurements) are described in detail in Chapters 7 and 8 offering a good physical insight into the light emitting processes in the most important LED materials GaAs, GaP and GaAsP.

In Chapter 9 a survey of light emitting diodes is given together with the discussion of the relationship between aspects of LED design and the electro-optical characteristics. The remainder of the Chapter reviews the progress achieved in producing LED's from different materials.

The book ends with the application aspects of LED products, which are divided into three main groups: (a) LED indicator lamps, (b) LED displays, (c) optically coupled devices.

Although this book is written for post-graduate students, it seems to be useful to a much wider range of readers who would like to know more about LED and the materials from which it is made.

T. GÖRÖG

Gánti, Tibor:

A THEORY OF BIOCHEMICAL SUPER-SYSTEMS. Its application to problems of natural and artificial biogenesis

The *chemoton theory* represents a conceptionally new approach to the deduction of the simplest physical—chemical, macromolecular super-systems satisfying those criteria of life which have been reformulated by the author almost axiomatically, in a more exact presentation than commonly known from the literature. The prospects of the further development of the theory are promising, because the principles of the chemoton model are simple and clear, making the deduction of many basic biological phenomena possible already in its present form, and offering a feasible explanation for the origin of living systems from which the outlines of the strategy for the artificial synthesis of living systems also emerge.

In English — Approx. 80 pages — 17×25 cm — ISBN 963 05 1719 1 — Cloth

AKADÉMIAI KIADÓ, Budapest
Publishing House of the Hungarian Academy of Sciences

Vértes, Attila — Korecz, László — Burger, Kálmán:

MÖSSBAUER SPECTROSCOPY

The introductory part of the book summarizes the physical fundamentals of Mössbauer spectroscopy, the purport of information obtainable from the parameters characterizing the spectrum, and the technique of measurement. The other chapters review the results obtained by applying Mössbauer spectroscopy in the chemistry of solutions, coordination chemistry, quantum chemistry, metallurgy and biochemistry. The material contained in these chapters enables researchers to collect information in their respective branches of science, in addition, they are able to gain insight into the possibilities of the useful applications of the Mössbauer effects for solving problems in their special field.

In English — Approx. 380 pages — Cloth — ISBN 963 05 1670 5

AKADÉMIAI KIADÓ, Budapest **ELSEVIER SCIENTIFIC PUBLISHING COMPANY, Amsterdam**

A new volume in the successful series

ABSORPTION SPECTRA IN THE INFRARED REGION

Ed. by L. LÁNG

Volume 5

This is the fifth volume of the series which presents the infrared spectra of selected organic compounds over the range 400—4000 cm^{-1}, together with full details of sample and experimental conditions. The empirical formula, molecular weight and melting point of each substance is also given. The choice of the spectra has been made by a panel of experienced spectroscopists, who have given primary considerations to covering compounds which have been isolated or synthetized recently. More familiar materials have also been included, generally because the spectra presented for them are more detailed than those of other published sources, or because they refer to different experimental conditions.

The volumes of ABSORPTION SPECTRA IN THE INFRARED REGION provide a valuable source of reference which complements and extends existing sources. Organic chemists and biochemists in academic and industrial laboratories, particularly in the petrochemicals and pharmaceuticals industries, will find this series an easily accessible source of clearly presented infrared spectra of an interesting range of compounds.

In English — Approx. 320 pages — Spectra of 300 compounds — 21×29 cm — ISBN 963 05 1768 X — Cloth

AKADÉMIAI KIADÓ, Budapest **E. KRIEGER PUBLISHING CO. INC., Huntington**

Printed in Hungary

A kiadásért felel az Akadémiai Kiadó igazgatója. Műszaki szerkesztő: Botyánszky Pál
A kézirat a kiadóba érkezett: 1979. II. 1. — A kézirat nyomdába érkezett: 1979. II. 6. — Terjedelem : 5,25 (A/5) ív, 25 ábra

79.6777 Akadémiai Nyomda, Budapest — Felelős vezető: Bernát György

NOTES TO CONTRIBUTORS

I. PAPERS will be considered for publication in Acta Physica Hungarica, only if they have not previously been published or submitted for publication elsewhere. They may be written in English, French, German or Russian.

Papers should be submitted to

Prof. I. Kovács, Editor
Department of Atomic Physics, Technical University
1521 Budapest, Budafoki út 8, Hungary

Papers may be either articles with abstracts or short communications. Both should be as concise as possible, articles in general not exceeding 25 typed pages, short communications 8 typed pages.

II. MANUSCRIPTS

1. Papers should be submitted in five copies.

2. The text of papers must be of high stylistic standard, requiring minor corrections only.

3. Manuscripts should be typed in double spacing on good quality paper, with generous margins.

4. The name of the author(s) and of the institutes where the work was carried out should appear on the first page of the manuscript.

5. Particular care should be taken with mathematical expressions. The following should be clearly distinguished, e.g. by underlining in different colours: special founts (italics, script, bold type, Greek, Gothic, etc.); capital and small letters; subscripts and superscripts, e.g. x_2. x^3; small *l* and 1; zero and capital O; in expressions written by hand: *e* and *l*, *n* and *u*, *v* and *v*, etc.

6. References should be numbered serially and listed at the end of the paper in the following form: J. Ise and W. D. Fretter, Phys. Rev., *76*, 933, 1949.

For books, please give the initials and family name of the author(s), title, name of publisher, place and year of publication, e.g.: J. C. Slater, Quantum Theory of Atomic Structures, I. McGraw-Hill Book Company, Inc., New York, 1960.

References should be given in the text in the following forms: Heisenberg [5] or [5].

7. Captions to illustrations should be listed on a separate sheet, not inserted in the text.

III. ILLUSTRATIONS AND TABLES

1. Each paper should be accompanied by five sets of illustrations, one of which must be ready for the blockmaker. The other sets attached to the copies of the manuscript may be rough drawings in pencil or photocopies.

2. Illustrations must not be inserted in the text.

3. All illustrations should be identified in blue pencil by the author's name, abbreviated title of the paper and figure number.

4. Tables should be typed on separate pages and have captions describing their content. Clear wording of column heads is advisable. Tables should be numbered in Roman numerals (I, II, III, etc.).

IV. MANUSCRIPTS not in conformity with the above Notes will immediately be returned to authors for revision. The date of receipt to be shown on the paper will in such cases be that of the receipt of the revised manuscript.

Reviews of the Hungarian Academy of Sciences are obtainable at the following addresses:

AUSTRALIA
C.B.D. LIBRARY AND SUBSCRIPTION SERVICE, Box 4886, G.P.O., *Sydney N.S.W. 2001*
COSMOS BOOKSHOP, 145 Acland Street, *St. Kilda (Melbourne), Victoria 3182*

AUSTRIA
GLOBUS, Höchstädtplatz 3, *1200 Wien XX*

BELGIUM
OFFICE INTERNATIONAL DE LIBRAIRIE, 30 Avenue Marnix, *1050 Bruxelles*
LIBRAIRIE DU MONDE ENTIER, 162 Rue du Midi, *1000 Bruxelles*

BULGARIA
HEMUS, Bulvar Ruszki 6, *Sofia*

CANADA
PANNONIA BOOKS. P.O. Box 1017, Postal Station "B", *Toronto, Ontario M5T 2T8*

CHINA
CNPICOR, Periodical Department, P.O. Box 50, *Peking*

CZECHOSLOVAKIA
MAD'ARSKÁ KULTURA, Národní třida 22, *115 66 Praha*
PNS DOVOZ TISKU, Vinohradská 46, *Praha 2*
PNS DOVOZ TLAČE, *Bratislava 2*

DENMARK
EJNAR MUNKSGAARD, Norregade 6, *1165 Copenhagen*

FINLAND
AKATEEMINEN KIRJAKAUPPA, P.O. Box 128, *SF-00101 Helsinki 10*

FRANCE
EUROPERIODIQUES S. A., 31 Avenue de Versailles, *78170 La Celle St.-Cloud*
LIBRAIRIE LAVOISIER, 11 rue Lavoisier, *75008 Paris*
OFFICE INTERNATIONAL DE DOCUMENTATION ET LIBRAIRIE, 48 rue Gay-Lussac, *75240 Paris Cedex 05*

GERMAN DEMOCRATIC REPUBLIC
HAUS DER UNGARISCHEN KULTUR, Karl-Liebknecht-Strasse 9, *DDR-102 Berlin*
DEUTSCHE POST ZEITUNGSVERTRIEBSAMT, Strasse der Pariser Kommüne 3—4, *DDR-104 Berlin*

GERMAN FEDERAL REPUBLIC
KUNST UND WISSEN ERICH BIEBER, Postfach 46, *7000 Stuttgart 1*

GREAT BRITAIN
BLACKWELL'S PERIODICALS DIVISION, Hythe Bridge Street, *Oxford OX1 2ET*
BUMPUS, HALDANE AND MAXWELL LTD., Cowper Works, *Olney*, Bucks *MK46 4BN*
COLLET'S HOLDINGS LTD., Denington Estate, *Wellingborough*, Northants *NN8 2QT*
W.M. DAWSON AND SONS LTD., Cannon House *Folkestone, Kent CT19 5EE*
H. K. LEWIS AND CO., 136 Gower Street, *London WC1E 6BS*

GREECE
KOSTARAKIS BROTHERS, International Booksellers, 2 Hippokratous Street, *Athens-143*

HOLLAND
MEULENHOFF-BRUNA B.V., Beulingstraat 2, *Amsterdam*
MARTINUS NIJHOFF B.V., Lange Voorhout 9—11, *Den Haag*
SWETS SUBSCRIPTION SERVICE, 347b Heereweg, *Lisse*

INDIA
ALLIED PUBLISHING PRIVATE LTD., 13/14 Asaf Ali Road, *New Delhi 110001*
150 B-6 Mount Road, *Madras 600002*
INTERNATIONAL BOOK HOUSE PVT. LTD., Madame Cama Road, *Bombay 400039*
THE STATE TRADING CORPORATION OF INDIA LTS., Books Import Division, Chandralok, 36 Janpath, *New Delhi 110001*

ITALY
EUGENIO CARLUCCI, P.O. Box 252, *70100 Bari*
INTERSCIENTIA, Via Mazzé 28, *10149 Torino*
LIBRERIA COMMISSIONARIA SANSONI, Via Lamarmora 45, *50121 Firenze*
SANTO VANASIA, Via M. Macchi 58, *20124 Milano*
D. E. A., Via Lima 28, *00198 Roma*

JAPAN
KINOKUNIYA BOOK-STORE CO. LTD., 17-7 Shinjuku-ku 3 chome, Shinjuku-ku, *Tokyo 160-91*
MARUZEN COMPANY LTD., Book Department, P.O. Box 5050 Tokyo International, *Tokyo 100-31*
NAUKA LTD. IMPORT DEPARTMENT, 2-30-19 Minami Ikebukuro, Toshima-ku, *Tokyo 171*

KOREA
CHULPANMUL, *Phenjan*

NORWAY
TANUM-CAMMERMEYER, Karl Johansgatan 41—43, *1000 Oslo*

POLAND
WĘGIERSKI INSTYTUT KULTURY, Marszałkowska 80, *Warszawa*
CKP I W ul. Towarowa 28 *00-958 Warsaw*

ROUMANIA
D. E. P., *Bucureşti*
ROMLIBRI, Str. Biserica Amzei 7, *Bucureşti*

SOVIET UNION
SOJUZPETCHATJ — IMPORT, *Moscow*
and the post offices in each town
MEZHDUNARODNAYA KNIGA, *Moscow G-200*

SPAIN
DIAZ DE SANTOS, Lagasca 95, *Madrid 6*

SWEDEN
ALMQVIST AND WIKSELL, Gamla Brogatan 26, *101 20 Stockholm*
GUMPERTS UNIVERSITETSBOKHANDEL AB, Box 346, *401 25 Göteborg 1*

SWITZERLAND
KARGER LIBRI AG, Petersgraben 31, *4011 Easel*

USA
EBSCO SUBSCRIPTION SERVICES, P.O. Box 1943, *Birmingham, Alabama 35201*
F. W. FAXON COMPANY, INC., 15 Southwest Park, *Westwood, Mass. 02090*
THE MOORE-COTTRELL SUBSCRIPTION AGENCIES, *North Cohocton, N. Y. 14868*
READ-MORE PUBLICATIONS, INC., 140 Cedar Street, *New York, N. Y. 10006*
STECHERT-MACMILLAN, INC., 7250 Westfield Avenue, *Pennsauken* N. J. 08110

VIETNAM
YXUNHASABA, 32, Hai Ba Trung, *Hanoi*

YUGOSLAVIA
JUGOSLAVENSKA KNJIGA, Terazije 27, *Beograd*
FORUM, Vojvode Mišiča 1, *21000 Novi Sad*

Index: 26.025
Acta Phys. Hung. Tom. 46. No. 1. Budapest, 30. VII. 1979 HU-ISSN 0001-6705

ACTA PHYSICA

ACADEMIAE SCIENTIARUM HUNGARICAE

TOMUS XLVI FASCICULUS 2

AKADÉMIAI KIADÓ, BUDAPEST

1979

ACTA PHYS. HUNG. APAHAQ 46 (2) 55–128 (1979)

ACTA PHYSICA

ACADEMIAE SCIENTIARUM HUNGARICAE

SZERKESZTI

KOVÁCS ISTVÁN

Az *Acta Physica* angol, német, francia vagy orosz nyelven közöl értekezéseket. Évente két kötetben, kötetenként 4—4 füzetben jelenik meg. Kéziratok a szerkesztőség címére (1521 Budapest XI., Budafoki út 8.) küldendők.

Megrendelhető a belföld számára az Akadémiai Kiadónál (1363 Budapest Pf. 24. Bankszámla 215-11488), a külföld számára pedig a „Kultura" Külkereskedelmi Vállalatnál (1389 Budapest 62, P.O.B. 149. Bankszámla 217-10990), vagy annak külföldi képviseleteinél.

The *Acta Physica* publish papers on physics in English, German, French or Russian, in issues making up two volumes per year. Subscription: $ 36.00 per volume. Distributor: "Kultura" Foreign Trading Company (1389 Budapest 62, P.O. Box 149) or its representatives abroad.

Die *Acta Physica* veröffentlichen Abhandlungen aus dem Bereich der Physik in deutscher, englischer, französischer oder russischer Sprache, in Heften, die jährlich zwei Bände bilden.

Abonnementspreis pro Band: $ 36.00. Bestellbar bei »Kultura« Außenhandelsunternehmen (1389 Budapest 62, Postfach 149) oder seinen Auslandsvertretungen.

Les *Acta Physica* publient des travaux du domaine de la physique en français, anglais, allemand ou russe, en fascicules qui forment deux volumes par an.

Prix de l'abonnement: $ 36.00 par volume. On peut s'abonner à l'Entreprise du Commerce Extérieur «Kultura» (1389 Budapest 62, P.O.B. 149) ou chez représentants à l'étranger.

«*Acta Physica*» публикуют трактаты из области физических наук на русском, немецком, английском и французском языках.

«*Acta Physica*» выходят отдельными выпусками, составляющими два тома в год.

Подписная цена — $ 36.00 за том. Заказы принимает предприятие по внешней торговле «Kultura» (1389 Budapest 62, P.O.B. 149) или его заграничные представительства.

ACTA PHYSICA

ACADEMIAE SCIENTIARUM HUNGARICAE

TOMUS XLVI FASCICULUS 2

AKADÉMIAI KIADÓ, BUDAPEST
1979

ACTA PHYS. HUNG.

INDEX

Acta Physica Academiae Scientiarum Hungaricae, Tomus 46 (2), pp. 55—59 (1979)

THE ROLE OF LITHIUM ATOMS IN THE STRUCTURAL CHANGES IN Al-Li ALLOY

By

R. KAMEL, A. R. ALI and Z. FARID

PHYSICS DEPARTMENT, FACULTY OF SCIENCE, CAIRO UNIVERSITY, CAIRO, EGYPT

and

F. ABD EL-SALAM

PHYSICS DEPARTMENT, FACULTY OF EDUCATION, AIN-SHAMS UNIVERSITY, CAIRO, EGYPT

(Received 9. XI. 1978)

The dependence of structural changes in precipitating Al-10 at% Li alloy on the annealing temperatures as traced by X-rays, electric resistivity and microhardness measurements revealed the formation and subsequent dissolution of Al-Li precipitates in the temperature range of 25—500 °C. The observed variations were attributed to the effect of the annealing temperature on the behaviour of Li atoms within the Al matrix. The increase of the Li concentration in the matrix due to the dissolution of Al-Li precipitates, being 3.75 at % Li as obtained from X-ray measurements agreed well with the value 4.0 at % Li obtained from resistivity measurements.

Introduction

It has been reported [1] that in supersaturated Al-Li alloys, the β-phase (Al-Li) precipitated by annealing in the temperature range of 150—300 °C and dissolved at higher temperatures leads to the dispersion of the excess Li atoms by diffusion through the matrix. Such structural changes affected largely both the electrical [2] and mechanical [1] properties of the alloy.

The present work aims at tracing the role of Li atoms in the Al matrix in the structural changes of different temperatures in the alloy from X-ray diffraction tests. Also, it is aimed at relating the variations in electric resistivity and microhardness to these structural changes.

Experimental

Samples of Al-10 at % Li were produced by a method previously described [3]. Quenching from 560 °C to room temperature with a rate of 3×10^3 °C/sec was carried out to bring the samples in a metastable standard condition of solid solution. Isochronal annealings were done by heat pulses of 10 min at temperatures successively increasing in steps of 20 °C. After each heat pulse the resistance of the samples was measured at room temperature using a standard potentiometric method [4]. A dummy sample helped to account for the effect of temperature variation. Microhardness measurements

were also carried out for the electropolished specimens after giving them the prescribed heat treatments [5].

X-ray tests were performed using the Debye—Scherrer film technique in a 114.6 mm diameter Philips camera [6]. Pure Al was used as a reference to ensure the accuracy of measurements and to detect the relative variations in the lattice parameter of the tested samples.

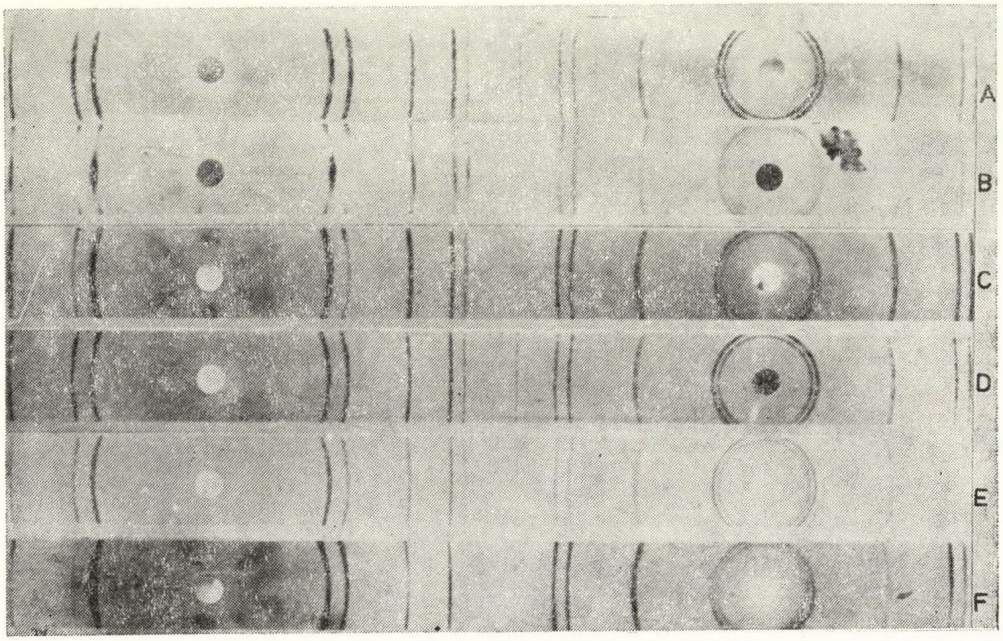

Fig. 1. Typical X-ray photographs for pure Al and Al-10 at % Li alloy

A — Pure Al from the stock.
B — Al-10 at % Li from the stock
C — Al-10 at % Li annealed at 250 °C
D — Al-10 at % Li annealed at 400 °C
E — Al-10 at % Li annealed at 450 °C
F — Al-10 at % Li annealed at 500 °C

Results

Typical X-ray photographs for differently annealed samples of the precipitating Al-10 at % Li alloy are shown in Fig. 1. The variation in the lattice parameter as calculated from (422) $K_{\alpha 1}$ line with the annealing temperature is shown in Fig. 2A. The lattice parameter initially decreased with the annealing temperature followed by an increase at 450 °C. Changes in electric resistivity and microhardness associated with the annealing temperature are also given in Fig. 2 (Band C). The electric resistivity of the precipitating alloy initially

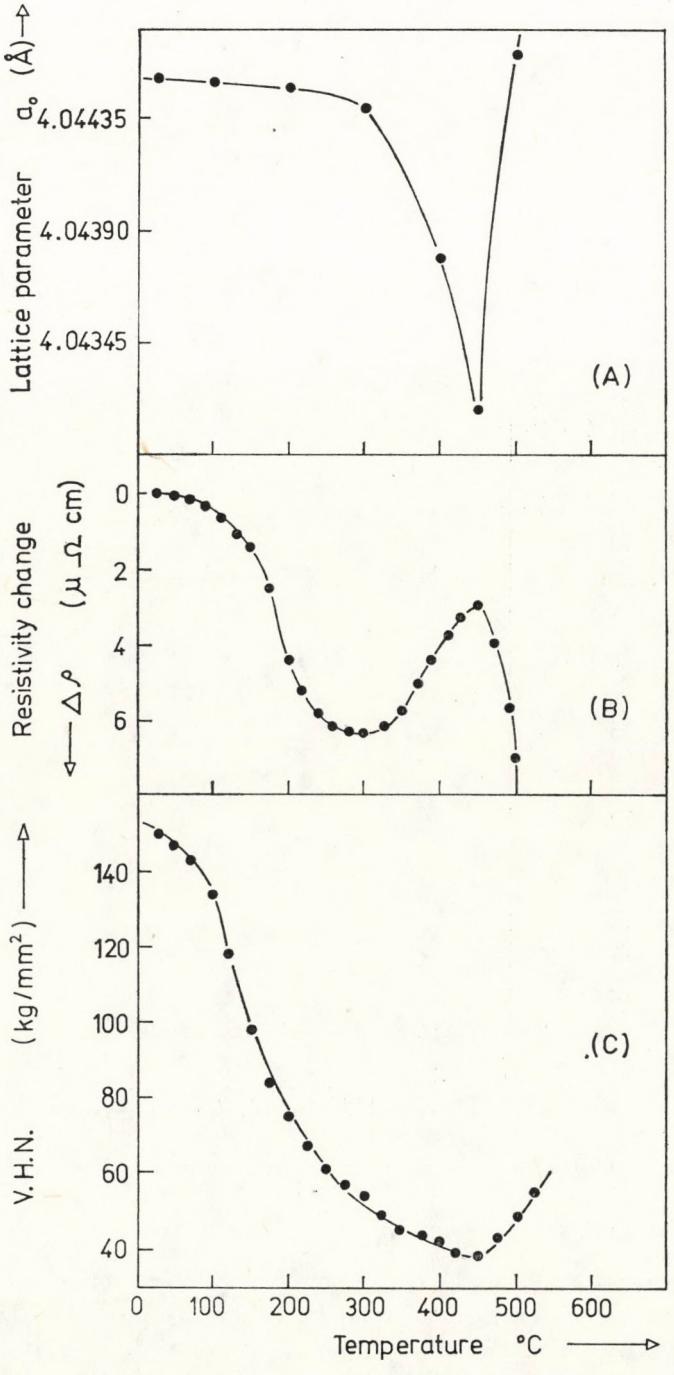

Fig. 2. The change of lattice parameter (curve A), electric resistivity (curve B) and microhardness (curve C) with the annealing temperature of Al-10 at % Li alloy

decreased to 300 °C after which an increase to a peak value was reached at 450 °C, followed by a sharp decrease at higher temperatures. The microhardness of Al-10 at % Li alloy decreased by annealing and reached a minimum value at 450 °C, then increased at higher temperatures (see Fig. 2C).

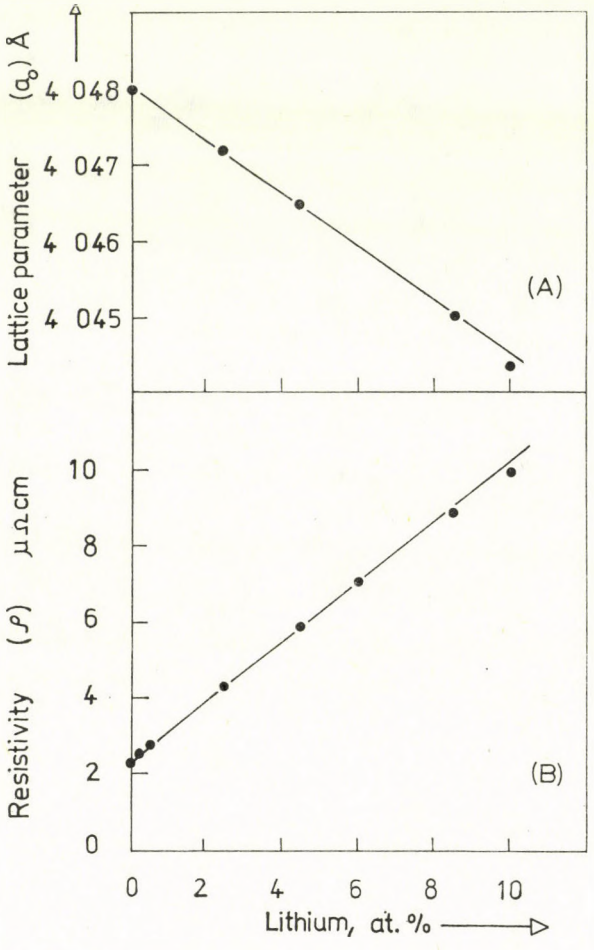

Fig. 3. Dependence of lattice parameter (a_0) and electric resistivity (ϱ) on lithium concentration

Lattice parameter and electric resistivity were found to be linearly dependent on Li concentration as shown in Fig. 3 A and B. The slopes of Fig. 3A and B assumed the values 0.0032 Å /at % Li and 0.81 $\mu\Omega$cm/ at % Li, which are in a good agreement with previous results [7, 8].

Discussion

The different recovery processes here observed in precipitating Al-10 at % Li alloy were first reported by KAMEL et al [2] using internal friction and electric resistivity measurements. Accordingly, the present observed recovery processes in the temperature range 25—450 °C might be ascribed to the growth of coherent Guinier-Preston zones formed at relatively lower temperatures [9] and the precipitation of the β-phase (Al-Li) in the temperature range 200—300 °C [1]. Since no precipitate except (Al-Li) exists, the dissolution of β-phase takes place in the temperature range 300—450 °C [1]. The redissolution of this precipitate caused an increase in the Li concentration existing within the matrix, leading to an increase in electric resistivity of 3.3 $\mu\Omega$cm (see Fig. 2B). The elimination of the strain fields surrounding the dissolved precipitates [10] may be the cause of softening observed in this temperature range.

The observed decrease in the lattice parameter due to dissolution of β-phase in Al-10 at % Li assumed the value 0.0012 Å (see Fig. 2A). From Fig. 3A, this decrease in the lattice parameter corresponds to an increase in Li concentration of about 3.75 at %. Also from Fig. 3B, the observed increase in electric resistivity in the temperature range 300—450 °C corresponds to an increase in Li concentration of 4.0 at % which agrees well with the present X-ray data.

It was reported [2] that above 450 °C Li atoms diffused to the surface of the specimen at which they are burnt. Above 450 °C the loss in Li concentration in the matrix seems to be responsible for the observed increase in lattice parameter and decrease in electric resistivity. Due to the existence of interaction energy between Li atoms and dislocations [1, 3], stabilization of dislocations takes place as a process of anneal hardening [11], which leads to the observed increase in hardness above 450 °C.

REFERENCES

1. S. SAKUI and M. TAMURA, Trans. Japan Isnt. Met., **10**, 343, 1969.
2. R. KAMEL, A. R. ALI and Z. FARID, Phys. Stat. Sol., **45A**, 419, 1978.
3. R. KAMEL, A. R. ALI and Z. FARID, Phys. Stat. Sol., **45A**, 47, 1978.
4. D. TURNBULL, H. S. ROSENBAUM and H. N. TREAFTS, Acta Met., **8**, 277, 1960.
5. R. KAMEL, T. H. YOUSSEF and D. SALAMA, Proc. Mat. Phys. Soc., Egypt, **44A**, 81, 1977
6. R. KAMEL, F. ABD EL-SALAM and S. A. KHAIRY, The First Arab Conference in Phys. and. Math., Baghdad, 1978.
7. H. J. AXON and W. HUME-ROTHERY, Proc. Roy. Soc. **A193**, 1, 1948.
8. K. R. VANHORN, Aluminium, **1**, 50, 1967, A. S. M.
9. S. CERESARA, A. GIARADA and A. SANCHEZ, Phil. Mag., **35**, 97, 1977.
10. K. HIRANO and K. ASANO, Trans Japan Inst. Met., **11**, 225, 1970.
11. P. HAASEN, Physical Metallurgy, North-Holland Publ. Co., Amsterdam, 1970, p. 1139.

Acta Physica Academiae Scientiarum Hungaricae, Tomus 46 (2), pp. 61—68 (1979)

PHONON DISPERSION RELATIONS IN *bcc* TRANSITION METALS

By

B. P. SINGH and M. P. HEMKAR

DEPARTMENT OF PHYSICS, UNIVERSITY OF ALLAHABAD, ALLAHABAD-211002, INDIA

(Received in revised form 5. XII. 1978)

Phonon dispersion relations for the normal modes of lattice vibration in *bcc* transition metals are computed along the three principal symmetry directions using the extended form of the FIELEK five-constant model. The calculated results are compared with the available experimental data obtained from inelastic neutron spectroscopy and a far better agreement than that obtained on the basis of other existing models has been achieved.

I. Introduction

In the recent past, a number of authors, such as BEHARI and TRIPATHI [1], SINGH and SHARMA [2], SHUKLA and PADIAL [3], MAHESH and DAYAL [4] and SHUKLA and CAVALHEIRO [5], have calculated the phonon dispersion relations of *bcc* transition metals using different lattice dynamical models. The main drawback with these approaches is that they have not considered the contribution of *d* shell — *d* shell central interactions. Consequently, their results were not in very good agreement with the experimental ones.

FIELEK [6] has developed a phenomenological model for *fcc* transition metals in which he has taken, for the first time, into account the contribution of *d* shell — *d* shell central interaction. We have successfully applied this model, in its simplified form, in the calculation of phonon dispersion relations of noble metals [7] and *fcc* transition metals [8].

In the present paper, we have used the extended form of the FIELEK five force-constant model for *bcc* transition metals, to calculate the phonon dispersion relations of α-iron, chromium, molybdenum and niobium along the symmetry directions [001], [110] and [111]. The motivation of this study is to check the accuracy of this model for *bcc* transition metals.

II. Theoretical formulation

The secular equation determining the angular frequencies $\omega(=2\pi\nu)$ of the normal modes of vibration in a cubic lattice can be expressed as:

$$| D(q) - M\omega^2 I | = 0, \tag{1}$$

where M is the mass of the atom and I is the unit matrix of order three, q is the phonon wave vector restricted to the first Brillouin Zone (BZ). The expressions for two typical elements of the dynamical matrix $D(q)$ are given below:

$$D_{11}(q) = -\frac{8}{3}\alpha_1(1 - C_1C_2C_3) - 4\alpha_2 S_1^2 - K + \frac{K^2}{N},$$
$$D_{12}(q) = -\frac{8}{3}\alpha_1 S_1 S_2 C_3, \tag{2}$$

where

$$C_i = \cos(aq_i), \qquad S_i = \mathrm{Sin}(aq_i) \quad i = 1, 2, 3.$$

a = Semi-lattice parameter and N can be expressed as

$$| D'(q) - NI | = 0. \tag{3}$$

The two typical elements of this determinant are:

$$D'_{11}(q) = \frac{8}{3}\beta(1 - C_1C_2C_3) + K - A'G(q),$$
$$D'_{12}(q) = \frac{8}{3}\beta S_1 S_2 C_3. \tag{4}$$

The expressions for the remaining elements can be derived in cyclic order from (2) and (4).

The other quantities appearing in Eqs. (2) and (4) are: the radial force constants α_1 and α_2, the nearest neighbours d shell — d shell central interaction force constant β, the ion core—d shell interaction force constant K, the d shell — conduction electrons interaction force constant A' and according to KREBS [9]

$$A'G(q) = A' \sum_H \left[\frac{(q + \mathbf{H})(q + \mathbf{H}_-) \cdot \mathbf{e}G^2(| q + \mathbf{H} | R_0)}{| q + \mathbf{H} |^2 + \left(\frac{a}{\pi}\right)^2 k_c^2(P)} - \right.$$
$$\left. - \frac{\mathbf{HH} \cdot \mathbf{e}G^2(| \mathbf{H} | R_0)}{| H^2 | + \left(\frac{\mathbf{a}}{\pi}\right)^2 k_C^2(P)} \right]. \tag{5}$$

Here $\mathbf{H}$ is the reciprocal lattice vector, $\mathbf{e}$ is polarisation vector, R_0 is Wigner—Seitz radius and $k_c(P)$ is the BOHM—PINE [10] screening parameter. The $G(x)$ in the expression (5) is given as

$$G(x) = 3x^{-3}(\sin x - x \cos x).$$

The five unknown parameters (α_1, α_2, K, β and A') involved in the solution of Eq. (1) are determined by expanding the elements of the determinant in the long wavelength limit ($q \to 0$) and relating them to the three elastic constants and two zone boundary frequencies ν_L and ν_T in [001] and [111] directions (for α-iron and niobium), respectively, but for molybdenum, the two zone boundary frequencies chosen are ν_L and ν_{T2} in [001] and [110] directions, respectively. In the case of chromium the two zone boundary frequencies ν_L and $\nu_{L'}$ are chosen corresponding to [001] and [110] directions, respectively. The resulting expressions are:

$$\alpha_1 + \beta = -3a\, C_{44}\,, \tag{6.a}$$

$$\alpha_2 = -a(C_{11} - C_{12})\,, \tag{6.b}$$

$$A' = 4a^3(C_{12} - C_{44})\, k_C^2(P)\,, \tag{6.c}$$

$$4\pi^2 M\nu_L^2 = -\frac{16}{3}\alpha_1 - K + \frac{K^2}{K + \frac{16}{3}\beta - A'G(q)}\,, \tag{6.d}$$

$$4\pi^2 M\nu_T^2 = -\frac{8}{3}\alpha_1 - 4\alpha_2 - K + \frac{K^2}{K + \frac{8}{3}\beta - A'G(q)}\,, \tag{6.e}$$

$$4\pi^2 M\nu_{T_2}^2 = -\frac{8}{3}\alpha_1 - K + \frac{K^2}{K + \frac{8}{3}\beta - A'G(q)}\,, \tag{6.f}$$

$$4\pi^2 M\nu_{L'}^2 = -\frac{16}{3}\alpha_1 - 4\alpha_2 - K + \frac{K^2}{K + \frac{16}{3}\beta - A'G(q)}\,. \tag{6.g}$$

The solution of these equations determines all the five force constants. The physical constants used in the computation work are listed in Table I, and the calculated values of force constants in Table II, respectively.

Table I

Physical constants

Metal	Elastic constants $\times 10^{11}$ dyn cm^{-2}			Lattice constant (2a) X10^{-8} cm	Zone boundary frequencies (THZ) [001]	[111]	[110]	
	C_{11}	C_{12}	C_{44}		ν_L	ν_T	ν_{T_2}	$\nu_{L'}$
α-Iron	23.31	13.55	11.78	2.8662	8.56	7.21	—	—
Chromium	35.00	6.78	10.08	2.8792	7.554	—	—	9.4
Molybdenum	44.077	17.243	12.165	3.1468	5.51	—	4.67	—
Niobium	23.50	12.10	2.82	3.3004	6.54	5.08	—	—

Table II

Calculated force constants in units of 10^3 dyn cm^{-1}

Metal	α_1	α_2	K	β	A'
α-Iron	−50.6804	−13.9871	0.2481	0.0346	18.4702
Chromium	−45.2785	−40.6255	−12.8488	1.7450	−34.7491
Molybdenum	−71.9092	−42.2206	−124.1429	14.4880	80.4750
Niobium	186.5581	−18.8123	7367.9475	−200.5188	152.2360

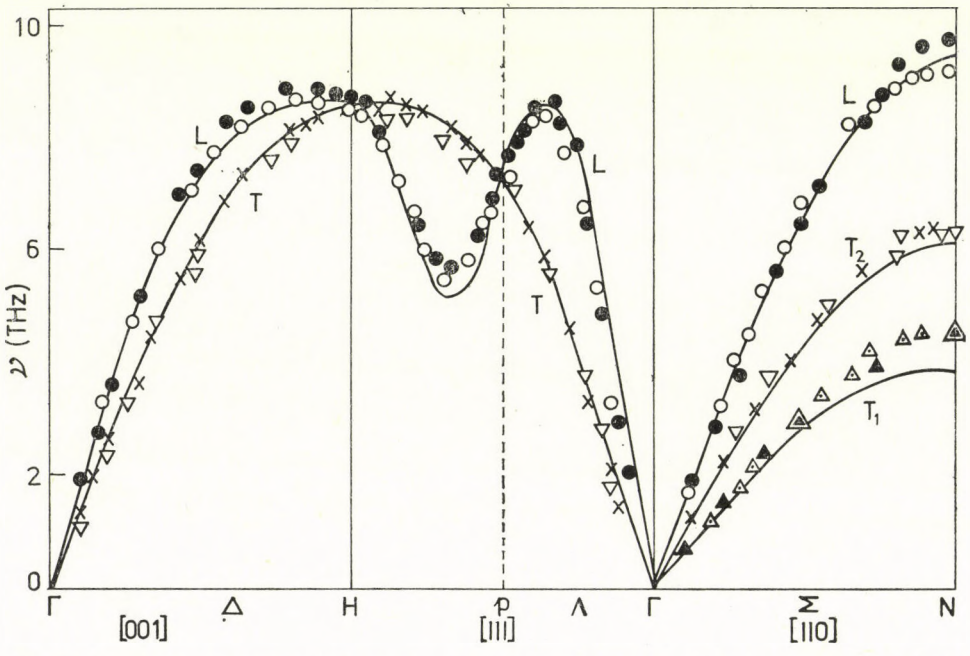

Fig. 1. Dispersion curves along the symmetry direction for α-iron at room temperature. Solid curves correspond to the computed frequencies. Experimental points are shown by ○, ▽, ▲ (MINKIEVICZ et al [11]) and ●, ×, △ (BERGSMA et al [12])

III. Results and discussion

1. *α-iron.* We have utilized here the experimental values of the elastic constants obtained by RAYNE and CHANDRASEKHAR [11] and the experimental phonon frequencies of MINKIEWICZ et al [12] and BERGSMA et al [13]. It is quite obvious from Fig. 1 that there is over all a satisfactory agreement between theoretical and experimental dispersion curves in all the directions except the Σ_{T_1} branch near the zone boundary.

2. *Chromium.* The computed phonon dispersion curves are plotted in Fig. 2 along with the experimental values of phonon frequencies of SHAW and MUHLESTEIN [14] obtained from neutron scattering measurements. The elastic constants used in this computational work are the measurements of BOLEF and DE KLERK [15]. Fig. 2 shows that three is no very satisfactory agreement between our curves and those obtained experimentally in the range P H.

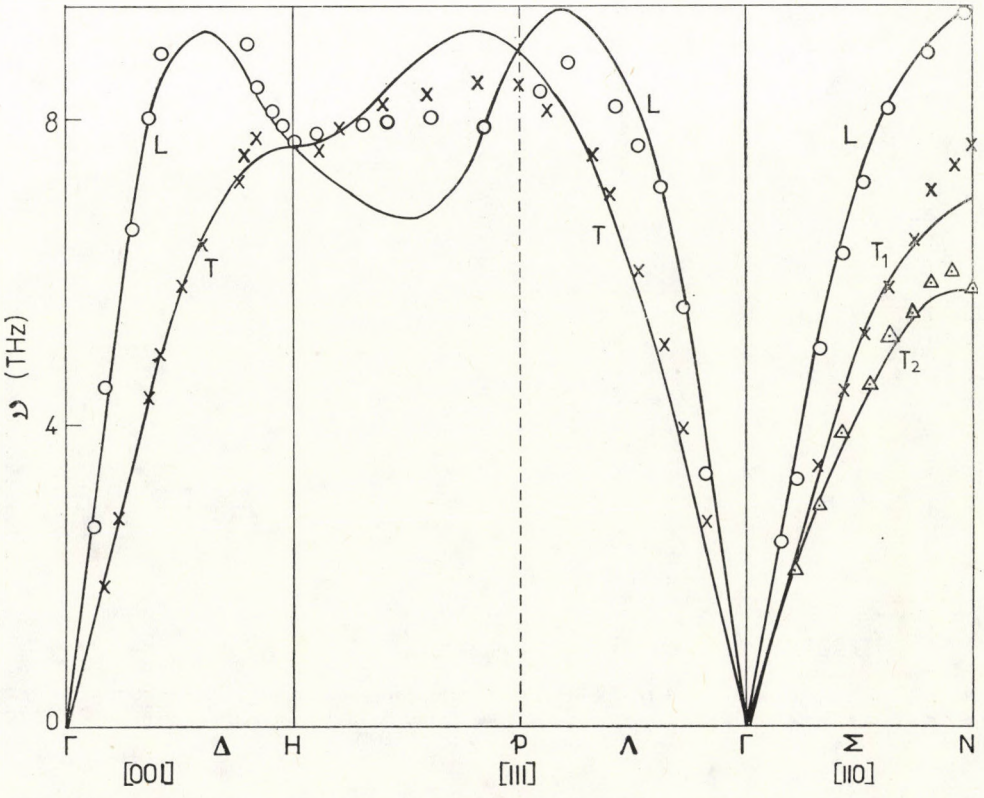

Fig. 2. Dispersion curves along the symmetry directions for chromium at room temperature. Solid curves correspond to present calculations. Experimental points are shown by ○, △, ×, (SHAW and MUHLESTEIN [13])

The agreement is not very good either in Σ_{T_1} branch near the zone boundary. However, they are better than the theoretical curves deduced from other existing models.

3. *Molybdenum.* In this case we have taken the measured values of the elastic constant due to FEATHERSTON and NEIGHBOURS [16]. The computed curves are plotted in Fig. 3. The overall agreement between our dispersion curves and those obtained by WOODS and CHEN [17] is quite satisfactory except in the Δ_L branch near the zone boundary and in the Σ_{T_1} branch.

4. *Niobium.* The phonon dispersion curves, calculated in the symmetry directions using elastic constants of WASILEWAKI [18] are presented in Fig. 4. They have been compared with the measured results of NAKAGAWA and WOODS [19]. The overall agreement of calculated phonon frequencies with the experimental data is quite satisfactory except for the fact that the model could not predict the crossing over of Δ_L and Δ_T branches. The Σ_L branch shows a disagreement with the experimentally obtained phonon frequencies

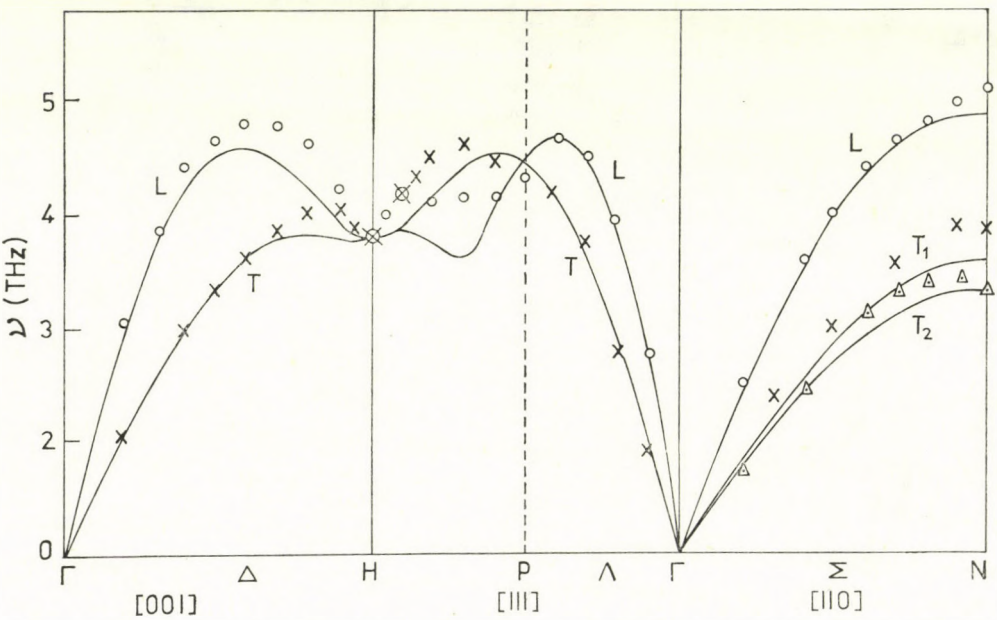

Fig. 3. Dispersion curves along the symmetry directions for molybdenum at room temperature. Solid curves correspond to present calculations. Experimental points are shown by ○, ×, △ (WOODS and CHEN [16])

near the zone boundary. The most salient feature of our computations is the crossing over of Σ_{T_1} and Σ_{T_2} branches, which has never been obtained from any model so far.

The existing discrepancies, may however, be attributed to:

1) The neglect of the contributions of second neighbours *d* shell and the angular interaction.
2) The neglect of ion core-conduction electrons interactions.
3) The form of dielectric function used (in present calculations Lindhard dielectric function).
4) Assumptions of short-range type interactions.
5) The neglect of flexibility of the *d*-orbitals in the present calculations.

A comparison of present study with earlier workers indicates that this model yields better results than those obtained with the models which do not consider the contribution of *d* shell — *d* shell interactions. So we can infer that our model is very suitable for the study of vibrational properties of *bcc* transition metals.

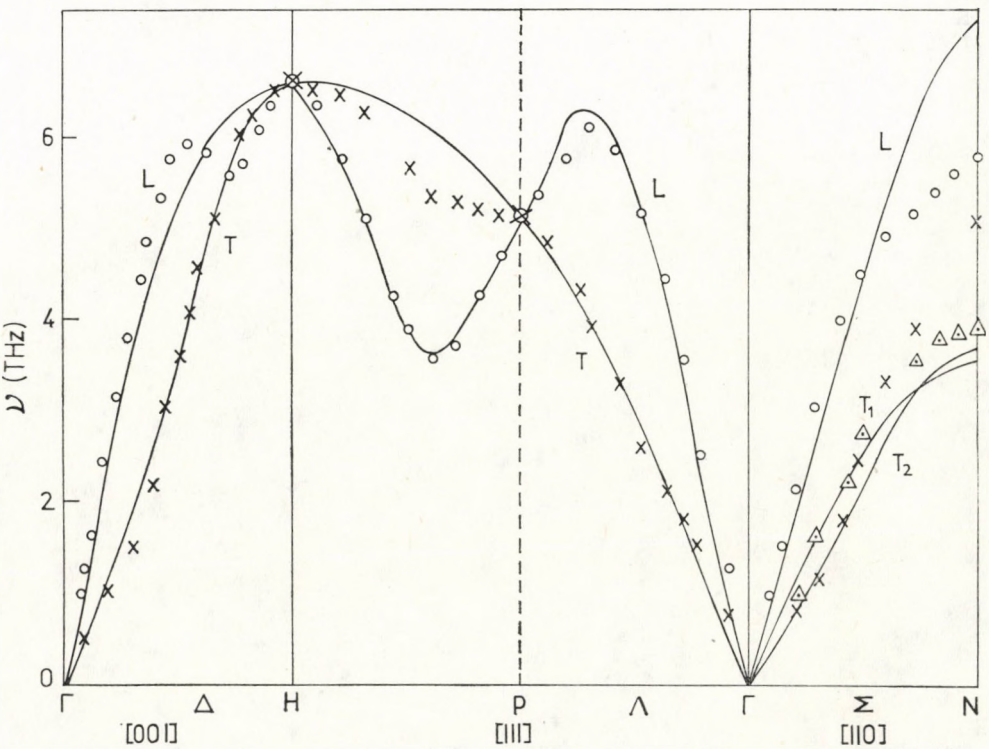

Fig. 4. Dispersion curves along the symmetry directions for niobium at room temperature. Solid curves correspond to the calculated frequencies. Experimental points are shown by ○, ×, △ (NAKAGAWA and WOODS [19])

Acknowledgement

The authors are very grateful to Professor VACHASPATI and Professor BIPIN K. AGARWAL for the encouragement and continued interest in the present study. We are also thankful to Mr. L. P. PATHAK and Mr. M. KUMAR for useful discussions. One of us (B.P.S.) wishes to extend his thanks to the authorities of U.G.C. New Delhi for awarding a 'Teacher fellowship'.

REFERENCES

1. J. BEHARI and B. B. TRIPATHI, J. Phys. Soc. Japan, **33**, 1207, 1972.
2. A. K. SINGH and P. K. SHARMA, J. Phys. Soc. Japan, **26**, 425, 1969.
3. M. M. SHUKLA and N. T. PADIAL, Nuovo Cimento Italy, **34B** Ser. 2, 103, 1976.

4. P. S. MAHESH and B. DANYL, Phys. Rev., **143**, 443, 1966.
5. M. M. SHUKLA and R. CAVALHEIRO, Acta Phys. Polonica, **49A**, 27, 1976.
6. B. L. FIELEK, J. Phys. F. Metal Physics, **5**, 17, 1975.
7. B. P. SINGH, L. P. PATHAK and M. P. HEMKAR, Acta Phys. Polonica, **54A**, 207, 1978.
8. B. P. SINGH, L. P. PATHAK and M. P. HEMKAR, J. Phys. Soc. Japan, **45**, 484, 1978.
9. K. KREBS, Phys. Rev., **138**, 143, 1965.
10. D. BOHM and D. PINES, Phys. Rev. **85**, 338, 1952; **92**, 609, 1953.
11. J. A. RAYNE and B. S. CHANDRASEKHAR, Phys. Rev., **122**, 1714, 1961.
12. V. J. MINKIEWICZ, G. SHIRANE and R. NATHANS, Phys. Rev., **162**, 528, 1967.
13. J. BERGSMA, C. VAN DIJK and D. TOCCHETTI, Phys. Lett., **24A**, 270, 1967.
14. W. M. SHAW and L. D. MUHLESTEIN, Phys. Rev., **B4**, 969, 1971.
15. D. I. BOLEF and J. DEKLERK, Phys. Rev., **129**, 1063, 1963.
16. F. H. FEATHERSTON and J. R. NEIGHBOURS, Phys. Rev., **130**, 1324, 1963.
17. A. D. B. WOODS and S. H. CHEN, Solid State Commun., **2**, 233, 1964.
18. R. J. WASILEWAKI, J. Phys. Chem. Solids, **26**, 1643, 1965.
19. Y. NAKAGAWA and A. D. B. WOODS, Phys. Rev. Letters, **11**, 271, 1963.

Acta Physica Academiae Scientiarum Hungaricae, Tomus 46 (2), pp. 69—76 (1979)

QUANTUM CHEMICAL STUDY OF INTERNAL ROTATIONS IN LIQUID CRYSTAL MOLECULES

By

S. KUGLER and G. NÁRAY-SZABÓ

QUANTUM THEORY GROUP, PHYSICAL INSTITUTE, TECHNICAL UNIVERSITY, BUDAPEST AND CHINOIN PHARMACEUTICAL AND CHEMICAL WORKS, BUDAPEST

(Received 13. II. 1979)

The rotational barriers of p-azoxy-anisole and dibutyl-phenyl-benzoyloxy-benzoates nematic liquid crystal molecules were calculated by the PCILO and CNDO/2 quantum chemical methods. It was found that motion in the side group is hindered to a given extent. According to chemical evidence the central part of the molecules is supposed to be completely rigid.

1. Introduction

The microdynamics of liquid crystal molecules has been studied earlier by means of quasi-elastic neutron scattering, NMR spectroscopy and dielectrical relaxation time measurements, respectively [1—4]. In this work quantum

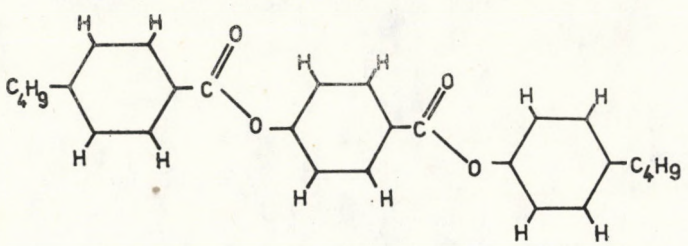

Fig. 1. The PAA molecule

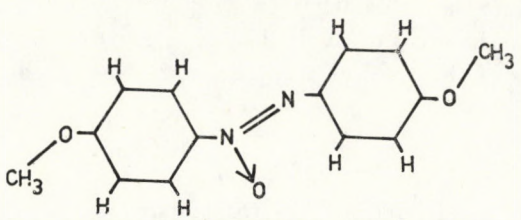

Fig. 2. The PB-DBB molecule

chemical results on p-azoxy-anisole PAA, (Fig. 1) and dibutyl-phenyl-benzoyloxy-benzoate DB-PBB, (Fig. 2) are summarized. The former is nematic in the temperature range of 116—136 °C, while the latter in the range of 85—183 °C, respectively.

The PCILO [5, 6] and CNDO/2 [7] methods were used simultaneously. It is known that both methods yield semiquantitative results for barriers to rotation around σ-bonds [8]. In case of delocalization serious discrepancies can arise [8]; the problem is discussed in case of our model molecules, too. These were used in order to reduce computer capacity necessary to the calculations. Details of calculations and results are given separately for both molecules in subsequent sections.

2. p-azoxy-anisole

Rotation of the methyl group

To examine the reliability of both quantum chemical methods for the rotation of methyl group around the CO σ-bond (see Fig. 1) methanol was examined as an example. PICLO yielded 0.79 kcal · mol^{-1}, the experimental

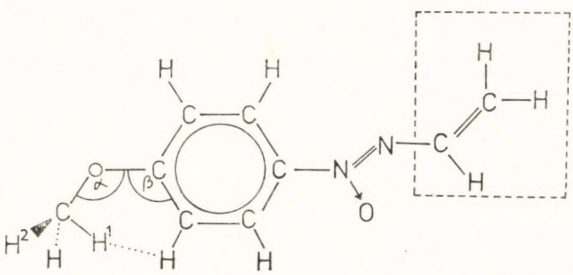

Fig. 3. Simplified model of the PAA molecule

value is 1.07 kcal · mol^{-1} [8]. According to literature data [10] the CNDO/2 method, combined with a rigid model of the molecule, yields 0.67 kcal · mol^{-1} for the barrier height. If a non-rigid molecular model is used, i.e. all bond angles and bond lengths are optimized during rotation, 1.29 kcal · mol^{-1} is obtained [11]. Thus the error of the PCILO and CNDO/2 methods, in reproducing barrier heights of the methyl group in molecules of the type CH_3-O-R, R stands for an aliphatic or aromatic group, can be estimated to be about 0.3 kcal · mol^{-1}.

To reduce computer time and capacity the PAA molecule was modelled as shown in Fig. 3. The adequacy of this model is proved as follows. First, the methyl and metoxy rotational barriers were calculated for the whole PAA molecule. It has been found that these values are in a good agreement with those obtained for the model of Fig. 1. The difference between both potential curves is smaller than 0.1 kcal · mol^{-1}. Secondly, rotating the molecular fragment, indicated in Fig. 3, by an angle of 180° around the N—C bond no significant change (0.1 kcal · mol^{-1}) of the barrier can be observed.

A rigid model of the methyl group rotation was considered first. The experimental molecular geometry, obtained by X-ray diffraction technique in the solid phase, was used [12]. PCILO gave 2.8 kcal · mol^{-1} while 3.0 kcal · mol^{-1} was obtained by CNDO/2 for the barrier to methyl rotation. According to very probable nonbonded H (benzene) — H (methyl) interactions as indicated by the enlarged COC angle 118.7° [12] instead of the normal tetrahedral value, 109.5°, the COC (α) and OCC (β) angles were optimized for each torsional angle. α and β were varied within the range of 109.7°—121.7° and 119.2°—128.2°, respectively. It is found that the effect of variation of both angles on the torsional potential curves is almost the same. This indicates that it is primarily the H...H distance which affects the barrier.

Using a nonrigid model, where the COC angle was optimized for each value of the torsional angle, τ, the potential curve for the rotation of the methyl group was investigated. Seven points, in the range of 0—60° in intervals of 10°, were calculated using the PCILO method. It is found that the curve, obtained numerically, is very close to the usually applied threefold expression:

$$V(\tau) = \frac{V_3}{2}(1 - \cos 3\tau)$$

with $V_3 = 3.85$ kcal · mol^{-1}. The maximum deviation between both curves does not exceed 2 per cent.

The rotational barrier was calculated with the CNDO/2 method, too. The experimental geometry was used except for the optimal COC angle which was taken from the PCILO calculation. The barrier height is 4.2 kcal · mol^{-1}. The equilibrium conformation was found to be, like in case of the PCILO calculations, the staggered one. The experimental barrier height, measured in the solid phase by NMR [3] and by neutron scattering [2], is 3.7 and 3.51 kcal · mol^{-1}, respectively. The fair agreement between experimental and theoretical values suggests that the rotation of the methyl group is governed by intramolecular forces. Interactions with neighbouring molecules may play a minor role only.

Rotation of the methoxy group

When rotating the methoxy group around the OC aromatic axis the COC angle was varied within the range of 100—120° while the OCC angle was put equal to 120° (see Fig. 1). Using the PCILO method 4.5 kcal · mol^{-1} is obtained for the barrier height as shown in Fig. 4. In equilibrium the C—O—C plane is perpendicular to the benzene one. According to X-ray diffraction studies these planes coincide in the solid phase. However, recent neutron

scattering measurements on the nematic phase [13] seem to confirm our results. It is supposed that, in this case, according to the weaker intermolecular forces, the conformation is similar to that of the free molecule.

The PCILO method gave somewhat contradictory results because, according to the localized orbitals. used in the calculations, the barrier height was found to be dependent on the Kekulé structure attached to the π-system. In the planar molecule a difference of 1 kcal · mol^{-1} was observed when the double bond of the Kekulé structure was positioned *cis* or *trans* with respect

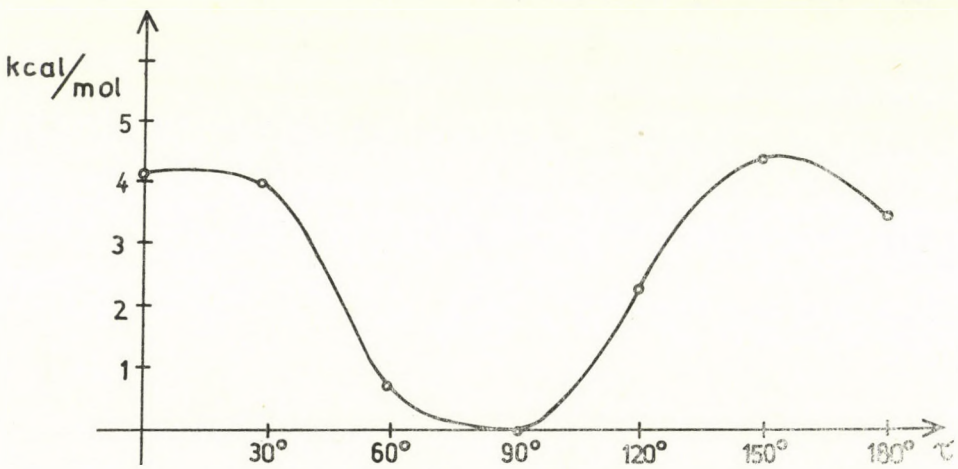

Fig. 4. Potential curve for the PAA methoxy rotation (nonrigid model)

to the methoxy group, respectively. We feel, however, that this discrepancy does not have an influence on the equilibrium position of the methoxy group.

Rotation around C—N bonds

As was mentioned before the PCILO method proved to be contradictory in this case, too. The difference in the barrier heights, calculated with different Kekulé structures, was found to be 2.5—3.0 kcal · mol^{-1} for all conformations. According to the failure of the CNDO/2 method to reproduce barrier heights, due to rotations around delocalized bonds [9], no calculations were performed.

3. Dibutyl-phenyl-benzoyloxy-benzoate

The DB-PBB molecule contains three benzene rings and two butyl substituents (see Fig. 2). As in case of the inner part of PAA, rotation around CC and CO bonds of DB-PBB cannot be described, using the CNDO/2 and

PCILO methods correctly. Therefore the butyl group was investigated only. A similar model as for PAA, combined with the PCILO method, was used (see Fig. 5).

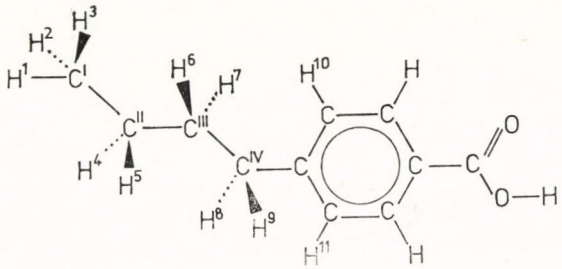

Fig. 5. Simplified model of the DB-PBB molecule

Methyl rotation around the $C^{I}C^{II}$ bond

A rigid model of rotation of the methyl group was considered first. The initial geometry was supposed to be a planar one as shown in Fig. 5. The C—C—C angle was put equal to the tetrahedral value. As in case of PAA, the potential curve for the methyl rotation was found to be of cosinusoidal type. $V_3 = 2.45$ kcal · mol^{-1} close to the PCILO value for ethane as calculated by us 1.99 kcal · mol^{-1}. This indicates that the methyl rotation is not very much affected by other parts of the molecule unlike to the case of PAA.

In the next step the $C^{I}C^{II}C^{III}$ angle was optimized. Using this non-rigid model no significant distortion (0.01 kcal · mol^{-1}) of the cosinusoidal potential curve was observed. $V_3 = 2.50$ kcal · mol^{-1} with 115° for the optimized $C^{I}C^{II}C^{III}$ angle. In energy minimum the methyl group is in a staggered position with respect to the $C^{II}H^{4}$ and $C^{II}H^{5}$ bonds.

Ethyl rotation around the $C^{II}C^{III}$ bond

A nonrigid model was used. The $H^{1}C^{I}C^{II}C^{III}$ dihedral angle was put equal to 180° but the $C^{I}C^{II}C^{III}$ angle was optimized under rotation of the ethyl group. It was varied within the range of 109—115°. Fig. 6 represents the change in energy in the course of a 360° rotation around the carbon-carbon bond. $\tau = 0°$ corresponds to the planar *trans*-form (see Fig. 5). The rotational barriers are: $V_3' = 2.2$ and $V_3 = 3.2$ kcal · mol^{-1}, respectively. The *ab initio* STO-3G values for *n*-butane are: $V_3 = 3.58$, $V_3' = 5.72$ kcal · mol^{-1}, respectively [14]. The PCILO method generally underestimates barriers to rotation around σ-bonds. For example the calculated and experimental (in parentheses [8]) values for ethane, methylamine and methanole are 1.99 (2.93), 1.49 (1.98) and 0.79 (1.07) kcal · mol^{-1}, respectively. Therefore the

comparison with the *ab initio* values indicates a qualitative agreement. The overall shape of the rotational curve is similar to the *ab initio* one. Thus it is concluded that, in DB-PBB the rotation of the ethyl group is similar to that in *n*-butane. The choice of the Kekulé structures was proved to be irrelevant in this case.

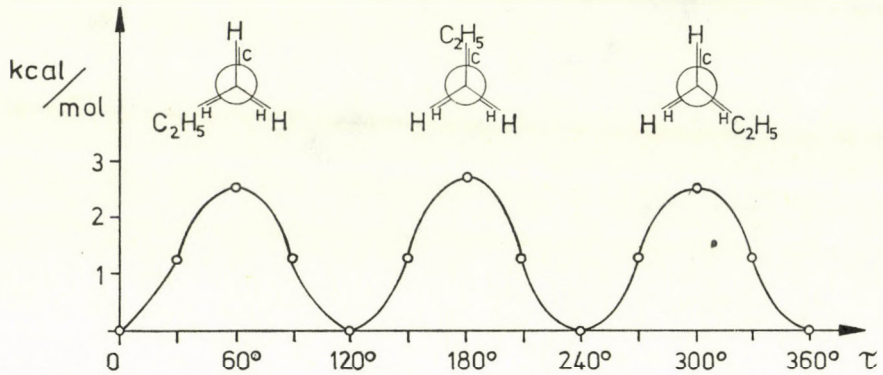

Fig. 6. Potential curve for the DB-PBB ethyl rotation (nonrigid model)

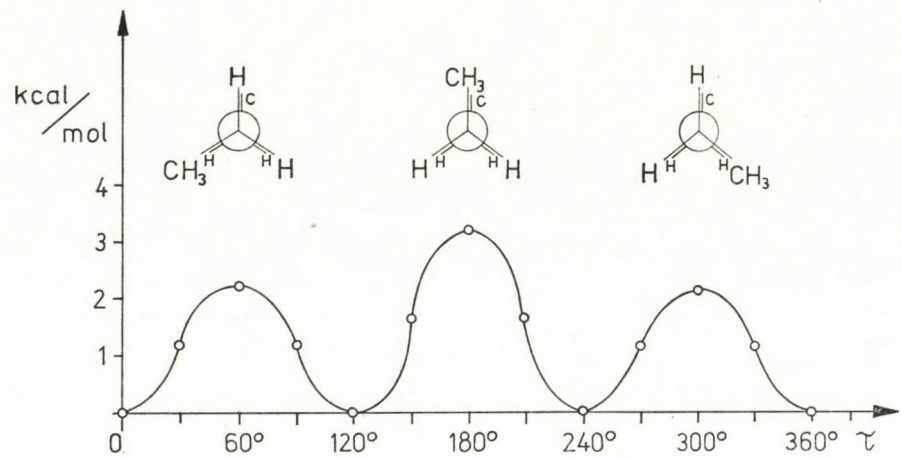

Fig. 7. Potential curve for the DB-PBB propyl rotation (nonrigid model)

Propyl rotation around the $C^{III}C^{IV}$ bond

In order to study this motion the phenyl ring had to be rotated by 90° around the $C^{IV}C$ (aromatic) bond in order to avoid close contact between hydrogen atoms of the aliphatic chain and the phenyl group, respectively. As it is seen in the subsequent subsection this is the equilibrium conformation of the butyl group. The carbon atoms of the propyl group were supposed to be in a planar arrangement during rotation. This choice is supported by the

results of the previous subsection. In energy minimum the propyl moiety was found to be planar. A nonrigid model was used the $C^{II}C^{III}C^{IV}$ angle was altered within the range or 112—115°. The potential curve is given in Fig. 7 yielding barrier heights: $V_3 = 2.4$ kcal · mol^{-1} and $V_3' = 2.6$ kcal · mol^{-1}, respectively. The overall character of the curve is similar to that obtained for the ethyl rotation. Changing the Kekulé structures a minor discrepancy (0.2—0.3 kcal · mol^{-1}) was observed in the calculated energy.

Butyl rotation around the $C^{IV}C$ (aromatic) bond

Using a nonrigid model the initial geometry was chosen to be a planar one as shown in Fig. 5. The $C^{III}C^{IV}C$ (aromatic) angle was altered within the range of 112°—115°. A considerable difference (0.7—1.0 kcal · mol^{-1}) in the

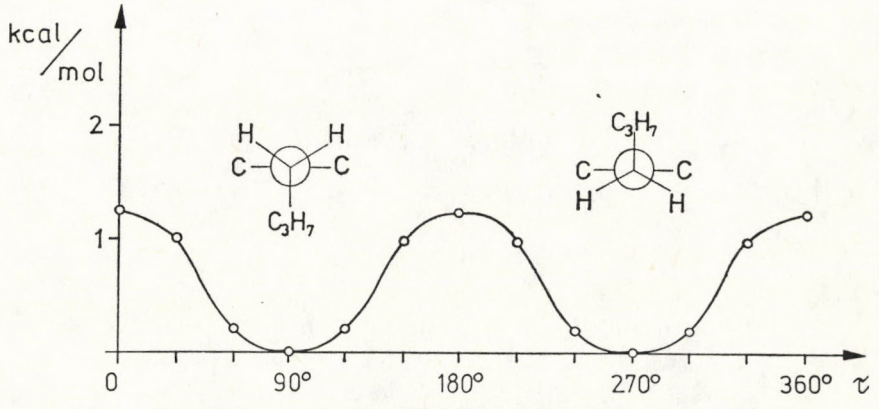

Fig. 8. Potential curve for the DB-PBB butyl rotation (nonrigid model)

calculated energy values, due to different Kekulé structures, was observed. The averaged potential curve is given in Fig. 8. The barrier height is 1.2 kcal · mol^{-1}. Due to this inconsistence of the PCILO method the barrier height was calculated by the CNDO/2 method, too. A similar curve with $V_3 = 2.2$ kcal · mol^{-1} was obtained. In equilibrium the butyl and phenyl planes were perpendicular to each other.

Conclusions

Computational results are summarized in Table I. The most important conclusions are the following:

1) Rotation in the methoxy group of PAA and in the butyl ones of DB-PBB is hindered to a given extent. However, barriers are not very high, thus a limited motion, especially at higher temperatures, is possible.

2) The equilibrium geometry *in vacuo* is similar in both molecules. The plane or the substituent is perpendicular to the phenyl one. In case of DB-PBB the butyl moiety has a planar zig-zag form.

Table I

Barriers to rotation of different groups in PAA and in DB-PBB (in kcal · mol^{-1})

Type	PCILO		CNDO/2 rigid
	rigid	nonrigid	
PAA methyl*	2.8	3.85	3.0, 4.2**
PAA methoxy	—	4.5	—
DB-PBB methyl§	2.45	2.50	—
DB-PBB ethyl§§	—	2.2, 3.2	—
DB-PBB propyl	—	2.4, 2.6	—
DB-PBB butyl	—	1.2	2.2

* Experimental values: 3.51 [2] and 3.7 [3].
** Optimal COC angle taken from the PCILO calculation.
§ For ethane 1.99 is obtained (experimental value: 2.93 [8]).
§§ *Ab initio* (STO-3G) values for *n*-butane are 3.58 and 5.72, respectively [14].

3) Rotation in the inner part of the molecules (—N(O)N— and —C(O)O—) is not to be described by either of the PCILO or the CNDO/2 methods. However, according to chemical intuition, a considerable delocalization through these parts of the molecules occurs. Therefore rotation around NN, CC and CO single bonds, present here, seems to be considerably hindered.

REFERENCES

1. L. Bata, I. Vizi and S. Kugler, Solid State Comm., **18,** 55, 1976.
2. H. Hervet, A. J. Dianoux, R. E. Lechner and F. J. Volino, J. Physique, **37,** 587, 1976.
3. I. Pócsik, K. Tompa, J. Lasanda, S. Kugler and G. Náray-Szabó, KFKI Preprint 1977—40, Budapest.
4. L. Bata, Á. Buka and G. Molnár, Mol. Cryst. Liq, Cryst., **38,** 155, 1977.
5. S. Diner, J. P. Malrieu, F. Jordan and M. Gilbert, Theoret. Chim. Acta, **15,** 100, 1969.
6. Quantum Chemistry Program Echange, No. 220. Indiana University, Bloomington, Indiana, USA.
7. J. A. Pople and D. L. Beveridge, Approximate Molecular Orbital Theory, McGraw Hill, New York, 1970.
8. A. Veillard, in: Quantum Mechanics of Molecular Conformations (Ed.: B. Bullman) Wiley-Interscience, London—New York—Sydney—Toronto, 1976. p. 1.
9. C. S. Sieiro, P. Gonzalez-Diaz and Y. G. Smeyers, J. Mol. Struct., **24,** 345, 1975.
10. M. S. Gordon, J. Amer. Chem. Soc., **91,** 3122, 1969.
11. K. Ösapay and G. Náray-Szabó, Adv. Mol. Rel. Proc., **12,** 97, 1978.
12. W. R. Krigbaum, Y. Chatami and P. G. Barber, Acta Cryst., **B26,** 97, 1970.
13. L. Bata, V. L. Bronde, V. G. Fedotov, N. Kroó, L. Rosta, J. Szabon, L. M. Umarov and I. Vizi, Mol. Cryst. Liq. Cryst., **44,** 71, 1978.
14. L. Radom and J. A. Pople, J. Amer. Chem. Soc., **92,** 4786, 1970.

Acta Physica Academiae Scientiarum Hungaricae, Tomus 46 (2), pp. 77—96 (1979)

FREE CONVECTION FLUCTUATING FLOW ON A HORIZONTAL MAGNETIZED PLATE

By

P. SINGH and R. L. VERMA

DEPARTMENT OF MATHEMATICS, INDIAN INSTITUTE OF TECHNOLOGY, KANPUR, INDIA

(Received 13. II. 1979)

The free convection flow of electrically conducting fluid along a semi-infinite horizontal magnetized plate is analysed, when the plate temperature oscillates about a constant mean. The basic steady flow is purely buoyancy induced, while the oscillations in the plate temperature cause a time-dependent boundary layer flow and heat transfer. The unsteady boundary layer equations are linearized and the first two approximations are considered. Two separate solutions valid for high and low frequency ranges are obtained by series expansion method in terms of frequency parameters. For very high frequencies, the oscillatory flow pattern is of 'shear-wave' type unaffected by the mean flow. The skin friction in the very high frequency solution has a phase lag of 45° while the phase of heat transfer oscillations is ahead of the plate temperature fluctuations by $\pi/4$.

1. Introduction

In unsteady laminar boundary layer theory one area of study which has received much attention in recent years deals with boundary layer responses to imposed oscillations. This theory was initiated by LIGHTHILL [1] to study the effect of free stream oscillations of flow and heat transfer along plates and cylinders. The extension of this theory for free convection boundary layers along a semi-infinite vertical plate was carried out by NANDA and SHARMA [2], ESHGHY, ARPACI and CLARK [3] and KELLEHER and YANG [4]. Recently MUHURI and MAITI [5] have studied the oscillatory free convection flow along a semi-infinite horizontal plate. It is, however, remarkable that the free convection oscillatory flow of an electrically conducting fluid along a semi-infinite horizontal plate has received no attention. The present investigation is, therefore, devoted to the study of a magneto-hydrodynamic free convection oscillatory flow of electrically conducting fluid along a semi-infinite horizontal plate, when the plate temperature oscillates about a constant mean. The specific aim of the present study is to gain further insight into the flow of conducting fluid of small viscosity when the magnetic field is applied at the plate itself. The possibility of setting up a uniform magnetic field in the plate has been very well discussed by ZHIGULEV [6]. The oscillatory flow and heat transfer problems are important in an engineering sense because such flow occurs very often in practice. The effect of surface temperature oscillations on the skin-friction and heat transfer from a surface to the surrounding flow is of special interest to the heat transfer engineer.

We consider a thin magnetized flat plate extending from 0 to ∞ in the x-direction where x measures the distance along the plate lying horizontally in quiescent electrically conducting viscous fluid (see Fig. 1). The plate is heated to a temperature T_w and is placed in an ambient at T_∞. Thus the basic flow is entirely due to buoyancy effect in the presence of externally applied magnetic field over a horizontal plate whose temperature differs from that of the free stream. The effect of the buoyancy force is to induce a longitudinal pressure gradient which causes flow. It is an interesting flow in its own right yielding a steady outer flow for the boundary layer as a result of free convec-

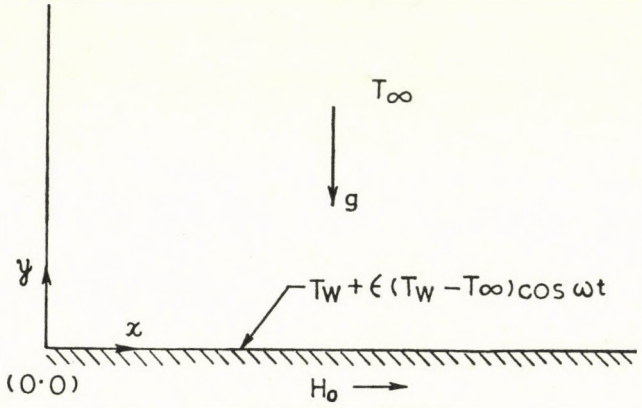

Fig. 1. The physical system

tion alone. Moreover this problem should be easily amenable to experiment in a laboratory. The steady free convection flow over the plate is perturbed due to a superimposed weak time-varying plate temperature distribution $\varepsilon(T_w - T_\infty) \cos \omega t$, where ω is the frequency of oscillations. The amplitude of the oscillations is assumed to be small (of order ε) compared with the mean flow induced by the convection. This enables us to employ the technique of the linearization for the perturbation due to oscillations.

The basic steady flow is considered using the Karman—Pohlhausen method and an approximate solution to be used in the subsequenty study of unsteady flow is obtained. Two different solutions for low and high frequency ranges are developed for perturbation equations. The method of solving the problem is essentially the same as developed by LIGHTHILL [1]. Here, of course, we have extended LIGHTHILL'S technique to obtain series solution for low and high frequencies. The matching between the two solutions is found to be quite satisfactory. For very high frequencies the amplitude of the rate of heat transfer fluctuations increases with ω and its phase is ahead of the plate temperature oscillations by 45°. On the other hand, the phase of skin friction oscillations lags behind that of the plate temperature oscillations by 45°.

2. The basic equations

We consider the two-dimensional free-convection boundary layer flow of an incompressible, viscous and electrically conducting fluid past a semi-infinite horizontal flat plate, when the magnetic Reynold's number is very small. There is no magnetic field in the distant fluid but in the boundary layer there is a field generated by external means within the plate itself. If (u, v) and (H_x, H_y) are the velocity and magnetic field components, respectively, the equations which govern the flow in the boundary layer, in MKS units, are

$$\varrho\left(\frac{\partial u}{\partial t}+u\frac{\partial u}{\partial x}+v\frac{\partial u}{\partial y}\right)=-\frac{\partial}{\partial x}\left(p+\frac{1}{2}\mu_e H_0^2\right)+\varrho\nu\frac{\partial^2 u}{\partial y^2}+ \\ +\mu_e\left(H_x\frac{\partial H_x}{\partial x}+H_y\frac{\partial H_x}{\partial y}\right), \tag{1}$$

$$0=-\frac{\partial}{\partial y}\left(p+\frac{1}{2}\mu_e H_0^2\right)-\varrho g\,, \tag{2}$$

$$\frac{\partial H_x}{\partial t}+u\frac{\partial H_x}{\partial x}+v\frac{\partial H_x}{\partial y}-\left(H_x\frac{\partial u}{\partial x}+H_y\frac{\partial u}{\partial y}\right)=\eta\frac{\partial^2 H_x}{\partial y^2}\,, \tag{3}$$

$$\frac{\partial u}{\partial x}+\frac{\partial v}{\partial y}=0\,, \tag{4}$$

$$\frac{\partial H_x}{\partial x}+\frac{\partial H_y}{\partial y}=0\,, \tag{5}$$

$$\frac{\partial\theta}{\partial t}+u\frac{\partial\theta}{\partial x}+v\frac{\partial\theta}{\partial y}=\alpha\frac{\partial^2\theta}{\partial y^2}\,, \tag{6}$$

where $\theta = T - T_\infty$, T being the temperature in the boundary layer. The fluid has density ϱ, kinematic viscosity ν, electric conductivity σ, magnetic permeability μ_e and thermal diffusivity α. g denotes the acceleration due to gravity and η is the magnetic diffusivity defined as

$$\eta=(\sigma\mu_e)^{-1}\,.$$

In accordance with the usual practice, we consider density variations only in the buoyancy force term, other density variations are neglected within the framework of incompressible fluids. The simplest way to do so is to take the equation of state in the form

$$\varrho=\varrho_\infty[1-\beta(T-T_\infty)]\,, \tag{7}$$

where β is the coefficient of thermal expansion and ϱ_∞ is the free stream density. Using (7) in (2) and eliminating

$$\left(p + \frac{1}{2}\mu_e H_0^2\right)$$

from (1) and (2) we obtain

$$\frac{\partial}{\partial y}\left(\frac{\partial u}{\partial t} + u\frac{\partial u}{\partial x} + v\frac{\partial u}{\partial y}\right) = \nu\frac{\partial^3 u}{\partial y^3} - g\beta\frac{\partial \theta}{\partial x} + \\ + \frac{\mu_e}{\varrho}\frac{\partial}{\partial y}\left[H_x\frac{\partial H_x}{\partial x} + H_y\frac{\partial H_x}{\partial y}\right]. \tag{8}$$

The boundary conditions of the problem are

$$y = 0: \quad u = 0, \quad v = 0, \quad H_x = H_0, \quad \theta = \theta_w(1 + \varepsilon\cos\omega t),$$
$$y \to \infty: \quad u \to 0, \quad \frac{\partial u}{\partial y} \to 0, \quad H_x \to 0, \quad H_y \to 0, \quad \theta \to 0; \tag{9}$$

where ω is the frequency of the temperature fluctuations and $\theta_w = T_w - T_\infty$. The magnetic field is applied at the plate in the x-direction.

The solutions of the above equations are obtained in terms of complex functions, the real parts of which have physical significance. The plate temperature which can be written as $\theta_w + \varepsilon\theta_w e^{i\omega t}$ consists of a basic steady distribution θ_w with a superimposed weak time-varying distribution $\varepsilon\theta_w e^{i\omega t}$. We assume the following forms for u, v, H_x, H_y and θ

$$\begin{aligned} u &= u_s + \varepsilon u_1 e^{i\omega t}, & v &= v_s + \varepsilon v_1 e^{i\omega t}, \\ H_x &= H_{xs} + \varepsilon H_{x1} e^{i\omega t}, & H_y &= H_{ys} + \varepsilon H_{y1} e^{i\omega t}, \\ \theta &= \theta_s + \varepsilon\theta_1 e^{i\omega t}, \end{aligned} \tag{10}$$

where u_s, v_s, H_{xs}, H_{ys} and θ_s satisfy the steady-state hydromagnetic free convection boundary layer equations

$$\frac{\partial}{\partial y}\left[u_s\frac{\partial u_s}{\partial x} + v_s\frac{\partial u_s}{\partial y}\right] = \nu\frac{\partial^3 u_s}{\partial y^3} - g\beta\frac{\partial \theta_s}{\partial x} + \\ + \frac{\mu_e}{\varrho}\frac{\partial}{\partial y}\left(H_{xs}\frac{\partial H_{xs}}{\partial x} + H_{ys}\frac{\partial H_{xs}}{\partial y}\right), \tag{11}$$

$$u_s\frac{\partial H_{xs}}{\partial x} + v_s\frac{\partial H_{xs}}{\partial y} - H_{xs}\frac{\partial u_s}{\partial x} - H_{ys}\frac{\partial u_s}{\partial y} = \eta\frac{\partial^2 H_{xs}}{\partial y^2}, \tag{12}$$

$$u_s \frac{\partial \theta_s}{\partial x} + v_s \frac{\partial \theta_s}{\partial y} = \alpha \frac{\partial^2 \theta_s}{\partial y^2} \,, \tag{13}$$

$$\frac{\partial u_s}{\partial x} + \frac{\partial v_s}{\partial y} = 0 \,, \tag{14}$$

$$\frac{\partial H_{xs}}{\partial x} + \frac{\partial H_{ys}}{\partial y} = 0 \,; \tag{15}$$

with the boundary conditions

$$y = 0: \quad u_s = 0, \quad v_s = 0, \quad H_{xs} = H_0, \quad \theta_s = \theta_w,$$

$$y \to \infty: \; u_s \to 0, \quad \frac{\partial u_s}{\partial y} \to 0, \quad H_{xs} \to 0, \quad H_{ys} \to 0, \quad \theta_s \to 0 \,. \tag{16}$$

Neglecting squares of ε and dividing by $e^{i\omega t}$, we find that u, v_1, H_{x1}, H_{y1} and θ_1 satisfy the oscillatory part of the boundary layer equations

$$\begin{aligned} &\frac{\partial}{\partial y}\left[i\omega u_1 + u_s \frac{\partial u_1}{\partial x} + v_s \frac{\partial u_1}{\partial y} + u_1 \frac{\partial u_s}{\partial x} + v_1 \frac{\partial u_s}{\partial y}\right] \\ &= \frac{\mu_e}{\varrho} \frac{\partial}{\partial y}\left[H_{xs} \frac{\partial H_{x1}}{\partial x} + H_{ys} \frac{\partial H_{xs}}{\partial y} + H_{x1} \frac{\partial H_{xs}}{\partial x} + H_{y1} \frac{\partial H_{xs}}{\partial y}\right] + \\ &\qquad + \nu \frac{\partial^3 u_1}{\partial y^3} - g\beta \frac{\partial \theta_1}{\partial x} \,, \end{aligned} \tag{17}$$

$$\begin{aligned} &i\omega H_{x1} + u_s \frac{\partial H_{x1}}{\partial x} + v_s \frac{\partial H_{x1}}{\partial y} + u_1 \frac{\partial H_{xs}}{\partial x} + v_1 \frac{\partial H_{xs}}{\partial y} - H_{xs} \frac{\partial u_1}{\partial x} - \\ &\qquad - H_{ys} \frac{\partial u_1}{\partial y} - H_{x1} \frac{\partial u_s}{\partial x} - H_{y1} \frac{\partial u_s}{\partial y} = \eta \frac{\partial^2 H_{x1}}{\partial y^2} \,, \end{aligned} \tag{18}$$

$$i\omega \theta_1 + u_s \frac{\partial \theta_1}{\partial x} + v_s \frac{\partial \theta_1}{\partial y} + u_1 \frac{\partial \theta_s}{\partial x} + v_1 \frac{\partial \theta_s}{\partial y} = \alpha \frac{\partial^2 \theta_s}{\partial y^2} \,, \tag{19}$$

$$\frac{\partial u_1}{\partial x} + \frac{\partial v_1}{\partial y} = 0 \,, \tag{20}$$

$$\frac{\partial H_{x1}}{\partial x} + \frac{\partial H_{y1}}{\partial y} = 0 \,, \tag{21}$$

with boundary conditions

$$y = 0: \quad u_1 = 0, \quad v_1 = 0, \quad H_{x1} = 0, \quad \theta_1 = \theta_w \,;$$

$$y \to \infty: \quad u_1 \to 0, \quad \frac{\partial u_1}{\partial y} \to 0, \quad H_{x1} \to 0, \quad H_{y1} \to 0 \,, \quad \theta_1 \to 0 \,. \tag{22}$$

3. The steady state solution

Equations (11) to (16) describe the steady state free convection flow of an electrically conducting fluid over a semi infinite horizontal magnetized flat plate maintained at a constant temperature T_w. These equations are the same as those obtained by GILL and CASAL [7] for electrically non-conducting fluids but the boundary conditions are different. They have assumed the existence of a uniform free stream velocity whereas in our case the free stream is assumed to be at rest. Thus the flow is purely due to buoyancy force which induces a longitudinal pressure gradient

$$\frac{\partial p}{\partial x} = -g\beta\varrho_\infty \frac{\partial}{\partial x}\int_y^\infty \theta \, dy \,. \tag{23}$$

This pressure gradient causes the flow (see SPARROW and MINKOWCZ [8]). For the flow below the plate, the coordinate y would be reversed to measure distances vertically downwards and the negtaive sign in Eq. (23) would be deleted. It follows that with a flow above the plate for which $T_w > T_\infty$ or for a flow below the plate for which $T_w < T_\infty$ the induced pressure gradient $\partial p/\partial x$ is negative resulting in an accelerated flow. For flow below the plate for $T_w > T_\infty$ or for flow above the plate for which $T_w < T_\infty$, the situation will be just reversed. It is therefore sufficient to consider only one of the four situations. For convenience we shall discuss flow above the plate for which $T_w > T_\infty$.

We shall employ the Karman—Pohlhausen method of integration to solve the steady state equations. Integrating Eqs. (11) to (13) over the width of the boundary layer, we obtain

$$\nu\left(\frac{\partial^2 u_s}{\partial y^2}\right)_{y=0} + g\beta\frac{\partial}{\partial x}\int_0^\infty \theta_s \, dy + \frac{\mu_e}{\varrho} H_0 \frac{dH_0}{dx} = 0 \,, \tag{24}$$

$$\eta\left(\frac{\partial H_{xs}}{\partial y}\right)_{y=0} = 0 \,, \tag{25}$$

$$\frac{\partial}{\partial x}\int_0^\infty u_s \theta_s \, dy + \alpha\left(\frac{\partial \theta_s}{\partial y}\right)_{y=0} = 0 \,. \tag{26}$$

We assume the steady state profile as:

$$u_s = UA(3\eta_1 - 8\eta_1^2 + 6\eta_1^3 - \eta_1^5) - UB(\eta_1 - 3\eta_1^2 + 3\eta_1^3 - \eta_1^4), \tag{27}$$

$$H_{xs} = H_0(1 - 6\eta_2^2 + 8\eta_2^3 - 3\eta_2^4) \,, \tag{28}$$

$$\theta_s = \theta_w(1 - 2\eta_1 + 2\eta_1^3 - \eta_1^4) \,, \tag{29}$$

where

$$A = \frac{H_0 U}{\delta_1^2}\left[\frac{30\,\delta\eta}{\frac{d}{dx}(H_0\,\delta_1)} - \frac{4\mu_e\,\delta^3}{15\,\varrho}\,\frac{d}{dx}(\delta_1 H_0)\right],$$

$$B = \frac{H_0 U}{\delta_1^2}\left[\frac{60\,\eta\delta}{\frac{d}{dx}(\delta_1 H_0)} - \frac{4\mu_e\,\delta^3}{5\varrho}\,\frac{d}{dx}(\delta_1 H_0)\right],$$

$$\eta_1 = y/\delta, \quad \eta_2 = y/\delta_1, \quad U = (g\beta\theta\omega)^{2/5}(\nu x)^{1/5}.$$

δ and δ_1 are the viscous and the magnetic boundary layer thicknesses, respectively, and these are to be determined with the help of integral equations (24) and (26). The expressions (27) to (29) satisfy the boundary conditions (16) and the steady boundary layer equations (11) to (13) at $y = 0$.

Substituting (27) to (29) into (24) and (26) and considering only the similarity cases, we get

$$(3\delta^* - 5s)\,\delta^{*2} = 50(8A - 3B), \tag{30}$$

$$\frac{10}{\sigma} = \delta^{*2}\left(\frac{89A}{420} - \frac{11B}{168}\right), \tag{31}$$

where

$$\delta = \delta^*\left(\frac{\nu^2}{g\beta\theta_w}\right)^{1/5} x^{2/5}, \qquad \delta_1 = \delta_1^*\left(\frac{\nu^2}{g\beta\theta_w}\right)^{1/5} x^{2/5},$$

$$A = \left(\frac{5s - 3\delta^*}{50} + \frac{15\,\lambda}{\delta^*\,\delta_1^{*3}}\right)\delta^{*2}, \quad B = \left(\frac{15s - 9\delta^*}{50} + \frac{4\lambda}{\delta^*\delta_1^{*3}}\right)\delta^{*2},$$

$$s = \frac{\mu_e H_0'^2}{\varrho\nu^2}\left(\frac{\nu^2}{g\beta\theta\omega}\right)^{4/5}, \qquad H_0 = H_0' x^{1/5},$$

$$\sigma = \nu/\alpha, \qquad \lambda = \eta/\nu.$$

It should be noted that the mean horizontal velocity induced by steady convection is zero at the leading edge of the plate, the analysis is invalid for small values of x. However, the mean velocity grows as $x^{1/5}$ and so the results are valid far downstream.

The results of practical interest are the skin friction and the rate of heat transfer from the plate to the fluid which can now be obtained easily. The skin frcition

$$\tau_s = \mu\left(\frac{\partial u_s}{\partial y}\right)_{y=0}$$

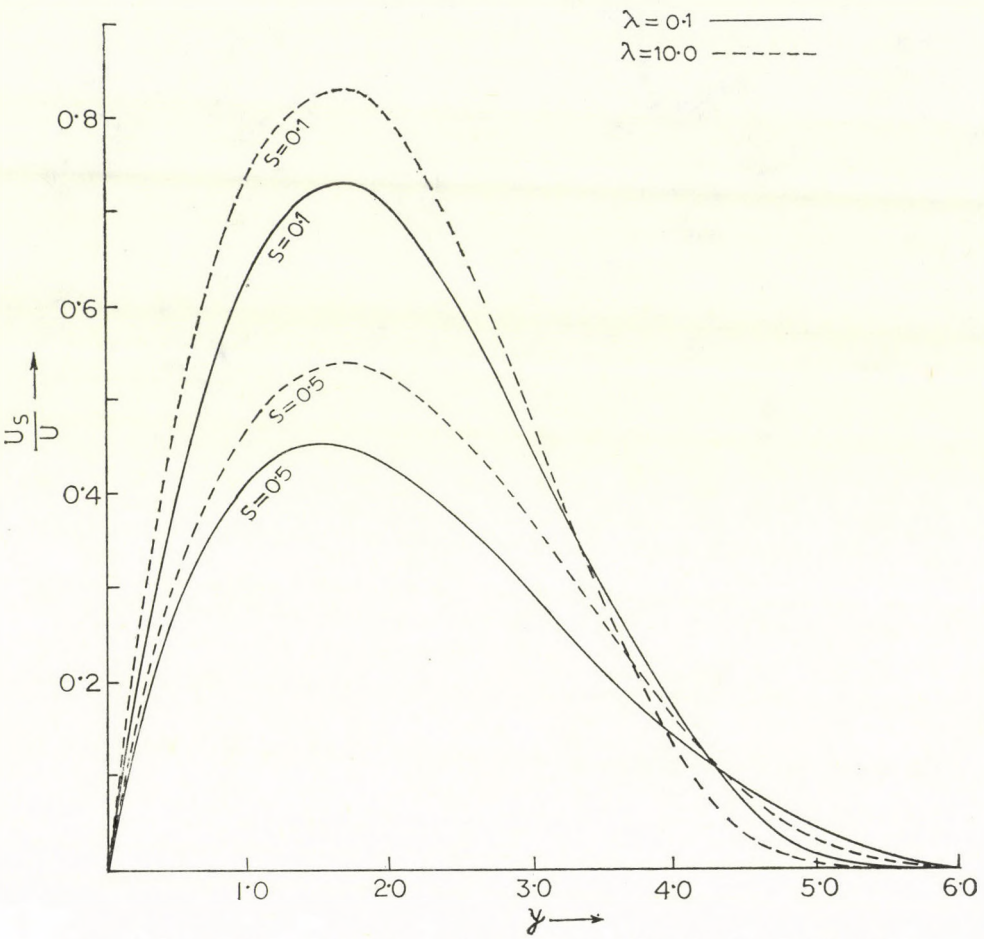

Fig. 2. The steady state velocity u_s/u vs y for $\lambda = 0.1$, 10 and $s = 0.1$, 0.5, 1

in the non-dimensional form is obtained as

$$\tau_s^* = \frac{(\nu x)^{1/5}}{(g\beta\theta_w)^{3/5}} \left(\frac{\partial u_s}{\partial y}\right)_{y=0} = \frac{3A - B}{\delta^*} . \tag{32}$$

The rate of heat transfer

$$q_s = - k \left(\frac{\partial T_s}{\partial y}\right)_{y=0}$$

in nondimensional form is

$$\begin{aligned} Nus &= - \frac{(\nu^2 x^2)^{1/5}}{\theta_w (g\beta\theta_w)^{1/5}} \left(\frac{\partial \theta_s}{\partial y}\right)_{y=0}, \\ &= 2/\delta^* , \end{aligned} \tag{33}$$

where *Nus* denotes the steady state Nusselt number.

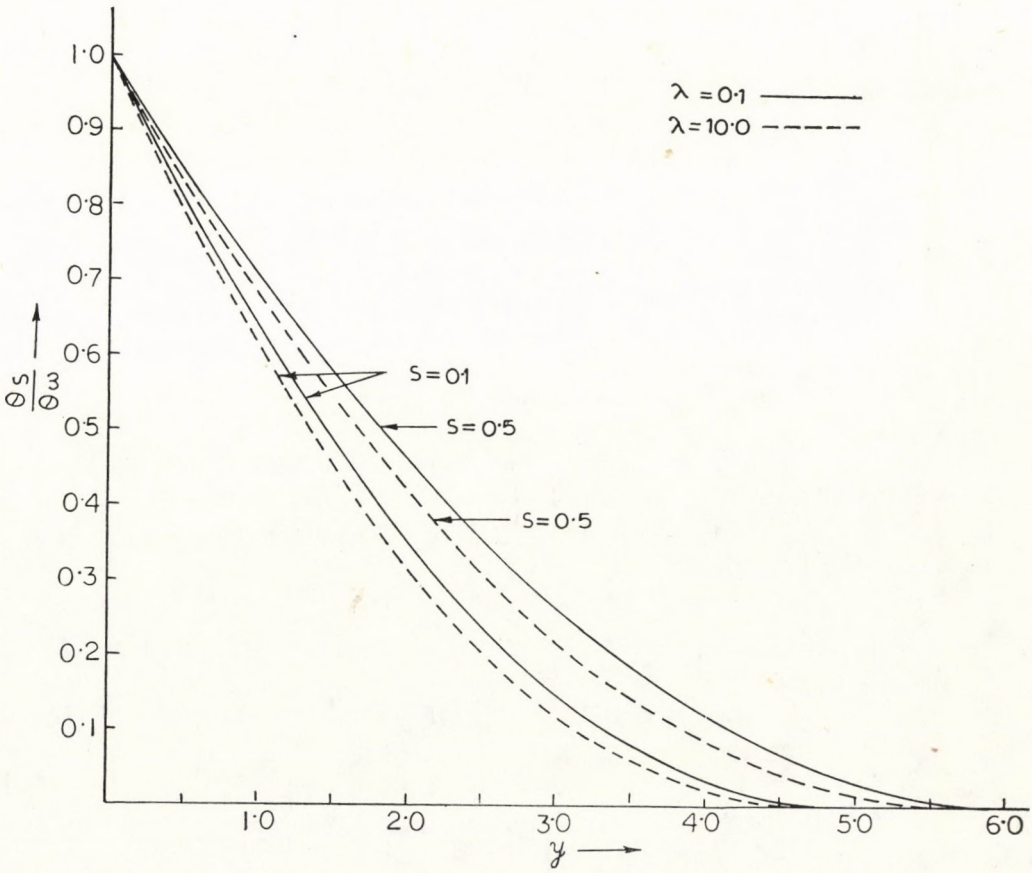

Fig. 3. The steady temperature field θ_s/θ_w vs y for $\lambda = 0.1$, 10 and $s = 0.1$, 0.5, 1

The solution of Eqs. (30) and (31) are obtained for $\sigma = 0.72$; $\lambda = 0.1$, 10 and $s = 0.1$, 0.5 and 1. Corresponding skin friction and the rate of heat transfer are calculated and the values are given in Table I.

Table I

	$\lambda = 0.1$		$\lambda = 10$	
S	τ_s^*	N_{us}	τ_s^*	N_{us}
0.1	0.908	0.355	0.890	0.380
0.5	0.894	0.283	0.599	0.309
1.0	0.793	0.190	0.304	0.256

It is obvious that the values of skin friction and the Nusselt number decrease with the increase of the magnetic field strength s. The effect of applied magnetic field on the velocity and temperature profiles are shown in Figs. 2 and 3. It is found that as s increases the velocity decreases and the boundary layer thickness increases, while the temperature inside the boundary layer increases with s. These results are expected from physical consideration too.

We, next, investigate the nature of the flow and the temperature fields due to the fluctuations in the plate temperature. Two separate solutions are obtained: one for small frequencies and the other for high frequencies.

4. Low frequency solution

We have already obtained the basic steady flow using Karman—Pohlhausen method, here again we shall employ the same method to solve Eqs. (17) to (22). Integrating (17) to (19) from $y=0$ to $y=\infty$, we obtain the averaging conditions

$$\nu\left(\frac{\partial^2 u_1}{\partial y^2}\right)_{y=0} + g\beta\frac{\partial}{\partial x}\int_0^\infty \theta_1 dy + \frac{\mu_e}{\varrho}\left(H_{ys}\frac{\partial H_{x1}}{\partial y} + H_{y1}\frac{\partial H_{xs}}{\partial y}\right)_{y=0} = 0\,, \tag{34}$$

$$i\omega\int_0^\infty H_{x1}\,dy = -\eta\left(\frac{\partial H_{x1}}{\partial y}\right)_{y=0}, \tag{35}$$

$$i\omega\int_0^\infty \theta_1\,dy + \frac{\partial}{\partial x}\int_0^\infty (u_s\theta_1 + u_1\theta_s)\,dy = -\alpha\left(\frac{\partial\theta_1}{\partial y}\right)_{y=0}. \tag{36}$$

Consistent with the boundary conditions (22), we assume the profiles for u_1, H_{x1} and θ_1

$$u_1 = UA_1(\eta_1 - 6\eta_1^3 + 8\eta_1^4 - 3\eta_1^5) + UB_1(\eta_1^2 - 3\eta_1^3 + 3\eta_1^4 + \eta_1^5), \tag{37}$$

$$\frac{H_{x1}}{H_0} = D_1(\eta_2 - 8\eta_2^3 + 2\eta_2^4) + D_2(\eta_2^2 - 2\eta_2^3 + \eta_2^4), \tag{38}$$

$$\frac{\theta_1}{\theta_w} = 1 - 4\eta_1^3 + 3\eta_1^4 + C_1(\eta_1 - 3\eta_1^3 + 2\eta_1^4) + \frac{i\omega\delta^2}{2\alpha}(\eta_1^2 - 2\eta_1^3 + \eta_1^4). \tag{39}$$

In (37) to (39) A_1, B_1, D_1, D_2 and C_1 are functions of x and ω and are to be determined. These profiles satisfy the conditions

$$i\omega\left(\frac{\partial u_1}{\partial y}\right)_{y=0} = \nu\left(\frac{\partial^3 u_1}{\partial y^3}\right)_{y=0} + \frac{\mu_e}{\varrho}\left[H_{xs}\frac{\partial^3 H_{x1}}{\partial y^2} + H_{ys}\frac{\partial^2 H_{x1}}{\partial y^2} + H_{y1}\frac{\partial^2 H_{xs}}{\partial y^2}\right]_{y=0}, \tag{40}$$

$$-\eta\left(\frac{\partial^2 H_{x1}}{\partial y^2}\right)_{y=0} = \left(H_{ys}\frac{\partial u_1}{\partial y} + H_{y1}\frac{\partial u_s}{\partial y}\right)_{y=0}, \tag{41}$$

$$i\omega\theta_w = \alpha\left(\frac{\partial^2\theta_1}{\partial y^2}\right)_{y=0}, \tag{42}$$

which are obtained by evaluating equations (17) to (19) at $y = 0$. Substituting (37) to (39) in (34) to (36), (40) and (41), we find that the unknowns A_1, B_1, D_1, D_2 and C_1 are given by

$$\begin{aligned}
A_1 &= -\frac{25}{3}\frac{\lambda\delta^*}{\delta_1^{*3}}D_2 - \frac{5}{12}(3A - B)\left(\frac{3}{5} + x\frac{d}{dx}\right)\left(\frac{3D_1}{2} + \frac{D_2}{3}\right), \\
B_1 &= -\frac{3}{25}sD_1\delta^{*2} - \frac{\delta^{*3}}{2}\left(\frac{2}{5} + x\frac{d}{dx}\right)\left(3/5 + \frac{i\omega^*\sigma}{60} + \frac{3}{20}C_1\right), \\
D_1 &= \frac{i\omega^*\delta_1^{*2}}{60\lambda\delta^{*2}}(9D_1 + 2D_2), \\
D_2 &= \frac{25\delta_1^*}{12s\delta^{*3}}[i\omega^*A_1 + 18(2A_1 + B_1)] - \frac{25}{12}\left[\left(x\frac{d}{dx} - \frac{1}{5}\right)D_1 - \right. \\
&\quad \left. - 6/5\left(3/5 + x\frac{d}{dx}\right)\left(\frac{3}{2}D_1 + \frac{1}{3}D_2\right)\right], \\
C_1 &= -\frac{i\omega^*\sigma}{60}(36 + 9C_1 + i\omega^*\sigma) - \sigma\delta^{*2}\left(\frac{3}{5} + x\frac{d}{dx}\right)\left[A\left(\frac{173}{1260} + \right.\right. \\
&\quad \left. + \frac{1}{30}C_1 + \frac{17\sigma}{5040}i\omega^*\right) - B\left(\frac{1}{24} + \frac{5}{504}C_1 + \frac{\sigma}{1008}i\omega^*\right) + \\
&\quad \left. + \frac{47}{1260}A_1 + \frac{13}{2520}B_1\right],
\end{aligned} \tag{43}$$

where $\omega^*\left(=\frac{\omega\delta^2}{\nu}\right)$ denotes the non-dimensional frequency parameter. Eqs. (43) may be solved by expanding A_1, B_1, D_1, D_2 and C_1 in the series of the form

$$\begin{aligned}
A_1 &= \sum_{n=0}^{\infty}(i\omega^*)^n A_{1n}, \qquad B_1 = \sum_{n=0}^{\infty}(i\omega^*)^n B_{1n}, \\
C_1 &= \sum_{n=0}^{\infty}(i\omega^*)^n C_{1n}, \qquad D_1 = \sum_{n=0}^{\infty}(i\omega^*)^n D_{1n}, \\
D_2 &= \sum_{n=0}^{\infty}(i\omega^*)^n D_{2n}.
\end{aligned} \tag{44}$$

Substituting (44) in (43) and comparing the coefficients of like powers of $(i\omega^*)$ on both sides, we get a series of simultaneous algebraic equations which can be easily solved for A_{1n}, B_{1n}, D_{1n}, D_{2n} and $C_{1n}(n = 0, 1, \ldots)$. It should be noted that the power series (44) probably will not converge for all values of ω^*, but they ought to be satisfactory for small values of frequency parameter.

The solution of Eqs. (17) to (20) in the limiting case $\omega \to 0$ is the quasi-steady solution to be denoted by (u_0, v_0), (H_{x0}, H_{y0}) and θ_0. These are the coefficients of ε in the velocity, temperature and magnetic field distributions for steady flow with an imposed plate temperature $\theta_w(1 + \varepsilon)$. Hence

$$(u_0, v_0) = \theta_w \frac{\partial}{\partial \theta_w}(u_s, v_s),$$

$$(H_{x0}, H_{y0}) = \theta_w \frac{\partial}{\partial \theta_w}(H_{xs}, H_{ys}),$$

$$\theta_0 = \theta_w \frac{\partial}{\partial \theta_w}\theta_s. \tag{45}$$

That this solves Eqs. (17) to (22) when $\omega \to 0$ can be verified by direct substitution. It can also be verified easily that this quasi-steady solution corresponds to $A_{10}, B_{10}, C_{10}, D_{10}$ and D_{20} in (44). Expressions (37) to (39) can be now expressed as the sum of the in-phase and out-phase components as

$$u_1 = u_0 + iu_2, \quad H_{x1} = H_{x0} + iH_{x2},$$
$$\theta_1 = \theta_0 + i\theta_2. \tag{46}$$

The velocity, the magnetic and the temperature fields may now be written in the form

$$u = u_s + \varepsilon R_1 \cos(\omega t + \alpha_1),$$
$$H_x = H_{xs} + \varepsilon R_2 \cos(\omega t + \alpha_2),$$
$$\theta = \theta_s + \varepsilon R_3 \cos(\omega t + \alpha_3), \tag{47}$$

where

$$R_1 = (u_0^2 + u_2^2)^{1/2}, \qquad \alpha_1 = \tan^{-1}\left(\frac{u_2}{u_0}\right),$$

$$R_2 = (H_{x0}^2 + H_{x2}^2)^{1/2}, \quad \alpha_2 = \tan^{-1}\left(\frac{H_{x2}}{H_{x0}}\right),$$

$$R_3 = (\theta_0^2 + \theta_2^2)^{1/2}, \qquad \alpha_3 = \tan^{-1}\left(\frac{\theta_2}{\theta_0}\right).$$

In free convection problems the skin friction and the rate of heat transfer at the plate are always of primary importance, we shall study the effect of magnetic field on these characteristics. The skin friction in the non-dimensional form is found to be

$$\tau_1^* = \varepsilon \ \text{Real}\left[\frac{e^{i\omega t}}{\delta^*}\sum_{n=0}^{\infty}(i\omega^*)^n A_{1n}\right],$$
$$= \varepsilon R_4 \cos(\omega t + \alpha_4) \quad \text{say.} \tag{48}$$

The rate of heat transfer for low frequency fluctuations is obtained in dimensionless form

$$Nu_1 = \varepsilon \ \text{Real}\left[-\frac{e^{i\omega t}}{\delta^*}\sum_{n=0}^{\infty}(i\omega^*)^n C_{1n}\right],$$
$$= \varepsilon R_5 \cos(\omega t + \alpha_5) \quad \text{say}. \tag{49}$$

5. High frequency oscillations

For very high frequencies LIGHTHILL [1] has shown that the oscillating flow is to a close approximation an ordinary "shear wave" unaffected by the mean flow. Following LIGHTHILL, we get the oscillatory component of temperature θ_1, as

$$\theta_1 = \theta_w \, e^{-\sqrt{i\omega/\alpha}\, y},$$

which is obtained by retaining the terms with the factor ω together with the derivatives of the highest order in (19). This shows that when the frequency of surface-temperature oscillation becomes very high, the thickness of the oscillatory boundary layer is of order $\sqrt{\alpha/\omega}$ and it should be confined in a very thin region adjacent to the plate. Here we again seek a series solution in the high frequency range, utilizing this limiting solution as the zeroth-order approximation. For this purpose we expand u_1, H_{x1} and θ_1 in the inverse powers of $\sqrt{\omega}$

$$u_1 = u_{10} + \frac{1}{\sqrt{\omega}} u_{11} + \frac{1}{\omega} u_{12} + \ldots -,$$

$$H_{x1} = H_{x10} + \frac{1}{\sqrt{\omega}} H_{x11} + \frac{1}{\omega} H_{x12} + \ldots, \tag{50}$$

$$\theta_1 = \theta_{10} + \frac{1}{\sqrt{\omega}} \theta_{11} + \frac{1}{\omega} \theta_{12} + \ldots.$$

Introducing the variable $z = \sqrt{\omega}\, y$, (17) to (19) take the form

$$\nu \frac{\partial^3 u_1}{\partial z^3} - i \frac{\partial u_1}{\partial z} = \frac{1}{\sqrt{\omega}} \frac{\partial}{\partial z}\left[v_s \frac{\partial u_1}{\partial z} + v_1 \frac{\partial u_s}{\partial z} - \right.$$

$$\left. - \frac{\mu_e}{\varrho}\left(H_{ys} \frac{\partial H_{x1}}{\partial z} + H_{y1} \frac{\partial H_{xs}}{\partial z}\right)\right] +$$

$$+ \frac{1}{\omega} \frac{\partial}{\partial z}\left[u_s \frac{\partial u_1}{\partial x} + u_1 \frac{\partial u_s}{\partial x} - \frac{\mu_e}{\varrho}\left(H_{xs} \frac{\partial H_{x1}}{\partial x} + H_{x1} \frac{\partial H_{xs}}{\partial x}\right)\right] -$$

$$- \frac{1}{\omega^{3/2}} g\beta \frac{\partial \theta_1}{\partial x}, \tag{51}$$

$$\eta \frac{\partial^2 H_{x1}}{\partial z^2} - iH_{x1} = \frac{1}{\sqrt{\omega}}\left[v_s \frac{\partial H_{x1}}{\partial z} + v_1 \frac{\partial H_{xs}}{\partial z} - H_{ys} \frac{\partial u_1}{\partial z} - H_{x1} \frac{\partial u_s}{\partial z}\right] +$$

$$+ \frac{1}{\omega}\left[u_s \frac{\partial H_{x1}}{\partial x} + v_1 \frac{\partial H_{xs}}{\partial x} - H_{xs} \frac{\partial u_1}{\partial x} - H_{x1} \frac{\partial u_s}{\partial x}\right],$$

$$\alpha \frac{\partial^2 \theta_1}{\partial z^2} - i\theta_1 = \frac{1}{\sqrt{\omega}}\left(v_s \frac{\partial \theta_1}{\theta z} + v_1 \frac{\partial \theta_s}{\partial z}\right) - \frac{1}{\omega}\left(u_s \frac{\partial \theta_1}{\partial x} + u_1 \frac{\partial \theta_s}{\partial x}\right).$$

Within the oscillatory boundary layer, the steady flow is approximated as

$$u_s = u_s(0) + y\left(\frac{\partial u_s}{\partial y}\right)_{y=0} + \frac{y^2}{L^2}\left(\frac{\partial^2 u_s}{\partial y^2}\right)_{y=0} + \ldots,$$

$$= (3A - B)\frac{Uz}{\sqrt{\omega}\,\delta} + \ldots\ldots\ldots.,$$

$$H_{xs} = H_{xs}(0) + y\left(\frac{\partial H_{xs}}{\partial y}\right)_{y=0} + \frac{y^2}{L^2}\left(\frac{\partial^2 H_{xs}}{\partial y^2}\right)_{y=0} + \ldots, \tag{52}$$

$$= H_0 - \frac{6H_0}{\omega\delta_1^2} z + \ldots\ldots\ldots,$$

$$\theta_s = \theta_s(0) + y\left(\frac{\partial \theta_s}{\partial y}\right)_{y=0} + \frac{y^2}{L^2}\left(\frac{\partial^2 \theta_s}{\partial y^2}\right)_{y=0} + \ldots,$$

$$= \theta_w - \frac{2\theta_w}{\sqrt{\omega}\,\delta} z + \ldots\ldots\ldots.$$

Substituting (50) in (51) and using (52), we get the following equations for u_{10}, H_{x10} and θ_{10}

$$\nu \frac{\partial^3 u_{10}}{\partial z^3} - i \frac{\partial u_{10}}{\partial z} = 0,$$

$$\eta \frac{\partial^2 H_{x10}}{\partial z^2} - i H_{x10} = 0, \tag{53}$$

$$\alpha \frac{\partial^2 \theta_{10}}{\partial z^2} - i\theta_{10} = 0,$$

with boundary conditions

$$\begin{aligned} &z = 0: \quad u_{10} = 0, \quad H_{x10} = 0, \quad \theta_{10} = \theta_w, \\ &z \to \infty: \quad u_{10} \to 0, \frac{\partial u_{10}}{\partial z} \to 0, \quad H_{x10} \to 0, \quad \theta_{10} \to 0. \end{aligned} \tag{54}$$

The solution of (53) is

$$u_{10} = 0, \quad H_{x10} = 0, \quad \theta_{10} = \theta_w e^{-\sqrt{i/\alpha}\, z}, \tag{55}$$

which is unaffected by the steady mean flow. Interaction terms, however, appear in the subsequent higher approximations. The next non-zero term in θ_1 is θ_{13} which satisfies the equation

$$\begin{aligned} &\alpha \frac{\partial^2 \theta_{13}}{\partial z^2} - i\theta_{13} = \frac{3A - B}{10\delta x} U \frac{\partial \theta_{10}}{\partial z} z^2, \\ &z = 0: \quad \theta_{13} = 0; \quad z \to \infty: \quad \theta_{13} \to 0. \end{aligned} \tag{56}$$

The solution of (56) is

$$\theta_{13} = \frac{\theta_w U}{20\alpha} \frac{3A - B}{\delta x} \left(\frac{z^3}{3} + \frac{z^2}{2\sqrt{i/\alpha}} + \frac{z}{2i/\alpha} \right) e^{-\sqrt{i/\alpha}\, z}. \tag{57}$$

The first non-zero term in u_1 is u_{16} which satisfies the equation

$$\begin{aligned} &\nu \frac{\partial^3 u_{16}}{\partial z^3} - i \frac{\partial u_{16}}{\partial z} = g\beta \frac{\partial \theta_{13}}{\partial x}, \\ &z = 0: \quad u_{16} = 0; \quad z \to \infty: \quad u_{16} \to 0, \frac{\partial u_{16}}{\partial z} \to 0. \end{aligned} \tag{58}$$

The solution of (58) is

$$u_{16} = \frac{3g\beta\theta_w\, U\,(3A - B)}{50\, v\alpha\delta x^2 (M^2 - m^2)} \left[\left(\frac{z^3}{3M} + \frac{7M^2 - 3m^2}{2\,M^2(M^2 - m^2)} z^2 + \right.\right.$$
$$+ \left.\left. \frac{31M^4 - 22\,M^2 m^2 + 7\,m^4}{2M^3 (M^2 - m^2)^2} z \right) e^{-MZ} + \right. \tag{59}$$
$$\left. + \frac{55\,M^6 - 45\,M^4 m^2 + 29\,M^2 m^4 - 7\,m^6}{2\,M^4 (M^2 - m^2)^3} (e^{-MZ} - e^{-mz}) \right],$$

where $M = \sqrt{i/\alpha}$, $m = \sqrt{i/\nu}$. The non-zero term in H_{x1} is H_{x17} which satisfies

$$\eta \frac{\partial^2 H_{x17}}{\partial z^2} - iH_{x17} = -\frac{6}{25} \frac{\delta_1 H_0}{x} \frac{\partial u_{16}}{\partial z}, \tag{60}$$
$$z = 0: \quad H_{x17} = 0: \quad z \to \infty: \quad H_{x17} = 0\,.$$

Solving the above equation, we get

$$H_{x17} = Pe^{-lZ} + \frac{9\, g\beta\theta_w\, UH_0\, \delta_1\,(3A - B)}{625\, v\alpha\eta\delta x^3 (M^2 - m^2)} \left[\frac{e^{-MZ}}{M^2 - l^2} \left\{ \frac{z^3}{3} + \frac{2M}{M^2 - l^2} z^2 + \right.\right.$$
$$+ \frac{2z(3M^2 + l^2)}{(M^2 - l^2)^2} + \frac{8M(M^2 + l^2)}{(M^2 - l^2)^3} + \frac{5M^2 - m^2}{2M(M^2 - m^2)} \left(z^2 + \frac{4Mz}{M^2 - l^2} + \right.$$
$$\left. + \frac{2(3M^2 + l^2)}{(M^2 - l^2)^2} \right) + \frac{17\,M^4 - 2\,M^2 m^2 + m^4}{2M^2 (M^2 - m^2)^2} \left(z + \frac{2M}{M^2 - l^2} \right) + \tag{61}$$
$$\left. + \frac{31M^4 - 22M^2 m^2 + 7m^4}{2M^3 (M^2 - m^2)^2} \right\} + \left(\frac{Me^{-MZ}}{M^2 - l^2} - \frac{me^{-mz}}{m^2 - l^2} \right) \times$$
$$\left. \times \frac{55\,M^6 - 45\,M^4 m^2 + 29M^2 m^4 - 7\,m^6}{2M^4 (M^2 - m^2)^3} \right],$$

where $l = \sqrt{i/\eta}$ and P is a constant of integration which can be obtained with the condition $H_{x17} = 0$ at $z = 0$.

For high frequency oscillations the rate of heat transfer and skin friction characteristics of the problem can now be obtained easily. The rate of heat transfer in dimensionless form is

$$N_{uh} = \frac{\varepsilon}{\delta^*} \left[\frac{\sigma\omega^*}{2} + \left(\sqrt{\frac{\overline{\sigma\omega*}}{2}} + \frac{3A - B}{40\omega^*} \delta^{*2} \right)^2 \right]^{1/2} \cos(\omega t + \alpha_6), \tag{62}$$

where

$$\alpha_6 = \tan^{-1} \left[1 + \frac{3A - B}{40\sqrt{\sigma}\,\omega^{*3/2}} \sqrt{2}\,\delta^{*2} \right].$$

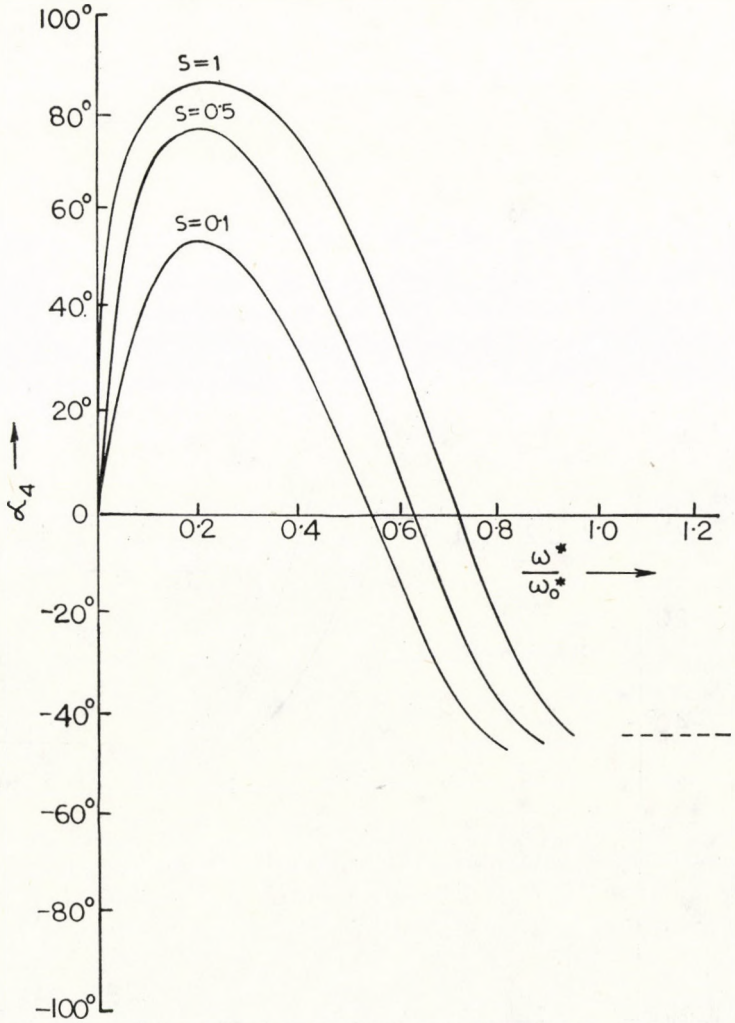

Fig. 4a. Phase angle α_4 of the oscillating skin friction vs ω^*/ω_0^* for $\lambda = 0.1$ and $s = 0.1, 0.5, 1$

The Nusselt number at the plate has a phase lead which tends to shear-wave value $\pi/4$ as $\omega \to \infty$. The skin friction in the non-dimensional form is obtained as

$$\tau_h^* = \varepsilon \frac{3\delta^{*4}(3A - B)}{100\omega^{*5/2}} \frac{24\sigma^{3/2} + 41\sigma + 28\sigma^{1/2} + 7}{\sigma^{3/2}(\sqrt{\sigma} + 1)^4} \cos(\omega t - \pi/4), \quad (63)$$

which has a phase lag of 45°. It is interesting to note that for very high frequencies the skin friction is extremely small being of the order of $\omega^{-5/2}$.

The high and low frequency solutions may be matched on the basis of the rate of heat transfer oscillations, taking the matching point as the frequency at which the low frequency solution predicts a phase advance equal to that

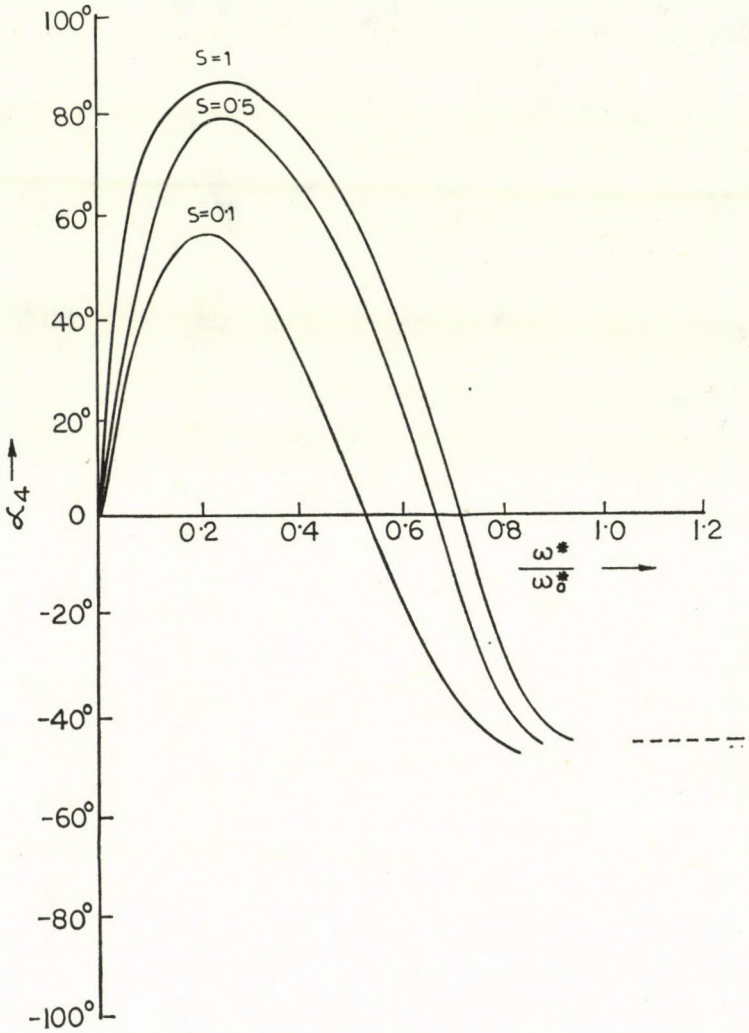

Fig. 4b. Phase angle α_4 of the oscillating skin friction vs ω^*/ω_0^* for $\lambda = 10$ and $s = 0.1, 0.5, 1$

of the 'shear wave' solution. We find the critical frequency parameter ω_0^* for which $\tan \alpha_5 = 1$, giving $\alpha_5 = \pi/4$. It is found that the critical frequency ω_0^* increases with s and λ. The values of ω_0^* for various s and λ are given in Table II.

Table II

λ \ S	0.1	0.5	1
0.1	7.1	15.1	16.9
10	11	44.4	92.4

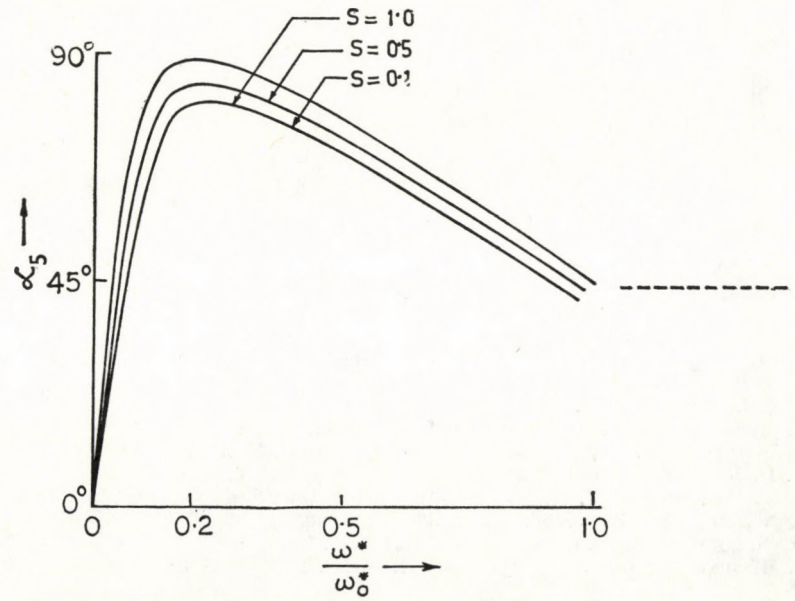

Fig. 5a. Phase angle α_5 of oscillating heat transfer vs ω^*/ω_0^* for $\lambda = 0.1$ and $s = 0.1, 0.5, 1$

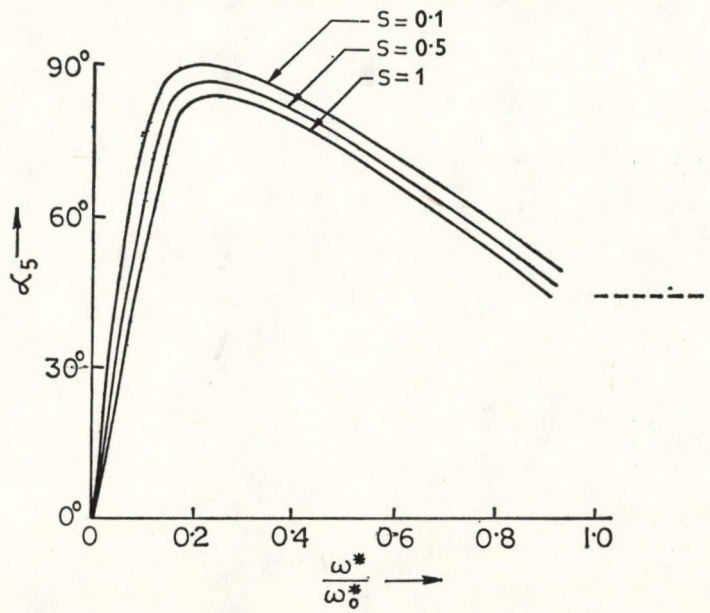

Fig. 5b. Phase angle α_5 of oscillating heat transfer vs ω^*/ω_0^* for $\lambda = 10$ and $s = 0.1, 0.5, 1$

The frequency response of the heat transfer and skin friction as functions of ω^*/ω_0^* are plotted in Figs. 4 and 5 for $\lambda = 0.1$, 10 and for $s = 0.1$, 0.5 and 1. The phase angle of the fluctuating component of heat transfer increases for small frequencies. The phase lead after reaching peak values begins to decrease for higher frequencies and attains the asymptotic value at ω_0^*. On the other hand, the phase angle of the skin friction, after attaining the maximum lead turns sharply towards the phase lag. From these Figures it is obvious that ω_0^* gives an approximate indication of the range of the validity of the two solutions.

REFERENCES

1. M. J. LIGHTHILL, Proc. Roy. Soc. A, **224**, 1, 1954.
2. R. S. NANDA and V. P. SHARMA, J. Fluid Mech., **15**, 419, 1963.
3. S. ESHGHY, V. S. ARPACI and J. A. CLARK, J. Appl. Mech., **32**, 183, 1965.
4. M. D. KELLEHER and K. T. YANG, ZAMP, **19**, 31, 1968.
5. P. K. MUHURI and M. K. MAITI, Int. J. Heat Mass Transfer, **10**, 717, 1967.
6. V. N. ZHIGULEV, Rev. Mod. Phys., **32**, 828, 1960.
7. W. N. GILL and E. D. CASAL, AIChE J., **8**, 515, 1962.
8. E. M. SPARROW and W. J. MINKOWYEZ, Int. J. Heat Mass Transfer, **5**, 505, 1962.

Acta Physica Academiae Scientiarum Hungaricae, Tomus 46 (2), pp. 97—100 (1979)

INTERPRETATION SIMPLE DU PARAMETRE ANHARMONIQUE ($\gamma\beta T$) D'UN SOLIDE

Par

Y. THOMAS

et

B. TARAVEL

INSTITUT DE RECHERCHES SCIENTIFIQUES ET TECHNIQUES
40945 ANGERS CEDEX (FRANCE)

(Reçu 13. II. 1979)

Un paramètre empirique mesurant l'anharmonicité des solides est interprêté, comparé avec les autres paramêtres utilisés jusqu'ici et calculé pour quelques solides ioniques et quelques métaux.

Si γ est le paramètre de GRUNEISEN, β le coefficient de dilatation cubique et T la température d'un solide, DUGDALE et MACDONALD [1] suggèrent que la quantité sans dimension ($\gamma\beta T$) mesure l'anharmonicité des vibrations thermiques de ce solide. Nous proposons une justification simple de ce paramètre et nous le calculons pour quelques solides.

L'énergie potentielle d'une paire d'atomes peut s'écrire, à une constante près:

$$V(x) = \frac{a}{2}x^2 + bx^3 + cx^4 + \ldots$$

où a, b, c sont des coefficients et $x = r - r_0$ est la variation de la distante r entre les atomes à partir de la position d'équilibre r_0. La force entre ces deux atomes est:

$$F(x) = -ax\left(1 + \frac{3b}{a}\bar{x} + \frac{4c}{a}x^2 + \ldots\right) = -ax(1+\varepsilon)$$

où ε est l'écart par rapport à la loi de HOOKE. Sa valeur moyenne — sans dimension — au second ordre peut donc mesurer l'anharmonicité:

$$\bar{\varepsilon} = \frac{3b}{a}\bar{x} + \frac{4c}{a}\bar{x}^2 .$$

Dans l'approximation du solide d'EINSTEIN, si E est l'énergie thermique d'un oscillateur:

$$\bar{\varepsilon} = -\frac{9b^2}{a^3}E - \left(\frac{27b^2c}{a^5}E^2 - \frac{4c}{a^2}E\right)$$

d'où le coefficient de dilatation cubique (si θ est la température de DEBYE, à $T \geq \theta$: $E \simeq kT$ et C_v la chaleur spécifique est quasi constante):

$$\beta = \frac{3}{r_0}\frac{d\bar{x}}{dT} = -\frac{9bC_v}{r_0 a^2}\left(1 + \frac{6c}{a^2}E\right) \cong -\frac{9bk}{r_0 a^2}$$

permettant de donner une signification très générale à $\bar{\varepsilon}$:

$$\bar{\varepsilon} \cong \frac{br_0}{a}\beta T = \frac{(\bar{x})^2}{\overline{x^2}} . \tag{1}$$

Si on adopte le potentiel de MIE LENNARD-JONES:

$$V = -\frac{A}{r^m} + \frac{B}{r^n}$$

où A et B sont des constantes, m et n des exposants ($n > m > 0$), on a $a = \frac{mn}{r_0^2} V_0$ et $b = -\frac{mn(m+n+3)}{6r_0^3} V_0$ où V_0 est l'énergie de dissociation d'une paire de particules. Pour un réseau de type quelconque, si N est le nombre d'Avogadro et f l'indice de coordination, l'énergie $\Phi_0 = \frac{V_0 Nf}{2}$. Or $\gamma = \frac{br_0}{a} = \frac{m+n+3}{6}$ d'où l'égalité fondamentale :

$$\bar{\varepsilon} = \frac{(m+n+3)^2 E}{4\, mn V_0} = (\gamma\beta T) . \tag{2}$$

Remarquons que:

$$\beta \cong \frac{3k\gamma}{mnV_0} \text{ soit } \beta V_0 \simeq \text{constante [2]}$$

on retrouve aussi un paramètre parfois utilisé comme mesure de l'anharmonicité [3]:

$$\bar{\varepsilon}' = \frac{d\bar{\varepsilon}}{dT} = \gamma\beta .$$

Etant donné les lois approximatives adoptées pour l'énergie et le potentiel, ces équations ont principalement l'intérêt de mettre clairement en évidence les lois de variation et les dépendances qualitatives en fonction des divers paramètres caractérisant un solide anharmonique.

Application à quelques solides ioniques:

On adopte le potentiel de MIE LENNARD-JONES

Tableau I

Résultats pour quelques solides ioniques. ($T = 300$ K) [5]

Solides	$\beta \cdot 10^6\,\mathrm{K}^{-1}$	γ	$\bar{\varepsilon}10^4 = \frac{(n+4)^2}{4nV_0}\,\mathrm{E}\cdot 10^4$	$\beta V_0(6N)$
LiF	102	1,34	260,8	244,9
Licl	132	1,52	335,1	255,1
LiBr	150	1,70	364,2	254,1
NaCl	330	1,63	376,5	594,0
NaBr	337	1,56	401,4	601,9
KF	300	1,45	355,8	511,2
Kcl	303	1,60	430,5	498,0
KBr	330	1,68	459,3	527,1
KI	375	1,63	504,9	528,2
RbBr	312	1,37	484,2	462,1
RbI	357	1,41	534,0	471,3

A $T = 300$ K, le caractère anharmonique croit (alors que le degré d'ionisation décroit) pour les composés de masse croissante d'un métal donné.

Application à quelques métaux:

On adopte le potentiel:

$$V = -\frac{A'}{r} + \frac{B'}{r^2}$$

où r est la distance entre deux atomes voisins et A', B' sont des constantes [4]. L'anharmonicité des métaux varie dans le même ordre que celle — plus faible — de leurs composés ioniques. A $T = 300$ K, pour des corps de structure identique, $\bar{\varepsilon}$ — proportionnel à V_0^{-1} — varie toujours dans le sens de β qui semble une meilleure caractéristique de l'anharmonicité que γ ou $(\gamma\beta)$ parfois utilisés.

Le coefficient b varie comme β^{-1} et ne peut caractériser l'anharmonicité du solide.

Tableau II

Résultats pour quelques métaux ($T = 300$ K) [5]

Métaux	$\beta \cdot 10^6\,K^{-1}$	γ	$\bar{\varepsilon} \cdot 10^4 = \frac{4{,}5E}{V_0} 10^4$	f
W	12,9	1,62	223,5	
Mo	15,3	1,57	235,8	8
Ta	19,5	1,75	318,8	
Fe	33,5	1,60	476,1	
Li	180	1,17	1171,1	
Na	216	1,25	1713,9	8
K	252	1,34	1828,8	
Rb	270	1,48	2202,3	
Cs	291	1,29	2401,2	
Pt	26,85	2,54	525,6	
Ni	40,2	1,88	666,3	12
Au	42,45	3,03	749,1	
Cu	50,1	1,96	840,3	12
Ag	58,5	2,40	1014,3	

Les résultats expérimentaux [5] montrent que l'équation (2) n'est pas rigoureusement vérifiée. Cela est principalement dû à la dépendence explicite de θ avec la température qui permet de formuler une mesure plus précise de l'anharmonicité [6]:

$$n\gamma\beta = -\frac{d \log \theta}{dT}$$

où n est un coefficient fonction de la température pouvant être déterminé par:

$$\left[\frac{\bar{\varepsilon}}{\gamma\beta T}\right]_i = n_i$$

à la température T_i.

BIBLIOGRAPHIE

1. J. S. Dugdale and D. K. C. Macdonald, Phys. Rev., **98,** 1751, 1955.
2. D. K. C. Macdonald and S. K. Roy, Phys. Rev., **97,** 675, 1955.
3. Y. Thomas, C. R. Acad. Sc. Paris, **265B,** 1339, 1967.
4. Ya. I. Frenkel', Introduction à la théorie des Métaux, GITTL, Moscou, 1950.
5. F. Seitz, Théorie moderne des solides, Masson, Paris, 1949.
   J. C. Slater, Introduction to Chemical Physics, McGraw-Hill Book Company Inc., New York, 1939.
6. Y. Thomas, Phys. Stat. Sol., (b)**87,** K13, 1978.

Acta Physica Academiae Scientiarum Hungaricae, Tomus 46 (2), pp. 101—112 (1979)

ELECTRICAL CONDUCTIVITY IN THIN POLYCRYSTALLINE p-QUATERPHENYL LAYERS

By

J. SWIĄTEK

INSTITUTE OF PHYSICS, TECHNICAL UNIVERSITY OF ŁÓDZ, ŁÓDZ, POLAND

and

D. C. LARSON

DEPARTMENT OF PHYSICS AND ATMOSPHERIC SCIENCE, DREXEL UNIVERSITY, PHILADELPHIA, Pa., USA

(Received 15. II. 1979)

The electric conductivity of metal-*p*-quaterphenyl-metal thin polycrystalline layers sandwich structures have been investigated as a function of voltage, thickness, and temperature. The films which ranged in thickness from 0.9 to 1.6 μm were measured in the temperature range of 100—370 K. The experimental data may be explained by space charge effects with contribution of Richardson—Schottky mechanism or in terms of injection modified by space charge effects.

1. Introduction

In recent years there has been increasing interest in research on the physical, especially electrical, properties of organic materials [1—6]. Organic substances are interesting as new materials which can be used in microelectronics because of their semiconducting properties. They are also interesting due to their structural similarity to biologically important materials.

In this paper the dark electrical conductivity of polycrystalline *p*-quaterphenyl layers in the temperature range 100—370 K have been investigated. The study of the current-voltage characteristics gives information concerning the position of trapping levels and their spatial density and the analysis of the current — thickness dependences is very important for selecting the pertinent model of the conductivity.

Because the current — voltage characteristics in examined films showed a nearly vertical region we have tried to adopt one carrier space charge limited currents (SCLC) theory to interpret the results obtained. We have not been able to fit any of existing SCLC models [7, 8] to the experimental points in spite of the fact that current — thickness characteristics give incorrect slope if one carrier SCLC theory is taken into account.

The experimental data may be interpreted in terms of injection theory proposed by ASHLEY and MILNES [9] or by SCLC with contribution of Richardson—Schottky mechanism.

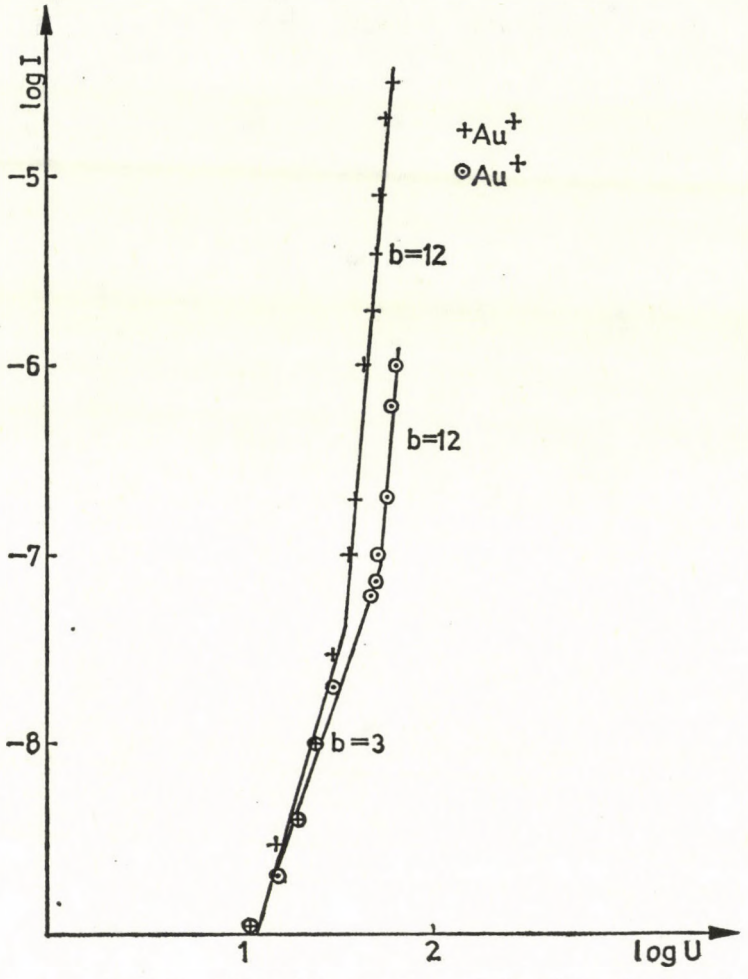

Fig. 1. Dependence of the logarithm of the current on the logarithm of voltage for *p*-quaterphenyl layer with Al—Au electrodes. Thickness of the layer 0.9 μm. Temperature 300 K

2. Experimental

The layers of *p*-quaterphenyl were prepared by vacuum sublimation from a quartz crucible. The evaporation process was carried out in a vacuum of 10^{-7} torr on a glass substrate being at a temperature of 300 K. Vacuum evaporated metallic electrodes of gold and aluminium in sandwich configuration were applied. Film thicknesses (0.9—1.6 μm) were measured by an interference method and by measuring film capacitance. The optical measurements were made with the MIN-4 interference microscope, which has an accuracy of ± 50 Å and the capacitance measurements were made with a General Radio impedance bridge and checked with a General Radio model 1673 capacitance bridge.

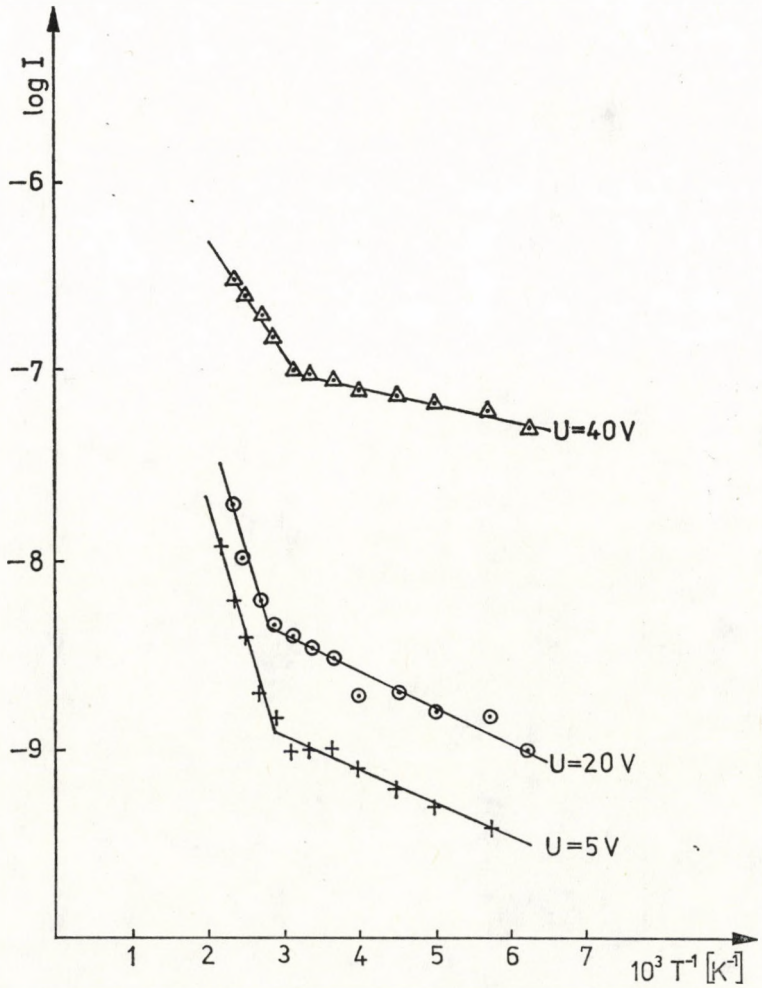

Fig. 2. Dependence of the logarithm of the current on the temperature reciprocal for different voltages. Thickness of the layer 0.9 μm

The current measurements were carried out in a vacuum of 10^{-3} torr using the Keithley model 25054 solid state logarithmic response picoammeter and a Hewlett—Packard model 7005A X—Y recorder to record the data.

As a power source the Hewlett—Packard model 202A function generator and Harrison model 682A Power Supply-Amplifier were used since it produced a very low frequency (0.01 Hz) triangular wave which made it suitable for making d.c. measurements.

A Leeds and Northrop model 1992 temperature-milivolt transmitter with copper-constantan thermocouple was used for recording the sample temperature.

3. Results

The typical current — voltage characteristics for different gold electrode bias drawn in a lgI — lgU plot at room temperature are shown in Fig. 1.

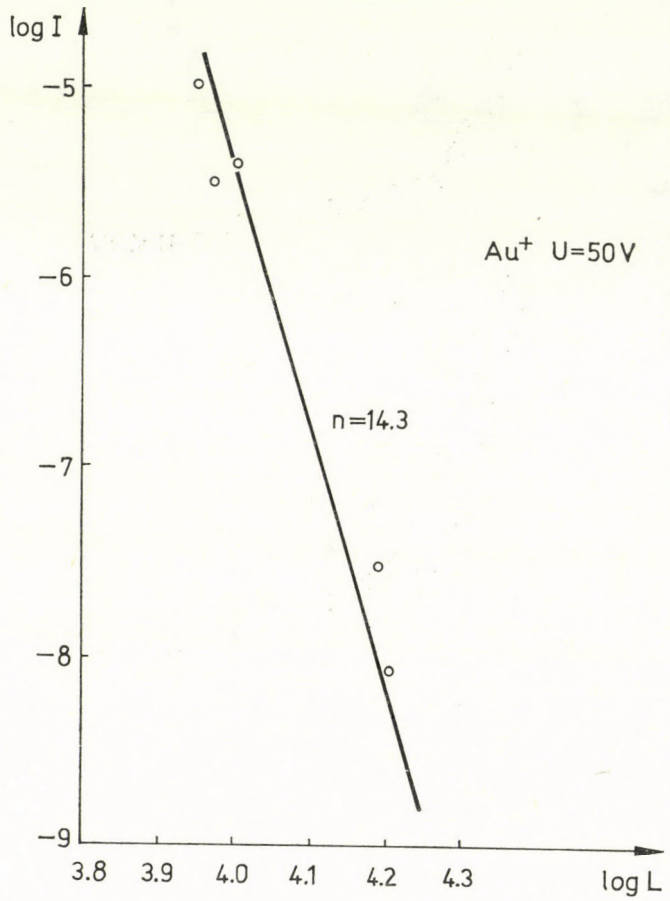

Fig. 3. Dependence of the logarithm of the current on the logarithm of the thickness for *p*-quaterphenyl layers. Voltage $U = 50$ V

Fig. 2 shows the dependence of the logarithm of the current on the temperature reciprocal for different voltages. The slope of these plots enables one to calculate the activation energy.

Fig. 3 shows the dependence of the logarithm of the current on the logarithm of the thickness for examined *p*-queterphenyl layers.

Fig. 4 shows lg I/L versus U/L^2 dependence. The general scaling relationships proposed by MURGATROYD [10, 11] for space charge limited currents show

how shape of the current — voltage characteristic depends on the trap distribution and the sample thickness.

Fig. 5 shows the Fermi level dependence on the logarithm of the voltage for the investigated *p*-quaterphenyl layers.

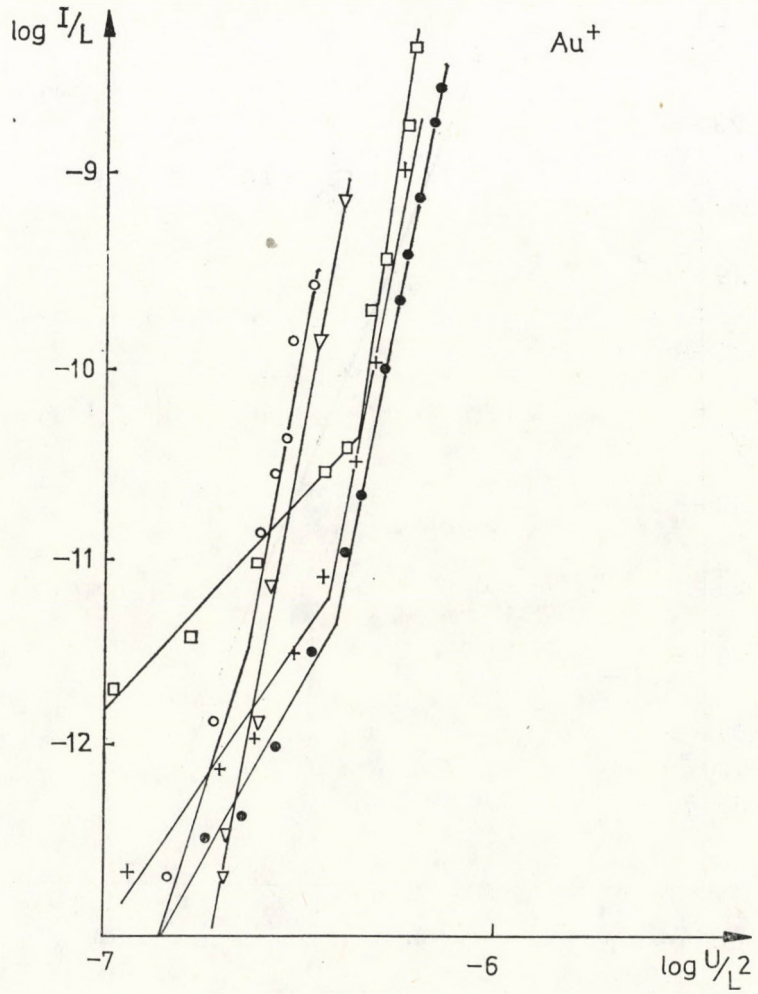

Fig. 4. Dependencce of the lg I/L versus lg U/L^2 for *p*-quaterphenyl layer. Gold electrode on positive bias. Thickness of the layers: + 0.9 μm, ● 0.93 μm, □ 1.01 μm, ▽ 1.56 μm, ○ 1.59 μm

4. Discussion of the results

4.1 *Space charge limited currents*

The SCLC theory in dielectric materials predicts that the slope of the current — voltage characteristics depends on the trap distribution. In the

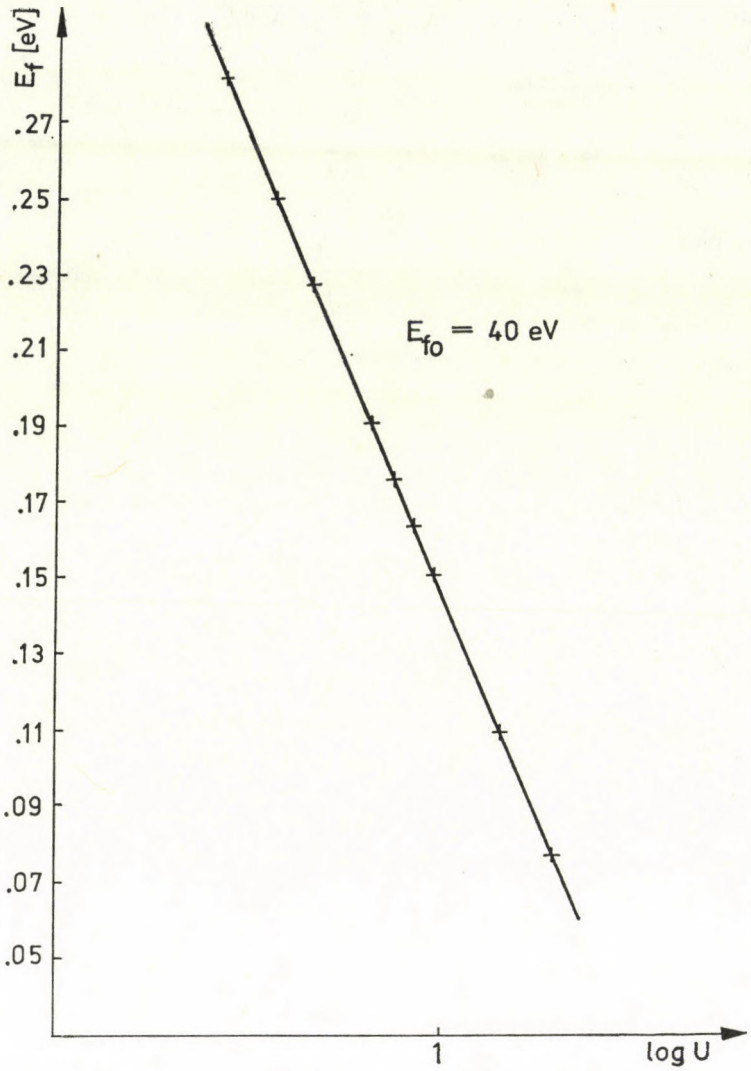

Fig. 5. Dependence of the Fermi level on the logarithm of voltage

most papers an exponential trap distribution has generally been assumed [1—3, 8] and the current density — voltage dependence is given by the following equation

$$j = N_c e\mu \left[\frac{\varepsilon\varepsilon_0 \cdot l}{eH(l+1)}\right]^l \cdot \left[\frac{2l+1}{l+1}\right]^{l+1} \cdot \frac{U^{l+1}}{L^{2l+1}}, \tag{1}$$

where N_c is the effective density of states in the valence band, ε_0 is the vacuum permittivity, ε is the dielectric constant of the material, μ is the free carrier

mobility, H the number of the traps per unit volume, U is the applied voltage, L is the thickness of the sample, and $l = T_c/T$.

The slope of the high voltage part of the lg I versus lg U characteristic $b = T_c/T + 1$ gives the "characteristic temperature" T_c and the characteristic energy of the trap distribution.

The value of the critical volrage at which the current increases steeply corresponds to the trap density, H, in the solid by the expression [8, 11]

$$U_{TFL} = \frac{eL^2}{\varepsilon\varepsilon_0} \cdot \left[\frac{9}{8} \cdot \frac{H^b}{N_c} \cdot \left(\frac{b+1}{b}\right)^b \cdot \left(\frac{b+1}{2b+1}\right)^{b+1}\right]^{(b+1)^{-1}}, \tag{2}$$

when $b \to \infty$

$$U_{TFL} = \frac{eHL^2}{2\varepsilon\varepsilon_0}. \tag{3}$$

Our experimental results give average value for $T_c = 2940$ K and characteristic energy of the trap distribution $kT_c = 0.25$ eV. The trap density changed from $0.5 \cdot 10^{22}$ m^{-3} to $2.35 \cdot 10^{22}$ m^{-3} for different p-quaterphenyl samples and average value equals $H = 1.6 \cdot 10^{22}$ m^{-3}.

From the logarithm of the current versus reciprocal temperature and logarithm of the current versus logarithm of the voltage plots we have obtained an energy of activation and the value for $N_c\mu$.

The values of activation energy of 0.14, 0.09, 0.05 and 0.10 eV for different voltages have been obtained. At low temperatures there were smaller values of the energy of activation. At a temperature about 300 K the activation energy changed to higher values.

These values are in good agreement with the activation energy obtained by SZYMANSKI [1].

The SCLC theory predicts a logarithmic dependence of current on thickness for the exponential trap distribution. It can be seen in Fig. 3 that lg I versus lg L plot gives a straight line what is typical for the exponential trap distribution.

The dependence of the Fermi level, for the exponential trap distribution, on voltage is given by the following equation:

$$E_F = kT_c \frac{(b+1)^2}{b(2b+1)} \cdot \frac{eHL^2}{\varepsilon\varepsilon_0 U}. \tag{4}$$

As b is known from the logarithm of the current versus logarithm of the voltage characteristics one can evaluate the Fermi level for different voltages. Fig. 5 shows the dependence of the Fermi level on the logarithm of voltage. It can be seen that this plot gives a straight line. This can be taken as evidence that traps are exponentially distributed in material.

The value of the activation energy for the exponential trap distribution can be interpreted as maxima situated on this distribution.

From the SCLC theory the slope of lg I versus lg L plot for the exponential trap distribution ought to have a twice higher value than the slope of the lg I versus lg U characteristic [8, 11], which does not agree with our results. As can be seen in Fig. 3 the slope of the plot is about 14. It is less than we expected from SCLC theory.

This result and the very low $N_c\mu$ value (about 10^{10} $m^{-1} V^{-1} s^{-1}$) show that the SCLC theory only partially describes electric conductivity in the investigated p-quaterphenyl layers. This may be explained by the following physical reasons.

At reasonably strong applied electric fields there is a sufficient supply of carriers available to enter the insulator from the electrode and current — voltage characteristics are determined by the bulk properties of the investigated material. At high fields, or if the injecting properties of the contact are not very good, the current is less than what the bulk of the dielectric is capable of carrying. Under these conditions the I — U characteristics of the sample are controlled not only by the bulk properties but also by conditions existing at the electrode — material interface. The current controlled by the space charge may be still predominant conductivity mechanism but it ought to be weaker dependent on the thickness of the sample than predicted by the one carrier SCLC theory.

If the electrode saturates we will expect the field to be uniform through the sample with

$$\frac{I}{L} = \frac{A}{L} \exp\left[BL^{1/2} \cdot \left(\frac{U}{L^2}\right)^{1/2}\right]. \tag{5}$$

as it was pointed out by MURGATROYD [12].

Then we can expect that the upper part of the lg $_2/L$ versus lg U/L^2 plot is to be ordered in the manner sketched in Fig. 6. The maximum field that may be applied to the insulator before the electrode saturates is given by:

$$E_c = \frac{\bar{c}}{4\mu}, \tag{6}$$

where $\bar{c}$ is the thermal velocity of the carriers, u is the mobility of the charge carriers.

The thermal velocity may be estimated for organic materials from the field at which the mobility of the carriers equals the drift velocity. For tetracene thin films this field is about 10^4 V/cm [13]. Similar results have been obtained for p-quaterphenyl layers [14]. As we can see from the experimental data at field order of 10^4 V/cm the current is controlled by space charge. So

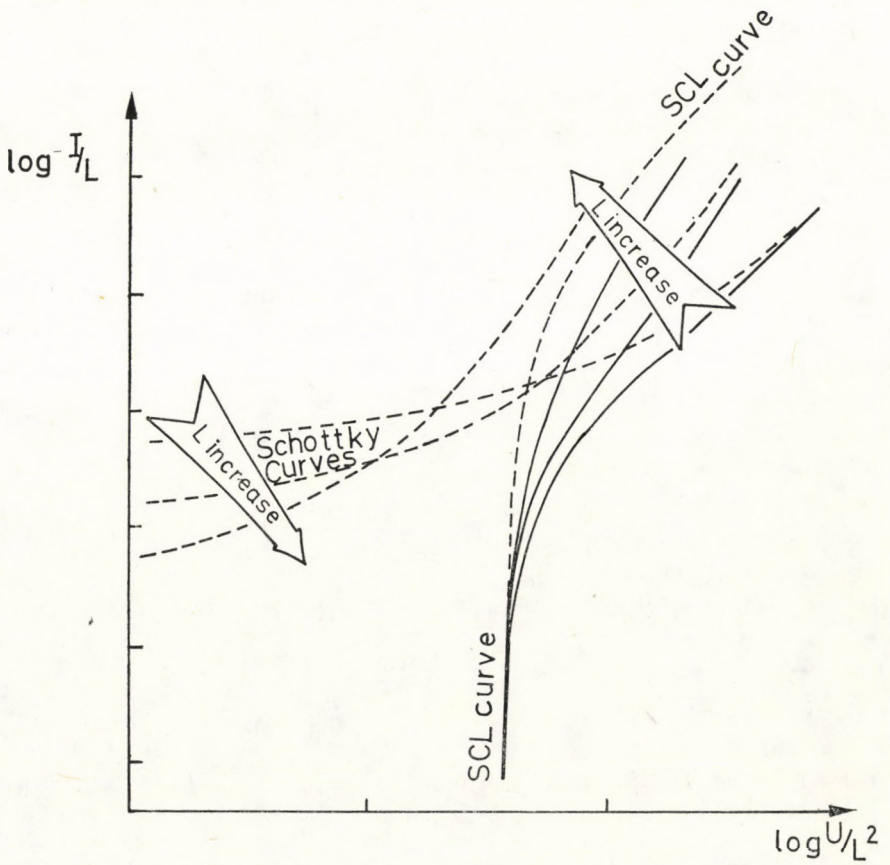

Fig. 6. Ordering due to electrode limiting (redrawn from [12])

we can suppose that in the investigated thin polycrystalline *p*-quaterphenyl layers the conditions at metal — organic material interface play a significant role during the current passing through the layer. It may be confirmed by the data presented in Fig. 4 which was drawn in the general scaling rule for space charge currents proposed by MURGATROYD [10].

The next point which ought to be explained is the low value for $N_c\mu$. This problem is typical for organic materials. We suppose that the theoretical interpretation is responsible for the discrepancy. The current — voltage and current — thickness dependences have been calculated with assumptions that the mobility of the carriers is independent of the applied field and the sample thickness. The experimental data obtained by MYCIELSKI [13] for tetracene thin films have shown that the carrier mobility depends as well on applied field (above 10^4 V/cm) as on the film thickness (below about 5 μm). The mentioned problem is unsolved. It requires further intensive experimental as well as theoretical research.

4.2 *Injection currents*

The SCLC theory predicts a power law dependence of a current on a thickness for the exponential trap distribution. It can be seen in Fig. 3 that the lg I versus lg L plot gives a straight line typical for the exponential trap distribution, but according to the SCLC theory the slope of this characteristic ought to have a value about twice higher than the slope of the lg I versus lg U dependence [8, 15], which does not agree with our results. As can be seen in Fig. 3 the slope of the lg I — lg L plot is about 14 what is not in conformity with one carrier SCLC theory. This means that the measured current is closed to the $(U/L)^n$ relation and may indicate the relative unimportance of space charge effects.

The results obtained are in a good agreement with the ASHLEY—MILNES model in which the charge carrier mobility and/or the cross-section for trapping depend on the electric field [8].

The exponential increase of the current with voltage is mainly related to injecting of the carriers from the electrode. If diffusion processes may be neglected, in the high electric field the current density is given by

$$j = (\mu_p p + \mu_n n)\, eE\,, \tag{7}$$

where p and n are the concentration of the free hole and electron, respectively, μ_p and μ_n their mobility, j the total current density and e is the charge of an electron, E is the electric field.

The value of n may be obtained from the particle conservation equation

$$\frac{n}{\tau_n} = \frac{1}{e}\frac{dj_n}{dx} = -\frac{1}{e}\frac{dj_p}{dx}\,, \tag{8}$$

where j_n and j_p are the electron and hole current density, respectively, τ_n and τ_p are the electron and hole life time, respectively.

The life times of the carriers are given by the following expressions:

$$\tau_n = (\sigma_n \bar{c}_n N_{Tn})^{-1} \quad \text{and} \quad \tau_p = (\sigma_p \bar{c}_p N_{Tp})^{-1} \tag{9}$$

where $\bar{c}_n$ and $\bar{c}_p$ are the thermal velocities of electrons and holes, respectively, N_{Tn} and N_{Tp} are the concentration of the electron and hole traps, respectively, σ_n and σ_p are cross-section for trapping of electrons and holes, respectively.

We know that in high electric fields the mobility of the carriers depends on the field and decreases with increasing of the electric field (see for example [13]). In weak fields the mobility is constant and its variations occur above a certain critical value of the field, E_c, and velocity of the carriers increases with field. In a high enough field the optical phonons are excited, the velocity of the carriers begins to saturate and mobility decreases with the field.

Let the mobility of the carriers and the capture-cross-section depend on the field as follows:

$$\mu_p = \mu_{p0}\left(\frac{E_c}{E}\right)^{1/\beta_p - 1/2}, \tag{10}$$

$$\mu_n = \mu_{n0}\left(\frac{E_c}{E}\right)^{1/\beta_n - 1/2} \tag{11}$$

and

$$\sigma_n = \sigma_{n0}\left(\frac{E_c}{E}\right)^{\alpha_n - 1/2}, \tag{12}$$

where μ_{p0} and μ_{n0} are the mobilities of the holes and electrons at the low electric field, respectively, β_0 and α_0 are constants, σ_{n0} is the capture cross-section for the trapping of electrons at low electric field.

With the above equations, the expression for the current — voltage dependence, obtained by ASHLEY and MILNES in ASHLEY—MILNES regime is

$$j = K\frac{U^{\alpha_n - 1/\beta_p + 1}}{L^{\alpha_n - 1/\beta_p + 2}}, \tag{13}$$

where K is a constant.

As can be seen from Eq. (13) the dependence of the cross-section for trapping on the electric field may be obtained from the slope of the current — thickness dependence.

We also see that the slopes of the $\lg I - \lg L$ and $\lg I - \lg U$ dependences ought to be very similar, as it was observed in our experiments.

We have only one information about field dependence of the carrier mobility in *p*-quaterphenyl layers [14] which is similar to that obtained by MYCIELSKI et al [13] for thin tetracene films e.g. the mobility depends on the field as E^{-n}, where n varied between 0.5 and 1, the β_p ought to have values varying between 1 and 2/3. For these values of β_p, the field-dependence of the capture cross-section for trapping changes with the field as E^{-12}. It is of course an unphysical result and we can suppose that the mechanism of the conductivity is determined by injection from the electrodes without changes of the capture cross-section for trapping.

Acknowledgement

One of us (JS) would like to acknowledge the support of the International Research and Exchange Board who provided a grant to enable the experimental part of this work to be carried out at Drexel University (Philadelphia).

REFERENCES

1. A. SZYMANSKI, Mol. Cryst. and Liquid Cryst., **3**, 339, 1968.
2. P. J. REUCROFT and F. D. MULLINS, J. Phys. Chem. Solids, **35**, 347, 1974.
3. J. SWORAKOWSKI, Mol. Cryst. and Liquid Cryst., **11**, 1, 1970.
4. A. K. WITT and D. C. LARSON, Thin Solid Films, **36**, 85, 1976.
5. A. SZYMANSKI and N. M. LABES, J. Chem. Phys., **50**, 1898, 1969.
6. J. SWIĄTEK, phys. stat. solidi (a), **36**, 285, 1976.
7. J. SWORAKOWSKI and K. PIGON, J. Phys. Chem. Solids, **30**, 491, 1969.
8. P. MARK and W. HELFRICH, J. Appl. Phys., **33**, 205, 1962.
9. K. L. ASHLEY and A. G. MILNES, J. Appl. Phys., **35**, 369, 1964.
10. P. N. MURGATROYD, phys. stat. solidi (a), **11**, 137, 1972.
11. W. HELFRICH, in "Physics and Chemistry of the Organic Solid State", ed. Fox, Labes, Weissberger, vol. III, Interscience, New York.
12. P. N. MURGATROYD, Thin Solid Films, **17**, 335, 1973.
13. W. MYCIELSKI and A. LIPINSKI, Thin Solid Films, **48**, 133, 1978.
14. A. LIPINSKI, J. KONDRASIUK and A. SZYMANSKI, Mol. Cryst. and Liquid Cryst., **13**, 381, 1971.
15. A. M. LAMPERT and P. MARK, Current Injection in Solids, Academic Press, New York. 1970.

Acta Physica Academiae Scientiarum Hungaricae, Tomus 46 (2), pp. 113—123 (1979)

ON CONCENTRATION DEPENDENCE OF LUMINESCENCE DECAY TIME OF MOLECULES IN ISOTROPIC MEDIA

By

C. BOJARSKI and E. GRABOWSKA

INSTITUTE OF PHYSICS, TECHNICAL UNIVERSITY, GDANSK, POLAND*

(Received in revised form 22. II. 1979)

Assuming that only monomers and non-luminescent dimers appear in the solution and non-radiative electronic energy transfer results from a dipole-dipole interaction we have obtained an expression for the dependence of luminescence decay time on the reduced concentration γ of the dye molecules in the solution. In order to compare the obtained theoretical results with the experiments, measurements have been carried out on the concentration changes of luminescence decay time of Na-fluorescein in glycerol-alcohol solutions.

After corrections for reabsorption and influence of the secondary fluorescence, the obtained experimental results show a satisfactory agreement with the theoretical prediction. The subsequent slight increase and decrease of τ found at the increasing concentration can be attributed to the competition between the electronic excitation energy diffusion process among the monomers and the process of photoluminescence concentration quenching by dimers, as well as by monomers.

1. Introduction

The concentration increase of luminescent molecules in solutions is often seen in the changes of quantum yield η of photoluminescence (PL), emission anisotropy r and also in the changes of PL decay time τ of active molecules. Many authors have dealt with the mentioned concentration effects [1—4]. Recently we worked out the theory of PL concentration quenching (PLCQ) and PL concentration depolarization (PLCD) where we took into account the association of active molecules and the multi-step mechanism of non-radiative transfer of electronic excitation energy [5, 6].

Regarding these real phenomena accompanying the concentration effects it is possible to describe the experimental results correctly over a wide range of concentrations [7—9].

In Section 2 we present a theoretical description of the concentrational changes of PL decay time obtained after taking into account the above mentioned processes. Sections 3 and 4 contain the results of measurements of PL decay time of Na-fluorescein in glycerin-alcohol solutions, their comparison with the theory and a discussion.

*Address: Instytut Fizyki, Politechnika Gdańska, Gdańsk—Wrzeszcz, Majakowskiego 11/12, Poland

2. Theoretical considerations

Similarly as in [5, 6] we accept that in an inactive medium there are statistically distributed molecules of donor D and acceptor A treated as electrical dipoles. The absorption and emission spectra of the donor as well as the emission spectrum of the donor and the absorption spectrum of the acceptor partially overlap. All molecules D^x can undergo deactivation as a result of the following processes: light emission, internal quenching, non-radiative energy transfer to a non-excited molecule of type D or to a molecule A with rate constants k_F, k_q, k_{DD} and k_{DA}, respectively. We assume that the non-radiative transfer occurs as a result of dipole-dipole interaction for which the rate constant [1] amounts to:

$$k_{DA} = (k_F + k_q)\left(\frac{R_{0A}}{R}\right)^6, \tag{1}$$

R_{OA} is the critical distance of energy transfer from an excited molecule of donor D^x to a molecule of acceptor A, R are the distance between the interacting molecules.

In the theory of concentration effects [5] developed formerly, all luminescence centres were divided into groups, according to configuration[1] σ of non-excited molecules D and A, in the environment of D^x, in order to characterize the spatial distribution of the active molecules in the solution.

In order to characterize the time evolution of energy migration process all molecules D^x were divided additionally as follows: molecule D^x belongs to the group of molecules $D^{(n)}$ of the n^{th} order if it obtained excitation energy after its "n" non-radiative transfers. We denote molecules $D^{(n)}$, characterized by configuration σ, with $D_\sigma^{(n)}$ and the number of molecules of such type after time t, from the moment of an impulsive excitation, with $N_\sigma^{(n)}(t)$. The luminescence decay time can be calculated from relation:

$$\tau = \sum_{n=0}^{\infty} \sum_{\sigma} \int_0^{\infty} N_\sigma^{(n)}(t)\, t\, dt \Big/ \sum_{n=0}^{\infty} \sum_{\sigma} \int_0^{\infty} N_\sigma^{(n)}(t)\, dt, \tag{2}$$

if we know the analytical form of function $N_\sigma^{(n)}(t)$. These functions satisfy the system of equations [5]:

$$\begin{aligned} \frac{dN_\sigma^{(0)}(t)}{dt} &= -k_\sigma N_\sigma^{(0)}(t), \\ \frac{dN_\sigma^{(n)}(t)}{dt} &= -k_\sigma N_\sigma^{(n)}(t) + \left(\sum_{\sigma'} k_{\sigma'} N_{\sigma'}^{(n-1)}(t)\, P_\sigma\right), \\ &\text{for } n = 1, 2, 3, \ldots, \end{aligned} \tag{3}$$

[1] We accept that this configuration is determined by distances $R_1, \ldots, R_{N_D-1}$ and $R_1, \ldots, R_{N_A}$ of all the non-excited molecules D and A from the molecule D^x; N_D and N_A denote the number of molecules D and A in the system.

where $k_\sigma = k_F + k_q + k_{\sigma DD} + k_{\sigma DA}$ and P_σ means the probability that the excited molecule of the donor has environment σ of the donors and acceptors. The concentration dependence of PL decay time should be calculated in a different way, because it is difficult to find the functions $N_\sigma^{(n)}(t)$ from the system of equations (3).

Let $\tau^{[n]}$ denote the mean time that elapsed from the moment of photon absorption by a molecule of type $D^{(0)}$ to its emission by a molecule of type $D^{(n)}$, and $\tau^{(n)}$ denote the mean time of excitation energy localization on molecules $D^{(n)}$. In the case of a very weak coupling, according to FÖRSTER's classification [10], the excitation can be treated as temporarily localized on one single molecule and the process of excitation energy transfer as an incoherent motion of this kind of localized excitation. Thus, time $\tau^{[n]}$ is the sum of localization times of excitation energy on the molecules of each order:

$$\tau^{[n]} = \sum_{k=0}^{n} \tau^{(k)} . \tag{4}$$

In the case of a very weak coupling the vibrational relaxation in excited state occurs completely before each act of energy transfer (before each jump). Therefore, it seems to be justified to accept the mean times $\tau^{(k)}$ being identical for the molecules of an arbitrary order.

Hence

$$\tau^{[n]} = (n + 1)\tau^{(0)}, \tag{5}$$

where n is the number of acts of non-radiative energy transfer, $\tau^{(0)}$ is the mean lifetime of molecules excited directly by light absorption. We also accepted a simplified assumption that at fixed concentrations of molecules D and A the localization time $\tau^{(n)}$ was independent of configuration σ. Actually $\tau^{(n)}$ depends on configuration σ, particularly in the range of low concentrations where the fluctuations of molecule numbers D and A are pronounced in the nearest environment of molecule $D^{(n)}$. It leads to an earlier deactivation of these luminescence centres which are characterized by a favourable configuration σ for the non-radiative energy transfer from molecules $D^{(n)}$ to molecules D or A.

At stationary excitation the PL decay time of molecules D can be calculated on the basis of relation:

$$\tau = \sum_{n=0}^{\infty} \tau^{[n]}\eta^{(n)} \Big/ \sum_{n=0}^{\infty} \eta^{(n)}, \tag{6}$$

where $\eta^{(n)}$ denotes the PL quantum yields of molecules $D^{(n)}$, at which [5]

$$\eta^{(n)} = P_F \cdot P_{DD}^n . \tag{7}$$

Taking into account relations (5) and (7) in Eq. (6) we obtain:

$$\tau = \tau^{(0)} \sum_{n=0}^{\infty} (n+1) P_{DD}^n \Big/ \sum_{n=0}^{\infty} P_{DD}^n \,. \tag{8}$$

P_F and P_{DD} denote the relative probabilities of PL emission and non-radiative energy transfer from D^x to D, respectively, at which [5]:

$$P_F = \eta_0[1 - f(\gamma)] \,, \tag{9}$$

$$P_{DD} = \alpha f(\gamma) \,, \tag{10}$$

where

$$f(\gamma) = \sqrt{\pi}\,\gamma \exp(\gamma^2)[1 - erf(\gamma)] \,, \tag{11}$$

$$\alpha = \gamma_D/\gamma \,, \tag{12}$$

$$\gamma = \gamma_D + \gamma_A = \frac{\sqrt{\pi}}{2}\left(\frac{C_D}{C_{0D}} + \frac{C_A}{C_{0A}}\right) , \tag{13}$$

η_0 is absolute PL yield of the donor molecules at $\gamma \to 0$, C_D and C_A as well as C_{OD} and C_{OA} denote concentrations and critical concentrations of the donor and acceptor, respectively. Taking into account relation (10) and condition $P_{DD} < 1$ in Eq. (8) we get:

$$\tau = \tau^{(0)}/[1 - \alpha f(\gamma)] \,. \tag{14}$$

The PL decay time $\tau^{(0)}$ of molecules $D^{(0)}$ depends on the concentrations of molecules D and A in solution. This dependence can be found on the basis of relation (2), because function

$$\sum_{\sigma} N_{\sigma}^{(0)}(t) \equiv N^{(0)}(t)$$

is known. According to FÖRSTER's calculations [11], as well as to other authors' [12—16]:

$$N^{(0)}(t) = N^{(0)}(0) \exp\left[-\frac{t}{\tau_0^{(0)}} - 2\gamma\sqrt{\frac{t}{\tau_0^{(0)}}}\right] . \tag{15}$$

This function takes into account the averaging all the configurations of molecules D and A in the environment of $D^{(0)}$ and represents the number of $D^{(0)}$ molecules after time t from the moment of impulsive excitation.

Using (15) GALANIN [16] obtained:

$$\tau^{(0)} = \frac{\int_0^{\infty} tN^{(0)}(t)\,dt}{\int_0^{\infty} N^{(0)}(t)\,dt} = \tau_0^{(0)} \frac{1 + \gamma^2 - \left(\frac{3}{2} + \gamma^2\right) f(\gamma)}{1 - f(\gamma)} \,, \tag{16}$$

where $\tau_0^{(0)}$ is mean PL decay time of molecules $D^{(0)}$ at $C_D \to 0$ and $C_A \to 0$[2]. Taking into consideration Eq. (16) in (14) and denoting $\tau_0^{(0)}$ by τ_0 we finally obtain:

$$\frac{\tau}{\tau_0} = \frac{1 + \gamma^2 - \left(\frac{3}{2} + \gamma^2\right) f(\gamma)}{[1 - f(\gamma)]\,[1 - \alpha_0 \alpha f(\gamma)]} \,. \tag{17}$$

Eq. (17) describes the changes of mean PL decay time as the function of reduced concentration $\gamma = \gamma_D + \gamma_A$.

In the case of a one-component system the role of the acceptor can be played by the dimers of molecules D. If dimers $D_{||}$ are characterized by a smaller PL quantum yield than molecules D, then the non-radiative energy transfer from D^x to $D_{||}$ leads to concentrational quenching and thus to a drop of quantum yield in the range of high concentrations.

The same effect is also responsible for the drop of τ/τ_0. When, apart friom PL quenching by dimers in solution, also monomer quenching takes place, factor α, which occurred in the expression for PL quantum yield (cf. Eq. (41‴) in [5]), should be replaced by $\alpha_0\alpha$. Here α_0 is the probability that excitation degradetion during its transfer between monomers does not occur.[3] On account of the above mentioned reasons factor α_0 was introduced into Eq. (17). The concentration dependences of PL decay time at several values of dimerization constant[4] K_γ and probability α_0 are presented in Fig. 1. A characteristic feature of the majority of the presented course of τ/τ_0 is a maximum whose value depends remarkably on K_γ and α_0. In the case of a pronounced monomer quenching (curve 4) practically there is no maximum. The noticeable maximum τ/τ_0 predicted by formula (17) in the case of small K_γ and $\alpha_0 = 1$ has not been observed in experiment so far. The measurements of τ/τ_0 versus c in one-component systems exhibited a constancy of τ in the wide range of concentrations and their drop at high c [16, 18—26]. However, no satisfactory theoretical description of such concentration courses like that of τ/τ_0 has been given up to now. Since the formula (16) predicts a drop of τ/τ_0 at comparatively low concentrations (at $\gamma = c/c_0 = 1$, τ/τ_0 amounts to only 0.434; cf. curve 2 in Fig. 3) this drop has been ascertained at $c > c_0 \approx$

[2] In [16] all the non-excited active molecules in solutions are treated as acceptor molecules; $\tau^{(0)}$ and $\tau_0^{(0)}$ correspond to τ_1 and τ_{10} in GALANIN's denotations.

[3] α_0 can also be interpreted as mean value of the probability of the so called non-active transfer [17].

[4] The non-dimensional dimerization constant $K_\gamma = \gamma_D/\gamma_{D_{||}}^2$ is connected with the equilibrium constant $K = C''/C'^2$ by dependence

$$K_\gamma = 2KC_0'^2/\sqrt{\pi}C_0'', \tag{18}$$

where C', γ_D, C_0' and C'', $\gamma_{D_{||}}$, C_0'' denote concentrations, reduced and critical concentrations, respectively.

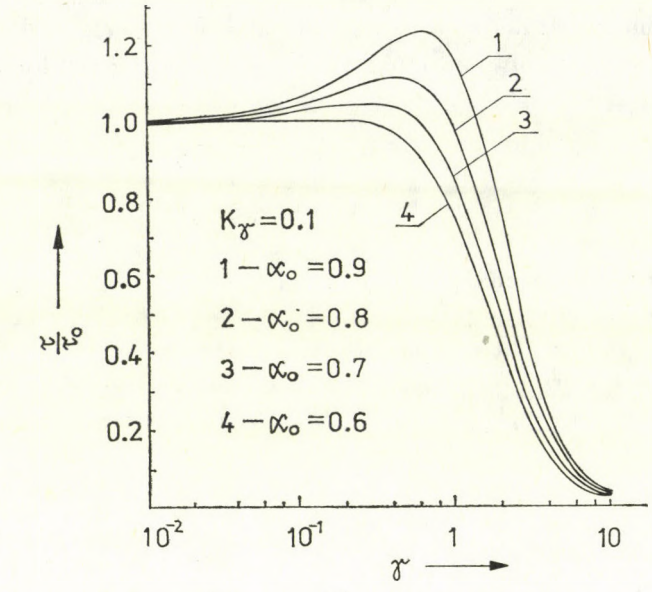

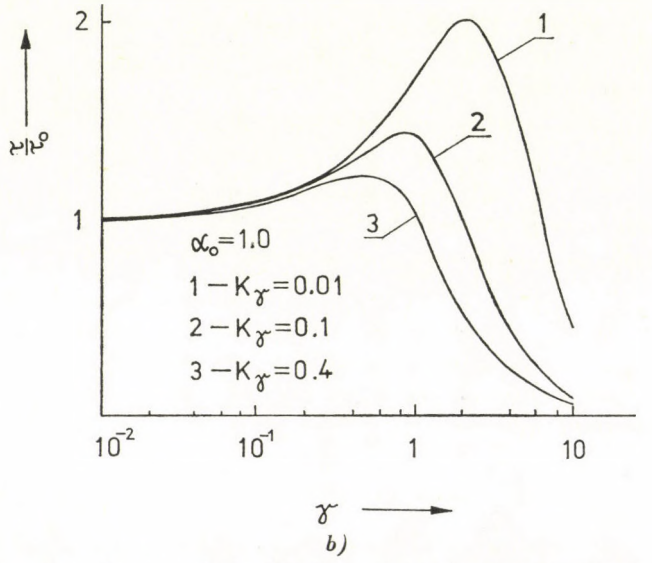

Fig. 1. Concentration changes of the PL-decay time τ/τ_0 versus reduced concentration γ calculated for several values of dimerization constant K_γ on the basis of Eq. (17) taking into account (Fig. 1a) and neglecting (Fig. 1b) monomer quenching

$\approx 10^{-3}$ M/l i.e. at $\gamma > 1$ in the course of the experiments. Below we present the experimental results of τ/τ_0 versus c corrected for reabsorption and secondary fluorescence, their comparison with Eq. (17) and also the discussion of the results.

3. Experiments

Glycerol-alcohol solutions of Na-fluorescein were prepared to test Eq. (17) experimentally. The characteristics of these solutions were given in Table I. The PL decay times were measured on a phase-fluorometer constructed in our laboratory [27]. The samples were excited by wavelength $\lambda = 475$ nm of 50 W halogen lamp. An SPM-2 monochromator was used for the excitation. On the observation side an OG-1 cutoff filter ($\lambda > 530$ nm) was employed. The absorption spectra were measured on a VSU-P spectrophotometer and the fluorescence spectra and quantum yield on the device described earlier [28]. The fluorescence spectra were corrected for the spectral sensitivity of the photomultipier and for reabsorption [29].

In order to obtain the true values of τ it is indispensable to take into account the effect of reabsorption and secondary fluorescence or to use sufficiently thin layers.

According to KETSKEMÉTY et al [30] the secondary effects can be neglected if

$$2.3\varepsilon_{\max} cd < 0.1\,, \tag{19}$$

where $\varepsilon_{\max}$ denotes the maximum value of the absorption coefficient, c is concentration, and d the thickness of the luminophore layer. In our investigation cuvettes of thicknesses smaller than 10 μm already for $c > 5{,}8 \cdot 10^{-4}$ M/l ($\varepsilon_{\max} = 0.75 \cdot 10^5$ l/Mcm) are required to fulfil the condition (19). Since the investigation of concentration changes of τ was intended to be realized over a wide range of concentrations (from 10^{-5} M/l to $5 \cdot 10^{-2}$ M/l) the measurements of τ were carried out in a cuvette of a relatively big thickness ($d = 0.2$ cm), taking into account the influence of secondary effects on the basis of relation [25]:

$$\tau = \tau'(1 - \varkappa)\,, \tag{20}$$

where $\varkappa = I_2/I_1$, I_1 and I_2 denoting the intensities of primary and secondary fluorescences. The concentration dependence of coefficient $\varkappa$ indispensable for obtaining the corrected values of τ, can be found basing on the exact theory of the influence of secondary effects on luminescent properties of solutions, worked out by BUDÓ and KETSKEMÉTY [31].

Values of $\varkappa$ found in this way for the system of Na-fluorescein in glycerol-alcohol solutions were taken from [32].

4. Results and discussion

In Fig. 2 the dependence of PL decay time τ of Na-fluorescein in glycerol-alcohol solution versus concentration is presented. The crosses and empty circles stand for the values of τ uncorrected and corrected for secondary effects,

respectively. It can be seen that the neglect of the reabsorption and secondary fluorescence causes a strong deformation of the course of concentrational changes of PL decay time. It is known that such a deformation appears if there exists a partial overlap of the absorption and emission spectra and the measurements are carried out in thick layers [16, 19]. Let us remark that regarding the secondary effects essentially decreases the values of τ, still the character of the course of $\tau(c)$ remains the same. A characteristic feature of the $\tau(c)$ courses is a maximum at a certain concentration of dye molecules.

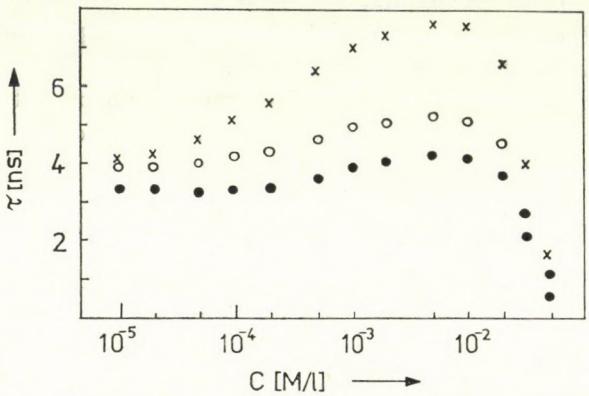

Fig. 2. Dependence of PL decay time τ of Na-fluorescein in glycerol-alcohol solution versus concentration c; x, ○ — experimental points uncorrected and corrected for secondary effects, ● — points corrected on the basis of the values of χ according to [25]

In order to verify the values of τ, marked by empty circles, Fig. 2 also presents the values of τ corrected on the basis of the known concentration changes of coefficient $\varkappa$ calculated for the same system by BUDÓ and SZALAY [25] (full circles). As can be seen in the Figure, the values of τ, corrected in this way, are slightly lower than the previous ones, while the courses of τ/τ_0 are in both cases practically identical. In Fig. 3 the theory is compared with the experimental values of τ (marked in Fig. 2 by empty circles). The solid line shows the theoretical curve calculated on the basis of Eq. (17) for $K_\gamma = 7 \cdot 10^{-4}$ and $\alpha_0 = 0.91$. Value K_γ was found on the basis of (18) from the known dimerization constant K. This latter as well as critical concentrations c_0' and c_0'' were found experimentally, but parameter α_0 was found with the best fitting of the theoretical curve and experimental points. The values of the above mentioned quantities are listed in Table I. In Fig. 3 the dashed line presents the concentration changes of τ based on Eq. (16) given by GALANIN [16]. It can be seen that the drop of the experimental values of τ occurs at much higher concentrations than it is predicated by formula (16). The latter one is right only in the case when two kinds of molecules of donor D and

acceptor A appear in the solution and when condition $C_A \gg C_D$ is fulfilled. In this case the non-radiative energy transfer occurs mainly in one step from D to A. As we proved before [33] the multi-step mechanism of energy transfer from D^* to A, occurring according to the scheme

$$\begin{aligned} &D^* + D + \ldots + D + A \xrightarrow{k_{DD}} D + D^* + \ldots + D + A \longrightarrow \\ &\ldots \xrightarrow{k_{DD}} D + D + \ldots + D^* + A \xrightarrow{k_{DA}} D + D + \ldots + D + A^* \end{aligned} \tag{21}$$

had a pronounced effect on the concentration changes of PL quantum yield. The comparison of curves 1 and 2 in Fig. 3 proves that the influence of this mechanism on the course of the changes of PL decay time is essential as well.

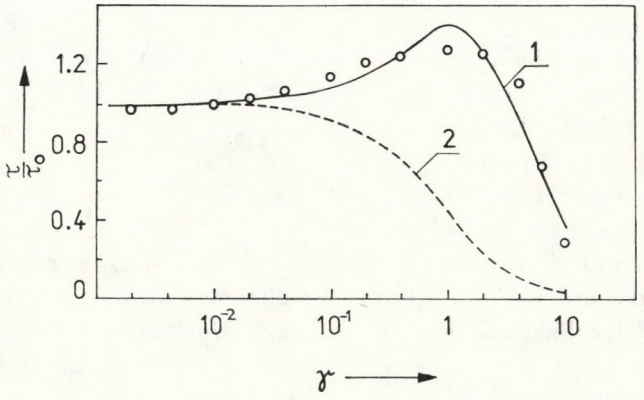

Fig. 3. Comparison of the experimental values of τ of Na-fluorescein in glycerol-alcohol solution versus reduced concentration γ with Eq. (17); o — experimental points corrected for secondary effects; 1 — theoretical curve for $K_\gamma = 7 \cdot 10^{-4}$ and $\alpha_0 = 0.91$; 2 — curve plotted on the basis of Eq. (16) according to [16]

Table I

Values of some parameters characterizing Na-fluorescein in glycerol-alcohol solutions[a]

System	Solution	viscosity (poise)	T[b] / K	C_0'	C_0''	R_0'	R_0''	α_0	K_γ	K	η_0
				10^{-3} M/l		Å			10^{-4}	L/M	
Na-fluorescein	glycerol										
$C_{20}H_{10}O_5Na_2$;	5% Methanol										
MW = 376.29	0.4% H_2O	6.0	293	4.395	3.084	44.1	50.5	0.91	7	0.1	0.8
	0.1% NaOH										

[a] the quoted values of parameters are very close to those of Na-fluorescein in glycerol-water solutions.

[b] measurements of τ were carried out for $T = 300$ K.

As is seen in the Figure, an approximate agreement of the experimental results with Eq. (17) is obtained. This result can be regarded as satisfactory, the more so as all the parameters (except for α_0) indispensable for the comparison of the theory with the experiment were found experimentally. Moreover, it seems to be worth mentioning that Eq. (17) predicts the concentration range correctly, in which the drop of τ/τ_0 is really observed. This fact we consider as the main result of the present paper.

The measured values of τ marked by crosses presented in Fig. 2 exhibit a distinct maximum also characteristic for other systems of partially overlapping absorption and emission spectra in case the measurements are carried out in thick cuvettes. Such a maximum can be explained [19] with the influence of secondary effects leading to a lengthening of τ and with the influence of concentration quenching leading to a shortening of τ.

The explanation of the increase of τ merely on the influence of secondary effects is based on the tacit assumption[5] that the non-radiative excitation energy transfer in an ensemble of molecules of the same kind does not change the value of τ until the processes leading to energy degradation appear in this ensemble.

In the present paper we have accepted that the non-radiative electronic excitation energy transfer causes, on the one hand, the lengthening of τ on account of the independence of the destiny of excitation energy in a molecule of an arbitrary order $D^{(k)}$ on its former history and, on the other hand, the shortening of localization time $\tau^{(k)}$ of excitation energy on molecules $D^{(k)}$ because of the possibility of the transfer of this energy to all the active molecules in the solution treated as acceptors.

The calculations based on this assumption proved that the above mentioned effects causing the change of τ in opposite directions did not compensate each other (cf. curves in Fig. 1). It can be explained by monomer quenching that the calculations predict a relatively large increase of τ/τ_0, especially for small K_γ, whereas in the experiment only a slight increase, constancy in the wide concentration range or a monotonic drop of τ with the concentration is observed.

It was found in the experiments on concentration quenching, concentration depolarization and sensibilized fluorescence that this kind of quenching could not be neglected [8, 34, 35].

It is also possible that the divergence between the experimental and theoretical values of τ/τ_0 (when $\alpha_0=1$) results, to some extent, from the simplification of the calculation of τ/τ_0. The course of concentration changes of PL decay time found experimentally and theoretically in this work suggests that, apart

[5] Unfortunately we have not found any quantitative justification of such an assumption in the literature on this subject.

from the radiative energy transfer, the process of non-radiative energy transfer is also partially responsible for the lengthening of τ. Still the shortening of τ is conditioned by PL concentrational quenching by non-luminescent dimers as well as by monomer quenching mentioned above.

To verify formula (17) fully it is indispensable to carry out further precise measurements on concentration changes of PL decay time in the systems of remarkably differing values of dimerization constant.

This work was supported by the Polish Academy of Sciences under project MR. I. 9. — 4.5.3.

REFERENCES

1. Th. Förster, Fluoreszenz Organischer Verbindungen. Vandenhoeck und Ruprecht, Göttingen 1951.
2. A. Schmillen and R. Legler, Landolt-Börnstein, Zahlenwerte und Funktionen aus Naturwissenschaften und Technik. Neue Serie, Gruppe II, Bd. 3, Lumineszenz organischer Substanzen, Springer-Verlag, Berlin 1967.
3. A. M. Sarzhewskij and A. N. Sevchenko, Anisotropija pogloschenija i ispunskanija sweta molekulami, Minsk, 1971.
4. A. Ore and L. Eriksen, Phys. Norveg, **5**, 57, 1971.
5. C. Bojarski and J. Domsta, Acta Phys. Hung., **30**, 145, 1971.
6. C. Bojarski, J. Luminescence, **5**, 413, 1972.
7. C. Bojarski and J. Dudkiewicz, Z. Naturforsch., **27a**, 1751, 1972.
8. C. Bojarski, A. Bujko, J. Dudkiewicz, J. Kusba and G. Obermueller, Acta Phys. Polon., **A45**, 71, 1974.
9. I. N. Kozlov, V. T. Koyava, N. I. Popetschits, A. M. Sarzhewskij and A. N. Sevchenko, Dokl. Akad. Nauk BSSR, **22**, 119, 1978.
10. Th. Förster, Modern Quantum Chemistry, Istambul Lectures, Vol. 3 Academic Press, New York, p. 93, 1966.
11. Th. Förster, Z. Naturforsch., **4a**, 321, 1949.
12. W. W. Antonow-Romanowskij and M. D. Galanin, Optika i Spektr., **3**, 389, 1957.
13. I. M. Rozman, Optika i Spektr., **4**, 536, 1958.
14. J. A. Kurskij and A. S. Selivanenko, Optika i Spektr., **8**, 340, 1960.
15. K. B. Eisenthal and S. Siegel, J. Chem. Phys. **41**, 652, 1964.
16. M. D. Galanin, Trudy Fiz. Inst. Akad, Nauk USSR, **12**, 3, 1960.
17. I. Ketskeméty, Z. Naturforsch., **17a**, 666, 1962.
18. S. I. Vavilov, J. Physics USSR, **7**, 141, 1943.
19. A. Schmillen, Z. Physik, **135**, 294, 1953.
20. L. Gáti and I. Szalma, Acta Phys. et Chem. Szeged, **13**, 3, 1968.
21. E. R. Dale and R. K. Bauer, Acta Phys. Pol., **A40**, 853, 1971.
22. J. A. Ferreira and G. Porter, Faraday Trans., II, **73**, 341, 1977.
23. K. A. Selanger, J. Falnes and T. Sikkeland, J. Phys. Chem., **81**, 1960, 1977.
24. J. Knof, F. J. Theiss and J. Weber, Z. Naturforsch., **33a**, 98, 1978.
25. A. Budó and L. Szalay, Z. Naturforsch., **18a**, 90, 1963.
26. A. Kawski and J. Kaminski, Z. Naturforsch., **3a**, 15, 1975.
27. J. Tyrzyk, Z. Nauk Politechn. Gdansk. **242**, 111, 1975.
28. C. Bojarski, G. Obermueller and J. Kusba, Z. Nauk. Politechn. Gdansk, **181**, 3, 1971.
29. A. Baczynski and M. Czajkowski, Bull. Acad. Polon., III, 8, 691, 1960.
30. I. Ketskeméty, J. Dombi, R. Horvai and L. Kozma, Acta Phys. et Chem., Szeged, **7**, 17, 1961.
31. A. Budó and I. Ketskeméty, Acta Phys. Hung., **7**, 207, 1957; **14**, 167, 1962.
32. J. Dudkiewicz, in preparation.
33. C. Bojarski, J. Kusba and G. Obermueller, Acta Phys. Polon. **A48**, 85, 1975.
34. I. Ketskeméty and J. Kusba, Acta Phys. et Chem., Szeged, **20**, 239, 1974.
35. C. Bojarski and G. Obermueller, Acta Phys. Polon., **A50**, 389, 1976.

RECENSIONES

L. VÁLYI: Atom and Ion Sources

Akadémiai Kiadó, Budapest, 1977

Atom and ion sources have been playing a fundamental role in experiments ever since the very beginning of nuclear sciences. These days they are more and more extensively used in various fields of science and technology, thereby creating the need for an up-to-date compilation which surveys the different types of particle sources. The aim of the present monograph — as is pointed out in the author's preface — is to provide specialists not only with a textbook on the physical processes taking place in atom and ion sources but also with a manual on the available types; this enables the most appropriate source to be selected for a given task.

The first Chapter of the book deals with elementary physical processes (excitation, ionization, recombination, charge transfer, etc.) a knowledge of which is important in understanding the working principles of particle sources. Not only the relevant theoretical background but also numerous experimental results are given in this part. Gaseous and thermal sources for the production of neutral particle beams are discussed in the next Chapter where high intensity and high energy sources, suitable for special physical, chemical and technological processes, are also described. In the third Chapter the reader is able to acquaint himself thoroughly with the large variety of conventional ion sources applied in mass spectroscopy, in low and high energy accelerators, in isotope separators, etc., beginning with the many different types of discharge sources and ending with those ionizing atoms of solid materials. It is mainly in nuclear and particle physics that use is made of the special ion sources, such as those of negative and multiple ionized beams, described in Chapter IV. This Chapter also deals with the technique of producing pulsed and polarized beams. The last part of the book (Chapters V and VI) is devoted to the treatment of some important characteristics of ion beams and to methods of their measurement. Tables of physical quantities and a reference list containing almost 1500 items complete the book.

The obvious intention of the author was to provide as comprehensive coverage as possible. This is already obvious in the introductory part and the same effect is reflected throughout the whole book by the presentation of a large number of actual devices with numerous illustrations showing technical details. There are only a few results in the given topic which are not mentioned or at least referred to. The presentation of the devices and their illustration is useful not only to researchers who wish to choose an adequate particle source for their work but also to those designing and constructing new devices as they are able to find many versions of construction and a great number of data on working parameters. The volume presents the theoretical and the practical aspects in a good proportion demonstrating that the author has his own experience in the use as well as in the development of different kinds of particle sources.

The effort to present the material in a comprehensive form has, besides the above mentioned advantages, its own drawbacks, the principal one being that it is difficult to distinguish between well proved devices and those which are important solely from an historical point of view. A critical evaluation of the many different types of atom and ion sources presented in the monograph would be very helpful to the reader and the need for this is substantiated by the fact that the majority of the references are more than 10 years old. The style of the book, especially when describing devices, is clear and concise enough. Unfortunately the general, physical treatments contain some obscure parts which are not easy to follow and one has the feeling that this may be largely due to the translation.

J. ERŐ

Electroluminescence

[Edited by J. I. Pankove. Springer-Verlag, Berlin, Heidelberg, New York, 1977
127 figures, 16 tables, XI + 212 pages

Electroluminescence has been known for more than half a century, its utilization has become practical only within the last years. The major attributes of electroluminescent devices are compactness, ruggedness, and long operational life. But much progress remains to be achieved with respect to efficiency, cost, for large-area displays, etc.

The contributors to this book were selected for their long and continuing expertise in the study of luminescence in selected compounds. They are:

J. I. PANKOVE: Introduction
Y. M. TAIROV and Y. A. VODAKOV: Group IV. Materials (Mainly SiC).
P. J. DEAN: III—V. Compound Semiconductors
Y. S. PARK and B. K. SHIN: Recent Advances in Injection Luminescence in II—XI. Compounds.
S. WAGNER: Chalcopyrites
T. INOGUCHI and S. MITO: Phosphore Films

The book serves two purposes: 1. to educate newcomers to this exciting area of physics and technology; 2. to provide specialists with useful references and new insights in adjoining areas of luminescence.

Since the boundaries of present knowledge have been outlined by each author, this volume of the Topics in Applied Physics should serve as a first stepping stone for future progress.

Z. BODÓ

Amorphous Semiconductors '76

Proceedings of the International Conference,
Balatonfüred, Hungary, 20—25 September 1976
Edited by I. Kósa Somogyi, Akadémiai Kiadó, Budapest, 1977, 554 pages,
Author and Subject Index

The high activity in the field of amorphous semiconductors is also demonstrated by the conferences organized periodically. This Conference "Amorphous Semiconductors 76" was the third in the series of regional conferences on this topic. The previous conferences were held in Sofia (1972) and Reinhardsbrunn, GRD (1974).

This Conference like the preceding ones covered all aspects of amorphous semiconductor research and application. Beside chalcogenide bulk glassy semiconductors, the problems of thin films were discussed from different angles.

The contributions represented also the tendency to get more quantitative information on the structure of the different materials as well as to establish correlations between structural and physical properties. The effect of additives and impurities on the physical properties was discussed in numerous papers. Switching, structural transformations and photostimulated processes as well as devices were also included in the program. Several sessions were dedicated to the theory as well as to optical and electrical properties.

Practically, all laboratories in Central Europe carrying out research work on amorphous semiconductors or dealing with the development of devices were represented by prominent experts, authors of the 90 papers collected in the Conference Proceedings.

The papers are grouped under the following headings: Switching, Devices, Theory, Effect of Doping and Impurities, Optical Properties, Electrical Properties, Structural Transformations, Structure and Characterization of Materials.

P. B. BARNA

HERMANN HAKEN:

Synergetics — An Introduction

(Second Enlarged Edition), Springer-Verlag, Berlin, Heidelberg, New York, 1978
(pp. XI + 355 with 152 Figures)

Synergetics is a new field of interdisciplinary research which deals with nonequilibrium phase transitions and self-organization in physics, chemistry, biology and other fields. It investigates the spontaneous formation of many subsystems and phenomena, etc. (See further details in the review on the first edition: Acta Phys. Hung., *43*, 352, 1977.)

The publication of this second edition was motivated, first of all, by the fact that the first edition had been sold out in less than one year. Of course, the author has used this opportunity to include some of the most interesting recent developments. For example, he has added a whole new chapter on the fascinating and rapidly growing field of irregular motion caused by deterministic forces. This kind of phenomenon is presently found in diverse fields ranging from physics to biology. Furthermore he has included a new section on the analytical treatment of a morphogenetic model using the order parameter concept first developed in this edition. Needless to say that the few minor misprints and errors of the first edition have also been eliminated.

This edition, similarly to the first one, is also beautifully presented by the famous Springer-Verlag. The book can be recommended to physicists, chemists, biologists, etc. and is really indispensable to university libraries, especially libraries of research centres of physics, chemistry and biology.

I. GYARMATI

The Ta-You Wu Festschrift
Science of Matter

Edited in Honor of Professor Ta-You Wu by Shigeji Fuyita
Gordon and Breach Science Publishers, New York, Paris, London, 1978

This volume is a collection of papers covering a wide range of subjects, edited and published to pay tribute to Professor TA-YOU WU on the occasion of his seventieth birthday. An outstanding scientist himself in the field of atomic and molecular physics and several other fields and an enthusiastic teacher, Professor WU became associated with a number of distinguished scientists (mostly his former students and colleagues) during his 50-year research and teaching career, who joined in celebrating the anniversary by contributing some up-to-date review papers and also some original reports. Naturally, the papers submitted are heterogeneous in nature, reflecting the variety of interests of their contributors.

The fields covered by the papers are: Philosophy, Particles and Fields, Phase Transition, Statistical and Plasma Physics, Solid State Physics, Molecular Physics, Mathematics and Applied Mathematics, Astronomy, Biophysics.

E. FEHÉR

English—Russian Physics Dictionary

Editor: D. M. Tolstoi, USSR, Pergamon Press, Oxford, New York, Toronto, Sydney, Paris, Frankfurt, 1978. 848 pages, $ 50.00, £ 25.00

The volume is a comprehensive work of reference containing the Russian equivalents of some 60.000 terms from all basic areas of modern physics including general, theoretical and applied mechanics; molecular physics; statistical physics; thermodynamics and thermophysics, geophysics and physics of the atmosphere; astrophysics; solid-state physics; macroscopic electrodynamics; atomic and nuclear physics; optics; theory of relativity; quantum mechanics; high energy physics; physical chemistry and computer science.

By this publication Pergamon Press has met a long-felt demand for a reliable and really up-to-date English—Russian physics dictionary, which can be recommended for use to scientists, engineers, teachers and students at senior level in physics and related fields. The dictionary provides an especially valuable tool for translators, editors of technical journals and librarians.

The dictionary is neatly printed and easy to handle. One minor critical remark: headwords introducing longer entries are rather hard to look up; these should have been set in a different type or positioned more to the left of the column of the text.

E. FEHÉR

Printed in Hungary

A kiadásért felel az Akadémiai Kiadó igazgatója Műszaki szerkesztő: Botyánszky Pál

A kézirat a kiadóba érkezett: 1979. III. 26. — A kézirat nyomdába érkezett: 1979. III. 30. — Terjedelem: 6,5 (A/5) 30 ábra

79.7019 Akadémiai Nyomda, Budapest — Felelős vezető: Bernát György

NOTES TO CONTRIBUTORS

I. PAPERS will be considered for publication in Acta Physica Hungarica, only if they have not previously been published or submitted for publication elsewhere. They may be written in English, French, German or Russian.

Papers should be submitted to

Prof. I. Kovács, Editor
Department of Atomic Physics, Technical University
1521 Budapest, Budafoki út 8, Hungary

Papers may be either articles with abstracts or short communications. Both should be as concise as possible, articles in general not exceeding 25 typed pages, short communications 8 typed pages.

II. MANUSCRIPTS

1. Papers should be submitted in five copies.

2. The text of papers must be of high stylistic standard, requiring minor corrections only.

3. Manuscripts should be typed in double spacing on good quality paper, with generous margins.

4. The name of the author(s) and of the institutes where the work was carried out should appear on the first page of the manuscript.

5. Particular care should be taken with mathematical expressions. The following should be clearly distinguished, e.g. by underlining in different colours: special founts (italics, script, bold type, Greek, Gothic, etc.); capital and small letters; subscripts and superscripts' e.g. x^2, x_3; small l and 1; zero and capital O; in expressions written by hand: e and l, n and u, v and v, etc.

6. References should be numbered serially and listed at the end of the paper in the following form: J. Ise and W. D. Fretter, Phys. Rev., *76*, 933, 1949.

For books, please give the initials and family name of the author(s), title, name of publisher, place and year of publication, e.g.: J. C. Slater, Quantum Theory of Atomic Structures, I. McGraw-Hill Book Company, Inc., New York, 1960.

References should be given in the text in the following forms: Heisenberg [5] or [5].

7. Captions to illustrations should be listed on a separate sheet, not inserted in the text.

III. ILLUSTRATIONS AND TABLES

1. Each paper should be accompanied by five sets of illustrations, one of which must be ready for the blockmaker. The other sets attached to the copies of the manuscript may be rough drawings in pencil or photocopies.

2. Illustrations must not be inserted in the text.

3. All illustrations should be identified in blue pencil by the author's name, abbreviated title of the paper and figure number.

4. Tables should be typed on separate pages and have captions describing their content. Clear wording of column heads is advisable. Tables should be numbered in Roman numerals. (I, II, III, etc.).

IV. MANUSCRIPTS not in conformity with the above Notes will immediately be returned to authors for revision. The date of receipt to be shown on the paper will in such cases be that of the receipt of the revised manuscript.

Reviews of the Hungarian Academy of Sciences are obtainable at the following addresses:

AUSTRALIA
C.B.D. LIBRARY AND SUBSCRIPTION SERVICE, Box 4886, G.P.O., *Sydney N.S.W. 2001*
COSMOS BOOKSHOP. 145 Acland Street, *St. Kilda (Melbourne), Victoria 3182*

AUSTRIA
GLOBUS, Höchstädtplatz 3, *1200 Wien XX*

BELGIUM
OFFICE INTERNATIONAL DE LIBRAIRIE, 30 Avenue Marnix, *1050 Bruxelles*
LIBRAIRIE DU MONDE ENTIER, 162 Rue du Midi, *1000 Bruxelles*

BULGARIA
HEMUS, Bulvar Ruszki 6, *Sofia*

CANADA
PANNONIA BOOKS, P.O. Box 1017, Postal Station "B", *Toronto, Ontario M5T 2T8*

CHINA
CNPICOR, Periodical Department, P.O. Box 50, *Peking*

CZECHOSLOVAKIA
MAD'ARSKÁ KULTURA, Národní třida 22, *115 66 Praha*
PNS DOVOZ TISKU, Vinohradská 46, *Praha 2*
PNS DOVOZ TLAČE, *Bratislava 2*

DENMARK
EJNAR MUNKSGAARD, Norregade 6, *1165 Copenhagen*

FINLAND
AKATEEMINEN KIRJAKAUPPA, P.O. Box 128, *SF-00101 Helsinki 10*

FRANCE
EUROPERIODIQUES S. A., 31 Avenue de Versailles, *78170 La Celle St.-Cloud*
LIBRAIRIE LAVOISIER, 11 rue Lavoisier, *75008 Paris*
OFFICE INTERNATIONAL DE DOCUMENTATION ET LIBRAIRIE, 48 rue Gay-Lussac, *75240 Paris Cedex 05*

GERMAN DEMOCRATIC REPUBLIC
HAUS DER UNGARISCHEN KULTUR, Karl-Liebknecht-Strasse 9, *DDR-102 Berlin*
DEUTSCHE POST ZEITUNGSVERTRIEBSAMT, Strasse der Pariser Kommüne 3—4, *DDR-104 Berlin*

GERMAN FEDERAL REPUBLIC
KUNST UND WISSEN ERICH BIEBER, Postfach 46, *7000 Stuttgart 1*

GREAT BRITAIN
BLACKWELL'S PERIODICALS DIVISION, Hythe Bridge Street, *Oxford OX1 2ET*
BUMPUS, HALDANE AND MAXWELL LTD., Cowper Works, *Olney*, Bucks *MK46 4BN*
COLLET'S HOLDINGS LTD., Denington Estate, *Wellingborough*, Northants *NN8 2QT*
W.M. DAWSON AND SONS LTD., Cannon House *Folkestone, Kent CT19 5EE*
H. K. LEWIS AND CO., 136 Gower Street, *London WC1E 6BS*

GREECE
KOSTARAKIS BROTHERS, International Booksellers, 2 Hippokratous Street, *Athens-143*

HOLLAND
MEULENHOFF-BRUNA B.V., Beulingstraat 2, *Amsterdam*
MARTINUS NIJHOFF B.V., Lange Voorhout 9—11, *Den Haag*
SWETS SUBSCRIPTION SERVICE, 347b Heereweg, *Lisse*

INDIA
ALLIED PUBLISHING PRIVATE LTD., 13/14 Asaf Ali Road, *New Delhi 110001*
150 B-6 Mount Road, *Madras 600002*
INTERNATIONAL BOOK HOUSE PVT. LTD., Madame Cama Road, *Bombay 400039*
THE STATE TRADING CORPORATION OF INDIA LTS. Books Import Division, Chandralok, 36 Janpath, *New Delhi 110001*

ITALY
EUGENIO CARLUCCI, P.O. Box 252, *70100 Bari*
INTERSCIENTIA, Via Mazzé 28, *10149 Torino*
LIBRERIA COMMISSIONARIA SANSONI, Via Lamarmora 45, *50121 Firenze*
SANTO VANASIA, Via M. Macchi 58, *20124 Milano*
D. E. A., Via Lima 28, *00198 Roma*

JAPAN
KINOKUNIYA BOOK-STORE CO. LTD., 17-7 Shinjuku-ku 3 chome, Shinjuku-ku, *Tokyo 160-91*
MARUZEN COMPANY LTD., Book Department, P.O. Box 5050 Tokyo International, *Tokyo 100-31*
NAUKA LTD. IMPORT DEPARTMENT, 2-30-19 Minami Ikebukuro, Toshima-ku, *Tokyo 171*

KOREA
CHULPANMUL, *Phenjan*

NORWAY
TANUM-CAMMERMEYER, Karl Johansgatan 41—43, *1000 Oslo*

POLAND
WĘGIERSKI INSTYTUT KULTURY, Marszałkowska 80, *Warszawa*
CKP I W ul. Towarowa 28 *00-958 Warsaw*

ROUMANIA
D. E. P., *Bucureşti*
ROMLIBRI, Str. Biserica Amzei 7, *Bucureşti*

SOVIET UNION
SOJUZPETCHATJ — IMPORT, *Moscow*
and the post offices in each town
MEZHDUNARODNAYA KNIGA, *Moscow G-200*

SPAIN
DIAZ DE SANTOS, Lagasca 95, *Madrid 6*

SWEDEN
ALMQVIST AND WIKSELL, Gamla Brogatan 26, *101 20 Stockholm*
GUMPERTS UNIVERSITETSBOKHANDEL AB, Box 346, *401 25 Göteborg 1*

SWITZERLAND
KARGER LIBRI AG, Petersgraben 31, *4011 Basel*

USA
EBSCO SUBSCRIPTION SERVICES, P.O. Box 1943, *Birmingham, Alabama 35201*
F. W. FAXON COMPANY, INC., 15 Southwest Park, *Westwood, Mass. 02090*
THE MOORE-COTTRELL SUBSCRIPTION AGENCIES, *North Cohocton, N. Y. 14868*
READ-MORE PUBLICATIONS, INC., 140 Cedar Street, *New York, N. Y. 10006*
STECHERT-MACMILLAN, INC., 7250 Westfield Avenue, *Pennsauken* N. J. 08110

VIETNAM
YXUNHASABA, 32, Hai Ba Trung, *Hanoi*

YUGOSLAVIA
JUGOSLAVENSKA KNJIGA, Terazije 27, *Beograd*
FORUM, Vojvode Mišiča 1, *21000 Novi Sad*

Index: 26.022
Acta Phys. Hung. Tom. 46. No. 2. Budapest, 20. IX. 1979 HU-ISSN 0001-6705

ACTA PHYSICA

ACADEMIAE SCIENTIARUM HUNGARICAE

TOMUS XLVI FASCICULUS 3

AKADÉMIAI KIADÓ, BUDAPEST
1979

ACTA PHYS. HUNG. APAHAQ 46 (3) 129—216 (1979)

ACTA PHYSICA

ACADEMIAE SCIENTIARUM HUNGARICAE

SZERKESZTI

KOVÁCS ISTVÁN

Az *Acta Physica* angol, német, francia vagy orosz nyelven közöl értekezéseket. Évente két kötetben, kötetenként 4—4 füzetben jelenik meg. Kéziratok a szerkesztőség címére (1521 Budapest XI., Budafoki út 8.) küldendők.

Megrendelhető a belföld számára az Akadémiai Kiadónál (1363 Budapest Pf. 24. Bankszámla 215-11488), a külföld számára pedig a „Kultura" Külkereskedelmi Vállalatnál (1389 Budapest 62, P.O.B. 149. Bankszámla 217-10990), vagy annak külföldi képviseleteinél.

The *Acta Physica* publish papers on physics in English, German, French or Russian, in issues making up two volumes per year. Subscription: $ 36.00 per volume. Distributor: "Kultura" Foreign Trading Company (1389 Budapest 62, P.O. Box 149) or its representatives abroad.

Die *Acta Physica* veröffentlichen Abhandlungen aus dem Bereich der Physik in deutscher, englischer, französischer oder russischer Sprache, in Heften, die jährlich zwei Bände bilden.

Abonnementspreis pro Band: $ 36.00. Bestellbar bei »Kultura« Außenhandelsunternehmen (1389 Budapest 62, Postfach 149) oder seinen Auslandsvertretungen.

Les *Acta Physica* publient des travaux du domaine de la physique en français, anglais, allemand ou russe, en fascicules qui forment deux volumes par an.

Prix de l'abonnement: $ 36.00 par volume. On peut s'abonner à l'Entreprise du Commerce Extérieur «Kultura» (1389 Budapest 62, P.O.B. 149) ou chez représentants à l'étranger.

«*Acta Physica*» публикуют трактаты из области физических наук на русском, немецком, английском и французском языках.

«*Acta Physica*» выходят отдельными выпусками, составляющими два тома в год.

Подписная цена — $ 36.00 за том. Заказы принимает предприятие по внешней торговле «Kultura» (1389 Budapest 62, P.O.B. 149) или его заграничные представительства.

ACTA PHYSICA

ACADEMIAE SCIENTIARUM HUNGARICAE

TOMUS XLVI FASCICULUS 3

AKADÉMIAI KIADÓ, BUDAPEST
1979

ACTA PHYS. HUNG.

INDEX

Acta Physica Academiae Scientiarum Hungaricae, Tomus 46 (3), pp. 129—136 (1979)

FREE CONVECTION EFFECTS ON THE FLOW PAST A VERTICAL POROUS PLATE SET IMPULSIVELY INTO MOTION WITH NEGLIGIBLE DISSIPATION

By

A. R. BESTMAN

DEPARTMENT OF MATHEMATICS, COLLEGE OF SCIENCE AND TECHNOLOGY, PORT HARCOURT, NIGERIA

(Received in revised form 17. I. 1979)

The flow induced by the impulsive motion of a vertical porous plate is analysed under the following assumptions: (i) that the flow is incompressible, (ii) that the suction normal to the plate is constant, (iii) that the temperature difference between the plate and the free-stream, $T_w - T_\infty$, is large enough for free convection currents to flow, and (iv) that the flow is slow enough for dissipation to be neglected. By employing the Laplace transform techniques solutions for the linear coupled differential equations are obtained in a closed form. It is observed that the temperature distribution (and hence the heat transfer at the wall) is unaffected by the free convection currents. Only the velocity and the shear stress vary with free convection currents.

1. Introduction

MENOLD and YANG [1] presented an analytical solution of an unsteady, incompressible laminar free convection flow past at infinite vertical flat plate. A review of much of the previous work is presented in this paper. POP and SOUNDALGEKAR [2] have extended this study to the case of compressible free convection flow.

In all quoted authors, the flat plate is assumed to be impermeable and the effects of forced convection are absent. It is now a well-known fact in areodynamics that suction has a stabilizing effect on boundary layer growth. Also from the technological point of view forced convections are prevalent. The object of this note is therefore to study the combined effect of free and forced convection flow of an incompressible Newtonian fluid past a vertical porous wall. The model used is a vertical porous flat plate which is set impulsively into motion with a step change in surface temperature. In Section 2 the governing equations are derived and in Section 3 the solutions are deduced by employing the Laplace transform techniques. The solutions obtained are discussed in Section 4.

2. Formulation of the problem

The physical problem consists of a vertical infinite porous flat plate, stationary at time $t' < 0$, and in contact and at the same temperature T_∞ with the fluid occupying the semi-infinite space $y' \geqslant 0$. Here a Cartesian coordinate system is employed with y' perpendicular to the plate. At time $t' \geqslant 0$ the plate is simultaneously raised to a constant temperature T_w and moved in its own plane with velocity U_0 while fluid is sucked with constant velocity V_0 normal to it. It is assumed that the difference between the temperatures of the plate and the freestream is moderately large for free convection currents to flow. If (u', v') are the velocity components, then under these assumptions the continuity equation reduces to

$$v' = -V_0$$

and employing this the momentum and energy equations become

$$\varrho'\left(\frac{\partial u'}{\partial t'} - V_0\frac{\partial u'}{\partial y'}\right) = -\frac{\partial p'}{\partial x'} + \mu\frac{\partial^2 u'}{\partial y'^2} - \varrho' g\,,$$

$$0 = -\frac{\partial p'}{\partial y'}\,, \qquad \text{(1a, b, c)}$$

$$\varrho' C_p\left(\frac{\partial}{\partial t'} - V_0\frac{\partial}{\partial y'}\right)(T' - T_\infty) = k\frac{\partial^2}{\partial y'^2}(T' - T_\infty) + \mu\left(\frac{\partial u'}{\partial y'}\right)^2,$$

where the dashes are dimensional variables and all the physical quantities have their usual meaning. The boundary conditions are

$$\left.\begin{aligned} u'|_{y'=0} &= U_0\,, \quad T'|_{y'=0} = T_w\,, \\ u'|_{y'\to\infty} &= 0\,, \quad T'|_{y'\to\infty} = T_\infty\,, \end{aligned}\right\} t' > 0 \qquad \text{(2a)}$$

$$u' = 0\,, \quad T' = T_\infty\,. \qquad t' \leq 0 \qquad \text{(2b)}$$

Equations (1a, b) and (2a) can be combined to give

$$\varrho'\left(\frac{\partial u'}{\partial t'} - V_0\frac{\partial u'}{\partial y'}\right) = \mu\frac{\partial^2 u'}{\partial y'^2} + (\varrho_\infty - \varrho')g\,. \qquad (3)$$

Under the Boussinesq approximations, fluid properties are assumed constant except in the buoyancy term where the density varies according to the law

$$\varrho_\infty - \varrho' = \varrho_\infty\beta(T' - T_\infty)\,. \qquad (4)$$

By virtue of (4), the approximate forms of (1c) and (3) are

$$\varrho_\infty \left(\frac{\partial u'}{\partial t'} - V_0 \frac{\partial u'}{\partial y'}\right) = \mu \frac{\partial^2 u'}{\partial y'^2} + \varrho_\infty g\beta(T' - T_\infty),$$

$$\varrho_\infty C_p \left(\frac{\partial}{\partial t'} - V_0 \frac{\partial}{\partial y'}\right)(T' - T_\infty) = k \frac{\partial^2}{\partial y'^2}(T' - T_\infty) + \mu \left(\frac{\partial u'}{\partial y'}\right)^2. \quad (5)$$

To facilitate analysis it is expedient to introduce the non-dimensional variables

$$y = \frac{y' V_0}{r}, \quad u = u' / V_0, \quad t = \frac{t' V_0^2}{4\nu}, \quad \theta = \frac{T' - T_\infty}{T_w - T_\infty},$$

$$\sigma = \frac{\mu C_p}{k}, \quad G = \frac{\nu g\beta(T_w - T_\infty)}{U_0 V_0^2}, \quad E = \frac{U_0^2}{C_p(T_w - T_\infty)}. \quad (6)$$

Here G is the free convection parameter or the Grashof number, ν the Prandtl number and E the Eckert number. Substituting (6) in (2) and (5) we get

$$\frac{1}{4}\frac{\partial u}{\partial t} - \frac{\partial u}{\partial y} = \frac{\partial^2 u}{\partial y^2} + G\theta,$$

$$\sigma\left(\frac{1}{4}\frac{\partial \theta}{\partial t} - \frac{\partial \theta}{\partial y}\right) = \frac{\partial^2 \theta}{\partial y^2} + \sigma E\left(\frac{\partial u}{\partial y}\right)^2, \quad (7a, b)$$

and

$$\left.\begin{aligned} u|_{y=0} &= \theta|_{y=0} = 1, \\ u|_{y\to\infty} &= \theta|_{y\to\infty} = 0, \end{aligned}\right\} \; t > 0 \quad (8)$$

$$u = 0, \quad \theta = 0 \qquad t \leq 0. \quad (9)$$

The problem is now reduced to mathematical terms. It is required to solve (7) subject to boundary and initial conditions (8) and (9). But this problem is coupled and nonlinear and is not amenable to analytical treatment. However, when the flow velocities induced are small, the dissipation term in (7b) is also negligibly small. The analysis in this note will be restricted to this state of affairs.

3. Solution for negligible dissipation

When $E \doteqdot 0$ in (7b), let us define the Laplace transform and its inverse as

$$\bar{f}(y, s) = \int_0^\infty e^{-st} f(y, t)\, dt,$$

$$^* L^{-1}\bar{f}(y, s) = f(y, t) = \frac{1}{2\pi i}\int_{\gamma - i\infty}^{\gamma + i\infty} e^{st}\bar{f}(y, s)\, ds = \frac{1}{2\pi i}\int_{\mathrm{Br}_1} e^{st}\bar{f}(y, s)\, ds.$$

* Br_1 and Br_3 represent Bromwich contour of the first and third kinds.

Then the equations satisfied by $\bar{u}$ and $\bar{\theta}$ are

$$\frac{1}{4}s\bar{u} - \frac{d\bar{u}}{dy} = \frac{d^2\bar{u}}{dy^2} + G\bar{\theta},$$

$$\sigma\left(\frac{1}{4}s\bar{\theta} - \frac{d\bar{\theta}}{dy}\right) = \frac{d^2\bar{\theta}}{dy^2},$$

$$\bar{u}\,|_{y=0} = \bar{\theta}\,|_{y=0} = \frac{1}{s},$$

$$\bar{u}_{y\to\infty}\,| = \bar{\theta}_{y\to\infty} = 0.$$

The solutions of these are

$$\bar{\theta} = \frac{1}{s}e^{-my}, \tag{10}$$

$$\bar{u} = \left[\frac{1}{s} + \frac{Gy}{s(s+1)^{1/2}}\right]e^{-ny}; \quad \sigma = 1, \tag{11}$$

and

$$\left.\begin{aligned}\bar{u} &= \frac{1}{s}e^{-ny} + \frac{4G}{\sigma-1}\left[\frac{e^{-ny} - e^{-my}}{s\{2\sigma + s + 2(\sigma^2+\sigma s)^{1/2}\}}\right],\\ &= \frac{1}{s}e^{-ny} + \frac{4G}{\sigma-1}\left[\frac{e^{-ny} - e^{-my}}{s\{(\sigma+s)^{1/2} + \sigma^{1/2}\}^2}\right],\end{aligned}\right\} \tag{12}$$

where

$$n = \frac{1}{2}[\sigma + (\sigma^2+\sigma s)^{1/2}], \quad n = \frac{1}{2}[1 + (1+s)^{1/2}].$$

To obtain the inverse Laplace transforms, we will require the following integrals

$$\frac{1}{2\pi i}\int_{\mathrm{Br}_1}\frac{\exp\{zt - b(z+a^2)^{1/2}\}}{z}dz =$$

$$= \frac{1}{2}\{e^{ab}\operatorname{erfc}[(b+2at)/2t^{1/2}] + e^{-ab}\operatorname{erfc}[(b-2at)/2t^{1/2}]\}, \tag{13}$$

and

$$\frac{1}{2\pi i}\int_{\mathrm{Br}_2}\frac{\exp(\xi^2 t - a\xi)}{\xi \pm b}d\xi = \frac{1}{2}\exp(b^2t \pm ab)\operatorname{erfc}[(a \pm 2bt)/2t^{1/2}], \tag{14}$$

which are given in McLachlan [3]. By a straightforward application of (13), (10) can be inverted as

$$\theta = \frac{1}{2}\exp\left[\sigma^{1/2}\left(\frac{1}{2}y + 2t\right)\Big/2t^{1/2}\right] + \frac{1}{2}e^{-\sigma y}\operatorname{erfc}\left[\sigma^{1/2}\left(\frac{1}{2}y - 2t\right)\Big/2t^{1/2}\right]. \tag{15}$$

To invert (11) it is necessary to consider the second term only. The first term can be obtained from (15) by putting $\sigma = 1$. Thus

$$L^{-1}\left\{\frac{e^{-ny}}{s(s+1)^{1/2}}\right\} = e^{-\frac{1}{2}y}\cdot\frac{1}{2\pi i}\int_{\mathrm{Br}_1}\frac{\exp\left\{st-\frac{1}{2}y(s+1)^{1/2}\right\}}{s(s+1)^{1/2}}\,ds\,,$$

$$= e^{-\frac{1}{2}y-t}\cdot\frac{1}{\pi i}\int_{\mathrm{Br}_2}\frac{\exp\left(\xi^2 t-\frac{1}{2}\xi y\right)}{\xi^2-1}\,d\xi\,,$$

where the second equation is obtained by putting

$$(s+1)^{1/2} = \xi\,.$$

Therefore

$$L^{-1}\left\{\frac{e^{-ny}}{s(s+1)^{1/2}}\right\} = e^{-\frac{1}{2}y-t}\cdot\frac{1}{2\pi i}\int_{\mathrm{Br}_2}\left(\frac{1}{\xi-1}-\frac{1}{\xi+1}\right)\exp\left(\xi^2 t-\frac{1}{2}\xi y\right)d\xi\,,$$

and the integrals can now be evaluated in virtue of (14). We get

$$u = \frac{1}{2}\left\{\operatorname{erfc}\left[\left(\frac{1}{2}y+2t\right)\Big/2t^{1/2}\right]+e^{-y}\operatorname{erfc}\left[\left(\frac{1}{2}y-2t\right)\Big/2t^{1/2}\right]\right\}+$$
$$+\frac{1}{2}Gy\left\{e^{-y}\operatorname{erfc}\left[\left(\frac{1}{2}y-2t\right)\Big/2t^{1/2}\right]-\operatorname{erfc}\left[\left(\frac{1}{2}y+2t\right)\Big/2t^{1/2}\right]\right\};\quad \sigma = 1\,. \tag{16}$$

Finally to invert (12), we first consider

$$L^{-1}\left[\frac{e^{-my}}{s\{(\sigma+s)^{1/2}+\sigma^{1/2}\}^2}\right] = e^{-\frac{1}{2}\sigma y}\cdot\frac{1}{2\pi i}\int_{\mathrm{Br}_1}\frac{\exp\left\{st-\frac{1}{2}\sigma^{1/2}y(s+\sigma)^{1/2}\right\}}{s\{(s+\sigma)^{1/2}+\sigma^{1/2}\}^2}\,ds\,.$$

Putting $(s+\sigma)^{1/2} = \xi$ in this we obtain

$$L^{-1}\left[\frac{e^{-my}}{s\{(\sigma+s)^{1/2}+\sigma^{1/2}\}^2}\right] = e^{-\frac{1}{2}\sigma y-\sigma t}\cdot\frac{1}{\pi i}\int_{\mathrm{Br}_2}\frac{\exp\left\{\xi^2 t-\frac{1}{2}\sigma^{1/2}y\xi\right\}}{(\xi^2-\sigma)(\xi+\sigma^{1/2})^2}$$
$$= e^{-\frac{1}{2}\sigma y-\sigma t}\cdot\frac{1}{2\pi i}\int_{\mathrm{Br}_2}\left[\frac{1}{4\sigma(\xi-\sigma^{1/2})}-\frac{1}{4\sigma(\xi+\sigma^{1/2})}-\right.$$
$$\left.-\frac{1}{2\sigma^{1/2}(\xi+\sigma^{1/2})^2}+\frac{1}{(\xi+\sigma^{1/2})^3}\right]\exp\left\{\xi^2 t-\frac{1}{2}\sigma^{1/2}y\xi\right\}d\xi\,.$$

The integrals appearing in the above equation can be evaluated directly using (14) or by differentiating (14) with respect to b under the integral sign which is valid by virtue of absolute convergence. We invert the middle term in (12) by employing the formula

$$\frac{1}{2\pi i}\int_{\mathrm{Br}_1}\frac{e^{st}}{(s^{1/2}+a^{1/2})^2}\,ds = 1 - 2\pi^{-1/2}a^{1/2}t^{1/2} + (1-2at)\,e^{at}[\operatorname{erfc}(a^{1/2}t^{1/2}) - 1],$$

(which is equation (10) in [4], p. 234), and the convolution theorem. Putting all together the inversion of (12) may be deduced as

$$\begin{aligned}
u = {} & \frac{1}{2}\left\{\operatorname{erfc}\left[\left(\frac{1}{2}y+2t\right)\Big/2t^{1/2}\right] + e^{-y}\operatorname{erfc}\left[\left(\frac{1}{2}y-2t\right)\Big/2t^{1/2}\right]\right\} - \\
& - \frac{4G}{\sigma-1}\left\{\frac{1}{8\sigma}\left(e^{-\sigma y}\operatorname{erfc}\left[\sigma^{1/2}\left(\frac{1}{2}y-2t\right)\Big/2t^{1/2}\right] - \operatorname{erfc}\left[\sigma^{1/2}\left(\frac{1}{2}y+2t\right)\Big/2t^{1/2}\right]\right) - \right. \\
& - \frac{1}{4\sigma^{1/2}}\left(\frac{2t^{1/2}}{\pi^{1/2}}\exp\left[-\frac{\sigma\left(\frac{1}{2}y+2t\right)^2}{4t}\right] - \right. \\
& \left. - \sigma^{1/2}\left(\frac{1}{2}y+2t\right)\operatorname{erfc}\left[\sigma^{1/2}\left(\frac{1}{2}y+2t\right)\Big/2t^{1/2}\right]\right) + \\
& + \frac{1}{4}\left(\left[\sigma\left(\frac{1}{2}y+2t\right)^2+2t\right]\operatorname{erfc}\left[\sigma^{1/2}\left(\frac{1}{2}y+2t\right)\Big/2t^{1/2}\right] - \right. \\
& \left.\left. - \frac{2\sigma^{1/2}t^{1/2}}{\pi^{1/2}}\left(\frac{1}{2}y+2t\right)\exp\left[-\frac{\sigma\left(\frac{1}{2}y+2t\right)}{4t}\right]\right)\right\} + \\
& + \frac{2G}{\sigma-1}e^{-\frac{1}{2}y}\int_0^t\left\{\operatorname{erfc}\left[\left(\frac{1}{2}y+2\tau\right)\Big/2\tau^{1/2}\right] + e^{-y}\operatorname{erfc}\left[\left(\frac{1}{2}y-2\tau\right)\Big/2\tau^{1/2}\right]\right\}\times \\
& \times\left\{e^{-\sigma(t-\tau)}\left[1-\frac{2\sigma^{1/2}(t-\tau)^{1/2}}{\pi^{1/2}}\right] - [1-2\sigma(t-\tau)]\operatorname{erfc}[\sigma^{1/2}(t-\tau)^{1/2}]\right\}d\tau. \quad (17)
\end{aligned}$$

Also of importance in technological applications are the heat transfer rates and the shear stress, both at the wall. The heat transfer is given by

$$q' = -k\left.\frac{\partial T'}{\partial y'}\right|_{y'=0},$$

and employing (6) a non-dimensional form will be

$$q = -\frac{q'v}{kV_0(T_w - T_\infty)} = \left.\frac{\partial\theta}{\partial y}\right|_{y=0}. \tag{18}$$

By virtue of (12) we get

$$\begin{aligned} q &= -\frac{1}{2}\left[\frac{\sigma^{1/2}}{\pi^{1/2}t^{1/2}}\, e^{-\sigma t} + \sigma \operatorname{erfc}\left(-\sigma^{1/2}t^{1/2}\right)\right], \\ &= -\frac{1}{2}\left[\frac{\sigma^{1/2}}{\pi^{1/2}t^{1/2}}\, e^{-\sigma t} + \sigma\{1 + \operatorname{erf}\left(-\sigma^{1/2}t^{1/2}\right)\}\right]. \end{aligned} \tag{19}$$

Finally the shear stress is

$$\tau' = \mu \left.\frac{\partial u'}{\partial y'}\right|_{y'=0},$$

which by virtue of (6) reduces to the non-dimensional form

$$\tau = \tau'/\varrho_\infty V_0 U_0 = \left.\frac{\partial u}{\partial y}\right|_{y=0}. \tag{20}$$

For flow with unit Prandtl number, we can deduce the result

$$\tau = -\frac{1}{2}\left[\frac{1}{\pi^{1/2}t^{1/2}}\, e^{-t} + 1 + \operatorname{erf}\left(t^{1/2}\right)\right] + G \operatorname{erf}\left(t^{1/2}\right). \tag{21}$$

When $\sigma \neq 1$, the expression for the shear stress is cumbersome and the integrals involved are not expressible in a closed form.

4. Discussion

In the previous two Sections we have formulated and solved an unsteady flow problem involving combined forced and free convections when dissipation effects are negligible. It is observed that the temperature field is in no way affected by the free convection currents. However, the temperature and velocity fields consist of forward and backward propagating waves of non-dimensional velocity 4. The forward moving wave has an amplitude which decays exponentially.

The heat transfer rate at the wall is negative for all $t > 0$ and tends to $-\sigma$ as $t \to \infty$. Hence the heat transfer rate is numerically equal to the Prandtl number at the ultimate steady state condition. For the shear stress

at the wall we restrict our discussion to $\sigma = 1$. This, though hypothetical, is not too separated from the real life since $\sigma = 0.71$ for air. Thus the shear stress is negative for an externally heated plate ($G < 0$). However, positive shear stresses are possible when the plate is externally cooled ($G > 0$) and G fairly large. The ultimate steady state shear stress is $G - 1$. Hence the steady state velocity is of the separation type when $G = 1$.

Acknowledgement

The work reported in this note was initiated when the author was visiting I. I. T. Delhi. He is therefore indebted to Prof. M. P. SINGH and members of the Mathematics Department for their hospitality and the College of Science and Technology for a financial support.

REFERENCES

1. E. R. MENOLD and K. T. YANG, J. Appl. Mech., Trans. ASME Ser. E **29**, 124, 1962.
2. I. POP and V. M. SOUNDALGEKAR, Rev. Roum. Phys., **8**, 843, 1975.
3. N. W. MCLACHLAN, Complex Variable Theory and Transform Calculus with Technical Applications, Cambridge University Press, 1963.
4. A. ERDELYI, Tables of Integral Transform, Vol. 1, McGraw-Hill Inc., 1954.

Acta Physica Academiae Scientiarum Hungaricae, Tomus 46 (3), pp. 137—152 (1979)

THE HALL EFFECTS ON HYDROMAGNETIC FLOW OVER A PERMEABLE BED

By

V. VIDYANIDHI and P. C. L. NARAYANA

DEPARTMENT OF ENGINEERING MATHEMATICS, ANDHRA UNIVERSITY, WALTAIR, INDIA

(Received 20. II. 1979)

Hydromagnetic forced convection in a parallel plate channel bounded by a rigid insulated plate and a permeable bed and permeated by a uniform transverse magnetic field has been considered taking Hall effects into account. Solutions for the flow above the bed, Zone 1 and that below the bed, Zone 2 are obtained using the matching conditions at the interface and also suitable boundary conditions at the bed. The primary flow, secondary flow, induced magnetic field components and the temperature distribution are found. The shear stresses and the Nusselt number at the bed and at the plate are calculated. Hall currents are found to exert a profound influence on the flow and heat transfer characteristics.

1. Introduction

The importance of flows through and past porous media in technology, geohydrology, petroleum industry and geophysics is indisputable. The flow through porous media is usually determined using Darcy's empirical formula. BEAVERS and JOSEPH [1], SAFFMANN [2], TAYLOR [3] and RAJASEKHAR [4] have investigated flow past horizontal porous beds. The temperature distribution for a Poiseuille was examined by VIDYANIDHI, SITHAPATI and NARAYANA [5] and for plane couette fow in the presence of buoyancy forces was studied by RUDRAIAH and VEERABHADRAIAH [6]. The Hartmann flow past a permeable bed in the presence of a transverse magnetic field was investigated by RUDRAIAH, RAMAIAH and RAJASEKHAR [7] to illustrate the experimental work of WALLACE, PIERCE and SWAYER [8]. The aim of this paper is to take into consideration the Hall effects and study these effects on the flow and heat transfer characteristics. Such a study will be of some use in the problem of cooling nuclear reactors where very strong magnetic fields are used and also in the utilization of the enormous power beneath the Earth's crust in the geothermal fields, which are clearly a problem of flow past a porous medium with the Earth's surface as a naturally permeable bed.

Here we consider the flow of an electrically conducting liquid through a parallel plate channel $z' = \pm 1$ bounded below by a permeable bed. We suppose that strong uniform magnetic field H_0 acts along the z'-axis. A uniform pressure gradient is maintained in the longitudinal direction in both the channels and the permeable material. In Zone 1 the flow is laminar and

is governed by magnetohydrodynamic equations (with Hall effects included) while the flow in the Zone 2 is determined by the modified Darcy's law. We use the slip velocity boundary condition [1] at the permeable bed. We further assume that the upper plate is at temperature $T = T_1$ while on the permeable bed we adopt the thermal slip boundary condition considered by RUDRAIAH and VEERABHADRAIAH [6] and also independently by VIDYANIDHI and NARAYANA [9]. It is well known that the introduction of Hall effects produces a cross flow [10]. The present investigation thus gives a complete picture of the flow and heat transfer characteristics when the Hall parameter is present.

2. Mathematical formulation

The physical model consists of two Zones; in one Zone, from the impermeable upper rigid plate up to the permeable bed, the flow called the modified Hartmann flow (due to Hall effects) is governed by magnetohydrodynamic equations and in the other Zone below the permeable bed, the flow is determined by the modified Darcy flow. In the following, we shall call the former Zone 1 and the latter Zone 2. The basic equations and the corresponding boundary conditions are set up for Zone 1 and 2, respectively. Solving these equations, the solutions are matched at the interface to get uniformly valid solutions throughout the region of flow.

The basic equations [10] are

$$\nabla' \cdot \vec{V}' = 0\,,$$

$$(\vec{V}' \cdot \nabla')\vec{V}' = -\frac{1}{\varrho}\nabla' p' + \nu\nabla'^2\vec{V}' + \frac{\mu_e}{\varrho}\vec{J}'\times\vec{H}_0'\,. \tag{1}$$

Maxwell's equations are

$$\nabla'\times\vec{E}' = 0, \quad \nabla'\times\vec{H}' = \vec{J}'$$

along with Ohm's law including Hall effects given by

$$\vec{J}' + \frac{\omega\tau}{H_0}\vec{J}'\times\vec{H}' = \sigma_e[\vec{E}' + \mu_e\vec{V}'\times\vec{H}']\,, \tag{2}$$

where $\vec{J}'$, ω, τ, μ_e, σ_e denote the current density, electron Larmor frequency, electron collision time, magnetic permeability and the electrical conductivity, respectively. In writing the Eq. (2), the ion slip effects arising out of imperfect coupling between ions and neutrals as well as electron pressure gradient are neglected.

The equations of energy including viscous dissipation term φ and ohmic dissipation is

$$\varrho c_p(\vec{V}' \cdot \nabla')\, T' = K\nabla'^2 T' - \varphi + \frac{\vec{J}' \cdot \vec{J}'}{\sigma_e}, \tag{3}$$

where K is the thermal conductivity of the liquid and T' the temperature.

We choose the coordinate system such that the z'-axis is perpendicular to the bed $z' = 0$ and the upper plate $z' = l$. There is a uniform magnetic field H_0 along the z'-axis. At large distances from the entry section the flow will be fully developed and in the steady state, all the physical variables depend on z'. Following SHERMANN and SUTTON [10], we assume

$$\vec{V}' = (u', v', 0), \quad \vec{H}' = (h_x', h_y', H_0), \quad \vec{J}' = (J_x', J_y', 0),$$
$$\vec{E}' = (E_x' = c_1, E_y' = c_2, E_z').$$

We use further that the non-dimensional variables

$$\vec{V} = \frac{\vec{V}'}{cl^2}, \quad \vec{J} = \frac{\vec{J}'}{\sigma_e \mu_e H_0 cl^2}, \quad \vec{H} = \frac{\vec{H}'}{H_0},$$

$$\vec{E} = \frac{\vec{E}'}{\mu_e cl^2 H_0}, \quad \theta = \frac{T' - T_0}{T_1 - T_0}, \quad c = -\frac{1}{\mu}\frac{\partial p'}{\partial K},$$

in which T', the temperature in the flow is assumed to be

$$T'(x', z') = Ax' + T'(z'),$$

and the dimensionless parameters defined by

$$M = \frac{\mu_e^2 H_0^2 l^2 \sigma_e}{\mu}, \quad R_m = cl^3 \mu_e \sigma_e, \quad Pr = \frac{\mu c_p}{K}, \quad \varkappa = \frac{K}{\varrho c_p},$$

$$Pe = \frac{\varrho_0 c_p cl^3}{K}, \quad Ec = \frac{c^2 l^4}{c_p(T_1 - T_0)}, \quad A_0 = \frac{Al}{(T_1 - T_0)},$$

where T_1 is the temperature of the plate and T_0 is the ambient temperature.

Introducing

$$q = u + iv, \quad J = J_y - iJ_x, \quad e = e_y - ie_x, \quad h = h_x + ih_y,$$

the foregoing equations reduce to

Zone 1:

$$\frac{d^2q}{dz^2} - m^2q = -1 - m^2e\,, \tag{4}$$

$$J = \frac{1}{1 - i\omega\tau}(e - q) = \frac{1}{R_m}\frac{dh}{dz}\,, \tag{5}$$

$$\frac{d^2\theta}{dz^2} = -PeA_0\ (\text{Real part of } q) - PrEc\left(\frac{dq}{dz}\frac{d\bar{q}}{dz} + M^2\frac{dh}{dz}\frac{d\bar{h}}{dz}\right), \tag{6}$$

where the bars represent the complex conjugates and

$$m = \alpha + i\beta = \frac{M}{\sqrt{(1 - i\omega\tau)}}\,.$$

For Zone 2: The modified Darcy law for Q^* and the equations corresponding to (4) and (6) are

$$Q^* = \frac{1 + m^2e}{m^2 + \sigma^2}\,, \tag{7}$$

$$\frac{d^2q}{dz^2} - (m^2 + \sigma^2)q = -1 - m^2e\,, \tag{8}$$

$$\frac{d^2\theta}{dz^2} = -PeA_0\,(\text{Real part of } q) - PrEc\left(\frac{dq}{dz}\frac{d\bar{q}}{dz} + \sigma^2q\bar{q} + M^2\frac{dh}{dz}\frac{d\bar{h}}{dz}\right). \tag{9}$$

In this Zone we have the additional dimensionless parameter $\sigma = 1/\sqrt{k}$, k is the permeability of the porous medium. Boundary conditions: At the impermeable rigid plate, we use the condition for no slip

$$q = 0 \ \text{ at } \ z = 1\,, \tag{10}$$

while at the permeable bed we adopt the BEAVERS and JOSEPH [1] condition, which in this case, becomes

$$\left.\frac{dq}{dz}\right|_{z=0+} = \alpha_*\sigma[q(0) - Q^*]\,, \tag{11}$$

$$h = 0 \ \text{ at } \ z = 1\,. \tag{12}$$

Supposing the rigid plate to be made up of insulating material, we also adopt the thermal slip condition [6], [8]

$$\frac{\partial T'}{\partial z} = \beta_*[T(0) - T_0]\,, \tag{13}$$

where β_* is the Biot number, T_0 the temperature in the porous bed. This reduces to

$$\frac{d\theta}{dz} = \beta_* \sigma\theta \quad \text{at} \quad z = 0\,, \tag{14}$$

and

$$\theta = 1 \quad \text{at} \quad z = 1\,. \tag{15}$$

In addition we have the continuity of q, h and θ across the interface $z = 0$.

The conditions (11) and (13) can be equivalently represented in Zone 2 by

$$q \to Q^* \quad \text{when} \quad z = -1/\alpha_* \sigma\,, \tag{16}$$

and

$$\theta \to 0 \quad \text{when} \quad z = -1/\beta_* \sigma\,. \tag{17}$$

For simplicity, we choose $e_x = 0$. The total current flowing through the circuit in Zone 1 is given by $I = \int_0^1 J_y' \, dz'$. For Hartmann flow (flow water) we require $I = 0$. This gives the value of e required to achieve the Hartmann flow, i.e.,

$$e = \text{Real part of } (1 - i\omega\tau) \int_0^1 q \, dz = e^* \quad \text{(say)}.$$

The solutions for the two Zones are obtained separately and are matched at the interface to get a continuous velocity distribution. Thus for Zone 1, from (4) subject to (10) and (11) using (7), we have

$$q = -\frac{1 + m^2 e}{m^2} (c_1 \operatorname{sh} mz + c_2 \operatorname{ch} mz - 1)\,, \tag{18}$$

where ch, sh denote hyperbolic functions and c_1, c_2 are complex constants given by

$$c_1 = \frac{\alpha_* \sigma m}{(\sigma^2 + m^2)\left(1 + \alpha_* \sigma \dfrac{\tanh m}{m}\right)} \left[1 + \frac{1 - \operatorname{ch} m}{m^2 \operatorname{ch} m} (\sigma^2 + m^2)\right] =$$

$$= a_1 + i b_1 \quad \text{(say)},$$

$$c_2 = \frac{1 - c_1 \operatorname{sh} m}{\operatorname{ch} m} = a_2 + i b_2 \ \text{(say)},$$

where

$$a_1 = \frac{\alpha_* \sigma p_1}{f(\alpha, \beta)}, \quad b_1 = \frac{\alpha_* \sigma q_1}{f(\alpha, \beta)},$$

$$a_2 = \frac{2 \operatorname{ch} \alpha \cos \beta - a_1 \operatorname{sh} 2\alpha + b_1 \sin 2\beta}{\operatorname{ch} 2\alpha + \cos 2\beta},$$

$$b_2 = -\frac{(2 \operatorname{sh} \alpha \sin \beta + a_1 \sin 2\beta + b_1 \operatorname{sh} 2\alpha)}{\operatorname{ch} 2\alpha + \cos 2\beta},$$

$$p_1 = \alpha(\sigma^2 + \alpha^2 - 3\beta^2)(p_2p_4 + q_2q_4) + \beta(\sigma^2 + 3\alpha^2 - \beta^2)(p_4q_2 - q_4p_2),$$

$$q_1 = \alpha(\sigma^2 + \alpha^2 - 3\beta^2)(p_2q_4 - q_2p_4) + \beta(\sigma^2 + 3\alpha^2 - \beta^2)(q_2q_4 + p_2p_4),$$

$$f(\alpha, \beta) = [(\sigma^2 + \alpha^2 - \beta^2)^2 + 4\alpha^2\beta^2]\left[1 + \alpha_*\sigma\left(\frac{2}{\alpha^2 + \beta^2}\,\frac{\alpha \operatorname{sh} 2\alpha + \beta \sin 2\beta}{\operatorname{ch} 2\alpha + \cos 2\beta}\right) + \right.$$

$$\left. + \alpha_*^2\sigma^2\left(\frac{1}{\alpha^2 + \beta^2}\,\frac{\operatorname{sh}^2 2\alpha - \sin^2 2\beta}{\operatorname{ch} 2\alpha + \cos 2\beta}\right)\right],$$

wherein

$$p_2 = 1 + \frac{\alpha_*\sigma}{(\alpha^2 + \beta^2)(\operatorname{ch} 2\alpha + \cos 2\beta)}(\alpha \operatorname{sh} 2\alpha + \beta \sin 2\beta),$$

$$q_2 = \frac{\alpha_*\sigma}{(\alpha^2 + \beta^2)(\operatorname{ch} 2\alpha + \cos 2\beta)}(\alpha \sin 2\beta - \beta \operatorname{sh} 2\alpha),$$

$$p_3 = (\alpha^2 - \beta^2) \operatorname{ch} \alpha \cos \beta - \frac{(\alpha^2 - \beta^2)}{2}(\operatorname{ch} 2\alpha + \cos 2\beta) + 2\alpha\beta \operatorname{sh} \alpha \sin \beta,$$

$$q_3 = 2\alpha\beta \operatorname{ch} \alpha \cos \beta - \alpha\beta(\operatorname{ch} 2\alpha + \cos 2\beta) - (a^2 - \beta^2) \operatorname{sh} \alpha \sin \beta,$$

$$p_4 = \frac{2}{(\alpha^2 + \beta^2)^2(\operatorname{ch} 2\alpha + \cos 2\beta)}[p_3(\sigma^2 + \alpha^2 - \beta^2) + 2q_3\alpha\beta] + 1.$$

$$q_4 = \frac{2}{(\alpha^2 + \beta^2)^2(\operatorname{ch} 2\alpha + \cos 2\beta)}[q_3(\sigma^2 + \alpha^2 - \beta^2) - 2\alpha\beta p_3].$$

Separating the real and imaginary parts of q from (18)

$$u = -\left[\left\{\frac{\alpha^2 - \beta^2}{(\alpha^2 + \beta^2)^2} + e\right\}(p_5 - 1) - \frac{2\alpha\beta}{(\alpha^2 + \beta^2)^2}q_5\right], \tag{19}$$

$$v = -\left[\frac{2\alpha\beta}{(\alpha^2 + \beta^2)^2}(p_5 - 1) + \left\{\frac{\alpha^2 - \beta^2}{(\alpha^2 + \beta^2)^2} + e\right\}q_5\right], \tag{20}$$

where

$$p_5 = a_2 \operatorname{ch} \alpha z \cos \beta z - b_2 \operatorname{sh} \alpha z \sin \beta z + a_1 \operatorname{sh} \alpha z \cos \beta z - b_1 \operatorname{ch} \alpha z \sin \beta z,$$

$$q_5 = b_2 \operatorname{ch} \alpha z \cos \beta z + a_2 \operatorname{sh} \alpha z \sin \beta z + b_1 \operatorname{sh} \alpha z \cos \beta z + a_1 \operatorname{ch} \alpha z \sin \beta z.$$

The magnetic field is obtained from (2) using the condition (12)

$$h_x = \frac{R_m}{1 + \omega^2\tau^2}\left[e(z - 1) + \left\{\frac{\alpha^2 - \beta^2}{(\alpha^2 - \beta^2)^2} - \frac{2\alpha\beta}{(\alpha^2 + \beta^2)^2}\omega\tau + e\right\}f_1(\alpha, \beta) - \right.$$

$$\left. - \left\{\frac{2\alpha\beta}{(\alpha^2 + \beta^2)^2} + \frac{\alpha^2 - \beta^2}{(\alpha^2 + \beta^2)^2}\omega\tau + \omega\tau e\right\}g_1(\alpha, \beta)\right], \tag{21}$$

$$h_y = -\frac{R_m}{1+\omega^2\tau^2}\left[\omega\tau e(1-z) - \left\{\frac{\alpha^2-\beta^2}{(\alpha^2+\beta^2)^2}\,\omega\tau + \frac{2\alpha\beta}{(\alpha^2+\beta^2)^2} + \right.\right.$$

$$\left.\left. + \omega\tau e\right\} f_1(\alpha,\beta) - \left\{\frac{\alpha^2-\beta^2}{(\alpha^2-\beta^2)^2} - \frac{2\alpha\beta}{(\alpha^2+\beta^2)^2}\,\omega\tau + e\right\} g_1(\alpha,\beta)\right], \tag{22}$$

where

$$f_1(\alpha,\beta) = \frac{1}{\alpha^2+\beta^2}\,[(a^2\alpha + b_2\beta)(\operatorname{sh}\alpha z\cos\beta z - \operatorname{sh}\alpha\cos\beta) +$$

$$+ (b_2\alpha - a_2\beta)(\operatorname{ch}\alpha\sin\beta - \operatorname{ch}\alpha z\sin\beta z) +$$

$$+ (a_1\alpha + b_1\beta)(\operatorname{ch}\alpha z\cos\beta z - \operatorname{ch}\alpha\cos\beta) +$$

$$+ (b_1\alpha - a_1\beta)(\operatorname{sh}\alpha\sin\beta - \operatorname{sh}\alpha z\sin\beta z)] - z + 1,$$

$$g_1(\alpha,\beta) = \frac{1}{a^2+\beta^2}\,[(b_2\alpha - a_2\beta)(\operatorname{sh}\alpha z\cos\beta z - \operatorname{sh}\alpha\cos\beta) -$$

$$- (a_2\alpha + b_2\beta)(\operatorname{ch}\alpha\sin\beta - \operatorname{ch}\alpha z\sin\beta z) +$$

$$+ (b_1\alpha - a_1\beta)(\operatorname{ch}\alpha z\cos\beta z - \operatorname{ch}\alpha\cos\beta) -$$

$$- (a_1\alpha + b_1\beta)(\operatorname{sh}\alpha\sin\beta - \operatorname{sh}\alpha\sin\beta z)].$$

The shear stresses at the plate and at the bed are given by

$$\left.\frac{du}{dz}\right|_{z=1} = -\left[\left\{\frac{\alpha^2-\beta^2}{(\alpha^2+\beta^2)^2} + e\right\} p_6 - \frac{2\alpha\beta}{(\alpha^2+\beta^2)^2}\,q_6\right], \tag{23}$$

$$\left.\frac{dv}{dz}\right|_{z=1} = -\left[\frac{2\alpha\beta}{(\alpha^2+\beta^2)^2}\,p_6 + \left\{\frac{\alpha^2-\beta^2}{(\alpha^2+\beta^2)^2} + e\right\} q_6\right], \tag{24}$$

$$\left.\frac{du}{dz}\right|_{z=0} = -\left[\left\{\frac{\alpha^2-\beta^2}{(\alpha^2+\beta^2)^2} + e\right\}(a_1\alpha - b_1\beta) - \frac{2\alpha\beta}{(\alpha^2+\beta^2)^2}(a_1\beta + b_1\alpha)\right], \tag{25}$$

$$\left.\frac{dv}{dz}\right|_{z=0} = -\left[\left\{\frac{\alpha^2-\beta^2}{(\alpha^2+\beta^2)^2} + e\right\}(b_1\alpha + a_1\beta) + \frac{2\alpha\beta}{(\alpha^2+\beta^2)^2}(a_1\alpha - b_1\beta)\right], \tag{26}$$

where

$$p_6 = (a_2\alpha - b_2\beta)\operatorname{sh}\alpha\cos\beta - (b_2\alpha + a_2\beta)\operatorname{ch}\alpha\sin\beta +$$

$$+ (a_1\alpha - b_1\beta)\operatorname{ch}\alpha\cos\beta - (b_1\alpha + a_1\beta)\operatorname{sh}\alpha\sin\beta,$$

$$q_6 = (b_2\alpha + a_2\beta)\operatorname{sh}\alpha\cos\beta + (a_2\alpha - b_2\beta)\operatorname{ch}\alpha\sin\beta +$$

$$+ (b_1\alpha + a_1\beta)\operatorname{ch}\alpha\cos\beta + (a_1\alpha - b_1\beta)\operatorname{sh}\alpha\sin\beta.$$

The temperature distribution for Zone 1, by solving (6) using the boundary conditions (14) and (15) is

$$\theta = k_1 + k_2 z - Pe\, A_0 F(z) - Pr\, Ec\, G(z)\,, \tag{27}$$

where

$$k_1 = \frac{1}{1+\beta_* \sigma}\left[1 - Pe\, A_0\{F'(0) - F(1) - \beta_* \sigma F(0)\} - \right.$$
$$\left. - Pr\, Ec\{G'(0) - G(1) - \beta_* \sigma\, G(0)\}\right]\,,$$
$$k_2 = 1 - k_1 + Pe\, A_0 F(1) + Pr\, Ec\, G(1)\,.$$

(here dashes denote differentiation with respect to z)

$$F(z) = -\left[\left\{\frac{\alpha^2-\beta^2}{(\alpha^2+\beta^2)^2} + e\right\}\left\{\frac{a_2p_7 - b_2q_7 + q_1p_8 - b_1q_8}{(\alpha^2+\beta^2)^2} - \frac{z^2}{2}\right\} - \right.$$
$$\left. - \frac{2\alpha\beta}{(\alpha^2+\beta^2)^4}\{b_2p_7 + a_2q_7 + b_1p_8 + a_1q_8\}\right],$$

$$G(z) = (a^2+b^2)\left[\frac{1}{(\alpha^2+\beta^2)^2} + \frac{2e(\alpha^2-\beta^2)}{(\alpha^2+\beta^2)^2} + e^2\right]\left[\frac{a_2^2+b_2^2}{8}\left(\frac{\operatorname{ch} 2\alpha z}{\alpha^2} + \right.\right.$$
$$\left. + \frac{\cos 2\beta z}{\beta^2}\right) + \frac{a_1^2+b_1^2}{8}\left(\frac{\operatorname{ch} 2\alpha z}{\alpha^2} - \frac{\cos 2\beta z}{\beta^2}\right) +$$
$$\left. + \frac{1}{4}\left\{\frac{(a_1a_2 + b_1b_2)\operatorname{sh} 2\alpha z}{\alpha^2} - \frac{(a_2b_1 - a_1b_2)\sin 2\beta z}{\beta^2}\right\}\right] +$$
$$+ \frac{M^2}{1+\omega^2\tau^2}\left[\frac{e^2z^2}{2} + 2e\left\{\left(\frac{\alpha^2-\beta^2}{(\alpha^2+\beta^2)^2} + e\right)\left(\frac{a_2p_7 - b_2q_7 + a_1p_8 - b_1q_8}{(\alpha^2+\beta^2)^2} - \right.\right.\right.$$
$$\left.\left.\left. - \frac{z^2}{2}\right) + \frac{2\alpha\beta}{(\alpha^2+\beta^2)^2}(b_2p_7 + a_2q_7 + b_1p_8 + a_1q_8)\right\} +\right.$$
$$\left. + \left\{\frac{1}{(\alpha^2+\beta^2)^2} + \frac{2e(\alpha^2-\beta^2)}{(\alpha^2+\beta^2)^2} + e^2\right\}\left\{\frac{a_2^2+b_2^2}{8}\left(\frac{\operatorname{ch} 2\alpha z}{\alpha^2} - \frac{\cos 2\beta z}{\beta^2}\right) + \right.\right.$$
$$\left.\left. + \frac{a_1^2+b_1^2}{8}\left(\frac{\operatorname{ch} 2\alpha z}{\alpha^2} + \frac{\cos 2\beta z}{\beta^2}\right) + \frac{z^2}{2} + \frac{(a_1a_2 + b_1b_2)\operatorname{sh} 2\alpha z}{4\alpha^2} + \right.\right.$$
$$\left.\left. + \frac{(a_2b_1 - a_1b_2)\sin 2\beta z}{4\beta^2} - \frac{2}{(\alpha^2+\beta^2)^2}(a_2p_7 - b_2q_7 + a_1p_8 - b_1q_8)\right\}\right],$$

wherein

$$p_7 = (\alpha^2-\beta^2)\operatorname{ch}\alpha z \cos\beta z - 2\alpha\beta \operatorname{sh}\alpha z \sin\beta z\,,$$
$$q_7 = 2\alpha\beta \operatorname{ch}\alpha z \cos\beta z + (\alpha^2-\beta^2)\operatorname{sh}\alpha z \sin\beta z\,,$$

$$p_8 = (\alpha^2 - \beta^2)\,\mathrm{sh}\,\alpha z \cos \beta z - 2\alpha\beta\,\mathrm{ch}\,\alpha z \sin \beta z\,,$$

$$q_8 = 2\alpha\beta\,\mathrm{sh}\,\alpha z \cos \beta z + (\alpha^2 - \beta^2)\,\mathrm{ch}\,\alpha z \sin \beta z\,.$$

For Zone 2, the velocity and temperature distribution from (8) and (9) using (7) subject to (16) and (17) are

$$q = c_3\,\mathrm{ch}\,\sqrt{m^2 + \sigma^2}\,z + c_4\,\mathrm{sh}\,\sqrt{m^2 + \sigma^2}\,z + \frac{1 + m^2 e}{m^2 + \sigma^2}\,, \tag{28}$$

$$\theta = k_3 + k_4 z - Pe\,A_0 R(z) - Pr\,Ec\,S(z)\,, \tag{29}$$

where $c_3 = a_3 + ib_3$ (say), $c_4 = a_4 + ib_4$ (say) and $\sqrt{(m^2 + \sigma^2)} = \psi + i\chi$. Separating the real and imaginary parts of (28),

$$u = \frac{[1 + (\alpha^2 - \beta^2)\,e]\,[\sigma^2 + \alpha^2 - \beta^2] + 4\alpha^2\beta^2 e}{(\sigma^2 + \alpha^2 - \beta^2)^2 + 4\alpha^2\beta^2} + p_9\,, \tag{30}$$

$$v = \frac{(\sigma^2 + \alpha^2 - \beta^2)\,2\alpha\beta\,e - 2\alpha\beta[1 + (\alpha^2 - \beta^2)\,e]}{(\sigma^2 + \alpha^2 - \beta^2)^2 + 4\alpha^2\beta^2} + q_9\,, \tag{31}$$

where

$$a_3 = -\frac{1}{(\sigma^2 + \alpha^2 - \beta^2)^2 + 4\alpha^2\beta^2}\,[(\sigma^2 + \alpha^2 - \beta^2)\,(1 + \alpha^2 e - \beta^2 e) + 4\alpha^2\beta^2 e] -$$

$$- \frac{1}{(\alpha^2 + \beta^2)^2}\,[(\alpha^2 - \beta^2)\,\{(1 + \alpha^2 e - \beta^2 e)\,(a_2 - 1) -$$

$$- 2\alpha\beta\,b_2 e\} + 2\alpha\beta\,\{2\alpha\beta\,e(a_2 - 1) + b_2(1 + \alpha^2 e - \beta^2 e)\}]\,,$$

$$b_3 = -\frac{1}{(\sigma^2 + \alpha^2 - \beta^2)^2 + 4\alpha^2\beta^2}\,[2\alpha\beta\,e(\sigma^2 + \alpha^2 - \beta^2) - 2\alpha\beta(1 - \alpha^2 e + \beta^2 e)] -$$

$$- \frac{1}{(\alpha^2 + \beta^2)^2}\,[(\alpha^2 - \beta^2)\,\{2\alpha\beta\,e(a_2 - 1) + b_2(1 + \alpha^2 e - \beta^2 e)\} -$$

$$- 2\alpha\beta\{(1 + \alpha^2 e - \beta^2 e)\,(a_2 - 1) - 2\alpha\beta\,b_2 e\}]\,,$$

$$a_4 = \frac{a_3\,\mathrm{sh}\,2\psi z - b_3 \sin 2\chi z}{\mathrm{ch}\,2\psi z - \cos 2\chi z}\,,$$

$$b_4 = \frac{b_3\,\mathrm{sh}\,2\psi z + a_3 \sin 2\chi z}{\mathrm{ch}\,2\psi z - \cos 2\chi z}\,,$$

$$p_9 = a_3\,\mathrm{ch}\,\psi z \cos \chi z - b_3\,\mathrm{sh}\,\psi z \sin \chi z + a_4\,\mathrm{sh}\,\psi z \cos \chi z -$$

$$- b_4\,\mathrm{ch}\,\psi z \sin \chi z\,,$$

$$q_9 = b_3 \operatorname{ch} \psi z \cos \chi z + a_3 \operatorname{sh} \psi z \sin \chi z + b_4 \operatorname{sh} \psi z \cos \chi z +$$
$$+ a_4 \operatorname{ch} \psi z \sin \chi z ,$$

$$k_3 = k_1 - Pe\, A_0[F(0) - R(0)] - Pr\, Ec\, [G(0) - S(0)] ,$$

$$k_4 = \frac{1}{\beta_* \sigma}\left[k_3 - Pe\, A_0 R\left(-\frac{1}{\beta_* \sigma}\right) - Pr\, Ec\, S\left(-\frac{1}{\beta_* \sigma}\right)\right],$$

$$R(z) = \frac{1}{(\sigma^2 + \alpha^2 - \beta^2)^2 + 4\alpha^2\beta^2}\left[\frac{z^2}{2}\{(\sigma^2 + \alpha^2 - \beta^2)(1 + \alpha^2 e - \beta^2 e) +\right.$$
$$\left. + 4\alpha^2\beta^2 e\} + (\sigma^2 + \alpha^2 - \beta^2)(p_{10} + p_{11}) + 2\alpha\beta(q_{10} + q_{11})\right],$$

$$S(z) = (\psi^2 + \chi^2)\left[\frac{a_3^2 + b_3^2}{8}\left(\frac{\operatorname{ch} 2\psi z}{\psi^2} + \frac{\cos 2\chi z}{\chi^2}\right) + \frac{a_4^2 + b_4^2}{8}\left(\frac{\operatorname{ch} 2\psi z}{\psi^2} -\right.\right.$$
$$\left. - \frac{\cos 2\chi z}{\chi^2}\right) + \frac{(a_3 a_4 + b_3 b_4) \operatorname{sh} 2\psi z}{4\psi^2} + \frac{(a_3 b_4 - b_3 a_4) \sin 2\chi z}{4\chi^2}\Big] +$$
$$+ \frac{M^2}{1 + \omega^2\tau^2}\left[\frac{e^2 z^2}{2} - \frac{2e}{(\sigma^2 + \alpha^2 - \beta^2)^2 + 4\alpha^2\beta^2}\left\{\frac{z^2}{2}[(\sigma^2 + \alpha^2 -\right.\right.$$
$$- \beta^2)(1 + \alpha^2 e - \beta^2 e) + 4\alpha^2\beta^2 e] + (\sigma^2 + \alpha^2 - \beta^2)(p_{10} + p_{11}) +$$
$$\left.\left. + 2\alpha\beta(q_{10} + q_{11})\right\} + Q(z)\right] + \sigma^2 Q(z) ,$$

$$Q(z) = \frac{(1 + \alpha^2 e - \beta^2 e)^2 + 4\alpha^2\beta^2 e}{(\sigma^2 + \alpha^2 - \beta^2)^2 + 4\alpha^2\beta^2}\,\frac{z^2}{2} + \frac{(a_3^2 + b_3^2)}{8}\left(\frac{\operatorname{ch} 2\psi z}{\psi^2} - \frac{\cos 2\chi z}{\chi^2}\right) +$$
$$+ \frac{(a_4^2 + b_4^2)}{8}\left(\frac{\operatorname{ch} 2\psi z}{\psi^2} + \frac{\cos 2\chi z}{\chi^2}\right) + \frac{(a_3 a_4 + b_3 b_4) \operatorname{sh} 2\psi z}{4\psi^2} -$$
$$- \frac{(a_3 b_4 - a_4 b_3) \sin 2\chi z}{\chi^2} + \frac{2}{(\sigma^2 + \alpha^2 - \beta^2)^2 + 4\alpha^2\beta^2}[(1 + \alpha^2 e -$$
$$- \beta^2 e)(p_{10} + p_{11}) + 2\alpha\beta\, e(q_{10} + q_{11})] ,$$

$$p_{10} = a_3 \operatorname{ch} \psi z \cos \chi z - b_3 \operatorname{sh} \psi z \sin \chi z ,$$
$$q_{10} = b_3 \operatorname{ch} \psi z \cos \chi z + a_3 \operatorname{sh} \psi z \sin \chi z ,$$
$$p_{11} = a_4 \operatorname{sh} \psi z \cos \chi z - b_4 \operatorname{ch} \psi z \sin \chi z ,$$
$$q_{11} = b_4 \operatorname{sh} \psi z \cos \chi z + a_4 \operatorname{ch} \psi z \sin \chi z .$$

The Nusselt numbers at the lower plate Nu_0, and the upper plate Nu_1 are given by

$$Nu_0 = \frac{\left(\frac{d\theta}{dz}\right)_{z=0}}{\theta_m - \theta(0)}, \tag{32}$$

$$Nu_1 = \frac{\left(\frac{d\theta}{dz}\right)_{z=1}}{\theta_m - \theta(1)}, \tag{33}$$

where $\theta_m = \int_1^0 \theta \, dz$ is the average temperature.

3. Results and discussion

Throughout this paper we take $\alpha_* = 0.1$, $\beta_* = 1$. As our primary interest is to examine the interactions of the Hall parameter $\omega\tau$, Hartmann number M and Darcy's number σ, we allow these to vary. We have plotted $u(z)$ and $-v(z)$ for some typical values of $\omega\tau$, M and σ for short circuited circumstances $e = 0$ and for flow meter $e = e^*$. Fig. 1 shows that $u(z)$ increases with increase in $\omega\tau$, while Fig. 2 shows a similar result for the cross flow $-v(z)$. The flattening effect of magnetic field in the velocity profiles is clearly discernible in the Figures. The effect of the permeability of the medium k, characterised by the parameter σ, is to increase the velocity. We find that the slip velocity at the permeable bed decreases as σ increases for given M

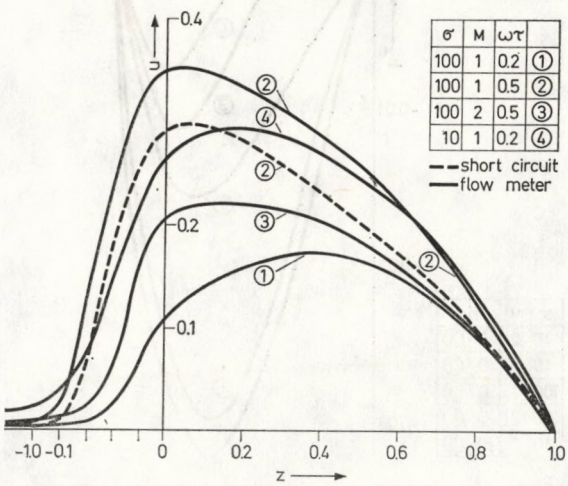

Fig. 1. Primary flow

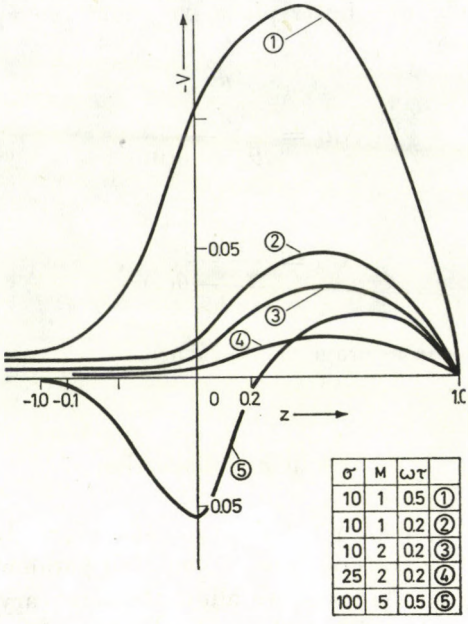

σ	M	ωτ	
10	1	0.5	①
10	1	0.2	②
10	2	0.2	③
25	2	0.2	④
100	5	0.5	⑤

Fig. 2. Secondary flow

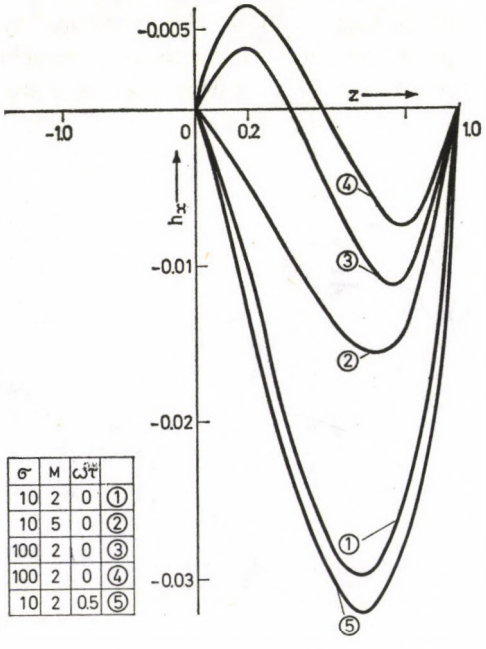

σ	M	ωτ	
10	2	0	①
10	5	0	②
100	2	0	③
100	2	0	④
10	2	0.5	⑤

Fig. 3. Primary induced magnetic field

and $\omega\tau$. The curve 5 in Fig. 2 reveals that the cross flow due to the Hall effects shows an incipient flow reversal, although the primary flow does not. Also the velocity profiles are found to increase with e in each case.

The Figs. 3 and 4 indicate that the dissipation of the induced magnetic field is in accord with the pulling of the line of force by the convection channel.

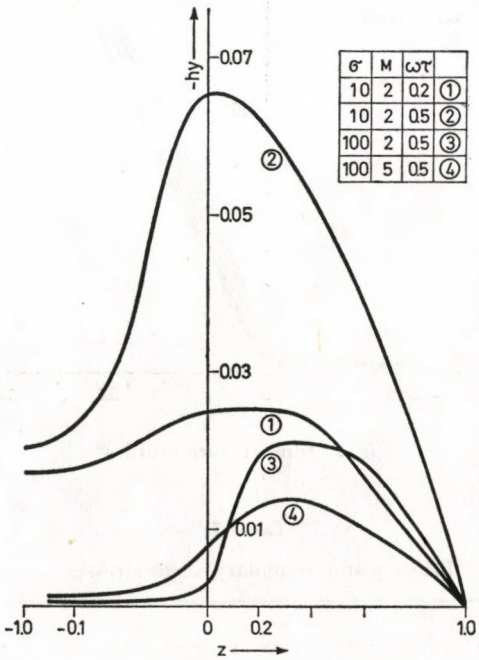

Fig. 4. Secondary induced magnetic field

It is interesting to note that non-zero values of h_y exist at the permeable bed for the flow meter circumstances; of course h_x vanishes at this bed in agreement with RUDRAIAH, RAMAIAH and RAJASEKHAR [7] in the absence of Hall effects. Fig. 5 shows the temperature distribution. It is found to increase with $\omega\tau$, decreases as M or σ increases. The effect of e is to increase the temperature. The results are anticipated on physical ground judging from the behaviour of the velocity profiles.

When the Hall effects are absent, the skin friction for the primary flow of the bed is found to increase as σ increases and decreases. However, as $\omega\tau$ increases, it decreases, passes through zero and changes its direction for fixed σ and M. Such behaviour is ruled out for the primary stresses at the plate and for the secondary stresses both at the plate and at the bed. The effect of e is in general to increase the skin friction. The results are inferred from a sample of data presented in Table I.

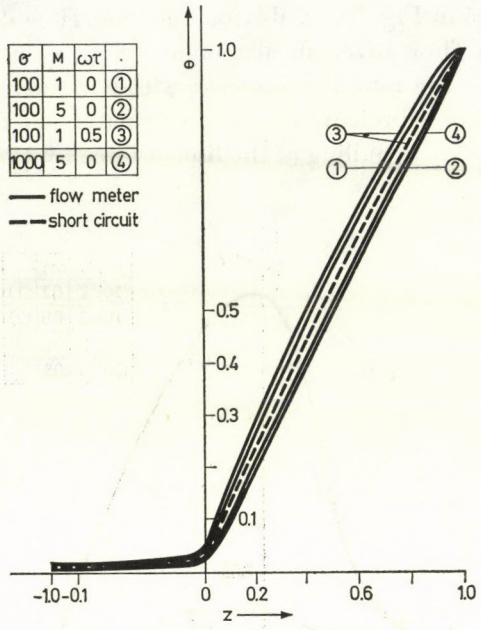

Fig. 5. Temperature profiles

Table I

Primary and secondary shear stresses

σ	M	$\omega\tau$	$z=0$		$z=1$	
			$e=0$	$e=e^*$	$e=0$	$e=e^*$
			Primary shear stresses			
10	1	0.	0.19417	0.23396	−0.63576	−0.76604
10	2	0	0.11736	0.20656	−0.45082	−0.79344
1000	1	0	0.45613	0.49465	−0.46599	−0.50535
1000	2	0	0.37306	0.49352	−0.38285	−0.50648
10	1	0.5	−0.04434	−0.03160	−0.54231	−0.71926
1000	1	0.5	−0.11552	−0.09559	−0.56371	−0.69136
			Secondary shear stresses			
10	1	0.5	−0.19877	−0.24991	0.44427	0.48434
1000	1	0.5	−0.44836	−0.54116	0.26509	0.26201

Table II gives the computed values of e^* needed to achieve the Hartmann flow. When $e < e^*$, the channel is short circuited (in our analysis we have taken $e = 0$ for this case) and all the currents flow in one direction and the net current flow is clearly non zero. When $e > e^*$, all the currents flow in

Table II

Computed values of e^*

σ	M \ $\omega\tau$	0	0.1	0.2	0.5
10	1	0.20492	0.20841	0.21882	0.28934
	2	0.19000	0.19232	0.19934	0.25089
	3	0.17150	0.17343	0.17928	0.22177
	4	0.15332	0.15507	0.16036	0.19868
	5	0.13711	0.13873	0.14360	0.17909
1000	1	0.08445	0.09044	0.10830	0.22918
	2	0.08073	0.08328	0.09102	0.14944
	3	0.07548	0.07681	0.08817	0.11054
	4	0.06962	0.07051	0.07319	0.09238
	5	0.06379	0.06450	0.06662	0.08142

the opposite direction and this corresponds to magnetohydrodynamic accelerator or pump. The parameter e modifies the usual Hartmann flow in that current distribution changes as does the induced magnetic field.

Table III

Values of the Nusselt number for e^*

σ	M	$\omega\tau$	Nu_0	Nu_1
10	1	0.2	2.06292	−1.50459
10	5	0.2	2.41072	−1.68197
10	1	0.5	2.28051	−1.52632
100	1	0.2	2.06840	−1.58278
1000	1	0.2	2.07201	−1.59124

Table III gives the computed values of the Nusselt numbers. These are in general found to increase with M or σ or $\omega\tau$ at the bed and at the plate. The negative sign in Nusselt number indicates the direction of the heat flow from the liquid to the plate.

The foregoing analysis reveals that the inclusion of the Hall currents exerts a profound influence on the flow and the heat transfer characteristics. It is also observed that the viscous and ohmic dissipation terms have significant effect in increasing the heat transfer coefficients.

REFERENCES

1. G. S. Beavers and D. D. Joseph, J. Flu. Mech., **30**, 197, 1967.
2. P. G. Saffmann, Stud. Appl. Math., **50**, 93, 1971.
3. G. I. Taylor, J. Fluid Mech., **49**, 319, 1971.
4. B. M. Rajasekhar, Experimental and theoretical study of flow past porous media, Ph. D. Thesis, Bangalore University, 1975.
5. V. Vidyanidhi, A. Sithapati, and P. C. L. Narayana, Pro. Indian Acad. Sci., **86A**, 557, 1977.
6. N. Rudraiah and R. Veerabhadraiah, Pro. Indian Acad. Sci., **86A**, 537, 1977.
7. N. Rudraiah, B. K. Ramaiah and B. M. Rajasekhar, Int. J. Engng. Sci., **13**, 1, 1975.
8. W. E. Wallace, C. I. Pierce and W. K. Swayer, U.S. Bureau of Mines, TN23, U7, No. 7259, 1969.
9. V. Vidyanidhi and P. C. L. Narayana, Current Sci., **47**, 713, 1978.
10. A. Sherman and G. W. Sutton, Magnetohydrodynamics (Edited by A. B. Cambel), North-Western University Press, Evanston, Illinois, 1962.

Acta Physica Academiae Scientiarum Hungaricae, Tomus 46 (3), pp. 153—156 (1979)

POTENTIAL ENERGY CURVES AND DISSOCIATION ENERGY OF $X^2\Sigma$ STATE OF ScO MOLECULE

By

V. M. RAO, M. L. P. RAO and P. T. RAO

DEPARTMENT OF PHYSICS, ANDHRA UNIVERSITY, WALTAIR, INDIA

(Received 7. III. 1979)

The potential energy curve of the $X^2\Sigma$ state of the astrophysically important ScO molecule has been constructed by R—K—R—V method and its dissociation energy has been evaluated by fitting the electro-negativity potential function to the experimental potential curve.

1. Introduction

The accurate determination of dissociation energies is of considerable importance in the study of chemical binding. The dissociation energies are generally determined by spectroscopic, thermochemical and mass spectrometric methods. Of these, the BIRGE—SPONER extrapolation [1] is suitable in cases where an appreciable number of vibrational quanta are known. However, this method is not quite reliable for molecules where ionic forces contribute considerably to the binding. Various empirical potential functions have been proposed based on certain physical and chemical models leading to information about the chemical bond.

The LIPPINCOTT [2] three parameter potential function based on a δ-type model of binding is indispensably covalent in nature. For molecular binding where ionic contribution becomes important, the SZÖKE and BAITZ [3] potential function which includes explicitly the electronegativities of the constituent atoms, yields better results. The ionic contribution in the bond of ScO molecule is quite considerable and hence it is expected that the electronegativity potential function would yield a reliable estimate of dissociation energy of this molecule. In the present work, this method has been applied and the results are presented.

2. Computational procedure

The potential function proposed by SZÖKE and BAITZ is

$$U(r) = D_e\left[1 - \exp\left(\frac{-n(r-r_e)^2}{2r}\right)\right] \times \left[1 - a\left(\frac{b^2 n}{2r}\right)^{1/2}(r-r_e)\exp\left\{-\left(\frac{b^2 n}{2r_e}\right)^{1/2}(r-r_e)\right\}\right], \qquad (1)$$

where n is defined by the relation $n = de/D_e^{1/2}$, d is a proportionality factor which is constant for molecules of the same bond type and related to the force constant by the relation $k_e = d\,(e_1 e_2\, D_e)^{1/2}\, r_e^{-1}$, e is the geometric mean of the PAULING [4] electronegativities e_1, e_2 of the constituent atoms. a and b are empirical parameters: $a = 0.35\ e^{1/2}$ and b is a universal constant (1.065) being independent of the bond type. D_e and r_e have the usual spectroscopic meanings.

By using the RYDBERG—KLEIN—REES [5—7] method as modified by VANDERSLICE et al [8, 9], the turning points corresponding to each vibrational level have been computed. The values of $r_{\min}$ and $r_{\max}$ of each vibrational level are substituted in Eq. (1) and the corresponding U values are calculated for different D_e values. The correlation coefficient between the estimated values and the experimental values is determined. The particular values of D_e corresponding to maximum correlation coefficient is regarded as the true dissociation energy.

3. Results and discussion

The spectroscopic constants employed in the present work have been taken from [10—14]. The results of fitting the electronegativity potential function to the R—K—R—V curve are shown in Table I. It can be seen from the Table that the dissociation energy D_e is 5.39 eV, which corresponds to the maximum correlation coefficient. The values of the R—K—R—V turning point and the electronegativity potential energy values obtained for the estimated D_e value are shown in Table II.

GAYDON [15] recommends a value of 6 ± 1 eV for the dissociation energy of $X^2\Sigma$ state of ScO, whereas the value obtained by us using the three parameter LIPPINCOTT [2] function is 5.48 eV. The value obtained in the present study is 5.39 eV.

The dissociation energy of a molecule is closely related to the ionicity of the bond in question and it has been suggested that r_x/r_e gives its measure. r_x is the hypothetical crossing point between the ionic potential energy curve and the asymptote of the covalent potential curve and r_e is the equilibrium internuclear distance. For a diatomic molecule AB, r_x is given by the relation $r_x(A) = 14.40/(I.P.\,(A) - E.A.(B))$ where $I.P.$ and $E.A.$ are the ionisation potential of atom A and electron affinity of atom B respectively, both expressed in electron volts. For the $X^2\Sigma$ state of ScO, r_x/r_e is equal to 1.69. According to the definition of ionicity as given by HILDENBRAND [16] and HERZBERG [17], the bonding in ScO falls in an intermediate region where both ionic and covalent contributions are significant. As the SZÖKE and BAITZ potential function is based on ionic model alone, it gives a slightly lower estimate of the dissociation energy (5.39 eV) of $X^2\Sigma$ state of ScO molecule.

Table I

Correlation between the electronegativity and the R—K—R—V potential curves

D_e (eV)	Correlation coefficient
5.31	0.99999094
5.32	0.99999288
5.33	0.99999543
5.34	0.99999592
5.35	0.99999704
5.36	0.99999790
5.37	0.99999849
5.38	0.99999882
5.39	0.99999889
5.40	0.99999871
5.41	0.99999827
5.42	0.99999759
5.43	0.99999665
5.44	0.99999546
5.45	0.99999404
5.46	0.99999236
5.47	0.99999045
5.48	0.99998829
5.49	0.99998590
5.50	0.99998328

Table II

Potential energy curves of $X^2\Sigma$ state of ScO

V	U (cm^{-1})	r_{min} (Å)	r_{max} (Å)	U_{min} (cm^{-1})	U_{max} (cm^{-1})
0	484.84	1.614	1.723	484.97	485.85
1	1 447.43	1.579	1.768	1 448.84	1 450.82
2	2 402.55	1.556	1.800	2 404.11	2 407.49
3	3 350.13	1.538	1.828	3 352.10	3 357.49
4	4 289.93	1.523	1.853	4 290.19	4 297.30
5	5 221.91	1.510	1.877	5 223.81	5 232.82
6	6 145.84	1.498	1.898	6 145.93	6 155.91
7	7 061.67	1.488	1.919	7 056.08	7 065.94
8	7 969.60	1.478	1.939	7 962.68	7 971.55
9	8 869.69	1.469	1.958	8 863.49	8 870.05
10	9 761.97	1.461	1.977	9 769.86	9 772.25
11	10 646.09	1.453	1.996	10 654.80	10 649.93
12	11 522.01	1.446	2.014	11 533.16	11 517.86

Acknowledgements

The authors are thankful to U.G.C. and C.S.I.R. (New Delhi) and also to the authorities of the Computer Centre, Andhra University, Waltair.

REFERENCES

1. R. T. Birge and H. Sponer, Phys. Rev., **28,** 259, 1926.
2. D. Steele and E. R. Lippincott, J. Chem. Phys., **35,** 2065, 1961.
3. S. Szöke and E. Baitz, Can. J. Phys., **46,** 2563, 1968.
4. L. Pauling, The Nature of the Chemical Bond, Cornell University Press, New York, 1960.
5. R. Rydberg, Z. Physik, **73,** 376, 1931.
6. O. Klein, Z. Physik., **76,** 226, 1932.
7. A. L. G. Rees, Proc. Phys. Soc., (G. B.), **59,** 998, 1947.
8. J. T. Vanderslice, E. A. Maison, W. G. Maisch and E. R. Lippincott, J. Molec. Spectro., **3,** 17, 1959.
9. J. T. Vanderslice, E. A. Maison, W. G. Maisch and E. R. Lippincott, J. Molec. Spectro., **5,** 83, 1960.
10. L. W. Johnson and R. C. Johnson, Proc. Roy. Soc., A, **133,** 207, 1931.
11. W. F. Meggers and J. A. Wheeler, Bur. Stand. J. Res., **6,** 239, 1931.
12. A. Adams, W. Klemperer and T. M. Dunn, Can. J. Phys., **46,** 2213, 1968.
13. L. Akerlind, Ark. Fysik., **22,** 41, 1962.
14. M. L. P. Rao, D. V. K. Rao and P. T. Rao, Physica, **81C,** 392, 1976.
15. A. G. Gaydon, Dissociation Energies and Spectra of Diatomic Molecules, Chapman and Hall Ltd., London, 1953.
16. D. L. Hildenbrand, Advances in High Temperature Chemistry. Academic Press, New York, Vol. 1, 1967.
17. G. Herzberg, Molecular Spectra and Molecular Structure. I. Spectra of Diatomic Molecules, Van Nostrand, Princeton, 1965.

Acta Physica Academiae Scientiarum Hungaricae, Tomus 46 (3), pp. 157—165 (1979)

THE GROWTH AND DECAY OF WEAK DISCONTINUITIES IN RELATIVISTIC FLUIDS WITH VIBRATIONAL RELAXATION

By

RISHI RAM and H. N. SINGH

DEPARTMENT OF APPLIED SCIENCES, INSTITUTE OF TECHNOLOGY, B.H.U., VARANASI, INDIA

(Received 8. III. 1979)

The propagation of weak discontinuities in relativistic fluids with vibrational relaxation has been studied. The velocity of propagation of a relativistic weak discontinuity has been determined. The fundamental equation governing the growth and decay of a relativistic weak wave has been obtained and solved. The relativistic results are shown to be in full agreement with earlier results of classical gasdynamics. The problem of breakdown of weak discontinuities has also been investigated. The critical time t_c is determined when the breakdown of the wave will occur and consequently a shock wave will be formed due to non-linear steepening. It is shown that there exists a critical amplitude of the wave such that all compressive waves with an initial amplitude greater than the critical one will break down and a shock-type discontinuity will be formed, while an initial amplitude less than the critical one will result in a decay of the wave. The local and global behaviour of the wave amplitude is also discussed.

I. Introduction

Weak waves have been extensively studied during the last decade. BECKER [1] and BOWEN and CHEN [2] studied various properties of acceleration waves in non-equilibrium flows. RARITY [3] studied the problem of breakdown of acceleration waves in flows with vibrational relaxation.

The recent advances in space technology have drawn a great deal of attention towards the study of wave propagation in relativistic gasdynamics. ECKART [4] and TAUB [5] provided theoretical foundations of relativistic shock waves. The relativistic theory of propagation of weak waves in a perfect gas has been treated by SAINI [6], COBURN [7] and KANWAL [8]. The growth of weak waves in relativistic gasdynamics has also been studied by MCCARTHY [9] for an ideal perfect gas. Nonequilibrium effects on the breakdown of weak waves have been recently studied by RAM [10]. The main academic interest of the present paper is to study the problem of growth and decay of relativistic weak waves in gas flows with vibrational relaxation and to determine a critical stage when there occurs a breakdown of the weak wave and the consequent formation of a shock wave.

II. Basic preliminaries

The notations used in this paper are, with a few minor exceptions, identical with those employed by GROT and ERINGEN [11].

Let X^k be the rectangular coordinates of a material point in a three dimensional space. The motion of a material body can be described by a new set of coordinates x^k given by

$$x^k = x^k(X^i, x^4); \quad x^4 = ct, \quad (i, k = 1, 2, 3),$$

where t is the time and c is the constant velocity of light in vacuum. Let us introduce the concept of an Einstein—Riemann space V_4 by four coordinates $x^\alpha = (x^k, x^4)$ with a metric $ds^2 = \Gamma_{\alpha\beta} dx^\alpha dx^\beta$. The metric has constant components given by

$$\Gamma^{\alpha\beta} = \Gamma_{\alpha\beta};$$

$$\Gamma^{ij} = \Gamma_{ij} = \delta_{ij}, \quad \Gamma^{44} = \Gamma_{44} = -1.$$

The world velocity can be expressed as

$$U^\alpha(x^\beta) = \beta\left(\frac{v^k}{c}, 1\right), \quad U^\alpha U^1_\alpha = -1; \tag{2.1}$$

where

$$v^k = c\frac{\partial x^k}{\partial x^4}, \quad \beta = (1 - v^2/c^2)^{-1/2}. \tag{2.2}$$

Here the range of Latin indices is 1, 2, 3 and that of Greek indices is 1, 2, 3, 4. A dummy index will usually imply summation unless specified otherwise.

The invariant derivative of any function $\varphi(x^\alpha)$ can be expressed as

$$D\varphi = \frac{\beta}{c}\left(\frac{\partial\varphi}{\partial t} + v^i\varphi_{,i}\right) = U^\alpha\varphi_{,\alpha}. \tag{2.3}$$

The equations of motion of a gas with vibrational relaxation in a relativistically correct form can be written in the form:

$$(\varrho U^\alpha)_{,\alpha} = 0 \tag{2.4}$$

$$T^{\alpha\beta}_{,\beta} = 0, \tag{2.5}$$

$$Dq - \frac{\beta}{c}\varrho\Phi(\bar{q} - q) = 0, \tag{2.6}$$

where

$$T^{\alpha\beta} = \omega U^{\alpha} U^{\beta} + p s^{\alpha\beta},$$
$$s^{\alpha\beta} = U^{\alpha} U^{\beta} + \delta^{\alpha\beta},$$
$$\omega = \varrho c^2 (1 + e/c^2 + kq/c^2) .$$

Here p, ϱ, $T^{\alpha\beta}$, e, Φ and q, $\bar{q}$ respectively represent the gas pressure, the particle density per unit volume, the energy momentum tensor, the internal energy per unit mass, the relaxation frequency and the vibrational energy per unit mass of the gas, local equilibrium value of q. Here k is the constant specific heat of the internal energy reservoir. A comma followed by an index denotes partial differentiation with respect to the corresponding coordinate.

From (2.4) and (2.5) we get

$$\varrho\sigma c^2 DU^{\alpha} + s^{\alpha\beta} p_{,\beta} = 0 , \tag{2.7}$$

$$(\varrho\sigma c^2 U^{\beta})_{,\beta} - U^{\beta} p_{,\beta} = 0 , \tag{2.8}$$

where $\sigma = 1 + h/c^2$, $h = h(p, \eta, q)$ is the enthalpy of the system per unit mass.

The Eqs. (2.7) and (2.8), respectively, represent the conservation of momentum and energy in a relativistic fluid motion with vibrational relaxation. In view of (2.3) and (2.4) the Eq. (2.8) can be expressed in the form

$$\varrho Dh - Dp = 0 , \tag{2.9}$$

where

$$h = \frac{\gamma}{\gamma - 1} \frac{p}{\varrho} + kq , \tag{2.10}$$

γ is the ratio of specific heats of the gas.

In consequence of (2.9) and the first law of thermodynamics we have

$$D\eta = -\frac{k}{T} Dq , \tag{2.11}$$

where η is the entropy of the system per unit mass and T is the absolute temperature.

Using (2.10) in (2.9) we get

$$Dp - a_f^2 D\varrho + k(\gamma - 1)\Phi \frac{\beta}{c} \varrho^2 (\bar{q} - q) = 0 , \tag{2.12}$$

where a_f is frozen speed of sound given by

$$a_f^2 = \left(\frac{\partial p}{\partial \varrho}\right)_{\eta, q} .$$

III. Compatibility conditions on a time-like hyper surface

Let $\Sigma(x^\mu)$ be a regular surface in an Einstein—Riemann space with parametric equations

$$x^\mu = \psi^\mu(b^1, b^2, b^3)\,, \tag{3.1}$$

where b^1, b^2 and b^3 are parametric coordinates of the surface. The vectors $x^\alpha_{;\tau}$, where semicolon denotes covariant differentiation with respect to b^τ, are tangential to $\Sigma(x^\mu)$. The surface $\Sigma(x^\mu)$ is called a time-like hypersurface if N_α, the components of the unit normal vector to the surface, is a space-like vector, i.e.

$$N_\alpha N^\alpha = 1\,.$$

The time-like hypersurface $\Sigma(x^\mu)$ may be regarded as a surface $s(t)$ in space-time for which the parametric equations are

$$x^4 = ct, \quad x^i = x^i(b^1, b^2, x^4)\,. \tag{3.2}$$

If n_i are the components of the unit space normal to $s(t)$ and G is its speed of propagation, then we can write

$$N^\alpha = \bar\beta\{n^i, G/c\}; \quad N_\alpha = \bar\beta\{n_i, -G/c\}\,, \tag{3.3}$$

where

$$\bar\beta = (1 - G^2/c^2)^{-1/2}.$$

Let R be the region of the Einstein—Riemann space V_4 which is divided by the time-like hypersurface $\Sigma(x^\mu)$ into two regions R_1 and R_2. Let any flow parameter z with its first and second derivatives be continuous in $R_1 + \Sigma$ and $R_2 + \Sigma$, but suffer a discontinuity in its first and second derivatives across Σ. Such a discontinuity is called a 'weak discontinuity' or 'weak wave'. If $[z]$ denotes the jump in z across $\Sigma(x^\mu)$, the geometrical compatibility conditions to be satisfied across $\Sigma(x^\mu)$ are [12]

$$[z_{,\alpha}] = CN_\alpha\,, \tag{3.4}$$

$$[z_{,\alpha\beta}] = \bar C N_\alpha N_\beta + 2N_{(\alpha} x^\tau_{\beta)} C_{;\tau} - C b_{\tau\varphi} x^\tau_{(\alpha} x^\varphi_{\beta)}\,, \tag{3.5}$$

where

$$C = [z_{,\alpha}]\, N^\alpha, \qquad \bar C = [z_{,\alpha\beta}]\, N^\alpha N^\beta,$$

$$b_{\tau\varphi} = N_\alpha\, x^\alpha_{;\tau\varphi}\,, \quad x^\tau_\beta = \Gamma_{\alpha\beta} a^{\tau\varphi}\, x^\alpha_{;\varphi}\,,$$

$$M_{(\alpha\beta)} = \frac{1}{2}(M_{\alpha\beta} + M_{\beta\alpha})\,, \quad a_{\alpha\beta} = \Gamma_{\tau\varphi}\, x^\tau_{;\alpha}\, x^\varphi_{;\beta}\,.$$

IV. Law of propagation

Using (3.4) and the identity

$$a^{\tau\varphi} x^{\alpha}_{\tau} x^{\beta}_{\varphi} = \Gamma^{\alpha\beta} - N^{\alpha} N^{\beta},$$

we get

$$[Dz] = V[z_{,\beta} N^{\beta}] + \delta[z], \tag{4.1}$$

where

$$\delta[z] = U^{\mu}[z]_{,\mu} - VN^{\mu}[z]_{,\mu}. \tag{4.2}$$

Taking jumps in (2.4), (2.6), (2.7) and (2.12) and making use of (4.1) we get

$$V\nu + \varrho\lambda^{\alpha} N_{\alpha} = 0, \tag{4.3}$$

$$V\varepsilon = 0, \tag{4.4}$$

$$\varrho\sigma c^2 V\lambda^{\alpha} + \mu s^{\alpha\beta} N_{\beta} = 0, \tag{4.5}$$

$$V\mu - a_f^2 V\nu = 0 \tag{4.6}$$

where

$$\lambda^{\alpha} = [U^{\alpha}_{,\beta}] N^{\beta}, \quad \nu = [\varrho_{,\beta}] N^{\beta}, \quad \mu = [p_{,\beta}] N^{\beta},$$

$$\varepsilon = [q_{,\beta}] N^{\beta}, \quad V = U^{\alpha} N_{\alpha}. \tag{4.7}$$

From (4.3), (4.5) and (4.6) we get

$$V^2 = \frac{a_f^2}{c^2(\sigma - a_f^2/c^2)}. \tag{4.8}$$

Using (2.1) and (3.3) we get

$$V = -\beta\bar{\beta} G_0/c, \tag{4.9}$$

where $G_0 = G - v^i n_i$ is the local speed of propagation of the surface $s(t)$ in space-time, which coincides with G in the instantaneous rest frame. In consequence of (3.3), (4.2) and (4.9) we have in the local instantaneous rest frame:

$$c\delta[z] = \bar{\beta}^2 \frac{\delta}{\delta t}[z], \tag{4.10}$$

where $\delta/\delta t$ is THOMAS' delta derivative [13].

From (4.8) and (4.9) we get

$$G_0^2\{\sigma\beta^2 + a_f^2/c^2(1-\beta^2)\} + (2G_0 + v^i n_i)\, a_f^2/c^2\, n_i v^i = a_f^2. \tag{4.11}$$

In an instantaneous rest frame the Eq. (4.11) assumes the form

$$G_0^2 = a_f^2/\sigma. \tag{4.12}$$

The velocity of propagation G_0 given by (4.12) in an instantaneous rest frame is in full agreement with earlier results of RARITY [3] and MCCARTHY [9] in particular cases.

If the medium is in uniform state of rest ahead of the wave front and if the motion is studied in the rest frame of this uniform state, the speed of propagation G_0 is a constant.

V. The growth equation

In this Section we shall derive a fundamental growth equation which will govern the growth and decay of a weak discontinuity during its course of propagation.

Now we define the amplitude b of the wave $\Sigma(x^\mu)$ by the relation

$$b = c\lambda = c\lambda^\alpha N_\alpha = c\lambda^\alpha \overset{*}{N}_\alpha, \tag{5.1}$$

where $\overset{*}{N}{}^\alpha = s^{\alpha\beta} N_\beta$ are the space-like components of N^α.

Differentiating (2.4), (2.7) and (2.12) with respect to x^β and taking jumps across $\Sigma(x^\mu)$ with the help of (3.4) and (3.5) we get

$$\begin{aligned}
&\varrho\left(\sigma + \frac{a_f^2}{V^2c^2}\right)\delta(\lambda^\alpha N_\alpha) + \varrho V\left\{\sigma - \frac{a_f^2(1+V^2)}{V^2c^2}\right\}\bar{\lambda}^\alpha N_\alpha - \\
&- \varrho a_f^2 \frac{(1+V^2)}{Vc^2}\, x_\alpha^\tau \lambda^\alpha_{;\tau} - \varrho\sigma\lambda^\alpha\delta(N_\alpha) + \frac{a_f^2}{Vc^2}\lambda^\beta N_\beta N_\alpha s^{\alpha\gamma}\delta\left(\frac{\varrho N_\gamma}{V}\right) + \\
&+ \varrho\lambda^2\left\{(\gamma-1)\, a_f^2 \frac{(1+V^2)}{V^2c^2} + 2a_f^2\frac{(1+V^2)}{V^2c^2} - 3a_f^2/c^2\right\} + \\
&+ \varrho\lambda(\gamma-1)\Phi k\frac{\beta}{C}\left\{2\varrho(\bar{q}-q) + \varrho^2\left(\frac{\partial\bar{q}}{\partial p}\, a_f^2 + \frac{\partial\bar{q}}{\partial\varrho}\right)\right\}\frac{(1+V^2)}{V^2c^2} - \\
&- (\gamma-1)\Phi\varrho^2 k(\bar{q}-q)\frac{\beta^3}{c^3}\, v_i\lambda^i\, \frac{(1+V^2)}{Vc^2} = 0.
\end{aligned} \tag{5.2}$$

In view of (4.8) the coefficient of $\bar{\lambda}^{\alpha}N_{\alpha}$ in (5.2) vanishes and, therefore, we get the following equation to be satisfied by λ:

$$\varrho(2\sigma - a_f^2/c^2)\,\delta(\lambda) - \varrho\frac{a_f^2}{Vc^2}\{x_{\alpha}^{\tau}\overset{*}{N}{}^{\alpha}\lambda_{;\tau} + \lambda\overset{*}{N}{}^{\alpha}_{,\alpha}\} + \varrho\lambda^2\{(\gamma+1) - 3a_f^2/c^2\} +$$

$$+ \varrho\lambda(\gamma-1)\Phi\frac{\beta}{c}k\left\{2\varrho(\bar{q}-q) + \varrho^2\left(\frac{\partial\bar{q}}{\partial p}a_f^2 + \frac{\partial\bar{q}}{\partial\varrho}\right)\right\}\frac{\sigma}{a_f^2} -$$

$$- (r-1)\Phi\varrho^2k(\bar{q}-q)\frac{\beta^3}{c^3}v_i\lambda^i\sigma V/a_f^2 + \lambda\frac{a_f^2}{Vc^2}N_{\alpha}S^{\alpha\gamma}\delta(\varrho N_{\gamma}/V) -$$

$$- \varrho\sigma(1+V^2)^{-1}\lambda\overset{*}{N}{}^{\alpha}\delta(N_{\alpha}) = 0\,, \tag{5.3}$$

which is the required growth equation governing the global behaviour of the amplitude $c\lambda$ of a relativistic wave in gases with vibrational relaxation. In a local instantaneous rest frame for which $\overset{*}{N}{}^{\alpha} = (1+V^2)^{1/2}\ (n^i,\ 0)$, the Eq. (5.3) takes on a particularly simple form

$$A\frac{\delta b}{\delta t} - (\Omega - E)\,b + Bb^2 = 0\,, \tag{5.4}$$

where

$$\Omega = -\frac{1}{2}\frac{\partial n^i}{\partial x^i}\,,$$

$$A = \frac{G_0}{2a_f^2}\,\frac{2\sigma - a_f^2/c^2}{1 - G_0^2/c^2}\,,$$

$$B = \frac{G_0}{2a_f^2}\{(\gamma+1)\sigma - 3a_f^2/c^2\}\,,$$

$$E = \frac{G_0}{2a_f^4}\sigma(\nu-1)\Phi k\left\{2\varrho(\bar{q}-q) + \varrho^2\left(\frac{\partial\bar{q}}{\partial p}a_f^2 + \frac{\partial\bar{q}}{\partial\varrho}\right)\right\}.$$

Here Ω is the mean curvature of the propagating surface $s(t)$ in space-time.

VI. Local and global behaviour of waves

In this Section we shall study the local and global behaviour of weak discontinuity in an instantaneous rest frame. If s denotes the distance traversed by the wave along its normal trajectory in time t, we have

$$\frac{\delta s}{\delta t} = G_0\,, \tag{6.1}$$

which gives a relation $s = G_0 t$, where G_0 is the constant speed of the wave front propagating in a uniform state ahead of it in the rest frame of this uniform state. For non-plane waves $\Omega \neq 0$ and is calculated in the form [14]

$$\Omega = \frac{\Omega_0 - K_0 s}{1 - 2\Omega_0 s + K_0 s^2}, \tag{6.2}$$

where Ω and K_0 are the values of the mean and Gaussian curvatures of the initial wave front.

Using (6.1) and (6.2) in (5.4) and integrating we get

$$b(t) = b_0 F(t) \left\{1 + \frac{B b_0}{A} \int_0^t F(\tau)\, d\tau\right\}^{-1}, \tag{6.3}$$

where

$$F(t) = e^{-Et}\{(1 - K_1 G_0 t)(1 - K_2 G_0 t)\}^{-1/2AG_0}. \tag{6.4}$$

Here b_0 is the initial wave amplitude at time $t = 0$ and K_1, K_2 are the principal curvatures of the initial wave front which are negative for diverging waves and positive for converging waves.

Let us consider the case of a diverging wave with initial amplitude $b_0 > 0$. From (6.4) we observe that $F(t)$ is a bounded and monotonically decreasing function of t and tends to zero as $t \to \infty$. Thus for the interval $(0, \infty)$ of t we have

$$0 \leq F(t) \leq 1, \quad 0 \leq \int_0^t F(\tau)\, d\tau < \infty. \tag{6.5}$$

Using (6.5) in (6.3) we get

$$\lim_{t \to \infty} b(t) = 0,$$

which shows that the wave will continuously decay and will be damped out ultimately. On the other hand if $b_0 < 0$ (the case of a compressive wave) there exists a critical value b_c of $|b_0|$ for diverging waves given by

$$b_c = \frac{A}{B}\left\{\int_0^\infty F(t)\, dt\right\}^{-1}.$$

For compressive waves with initial amplitude b_0 numerically less than b_c we have

$$0 < 1 + \frac{B}{A} b_0 \int_0^t F(\tau)\, d\tau < 1 \quad \text{for} \quad 0 < t < \infty. \tag{6.6}$$

Since K_1 and K_2 are negative for diverging waves, we have

$$\lim_{t \to \infty} F(t) = 0. \tag{6.7}$$

In consequence of (6.6) and (6.7) we have

$$\lim_{t\to\infty} b(t) = 0 \tag{6.8}$$

when $|b_0| > b_c$, there exists a finite critical time t_c given by

$$\int_0^{t_c} F(t)\,dt = \frac{A}{B|b_0|}, \tag{6.9}$$

such that

$$\lim_{t\to t_c} b(t) = \infty\,. \tag{6.10}$$

From (6.8) and (6.10) we conclude that a weak compressive wave with initial amplitude numerically less than b_c will decay, while a weak compressive wave with initial amplitude numerically greater than b_c will grow and after a finite critical time t_c it will terminate into a shock wave in consequence of (6.10). The underlying mathematical fact is that due to non-linear steepening the flow parameters themselves suffer a discontinuity culminating into a shock wave.

From (6.9) we get

$$\frac{dt_c}{dE} = \int_0^{t_c} t\,F(t)\,dt/F(t_c) > 0\,,$$

which proves that the critical time t_c increases with relaxation effects. This shows that the relaxation process will delay the shock formation and thus has a stabilizing effect.

REFERENCES

1. E. Becker, Areo. J., **74**, 736, 1970.
2. R. M. Bowen and P. J. Chen, J. Math. Phys., **13**, 958, 1972.
3. B. S. H. Rarity, J. Fluid Mech., **27**, 49, 1967.
4. C. Eckart, Phys. Rev., **58**, 919, 1940.
5. A. H. Taub, Phys. Rev., **74**, 328, 1948.
6. G. Saini, Proc. R. Soc., **A260**, 61, 1961.
7. N. Coburn, J. Math. Mech., **10**, 361, 1961.
8. R. P. Kanwal, J. Math. Mech., **15**, 379, 1966.
9. M. F. McCarthy, Int. J. Engng. Sci., **7**, 209, 1969.
10. R. Ram, Acta Phys. Hung., **44**, 195, 1978.
11. R. A. Grot and A. C. Eringen, Int. J. Engng. Sci., **4**, 611, 1966.
12. C. Trusedell and R. A. Toupin, The Classical Field Theories, in Handbuch der Physik, **111/1** Springer, 1960.
13. T. Y. Thomas, J. Math. Mech., **6**, 311, 1957.
14. T. Y. Thomas, Concepts from Tensor Analysis and Differential Geometry, 2nd edition, Academic Press, 1963.
15. R. A. Grot, Int J. Engng. Sci., **6**, 295, 1968.

Acta Physica Academiae Scientiarum Hungaricae, Tomus 46 (3), pp. 167—175 (1979)

ON THE EXCITATION MECHANISM OF HOLLOW CATHODE CW NOBLE GAS MIXTURE ION LASERS

By

M. JÁNOSSY

CENTRAL RESEARCH INSTITUTE FOR PHYSICS, H-1525 BUDAPEST, P.O.B. 49

and

P. TUOVINEN

HELSINKI UNIVERSITY OF TECHNOLOGY, DEPARTMENT OF TECHNICAL PHYSICS
RAKENTAJANAUKIO 1, SF-02150 ESPOO 15, FINLAND

(Received 27. III. 1979)

CW laser operation was observed at transitions of Kr II, Ar II and Xe II in noble gas mixture hollow cathode discharges. The laser transitions are excited in two steps: 1) ionization of atoms, 2) excitation of ions to the upper laser state. It is shown that in contrast to the pulsed positive column system the dominant process of ionization of Kr atoms is not Penning collisions but electron impact. This result is found to be valid also for the CW He-Ar and He-Ne-Xe hollow cathode ion lasers. Excitation of ground state ions to the upper laser state is considered to be second kind collisions with metastable atoms.

1. Introduction

Pulsed laser oscillation in positive column He-Kr and Ne-Xe noble gas mixture discharges was obtained first by DANA and LAURES [1]. Lasing at various Kr and Xe ion transitions was observed in the afterglow 5—15 μsec after the discharge pulse. The Kr and Xe ions were assumed to be produced by Penning ionization by metastable He and Ne atoms, respectively, and excitation of these ions to the upper laser state was considered to be second kind collisions with He 2^3S (Ne 1s) metastables.

Further investigation of these pulsed laser systems has been performed by BRETON [2] and KATO [3—5].

On the basis of the two step excitation mechanism laser oscillation at the 4765 Å transition of Ar II was obtained in the afterglow of a pulsed He-Ar positive column discharge [6]. Investigations on pulsed positive column ion lasers (He-Cd 5378 Å and He-Kr 4694 Å) [7], and on the CW hollow cathode He-Cd laser [8], raised the possibility for CW operation in various noble gas mixture hollow cathode discharges.

CW laser oscillation was obtained first at the 4694 Å transition of Kr II in a hollow cathode He-Kr discharge [9]. In this experiment efforts aiming to obtain CW oscillation in the other two noble gas mixture systems were unsuccessful.

CW laser operation in He-Ar was obtained using an improved hollow cathode tube construction [10]. Experiments in the Ne-Xe system were successful by using a special high voltage hollow cathode discharge [11], and it was found that addition of He significantly increases laser output power. New CW Kr and Ar ion transitions were obtained in a high voltage hollow cathode discharge of 160 cm active length [12]. The CW noble gas mixture ion laser transitions with main operation data are summarized in Table I. An output

Table I

CW noble gas mixture ion laser transitions

Gas mixture	Wavelength (Å)	Upper state energy (eV)	Threshold current* (A)
He-Kr	Kr II		
12 torr He	6510	19.47	2.1
75 mtorr Kr	5126	19.57	4.4
	4694	19.47	1.1
	4583	19.57	4.2
	4387	19.47	4.5
	4318	19.47	2
He-Ar	Ar II		
11 torr He	6861	19.87	2.3
0.7 torr Ar	6483	19.97	2.5
	4765	19.87	2.2
	4579	19.97	4.2
	4545	19.87	3.5
He-Ne-Xe	Xe II		
7 torr He	5314	16.43	4
4 torr Ne	4863	16.43	12
45 mtorr Xe			
Energy of exciting	He 2^3S	19.82	
metastable states	Ne $1s_5$	16.62	

* Threshold currents measured in a high voltage hollow cathode discharge tube of 160 cm active length

power of 100 mW was observed at the strongest 4694 Å Kr II transition. CW laser action in flute type and segmented bore He-Kr hollow cathode discharge tubes was investigated recently [13, 14].

In this paper the excitation mechanism of the cw hollow cathode He-Kr ion laser is considered in detail. It is shown by calculations that

contrary to the pulsed positive column system, the dominant process of ionization of Kr atoms is not Penning ionization but electron impact. This result is found to be valid also for the CW He-Ar and He-Ne-Xe hollow cathode lasers.

2. Excitation processes

For excitation of the CW He-Kr hollow cathode ion laser a two step process is considered: 1) ionization of Kr atoms, 2) excitation of these ions to the upper laser level. This is shown schematically in Fig. 1, in which relevant energy levels of the Kr ion and the exciting He metastable are also shown.

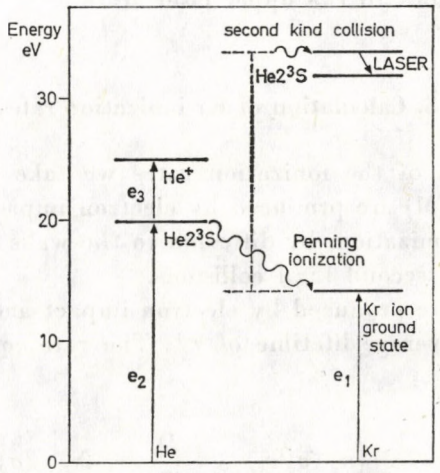

Fig. 1. Partial energy level diagrams of Kr and He (e = electron impact)

In our considerations population of the lower laser level is assumed to be negligible.

In ionization of Kr atoms (1) the following atomic processes are relevant: electron impact ionization

$$\mathrm{Kr} + \mathrm{e} \rightarrow \mathrm{Kr}^+ + \mathrm{e} + \mathrm{e}$$

and Penning ionization

$$\mathrm{He}\ 2^3\mathrm{S} + \mathrm{Kr} \rightarrow \mathrm{He} + \mathrm{Kr}^+ + \mathrm{e} + \Delta\mathrm{E}\,.$$

He 2^3S metastables are produced by electron impact excitation

$$\mathrm{He} + \mathrm{e} \rightarrow \mathrm{He}\ 2^3\mathrm{S} + \mathrm{e}$$

and they are de-excited mainly by electron impact ionization:

$$\mathrm{He}\ 2^3\mathrm{S} + \mathrm{e} \rightarrow \mathrm{He}^+ + \mathrm{e} + \mathrm{e}\,.$$

In step (2) Kr ions are excited by second kind collisions between metastable He atoms and ground state Kr ions

$$\mathrm{He}\ 2^3\mathrm{S} + \mathrm{Kr}^+ \rightarrow \mathrm{Kr}^{+*} + \mathrm{He}\,.$$

First a calculation of Penning and electron impact ionization rates is given to determine which of these mechanisms is dominant in producing ground state Kr ions. This is followed by a discussion, which deals with excitation of ground state Kr ions to the upper laser state.

3. Calculation of Kr ionization rates

For calculation of the ionization rates we take the following model: He 2^3S metastables (M) are produced by electron impact excitation and lost by electron impact ionization, by diffusion to the walls of the discharge tube and by Penning and second kind collisions.

Kr ions (N^+) are produced by electron impact and Penning ionization, and they have an average lifetime of τ^+. The rate equations are then the following:

$$\frac{dM}{dt} = N_{\mathrm{He}} n_e \langle \sigma_e^M v_e \rangle - M\left(n_e \langle \sigma_e^D v_e \rangle + \frac{D}{\Lambda^2 p} + N_{\mathrm{Kr}} \langle \sigma_p v \rangle + N^+ \langle \sigma_c v \rangle\right), \quad (1)$$

$$\frac{dN^+}{dt} = N_{\mathrm{Kr}} n_e \langle \sigma_e^+ v_e \rangle + M N_{\mathrm{Kr}} \langle \sigma_p v \rangle - N^+\left(\frac{1}{\tau^+} + M \langle \sigma_c v \rangle\right), \quad (2)$$

where

N_{He} = density of ground state He atoms;
n_e = electron density;
σ_e^M = cross section for He 2^3S production by electron impact;
v_e = velocity of electron;
σ_e^D = He 2^3S destruction (ionization) cross section by electron impact;
D = diffusion constant of He 2^3S in He;
Λ = characteristic diffusion length of He 2^3S in He;
σ_p = Penning ionization cross section of Kr atoms by He 2^3S atoms;
σ_c = cross section for second kind collision of Kr ions and He 2^3S atoms;

p = He pressure;
v = relative velocity of colliding atoms;
σ_e^+ = total electron impact ionization cross section of Kr.

In a stationary state,

$$\frac{dM}{dt} = 0, \quad \frac{dN^+}{dt} = 0. \tag{3}$$

Then, from (1), taking into account that $N^+ \ll N_{\mathrm{Kr}}$ the metastable density in steady state is,

$$M = \frac{N_{\mathrm{He}} n_e \langle \sigma_e^M v_e \rangle}{n_e \langle \sigma_e^D v_e \rangle + D/\Lambda^2 p + N_{Kr} \langle \sigma_p v \rangle} \tag{4}$$

and the ratio of electron impact and Penning ionization rates of Kr is

$$R = \frac{N_{\mathrm{Kr}} n_e \langle \sigma_e^+ v_e \rangle}{M N_{\mathrm{Kr}} \langle \sigma_p v \rangle} = \frac{n_e \langle \sigma_e^+ v_e \rangle}{M \langle \sigma_p v \rangle}. \tag{5}$$

In order to calculate the metastable density M and then the ionization ratio R, following data are needed: electron density, cross sections as a function of energy, electron energy distribution function, He metastable diffusion coefficient and diffusion length.

The following rate integrals have to be calculated: $\langle \sigma_e^M v_e \rangle$, $\langle \sigma_e^D v_e \rangle$, $\langle \sigma_e^+ v_e \rangle$, $\langle \sigma_p v \rangle$. The last integral is approximated by $\bar{\sigma}_p \bar{v}_{\mathrm{He}}$, where average values $\bar{\sigma}_p = 9.7 \times 10^{-16}$ cm^2 [15] and $\bar{v}_{\mathrm{He}} = 1.5 \times 10^5$ cm/s are used.

The remaining three integrals are all of the same type:

$$\langle \sigma_i v_e \rangle = \left(\frac{2}{m_e} \right)^{1/2} \int_0^\infty E^{1/2} f(E) \, \sigma_i(E) dE, \tag{6}$$

where $\sigma_i = \sigma_e^M$, σ_e^D or σ_e^+, and $f(E)$ is the electron energy distribution function. The cross sections used in the calculation are shown in Fig. 2. σ_e^D is obtained from [16], σ_e^M from [17] and σ_e^+ from [18]. Because the cross sections are zero below the threshold energies (see Fig. 2), integration is carried out from $E_{th,i}$ to infinity. The integrals have been calculated in two cases: first assuming a Maxwellian electron energy distribution function with (somewhat arbitrarily) $kT_e = 5$ eV and then using data from [19], where electron energy distributions have been measured in the negative glow of an abnormal glow discharge. Functions $f(E)$ in both cases are shown in Fig. 3. In case of Maxwellian distribution the integrals can be calculated exactly, but in the other case numerically.

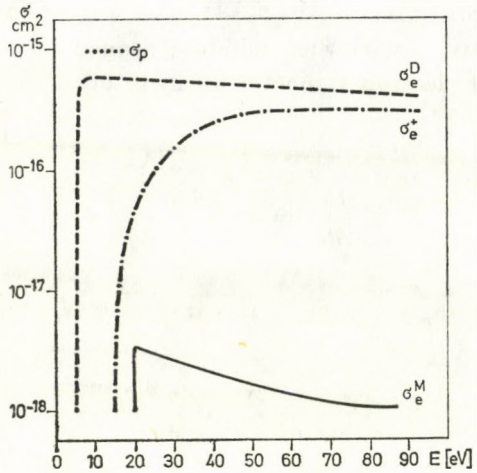

Fig. 2. Electron impact cross sections relevant to the CW He-Kr hollow cathode ion laser as a function of electron energy (σ_e^M = He 2^3S production cross section, σ_e^D = He 2^3S destruction cross section and σ_e^+ = Kr ionization cross section). The value of the Penning ionization cross section σ_p is also shown

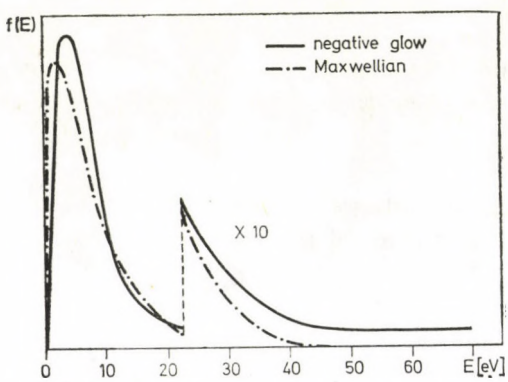

Fig. 3. Maxwellian distribution function with $kT_e = 5$ eV and electron energy distribution measured in [19] in the negative glow at 1.5 mm from the cathode surface (He pressure 10 torr, discharge current 3.5 mA)

In the calculation of R $p_{\mathrm{He}} = 15$ torr was taken. The diffusion coefficient is $D = 470$ cm^2 torr s^{-1} [20]. For a cylinder of radius r and height h the following expression of the diffusion length is used [21]:

$$\Lambda^2 = \left[\left(\frac{\pi}{h}\right)^2 + \left(\frac{2 \cdot 4}{r}\right)^2\right]^{-1}. \tag{7}$$

The first term in (7) can be neglected. For a typical hollow cathode diameter $2r = 5$ mm and $\Lambda^2 = 1.1 \times 10^{-2}$ cm^2 results.

Electron density has been obtained by extrapolating the data given in [22] up to a current of 40 mA/cm at 8 torr He pressure. The value of n_e is then $1.5 \times 10^{13}/\text{cm}^3$. No data of n_e are given in [22] for higher He pressures, but since electron density does not change very strongly with He pressure, this value is taken for the calculation at 15 torr. Recent measurements on electron density [23, 24] give values near to that obtained in this way.

4. Discussion

When using a Maxwellian distribution function a value of 0.3 is obtained for the ionization ratio R, whereas using the electron energy distribution measured in the negative glow, $R = 120$ results. In the former case it can be said that electron impact ionization and Penning ionization rates are about of the same order of magnitude but in the latter case electron impact ionization is dominant.

The former result is not valid for our case, however, because a Maxwellian distribution is not a good approximation for a hollow cathode discharge since this is known to have much more high and low energy electrons.

Possible sources of error in our calculation are the following: The measured cross sections are known to be accurate to 10—20 per cent. The electron density value may deviate by 50 to 100 per cent from the actual value. The main source of error is in the electron energy distribution, because the measured data do not correspond exactly to our experimental situation. It is difficult to estimate exactly this error, but even if the value of R has an error of a factor of ten, which is with high probability an upper limit, the final result remains the same, i.e. in the He-Kr hollow cathode discharge electron impact ionization is dominant over Penning collisions in producing Kr ions. Comparing this result with that obtained using a Maxwellian distribution it can be seen that the high energy electrons play an important role in producing Kr ions in the hollow cathode discharge.

It was observed that output power and efficiency increases in a high voltage hollow cathode He-Kr laser. This is due to the larger number of high energy electrons in such a tube, thus in this case electron impact ionization of Kr is even more effective than in a conventional hollow cathode discharge.

In the pulsed positive column He-Kr discharge laser oscillation occurs in the afterglow when the electrons have lost most of their energy and no electron impact ionization takes place. This means that in the pulsed laser system Penning ionization is the process producing ground state Kr ions.

Because the relevant cross sections in the case of Ar and Xe do not differ much from those of Kr [18], our conclusions are valid for the other noble gas mixture ion lasers as well.

Since the Maxwellian electron energy distribution is more or less valid for a positive column, from our results it follows that in this case the Kr ion density is much less. This shows that it should not be easy to obtain cw laser oscillation in a positive column He-Kr discharge and may explain why efforts aiming on this were unsuccessful [25].

5. Excitation of the upper laser state

In the following some aspects of excitation of ground state ions to the upper laser level are discussed. It is known that only those Kr ion laser transitions oscillate in which the upper level is in near resonance with the He 2^3S state. Also these laser transitions do not operate in pure Kr. From these facts it can be concluded that excitation of ground state Kr ions to the upper laser state is due to second kind collisions between ground state Kr ions and He 2^3S metastables.

Although the energy of the excited state of Ar ion is a little higher than that of He 2^3S (Table I), the second kind collision is assumed to be energetically possible because the Ar ions have large enough kinetic energy in the discharge to cover the energy difference [26].

The role of He in enhancing laser output in the He-Ne-Xe laser is probably the following: Electron density and the component of high energy electrons is larger in the He-Ne-Xe mixture than in Ne-Xe and thus much more Ne metastables and Xe ions are excited. In the He-Ne mixture second kind collisions between He metastables and Ne also lead to an enhancement of Ne metastable density.

6. Summary

Excitation mechanism of the cw He-Kr hollow cathode ion laser has been studied. Considering a two step excitation process it has been shown that the dominant process in producing Kr ions is electron impact. The second step, excitation of these ground state ions, is due to second kind collisions between Kr ions and He triplet metastable atoms. This kind of mechanism is found to be valid for the other cw noble gas mixture ion lasers as well.

Acknowledgement

Discussions on this work with K. Rózsa, L. Csillag and J. Bergou are gratefully acknowledged. One of the authors (P. T.) thanks the Hungarian Academy of Sciences for providing him a scholarship.

REFERENCES

1. L. DANA and P. LAURES, Proceedings of the IEEE, **53,** 78, 1965.
2. J. BRETON, IEEE Journal of Quantum Electronics, QE—**9,** 854, 1973.
3. I. KATO, M. NAKAYA and T. SHIMIZU, Japanese Journal of Applied Physics, **14,** 2001, 1975.
4. I. KATO, T. SATAKE and T. SHIMIZU, Japanese Journal of Applied Physics, **16,** 597, 1977.
5. I. KATO, A. IWASAKI and T. SHIMIZU, Japanese Journal of Applied Physics, **16,** 1219, 1977.
6. M. JÁNOSSY, L. CSILLAG, K. RÓZSA and T. SALAMON, Physics Letters, **47A,** 411, 1974.
7. See M. JÁNOSSY, Thesis, Budapest 1974 (in Hungarian).
8. K. RÓZSA, L. CSILLAG, M. JÁNOSSY and T. SALAMON, Reports of the Central Research Institute for Physics No. 39, 1973; Kvantovaja Elektronika, **1,** 671, 1974.
9. M. JÁNOSSY, L. CSILLAG, K. RÓZSA and T. SALAMON, Physics Letters, **46A,** 379, 1974.
10. M. JÁNOSSY, L. CSILLAG and K. RÓZSA, Physics Letters, **63A,** 84, 1977.
11. K. RÓZSA, M. JÁNOSSY, J. BERGOU and L. CSILLAG, Optics Communications, **23,** 15, 1977.
12. M. JÁNOSSY, K. RÓZSA, L. CSILLAG and J. BERGOU, Physics Letters, **68A,** 317, 1978.
13. N. K. VUCHKOV, M. G. GROZEVA and N. V. SABOTINOV, Optics Communications, **27,** 114, 1978.
14. Y. PACHEVA, M. STEFANOVA and P. PRAMATAROV, Optics Communications, **27,** 121, 1978.
15. K. L. BELL, A. DALGARNO and A. E. KINGSTONE, Journal of Physics B, ser. 2, **1,** 18, 1968.
16. D. R. LONG and R. GEBALLE, Phys. Rev. A, **1,** 260, 1970; P. GILL, Thesis, Oxford, 1975.
17. B. L. MOISEIWITSCH and S. J. SMITH, Rev. Mod. Phys., **40,** 238, 1968.
18. F. EGGER and T. D. MÄRK, Proceedings of the Symposium on Atomic and Surface Physics, Tirol 1978, p. 51.
19. P. GILL and C. E. WEBB, Journal of Physics D, Applied Physics, **10,** 299, 1977.
20. A. V. PHELPS, Phys. Rev. **99,** 1307, 1955.
21. See e.g. C. S. WILLETT, An Introduction to Gas Lasers: Population Inversion Mechanisms, Pergamon Press, 1974, p. 77.
22. A. N. SOLDATOV, Optics and Spectroscopy, **31,** 181, 1977.
23. I. K. BELAL and M. H. DUNN, Journal of Physics D, Applied Physics, **11,** 313, 1978.
24. P. GILL and C. E. WEBB, Journal of Physics D, Applied Physics, **11,** 245, 1978.
25. L. DANA, J. BRETON, private communications.
26. G. FRANCIS, Handbuch der Physik, **23,** Springer, Berlin 1956, p. 136.

Acta Physica Academiae Scientiarum Hungaricae, Tomus 46 (3), pp. 177—183 (1979)

ROLE OF POINT-DEFECT SCATTERING IN THE LATTICE THERMAL CONDUCTIVITY OF AN INSULATOR: APPLICATION TO GaAs

By

M. C. AL-EDANI and K. S. DUBEY

DEPARTMENT OF PHYSICS, COLLEGE OF SCIENCE, UNIVERSITY OF BASRAH, BASRAH, IRAQ

(Received in revised form 27. III. 1979)

The role of the point-defect scattering relaxation rate has been studied in the lattice thermal conductivity of an insulator by calculating the lattice thermal conductivity of GaAs for the different values of the point-defect scattering strength. All calculations have been performed in the frame of the recently proposed model of DUBEY and MISHO of the phonon conductivity of an insulator. The study is made for low as well as high values of the point-defect scattering strength in the entire temperature range 4—100 K.

The lattice thermal resistivity of an insulator has been studied by several workers and is found that the transportation of heat by lattice waves in a solid is governed by the anharmonicities of the lattice forces such as various imperfections of the crystal lattice and by the external boundary. It is well known [1—4] that the point-defects (isotopic impurities) are one of the very important scatterers of phonons at temperatures near the conductivity maxima, and the lattice thermal resistivity of an insulator is mainly due to the point-defect scattering relaxation rate at these temperatures. Thus, there is a need to study the role of the point-defect scattering relaxation rate in the calculation of the lattice thermal conductivity. Recently, the authors [4, 6] studied the phonon conductivity of GaAs in the entire temperature range 2—800 K. But their studies are confined to see the role of the three phonon and boundary scattering processes only, while the study of the role of the point-defect scattering has been totally ignored in their previous studies. In continuation of the earlier study, the aim of the present note is to study the role of the point-defect scattering relaxation rate in the calculation of the lattice thermal conductivity. The study is performed by introducing a new parameter "p" which is the ratio of the point-defect scattering strengths of the normal sample and the sample under study (having an impurity concentration different from the normal sample), similar to the previous study of the role of the boundary scattering [6]. The new parameter "p" can be defined as p = (point-defect scattering strength for the sample under study)/(point-defect scattering strength of the normal sample) and it depends totally on the extra impurities present in the normal sample. GaAs is taken as an example and its lattice thermal conduc-

tivity has been calculated in the entire temperature range 4—100 K for the different values of "p".

Following DUBEY and MISHO [7, 8] the phonon conductivity of an insulator can be expressed as

$$K = K_T + K_L, \tag{1}$$

$$K_T = (C/v_{T1}) \int_0^{\theta_1/T} \tau_{c,T} F_1(x)\, dx + (C/v_{T2}) \int_{\theta_1/T}^{\theta_2/T} \tau_{c,T} F_2(x)\, dx, \tag{2}$$

$$K_L = (C_1/v_{L1}) \int_0^{\theta_3/T} \tau_{c,L} F_3(x)\, dx + (C_1/v_{L2}) \int_{\theta_3/T}^{\theta_4/T} \tau_{c,L} F_4(x)\, dx, \tag{3}$$

where $C = 2C_1 = (k_B/3\pi^2)(k_BT/\hbar)^3$, $\tau_{c,i}^{-1} = \tau_B^{-1} + \tau_{pt}^{-1} + \tau_{3ph,i}^{-1}$; $i = T$ and L, $F_i = x^4e^x(e^x - 1)^{-2}(1 + R_iT^2x^2)^2\,(1 + 3R_iT^2x^2)^{-1}$; $i = 1, 2, 3$ and 4, k_B is the Boltzmann constant, $\hbar$ is the Planck constant divided by 2π, v's are the phonon velocities, R's are the constants and depend on the dispersion curve of the sample under study, θ's are the characteristic temperatures, τ_B^{-1}, τ_{pt}^{-1} and τ_{3ph}^{-1} are the scattering relaxation rates due to boundary [9], point-defects [10] and three phonon [7, 8] scattering processes, respectively (for details, see [5]). The boundary scattering relaxation rate used in the present analysis is due to CASIMIR [9] and it can be expressed as $\tau_B^{-1} = v/L$, where L is the CASIMIR length of the crystal. The expression for τ_{3ph}^{-1} used in the present study includes both three phonon normal and umklapp processes and it is the same as proposed by DUBEY and MISHO [7, 8]. In writing Eq. (1), the correction term [11] due to the three phonon normal processes has been neglected due to its very small contribution [12—15].

As stated above, our aim is to study the role of the point-defect scattering relaxation rate [10]. Therefore, before giving the details of the calculations, it is needed to give a few lines about the point-defect scattering relaxation rate τ_{pt}^{-1}. When the wave length of the phonons is large compared to an imperfection in the crystal, the scattering can be treated classically in the manner of Lord RAYLEIGH. KLEMENS [10] has treated the problem by perturbation theory and derived an expression for the asymptotic limit of low temperature and low frequency of phonons which does not include the dispersion of phonons. He finds as expected $\tau_{pt}^{-1} \propto w^4$ which can also be expressed as $\tau_{pt}^{-1} = Aw^4$. The proportionality constant A (which is known as the point-defect scattering strength) depends on both mass difference and force constant difference between the host lattice and imperfections, the latter difference is difficult to estimate both because input data for new binding scheme may not available and because the strain field associated with the point imperfection can cause small changes in the force constants in the crystal. According to KLEMENS, the point-defect scattering strength A can be expressed as

$$A = (V/4\pi v^3) \sum_i f_i(1 - m_i/m)^2,$$

where V is the volume, v is the average phonon velocity, m_i is the mass of an impure atom, m is the average mass of all atoms, f_i is the fraction of atoms with mass m_i and suffix i is used to denote impure atoms. The above stated expression for the point-defect scattering relaxation rate has been used by several workers and it is found that it gives very good response to the experimental data of the lattice thermal conductivity.

If A_N is the point-defect scattering strength of a normal sample, any change in the impurity concentration or presence of any other defect (mass difference), causes a change in A_N. Following the earlier work of the authors [6] and introducing a new parameter "p", the point-defect scattering strength A of the new crystal (after increasing impurities in it) under study can be expressed as a function of A_N as $A = A_N p$. Thus, it is clear that p measures the ratio of the point-defect scattering strengths of the normal sample and the sample under study. The value of "p" totally depends on the extra impurities present inside the normal sample. Assigning the different values for "p" as $p = 0.1, 0.2, 0.3, \ldots, 1$ and $10, 10^2, \ldots, 10^5$, and using the conductivity integ-

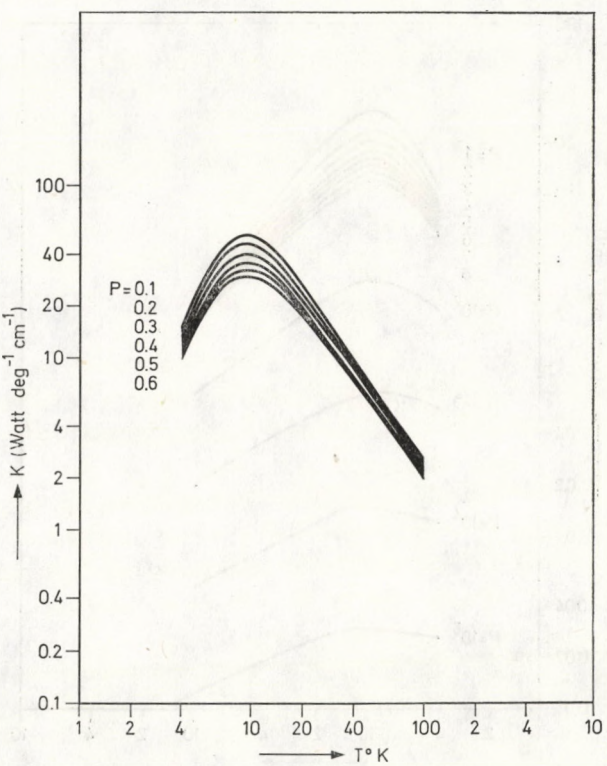

Fig. 1a. Phonon conductivity of GaAs in the entire temperature range 4—100 K for the different values of "p" in the range 0.1—0.6

rals stated in Eq. (2) and (3), the lattice thermal conductivity of GaAs has been calculated in the entire temperature range 4—100 K for the different values "p". The study is limited upto 100 K only, due to the fact that above this temperature the point-defect scattering relaxation rate does not make a significant contribution to the combined scattering relaxation rate and the lattice thermal resistivity is mainly due to phonon-phonon scattering processes.

The constants used in the present analysis are taken from the earlier report of the authors [5] for GaAs and results obtained are shown in Figs. 1*a*, 1b, 2a and 2b. The percentage change the the phonon conductivity due to a change in the point-defect scattering strength A (i.e. for the different values of "p") is also calculated and the results are listed in Table I. From Figs. 1a and 1b (corresponding to $p < 1$ and to $p > 1$, respectively), it is clear that the position of the conductivity maxima in K vs T curve is shifted from its normal position due to a change in the point-defect scattering strength A. If $A < A_N$ (i.e. $p < 1$), it shifts towards the higher temperature whereas it is shifted to lower temperature for $p > 1$, and it can be explained looking at the role of the boundary scattering relaxation rate [6]

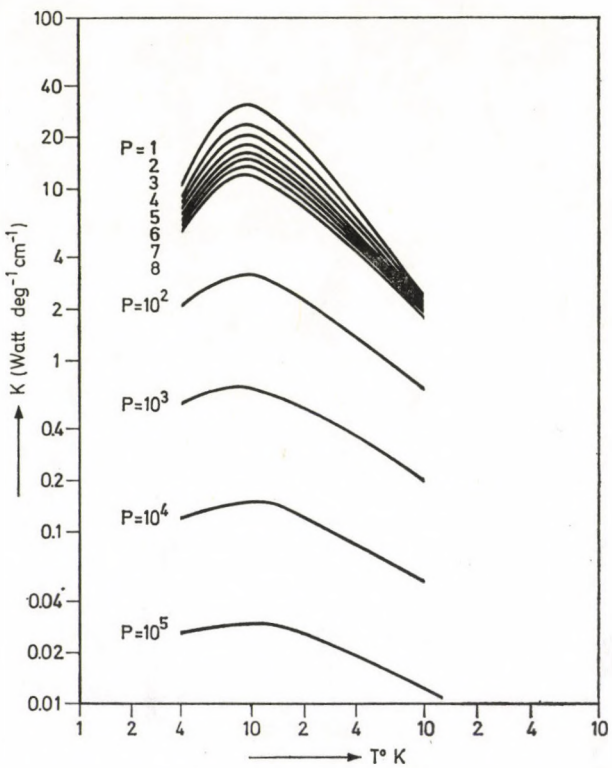

Fig. 1b. Phonon conductivity of GaAs in the entire temperature range 4—100 K for the different values of "p" in the range 10^0—10^5

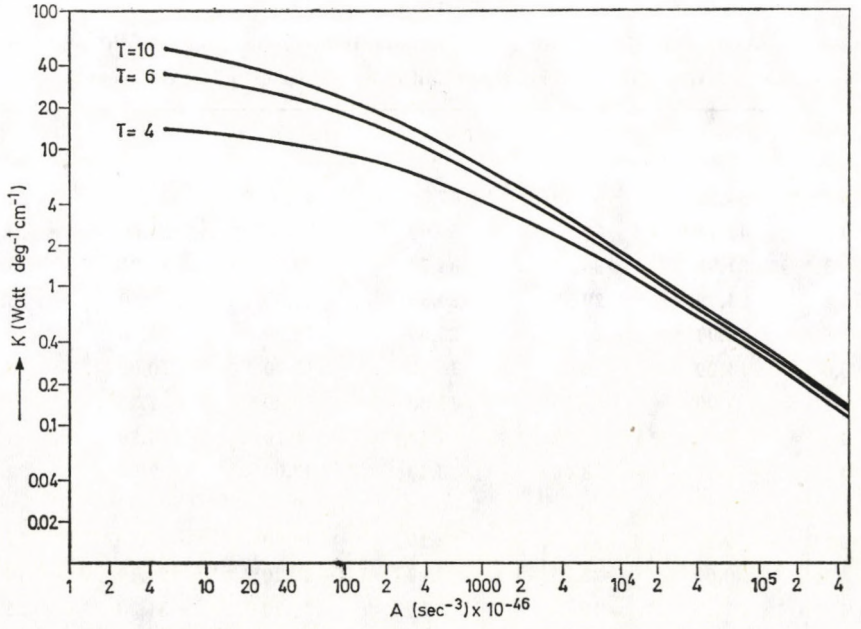

Fig. 2a. Variation of the phonon conductivity of GaAs with respect to the point defect scattering strength A at different temperatures in the range 4—10 K

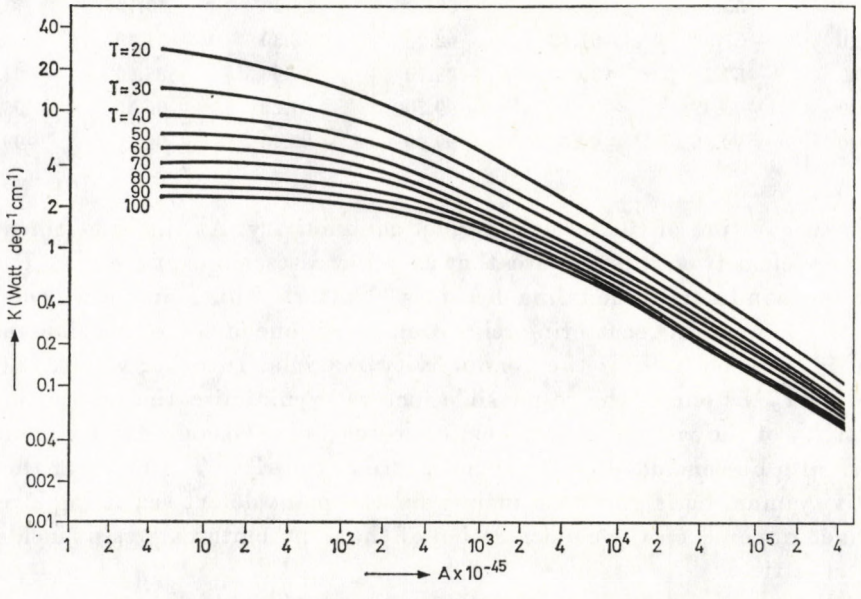

Fig. 2b. Variation of the phonon conductivity of GaAs with respect to the point defect scattering strength A at different temperatures in the range 20—100 K

Table I

The percentage change in the lattice thermal conductivity of GaAs for the different values of the point-defect scattering strength i.e. for the different values of "p" at different temperatures

p	$T=6$	$T=8$	$T=10$	$T=20$	$T=30$	$T=40$
0.1	54.26	67.50	47.50	47.50	30.00	22.30
0.2	41.14	50.16	51.60	37.60	24.60	18.80
0.3	31.91	38.50	34.50	29.90	20.20	15.80
0.4	24.79	29.53	30.30	23.60	16.40	13.10
0.5	18.97	22.43	23.00	18.30	13.00	10.80
0.6	14.09	16.56	16.90	13.70	10.00	8.30
0.7	9.90	11.56	11.80	9.80	7.30	6.60
0.8	6.21	7.22	7.40	6.10	4.80	4.70
0.9	2.94	3.40	3.40	3.00	2.50	2.00
1.0	0	0	0	0	0	0
2	−19.23	−21.61	−22.10	−19.20	−14.80	−11.00
3	−30.00	−33.25	−33.80	−30.20	−24.40	−19.30
4	−37.25	−40.90	−41.60	−37.70	−31.30	−25.50
5	−42.61	−46.45	−47.20	−43.10	−26.50	−20.40
6	−46.79	−50.72	−51.40	−47.40	−41.70	−34.40
7	−50.17	−54.15	−54.90	−50.90	−44.20	−37.90
8	−53.00	−56.98	−47.70	−53.80	−47.10	−40.80
9	−55.40	−59.38	−601.0	−56.20	−49.70	−43.30
10	−57.90	−61.43	−62.20	−48.30	−51.80	−45.50
100	−87.29	−89.32	−89.70	−89.90	−85.00	−81.70
1 000	−96.97	−97.58	−99.70	−97.20	−96.30	−95.30
10 000	−99.36	−99.50	−99.90	−99.40	−99.20	−99.00

in the calculation of the lattice thermal conductivity. At the same time, it is also very clear from these Figures that as A increases, slope of the K vs T curve near the conductivity maxima becomes flatter. Thus, one can conclude that the point-defect scattering relaxation rate is one of the responsible factors to assign the position of the conductivity maxima. In other words, one can say that τ_{pt}^{-1} is one of the responsible factors to minimise the lattice thermal resistivity of the sample at these temperatures (near the conductivity maxima). It can also be concluded that the curvature of the K vs T curve near the conductivity maxima is governed mainly by the point-defect scattering strength A which depends on the concentration of the impure atoms present inside the crystal lattice.

From Figs. 2a and 2b (corresponding to $T < 10$ K and $T > 10$ K, respectively) it can be seen that the lattice thermal conductivity decreases

with an increase in the point-defect scattering strength A at every temperature. In other words, the lattice thermal resistivity increases with an increase of the impurity concentration. From these Figures as well as with the help of Table I it can be seen that the maximum effect of A on the lattice thermal conductivity is at 10 K which corresponds to the conductivity maxima.

*

The authors wish to express their thanks to Dr. R. A. RASHID and Dr. R. H. MISHO for their interest in the present work.

REFERENCES

1. T. H. GEBALLE, J. Appl. Phys., **30,** 1153, 1959.
2. J. CALLAWAY and H. C. V. BAEYER, Phys. Rev., **120,** 1149, 1960.
3. P. G. KLEMENS, J. Phys. Chem. Solids, **8,** 345, 1959.
4. R. BERMAN and E. L. FOSTER, Proc. Roy. Soc. (London), **237,** 344, 1956.
5. M. C. AL-EDANI and K. S. DUBEY, Phys. Stat. Solidi (b)**86,** 741, 1978.
6. M. C. AL-EDANI and K. S. DUBEY, Phys. Stat. Solidi (b)**87,** K47, 1978.
7. K. S. DUBEY and R. H. MISHO, J. Therm. Anal., **12,** 223, 1977.
8. K. S. DUBEY and R. H. MISHO, Phys. Stat. Solidi (b)**84,** 69, 1977.
9. H. B. G. CASIMIR, Physica, **5,** 495, 1938.
10. P. G. KLEMENS, Solid State Physics, **7,** 1, 1958.
11. J. CALLAWAY, Phys. Rev., **113,** 1046, 1959.
12. K. S. DUBEY, J. de Physique, **37,** 267, 1976.
13. K. S. DUBEY, Phys. Stat. Solidi (b)**79,** K119, 1977.
14. K. S. DUBEY, Phys. Stat. Solidi (b)**81,** K83, 1977.
15. K. S. DUBEY, Solid State Comms., **23,** 963, 1977.

Acta Physica Academiae Scientarum Hungaricae, Tomus 46 (3), pp. 185—191 (1979)

DETERMINATION OF THE POLARIZABILITY AND THE DIPOLE MOMENT OF ANTHRACENE DERIVATIVES*

By

JANINA HELDT and JÓZEF HELDT

INSTITUTE OF PHYSICS, UNIVERSITY OF GDANSK, GDANSK, POLAND

(Received in revised form 3. IV. 1979)

The difference of dipole moments between the excited and ground state was determined to be 1.9 and 1.8 Debye for 9-acetoxyanthracene and 10-phenyl-9-acetoxyanthracene from the frequency shifts of absorption and emission spectra. The polarizability of these two compounds is 36×10^{-24} and 54×10^{-24} cm^3, respectively. The measured natural lifetimes are compared with those calculated from the absorption integral taking into account the effect of intermolecular interactions on the optical properties of dissolved molecules.

1. Introduction

Among meso-substituted anthracenes only a few lasing dyes are known [1—3]. Recently we found [4a] that some of 9-acetoxyanthracene derivative show the lasing action in toluene and dioxan. The selection of aromatic hydrocarbons as laser dyes can be facilitated, taking into consideration all spectroscopic data available for the group of dyes. Further these experimental data are of great importance concerning many theoretical investigations of the anthracene derivatives since they allow the comparison with theoretical values. In earlier papers [4, 5] we reported the results of studies on the absorption and emission spectra, quantum yields and mean decay times of the fluorescence of 9-acetoxyanthracene derivatives. In this paper we report the polarizability, α, and the difference of the dipole moments of the excited and ground states, $\Delta\vec{\mu} = \vec{\mu}_e - \vec{\mu}_g$, of the 9-acetoxyanthracene (I) and 10-phenyl-9-acetoxyanthracene (II). They are determined from the changes of intensities of absorption spectra and from the frequency shifts of absorption and emission spectra when the dyes are dissolved in various solvents.

2. Effect of the internal field in solution on the electronic absorption and emission spectra and on the lifetimes of the molecules in the excited state

The shift of the electronic absorption and emission spectra in the solution from their position in the gas phase is related to the dielectric constant (D) and the refractive index (n) of the solvent.

* This work was carried on under the Research Project 10.2

The theoretical explanation of this shift was given by BAYLISS [6], OOSHIKA [7], LIPPERT [8], BILOT et al. [9], LIPTAY [10], and MATAGA et al [11]. A review of the above mentioned theories is given in the book of MATAGA and KUBOTA [12].

The comprehensive treatment of solvent effects on electronic spectra of dissolved polyatomic molecules gives the following formula which explains the frequency shift (see [9] and [10]) of the absorption and emission maxima in various solvents:

$$\Delta\tilde{\nu} = \tilde{\nu}_a - \tilde{\nu}_e = m \cdot d(n, D) + \text{const}, \tag{1}$$

where

$$m = \frac{2(\vec{\mu}_e - \vec{\mu}_g)^2}{hcr^3}, \tag{2}$$

$$d(n, D) = \frac{\dfrac{D-1}{2D+1} - \dfrac{n^2-1}{2n^2+1}}{\left(1 - \dfrac{2\alpha}{r^3}\,\dfrac{n^2-1}{2n^2+1}\right)\left(1 - \dfrac{2\alpha}{r^3}\,\dfrac{D-1}{2D+1}\right)} \tag{3}$$

and where r is the radius of the cavity in Onsager's theory, $\vec{\mu}_g$ and $\vec{\mu}_e$ are the dipole moments of the ground and excited singulet state and α is the real part of the complex polarizability of the molecule under investigation.

It results from Eq. (1) that a graph of $\Delta\tilde{\nu}$ versus $d(nD)$ should be a straight line, the slope of which is given in Eq. (2). To perform this plot, the value of α/r^3 must be known in order to determine the variable $d(n, D)$ for various solutions.

The value α/r^3 of dissolved molecules can be determined (the appropriate method is due to SCHUYER [12]), if the oscillator strength, f, is treated as an invariant quantity in transition from vapour to solution where only dielectric effects appear. The dielectric effects have no direct influence upon the transition probabilities and solely effect the internal field strength of the light wave acting on the molecule, and thus they are of a universal nature.

In this case when the solvent as an external physical medium has no direct influence on the changes in transition probability the expression for the oscillator strength f of a dissolved molecule can be written in the form [13]

$$\varphi(n)\,\frac{3mc}{\pi e^2}\int \varepsilon_{\tilde{\nu}M}\,d\tilde{\nu} = f \equiv B, \tag{4}$$

where $\int \varepsilon_{\tilde{\nu}M}\,d\tilde{\nu}$ is the experimental value of the absorption integral of the solution, c is the velocity of the light and m, e are the mass and the charge

of the electron, respectively. The correction function $\varphi(n)$ depends on the effective internal electric field acting on a molecule in the solution. Considering the solvent to be a continuous, structureless dielectric characterized by the refractive index n, the simple relation

$$\varphi(n) = n \tag{5}$$

holds. But taking into account the individual properties of the dissolved molecules and the polarization resulting from the dipole induced in the molecule under the effect of the light wave [14], the correction function is:

$$\varphi(n) = \frac{(2n^2+1)^2}{9n^3}\left(1 - \frac{\alpha}{r^3}\,\frac{2n^2-2}{2n^2+1}\right). \tag{6}$$

Substituting the above expression (Eq. (6)) for $\varphi(n)$ in Eq. (4) and rewriting it in the form:

$$\frac{1}{\left(g'\int \varepsilon_{\tilde{\nu}M}\,d\tilde{\nu}\right)^{1/2}} = \frac{1}{B^{1/2}} - \frac{\alpha}{r^3}\,\frac{1}{B^{1/2}}\,\frac{2n^2-2}{2n^2+1}, \tag{7}$$

where $g' = 3mc/\pi e^2\,(2n^2+1)^2/9n^3$ and the other quantities are as defined earlier a linear dependence between $(g'\int \varepsilon_{\tilde{\nu}M}\,d\tilde{\nu})^{-1/2}$ and $(2n^2-2)/(2n^2+1)$ is obtained.

The line in the graph of Eq. (7) intersects the axis of ordinates in the point $B^{-1/2}$ and has a slope equal to $\alpha/(r^3\sqrt{B})$. The quotient of the two quantities yields the required parameter α/r^3.

Taking into account the influence of the solvent and the width of the spectra of complex molecules [13] the following expression is obtained relating the integral probability of absorption to the lifetime of the molecule in the excited state:

$$\tau\,[ns] = 3.43\times 10^8\,\frac{1}{\int \tilde{\nu}^2\,\varepsilon_{\tilde{\nu}M}\,d\tilde{\nu}}\,\frac{1}{n\varphi(n)}. \tag{8}$$

From the above relations it follows that the data obtained from absorption and emission spectra of dissolved molecules in various solvents can be used by means of Eq. (1) and Eq. (7) to determine the dipole moment of the excited molecule $\vec{\mu}_e$(or the value $\Delta\vec{\mu} = \vec{\mu}_e - \vec{\mu}_g$) and the real part of the complex polarizability α. The additional knowledge of the lifetime τ and the quantum yield Q of fluorescence of the investigated molecules give a possibility to check these values.

3. Results and discussion

The synthesis of the investigated compounds is given in our former paper [4]. The structural formulas are shown in Fig. 1. The compounds were recrystallized from ethanol before use. The solvents were spectroscopic pure. The concentration of the compounds in the solution was 2×10^{-5} gcm^{-3}. The absorption spectra were measured with a Zeiss-Jena type VSU-2 spectrometer.

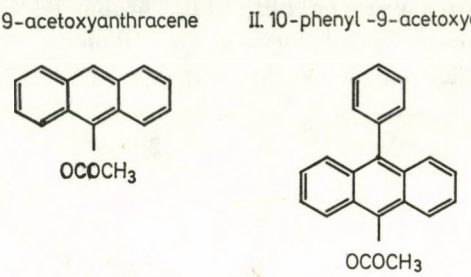

Fig. 1. The structural formulae of 9-acetoxyanthracene and 10-phenyl-9-acetoxyanthracene

The emission spectra and the quantum yield (for n-heptane solutions only) were obtained using the apparatus described in [5]. The measurements of fluorescence lifetime in n-heptane solutions were performed by means of a phase fluorometer [16].

The obtained experimental data are collected in Table I. The frequencies $\tilde{\nu}_a$ and $\tilde{\nu}_e$ give the value of the lowest vibrational peak of the absorption and

Table I

The physical parameters of the used solvents and frequencies of the lowest vibrational peak of the absorption and emission spectra

	Solvent	Refractive index	Dielectric const.	9-Acetoxyanthracene			10-Phenyl-9-acetoxyanthracene		
				$d(nD)$	$\tilde{\nu}_a$[cm^{-1}]	$\tilde{\nu}_e$[cm^{-1}]	$d(nD)$	$\tilde{\nu}_a$[cm^{-1}]	$\tilde{\nu}_e$[cm^{-1}]
1	Methanol	1.3290	31.20	0.939	29 100	25 650	0.8183	28 450	24 950
2	Ethanol	1.3623	25.00	0.8857	29 000	25 550	0.7726	28 250	24 650
3	n-propanol	1.3854	21.80	0.8483	28 900	25 600	0.7405	28 350	24 750
4	n-heptane	1.3867	1.97	0.0102	29 000	25 750	0.0096	28 500	25 000
5	n-butylchlorate	1.4022	7.39	0.5497	28 900	25 700	0.4927	28 250	24 700
6	Tetrahydrofurane	1.4045	7.39	0.5483	28 900	24 450	0.4915	28 300	24 750
7	n-heptanol	1.4250	12.10	0.6915	28 850	25 650	0.6099	28 200	24 750
8	Cyclohexane	1.4464	2.23	0.2654	28 800	25 700	0.2494	28 200	24 750
9	Chloroform	1.4467	5.14	0.3851	28 750	25 500	0.3491	28 520	24 550
10	Cyclohexanol	1.4648	15.00	0.7227	28 850	25 600	0.6325	28 200	24 700
11	Benzene	1.5014	2.28	0.0049	28 800	25 650	0.0045	28 100	24 850

emission spectra. The dielectric constants and the refractive index were taken from the tables in "Technique of Organic Chemistry", Volume VII [17].

Using the values of n, D from the Tables and $\int \varepsilon_{\tilde{\nu}M} d\tilde{\nu}$ from our measurements the coefficients α/r^3 were determined on the basis of Eq. (7). Fig. 2 shows the graph obtained for the dependence $(g' \int \varepsilon_{\tilde{\nu}M} d\tilde{\nu})^{-1/2}$ versus $(2n^2 - 2)/(2n^2 + 1)$ for 9-acetoxyanthracene. In Fig. 2 the crosses give the dependence $(g' \int \varepsilon_{\tilde{\nu}M} d\nu)^{-1/2}$ versus $(2n^2 - 2)/(2n^2 + 1)$ for non-dipole (4) and (11) and mixtures of two non-dipole solvents, respectively.

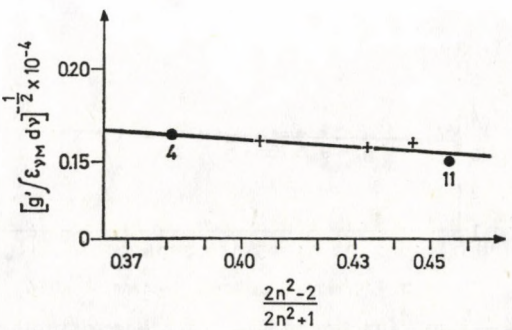

Fig. 2. $(g \int \varepsilon_{\nu M} d\nu)^{-1/2}$ as a function of $(2n^2 - 2)/(2n^2 + 1)$ for 9-acetoxyanthracene in various solvents. The figures near the points refer to the sample No. as in Table I. The points marked by crosses give the above dependence for n-heptane (4) and benzene (11) mixtures for different proportions

As can be seen in Fig. 2 the experimental points approach the straight line well.

The values of the α/r^3 coefficient, calculated for the 9-acetoxyanthracene and 10-phenyl-9-acetoxyanthracene (the graph of the dependence $(g' \int \varepsilon_{\tilde{\nu}M} d\tilde{\nu})^{-1/2}$ versus $(2n^2 - 2)/(2n^2 + 1)$ is similar to the one in Fig. 2) are equal to 0.62 and 0.54, respectively. Utilizing the above values the variable $d(n, D)$ were calculated for the solutions given in Table I. In these calculations for the radius of the spherical cavity with a point dipole at the centre the mean radius of the molecule has been calculated from the length of the chemical bonds.

The dependence $\Delta\tilde{\nu} = \tilde{\nu}_a - \tilde{\nu}_e$ as the function of $d(n, D)$ of the two compounds is given in Figs. 3a and 3b. In this case the scattering of the experimental points is negligible. The values of the Onsager radius r, the direction coefficients m (for the straight lines in Figs. 3a and 3b) and the values of $\Delta\vec{\mu}$ calculated by means of Eq. (2) are collected in Table II. The values obtained for $\Delta\vec{\mu}$ show that the dipole moment of the excited state differs from the ground state value for both molecules. The changes are not so large as for some other molecules (see [8]).

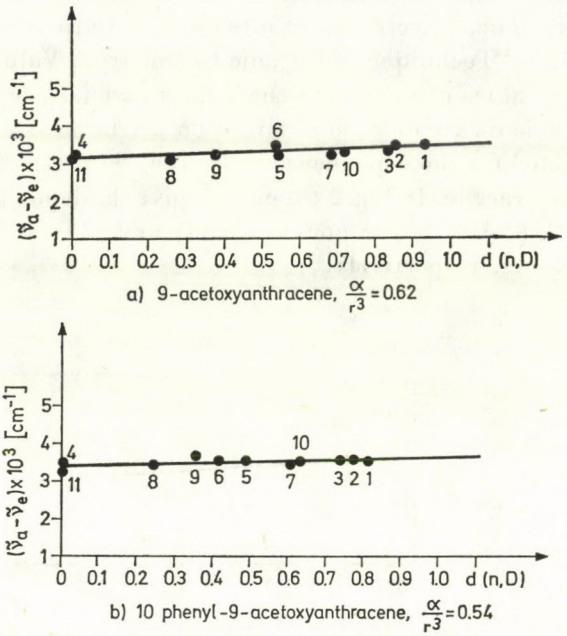

Fig. 3. The values of $\tilde{\nu}_a - \tilde{\nu}_e$ as a function of $d(n, D)$ for 9-acetoxyanthracene and 10-phenyl-9-acetoxyanthracene. The figures near the points refer to the sample No as in Table I

Applying the same values of r, the polarizability of the 9-acetoxyanthracene and 10-phenyl-9-acetoxyanthracene molecules is determined to be equal to 36×10^{-24} and 56×10^{-24} cm^3, respectively.

Since the expressions used for the determination of $\Delta\vec{\mu}$ and α are obtained using the simplified form of the Onsager's reaction field model [12] it is very

Table II

The mean polarizability α and $\Delta\vec{\mu} = \vec{\mu}_e - \vec{\mu}_g$ values of 9-acetoxyanthracene and 10-phenyl-9-acetoxyanthracene.

Compound	$\frac{\tau_{exp}}{Q}$ [ns]	$\left.\begin{matrix}\tau_2^{cal}\\ \tau_1^{cal}\end{matrix}\right\}$ [ns]	$\frac{\alpha}{1^{-3}}$	r [Å] m (cm^{-1}]	$\Delta\vec{\mu}$ [Debye]	$\alpha \times 10^{24}$ [cm^3]
Anthracene			0.66[b]	3.61	0 ± 0.4[b]	26.2[a]
						31 ± 3[b]
						30.4[c]
9-Acetoxyanthracene	10.56	11.07	0.62	3.89	1.9	36
		5.97		289		
10-Phenyl-9-acetoxy-	9.15	9.18	0.54	4.75	1.8	54
anthracene		5.10		292		

[a] N. G. BAKHSHIEV et al., Optika i Spektrosk., **24**, 901, 1968.
[b] W. LIPTAY et al., Z. Naturforsch., **26a**, 2020, 1971.
[c] YU. B. MALIHANOV, Optika i Spektrosk., **43**, 431, 1977.

difficult to state how reliable the data determined in this work are. Some answers to this question can be obtained when the result is compared with the data known for anthracene or other similar molecules. As can be seen in Table II the mean polarizability α and the $\Delta\vec{\mu} = \vec{\mu}_e - \vec{\mu}_g$ values of 9-acetoxy-anthracene and 10-phenyl-9-acetoxyanthracene are larger than those of anthracene. These differences are not very large if one considers that the investigated molecules have only an identical frame in which the electronic transition takes place. Our results agree with the data obtained for 9-bromo-anthracene ($\Delta\vec{\mu} = 1.7\ D$ [18]) and 9,9-bianthryl ($\alpha \times 10^{24}\ \mathrm{cm}^3 = 56 \pm 3$ [19]).

Another way of testing the correctness of the α, $\Delta\vec{\mu}$ and r value may be the comparison of measured and calculated natural lifetimes using Eq. (8). For this aim the absorption spectra of n-heptane solutions were selected. The results of these calculations are collected in Table II too. The τ_1^{cal} and τ_2^{cal} are calculated for the two cases where the solvent is considered to be a continuous, structureless dielectric and where the individual properties of the dissolved molecules and the polarization resulting from the dipole induced in the molecule are taken into account. The comparison of measured natural lifetimes τ_{exp}/Q (see Table II) with those calculated from the absorption integral shows good agreement only for those values for which the quantity α/r^3 was taken into account.

This agreement gives confidence for the correct determination of the polarizability and $\Delta\vec{\mu}$ value of these two compounds.

REFERENCES

1. J. A. Myer, C. L. Johnson, E. Kierstead, R. D. Sharmo and I. Itzka, Appl. Phys. Letters, **15**, 3, 1970.
2. J. Ferguson and A. W. H. Mau, Chem. Phys. Letters, **14**, 245, 1972.
3. F. P. Schäfer, Topics in Applied Physics, Vol. 1. Springer-Verlag, Heidelberg, 1973.
4. J. R. Heldt, J. Gronowska and J. Heldt, Acta Phys. Polon, *A47*, 613, 1974.

4a. Janina Heldt and J. Heldt, Acta Phys. Polon., **A55**, 79, 1979.

5. Janina Heldt, Józef Heldt and Janina Gronowska, Z. f. Naturforschg., **30a**, 612, 1975.
6. N. S. Bayliss, J. Chem. Phys., **18**, 292, 1950.
7. Y. Ooshika, J. Phys. Soc. Japan, **9**, 594, 1954.
8. E. Lippert, Z. Elektrochem, **61**, 962, 1957.
9. L. Bilot and A. Kawski, Z. f. Naturforschg., **17a**, 621, 1962.
10. W. Liptay, Z. f. Naturforschg., **20**, 1441, 1965.
11. N. Mataga, Y. Kaifu and M. Koizumi, Bull. Chem. Soc. Japan, **29**, 465, 1956.
12. N. Mataga and T. Kubota, Molecular Interactions and Electronic Spectra, New York, Dekker, 1970.
13. I. Schuyer, Rec. Trav. Chim., **72**, 933, 1953.
14. B. S. Neporent and N. G. Bakhshiev, Optik i Spektrosk., **5**, 634, 1958.
15. H. Onsager, J. Amer. Chem. Soc., **58**, 1986, 1936.
16. R. K. Bauer and A. Kowalczyk, Raport techniczny Nr 3, Nicholas Copernicus University, Torun, 1974.
17. Technique of Organic Chemistry, Arnold Wiessberger, Editor Vol. VII, Interscience Publishers Inc., New York, 1956.
18. B. Pasztor-Bartoszewicz, Zeszyty Naukowe, WSP Gdansk, **8**, 55, 1968.
19. W. Liptay, G. Walz, W. Baumann, H. J. Schlosser, H. Deckers and N. Detzer, Z. Naturforsch., **26a**, 2020, 1971.

Acta Physica Academiae Scientiarum Hungaricae, Tomus 46 (3), pp. 193—201 (1979)

PSEUDOHARMONIC EFFECTS OF PHONONS IN HEAT CONDUCTIVITY

By

C. MALINOWSKA-ADAMSKA[a] and L. WOJTCZAK[b]

INSTITUTE OF PHYSICS, TECHNICAL UNIVERSITY OF ŁÓDŹ[a]
AND INSTITUTE OF PHYSICS, UNIVERSITY OF ŁÓDŹ[b], POLAND

(Received 3. IV. 1979)

The temperature behaviour of the heat conductivity of metals is investigated in the case when the anharmonic properties of phonons are taken into account in the pseudoharmonic approximation. The results show that the pseudoharmonic effects of lattice vibrations are not negligible in calculations concerning the high temperature region. A comparison with experimental data is given for copper, silver and gold theoretically described by various potential functions.

1. Introduction

Some years ago the influence of the pseudoharmonic effects of lattice vibrations on the temperature behaviour of the electrical conductivity was shortly reported [1]. The theoretical results corrected by means of the anharmonicity of phonons come much closer to experimental data than the corresponding ones calculated in the harmonic approximation. The illustrative considerations were presented for the model discussed by PAL [2] and by PRAKASH and SHARMA [3] applied to the description of the electrical conductivity while the pseudoharmonic correction was introduced by means of the evaluations given by SIKLÓS [4] on the basis of the Morse potential. The above calculations showed that the pseudoharmonic effects should not really be neglected in considerations of thermal properties of transport phenomena. Thus, it seems to be natural to check this suggestion studying not only electrical conductivity but also other phenomena. For this reason, the aim of the present paper is to analyse the temperature behaviour of the heat conductivity in the high temperature limit of the pseudoharmonic procedure.

On the other hand, we are stimulated for further applications of the pseudoharmonic procedure to transport phenomena because of the interesting fact that there exists a very simple relation for the renormalization of the temperature in standard formulas derived in the harmonic approximation [1]. This feature allows us in fact to draw the temperature behaviour of the kinetic coefficients without any additional procedure in their determination except for the change for the phonon basic frequency.

In order to find the lattice vibration parameters the self-consistent theory of anharmonic crystals developed by PLAKIDA and SIKLÓS [5] can be used. The above approach is based on the Green's function method which allows us to describe dynamic as well as thermodynamic and elastic properties of crystals. In its general form the theory can be formulated for an arbitrary potential function leading to the results taking all higher-order terms of the lower-order perturbation theory into account in a self-consistent way and including the damping effects [6—8]. In the frames of the first approximation of this theory, the so called the pseudoharmonic approach or the approximation of the self-consistent phonons, in which the damping processes are not taken into considerations, the self-consistent equations were obtained for physical quantities in systems of the three-dimensional face centred cubic lattice with the central pair interaction in the nearest neighbours approximation [4, 9]. This level of approximation is a starting point for calculations connected with the temperature renormalization of phonon spectra in the present paper.

Usually, the exemplification of the general procedure derived for the pseudoharmonic theory is done by means of the Morse potential function which is very useful for numerical calculations because of its quite simple form in the pseudoharmonic representation. However, the Morse curve is one of the simplest potentials used for the description of the diatomic interaction in molecules as well as in crystals. Therefore, the detailed analysis was performed also for potentials typical for crystals as the Lennard-Jones one [10] and other various curves discussed in the theory of molecules [11]. One of the conclusions obtained was quite unexpectable since it seems to be very strange, but extremely interesting, that some kinds of potential curves satisfying the VARSHNI's criteria [13] cannot be applicable in low-temperature limit where the pseudoharmonic approach leads to the negative values of the force constants. In any case, the above fact implies a careful choice of the initial interaction function which should be tested not only before but also after the renormalization procedure. The analysis recently done [11, 12] shows that the Rydberg potential function leads to sufficiently good results for the large class of various properties.

In the present paper we also consider the properties of the heat conductivity in metals by means of the model function suggested by VARSHNI [14] in the case of an arbitrary external pressure. The choice of the VARSHNI's potential follows from the fact that its testing with respect to the VARSHNI's criteria gives better results for the Sutherland's parameter than for the Morse as well as Rydberg functions [13]. It is worth-while to remark that the Sutherland's parameter plays an essential role in molecular investigation [15] and therefore the recognition for applicability of the VARSHNI's shape potential to solids is very fruitful.

2. Heat conductivity in pseudoharmonic approximation

In order to determine the heat conductivity it is usual to apply the Boltzmann equation for the transport in the crystalline lattice. The scattering mechanisms for propagating phonons are considered in fact by the phonon reciprocal relaxation time which is assumed to be taken as the sum of the relaxation times for each phonon scattering because of their proportionality to the cross sections. In the case of an ideal lattice the main scatterers are expected to be sample boundaries and point defects as impurities, displacement, local electronic density inhomogeneities or fluctuations. The phonon processes, i.e. the anharmonic effects of phonons, are usually neglected since the mean free path of phonons is sufficiently large compared to sample dimensions at low temperatures.

Independently of the method for derivation of the formula for thermal resistivity determining the heat transport properties its essential dependence on temperature T is expressed by the variable $\hbar\omega^0/k_BT$, where the symbols $\hbar$ and k_B have their usual meaning as the Planck's and Boltzmann's constants, respectively. The phonon frequency ω^0 is given in the harmonic approximation and then the thermal resistivity can be written in the form:

$$W_0(T) = \left(\frac{1}{k_BT}\right)^q f(\hbar\omega^0/k_BT)\,, \tag{1}$$

with $q = 3$ for insulators [16] and $q = 2$ for metals [2, 3]. The expression (1) is of a quite general form as far as a pure boundary mechanism of phonon scattering in the heat conductivity is considered. This situation is well satisfied in insulators while some discrepancies between the general formulation (1) of the theory for metals and corresponding experimental results can follow from the use of the free electron model in which the electron-phonon matrix elements ignore usually the exchange and correlation effects. It is well known that the transport coefficient of metals is very sensitive to the form of the matrices used for electron-ion interactions [3]. However, this sensitivity concerns not only thermal, but first of all electric conductivity which can be related to the former by means of the Lorentz number. Since the experience of the previous investigations connected with the electric conductivity [1, 17] indicates that only the phonon frequency renormalization is even enough reason to conclude on the important role of the pseudoharmonic corrections to the temperature behaviour of the electric resistivity and taking into account that the Lorentz number is a linear function of temperature at sufficiently high temperature, we can really assume that the essential contribution to the heat conductivity in the high temperature limit is caused by the phonon properties. In other words, from the physical point of view this means that the reciprocal

relaxation time of the phonon-phonon collision process is more significant than other kinds of relaxation mechanisms, of course, the phonon-phonon interaction plays a decisive role in the temperature interval above the maximum point of curves obtained in the harmonic approximation where the influence of the other, above mentioned scatterers, seems to be well established.

In terms of the pseudoharmonic theory of phonons the frequencies of lattice vibrations ω are related to those ω^0 found in the harmonic approximation by means of a very simple renormalization factor $\alpha(T)$ as:

$$\omega_\lambda(\vec{h}) = \alpha(T)\,\omega_\lambda^0(\vec{h}), \tag{2}$$

while the dependence on the wave vector $\vec{h}$ of the phonon modes remains unchanged as well as the polarization λ is the isotropic character. For this reason the renormalization factor $\alpha(T)$ scales the temperature only leading to the relation:

$$W(T) = \left(\frac{1}{\alpha(T)}\right)^q W_0\big(T/\alpha(T)\big), \tag{3}$$

which can be obtained immediately by substituting the expression (2) into the general formula (1) for the heat resistivity. In this way, the formula (3) allows to include very easily the phonon-phonon interaction in the pseudoharmonic approximation into the heat resistivity by the simple renormalization procedure for temperature in conventional expressions.

3. Phonon frequency renormalization in pseudoharmonic approximation

The renormalization factor $\alpha(T)$ appearing in the dispersion relation (2) is well defined by the pseudoharmonic approach to the problem in question [4] namely:

$$\alpha^2(T) = \frac{f(T, l_e)}{f^0(r_e)}, \tag{4}$$

where $f^0(r_e)$ is the harmonic force constant determined by the second derivative of the initial, pair interaction potential $\Phi(r)$, taken at the equilibrium point $r = r_e$. Analogously, the pseudoharmonic force constant $f(T, l_e)$ is expressed by the second derivative of the self-consistent potential $\tilde{\Phi}(T, r)$ taken at the equilibrium point $r = l_e$ in which the first derivative of $\tilde{\Phi}(T, r)$ vanishes. In order to complete all the equations necessary in calculations of this paper we remember the shape of $\tilde{\Phi}(T, r)$ as follows [4]:

$$\tilde{\Phi}(T, r) = \sum_{n=0}^{\infty} \frac{1}{n!} \left(\frac{1}{2}\,\overline{u^2}\right)^n \Phi^{(2n)}(r), \tag{5}$$

where the mean square displacement of neighbouring atoms $\overline{u^2}(T)$ related to the square of the equilibrium value l_e determines the temperature behaviour of the effective potential (5) by the well known relation:

$$\overline{u^2}(T) = \frac{1}{zNf(T, l_e)} \sum_{h,\lambda} \omega_\lambda(h) \operatorname{cth} \frac{\omega_\lambda(h)}{2k_B T}, \tag{6}$$

for $z = 12$ in the case of the f.c.c. lattices. In the high temperature limit we can reduce the relation (6) to the linear function of $\overline{u^2}(T)$ with respect to the temperature independently of the dispersion law for phonon branches. In better approximation the following expression is used [18, 19]:

$$\overline{u^2} = \frac{6k_B T}{f^0(r_e)\,\alpha^2} + \frac{3k^2}{10 f^0(r_e)\,k_B T} - \frac{\alpha k^4}{6.22 f^0(r_e)\,(k_B T)^3}, \tag{7}$$

where $k = \sqrt[3]{18\,\pi^2}\,\hbar v/a$, with v denoting the velocity of sound and a the lattice constant.

The detailed calculations performed in the present paper concern three cases with respect to the initial potential curves: a) Morse potential widely discussed by SIKLÓS (e.g. [20]) as a model potential for the description of thermodynamic properties of anharmonic csystals, b) Rydberg potential expressed in the pseudoharmonic approximation in which the accuracy of thermodynamic properties is the best in fact in comparison with other kinds of potential curves still considered [11], c) VARSHNI potential which is tested for crystals because of its very good applicability for molecules in gaseous medium [13, 14]. The initial potential functions are:

$$\Phi(r) = D_e\{[\exp(-b(r - r_e)) - 1]^2 - 1\}, \tag{8}$$

$$\Phi(r) = -D_e[1 + b(r - r_e)] \exp[-b(r - r_e)], \tag{9}$$

$$\Phi(r) = D_e\{(1 - \exp[-b(r^2 - r_e^2)])^2 - 1\}, \tag{10}$$

for MORSE, RYDBERG and VARSHNI approximations, respectively.

The constants have their characteristic values for crystals considered [21] and they are collected in Table I for copper, silver and gold in which we are interested from the point of view of the heat transport behaviour.

In this way we obtained a closed system of equations (4)—(10) which determine the renormalization factor $\alpha(T)$ appearing in the formula (3) found in the harmonic approximation. It is worth-while to strongly underline that the described procedure based on the renormalization $\alpha(T)$ allows us to obtain directly the corrected thermal resistivity $W(T)$ using the known values for $W_0(T^*)$, where $T^* = T/\alpha(T)$. Moreover, the same relation should be satisfied

Table I

Numerical values of the parameters of the interaction potentials of MORSE, RYDBERG and VARSHNI types for copper, silver and gold

Metals	Curve	$b\left[\frac{1}{\text{nm}}\right]$	r_e [nm]	$D_e \cdot 10^{-20}$ [J]
Copper	MORSE	13.649220	0.286074	5.424099
	RYDBERG	20.027270	0.281625	6.096274
	VARSHNI	28.943860 × α_1^*	0.271097	7.571969
Silver	MORSE	13.501210	0.312624	5.091160
	RYDBERG	19.657010	0.309035	5.605234
	VARSHNI	24.789800 × α_1	0.301363	6.585555
Gold	MORSE	16.243880	0.299983	7.583399
	RYDBERG	24.407570	0.297946	8.113146
	VARSHNI	29.177310 × α_1	0.294382	8.909224

$^* \alpha_1 = 1\left[\frac{1}{\text{nm}}\right]$

in the case of the electric resistivity or another quantity. So, we can see that the phonon frequency renormalization factor is of a universal character and for this reason we present it not only by graphs (Fig. 1) but also in Table II for several metals in the case of the Rydberg function which leads to the best results for the correction of the heat conductivity.

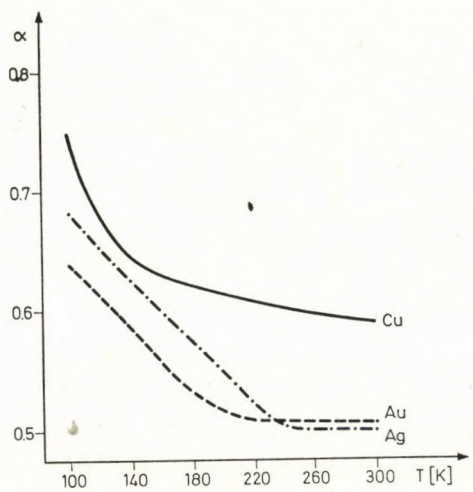

Fig. 1. The phonon frequency renormalization factor $\alpha(T)$ for the Rydberg interatomic potential determined in the case of copper, silver and gold

Table II

Phonon frequency renormalization factor $\alpha(T)$ of the Rydberg potential for copper, silver and gold

T [K] \ Metal	Copper	Silver	Gold
100	0.751414	0.685448	0.651599
120	0.675132	0.651114	0.602830
140	0.640422	0.618285	0.587305
160	0.632578	0.611726	0.556515
180	0.626309	0.577790	0.527131
200	0.620045	0.553640	0.522183
220	0.613788	0.519136	0.519647
240	0.607538	0.508814	0.516368
260	0.601297	0.505376	0.513190
280	0.595064	0.503754	0.510432
300	0.578840	0.501982	0.507916

4. Results and discussion

Numerical results for the temperature dependence of the thermal resistivity $W(T)$ are given by graphs for copper (Fig. 2), silver (Fig. 3) and gold (Fig. 4). Calculations are based on the theoretical results published by PRAKASH and SHARMA [3] in the harmonic approximation and compared with experimental data reported by WHITE [22—24].

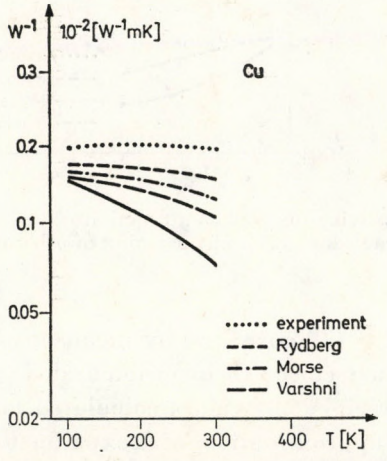

Fig. 2. The thermal resistivity for copper as a function of temperature. The solid line shows the results in the harmonic approximation [3]. The points refer to the experimental data [22]. The dashed curves represent the results calculated for the phonon spectrum renormalized by the pseudoharmonic theory for the MORSE, RYDBERG and VARSHNI potentials

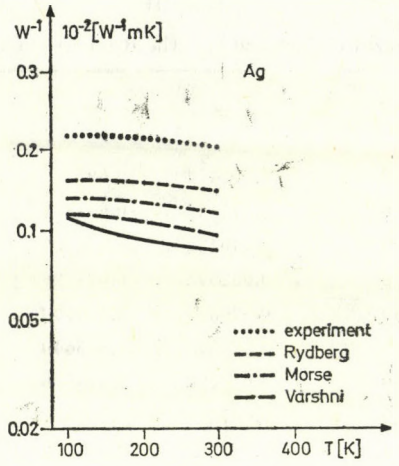

Fig. 3. The thermal resistivity for silver as a function of temperature. The points refer to the experimental data [23]. The meaning of other curves as in Fig. 2

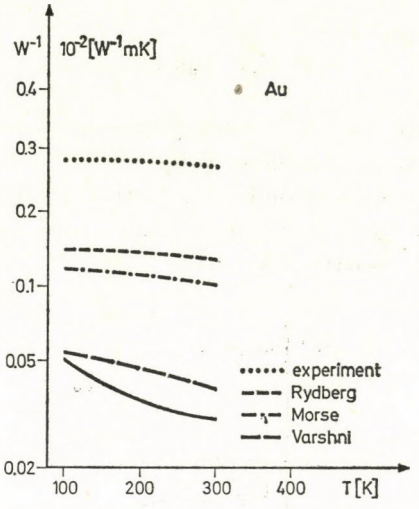

Fig. 4. The thermal resistivity for gold as a function of temperature. The points refer to the experimental data [24]. The meaning of other curves as in Fig. 2

The results for $W(T)$ corrected by means of the anharmonicity of lattice vibrations come much closer to experimental data in the high-temperature region. The best agreement of values calculated for the thermal resistivity in the pseudoharmonic approximation with experimental data was obtained for the Rydberg interatomic potential. Let us remember here, that this function used earlier [11] to describe the thermodynamic functions in the pseudoharmonic approximation gave also quite good results in comparison with

other potentials. The conclusions following from the thermal resistivity on the temperature limit are in agreement with those obtained from the analysis of the electrical resistivity for which the Rydberg potential leads to the best correction [17]. The last remark seems to be very important, as it allows us to formulate a new kind of the criterion for the correctness of interatomic interactions applied to solids. We can see, in fact, that some effective self-consistent potentials can be more suitable for cyrstals than others although they were more accurate in harmonic approximation (e.g. VARSHNI'S function). It is also worth-while to notice that the agreement between results for thermal and electric resistivities is not unexpectable because of the mentioned relation formulated by the Lorentz number. The existence of this agreement can be treated as an additional test of the correct formulation for presented considerations.

In general we would like to conclude that the pseudoharmonic approach to the transport problems connected with phonon processes leads to a very useful method of taking the pair anharmonic terms into account and the proposed procedure of temperature renormalization is a very convenient tool for the description of the temperature behaviour of transport coefficients.

REFERENCES

1. L. WOJTCZAK and K. STACHULEC, Phys. Stat. Solidi, b**70**, K 165, 1975.
2. S. PAL, J. Phys. Soc. Japan, **35**, 760, 1973.
3. J. PRAKASH and P. SHARMA, Acta Phys. Polon., A**40**, 269, 1971.
4. T. SIKLÓS, Acta Phys. Hung., **30**, 193, 1971.
5. N. M. PLAKIDA and T. SIKLÓS, Phys. Stat. Solidi, **33**, 103, 1969.
6. N. M. PLAKIDA and T. SIKLÓS, Phys. Stat. Solidi, **39**, 171, 1970.
7. T. SIKLÓS and V. L. AKSIENOV, Acta Phys. Hung., **31**, 335, 345, 1972.
8. T. SIKLÓS and V. L. AKSIENOV, Phys. Stat. Solidi, **50**, 171, 1972.
9. N. M. PLAKIDA, FTT **11**, 700, 1969.
10. VO HONG ANH, Acta Phys. Hung., **30**, 259, 1971.
11. C. MALINOWSKA-ADAMSKA, Acta Phys. Hung., **42**, 295, 1977.
12. A. B. SANNIGRAHI and S. NOOR MOHAMMAD, Ind. J. pure appl. Phys., **13**, 35, 1975; Molec. Phys., **31**, 963, 1976.
13. Y. P. VARSHNI, Rev. Mod. Phys., **29**, 664, 1957.
14. Y. P. VARSHNI and R. C. SHUKLA, Trans. Faraday Soc., **57**, 537, 1961.
15. C. MALINOWSKA-ADAMSKA, Bull. Soc. Sci. Letters, (Łódź) XXIV, 1, 1974.
16. J. CALLAWAY, Phys. Rev., **113**, 1046, 1959.
17. C. MALINOWSKA-ADAMSKA, Bull. Soc. Sci. Letters, (Łódź) (to be published).
18. N. M. PLAKIDA and T. SIKLÓS, Acta Phys. Hung., **26**, 387, 1969.
19. C. MALINOWSKA-ADAMSKA, Bull. Soc. Sci. Letters (Łódź) XXVIII, 15, 1978.
20. T. SIKLÓS, Acta Phys. Hung., **30**, 301, 1971.
21. C. MALINOWSKA-ADAMSKA, Acta Phys. Hung., **45**, 221, 1978.
22. G. K. WHITE, Aust. J. Phys., **6**, 397, 1953.
23. G. K. WHITE, Proc. Phys. Soc., A**66**, 844, 1953.
24. G. K. WHITE, Proc. Phys. Soc., A**66**, 559, 1953.

Acta Physica Academiae Scientiarum Hungaricae, Tomus 46 (3), pp. 203—213 (1979)

INVESTIGATION OF PIEZOELECTRICALLY INDUCED ACOUSTIC TRANSIENTS IN KDP CRYSTALS

By

J. Bakos, Zs. Sörlei

CENTRAL RESEARCH INSTITUTE FOR PHYSICS, BUDAPEST

and

Cs. Kuti, S. Szikora

INSTITUTE OF PHYSICS, TECHNICAL UNIVERSITY, BUDAPEST

(Received 26. IV. 1979)

Acoustic transients generated by high voltage pulses in longitudinal KDP modulator crystals were investigated. Photographic method has been developed to visualize the acoustic waves. The experiments directly demonstrate the piezoelectric acoustic wave generation, the acoustic wave propagation, the reflexion, diffusion and diffraction of acoustic waves and the interaction of acoustic waves with crystal imperfections. From the experimental results the velocity of shear waves and the related elastic constant can be evaluated.

1. Introduction

For quantum-electronic applications devices based on the linear electrooptic effect [1] are widely used. Crystals having good linear electrooptic properties are usually strongly piezoelectric [2]. An electric field applied to linear electrooptic crystals acts on their refractive properties by two distinguishable mechanisms. The primary effect is direct interaction between the electric field and the electrons and optical phonons of the crystals. The mechanical strains caused by the inverse piezoelectric effect give secondary contributions to the change of refractive indices by the strain optic effect, which is known as the secondary electrooptic effect.

Several papers [3—18] have been published on problems originating from the secondary electrooptic effect. Such problems are, e.g., the separation of the primary from the secondary effect, the disagreements between the results of different measurements of the linear electrooptic characteristics of crystals [3—7], and, mainly in the area of applications, the influence of the secondary effects on the operation of electrooptic devices [6—18].

The origin of these problems essentially lies in the different time-dependences of the primary and secondary effects. The primary effect follows quasi simultaneously the applied electric field. The secondary-strain-optic contribution reacts with delay according to the inertia and resistance of the lattice to mechanical deformations.

Moreover, piezoelectrically induced lattice deformations are generated locally in the crystals and they are sources of acoustic waves [19]. The acoustic waves propagating across the crystal result in spatial and time-dependent changes of refractive properties which may cause, e.g. undesirable transient effects in the operation of electrooptic light shutters [6—14] or resonance in the frequency transfer characteristic of periodically driven electrooptic modulators [15—18].

We have investigated the behaviour of acoustic transients generated by relatively short, high voltage pulses applied to 0 °Z cut KDP crystals. The methods published in the literature are based on measuring the pulse response of the transmission of modulators made of electrooptic crystals.

Most of these investigations give the time-dependence of the transmission averaged on the aperture of the crystal [8—13]. In references [7] narrow light beams were used to investigate the acoustic transients in discrete points of the aperture.

In our experiments we have developed a method to obtain better spatial resolution [14]. The transmission pictures of KDP crystals, placed between crossed polarizers, have been photographed with relatively short exposure times. The photos were taken with variable delays after the high voltage pulses. The delay times were changed in μsec steps, thereby giving a good temporal resolution as well. Photos taken in such a way provide very informative pictures about the transient processes.

By this method phenomena such as propagation, reflection, superposition, interference and dispersion of piezoelectrically induced acoustic transients can be observed. The photos also give information on the interaction of acoustic waves with the crystal imperfections.

2. Principles of investigations

The features of acoustic wave propagation in anisotropic media can be obtained by solving the equation [19, 20].

$$\varrho \frac{\partial^2 u_j}{\partial t^2} = \frac{\partial T_{ij}}{\partial x_i}. \tag{1}$$

Here ϱ is the density of the crystal; x_j is the particle position vector-component in the crystallographic coordinate system; u_j is the particle displacement component; T_{ij}-s are the components of the stress tensor, which depends on the

$$S_{kl} = \frac{1}{2}\left(\frac{\partial u_k}{\partial x_e} + \frac{\partial u_e}{\partial x_k}\right) \tag{2}$$

strain tensor component and on the E_k electric field components as follows:

$$T_{ij} = c_{ijkl} \cdot S_{k1} - e_{kij} E_k \,. \tag{3}$$

Here c_{ijkl}-s are the components of the stiffness tensor and e_{kij}-s are the tensor components describing direct relations between the electric field and the piezoelectrically induced stress. The repetition of the indices implies summation.

In the case of the KDP sample investigated in our experiments the KDP crystal is cut perpendicular to the crystallographic axes with edges a, a, l and the electric field is applied along the [0 0 1] direction (Fig. 1). The electric field, taking into account the $\bar{4}2m$ symmetry of KDP crystals, causes T_{12} and T_{21} non zero stress components by the inverse piezoelectric effect. T_{12} is the shear stress producing displacement u_2 along the [0 1 0] direction. Similarly, T_{21} induces displacements u_1 in the [1 0 0] direction.

According to the symmetry of the arrangement and neglecting the influence of the lateral surfaces the shear displacement u_1 spatially depends on the x_2 coordinate only and u_2 depends on x_1, respectively. This means that all planes parallel to the (100) and (010) surfaces of the sample are planes of constant phase and the wave can be treated one-dimensionally. In this way u_1 and u_2 are functions of the time and the x_2 or x_1 coordinate, respectively:

$$u_1 = u_1(x_2, t); \quad u_2 = u_2(x_1, t) \,. \tag{4}$$

From Eqs. (1)—(3), using condition (4), two relatively simple equations follow for the generation and propagation of piezoelectrically induced acoustic transients:

$$\frac{\partial^2 u_1}{\partial x_2^2} - \frac{1}{v^2} \frac{\partial^2 u_1}{\partial t^2} = \frac{\partial}{\partial x_2} (d_{36} E_3) \,, \tag{5}$$

$$\frac{\partial^2 u_2}{\partial x_1^2} - \frac{1}{v^2} \frac{\partial^2 u_2}{\partial t^2} = \frac{\partial}{\partial x_1} (d_{36} E_3) \,. \tag{6}$$

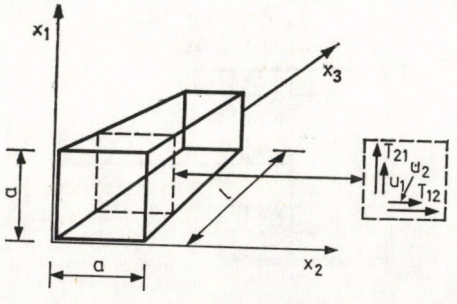

Fig. 1. The investigated KDP sample

Here the condensed matrix notation is used and the constants are:

$$d_{36} = e_{36}/c_{66}; \quad v^2 = c_{66}/\varrho .$$

Expressions (5) and (6) are inhomogeneous wave equations describing plane waves propagating with velocity v defined above. The sources of the waves are the gradients of the piezoelectrically induced strains. Assuming the electric field to be homogeneous within the sample, nonvanishing gradients of the piezoelectric strains are only at the (100) and (010) side surfaces of the sample. Thus, the sources of the acoustic waves are at the side surfaces of the KDP crystal sample.

The method for the solution of the inhomogeneous wave equations is given in papers [19] and [7]. The Green function method is used in the case of rectangular voltage pulses. The general conclusions can be applied in our case as well.

The spatial distribution of the source term according to the abrupt fall of the $(d_{36}E_3)$ term at the lateral surfaces of the crystal sample can be given by a very sharp distribution. The time dependence of the source term and the shape of the acoustic pulses is determined by the time-dependence of driving voltage (Fig. 2). The distribution of the strain in the acoustic pulses propagating in the KDP sample is expected to be as shown in Fig. 2. The lined strips represent the areas where the strain differs from zero. These strips are assumed to be propagated with constant velocity, neglecting the dispersion of Fourier components of acoustic pulses. Arriving at the opposite side faces of the sample the acoustic pulses are expected to be reflected back into the crystal.

The acoustic pulses shown in Fig. 2 can be made visible on the principle of the strain-optic birefringence. If the crystal is placed between crossed polarizers on the areas of the aperture where the strain differs from zero, a time-dependent, spatial transmission is expected which is determined by the strain distribution. The transmission in crossed polarizer arrangement, if the analyzer

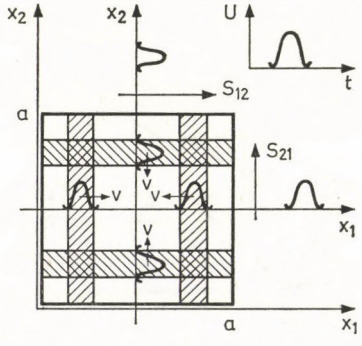

Fig. 2. Expected strain distribution

is parallel to the x_1 or the x_2 crystallographic axis depends on the retardation Γ as

$$T = T_{\max} \sin^2 \frac{\Gamma}{2}. \tag{7}$$

The retardation

$$\Gamma = 2\pi \frac{\Delta n \cdot l}{\lambda}, \tag{8}$$

where Δn is the strain-optic birefringence, l is the length of the crystal and λ is the wavelength of the transmitted light in vacuum.

The strain-optic birefringence linearly depends on the strain; in the acoustic pulses propagating along the x_1 axis

$$\Delta n = \frac{1}{2} n_0^3 p_{66} S_{12} \tag{9}$$

and in the acoustic pulses propagating along the x_2 axis, similarly

$$\Delta n = \frac{1}{2} n_0^3 p_{66} S_{21}. \tag{10}$$

n_0 is the ordinary refractive index of the uniaxial KDP crystal and p_{66} is the proper strain-optic coefficient, in condensed matrix notation.

As can be seen in Fig. 2 the areas in which the strain, and thus the transmission, differs from zero, are moving strips. Using relatively short light pulses, with variable delay to the high voltage pulses, we can follow the propagation of the acoustic pulses with a camera focussed on the exit face of the KDP crystal.

3. Experimental set-up

A detailed description of the experimental method has been reported [14]. The main part of the experimental set up can be seen in Fig. 3.

A 15 mm × 15 mm × 25 mm sample was cut from a KDP monocrystal grown by our group. The 25 mm edge is along the x_3 axis (see Fig. 1). The

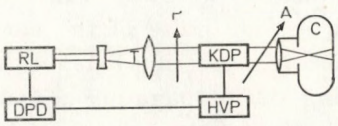

Fig. 3. Experimental set-up
KDP-crystal sample, P-polarizer, A-analyser, DPD-digital pulse delay generator, HVP-high voltage pulse generator, RL-ruby laser, T-Galilean telescope, C-camera

(001) end faces are polished. Copper plate electrodes with 13 mm diameter circular opening are pressed to the end faces of the sample by springs. The KDP sample is placed between crossed polarizers. The polarization direction of the polarizer (P) is parallel to x_1, and that of the analyser (A) is parallel to the x_2 crystallographic axis. The half-wave voltage measured under static conditions is about 17 kV for the wavelength of the He-Ne laser (6328 Å) in the middle point of the aperture. This high value can be explained by the non-uniform electric field distribution due to the large aperture diameter and by the high resistance of the junction between the copper plate electrode and the crystal surface.

The experimental system is controlled by an eight channel digital pulse delay generator (DPD). The delay of pulses of each channel can be set separately from each other in 1 μsec steps. The precision of the delay is about 50 nsec.

The KDP modulator is driven by 12 kV pulses of a high voltage pulse generator (HVP). The HVP generator is started by a pulse from a channel of the DPD generator. The rising and trailing edges of the high voltage pulses are about 50 nsec long and the pulse width is about 300 nsec.

The exposure light is given by a ruby laser (RL). The laser is controlled by another channel of the DPD generator. The halfwidth of the RL pulses is about 60 nsec. The laser radiates in TEM_{00} mode. The cross-section of the laser beam is enlarged and collimated by a Galilean telescope (T). This cross-section is about twice as large as the clear aperture. The delay of the exposure light pulses is changed in 1 μsec steps over the 1—150 μsec range.

The camera (C) is focussed on the exit face of the crystal and it takes a picture in every shot of the laser, setting variable delay for every shot after the high voltage pulse on the KDP crystal. So the camera takes a ciné film of the acoustic processes taking place in the crystal on shot by shot basis.

4. Experimental results

The frames of the ciné film of the acoustic processes can be seen in Figs. 4—7. The most characteristic propagating features of the acoustic pulse generated in the KDP crystal by the inverse piezoelectric effect are demonstrated on the frames. The pictures were taken in 1 μsec steps. The delay of the ruby-laser pulse to the driving pulse of the modulator is given at the bottom of every frame. The bright crossing bars on the frames are the transmission patterns representing the propagating acoustic pulses.

The velocity of propapation of the acoustic pulses was calculated from the distances measured on the photos. It was found to be the same in both directions of propagation. The calculated value is (1540 ± 100) m/s.

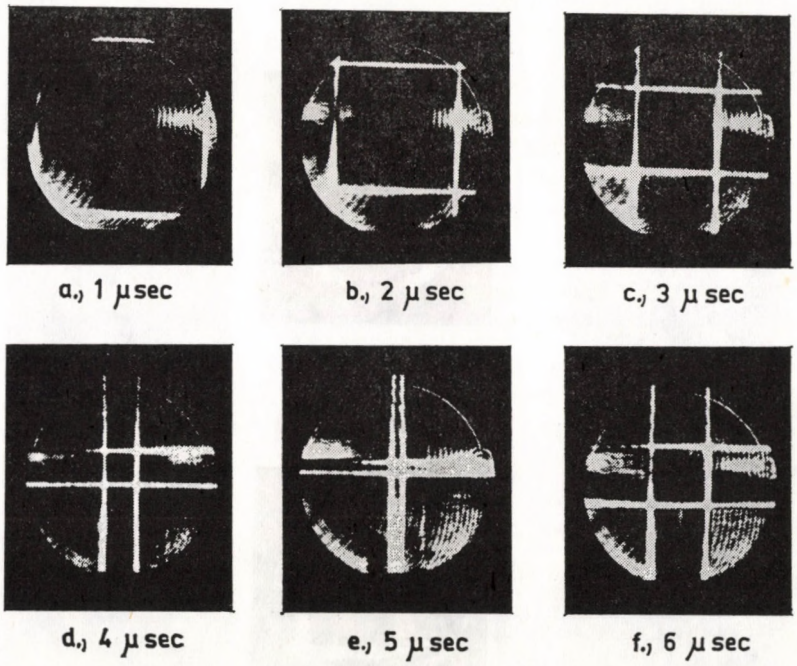

Fig. 4. The acoustic transients start from the side surfaces and propagate with constant velocity

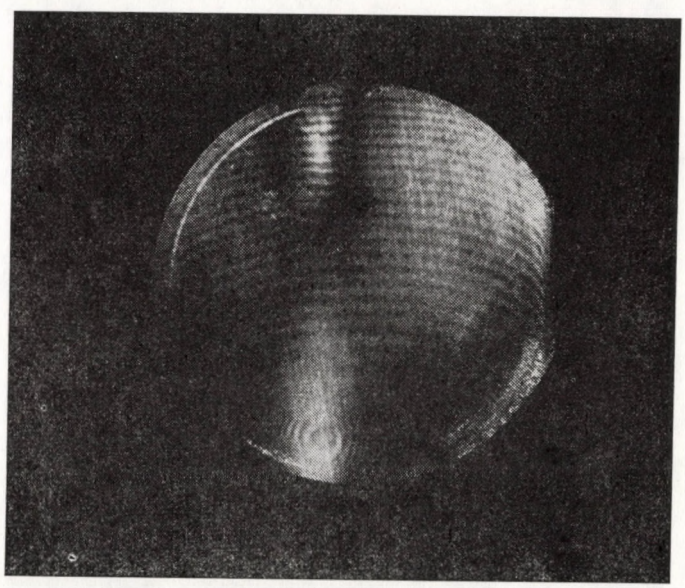

Fig. 5. The transmission background

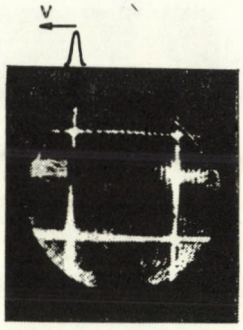

a., 7 μ sec

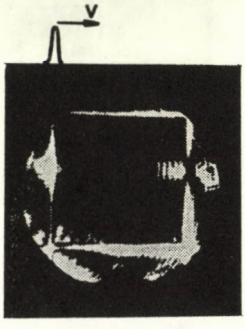

b., 11 μ sec

Fig. 6. The phase change at reflexion

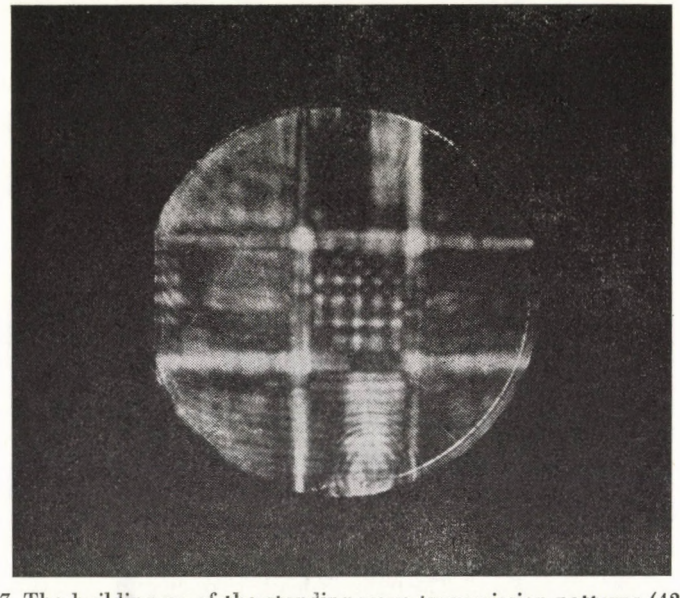

Fig. 7. The building up of the standing wave transmission patterns (42 μsec)

The acoustic pulses move from the side faces towards the centre of the crystal. They cross each other and move further to the opposite side faces as can clearly be seen on the frames. Arriving to the opposite faces the waves are reflected and start to move back into the crystal. This cycle is repeated again and again.

If we follow the propagation of the acoustic pulses, several phenomena can be observed.

The acoustic pulses interfere with each other. During their propagation they diffuse. Diffraction of the acoustic pulses can also be observed. There are areas on the aperture where the bright bars representing the acoustic pulses are significantly widened or they nearly disappear. Leaving these areas the bright bars are very regular parallel strips again as they were earlier.

In spite of these processes the acoustic pulses can be seen also at delays being as large as 150 μsec. But these processes causing the smearing off of the acoustic pulses give rise to the appearance at transmission of patterns similar to that well known from the work of STEPHANY [15].

5. Discussion

The frames in Fig. 4 give direct evidence that the sources of the acoustic waves are at the free surfaces of the crystal, as was concluded by JACOBSEN [19] (and was shown for longitudinal KDP modulators in reference [7]). More precisely, the sources exist in the crystal where the gradients of the $d_{36}E_3$ product differ from zero, as can be seen from wave equations (5) and (6). The assumption is valid only in a homogeneous electric field approximation that sources of acoustic waves are at the side surface of the crystal. Actually in our high aperture electrode arrangement the electric field has a non-uniform distribution inside the crystal and there are non-zero gradients of the $d_{36}E_3$ term. Since the electric field changes relatively slowly the source terms relating to the non-uniform electric field distribution inside the crystal can be neglected.

The acoustic pulses are composed of acoustic waves due to the Fourier components of the generating high voltage pulse. The composing acoustic waves must be in good approximation plane waves as can be concluded from the photos of the acoustic pulse (Fig. 4).

From the measured propagating velocity of the acoustic pulses and the density of the crystal the c_{66} elastic coefficient can be calculated. Its value is $(6.1 \pm 0.6) \cdot 10^9$ N/m^2 in good agreement with the value published by MASON [21].

At the intersection of the acoustic pulses a positive superposition of the acoustic pulses can be observed. This means that the acoustic pulses propa-

gating at right angles to each other cause in refractive indices changes of the same sign. From the similar brightness distribution in the acoustic pulses it can be concluded that they are very similar to each other regarding their strain distribution as well. Arriving at the opposite faces the acoustic pulses are reflected.

The transmission picture taken in the experiments can be separated into two parts. The primary one is the time-dependent part, i.e. the propagation of the bright bars representing the acoustic pulses as discussed above. Besides the primary part there is a transmission background which is constant in time as can be seen on every frame.

The transmission background is shown in the photo of Fig. 5 taken when no acoustic transient was present in the KDP sample. The curved strips are the fringes of equal thickness — the polished end faces of the crystal are not exactly parallel to each other and they are slightly spherical. As can be seen in the photos the density and the curvature of the fringes of equal thickness change on the aperture of the crystal. Besides these relatively regular interference fringes there are significant nonuniformities on the transmission pictures. The most obvious one can be seen slightly above the horizontal diameter of the aperture. This nonuniformity can be caused by a crystal imperfection across the crystal. The stress distribution in the imperfection causes the characteristic transmission distribution by the strain optic birefringence. The crystal was checked in a Mach—Zender interferometer KP-74 and the distortion of the interference fringes proved the assumption.

The stress field of this crystal imperfection interacts with the stress field of the propagating acoustic pulses. It can be seen in the frames of Fig. 4 that the stress field of the crystal imperfection and the acoustic pulse interfere positively on the right side of the imperfection and they cause each other diminish in the area on the left side. The stress field of the imperfection probably changes the sign from left to right. At the middle part of the aperture interference of the acoustic pulses with the assumed stress distribution cannot be observed (Figs. 4 d and e). This proves that the stress changes sign in the central part of the imperfection and therefore the stress in the middle part is negligible.

Returning to the reflection process it can be established that the stress field of the acoustic pulses changes sign during reflection. The vertical bright bar at the left side of Fig. 6a shows negative interference with the stress distribution of the crystal imperfection. After reflection nearly at the same place a remarkable positive interference can be observed (Fig 6b).

The diffusion of the acoustic pulses can be well observed after the first tén photos. The diffusion is the consequence of the dispersion of the Fourier components of the acoustic waves composing the acoustic pulse, and that of the diffraction in the reflection processes on the side faces.

The interaction with the crystal imperfections causes the spreading of the acoustic pulses. The short wavelength components exist longer and therefore the acoustic pulses are observable long after generation. The components of long wavelengths give rise to the appearance of transmission patterns similar to the typical standing wave transmission patterns which are developed in the case of periodical driving (Fig. 7).

6. Conclusion

The experiments prove the results calculated by the simplified mathematical model. The method developed for investigations makes a direct visualization of the acoustic transient processes possible.

The experimental results can be evaluated quantitatively, beside the sound velocity and related elastic constant, the elastoopic, piezoelectric and electrooptic properties of crystals can be calculated by the microdensitometric evaluation of the photos. Such measurements are planned.

The experimental method may be very useful in the design of electrooptic devices in which disturbing acoustic transients and resonances may take place.

REFERENCES

1. J. P. KAMINOW, An Introduction to Electrooptic Devices, Academic Press, New York and London, 1974.
2. A. C. SONIN and A. C. VASHILEVSKAYA, Elektroopticheskie Kristalli, Atomizdat, Moscow, 1971.
3. T. R. SLIKER and S. R. BURLAGE, J. Appl. Phys., **34**, 1837, 1963.
4. T. M. CHRISTMAS and C. G. WILDEY, Electr. Lett., **6**, 152, 1970.
5. W. D. FOUNTAIN, Appl. Opt., **10**, 972, 1971.
6. H. GERLACH, Appl. Phys. **1**, 279, 1973.
7. H. VEESER, U. BOGNER and W. EISENMENGER, Phys. Stat. Sol. (a) **37**, 161, 1976.
8. A. M. MARUGIN and V. M. OVSHINNIKOV, Opt. Mech. Prom., **37**, 79, 1969.
9. J. M. LEY, T. M. CHRISTMAS and C. G. WILDEY, Proc. IEE, **117**, 1057, 1970.
10. R. P. HILBERG and W. R. HOOK, Appl. Opt., **9**, 1939, 1970.
11. K. RASHIDI, Electric Lett., **7**, 114, 1971.
12. R. PEPPERL, Optica Acta, **24**, 413, 1977.
13. T. A. KUZOVKOVA, A. M. MARUGIN, E. V. NILOV and V. M. OVSHINNIKOV, Opt. Mech. Prom., **44**, 57, 1977.
14. J. BAKOS, Zs. SÖRLEI, Cs. KUTI and S. SZIKORA, Appl. Phys. **19**, 59, 1979.
15. J. F. STEPHANY, JOSA, **55**, 136, 1965.
16. F. HOFF and B. STADNIK, Electr. Lett., **2**, 293, 1966.
17. C. F. BROVEEV, A. J. CAUKOV and A. A. UGODENKO, P.T.E., 181, 1972.
18. T. A. KUZOVKOVA and E. V. NILOV, Opt. i Spektr., **42**, 687, 1977.
19. E. H. JACOBSEN, J. Acoust. Soc. Amer., **32**, 949, 1960.
20. W. P. MASON, Physical Acoustic Vol. I. A. Academic Press, New York and London, 1964.
21. W. P. MASON, Phys. Rev., **69**, 173, 1946.

RECENSIONES

WALTER THIRRING: Classical Dynamical Systems

Springer, New York, Wien, 1978, 258 pages

The author is respected for his exactly soluble models in the scientific world community. This book, the first in a series of four volumes, containing his lectures at the Vienna University, deals with classical mechanics. The theorems and problems treated are essentially the same as in any University course, but a special flavour is given by the full mathematical rigour. It is remarkable that this does not make the treatment longer, it has made it even more compact. The language of the book is the elegant Bourbaki language of modern mathematics, generally spoken among mathematicians and spreading among theoretical physicists. Looking at the contents of the different chapters, one discovers that the restricted motions and some approximation methods (relevant mainly for mechanical engineering) are omitted; they were inconsistent with the spirit of the book. On the other hand, a consequent use of configuration space, phase space and fourdimensional space time is offered, which is certainly the most powerful way to present the Newtonian dynamics from a 20th century point of view. In this framework e.g. the Liouville theorem, quasi ergod theorem, the asymptotic treatment of scattering problem have found a natural place. The book is strongly recommended to mathematics students, who are interested in learning hard physics in their own language. It is also recommended for those readers of physics, who are eager to present classical dynamics as a relevant part of 20th century physics.

G. MARX

Particles and Fields

Edited by David H. Boal and Abdul N. Kamal
Plenum Publishing Corporation, New York and London, 1978, viii + 462 pages

This book contains the invited lectures and seminars presented at the Banff Summer Institute on Particles and Fields, held at the Banff Center in Banff, Canada, from 25 August to 3 September, 1977. It presents recent experimental and theoretical developments in particle physics and field theory. The book contains such topics as extended objects, lattice gauge theories, quantum chromodynamics, Reggeon field theory, the theoretical interpretation of colliding electron-positron beam experiments and gauge theories of weak interaction. Experimental reviews of recent work in charmed particle and neutrino physics, as well as summaries of the theoretical implications of these experiments are also given.

The book includes eight lectures and six seminars. Lectures:

Contemporary Reggeon Physics (ABARBANEL)
Chromodynamic Structure and Phenomenology (APPELQUIST)
Charmed Particle Spectroscopy (FELDMAN)
Hadron Spectroscopy and the New Particles (GILMAN)
Extended Objects in Gauge Field Theories ('T HOOFT)

Classical and Semi-classical Solutions of the Yang-Mills Theory (JACKIV, NOHL and REBBI)
Some Recent Advances in Neutrino Physics (MANN)
Lattice Gauge Theories (WEINSTEIN)

Seminars :

Non-perturbative Method in Field Theory (CAIANIELLO, MARINARO and SCARPETTA)
Dimensional Regularisation and Hyperfunctions (FUJII)
Transverse Momentum Distribution of Partons in Quantum Chromodynamics (LAM)
Trimuons (PHILLIPS)
An Approach to Measurement in Quantum Mechanics (SUDARSHAN, SHERRY and GAUTAM)
A Survey of Vortices in Gauge Theories (TZE)

G. KNAPECZ

General Physics with Bioscience Essays

John Wiley & Sons, Inc, New York, Chichester, Brisbane, Toronto, 1979, pp. 555

This book is a text for a general introductory course in physics for students whose main interest and careers lie in other areas. The mathematical ability necessary to master the material presented is not great — high school algebra is used extensively and simple trigonometry is used where necessary. The Appendix summarizes all of the mathematical techniques required to understand the discussions and to solve the problems.

There is a strong emphasis on classical physics, with discussions of all the important topics but there is also a generous amount of material on modern physics.

To understand and appreciate the various concepts and applications of physics, considerable drill in problem solving is required. Each chapter contains a collection of worked examples covering all of the important points. Moreover, at the end of each chapter there is a list of questions to test the student's comprehension of the concepts and a generous number of problems to test his or her problem-solving abilities. The more difficult problems are indicated by an asterisk, and the answers to the odd-numbered problems are at the back of the book. Altogether, there are approximately one *thousand* questions and problems in the 20 chapters of this book. For the students who whish assistance in a planned study program, a Study Guide is available to accompany the text.

Many of the students who take an introductory physics course are looking towards careers in medicine, dentistry, nursing, medical technology, microbiology, chemistry, and a variety of other professions in or related to the life sciences. These students, in particular, sometimes wonder how the subject of physics plays a role in the behavior of living things. The attempt to provide a partial answer to this curiosity has led to the development of the unique aspect of this book, that is, the inclusion of a number of essays on bioscience topics that emphasize the importance of physical principles in the operation of living systems. Each essay is related directly to the material in the chapter of which it is a part. But the essays are supplementary to and separate from the material in the chapters themselves. That is, the essays are optional and can be completely skipped without loss in the flow of physics ideas. However, by omitting the essays, some of the most interesting physics in the book will be lost!

One of the ideas in preparing this collection of bioscience essays was to provide, for every main physics topic, some quantitative life-science application Therefore, each essay contains some numerical discussion of the topic and some numerical problems so the students can see how calculations are carried out in a different area of science. The essays here amount to about 13 percent of the text.

I. KOVÁCS

Quantentheorie elementarer Objekte

Von Prof. Dr. CARL-FRIEDRICH Frhr. von WEIZSÄCKER, Starnberg

(Nova Acta Leopoldina. Neue Folge. Nr. 230, Bd. 49)

1978. 19 Seiten
Broschiert 2,80 M

Carl-Friedrich Frhr. v. Weizsäcker, dessen Geltung und Kompetenz sowohl als Theoretischer Physiker, wie auch als Naturphilosoph weltweit unbestritten ist, greift die in der LEOPOLDINA mehrfach von verschiedenen Wissenschaftlern diskutierte Frage wieder auf, die man überspitzt formulieren könnte: »Sind Elementarteilchen elementar?« Der Autor entscheidet sich nach gründlicher Diskussion dafür, lieber von »elementaren Objekten« zu sprechen.

Ausgehend von der griechischen Atomistik und der klassischen Physik KEPLERs und NEWTONs zeigt er, wie mehrfach versucht wurde, die moderne Mikrophysik aus der klassischen Physik herzuleiten oder diese zumindest auf jene zurückzuführen. Er erläutert, wie das, was noch vor 2 Jahrzehnten für »elementar« gehalten wurde, heute wiederum in noch kleinere »Elemente« zerlegt wird, die Quarks. Mittlerweile gibt es davon auch schon wieder über 20 verschiedene. Nach einer Diskussion von Symmetrie- und Drehgruppen kommt er auf die in seinem Institut aktuell bearbeitete Uralternative zu sprechen, das Ur.

Die philosophische Interpretation der modernen Physik

Zwei Vorlesungen

Von Prof. Dr. Carl-Friedrich Frhr. v. WEIZSÄCKER, Starnberg

(Nova Acta Leopoldina. Neue Folge. Nr. 207, Bd. 37/2)

5. Auflage

1978. 39 Seiten

Broschiert 6,80 M

In den beiden Essays gibt der bekannte theoretische Physiker, der sich auf den Gebieten der Theorie der Elementarteilchen, der Kosmogonie und der Turbulenztheorie weltweit einen Namen gemacht hat, der aber gleichzeitig eine der markantesten Naturphilosophenpersönlichkeiten ist, einen Überblick über seine Sicht der derzeitigen philosophischen Problematik der modernen Physik. Er zeigt insbesondere neue und sehr originelle Gedanken über die Stellung der modernen Physik im Gesamtsystem der Naturwissenschaften überhaupt.

Bestellungen an den Buchhandel erbeten

JOHANN AMBROSIUS BARTH LEIPZIG

Printed in Hungary

A kiadásért felel az Akadémiai Kiadó igazgatója. Műszaki szerkesztő: Botyánszky Pál
A kézirat a kiadóba érkezett: 1979. V. 25. A kézirat nyomdába érkezett: 1979. VI. 6. — Terjedelem: 8 (A/5) ív, 26 ábra

80.7219 Akadémiai Nyomda, Budapest — Felelős vezető: Bernát György

NOTES TO CONTRIBUTORS

I. PAPERS will be considered for publication in Acta Physica Hungarica, only if they have not previously been published or submitted for publication elsewhere. They may be written in English, French, German or Russian.

Papers should be submitted to

Prof. I. Kovács, Editor
Department of Atomic Physics, Technical University
1521 Budapest, Budafoki út 8, Hungary

Papers may be either articles with abstracts or short communications. Both should be as concise as possible, articles in general not exceeding 25 typed pages, short communications 8 typed pages.

II. MANUSCRIPTS

1. Papers should be submitted in five copies.

2. The text of papers must be of high stylistic standard, requiring minor corrections only.

3. Manuscripts should be typed in double spacing on good quality paper, with generous margins.

4. The name of the author(s) and of the institutes where the work was carried out should appear on the first page of the manuscript.

5. Particular care should be taken with mathematical expressions. The following should be clearly distinguished, e.g. by underlining in different colours: special founts (italics, script, bold type, Greek, Gothic, etc.); capital and small letters; subscripts and superscripts, e.g. x_2, x^3; small *l* and 1; zero and capital O; in expressions written by hand: *e* and *l*, *n* and *u*, *v* and v, etc.

6. References should be numbered serially and listed at the end of the paper in the following form: J. Ise and W. D. Fretter, Phys. Rev., *76*, 933, 1949.

For books, please give the initials and family name of the author(s), title, name of publisher, place and year of publication, e.g.: J. C. Slater, Quantum Theory of Atomic Structures, I. McGraw-Hill Book Company, Inc., New York, 1960.

References should be given in the text in the following forms: Heisenberg [5] or [5].

7. Captions to illustrations should be listed on a separate sheet, not inserted in the text.

III. ILLUSTRATIONS AND TABLES

1. Each paper should be accompanied by five sets of illustrations, one of which must be ready for the blockmaker. The other sets attached to the copies of the manuscript may be rough drawings in pencil or photocopies.

2. Illustrations must not be inserted in the text.

3. All illustrations should be identified in blue pencil by the author's name, abbreviated title of the paper and figure number.

4. Tables should be typed on separate pages and have captions describing their content. Clear wording of column heads is advisable. Tables should be numbered in Roman numerals (I, II, III, etc.).

IV. MANUSCRIPTS not in conformity with the above Notes will immediately be returned to authors for revision. The date of receipt to be shown on the paper will in such cases be that of the receipt of the revised manuscript.

Reviews of the Hungarian Academy of Sciences are obtainable at the following addresses:

AUSTRALIA
C.B.D. LIBRARY AND SUBSCRIPTION SERVICE, Box 4886, G.P.O., *Sydney N.S.W.2001*
COSMOS BOOKSHOP, 145 Ackland Street, *St. Kilda (Melbourne), Victoria 3182*

AUSTRIA
GLOBUS, Höchstädtplatz 3, *1200 Wien XX*

BELGIUM
OFFICE INTERNATIONAL DE LIBRAIRIE, 30 Avenue Marnix, *1050 Bruxelles*
LIBRAIRIE DU MONDE ENTIER, 162 Rue du Midi, *1000 Bruxelles*

BULGARIA
HEMUS, Bulvar Ruszki 6, *Sofia*

CANADA
PANNONIA BOOKS, P.O. Box 1017, Postal Station "B", *Toronto, Ontario M5T 2T8*

CHINA
CNPICOR, Periodical Department, P.O. Box 50, *Peking*

CZECHOSLOVAKIA
MAD'ARSKÁ KULTURA, Národní třida 22, *115 66 Praha*
PNS DOVOZ TISKU, Vinohradská 46, *Praha 2*
PNS DOVOZ TLAČE, *Bratislava 2*

DENMARK
EJNAR MUNKSGAARD, Norregade 6, *1165 Copenhagen*

FINLAND
AKATEEMINEN KIRJAKAUPPA, P.O. Box 128, *SF-00101 Helsinki 10*

FRANCE
EUROPERIODIQUES S. A., 31 Avenue de Versailles, *78170 La Celle St.-Cloud*
LIBRAIRIE LAVOISIER, 11 rue Lavoisier, *75008 Paris*
OFFICE INTERNATIONAL DE DOCUMENTATION ET LIBRAIRIE, 48 rue Gay-Lussac, *75240 Paris Cedex 05*

GERMAN DEMOCRATIC REPUBLIC
HAUS DER UNGARISCHEN KULTUR, Karl-Liebknecht-Strasse 9, *DDR-102 Berlin*
DEUTSCHE POST ZEITUNGSVERTRIEBSAMT, Strasse der Pariser Kommüne 3—4, *DDR-104 Berlin*

GERMAN FEDERAL REPUBLIC
KUNST UND WISSEN ERICH BIEBER, Postfach 46, *7000 Stuttgart 1*

GREAT BRITAIN
BLACKWELL'S PERIODICALS DIVISION, Hythe Bridge Street, *Oxford OX1 2ET*
BUMPUS, HALDANE AND MAXWELL LTD., Cowper Works, *Olney, Bucks MK46 4BN*
COLLET'S HOLDINGS LTD., Denington Estate, *Wellingborough, Northants NN8 2QT*
W.M. DAWSON AND SONS LTD., Cannon House, *Folkestone, Kent CT19 5EE*
H. K. LEWIS AND CO., 136 Gower Street, *London WC1E 6BS*

GREECE
KOSTARAKIS BROTHERS, International Booksellers, 2 Hippokratous Street, *Athens-143*

HOLLAND
MEULENHOFF-BRUNA B.V., Beulingstraat 2, *Amsterdam*
MARTINUS NIJHOFF B.V., Lange Voorhout 9—11, *Den Haag*
SWETS SUBSCRIPTION SERVICE, 347b Heereweg, *Lisse*

INDIA
ALLIED PUBLISHING PRIVATE LTD., 13/14 Asaf Ali Road, *New Delhi 110001*
150 B-6 Mount Road, *Madras 600002*
INTERNATIONAL BOOK HOUSE PVT. LTD., Madame Cama Road, *Bombay 400039*
THE STATE TRADING CORPORATION OF INDIA LTD., Books Import Division, Chandralok, 36 Janpath, *New Delhi 110001*

ITALY
EUGENIO CARLUCCI, P.O. Box 252, *70100 Bari*
INTERSCIENTIA, Via Mazzé 28, *10149 Torino*
LIBRERIA COMMISSIONARIA SANSONI, Via Lamarmora 45, *50121 Firenze*
SANTO VANASIA, Via M. Macchi 58, *20124 Milano*
D. E. A., Via Lima 28, *00198 Roma*

JAPAN
KINOKUNIYA BOOK-STORE CO. LTD., 17-7 Shinjuku-ku 3 chome, Shinjuku-ku, *Tokyo 160-91*
MARUZEN COMPANY LTD., Book Department, P.O. Box 5050 Tokyo International, *Tokyo 100-31*
NAUKA LTD. IMPORT DEPARTMENT, 2-30-19 Minami Ikebukuro, Toshima-ku, *Tokyo 171*

KOREA
CHULPANMUL, *Phenjan*

NORWAY
TANUM-CAMMERMEYER, Karl Johansgatan 41—43, *1000 Oslo*

POLAND
WĘGIERSKI INSTYTUT KULTURY, Marszalkowska 80, *Warszawa*
CKP I W ul. Towarowa 28 *00-958 Warsaw*

ROMANIA
D. E. P., *Bucureşti*
ROMLIBRI, Str. Biserica Amzei 7, *Bucureşti*

SOVIET UNION
SOJUZPETCHATI — IMPORT, *Moscow* and the post offices in each town
MEZHDUNARODNAYA KNIGA, *Moscow G-200*

SPAIN
DIAZ DE SANTOS, Lagasca 95, *Madrid 6*

SWEDEN
ALMQVIST AND WIKSELL, Gamla Brogatan 26, *101 20 Stockholm*
GUMPERTS UNIVERSITETSBOKHANDEL AB, Box 346, *401 25 Göteborg 1*

SWITZERLAND
KARGER LIBRI AG, Petersgraben 31, *4011 Basel*

USA
EBSCO SUBSCRIPTION SERVICES, P.O. Box 1943, *Birmingham*, Alabama 35201
F. W. FAXON COMPANY, INC., 15 Southwest Park, *Westwood*, Mass. 02090
THE MOORE-COTTRELL SUBSCRIPTION AGENCIES, *North Cohocton, N. Y. 14868*
READ-MORE PUBLICATIONS, INC., 140 Cedar Street, *New York, N. Y. 10006*
STECHERT-MACMILLAN, INC., 7250 Westfield Avenue, *Pennsauken* N. J. 08110

VIETNAM
XUNHASABA, 32, Hai Ba Trung, *Hanoi*

YUGOSLAVIA
JUGOSLAVENSKA KNJIGA, Terazije 27, *Beograd*
FORUM, Vojvode Mišiča 1, *21000 Novi Sad*

Index: 26.022
Acta Phys. Hung. Tom. 46. No. 3. Budapest, 12. XII. 1979 HU-ISSN 0001-6705

ACTA PHYSICA

ACADEMIAE SCIENTIARUM HUNGARICAE

TOMUS XLVI FASCICULUS 4

AKADÉMIAI KIADÓ, BUDAPEST

1979

ACTA PHYS. HUNG. APAHAQ 46 (4) 217—342 (1979)

ACTA PHYSICA

ACADEMIAE SCIENTIARUM HUNGARICAE

SZERKESZTI

KOVÁCS ISTVÁN

Az *Acta Physica* angol, német, francia vagy orosz nyelven közöl értekezéseket. Évente két kötetben, kötetenként 4—4 füzetben jelenik meg. Kéziratok a szerkesztőség címére (1521 Budapest XI., Budafoki út 8.) küldendők.

Megrendelhető a belföld számára az Akadémiai Kiadónál (1363 Budapest Pf. 24. Bankszámla 215-11488), a külföld számára pedig a „Kultura" Külkereskedelmi Vállalatnál (1389 Budapest 62, P.O.B. 149. Bankszámla 217-10990), vagy annak külföldi képviseleteinél.

The *Acta Physica* publish papers on physics in English, German, French or Russian, in issues making up two volumes per year. Subscription: $ 36.00 per volume. Distributor: "Kultura" Foreign Trading Company (1389 Budapest 62, P.O. Box 149) or its representatives abroad.

Die *Acta Physica* veröffentlichen Abhandlungen aus dem Bereich der Physik in deutscher, englischer, französischer oder russischer Sprache, in Heften, die jährlich zwei Bände bilden.

Abonnementspreis pro Band: $ 36.00. Bestellbar bei »Kultura« Außenhandelsunternehmen (1389 Budapest 62, Postfach 149) oder seinen Auslandsvertretungen.

Les *Acta Physica* publient des travaux du domaine de la physique en français, anglais, allemand ou russe, en fascicules qui forment deux volumes par an.

Prix de l'abonnement: $ 36.00 par volume. On peut s'abonner à l'Entreprise du Commerce Extérieur «Kultura» (1389 Budapest 62, P.O.B. 149) ou chez représentants à l'étranger.

«*Acta Physica*» публикуют трактаты из области физических наук на русском, немецком, английском и французском языках.

«*Acta Physica*» выходят отдельными выпусками, составляющими два тома в год.

Подписная цена — $ 36.00 за том. Заказы принимает предприятие по внешней торговле «Kultura» (1389 Budapest 62, P.O.B. 149) или его заграничные представительства.

ACTA PHYSICA

ACADEMIAE SCIENTIARUM HUNGARICAE

TOMUS XLVI FASCICULUS 4

AKADÉMIAI KIADÓ, BUDAPEST
1979

ACTA PHYS. HUNG.

INDEX

Acta Physica Academiae Scientiarum Hungaricae, Tomus 46 (4), pp. 217—236 (1979)

LES NOMBRES QUANTIQUES COMME PARAMÈTRES CACHÉS DANS L'INTERPRÉTATION CAUSALE DE LA MÉCANIQUE ONDULATOIRE

Par

T. MÁTRAI

CHAIRE DE PHYSIQUE À L'ÉCOLE SUPÉRIEURE PÉDAGOGIQUE DE EGER, EGER, HONGRIE

(Reçu 16. I. 1979)

Ce travail adhère à la conception de M. L. DE BROGLIE [1]. Suivant celle-ci, la mécanique ondulatoire ne fournit que des données probables sur une microparticule seulement parce que celles-ci sont incomplètes et même imprecises. Point de besoin alors de considérer la particule comme par sa nature floue dans l'espace de ses cordonnées et de sa vitesse. Attribuons ici donc — à la particule — un lieu $\mathbf{r}(t)$ ponctuel, c'est-à-dire une orbite précise à un temps t arbitraire dans le système d'inertie[1] et prêtons l'incertitude Heisenbergienne seulement à l'intervention de mesure [4]. Cette étude même — profitant des enseigments de plusieurs tentatives précedentes [5—12] — cherche à interpréter un cas individuel à l'aide de la généralisation connue (jusqu'ici pensée formelle) de la point-dynamique Hamilton—Jacobienne.[2] Elle cherche, notamment sur le chemin, proposé également par BOHM [7], la solution totale de l'équation Jacobienne généralisée mais elle y explore par des considérations de correspondances les paramètres de dynamique, désignés habituellement dans la mécanique classique par α_j ainsi que β_j ($j = 1, 2, 3$), puis elle les suit jusqu'à leur dérobade. Il en dégage ainsi les paramètres, indiqués par α, sont contenus en fait dans les fonctions propres de mécanique ondulatoire, mais en dernière analyse, trivialement cachés dans le domaine, déterminé par les nombres quantiques, c'est-à-dire dégénérés en comptables. C'est pourquoi, dans la valabilité de la statistique quantique de bien beaucoup de particules, ne peuvent pas se présenter de changements séculaires qui, selon PAULI [14], peuvent être provoqués par les paramètres cachés. En effet, les statistiques quantiques comptaient même jusqu'ici avec des nombres quantiques, et cela est en concordance complète avec les expériences. Le travail présent démontre comment il faut ordonner une orbite à la particule et dans son état pur et son état mélangé, mais il montre aussi que les paramètres, indiqués par β ont leur rôle non seulement dans la détermination de l'orbite individuelle, mais dans celle de multitude statistique de particules à la mécanique ondulatoire même. Pendant la discussion, il devient également prouvé que, en général, la vraie impulsion ne correspond pas précisement à la canonique; entre elles se présente donc un rapport plus général que dans l'équation connue sous le nom équation de guidage [15]. Ainsi, le paradoxe de vitesse y mentionné ne peut être posé ici.

Remarques initiales aux précédents du sujet

M. BORN, à qui on attribue l'interprétation statistique de la fonction d'onde Broglienne et avec cela celle de la mécanique ondulatoire, croit expréssement pour impossible [16] — tout comme Newton la lentille achromatique — de pouvoir trouver une interprétation individuelle avant la même de la nature statistique. Sous ses arguments vraiment très pesants, selon la théorie

[1] On peut l'interpréter en vertu du principe de la relativité restreinte aussi [2], c'est-à-dire même, si dans la généralisation cherchée de la dynamique, la loi d'inertie ne conserve pas sa vigueur générale dans un cas individuel, et ainsi la définition de LANGE sur le système d'inertie [3] perd son sens.

[2] Sur un autre chemin plus approfondi, qui fait descendre la particule des ondes Brogliennes, voir [13].

devenue légitime: plus une particule est petite, moins elle est descriptible par le modèle de Laplace. C'est J. NEUMANN qui a établi les bases de ces conceptions dans un système d'axiomes — pareil à table de pierre — lequel [17] exclut même l'existence des paramètres «cachés» et par la formulation causale de la mécanique ondulatoire bien que cela fût pressée assidument par LORENTZ, PLANCK [18] et par EINSTEIN [19] à l'intérêt de «totalité». Mais plus récemment, même BELL a cru trouver une preuve à l'impossibilité des paramètres cachés laquelle a été réfutée efficacement par DE BROGLIE [20]. WIGNER a relevé, dans le cadre des conceptions Neumanniennes certaines difficultés de la notion de la particule «floue» [21], tandisque TISZA a essayé expressément la reconstruction de celle-la [22]. Ce travail ici serait inséré par les études polémiques de BORN parmi les «épreuves réactionnaires p-absolutisantes» (c'est-à-dire au genre, partant de la priorité de l'existence de la particule) dont plusieurs variantes se montraient jusqu'ici comme inachevées, ainsi les travaux de FRENKEL [5], ceux de BLOHINCEV [6], de BOHM [7] et celui de l'auteur [8—9], puis, adhérant au critère de la stabilité dynamique de Poincaré—Birkhof—Ljapunov—Chetaev: les études de CHAKO [10], de KALITZIN [11] et celui de PYRAGAS—ALEXANDROV [12]. A savoir, eux tous érigent des signaux de route instructifs pour sortir du labyrinthe du postulat à la totalité.

§ 1. L'algorithme Jacobien pour attribuer une orbite même à une particule de mécanique ondulatoire

a) *Pour début* et pour y faire tard des *références*, nous décrivons les équations de la mécanique ondulatoire et nous développons l'analogie formale à l'équation de point-dynamique de Hamilton—Jacobi. Nous commençons par l'équation de Schrődinger dépendant du temps, suivant laquelle pour une particule libre de masse m dans l'espace du potentiel réel

$$V \equiv V[\mathbf{r}, t] \tag{1a,1}$$

connu de la mécanique classique, s'accomplit l'équation:

$$-\frac{\hbar^2}{2m} \cdot \Delta\Psi + V \cdot \Psi = -\frac{\hbar}{i} \frac{\partial\Psi}{\partial t} . \tag{1a,2}$$

Ici, $2\pi\hbar \equiv h$ est le constant de Planck, $\Delta \equiv$ div grad est opérateur connu de Laplace et

$$\Psi \equiv \Psi(\mathbf{r}, t) \tag{1a,3}$$

est la fonction d'onde Broglienne (nommée état). Cela est forcément complexe en raison de la forme de (1a, 2). Grâce à la forme linéaire homogène de (1a, 2)

nous trouvons parfois pour (1a,2) une solution normalisée pour laquelle la condition

$$\int^{\infty} \Psi^* \cdot \Psi \cdot d^3\mathbf{r} = 1 \tag{1a,4}$$

sera remplie. Dans celle-ci, la Ψ^* signifie le complexe conjugué de Ψ, l'intégral de volume (par l'élément $d^3\mathbf{r}$) s'étand pourtant sur l'espace configurationnel infini (∞). Cette condition ne peut être accordée qu'avec la Ψ quadratiquement intégrable qui disparait dans $|\mathbf{r}| \equiv r \to \infty$. Conformément à l'expérience, la quantité

$$\Psi^* \cdot \Psi \equiv \varrho(\mathbf{r}, t) \leqq 1 \tag{1a,5}$$

donne la *densité* spatiale pour la *probabilité* (c'est-à-dire la fréquence) *de trouver* la particule au lieu $\mathbf{r}$ à l'instant t. En vertu de la règle d'addition des probabilités exclusives, cette affirmation est en accord avec la (1a,4) exprimant la certitude.[3] Si nous inversons la fonction d'onde, écrite sous forme trigonométrique:

$$\Psi \underset{+}{\equiv} \sqrt{\varrho} \cdot e^{iS/\hbar}, \tag{1a,6}$$

nous gagnons

$$S(\mathbf{r}, t) = \frac{\hbar}{2i} \cdot \ln \frac{\Psi}{\Psi^*} \tag{1a,7}$$

qui est même par sa forme réelle, nommée fonction principale. À l'aide de celle-ci, la complexe (1a,2) se décompose en deux équations réelles. L'une d'elles est:

$$\operatorname{div}\left\{\frac{\varrho}{m} \cdot \operatorname{grad} S\right\} + \frac{\partial \varrho}{\partial t} = 0\,, \tag{1a,8}$$

c'est-à-dire formellement une *équation de continuité* où, justement pour cela, il faut considérer le vecteur, mis en parenthèses graciles comme *densité de courant de probabilité*. Et l'autre équation:

$$\frac{1}{2m} \operatorname{grad}^2 S + V + U = -\frac{\partial S}{\partial t}, \tag{1a,9}$$

[3] Par la forme de l'équation (1a, 2), la solution (1a, 3) permet — outre les variables $\mathbf{r}$ et t, mises en parenthèses rondes — même d'autres variables (paramètres) qui ne figurent pas dans l'équation (1a, 2). De telles apparaissent nécessairement et habituellement dans la solution nommée totale et non générale des équations aux dérivées partielles. Une autre variable n'est d'accord avec l'affirmation (1a, 5) que si dans les périodes des épreuves répétées de retrouver certaines grandeurs, c'est-à-dire paramètres, prennent toujours la-même valeur.

se présente dans la forme élargie par U de *l'équation Hamilton—Jacobienne*, connue dans la point-dynamique où

$$U \equiv -\frac{\hbar^2}{2m} \cdot \frac{\Delta \sqrt{\varrho}}{\sqrt{\varrho}} \tag{1a,10}$$

est le *potentiel* subséquent de DE BROGLIE [15]. Si donc, $\hbar \to 0$, la (1a,9) passe dans la forme classique. On peut obtenir l'intégrale Ψ dans la forme (1a,6) par la solution sur S et ϱ des équations différentielles simultanées (1a,8—9).

Dans un espace potentiel, indépendant du temps, c'est-à-dire *conservatif*

$$V \equiv V[\mathbf{r}] \tag{1a,11}$$

on peut se contenter pour la plupart de la solution de forme simple, nommée *séparée*:

$$\Psi = \vartheta(t) \cdot \psi(\mathbf{r}). \tag{1a,12}$$

À savoir, dans un tel cas *stationnaire*, à l'aide de la constante B de séparation, qui doit être prise pour complexe (1a,2), peut être disloquée en deux équations complexes d'entre lesquelles l'une ne contient que la variable t et l'autre que la variable $\mathbf{r}$. Entre elles, l'intégrale complète de l'équation différentielle contenante t:

$$\vartheta(t) = e^{-\frac{i}{\hbar}(B \cdot t + D)}, \tag{1a,13}$$

où D est aussi une constante arbitraire complexe d'intégration. Et l'équation de $\mathbf{r}$ variable est:

$$\frac{\hbar^2}{2m} \Delta\psi + (B - V)\psi = 0 \tag{1a,14}$$

nommée *équation-amplitude*. Ici, pour la *fonction d'amplitude* ψ — qui peut être cherchée toujours même en forme complexe — est valable à cause de (1a,4):

$$\psi^* \cdot \psi = \varrho \tag{1a,15}$$

et puis, à cause de (1a,5) dans le cas de (1a, 4)

$$\int^{\infty} \psi^* \cdot \psi \, d^3\mathbf{r} = 1 \tag{1a,16}$$

est aussi remplissable. Introduisons la quantité réelle E:

$$E \equiv (B^* + B)/2. \tag{1a,17}$$

Maintenant, à cause de (1a,7) — représentée par $(D^* + D)/2 \equiv$ const. —:

$$S(\mathbf{r}, t) = -Et + \frac{\hbar}{2i} \ln \frac{\psi}{\psi^*} - \text{const.} \tag{1a,18}$$

C'est pourquoi, en cas conservatif la (1a,9) se réduit par l'abréviation:

$$S_r \equiv \frac{\hbar}{2i} \ln \frac{\psi}{\psi^*} \; (\not\equiv 0) \tag{1a,19}$$

à *l'équation Jacobienne*, nommée *abréviée*:

$$\frac{1}{2m} \operatorname{grad}^2 S_r + V + U = E \tag{1a,20}$$

où alors, à cause de (1a,15) et (1a,10), ni ϱ, ni U ne dépendent du t. Et (1a,8) se réduit[4] comme cela:

$$\operatorname{div} \left\{ \frac{\varrho}{m} \cdot \operatorname{grad} S_r \right\} = 0 \; . \tag{1a,21}$$

b) *Calcul d'orbite dans l'état «pur»; les paramètres de caractère α et β*

Nous voulons que (1a,9) laquelle ensemble avec (1a,8) et (1a,10) est équivalente à (1a,2), non seulement par forme, mais aussi par contenu, soit la généralisation de l'équation Hamilton—Jacobienne classique ($\hbar \to 0$). C'est pourquoi nous n'acceptons q'une *solution totale* de forme: $S \equiv S[\mathbf{r}, t, \alpha_1, \alpha_2, \alpha_3]$. Par conséquent, à cause de (1a,7), il faut chercher dans la Ψ, donnée par (1a,3), outre les $\mathbf{r}$ et t encore trois paramètres réels α_j $(j = 1, 2, 3)$, c'est-à-dire, il faut la (1a,3) trouver dans la forme

$$\Psi \equiv \Psi[\mathbf{r}, t, \alpha_1, \alpha_2, \alpha_3] \tag{1b,1}$$

qui est dérivable non seulement par rapport à $\mathbf{r}$ et t, mais à α_j aussi, au moins deux fois (et même mélangée).[5] Nous remarquons que en expériences pour

[4] En cas de particule de charge électrique (1a, 21) doit exprimer la conservation de charge. Et cela ne peut être possible même en cas $V \equiv 0$ et stationnaire [23] que, si $S_r \not\equiv 0$, c'est-à-dire, si $\psi \not\equiv \psi^*$. C'est pourquoi, il faut construire tous les diviseurs de la ψ séparés selon les cordonnées en cas non trivial dans formes complexes (voir encore § 1/d, la note 6 et § 3/c, puis [24]).

[5] Les parenthèses rondes autour de $\mathbf{r}$ et t dans (1a, 3), veulent exprimer que la valeur de la fonction peut dépendre d'autres paramètres encore. Mais les parenthèses de crochets dans (1b, 1) excluent d'autres variables qui diffèrent des quantités contenues en elles.

déterminer la ϱ, donnée par (1a,5), il faut restituer les circonstances à chaque épreuve, et il ne faut varier que **r** et t. Ainsi, α_j caractérise, à vrai dire, l'entourage de départ.

Dans des cas conservatifs, p.e. dans les solutions *stationnaires* usuelles de (1a,2), des paramètres α se présentent d'habitude sous formes des constants de séparation mentionnée. Notamment, dans (1a,9), la séparation du temps et des cordonnées introduit dans (1a,20) la $\alpha_1 \equiv E$, et dans cette dernière, la séparation des trois cordonnées entre elles résulte nécessairement encore les valeurs réelles: α_2, α_3. Mais l'exigence de l'integrabilité quadratique et celle de l'univalence (à savoir de la *régularité)* choisit encore, pour α_1, α_2, α_3 jusqu'ici arbitraire réelle, un domaine discret, c'est-à-dire comptable par des *nombres*, nommés *quantiques*. En cas de potentiel central, il est d'usage de faire descendre α_1, α_2, α_3 p.e. des nombres quantiques connus: n, l, m. C'est pourquoi:

$$\alpha_j \equiv \alpha_j(n, l, m); \; j = 1, 2, 3, \tag{1b,2}$$

où

$$\frac{\partial(\alpha_1, \alpha_2, \alpha_3)}{\partial(n, l, m)} \not\equiv 0 .$$

Mais, même en cas non-stationnaire, se présente le paramètre α, p.e. chez le paquet d'ondes au mouvement linéaire de vitesse $v \equiv \alpha$ sans force (voir [8], p. 329.(3,2)). Dans la suite, nous examinons aussi les conséquences de l'apparition de tels paramètres.

Si pour (1a,2), nous avons vraiment trouvé une solution de forme (1b,1), nommée *pure*, alors d'après le *théorème* connu de Jacobi [25], — à l'aide de S, donnée par (1a,7) — l'*équation orbitale* cherchée sera donnée par le système d'équations:

$$\frac{\partial S[\mathbf{r}, t, \alpha_1, \alpha_2, \alpha_3]}{\partial \alpha_j} = \beta_j \; (j = 1, 2, 3), \tag{1b,3}$$

il est vrai: dans une forme implicite. Là, β_j — au moins dans le domaine de valeur du premier membre — signifie trois nombres réels arbitrairement choisissibles.

En cas mentionné du V conservatif et central, p.e. (1b,3) est de forme suivante d'après (1b,2):

$$\frac{\partial S}{\partial n} \cdot \frac{\partial n}{\partial \alpha_j} + \frac{\partial S}{\partial l} \cdot \frac{\partial l}{\partial \alpha_j} + \frac{\partial S}{\partial m_j} \cdot \frac{\partial m}{\partial \alpha_j} = \beta_j \quad (j = 1, 2, 3). \tag{1b,4}$$

Selon la fonction-amplitude complexe ψ et avec (1a,19), même la S peut-être exprimée dans une forme différentiable par rapport aux nombres n, l, m. À savoir, par la séparation de (1a, 14), se présentent des équations différentielles

auto-adjointes ordinaires. Mais la solution de telles sera donnée par des polynomes de l-ième degré (de valeur aux bords prescrite) qui sont produits d'habitude par formules recursives aussi. Par conséquent, ces polynomes peuvent être déduites — à la suite de Rodrigues — des l-ièmes dérivées d'une fonction génératrice convenable. Une telle dérivée peut être produite même dans une forme intégrale par le *théorème de Cauchy* ([26] p. 153), différentiable partiellement par rapport à l, comme paramètre. Dans (1b,4) donc, $\partial S/\partial l$ existe. P.e. la forme intégrale de la fonction sphérique «adjointe» connue — par abréviation $\mu \equiv \cos\vartheta$ — (voir [27]):

$$P_l^m(\mu) = \frac{C}{2\pi} \cdot \int_{-\pi}^{+\pi} \left(\mu + \sqrt{\mu^2 - 1} \cdot \cos\varphi\right)^l \cdot e^{-im\varphi} \cdot d\varphi.$$

Mais par la méthode ici mentinnée, même la fonction de Laguerre $L_n(r)$ peut être construite en forme différentiable par rapport à n. C'est pourquoi, d'après (1b,3) — en état pur l'orbite est vraiment déterminée.

Dans la suite, nous introduisons comme abréviation:

$$\begin{aligned} &\alpha \text{ au lieu de } \alpha_j \qquad j = 1, 2, 3. \\ &\beta \text{ au lieu de } \beta_j \qquad j = 1, 2, 3. \end{aligned} \tag{1b,5}$$

c'est-à-dire la représentation par des lettres deboutes et grosses, substituant l'index j. Ainsi, la forme explicite de l'équation orbitale (1b,3) est la suivante:

$$\mathbf{r} = \mathbf{r}[t, \alpha, \beta]. \tag{1b,6}$$

Mais, la détermination générale de celle-ci est un devoir grave, exigeant — même dans le plus simple cas — l'itération par calculatrice électronique. Pourtant, même sans cela concernant l'orbite, par (1b,3), on y peut conclure à des propriétés importantes (voir § 2a—b).

(En même temps le problème se pose ici de déciser si, l'orbite de la singularité d'une solution plus générale à (1a,2), mentionnée en [13], satisfait même la (1b,3), contenante de Ψ totale (1b,1), respectivement la (1c,5) subséquente.)

c) *Calcul d'orbite en état «mélangé», apparition de nouveaux paramètres*

Produisons dans l'argument des solutions (1b,1), qui appartiennent au même V de l'équation (1a,2), une suite α_l ($l = 1, 2, \ldots, n$) de paramètre α, parmi les éléments de laquelle ne doivent pas se trouver deux égaux. Comme chaque fonction de n'importe quel ordinal l de la suite de fonctions

$$\Psi_l \equiv \Psi[\mathbf{r}, t, \alpha_l] \qquad (l = 1, 2, \ldots, n) \tag{1c,1}$$

tirées ainsi de (1b,1), satisfait (1a,2), par conséquent, la combinaison linéaire

$$\Psi_l \equiv \sum_{l=1}^{n} c_l \cdot \Psi_l \tag{1c,2}$$

est aussi une solution de celle-là, où le complexe c_l est constant. C'est pourquoi, dans la forme trigonométrique de

$$c_l \equiv \gamma_l \cdot e^{i\delta_l/\hbar} \tag{1c,3}$$

$\gamma_l(\geqq 0)$ et δ_l sont des constants réels. La (1c, 2) décrit un *état mélangé* (autrement: celui même de superposition ou bien d'interférence) des états pours d'ordinal l dont la forma d'argument — par l'abréviation de (1b,5) — est la suivante:

$$\Psi \equiv \Psi[\mathbf{r}, t, \alpha_l, \gamma_l, \delta_l;\ l = 1, 2, \ldots, n]. \tag{1c,4}$$

De cela, le système d'équations

$$\sum_{l-1}^{n} \frac{\partial S[\mathbf{r}, t, \alpha_l, \gamma_l, \delta_l;\ l = 1, 2, \ldots, n]}{\partial \alpha_{lj}} = \beta_j \quad (j = 1, 2, 3) \tag{1c,5}$$

définie, d'une façon implicite, l'orbite par S, provenant de (1a,7), comme généralisation conséquente de (1b,3). Dans cela, même maintenant, la β_j signifie une valeur tripartite, choise arbitrairement du domaine de valeurs du premier membre. Cette orbite a caractère de mécanique ondulatoire porte même maintenant la forme suivante:

$$\mathbf{r} = \mathbf{r}[t, \alpha_l, \beta, \gamma_l, \delta_l;\ l = 1, 2, \ldots, n]. \tag{1c,6}$$

(Un état méiangé survient p.e. si, dans l'espace configurationnel voyagent certaines surfaces de guidages dans le long desquelles la direction de grad S ne peut être que tangente.)

Mais dans la (1c,4) les valeurs des paramètres γ_l et δ_l sont réglées par la normalisation de la Ψ, donnée par (1c,2). Notamment, par la forme trigonométrique de Ψ_l

$$\Psi^* \cdot \Psi \equiv \sum_{l}^{n} \gamma_l^2 \cdot \varrho_l + 2 \sum_{k,l}^{n} \gamma_l \cdot \gamma_k \cdot \sqrt{\varrho_k \varrho_l} \cdot \cos \frac{S_k - S_l + \delta_{kl}}{\hbar}$$

où

$$\delta_{kl} \equiv \delta_k - \delta_l . \tag{1c,7}$$

En étendant sur l'espace infinie l'intégrale de volume de cette équation et en y introduisant l'abréviation suivante:

$$A_{kl} \equiv \int^{\infty} (\Psi_l^* \Psi_k + \Psi_k^* \Psi_l)\, d^3\mathbf{r} = \int^{\infty} \sqrt{\varrho_k \varrho_l} \cdot \cos \frac{S_l - S_k + \delta_{lk}}{\hbar}\, d^3\mathbf{r} \tag{1c,8}$$

d'après (1a,4) nous gagnons:

$$\sum_{l}^{n} \gamma_l^2 + 2 \sum_{k,l}^{n} \gamma_n \cdot \gamma_l \cdot A_{nl} = 1 . \qquad (1c,9)$$

Et cela est une équation quadratique pour un, disons: justement pour le dernier paramètre γ_n, il y a seulement les précédents du nombre $(n - 1)$ qui peuvent être choisis arbitrairement. Mais, même alors, le γ_n, calculé d'eux, doit être constant dans le temps dont la condition nécessaire et suffisante est le système d'équation:

$$\frac{d}{dt} A_{nl} = 0 \quad (k, l = 1, 2, \ldots, n) . \qquad (1c,10)$$

Dans cela, le nombre des équations est $n(n - 1)/2$. La (1c,10) s'accomplit sans condition avec n arbitraire, si $A_{kl} \equiv 0$ et en se cas de (1c,9):

$$\sum_{l}^{n} \gamma_l^2 = 1 . \qquad (1c,11)$$

Nous notons que, en état stationnaire de l'espace V conservatif, le système des fonctions Ψ_l est orthogonal et ainsi $A_{kl} \equiv 0$.

Pourtant en cas général (1c,10) ne peut pas être satisfait pour les valeurs arbitraires de α_l, mais seulement pour les valeurs déterminées par elle. Néanmoins, le nombre des équations indépendantes, qui peuvent être produites de la $l = 1, 2, \ldots, n$, c'est-à-dire $n(n - 1)/2$, ne peut être plus grand que le nombre $3n + n = 4n$, d'ensemble des variables α_l, δ_l. Par conséquent, la condition (1c,10) ne peut être satisfaite sans contradiction qu'en cas, si $n \leqq 9$. Et cela indique le caractère causal de la mécanique ondulatoire, à savoir que le nombre n des états purs, qui peuvent se mélanger l'un avec l'autre, est en général limité.

d) *Calcul d'orbite en cas de mélange d'états purs à α égaux; apparition de nouveaux paramètres*

Il peut arriver que, en cas du-même V, la (1a,2) possède même deux solutions Ψ' et Ψ'', de forme (1b,1) mais avec α égaux, qui ne sont pas identiques entre elles (linéairement indépendantes):[6]

$$\Psi'[\mathbf{r}, t, \alpha] \not\equiv \Psi''[\mathbf{r}, t, \alpha]. \qquad (1d,1)$$

[6] Tel est p.e. le *polynome de Legendre* à I-er type (P_l) ainsi que le même à II-ième type (Q_l), à l'index l. Mais par un procédé universel ([26] p. 402), on peut construire pour une solution particulière de l'équation différentielle de Sturm-Liouville (p.e. même de Laguerre), une autre solution qui la complète entièrement. Par conséquent le facteur complexe de la ψ, mentionné dans la note 4, appartenant à la cordonnée ϑ, a la forme $P_l(\vartheta) + i\varepsilon Q_l(\vartheta)$ où le facteur ε est réel constant.

La restriction de numérotage dans le premier alinée de § 1|c exclut un tel cas. {Si Ψ' et Ψ'' sont stationnaires, c'est-à-dire tous les deux sont de forme (1a,12), il est à comprendre que les B' et B'' dans (1a,13—14) sont égaux.} Bornons-nous ici au cas $n = 1$ de (1c,4), c'est-à-dire aux fonctions d'état non sans faute stationnaire, quand en vertu de (1c,1) $\gamma = 1$ et $\delta = 0$, conformément à (1d,1). Alors la solution de (1a,2) est la combinaison linéaire

$$\Psi[\mathbf{r}, t, \alpha, c', c''] \equiv c' \cdot \Psi' + c'' \cdot \Psi'' \tag{1d,2}$$

aussi, si les c' et c'' y sont complexes constants. Écrivons même maintenant (1d,2) en forme trigonométrique, ainsi, en vertu de (1a,6):

$$\Psi' \equiv \sqrt[+]{\varrho'} \cdot e^{iS'/\hbar}; \quad \Psi'' \equiv \sqrt[+]{\varrho''} \cdot e^{iS''/\hbar} \tag{1d,3}$$

et

$$c' \equiv \varepsilon' \cdot e^{i\eta'/\hbar}; \quad ; \quad c'' \equiv \varepsilon'' \cdot e^{i\eta''/\hbar}, \tag{1d,4}$$

où ε', ε'' et η', η'' sont des constants réels, mais les $\varepsilon \geqq 0$. Avec ces nouveaux constants, la forme à argument de (1d,2) est en dernière analyse

$$\Psi[\mathbf{r}, t, \alpha, c', c''] \equiv \Psi[\mathbf{r}, t, \alpha, \varepsilon', \varepsilon'', \eta', \eta'']. \tag{1d,5}$$

{Mais puisque, d'après l'expérience, chaque état — satisfaisant (1a,2) — peut se produire, il faute donc normaliser même Ψ, donnée, par (1d,2), et cela par (1a,4—5). Par conséquent conformément à (1c,9) les constants ε', ε'' et η', η'' même ici ne peuvent pas être choisis tout indépendamment l'un de l'autre. Formons d'abord Ψ^*. Ψ par (1d,3—4):

$$\Psi^* \cdot \Psi \equiv \varepsilon'^2 \varrho' + \varepsilon''^2 \varrho'' + 2\varepsilon'' \varrho'^2 \cdot \varepsilon'' \varrho''^2 \cdot \cos \frac{S' - S'' + \eta}{\hbar} \tag{1d,6}$$

où

$$\eta \equiv \eta' - \eta''. \tag{1d,7}$$

De cela, l'exigence de normalisation de (1a,4) nous conduit à l'équation quadratique:

$$\varepsilon'^2 + \varepsilon''^2 + 2\varepsilon'\varepsilon'' \cdot A = 1 \tag{1d,8}$$

où

$$A \equiv \int_{+}^{\infty} \sqrt{\varrho' \varrho''} \cdot \cos \frac{S' - S'' + \eta}{\hbar} \, d^3 \mathbf{r} \,. \tag{1d,9}$$

En cas du constant $\varepsilon'(\geqq 0)$, (1d,8) peut être résolue selon ε''. Mais même ε'' ne peut pas dépendre du temps, c'est pourquoi une solution de forme (1d,2), resp. (1d,5) peuvent posséder un sens probabiliste dans le cas où

$$\frac{dA}{dt} = 0. \tag{1d,10}$$

La condition suffisante en est que, p.e. le V soit conservatif et la paire de solution Ψ', Ψ'' soient stationnaires, quand à cause de (1a,15), ϱ' et ϱ'' sont indépendants du temps, et S', S'' sont de forme (1a,18). Mais le discriminant de l'équation quadratique (1d,8) — quant à ε'', qui doit être réel — ne peut pas être négatif. Et cela peut arriver seulement, si

$$A^2 \geq (\varepsilon'^2 - 1)/\varepsilon'^2. \tag{1d,11}$$

Dans le cas général donc, à cause de (1d,8), parmi les ε', ε'' et η', η'' du second membre de (1d,5), seulement trois peuvent être choisis arbitrairement: p.e. ε' et η', η'', mais ε' doit satisfaire quand même (1d,11). C'est pourquoi, par l'indication $\varepsilon \equiv \varepsilon'$ et avec (1d,7) la fonction d'état du second membre de (1d,5) sera en définitive:

$$\Psi \equiv \Psi[\mathbf{r}, t, \boldsymbol{\alpha}, \varepsilon, \eta]. \tag{1d,12}$$

D'après les mentionnés Ψ peut être toujours construite en forme complexe aussi au plus sera irrégulière.[4]}

§ 2. Quelques conséquences dynamiques importantes

Ici nous répétons, mais avec généralité de mécanique ondulatoire (c'est-à-dire sans négliger $\hbar$), les déductions par lesquelles on a l'habitude de conclure dans la dynamique classique ($\hbar \to 0$) de Hamilton—Jacobi aux lois de mouvement Newtoniennes, resp. de conservation.

a) *L'espace à vitesse* de la particule est calculable d'une façon explicite, connaissant S et à l'aide de l'équation orbitale implicite (1c,5) en produisant sa dérivée totale par rapport au temps t (p.e. employant les cordonnées Cartesiennes dans $\mathbf{r} = \mathbf{i}x + \mathbf{j}y + \mathbf{k}z$):

$$\sum_l^n \frac{\partial^2 S}{\partial t\, \partial \alpha_{lj}} + \dot{x} \sum_l^n \frac{\partial^2 S}{\partial x \partial \alpha_{lj}} + \dot{y} \sum_l^n \frac{\partial^2 S}{\partial y\, \partial \alpha_{lj}} + \dot{z} \sum_l^n \frac{\partial^2 S}{\partial z\, \partial \alpha_{lj}} = 0; (j = 1, 2, 3). \tag{2a,1}$$

Le déterminant de ce système d'équations linéaires aux $\dot{x}, \dot{y}, \dot{z}$ est:

$$D \equiv \begin{vmatrix} \sum_l \partial^2 S/\partial x\ \partial \alpha_{l1} & \sum_l \partial^2 S/\partial y\ \partial \alpha_{l1} & \sum_l \partial^2 S/\partial t\, \partial \alpha_{l1} \\ \sum_l \partial^2 S/\partial x\ \partial \alpha_{l2} & \sum_l \partial^2 S/\partial y\ \partial \alpha_{l2} & \sum_l \partial^2 S/\partial z\ \partial \alpha_{l2} \\ \sum \partial^2 S/\partial x\ \partial \alpha_{l3} & \sum_l \partial^2 S/\partial y\ \partial \alpha_{l3} & \sum_l \partial^2 S/\partial z\ \partial \alpha_{l3} \end{vmatrix}. \tag{2a,2}$$

Supposons que

$$D \not\equiv 0, \tag{2a,3}$$

c'est-à-dire, excluons le cas trivial de $S_r \equiv 0$ (voir encore la note 4 et le dernier alinéa du § 2|b subséquent). En employant la règle de Cramer sur (2a,1):

$$\dot{x} = -D^{-1} \cdot \begin{vmatrix} \sum_l \partial^2 S/\partial t\ \partial\alpha_{l1} & \sum_l \partial^2 S/\partial y\ \partial\alpha_{l1} & \sum_l \partial^2 S/\partial z\ \partial\alpha_{l1} \\ \sum_l \partial^2 S/\partial t\ \partial\alpha_{l2} & \sum_l \partial^2 S/\partial y\ \partial\alpha_{l2} & \sum_l \partial^2 S/\partial z\ \partial\alpha_{l2} \\ \sum_l \partial^2 S/\partial t\ \partial\alpha_{l3} & \sum_l \partial^2 S/\partial y\ \partial\alpha_{l3} & \sum_l \partial^2 S/\partial z\ \partial\alpha_{l3} \end{vmatrix} \tag{2a,4}$$

et de même $\dot{y}, \dot{z}$. P.e. dans le cas d'une dimension et pour (c'est-à-dire cas d'argument $[x, t, \alpha]$):

$$\dot{x} = -\frac{\partial^2 S/\partial t\ \partial\alpha}{\partial^2 S/\partial x\ \partial\alpha}\,. \tag{2a,5}$$

La (2a,4) donne la vitesse de la particule, se trouvant dans le lieu **r** à un instant t. Pour la calculer, il faut connaitre l'orbite de forme (1c,6) explicite.

b) *La relation des impulsions «vraie» et canonique*

Les explications suivantes reposent sur une reconnaissance nouvelle (aussi pour la mécanique classique) selon laquelle, de l'équation Hamilton—Jacobienne (1a,9) et de l'équation orbitale (implicite), accessoire (1c,5), suit l'autre équation, appelée d'exprimer la relation des impulsions vraie et canonique, et avec cela les lois de conservation. Pour la recouvrir, il faut interpréter l'*impulsion vraie*:

$$\mathbf{I} \equiv m \cdot \dot{\mathbf{r}}\,. \tag{2b,1}$$

Et l'*impulsion canonique* sera définie par

$$\mathbf{p} \equiv \operatorname{grad} S. \tag{2b,2}$$

Calculons la *différence d'impulsion*

$$\mathbf{f} \equiv m\dot{\mathbf{r}} - \operatorname{grad} S. \tag{2b,3}$$

Pour ce but, il suffit de se borner à la composante x, notamment d'après (2a,4):

$$f_x = -m \cdot D^{-1} \cdot \begin{vmatrix} \sum_l \partial^2 S/\partial t\ \partial\alpha_{l1} & \sum_l \partial^2 S/\partial y\ \partial\alpha_{l1} & \sum_l \partial^2 S/\partial z\ \partial\alpha_{l1} \\ \sum_l \partial^2 S/\partial t\ \partial\alpha_{l2} & \sum_l \partial^2 S/\partial y\ \partial\alpha_{l2} & \sum_l \partial^2 S/\partial z\ \partial\alpha_{l2} \\ \sum_l \partial^2 S/\partial t\ \partial\alpha_{l3} & \sum_l \partial^2 S/\partial y\ \partial\alpha_{l3} & \sum_l \partial^2 S/\partial z\ \partial\alpha_{l3} \end{vmatrix} - \frac{\partial S}{\partial x}\,. \tag{2b,4}$$

Dans la première colonne du déterminant, signalé ici, nous pouvons substituer les éléments de forme $\partial^2 S/\partial t \partial\alpha_{lj}$ par des expressions, gagnées de (1a,9) en cela

dérivant partiellement par rapport à α_{lj}, mais d'où les dérivées $\partial V/\partial\alpha_{lj}$ tombent à cause de (1a,1). Ensuite, en vertu des théoremes d'échange des dérivations partielles ainsi que de transformation de déterminants:

$$f_x = m \cdot D^{-1} \cdot \begin{vmatrix} \sum_l \partial U/\partial\alpha_{l1} \sum_l \partial^2 S/\partial y\ \partial\alpha_{l1} \sum_l \partial^2 S/\partial z\ \partial\alpha_{l1} \\ \sum_l \partial U/\partial\alpha_{l2} \sum_l \partial^2 S/\partial y\ \partial\alpha_{l2} \sum_l \partial^2 S/\partial z\ \partial\alpha_{l2} \\ \sum_l \partial U/\partial\alpha_{l3} \sum_l \partial^2 S/\partial y\ \partial\alpha_{l3} \sum_l \partial^2 S/\partial z\ \partial\alpha_{l3} \end{vmatrix} \tag{2,5b}$$

et des expressions semblables se présentent pour f_y et f_z aussi. On voit que en général, $\mathbf{f} \not\equiv 0$. Dans un cas pur d'une dimension p.e.:

$$f_x = -m\partial U/\partial x. \tag{2b,6}$$

En même temps, $\mathbf{f} \not\equiv 0$ trahit que $\dot{\mathbf{r}}$ n'est pas un vecteur potentiel, et ainsi l'*équation de guidage* Broglienne [15] est valable dans une forme plus générale que dans la dynamique classique ($\hbar \to 0$), où notamment à cause de (1a,10) dans (2b,5) la colonne $\sum_l \partial U/\partial\alpha_{lj} \to 0$, mais même ici, tout au plus en cas de liaison scléronome. C'est pourquoi dans le cas classique l'équation $m\dot{\mathbf{r}} = \text{grad } S$ est en effet une conséquence directe des équations: $\partial S/\partial\alpha = \beta$ orbitale et Jacobienne. Par contre, toutes les interprétations de la mécanique ondulatoire qui n'élargissent pas l'équation de guidage, peuvent décrire tout au plus un cas spécial de mécanique ondulatoire, ainsi p.e. [8—9],[7] en plus les modèles de hydrodynamique, étudiés à la suite de E. Madelung.

Nous notons donc que, dans (2b,3), $\mathbf{f}$ est formellement analogue au membre additionnel $-e\mathbf{A}/c$ de l'impulsion classique de la charge e ponctuelle, si $\mathbf{A}$ signifie le potentiel vecteuriel dans le lieu de la charge ([28] p. 379.). En cas de ψ réel, $S_r \equiv 0$, par conséquent, à la fois $D \equiv 0$, et ainsi, p.e. dans un cas d'unidimension, $\mathbf{f} \equiv 0$ à cause de (2b,6), c'est-à-dire $m\dot{x} = \partial S_r/\partial x$ d'où provient le cas statique: $\dot{x} = 0$.

c) *La force, le travail, l'équation de mouvement*

Se bornant à l'espace potentiel (1a,1), on définie le *champ de force* $\mathbf{F}(\mathbf{r}, t)$ et le travail $W_{|\to||}$, accompli par lui sur la particule suivant l'orbite $\mathbf{r} = \mathbf{r}(t)$ dans un intervalle $t' < t''$, par les équations:

$$\mathbf{F} \equiv -\text{grad } V;\ W_{|\to||} \equiv \int_{\mathbf{r}'}^{\mathbf{r}''} \mathbf{F}\, d\mathbf{r}\ . \tag{2c,1}$$

[7] Mais [8] exige encore un élargissement, parce que elle a exprimé la ϱ de l'équation partielle-différentielle à continuité non dans une forme générale désirable (c'est-à-dire contenant des fonctions arbitraires), mais seulement dans celle d'une solution totale (c'est-à-dire, contenant des constantes arbitraires) pour éliminer la ϱ de (1a, 9) ici.

Nous en recevons la forme générale du *theorème* à «force vive», c'est-à-dire du même *à travail* par l'intégration du gradient de (1a,9), dans la forme suivante:

$$W_{|\to||} = \left[\frac{\operatorname{grad}^2 S}{2m} + \frac{\partial S}{\partial t} + U\right]_{t'}^{t''} - \\ - \int_{t'}^{t''} \left(\frac{\operatorname{grad} S}{m} \operatorname{grad} \frac{\partial S}{\partial t} + \frac{\partial^2 S}{\partial t^2} + \frac{\partial U}{\partial t}\right) dt. \tag{2c,2}$$

Il devient clair que le deuxième membre de $W_{|\to||}$ dépend de la forme de l'orbite aussi, et ce membre, en cas $\hbar \neq 0$, peut disparaître seulement en cas de potentiel conservatif (1a,11).

Nous arrivons à l'équation de mouvement — de même — par le gradient la (1a,9). Celui-ci est le suivant d'après (2b,3):

$$\frac{d}{dt}(m\dot{\mathbf{r}} - \mathbf{f}) - \frac{\mathbf{f}}{m} \cdot \operatorname{grad}(m\dot{\mathbf{r}} - \mathbf{f}) + \operatorname{grad} U = \mathbf{F} \tag{2c,3}$$

et correspond à l'*équation de Newton*. Notamment en cas (irréel) $\hbar \to 0$ (quand $\mathbf{f} = 0$ et $\operatorname{grad} U \equiv 0$), elle prend la forme connue: $d(m\dot{\mathbf{r}})/dt = \mathbf{F}$. Mais (2c,3) montre que, en cas de $\mathbf{F} \equiv 0$ (si $\hbar \neq 0$), $\dot{\mathbf{r}}$ n'est pas constant, c'est-à-dire, la *loi d'inertie* perd[2] sa valabilité générale. La (2c,3) en soi, n'est pas capable même de la détermination de l'orbite.

d) *Prévention contre un paradoxe de vitesse*

Il est connu que, en cas $V \equiv 0$, la solution de (1a,2) est même l'onde plane de forme de deux dimensions

$$\Psi_l \sim e^{2\pi i\nu\left(t - \frac{x \sin \vartheta_l + z \cos \vartheta_l}{c}\right)}.$$

Suivant (1a,7) y est $\mathbf{f}_l \equiv 0$, et par conséquent — à cause de (2b,1) et (2b,3) — la particule, toute comme la phase d'onde sont de vitesse c. Mais de deux telles ondes pures ($l = 1, 2$), peut être superposée une

$$\Psi \equiv \Psi_1 + \Psi_2$$

mélangée aussi, et cela correspond à (1c,2), de plus près: au cas physique aussi, où, devant un miroir plan imparfait, l'onde plan Ψ_1 rencontre la Ψ_2 reflétée ([15] Chap. X. § 5.). Ici, à l'α_{l1} correspond l'angle ϑ_l (incident $\vartheta_1 = -\vartheta_2$ de réflexion), à l'α_{l2} correspond en cas $l = 1, 2$ également ν et par l'indication de [15], la γ est déterminée par la reflexivité η. Selon la supposition de $m\dot{\mathbf{r}} =$

$=$ grad S, [15] a donc démontré que, dans l'espace de Ψ, la vitesse de la particule est, d'une façon paradoxe, toujours plus grande de c, lésant ainsi le principe de la relativité restreinte. Bien que dans une théorie, pas encore relativistiquement corrigée, une lèse comme cela peut être supportable, pourtant, en répétant les calculations mentionnées, nous pouvons nous persuader de ce qu'en cas Ψ mélangé: $\mathbf{f} \not\equiv 0$, donnée par (2b,5). Ainsi, au lieu de $m\dot{\mathbf{r}} = \text{grad } S$, il faut partir de (2b,4). Et cela coupera court au dressement du paradoxe.

En même temps, on peut établir que, ici la dynamique proposée est au fait un renouvellement de la théorie des *ondes pilotes de M. de Broglie* dans une forme élargie.

§ 3. Assujetissement des paramètres découvertes à la mécanique ondulatoire

a) *Le caractère statistique des paramètres de genre β et leur rapport à la densité ϱ des particules virtuelles*

Dans l'état général (mélangé), donné par (1c,4) à la particule, c'est-à-dire en cas de paramètres $[\alpha_l, \gamma_l, \delta_l\,;\, l = 1, 2, \ldots, n]$ fixés, en (1c,5) — dans le domaine de valeur du premier membre — le β du second membre peut être arbitrairement toujours et toujours autre. Nommément, dans une nouvelle «épreuve» — qui cherche à établir empiriquement ϱ, définie par (1a,5) — si β_j $(j = 1, 2, 3)$ diffère un peu de la précédente par $\delta\beta_j$, alors — selon la nouvelle épreuve dans l'instant t, c'est-à-dire $\delta t = 0$, correspondant au précédent —

$$\delta\mathbf{r} = \mathbf{i} \cdot \delta x + \mathbf{j}\, \delta y \cdot + \mathbf{k} \cdot \delta z$$

peut être calculée à la base de (1c,5) du système d'équations linéaires:

$$\delta\beta_j = \delta x \cdot \frac{\partial}{\partial x} \sum_l \frac{\partial S}{\partial \alpha_{lj}} + \delta y \cdot \frac{\partial}{\partial y} \sum_l \frac{\partial S}{\partial \alpha_{lj}} + \partial z \cdot \frac{\partial}{\partial z} \sum_l \frac{\partial S}{\partial \alpha_{lj}} \cdot (j = 1, 2, 3) \qquad (3a,1)$$

La particule se «déplace», c'est-à-dire migre dans la nouvelle épreuve avec $\delta\mathbf{r}$ relativement à la précédente. Par conséquent, même au prisme de diagonale principale $\delta\beta$, se trouvant dans l'espace β, correspond un parallélépipède de diagonale principle $\delta\mathbf{r}$ dans l'espace $\mathbf{r}$.

Suivant cette conception, l'*incertitude Heisenbergienne* peut être exprimée ici dans la forme suivante: Pour les épreuves de retrouver, interprétées après (1b,1), les circonstances de départ mentionnées déterminent *d'avance* avec précisité seulement les paramètres $[\alpha_l, \gamma_l, \delta_l\,;\, l = 1, 2, \ldots, n]$ caractéristiques à l'état de la particule et pas[8] le β, c'est-à-dire β est tout indéfini pendant

[8] Contrairement à la mécanique classique.

l'épreuve, seulement *après* l'épreuve peut on y tirer des conclusions à sa valeur, justement suivant le résultat de l'épreuve. Mais les épreuves rélèvent que, les β, appartenant aux épreuves, ont pourtant limite de distribution à densité certaine dans l'espace β.

Pour la calculer, il faut considérer que, dans l'ensemble d'orbites virtuelles, appartenant à l'état égal, le nombre des orbites, dont les paramètres desquels tombent dans l'intervalle $\beta_1' \pm d\beta_1/2$, est autre que, le nombre des orbites, dont les paramètres tombent dans l'intervalle $\beta_1'' \pm d\beta_1/2$, où $\beta_1'' \neq \beta_1'$. La distribution statistique de β_1 mentionnée consiste en cela que, dans l'intervalle $\beta' \pm d\beta_1/2$, les β_1 de certaines orbites (à savoir «atteinte») se placent avec une fréquence relative dp_1 (c'est-à-dire probabilité), ainsi:

$$dp_1 = P_1[\alpha_l, \gamma_l, \delta_l;\ l = 1, 2, \ldots, n;\ \beta'] \cdot d\beta \ (\leqq 1). \tag{3a,2}$$

Une relation analogue est valable pour β_2 et β_3 aussi. Partant, selon la règle de multiplication des probabilités indépendantes, la probabilité d^3p d'une atteinte, tombante dans l'intervalle $\beta_j' \pm d\beta_j/2$, est la suivante:

$$d^3p \equiv dp_1 \cdot dp_2 \cdot dp_3 = P_1 \cdot P_2 \cdot P_3 \cdot d\beta_1 \cdot d\beta_2 \cdot d\beta_3.$$

Omettant le signe de virgule déjà dispensable audessus de β, introduisons la fonction de «distribution à β»:

$$P_1 \cdot P_2 \cdot P_3 \equiv Q[\alpha_l, \gamma_l, \delta_l;\ l = 1, 2, \ldots, n;\ \beta]\,. \tag{3a,3}$$

Avec cela

$$d^3p = Q \cdot d\beta_1\, d\beta_2\, d\beta_3 \ (\leqq 1)\,, \tag{3a,4}$$

où la forme de la fonction Q sera déterminée par l'état, reproduit souvent des épreuves, et par le β. En tous cas, nous la considérons pour continue quant aux variables, au moins par étapes. Le nombre relatif p des atteintes qui tombent dans un domaine fini, signé (B) de l'espace β, gagnons — dans le sense de la règle d'addition des probabilités des événements exclusifs —:

$$p \equiv \int^{(B)} d^3p = \iiint^{(B)} Q \cdot d\beta_1\, d\beta_2\, d\beta_3 \ \ (\leqq 1)\,. \tag{3a,5}$$

Cette intégrale triple d'espace β peut être exprimée par intégrale d'espace r, c'est-à-dire selon les mentionnés, au sujet de (3a,1) nous pouvons projeter le domaine (B) — fixé dans l'espace β — à un domaine correspondant (R) qui erre dans l'espace r, notamment par la transformation d'intégrale à volume connue:

$$p \equiv \iiint^{(B)} Q \cdot d\beta_1 d\beta_2 d\beta_3 = \iiint^{(R)} Q \cdot D \cdot dx\, dy\, dz\,, \tag{3a,6}$$

où D est le déterminant de Jacobi de la transformation, donnée par (1c,5), mais qui correspond, par bonheur, à (2a,2). Mais ici le facteur Q de la fonction à intégrer doit être compris suivant (3a,3) et (1c,5) dans la forme $Q[\alpha_l, \gamma_l, \delta_l; l = 1, 2, \ldots, n; \sum_l \partial S/\partial\alpha_l]$. D'ailleurs puisque la (3a,6) doit accomplir n'importe quel volume *dxdydz*, la densité ϱ de la probabilité se trouve dans lieu $\mathbf{r}$ à l'instant t:

$$\varrho \equiv \frac{d^3 p}{dx\, dy\, dz} = Q \cdot D \,. \tag{3a,7}$$

Cela donne en même temps la fonction de distribution $Q = \varrho/D$ inconnue, mais au lieu de β, comme fonction de la variable $\mathbf{r}$. Si nous voulons donc savoir de quelle manière Q dépend le β, il faut substituer, au lieu de la variable $\mathbf{r}$ dans ϱ/D le $\mathbf{r} = \mathbf{r}(t)$ exprimé de l'équations d'orbite implicite (1c,5). Par la, la détermination de Q est un devoir, égal à la calculation d'orbite.

b) *Le rôle des paramètres dynamiques dans les valeurs moyennes et dans le formalisme des opérateurs*

Nous avons vu dans a) que, calculant depuis le début de la durée des épreuves d'états concordants (mentionnés déjà dans la note 3 aussi) à l'instant t, la particule passe (ou bien peut être trouvée) en cas d'un autre β, dans un autre lieu $\mathbf{r}$. Tout comme la valeur la plus fréquente des éléments dans une suite de mesure — autour de laquelle la somme, c'est-à-dire l'intégrale des carrés d'écarts montre minimum — sera fournie par leur valeur moyenne arithmétique, de même ici: la *situation* $\bar{\mathbf{r}}$ la plus fréquente (c'est-à-dire probable) de la particule dans l'instant t, est donnée par la *valeur moyenne de mécanique ondulatoire* $\bar{\mathbf{r}}$ des situation, observées dans les épreuves:

$$\bar{\mathbf{r}}[t, \alpha_l, \gamma_l, \delta_l;\ l = 1, 2, \ldots, n] \equiv \int^{\infty} \varrho \mathbf{r}\, d^3\mathbf{r} = \int^{\infty} \Psi^* \mathbf{r} \Psi\, d^3\mathbf{r} \,, \tag{3b,1}$$

et cela analogue au centre de masse. De la même façon, la valeur probable $\bar{\mathbf{p}}$ de l'impulsion canonique $\mathbf{p}$ est:

$$\bar{\mathbf{p}} \equiv \int^{\infty} \varrho \cdot \operatorname{grad} S \cdot d^3\mathbf{r} \tag{3b,2}$$

qui sera à la base de (1a,5), (1a,7) et (1a,4)

$$\bar{\mathbf{p}}\,[t, \alpha_l, \gamma_l, \delta_l;\ l = 1, 2, \ldots, n] = \frac{\hbar}{i} \int^{\infty} \Psi^* \cdot \operatorname{grad} \Psi \cdot d^3\mathbf{r} \tag{3b,3}$$

De même, la valeur $\bar{E}$ probable de l'expression $-\partial S/\partial t$ peut être écrite d'une façon:

$$\bar{E}\,[t, \alpha_l, \gamma_l, \delta_l;\ l = 1, 2, \ldots, n] = -\frac{\hbar}{i}\int^{\infty} \Psi^* \cdot \frac{\partial \Psi}{\partial t}\, d^3\mathbf{r}\,. \tag{3b,4}$$

qui, dans un cas conservatif et stationnaire, est indépendant de t. Si, pour satisfaire même la (1a,4), nous nous bornons — dans la (1a,2) — à la solution de la Ψ disparaissant au moins à la manière de $1/r$ dans l'infini, en ce cas (p.e. selon [28] p. 111) à la base de $m\dot{\bar{\mathbf{r}}} = \bar{\mathbf{p}}$, c'est-à-dire de (2b,3) il existe en même temps:

$$\bar{\mathbf{f}} \equiv \bar{\mathbf{f}}\,[t, \alpha_l, \gamma_l, \delta_l;\ l = 1, 2, \ldots, n] \equiv 0\,. \tag{3b,5}$$

Par conséquent, l'introduction des paramètres cachés ne modifie pas le *théorème* connu d'Ehrenfest.

La (3b,3—4) trahit en même temps la règle des opérateurs aussi.

Dans cet élargissement de la dynamique Hamilton—Jacobienne, l'interprétation statistique de la mécanique ondulatoire consiste en ce que, nous faisons tomber les paramètres de caractère β par calcul de la moyenne, et ainsi, nous nous contentons des valeurs moyennes à mécanique ondulatoire, concernant les quantités physiques. La résolution de ce devoir, plus simple que le calcul d'orbite individuelle, crée en même temps, la relation en tout cas indispensable avec la physique macroscopique. C'est pourquoi, le développement de l'interprétation statistique mérite beaucoup d'honneur.

c) *Les paramètres de dynamique et le problème des valeurs propres*

En cas de Ψ stationnaire (grâce au V conservatif), même les équations (1a,11—21) permettent que les arguments contiennent, outre $\mathbf{r}$ et t, des paramètres dynamiques aussi. Mais on peut voir de (1a,18) que la séparation (1a,12) peut être accordée seulement avec la forme (1b,1) de Ψ, c'est-à-dire avec la forme pure, puisque la séparation ne peut être accomplie ni avec (1c,4) de $l > 1$, ni avec une fonction d'état mélangé (1d,2). Ainsi, l'argument de fonction possible de (1a,2) est illustré par la relation:

$$\Psi = \vartheta[t, \alpha] \cdot \psi[\mathbf{r}, \alpha] \tag{3c,1}$$

à la base de laquelle

dans (1a,13): $B \equiv B[\alpha];\ D \equiv D[\alpha]\,,$ (3c,2)

(1a,15): $\varrho \equiv \varrho[\mathbf{r}, \alpha]\,,$ (3c,3)

(1a,17): $E \equiv E[\alpha];$ dans (1a,19): $S_r = S_r[\mathbf{r}, \alpha]\,.$ (3c,4)

Mais à cause de (3c,3) dans (1a,10): $U \equiv U[\mathbf{r}, \alpha]$; ensuite $\mathbf{f} = \mathbf{f}[\mathbf{r}, \alpha]$ interprétée par (2b,3), enfin à la base de la (3c,4) la vitesse donnée par (2a,4): $\dot{\mathbf{r}} \equiv \mathbf{v}[\mathbf{r}, \alpha]$, c'est-à-dire elles sont de forme stationnaire.

Pour terminer la E, donnée par (1a,17), nous évoquons la discussion connue du problème des valeurs propres, afin de montrer que les paramètres de dynamique s'y conforment souplement. Dans

$$\Psi_l = e^{-i(B_l \cdot t + D_l)/\hbar} \cdot \psi_l ,$$

interpretée par (1a,12—13) et (1c,1), à cause de la forme d'argument (3c,1—2) de ψ_l:

$$\psi_l \equiv \psi_l[\mathbf{r}, \alpha_l]; \quad B_l \equiv B[\alpha_l]; \quad D_l \equiv D[\alpha] . \tag{3c,5}$$

Ici, selon la prescription de numérotage donnée dans le premier alinéa § 1|c, si $l \neq m$, l'inégalité: $\alpha_l \neq \alpha_m$ existe toujours et même inversement. A l'intéret de normalisabilité de Ψ_l, nous exigeons aussi que la fonction d'amplitude ψ_l disparaisse dans l'infini et cela plus lentement de $1/r$. Cela veut dire pluspréci-sement que dans n'importe quel lieu $r \equiv |\mathbf{r}|$, où $r \to \infty$, doit s'accomplir $\psi_l \cdot r^\lambda \to C_l$, et ici C_l est un constant fini, complexe et $\lambda \geqq 1$, réel. Pour tirer en usage des conséquences de la disparition dans l'infini, nous formons à la base de (1a,14)

$$I \equiv \int^\infty (\psi_m^* \Delta\psi_l - \psi_l^* \, \Delta\psi_m) \, d^3\mathbf{r} = -\frac{2m}{\hbar^2} (B_n^* - B_l) \int^\infty \psi_n^* \cdot \psi_l \cdot d^3\mathbf{r}. \tag{3c,6}$$

Après avoir transformée l'intégrale I de volume en superficielle par le théorème de Green, nous l'étendons sur la surface d'une sphère de rayon $r \to \infty$, dans l'élément de surface $r^2 \cdot d\Omega$ de laquelle l'angle solide, coupé par elle est $d\Omega$, c'est-à-dire:

$$I = \int_{r \to \infty} \left(\psi_m^* \cdot \frac{\partial \psi_l}{\partial r} - \psi_l^* \cdot \frac{\partial \psi_m}{\partial r} \right) r^2 \, d\Omega.$$

Mais selon la restriction la fonction à intégrer disparait en cas $r \to \infty$ et $\lambda = 1$ le moins favorable encore permis. C'est pourquoi $I \to 0$, et de (3c,6) devient

$$(B_m^* - B_l) \int^\infty \psi_m^* \cdot \psi_l \, d^3\mathbf{r} = 0 . \tag{3c,7}$$

Si ici $l = m$, c'est-à-dire dans le sens de l'adjonction d'indexe $\alpha_m = \alpha_l$ et par la $\psi_m = \psi_l$, alors en conséquence de (1a,16), de (3c,7) devient

$$B_l^* = B_l . \tag{3c,8}$$

Le constant B_l est donc réel, et ainsi de (1a,17) et de (1a,14)

$$B_l = E_l = -\frac{\hbar^2}{2m} \cdot \frac{\Delta\psi_l}{\psi_l} + V$$

devient une *valeur propre*, et dedans la *fonction* ψ_l, nommée *propre* qui la fournit. Mais dans (3c,7), $m \neq l$ et ainsi $\psi_l \neq \psi_m$ existe aussi. S'il y a un cas nondégénéré, c'est-à-dire $B_l \neq B_m$ (= à cause de (3c,8) B_m^*), alors de la forme connue:

$$\int^{\infty} \psi_m^* \cdot \psi_l \cdot d^3\mathbf{r} = 0$$

se suit la condition d'orthogonalité.

Le § 1/d a fait allusion que même les deux états $\Psi'[\mathbf{r}, t, \alpha] \not\equiv \Psi''[\mathbf{r}, t, \alpha]$ indépendants peuvent se mêler en cas de V conforme. La restriction de numérotage exclut un tel Ψ' du système des fonctions orthogonales contenant Ψ', c'est-à-dire un tel Ψ'' est l'élément d'un autre système de telles fonctions. C'est l'analyse des paramètres de dynamique qui nous a conduit à cet établissement.

Expression de remerciement

L'auteur exprime sa reconnaissance à Monsieur L. DE BROGLIE, secrétaire perpétuel de l'Académie des Sciences Française, pour l'encouragement par lettre, de plus à Monsieur Z. CSOMA pour ses remarques précieuses.

BIBLIOGRAPHIE

1. L. DE BROGLIE, Étude critique des bases de l'interprétation actuelle de la mécanique ondulatoire, Paris, Gauthier, 1963.
2. T. MÁTRAI, Acta Phys. Hung., **5**, 409, 1956.
3. L. LANGE, Die geschichtliche Entwicklung des Bewegungsbegriffs, 1886.
4. P. FÉVRIER, L'interprétation physique de la mécanique ondulatoire et des théories quantiques, V., Gauthier, Paris, 1956.
5. J. FRENKEL, Uszpehi fizicseszkih nauk, **42**, 69, 1950 et **44**, 110, 1951.
6. D. BLOHINCEV, Uszpehi fizicseszkih nauk, **42**, 76, 1950 et **44**, 104, 1951.
7. D. BOHM, Phys. Rev., **85**, 166 et 188, 1952.
8. T. MÁTRAI, Acta Phys. Hung., **28**, 323, 1970.
9. T. MÁTRAI, Acta Phys. Hung., **32**, 115, 1972.
10. N. CHAKO, C. R., 1960, 2e Sem. 645.
11. N. ST. KALITZIN, Journ. de Phys. et le Rad., **22**, 821, 1961.
12. K. A. PYRAGAS et A. N. ALEXANDROV, Tensor, N. S. **23**, 337, 1972.
13. L. DE BROGLIE, Found of Phys., **I**, 5, 1970.
14. A. MICHEL, L. de Broglie, le physicien et penseur, Paris, 1952.
15. L. DE BROGLIE, Einf. in die Wellenmech., Hirzel, Leipzig, 1926.
16. M. v. BORN, Études Sélectionnées, Édition "Gondolat", Budapest, p. 225, 1973 (en hongrois).
17. J. NEUMANN, Math. Grundl. der Quantenmech. Berlin, Springer, 1932. p. 167.
18. M. PLANCK, Études Sélectionnées, Édition "Gondolat", Budapest, p. 177, 1965 (en hongrois).
19. A. EINSTEIN, B. PODOLSKY, N. ROSEN, Phys. Rev., **47**, 777, 1935.
20. L. DE BROGLIE, C. R. Hebd. Seances Acad. Sc. **B. 278**, 721, 1974.
21. E. WIGNER, Revue Hongroise de Physique, XXVII, 81, 1977 (en hongrois).
22. L. TISZA, Revue Hongroise de Physique,XXVII, 46, 1977 (en hongrois).
23. F. HUND, Einf. in die theoretische Phys. V. p. 225. VEB, Leipzig, 1950.
24. G. MARX, Acta Phys. Hung., **1**, 104, 1951.
25. Á. BUDÓ, Theoretische Mechanik, Verl. Wissensch., p. 191, 1965.
26. F. SCHWANK, Randwertprobleme, Teubner, Leipzig, 1951.
27. A. SOMMERFELD, Partielle Differentialgleichungen d. Phys. Akad. Verl., Leipzig, p. 133 1954.
28. G. MARX, Kvantummechanika, Műsz. K. K., Budapest 1964 (en hongrois).

Acta Physica Academiae Scientiarum Hungaricae, Tomus 46 (4), pp. 237—245 (1979)

TWO-PHASE FLOW HEAT TRANSFER IN A CIRCULAR PIPE WHEN THE INLET TEMPERATURE VARIES PERIODICALLY WITH TIME

By

K. S. SHIRKOT and SURJIT SINGH

DEPARTMENT OF MATHEMATICS, HIMACHAL PRADESH UNIVERSITY, SIMLA-171005, INDIA

(Received 31. III. 1979)

The problem of two phase flow heat transfer in a circular pipe is analysed when the temperature of the dust particles and of the liquid varies sinusoidally with time. The effect of various parameters on the amplitudes of dust particles, liquid-dust mixture and clear liquid is calculated. Graphs have been drawn to compare the values. It is found that the effect of dust particles is to flatten the temperature profile and thus increase the heat transfer.

$\bar{T}_p$	temperature of dust particles
$\bar{T}$	temperature of liquid
C_p	specific heat of dust particles
C	specific heat of liquid
K_p	thermal conductivity of dust particles
K	thermal conductivity of liquid
ϱ	fluid density
μ	co-efficient of viscosity of liquid
ν	kinematic co-efficient of viscosity
P	Prandtl number ($= \mu C/K$)
R	Reynold's number ($= r\,\bar{u}/\nu$)
$\bar{t}$	time
r_1	radius of the pipe
$\bar{z}$	$\bar{z}$-flow direction
u	velocity component in $\bar{z}$-direction
$\bar{u}$	average velocity
mN	mass of dust particles per unit volume ($= mN_0 =$ constant)
h_p	heat transfer co-efficient for flow over dust particles
A_p	surface area of dust particles
V_p	volume of dust particles
T_ω	constant well temperature

The meaning of any other symbols is given in the text as it occurs.

1. Introduction

In the solution of the transient forced convection energy equation of dust particles and of liquid in a circular pipe SOO [1] has assumed that the inlet temperature of dust particles and of liquid is constant across the flow. SHIRKOT and SINGH [2] have analysed the two-phase laminar flow in a channel when the temperature varies linearly with time. It is found that the temperature of dust particles and of liquid decays exponentially along the channel. In the present paper an exact solution of a two-phase flow problem with fully

developed flow in a circular pipe is obtained under given boundary conditions when the inlet temperature of dust particles and of liquid varies sinusoidally with time. The effect of various parameters on the amplitude of dust particles (a_p), liquid dust mixture (a_s) and clear liquid (a) is calculated. Graphs have been drawn to compare the values. It is found that the effect of the presence of dust particles is to increase the heat transfer.

2. Formulation of the problem

We consider a steady laminar flow of a dusty viscous liquid with uniform distribution of dust particles in a circular pipe. The dust particles and the liquid entering the pipe have temperatures which are spatially uniform across the entrance section of the pipe but vary sinusoidally with time. Therefore we can write the inlet conditions as

$$\bar{T}_p(\bar{r}, 0, \bar{t}) = T_0 + (\Delta T)_0 \sin \bar{\omega}\bar{t}, \tag{1}$$

$$\bar{T}(\bar{r}, 0, \bar{t}) = T_0 + (\Delta T)_0 \sin \bar{\omega}\bar{t}, \tag{2}$$

where T_0 is the cycle mean temperature (ΔT_0), is the amplitude and $\bar{\omega}$ is the inlet frequency.

To obtain heat transfer performance and the temperature of dust particles and of liquid, it is necessary to set up two energy equations, one for the dust particles and one for the liquid dust mixture. They are given as follows:

$$\frac{\partial \bar{T}_p}{\partial \bar{t}} + \bar{u}_p \frac{\partial \bar{T}_p}{\partial \bar{z}} = G(\bar{T} - \bar{T}_p), \tag{3}$$

$$\frac{\partial \bar{T}_p}{\partial \bar{t}} + \bar{u}_p \frac{\partial \bar{T}_p}{\partial \bar{z}} + \frac{(mN_0)\, C_p}{\varrho C} \left(\frac{\partial \bar{T}_p}{\partial \bar{t}} + \bar{u}_p \frac{\partial \bar{T}_p}{\partial \bar{z}} \right) = \frac{\nu}{\varrho} \left(\frac{\partial^2 \bar{T}}{\partial \bar{r}^2} + \frac{1}{\bar{r}} \frac{\partial \bar{T}}{\partial \bar{r}} \right) + \beta_2 (\bar{T}_p - \bar{T}), \tag{4}$$

where

$$\beta_2 = \frac{(mN_0) C_p G}{\varrho C}, \quad G = \frac{h_p A_p}{(mN_0) C_p V_p}.$$

Simplifying (4), we get

$$\frac{\partial \bar{T}}{\partial \bar{t}} + \bar{u} \frac{\partial \bar{T}}{\partial \bar{z}} = \frac{\nu}{\varrho} \left(\frac{\partial^2 \bar{T}}{\partial \bar{r}^2} + \frac{1}{\bar{r}} \frac{\partial \bar{T}}{\partial \bar{r}} \right) + 2\beta_2 (\bar{T}_p - \bar{T}). \tag{5}$$

The inlet boundary conditions of the problem are as follows:

$$\left.\begin{aligned} \bar{T}_p &= T_0 + (\Delta T)_0 \sin \bar{\omega}\bar{t}, \\ \bar{T} &= T_0 + (\Delta T)_0 \sin \bar{\omega}\bar{t} \end{aligned}\right] \quad \text{at} \quad \bar{z} = 0, \tag{6}$$

$$\left(\frac{\partial \bar{T}_p}{\partial \bar{r}}\right)_{\bar{r}=0} = 0, \quad \left(\frac{\partial \bar{T}}{\partial \bar{r}}\right)_{\bar{r}=0} = 0; \quad \bar{T}_p = \bar{T} = T_\omega \text{ at } \bar{r} = r, \; \bar{t} > 0 . \tag{7}$$

The system satisfying Eqs. (3) and (4) is subjected to the following restrictions [1]:

(i) Radiation effect is neglected.
(ii) Each dust particle is small and maintains uniform temperature due to its high thermal conductivity K_p.
(iii) The liquid and the dust particle cloud have similar velocity profiles.
(iv) The dust particles are uniformly distributed throughout the pipe and the suspension is extremely dilute.
(v) The effect of collision with wall is neglected.
(vi) Axial conduction is negligible with respect to bulk transport in the direction. This is a reasonable assumption when Peclet number exceeds 100 [3].

Further, to simplify the method of analysis the case of constant velocity will be considered here. For this purpose, we substitute $u = \bar{u} = \bar{u}_p$ for the velocity profile in (3) and (4) or (5). We now introduce the following non-dimensional quantities:

$$\theta = \frac{\bar{T} - T_0}{(\Delta T)_0}, \; \theta_p = \frac{\bar{T}_p - T_0}{(\Delta T)_0}, \; \theta_0 = \frac{T_\omega - T_0}{(\Delta T)_0}, \; z = \frac{\bar{z}}{r_1},$$

$$\omega = \frac{r_1^2 \bar{\omega}}{\nu}, \; t = \frac{\nu \bar{t}}{r_1^2}, \; \beta_3 = \frac{r_1^2 G}{\nu}, \; \beta_4 = \frac{2r^2 \beta_2}{\nu}, \; r = \frac{\bar{r}}{r_1} .$$

Eqs. (3) and (5) then become

$$\frac{\partial \theta_p}{\partial t} + R \frac{\partial \theta_p}{\partial z} = \beta_3(\theta - \theta_p), \tag{8}$$

$$\frac{\partial \theta}{\partial t} + R \frac{\partial \theta}{\partial z} = \frac{1}{p}\left(\frac{\partial^2 \theta}{\partial r^2} + \frac{1}{r}\frac{\partial \theta}{\partial r}\right) + \beta_4(\theta_p - \theta) . \tag{9}$$

The inlet boundary conditions reduce to

$$\theta_p = \theta = \sin \omega t \text{ at } z = 0, \tag{10}$$

$$\left(\frac{\partial \theta_p}{\partial r}\right)_{r=0} = 0, \quad \left(\frac{\partial \theta}{\partial r}\right)_{r=0} = 0; \quad \theta_p = \theta = \theta_0 \text{ at } r = 1, \; t > 0 . \tag{11}$$

3. Method of solution

The above problem can be separated into two as follows:

$$\theta_p = \theta_{p_1}(r, z) + \theta_{p_2}(r, z, t)\,, \tag{12}$$

$$\theta = \theta_1(r, z) + \theta_2(r, z, t)\,, \tag{13}$$

where θ_1, θ_2, θ_{p_1} and θ_{p_2} satisfy the following equations

$$R\frac{\partial\theta_{p_1}}{\partial z} = \beta_3(\theta_1 - \theta_{p_1})\,, \tag{14}$$

$$R\frac{\partial\theta_1}{\partial z} = \frac{1}{\varrho}\left(\frac{\partial^2\theta_1}{\partial r^2} + \frac{1}{r}\frac{\partial\theta_1}{\partial r}\right) + \beta_4(\theta_{p_1} - \theta_1), \tag{15}$$

$$\theta_1 = 0,\ \theta_{p_1} = 0 \text{ when } z = 0\,, \tag{16}$$

$$\left(\frac{\partial\theta_1}{\partial r}\right)_{r=0} = 0,\ \left(\frac{\partial\theta_{p_1}}{\partial r}\right)_{r=0} = 0\,, \tag{17}$$

$$[\theta_1 = \theta_0,\ \theta_{p_1} = \theta_0] \text{ at } r = 1\,, \tag{18}$$

$$\frac{\partial\theta_{p_2}}{\partial t} + R\frac{\partial\theta_{p_2}}{\partial z} = \beta_3(\theta_2 - \theta_{p_2})\,, \tag{19}$$

$$\frac{\partial\theta_2}{\partial t} + R\frac{\partial\theta_2}{\partial z} = \frac{1}{\varrho}\left(\frac{\partial^2\theta_2}{\partial r^2} + \frac{1}{r}\frac{\partial\theta_2}{\partial r}\right) + \beta_4(\theta_{p_2} - \theta_2)\,, \tag{20}$$

$$[\theta_{p_2} = \sin\omega t,\ \theta_2 = \sin\omega t] \text{ when } z = 0\,, \tag{21}$$

$$\left(\frac{\partial\theta_2}{\partial r}\right)_{r=0} = 0\,,\ \left(\frac{\partial\theta_{p_2}}{\partial r}\right)_{r=0} = 0; \theta_2 = 0,\ \theta_{p_2} = 0 \text{ at } r = 1, t > 0. \tag{22}$$

Solving (14) and (15) under the conditions (16)—(18), we get

$$\theta_1(r, z) = \theta_0\left[1 - 2\sum_{n=1}^{\infty}\frac{J_0(r\alpha_n)}{\alpha_n J_1(\alpha_n)}\left\{\frac{\lambda_n}{\lambda_n - \mu_n}\left(1 - \frac{R\mu_n}{\beta_3}\right)e^{-\mu_n z} - \right.\right.$$
$$\left.\left. - \frac{\mu_n}{\lambda_n - \mu_n}\left(1 - \frac{R\lambda_n}{\beta_3}\right)e^{-\lambda_n z}\right\}\right], \tag{23}$$

$$\theta_{p_1}(r, z) = \theta_0\left[1 - 2\sum_{n=1}^{\infty}\frac{J_0(r\alpha_n)}{\alpha_n J_1(\alpha_n)}\left\{\frac{\lambda_n}{\lambda_n - \mu_n}e^{-\mu_n z} - \frac{\mu_n}{\lambda_n - \mu_n}e^{-\lambda_n z}\right\}\right], \tag{24}$$

where

$$2\lambda_n = \frac{\beta_3 + \beta_4}{R} + \frac{\alpha_n^2}{PR} + \left(\frac{\beta_3 + \beta_4}{R} + \frac{\alpha_n^2}{PR} - \frac{u\alpha_n^2}{PR^2}\beta_3\right)^{1/2}, \tag{25}$$

$$2\mu_n = \frac{\beta_3 + \beta_4}{R} + \frac{\alpha_n^2}{PR} - \left(\frac{\beta_3 + \beta_4}{R} + \frac{\alpha_n^2}{PR} - \frac{u\alpha_n^2}{PR^2}\beta_3\right)^{1/2}, \tag{26}$$

and α_n ($n = 1, 2, 3, \ldots$) are the positive roots of $J_0(\alpha) = 0$.

In order to obtain $\theta_{p_2}(r, z, t)$ and $\theta_2(r, z, t)$, we define the following auxiliary problem:

$$\frac{\partial \theta'_{p_2}}{\partial t} + R\frac{\partial \theta'_{p_2}}{\partial z} = \beta_3(\theta'_2 - \theta'_{p_2}), \tag{27}$$

$$\frac{\partial \theta'_2}{\partial t} + R\frac{\partial \theta'_2}{\partial z} = \frac{1}{p}\left(\frac{\partial^2 \theta'_2}{\partial r^2} + \frac{1}{r}\frac{\partial \theta'_2}{\partial r}\right) + \beta_4(\theta'_{p_2} - \theta'_2), \tag{28}$$

$$[\theta'_2 = \cos \omega t,\ \theta'_{p_2} = \cos \omega t] \text{ when } z = 0, \tag{29}$$

$$\left(\frac{\partial \theta'_2}{\partial r}\right)_{r=0} = 0,\ \left(\frac{\partial \theta'_{p_2}}{\partial r}\right)_{r=0} = 0;\ \theta'_2 = 0,\ \theta'_{p_2} = 0 \text{ at } r = 1,\ t > 0. \tag{30}$$

Let us define new temperature functions θ_{p_c} and θ_c such that $\theta_{p_c} = \theta'_{p_c} + i\theta_{p_2}$ and $\theta_c = \theta'_2 + i\theta_2$. Then the problem given by (19), (22) and (27)—(30) can be combined to give the following equations

$$\frac{\partial \theta_{p_c}}{\partial t} + R\frac{\partial \theta_{p_c}}{\partial z} + \beta_3(\theta_c - \theta_{p_c}), \tag{31}$$

$$\frac{\partial \theta_c}{\partial t} + R\frac{\partial \theta_c}{\partial z} = \frac{1}{\varrho}\left(\frac{\partial^2 \theta_c}{\partial r^2} + \frac{1}{r}\frac{\partial \theta_c}{\partial r}\right) + \beta_4(\theta_{p_c} - \theta_c), \tag{32}$$

$$(\theta_{p_c} = e^{i\omega t},\ \theta_c = e^{i\omega t}) \quad \text{when} \quad z = 0 \tag{33}$$

$$\left(\frac{\partial \theta_{p_c}}{\partial r}\right)_{r=0} = 0,\ \left(\frac{\partial \theta_c}{\partial r}\right)_{r=0} = 0;\ (\theta_{p_c} = 0,\ \theta_c = 0) \text{ at } r = 1,\ t > 0. \tag{34}$$

We now assume the periodic solutions of the form:

$$\theta_{p_c}(r, z, t) = e^{i\omega t}\psi(r, z), \tag{35}$$

$$\theta_c(r, z, t) = e^{i\omega t}\varphi(r, z), \tag{36}$$

where ψ and φ satisfy the following

$$i\omega\psi + R\frac{\partial \psi}{\partial z} = \beta_3(\varphi - \psi), \tag{37}$$

$$i\omega\varphi + R\frac{\partial \varphi}{\partial z} = \frac{1}{\varrho}\left(\frac{\partial^2 \varphi}{\partial r^2} + \frac{1}{r}\frac{\partial \varphi}{\partial r}\right) + \beta_4(\psi - \varphi), \tag{38}$$

$$(\psi = 1,\ \varphi = 1) \text{ when } z = 0, \tag{39}$$

$$\left(\frac{\partial \psi}{\partial r}\right)_{r=0} = 0,\ \left(\frac{\partial \varphi}{\partial r}\right)_{r=0} = 0;\ (\psi = 0,\ \varphi = 0) \quad \text{at} \quad r = 1,\ t > 0. \tag{40}$$

Solving (37) and (38) under the conditions (39) and (40), we get

$$\theta_2 = 2 \sin\left(\omega t - \frac{\omega}{R} z\right) \sum_{n=1}^{\infty} \frac{J_0(r\alpha_n)}{\alpha_n J_1(\alpha_n)} \left[\left(1 - \frac{R\mu_n}{\beta_3}\right)\left(\frac{\lambda_n}{\lambda_n - \mu_n}\right) e^{-\lambda_n z} - \left(1 - \frac{R\lambda_n}{\beta_3}\right)\left(\frac{\mu_n}{\lambda_n - \mu_n}\right) e^{-\lambda_n z}\right], \tag{41}$$

$$\theta_{p_e} = 2 \sin\left(\omega t - \frac{\omega}{R} z\right) \sum_{n=1}^{\infty} \frac{J_0(r\alpha_n)}{\alpha_n J_1(\alpha_n)} \left[\frac{\lambda_n}{\lambda_n - \mu_n} e^{-\mu_n z} - \frac{\mu_n}{\lambda_n - \mu_n} e^{-\lambda_n z}\right], \tag{42}$$

where

$$\lambda_n \mu_n = \frac{\alpha_n^2}{PR^2} \beta_3, \quad \lambda_n + \mu_n = \frac{\beta_3 + \beta_4}{R} + \frac{\alpha_n^2}{PR}, \tag{43}$$

$$\lambda_n - \mu_n = \left[\left(\frac{\beta_3 + \beta_4}{R} + \frac{\alpha_n^2}{PR}\right)^2 - \frac{4\alpha_n^2}{PR^2} \beta_3\right]^{1/2}. \tag{44}$$

4. Discussion

When the boundary conditions on the wall of the pipe for θ and θ_p are homogeneous, that is when θ_0 is zero, we have

$$\theta_p(r, z, t) = \theta_{p_s}(r, z, t), \tag{45}$$

$$\theta\,(r, z, t) = \theta_2(r, z, t)\,. \tag{46}$$

$\theta_{p_s}(r, z, t)$ and $\theta_2(r, z, t)$ show that the temperatures of dust particles and of liquid decay exponentially along the pipe. For a single phase system the number of dust particles per unit volume is zero ($\beta_4 = 0$), then

$$\theta_s(r, z, t) = 2 \sin\left(\omega t - \frac{\omega}{R} z\right) \sum_{n=1}^{\infty} \frac{J_0(r\alpha_n)}{\alpha_n J_1(\alpha_n)} \cdot C_n, \tag{47}$$

where

$$C_n = \exp\left(-\frac{\alpha_n^2}{PR} z\right).$$

In many applications, heat transfer in regions away from the inlet is of interest and for such situations, only the first term in (41), (42) and (47) is taken and for this case the temperature at $r = 0$ is given by

$$\theta = 2 \sin\left(\omega t - \frac{\omega}{R} z\right) a\,, \tag{48}$$

$$\theta_p = 2 \sin\left(\omega t - \frac{\omega}{R} z\right) a_p\,, \tag{49}$$

$$\theta_s = 2 \sin\left(\omega t - \frac{\omega}{R} z\right) a_s , \tag{50}$$

where

$$a_p = \frac{1}{\alpha_1 J_1(\alpha_1)} \left[\frac{\lambda_1}{\lambda_1 - \mu_1} e^{-\mu_1 z} - \frac{\mu_1}{\lambda_1 - \mu_1} e^{-\lambda_1 z} \right], \quad a_s = \frac{1}{\alpha_1 J_1(\alpha_1)} e^{-\frac{\alpha_1^2}{PR} z},$$

and

$$a = \frac{1}{\alpha_1 J_1(\alpha_1)} \left[\left(1 - \frac{R\mu_1}{\beta_3}\right) \left(\frac{\lambda_1}{\lambda_1 - \mu_1}\right) e^{-\mu_1 z} - \left(1 - \frac{R\lambda_1}{\beta_3}\right) \left(\frac{\mu_1}{\lambda_1 - \mu_1}\right) e^{-\lambda_1 z} \right],$$

are respectively the amplitudes of dust particles, liquid-dust mixture and clear liquid.

Remarks

By using Soo's trial solution, (Eq. (4.47) on p. 155 of [1]) we have obtained ordinary differential equations of Bessel's type. The resulting boundary value problem turned out to be a Sturm—Liouville system. This is important

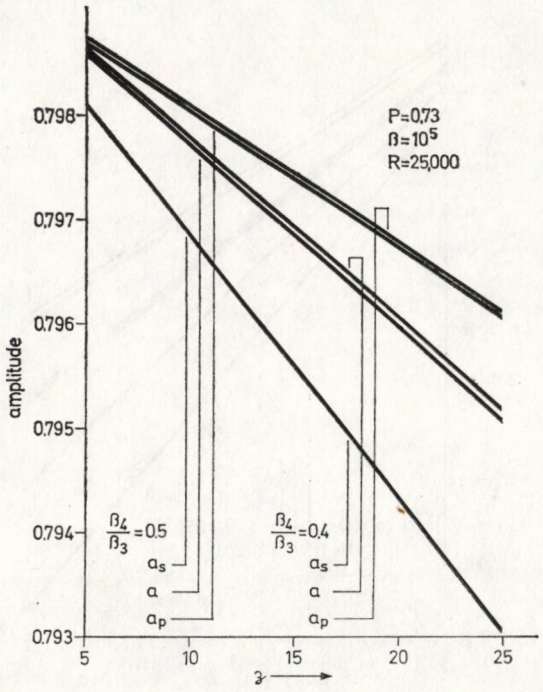

Fig. 1

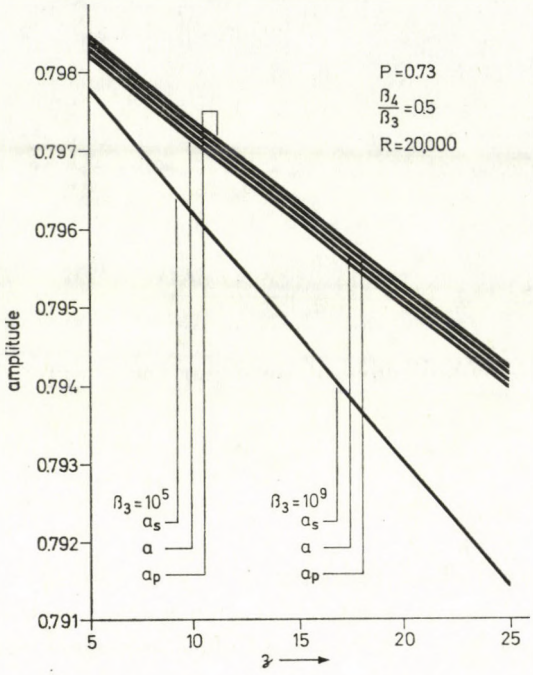
P=0.73
$\frac{\beta_4}{\beta_3}$=0.5
R=20,000
amplitude
0.798
0.797
0.796
0.795
0.794
0.793
0.792
0.791
5
10
15
20
25
$\beta_3=10^5$
$\beta_3=10^9$
a_s
a
a_p
γ

Fig. 2

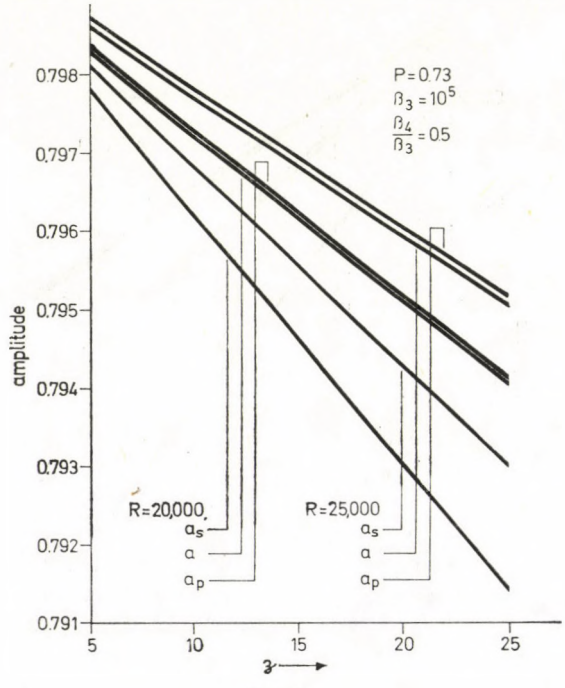
P=0.73
$\beta_3=10^5$
$\frac{\beta_4}{\beta_3}$=0.5
amplitude
0.798
0.797
0.796
0.795
0.794
0.793
0.792
0.791
5
10
15
20
25
R=20,000
R=25,000
a_s
a
a_p
γ

Fig. 3

because Soo obtained a Sturm—Liouville system for a degenerate case only. Eqs. (23) to (26) of this paper represent a general solution of the heat transfer problem.

(i) From Fig. 1 it is clear that the amplitudes increase with R and $a_p > > a > a_s$.

(ii) Fig. 2 shows that a_p decreases with the increase of β_3 (and so β_4) but a increases and $a_p > a > a_s$.

(iii) From Fig. 3 we find that the amplitude a_p and a increase with increasing β_4/β_3 and $a_p > a > a_s$ (at least for the values of various parameters occurring here).

Therefore the effect of dust particles is to flatten the temperature profile and consequently increase the heat transfer. The phase lags are the same for two-phase and single-phase system. Also, as the inlet frequency is increased the phase lag increases and as the Reynold number R is increased, the phase lag decreases.

REFERENCES

1. S. L. Soo, Fluid Dynamics of Multiphase Systems; Blaisdell Publishing Comp., London, 1967.
2. K. S. Shirkot and Surjit Singh, Acta Phys. Hung., **43**, 209, 1977.
3. P. J. Schneider, Trans. ASME, **79**, 765, 1957.

Acta Physica Academiae Scientiarum Hungaricae, Tomus 46 (4), pp. 247—252 (1979)

RAYLEIGH-TAYLOR INSTABILITY OF A COMPOSITE MIXTURE THROUGH POROUS MEDIUM

By

R. C. SHARMA and K. P. THAKUR

DEPARTMENT OF MATHEMATICS, HIMACHAL PRADESH UNIVERSITY, SIMLA-171005, INDIA

(Received 3. IV. 1979)

The frictional effect of collisions of ionized with neutral atoms on the Rayleigh—Taylor instability of a composite mixture through porous medium is considered in the presence of a horizontal magnetic field. For the case of two uniform fluids separated by a horizontal boundary, the magnetic field completely stabilizes certain wave-number band. For the case of exponentially varying density, the collisions are found to have no effect as such on the stratification. However for the stable stratification, the growth rates increase with the increase in permeability of the medium whereas for the unstable stratification, the growth rates may be both increasing or decreasing.

1. Introduction

CHANDRASEKHAR [1] has given a detailed account of the stability of superposed fluids in the presence of magnetic field through non-porous medium. When a fluid permeates a porous material, the actual path of an individual particle of fluid cannot be followed analytically. The effect, as the fluid slowly percolates through the pores of the rock, is represented by a macroscopic law. This is the usual Darcy's law. As a result of this, the usual viscous term in the equations of fluid motion is replaced by the resistance term $(\mu/k_1)\mathbf{q}$, where μ is the viscosity of the fluid, k_1 the permeability of the medium and $\mathbf{q}$ the velocity of the fluid, calculated from Darcy's law. WOODING [2] has considered the Rayleigh instability of a thermal boundary layer in flow through a porous medium.

It is quite frequent that the medium is not fully ionized and may be permeated with neutral atoms. The medium has been idealized therefore, following HANS [3], as a composite mixture of a hydromagnetic (ionized) component and a neutral component, the two interacting through mutual collisional (frictional) effects. HANS [3] and BHATIA [4] have shown that the collisions have a stabilizing effect on the Rayleigh—Taylor instability. However, for the Kelvin—Helmholtz configuration, RAO and KALRA [5] and HANS [3] have found that the collisional effects are in fact destabilizing for a sufficiently large collision frequency.

In the present paper we study the collisional and porosity effects on the Rayleigh—Taylor instability of a composite mixture through porous medium in hydromagnetics.

2. Perturbation equations

Consider an incompressible composite layer consisting of an infinitely conducting hydromagnetic fluid of density ϱ, permeated with neutrals of density ϱ_d, arranged in horizontal strata; through porous medium and acted on by gravity force $\mathbf{g}(0, 0, -g)$ and horizontal magnetic field $\mathbf{H}(H, 0, 0)$. Assume that both the ionized fluid and neutral fluid behave like continuum fluids and that effects on the neutral component resulting from the fields of gravity and pressure are neglected. The magnetic field interacts with the hydromagnetic component only.

Let $\delta\varrho$, δp, $\mathbf{q}(u, v\ w)$ and $\mathbf{h}(h_x, h_y, h_z)$ denote respectively the perturbations in density, pressure, velocity and magnetic field $\mathbf{H}$; $\mathbf{q}_d$, v_c, μ_e and μ denote the velocity of the neutral fluid, the mutual collisional (frictional) frequency between the two components of the composite medium, the magnetic permeability of the medium and the viscosity of the hydromagnetic fluid, respectively. Then the linearized perturbation equations governing the motion of the composite medium are

$$\varrho \frac{\partial \mathbf{q}}{\partial t} = -\nabla \delta p + \mathbf{g}\delta\varrho + \frac{\mu_e}{4\pi}(\nabla \times \mathbf{h}) \times \mathbf{H} + \varrho_d v_c(\mathbf{q}_d - \mathbf{q}) - \frac{\varrho \nu}{k_1}\mathbf{q}, \tag{1}$$

$$\frac{\partial \mathbf{q}_d}{\partial t} = -v_c(\mathbf{q}_d - \mathbf{q}), \tag{2}$$

$$\nabla \cdot \mathbf{q} = 0, \quad \nabla \cdot \mathbf{h} = 0, \tag{3}$$

$$\frac{\partial}{\partial t}\delta\varrho = -w\frac{d\varrho}{dz}, \tag{4}$$

$$\frac{\partial \mathbf{h}}{\partial t} = \nabla \times (\mathbf{q} \times \mathbf{H}). \tag{5}$$

Analyzing the disturbances into normal modes, we seek solutions whose dependence on space coordinates x, y, z and time t is of the form

$$f(z) \exp(ik_x x + ik_y y + nt), \tag{6}$$

where $k_x, k_y \left(k = \sqrt{(k_x^2 + k_y^2)}\right)$ are the wave numbers along x and y directions respectively, $f(z)$ is some function of z and n is a complex constant.

Eliminating $\mathbf{q}_d$ between Eqs. (1) and (2) and using (6), Eqs. (1)—(5) give

$$\left(n' + \frac{\nu}{k_1}\right)\varrho u = -ik_x \delta p, \tag{7}$$

$$\left(n' + \frac{\nu}{k_1}\right)\varrho v = -ik_y \delta p + \frac{\mu_e H}{4\pi}(ik_x h_y - ik_y h_x), \tag{8}$$

$$\left(n' + \frac{v}{k_1}\right) \varrho w = -D\delta p - \frac{\mu_e H}{4\pi}(Dh_x - ik_x h_z) - g\delta\varrho\,, \tag{9}$$

$$ik_x u + ik_y v + Dw = 0, \tag{10}$$

$$ik_x h_x + ik_y h_y + Dh_z = 0, \tag{11}$$

$$n\delta\varrho = -wD\varrho\,, \tag{12}$$

$$nh_x = ik_x Hu,\ nh_y = ik_x Hv,\ nh_z = ik_x Hw\,, \tag{13}$$

where

$$n' = n\left(1 + \frac{\alpha_0 \nu_c}{n + \nu_c}\right),\ \nu = \frac{\mu}{\varrho},\ \alpha_0 = \frac{\varrho_d}{\varrho} \quad \text{and} \quad D = \frac{d}{dz}\,.$$

Eliminating δp between Eqs. (7)—(9) and using Eqs. (10)—(13), we get

$$n'[D(\varrho Dw) - k^2\varrho w] + \frac{1}{k_1}[D(\varrho\nu Dw) - k^2\varrho\nu w] + \frac{\mu_e k_x^2 H^2}{4\pi n} \times (D^2 - k^2)w + \frac{gk^2}{n}(D\varrho)w = 0\,. \tag{14}$$

3. Two uniform fluids separated by a horizontal boundary

Consider the case of two uniform fluids of densities ϱ_1 (lower fluid) and ϱ_2 (upper fluid) separated by a horizontal boundary at $z = 0$. Eq. (14) for both regions of fluid reduces to

$$(D^2 - k^2)w = 0. \tag{15}$$

The general solution of Eq. (15) is

$$w = Ae^{+kz} + Be^{-kz}\,, \tag{16}$$

where A and B are arbitrary constants.

The boundary conditions to be satisfied in the present problem are as follows.

(i) The velocity w should vanish when $z \to +\infty$ (for the upper fluid) and $z \to -\infty$ (for the lower fluid).
(ii) $w(z)$ is continuous at $z = 0$.
(iii) The pressure should be continuous across the interface.

The continuity of pressure means that

$$n'\Delta_0(\varrho Dw) + \frac{1}{k_1}\Delta_0(\varrho\nu Dw) + \frac{\mu_e k_x^2 H^2}{4\pi n}\Delta_0(Dw) + \frac{gk^2}{n}\Delta_0(\varrho)w_0 = 0. \tag{17}$$

Applying the boundary conditions (i) and (ii), we can write

$$w_1 = Ae^{+kz}(z < 0)\,, \tag{18}$$

and

$$w_2 = Ae^{-kz}(z > 0)\,, \tag{19}$$

the same constant A has been chosen to ensure the continuity of w at $z = 0$.

Applying the condition (17) to the solutions (18) and (19), we get

$$n^3 + \left[\nu_c(\alpha_0 + 1) + \frac{1}{k_1}(\alpha_1\nu_1 + \alpha_2\nu_2)\right]n^2 + \left[\frac{\nu_c}{k_1}(\alpha_1\nu_1 + \alpha_2\nu_2) + 2k_x^2 v_A^2 + gk(\alpha_1 - \alpha_2)\right]n + [2k_x^2 v_A^2 + gk(\alpha_1 - \alpha_2)]\,\nu_c = 0\,, \tag{20}$$

where $v_A^2 = \mu_e H^2/4\pi(\varrho_1 + \varrho_2)$.

(a) Stable case ($\varrho_1 > \varrho_2$).

In this case, Eq. (20) does not allow any positive root as there is no change of sign. This means that the system is stable.

(b) Unstable case ($\varrho_2 > \varrho_1$).

In this case if

$$2k_x^2 v_A^2 < gk(\alpha_2 - \alpha_1)\,, \tag{21}$$

the constant term in Eq. (20) is negative. Eq. (20) therefore allows one change of sign and so has one positive root. The occurrence of positive root implies that the system is unstable. If

$$2k_x^2 v_A^2 > gk(\alpha_2 - \alpha_1)\,, \tag{22}$$

Eq. (20) does not admit of any change of sign and so no positive root occurs. The system is therefore stable.

Thus for the unstable case ($\varrho_2 > \varrho_1$), the system is stable or unstable according as $\varrho_2 - \varrho_1$ is less than or greater than $\mu_e H^2 k_x^2/2\pi gk$. In the absence of magnetic field, the system is unstable for $\varrho_2 > \varrho_1$, as one of the values of n given by Eq. (20) is positive. But the presence of magnetic field has got stabilizing effect and completely stabilizes the wave-number band $k > k_*$ where

$$k_* = \frac{2\pi g(\varrho_2 - \varrho_1)}{\mu_e H^2}\sec^2\theta\,, \tag{23}$$

and θ is the inclination of the wave vector **k** to the direction of magnetic field **H**.

4. The case of exponentially varying density

Let us consider the density stratification in a continuously stratified medium of depth d as

$$\varrho(z) = \varrho_0 e^{\beta z}, \tag{24}$$

where ϱ_0 and β are constants. Let us assume that $\beta d \ll 1$, i.e., the variation of density at two neighbouring points in the velocity field, which is much less than the average density, has a negligible effect on the inertia of the fluid.

Following CHANDRASEKHAR [1], the boundary conditions for the case of two free surfaces are

$$w = D^2 w = 0 \quad \text{at} \quad z = 0 \quad \text{and} \quad d\,. \tag{25}$$

The proper solution of Eq. (14) satisfying (25) is

$$w = A \sin \frac{m\pi z}{d}\,, \tag{26}$$

where A is a constant and m is any integer.

Substituting (26) in (14) and neglecting the effect of heterogeneity on the inertia, we get

$$\left[n' + \frac{v}{k_1} + \frac{k_x^2 v^2}{n}\right]\left\{\left(\frac{m\pi}{d}\right)^2 + k^2\right\} - \frac{g\beta k^2}{n} = 0, \tag{27}$$

which on simplification gives

$$\begin{aligned} n^3 + \left[v_c(\alpha_0 + 1) + \frac{v}{k_1}\right] n^2 + \left[\frac{v}{k_1} v_c + k_x^2 V^2 - \frac{g\beta k^2}{L}\right] n + \\ + \left[k_x^2 v^2 - \frac{g\beta k^2}{L}\right] v_c = 0\,, \end{aligned} \tag{28}$$

where

$$v^2 = \frac{\mu_e H^2}{4\pi\varrho_0} \quad \text{and} \quad L = \left(\frac{m\pi}{d}\right) + k^2.$$

For the stable stratification ($\beta < 0$), Eq. (28) does not have any positive root implying thereby that the system is stable. For the unstable stratification ($\beta > 0$) and for $k^2 > k_x^2 v^2 L/g\beta$, the constant term in Eq. (28) is negative. This means that Eq. (28) possesses one positive root implying thereby that the system is unstable. Let n_0 denote the positive root of Eq. (28). Then

$$\begin{aligned} n_0^3 + \left[v_c(\alpha_0 + 1) + \frac{v}{k_1}\right] n_0^2 + \left[\frac{v}{k_1} v_c + k_x^2 v^2 - \frac{g\beta k^2}{L}\right] n_0 + \\ + \left[k_x^2 v^2 - \frac{g\beta k^2}{L}\right] v_c = 0\,. \end{aligned} \tag{29}$$

To find the role of collisions concerning the growth rate of unstable modes, we examine the nature of dn_0/dv_c. Eq. (29) gives

$$\frac{dn_0}{dv_c} = -\frac{n_0^2(\alpha_0+1) + \frac{v}{k_1}n_0 + \left(k_x^2 v^2 - \frac{g\beta k^2}{L}\right)}{3n_0^2 + 2\left[v_c(\alpha_0+1) + \frac{v}{k_1}\right]n_0 + \left[\frac{v}{k_1}v_c + k_x^2 v^2 - \frac{g\beta k^2}{L}\right]}. \tag{30}$$

Therefore if, in addition to $k^2 > k_x^2 v^2 L/g\beta$, which is a sufficient condition for instability, we have either of the conditions

$$k_x^2 v^2 - \frac{g\beta k^2}{L} \gtrless -\left[\frac{v}{k_1}v_c + 2n_0\left\{v_c(\alpha_0+1) + \frac{v}{k_1}\right\} + 3n_0^2\right], \tag{31}$$

dn_0/dv_c is always negative. Thus with the increase in collisional frequency, the growth rate decreases.

We conclude therefore that for $k^2 > k_x^2 v^2 L/g\beta$, the system is unstable and the growth rate, under either of the conditions (31), decreases with the increase of collisions. If $k^2 < k_x^2 v^2 L/g\beta$, the system is stable.

To find the effect of permeability of the medium on growth rates, we examine the nature of dn_0/dk_1. Eq. (29) gives

$$\frac{dn_0}{dk_1} = \frac{\frac{v}{k_1^2}(n_0 + v_c)n_0}{3n_0^2 + 2n_0\left\{v_c(\alpha_0+1) + \frac{v}{k_1}\right\} + \left\{\frac{v}{k_1}v_c + k_x^2 v^2 - \frac{g\beta k^2}{L}\right\}}. \tag{32}$$

Eq. (32) implies that for stable stratification ($\beta < 0$), dn_0/dk_1 is positive; meaning thereby that with the increase in permeability of the medium, the growth rate increases for the stable stratification.

For unstable stratification ($\beta > 0$) and for

$$\frac{g\beta k^2}{L} \gtrless 3n_0^2 + 2n_0\left\{v_c(\alpha_0+1) + \frac{v}{k_1}\right\} + \left\{\frac{v}{k_1}v_c + k_x^2 v^2\right\}, \tag{33}$$

dn_0/dk_1 is negative or positive for the greater than or less than sign, respectively; meaning thereby that with the increase in permeability of the medium, the growth rates are both decreasing and increasing for the unstable stratification.

REFERENCES

1. S. CHANDRASEKHAR, Hydrodynamic and Hydromagnetic Stability, Oxford University Press, London, 1961, Chap. X.
2. R. A. WOODING, J. Fluid Mech., **9**, 183, 1960.
3. H. K. HANS, Nucl. Fusion, **8**, 89, 1968.
4. P. K. BHATIA, Nucl. Fusion, **10**, 383, 1970.
5. S. S. RAO and G. L. KALRA, Can. J. Phys., **45**, 2779, 1967.

Acta Physica Academiae Scientiarum Hungaricae, Tomus 46 (4), pp. 253—261 (1979)

SEMI-CONDUCTING PROPERTIES OF ORIENTED THIN TELLURIUM FILMS

By

A. H. EID, S. MAHMOUD and M. S. ELMANHARAWY

ELECTRON MICROSCOPY LABORATORY, NATIONAL RESEARCH CENTRE, DOKKI, CAIRO, EGYPT

(Received in revised form 8. V. 1979)

Oriented tellurium films have been deposited on mica at temperatures ranging between 333K and 423 K. The electrical properties are measured. The results are discussed in relation to those resulting from electron microscopical and optical investigations. The existence of two acceptor states in the band gap is demonstrated, these states act as sources of holes below 400 K. On annealing the samples in situ, the electrical properties and the Hall coefficient imply considerable influence on the semi-conducting behaviour by electrons from the conduction band. I. R. spectral measurements have revealed the presence of three different peaks corresponding to three activation energy values of 0.05 eV, 0.12 eV and 0.31 eV.

Introduction

The structure of thin semi-conducting films as well as the experimental conditions used in their preparation are known to affect the electrical properties of these films to a great extent. The mobility of carriers together with their concentrations represent two parameters which are most sensitive to the vacuum, the rate of deposition, the temperature of substrate and the annealing program. With regard to tellurium, the atoms have been found to possess high mobilities on heated substrates; thus allowing the structure to be very much governed by the surface free energies of the crystallites [1]. Thin films on cooled substrates have polycrystalline structures with dropletlike islands. On raising the temperature of the crystalline substrate, these droplet-like islands assume the dendritic shape with a considerable ability for nucleation of twins. Little information only is available in the existing literature on the correlation between the electrical properties and the microstructure of such oriented films. By careful selection of the experimental conditions, we were able to deposit oriented tellurium films on freshly-cleaved surfaces of mica. Electric resistivity and galvanomagnetic properties of these films were measured and the results were supported by further optical studies in the I.R. range.

Experimental

Thin tellurium films were thermally evaporated from heated silica crucible on freshly cleaved surface of mica under vacuum of 10^{-4} μbar. The mica employed was of Egyptian locality of muscovite type. The glide plane of muscovite

coincides with its cleavage plane and this makes it easy to be cleaved and produce thin sheets of extended crystalline layers. The cleaved surface is approximately atomically flat [2]. Before evaporating the tellurium films, the mica was heated up to 675 K for one hour to minimize the presence of any unavoidable surface impurities. Special mechanical diaphragms were used to evaporate thick layers of gold electrodes at the terminals of the mica sheets. Before the deposition of tellurium films, the mica was maintained at the required temperature. The experimental conditions (substrate type, substrate temperature and rate of deposition) which yield tellurium films of monocrystalline structure were selected from our previous work [3]. Accordingly, 20 nm/sec was a suitable rate, on a mica substrate maintained at a temperature of 423 K. Simultaneously prepared tellurium films on optical quality were used for measuring the film thickness by TOLANSKY method [4]. The electron microscope samples were detached from the tellurium films deposited on mica and treated under the same conditions. The mica with the film on it was gently immersed in distilled water on which few drops of petroleum ether were added. The floating pieces were fixed on the electron microscope grids. For I. R. studies some discs of mica simultaneously prepared and similarly treated were used.

Results and discussion

When the temperature of the substrate is close to that of the room, and the rate of deposition is above 10^{-7} cm/sec, the film is composed of polycrystalline islands of droplet-like shape as shown on Plate (1a). The corresponding electron diffraction pattern in Plate (1b) is a normal ring pattern indicating no

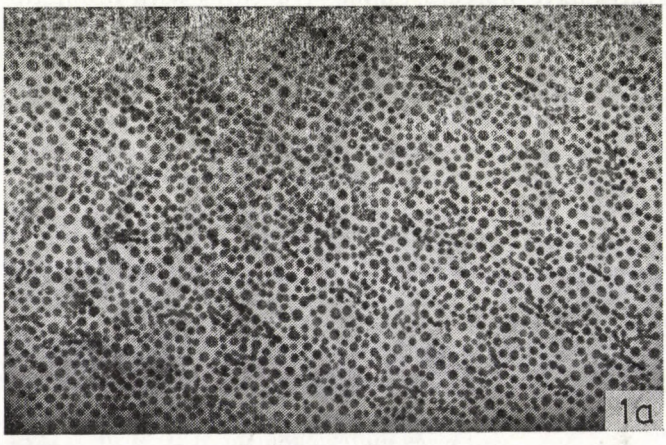

Plate (1a). 9000 times magnified photograph of Te film 0.05 μm thick deposited on cold mica substrate

preferred orientation even on tilting the film 30°. One should mention that when the rate of deposition ranged between 2×10^{-8} cm/sec and 10^{-7} cm/sec, the dendritic shape started to appear with a poor orientation, detected by the weak arcs which were superimposed on the ring pattern (Plate 2).

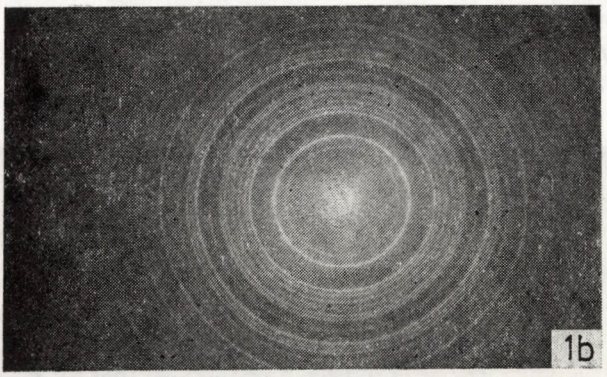

Plate (1b). Transmission electron diffraction from the same area recorded in Plate 1a

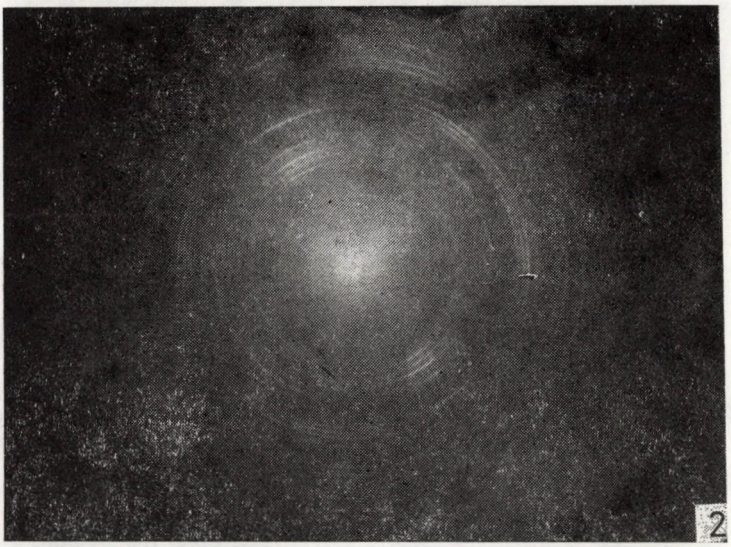

Plate (2). Transmission electron diffraction for Te film 0.05 μm thick deposited on mica with a smaller rate of deposition than that used for film recorded in Plate 1b

The details of the morphology and structure studies using different substrates are published elsewhere [3]. On raising the substrate temperature ranging between 333 K and 423 K, the transmission photographs show the dendritic growth confirmed by two superimposed electron diffractions as shown on Plates (3a) and (3b), (4a) and (4b). This type of electron diffraction

implies the presence of two groups of crystals inclined at an angle of about 68°, with a common zonal axis [$\bar{1}012$].

Similar results have been reported by WEIDMANN and ANDERSON [1]. This pattern represents twinning along the ($\bar{1}012$) plane. Annealing the film leads to a sharper electron diffraction and the disappearance of many peculiarities from the diffraction. These observations are due to increasing the average dendritic size, washing out most of the thermally unstable defects and a better ordering in the film.

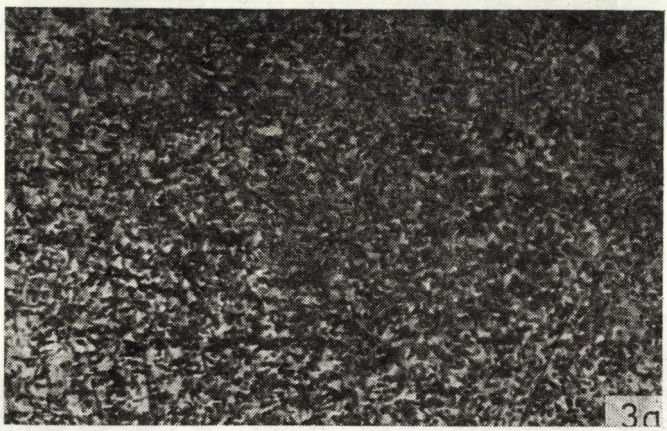

Plate (3a). 9000 times magnified photograph of Te film 0.06 μm thick, deposited on mica at 333 K, with a rate of deposition of about 50 nm/sec

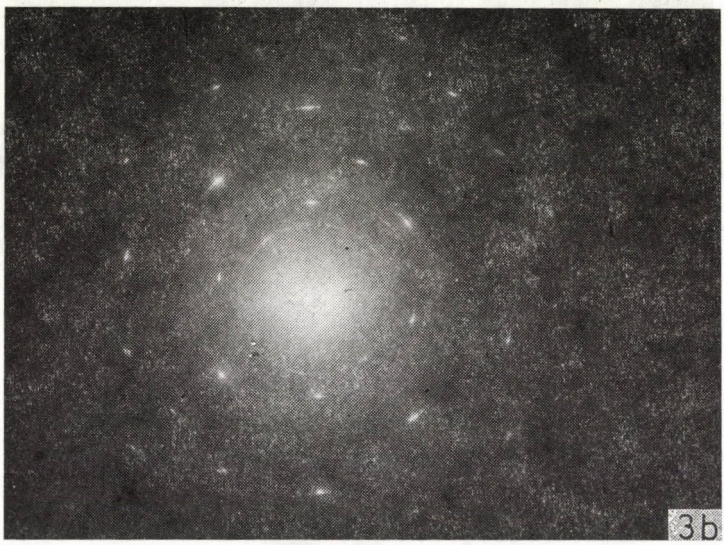

Plate (3b). Electron diffraction recorded from the area shown in Plate 3a

The electrical resistivity was measured in situ before and after annealing. The low temperature resistivity and galvanomagnetic behaviour were measured under atmospheric pressure. The irreversible changes, on admitting air to the specimen chamber, matched the resistivity data in situ in the different ranges of temperature.

For non-annealed films deposited on mica at room temperature and at a deposition rate exceeding 50 nm/sec, the resistivity — temperature relation-

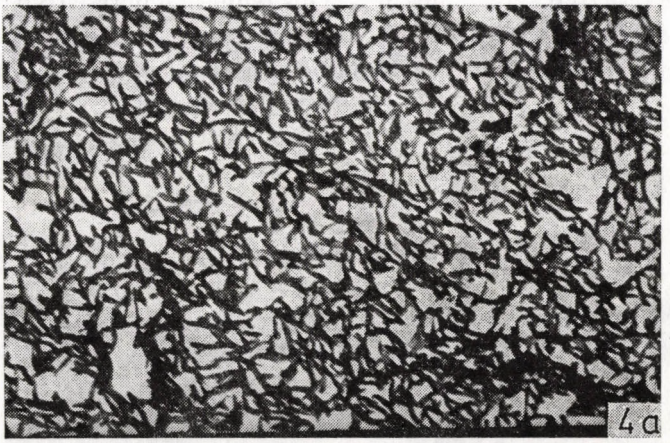

Plate (4a). 9000 times magnified photograph of Te film, 0.065 μm thick, deposited on mica substrate at 423 K, and left at this temperature for about 30 minutes before switching off the substrate temperature

Plate (4b). Electron diffraction pattern recorded from the area shown in Plate 4a

ship was found not to differ much from that for films deposited on glass under the same experimental conditions [3]. Below 10 °C, the relation yields an activation energy of 0.05 eV with a minor dependence on temperature. As the temperature exceeds 10 °C, a linear temperature-dependent relation is obtained with an activation energy of 0.14 eV for films of thicknesses greater than 0.2 μ. For thinner films, the second activation energy value increased to about 0.19 eV. The reason for this is the disturbance by tunneling activation energy in thinner films [5, 6]. Annealing the film in situ at 423 K for three hours reduced the resistivity by about 20%. This reduction in resistivity is attributed to increasing the mobility of the charge carriers due to the increase in the average dendritic size and the reduction in concentration of lattice defects [7, 8].

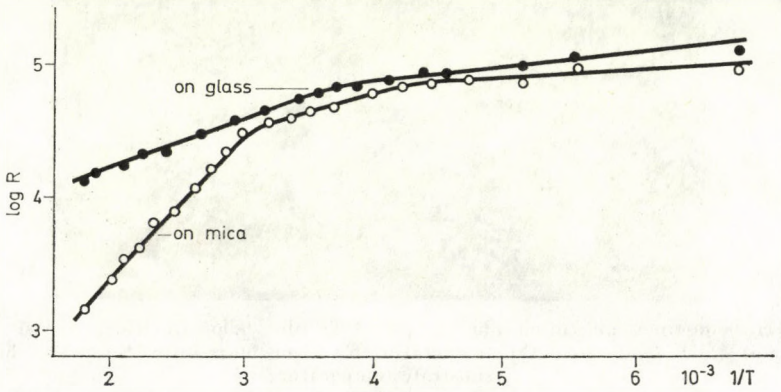

Fig. 1. Log resistance vs $1/T$ for Te films deposited on glass at room temperature and for that deposited on mica with the experimental conditions mentioned for Plate 4a

As a matter of fact, if the mica substrate is kept at its temperature after deposition for a time exceeding thirty minutes, the reduction in resistivity is about to stop. Admitting air thereafter did not alter the resistivity. On the other hand admitting of air just after stopping film deposition increases the resistivity by about 5% for films deposited on heated substrates and 20% for films deposited on cold ones.

Fig. 1 is just a representative run for the variation of log R vs the reciprocal of the absolute temperature. For this run a tellurium film was deposited on mica maintained at 423 K with a rate of deposition of 20 nm/sec. The mica substrate was kept at the temperature mentioned for about thirty minutes after the deposition ceased. One has to state that it took about fifty minutes for the film to cool down to room temperature before the first run was taken. The resistivity — temperature relationship shown in Fig. 1 can be easily divided into three distinct regions. Above 80 K to about 240 K, the resistivity is nearly independent of temperature and the activation energy amounts to 0.05 eV.

The second region extends over a temperature range of 240 K to 400 K, the dependence of resistivity on temperature is quite evident and appears to be due to a deep-lying acceptor state which starts to show itself above 200 K with an activation energy of 0.12 eV. In the third region, the dependence of resistivity on temperature yields an activation energy of about 0.31 eV. As a matter of fact, samples annealed for three hours in situ showed similar trends but slight shifts in those three regions to lower temperatures occurred. This observation implies that the concentration of the thermally unstable impuri-

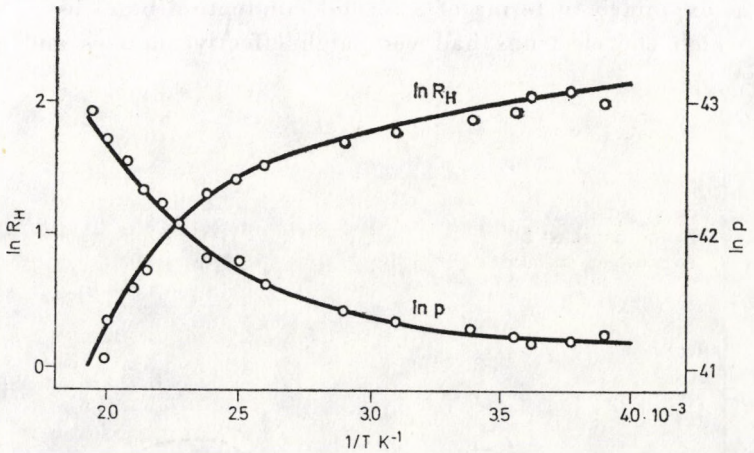

Fig. 2. Ln R_H and ln P vs the reciprocal of the absolute temperature for Te film deposited on mica with the experimental conditions of Fig. 1

ties was too high. On admitting air to the specimen chamber, the same type of relation still existed but with a shift towards high temperatures by about 100 K. Unfortunately, it was not possible to raise the temperature above 550 K because the resistivity increased by few orders of magnitude due to film rolling, cracking and re-evaporation. It seems that above 450 K, the resistivity is very much influenced by electrons from the conduction band.

The Hall coefficient was measured at about 0.5 T, the results are presented in Figs. (1—2). The dependence of R_H on temperature does not differ much from that of resistivity and is similar to that reported by ALBERS and LINK [9] with some shift in the transition temperature between three regions. These authors were able to discuss their results in terms of a model already valid for single crystals. Accordingly, the hole concentration P below 400 K was expressed as:

$$P(T) = p_1 + p_2(T),$$

where p_1, the temperature-independent concentration of shallow traps and diffused oxygen, is associated with the least activation energy (0.05 eV),

while the second parameter represents the concentration of deep traps due to lattice defects and is temperature-dependent. $p_2(T)$ can be written as:

$$p_2^+(T) = p_2 \left(2 \exp \frac{E_2 - E_F}{kT} - 1\right)^{-1},$$

E_2 being the activation energy of deep traps and E_F the Fermi level. The value of E_2 estimated by ALBERS and LINK amounted to 0.115 eV which is in good agreement with our value of 0.12 eV deduced from the second region. The third region was explained in terms of a second conduction band as a source of holes in which the electrons had very high effective masses and negligible mobility.

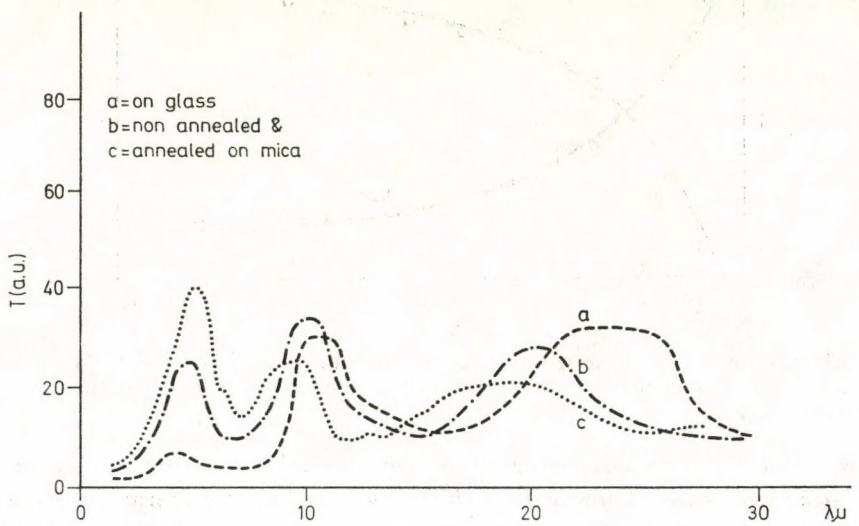

Fig. 3. Variation of transmittance with wavelength in I. R. region for Te film deposited on mica with experimental conditions as in Fig. 1

Since the third region gives an activation energy of about 0.31 eV which is very close to the band gap of tellurium, one may assume that in this region the film has an intrinsic behaviour and the total impurities are depleted. The uncertainty in measuring the Hall coefficient in this range of temperature makes it, however, difficult to draw definite conclusions. Moreover, the variations in the structure, confirmed by electron microscopy in this range of temperature which showed the casual disappearance of the dendritic shape with a filament growth in the film [3] adds to the previous reason.

The transition from extrinsic to intrinsic behaviour is confirmed by optical measurements on some samples in the infra-red range (2 μm—25 μm). The existence of three band-to-band transitions is clear in Fig. 3. These

bands have depths of 0.04 eV, 0.14 eV and 0.33 V measured from the valence band of tellurium. Future measurements of the Hall coefficient under I. R. stimulation as well as thermal glow curves will undoubtedly furnish additional important information with regard to the type of carriers and energy levels created in the band gap.

REFERENCES

1. E. J. WEIDMANN and J. C. ANDERSON, Thin Solid Films, **7**, 265 1971.
2. R. I. DAWOOD, A. H. EID and KH. A. MADY, Egypt. J. Phys. **3**, 37, 1972.
3. A. H. EID, E. A. ABOU-SEIF, N. E. ABDEL-AZIZ and S. KISHK, Proc. Phys. and Math. Soc. Egypt.
4. S. TOLANSKY, Introduction to Interferometry, Longmans Green Co., London, 157 (1955).
5. A. GOSWAMI and R. H. JOG, Indian J. Pure and Appl. Phys., **6**, 416, 1968.
6. C. A. NEUGEBAUER and M. B. WEBB, J. Appl. Phys., **33**, 74, 1962.
7. M. A. DINNO, M. SCHWARTZ and B. GIAMMARA, J. Appl. Phys., **45**, 3328, 1974.
8. J. J. CAPERS and M. WHITE, Thin Solid Films, **15**, 5, 1973.
9. C. ALBERS and R. LINK, Phys. Stat. Sol., A**12**, 89, 1972.

Acta Physica Academiae Scientiarum Hungaricae, Tomus 46 (4), pp. 263—276 (1979)

THE DIFFERENTIAL GEOMETRY OF SURFACES*

By

M. J. MARCINKOWSKI

ENGINEERING MATERIALS GROUP AND DEPARTMENT OF MECHANICAL ENGINEERING
UNIVERSITY OF MARYLAND, COLLEGE PARK, MARYLAND 20742, USA

(Received 15. V. 1979)

A differential geometric analysis has been made with respect to free surfaces in both undeformed and deformed crystals. It has been shown that such well-defined tensor quantities as distortion, torsion, anholonomic object, Burgers vector and Burgers circuit may be defined with respect to such a surface.

Introduction

It has already been shown that internal surfaces such as grain boundaries [1] and two-phase interfaces [2] can be described in terms of well-defined dislocation arrays. A problem closely related to this concerns the nature of a free surface. In particular, one wishes to know the exact configuration of the Burgers circuit and the corresponding tensor quantities associated with these free surfaces. The purpose of the present study is thus to employ the techniques of differential geometry in the analysis of this particular problem

Burgers circuit associated with a simple surface

Consider the perfect crystal shown in Fig. 1a. A reference circuit may now be constructed within such a crystal as shown by the arrows along the path 1-2-3-4-5-6-1. If now the crystal in Fig. 1a is cut along the dotted line which passes through points 3 and 6, and the right half of the crystal removed, we obtain the configuration shown in Fig. 1b. It is seen that a closure failure shown by the dotted arrows between points 3 and 6 now exists. The purpose of what follows is to discuss quantitatively the meaning of these Burgers circuits.

In general, the closure failure b^k associated with a given Burgers circuit may be written as [3]

$$b^k = \oint A^k_K \, dx^K, \tag{1}$$

* The present research effort was supported by the United States Energy Research and Development Administration under Contract No. AT-(40-1)-3935 and by an award from The Alexander von Humboldt Stiftung.

where A_K^k is defined as the distortion tensor which relates the local coordinates in the initial or undeformed state (K) to those in the torn or natural state (k) [4]. In the present study, lower case Latin letters will be used to denote

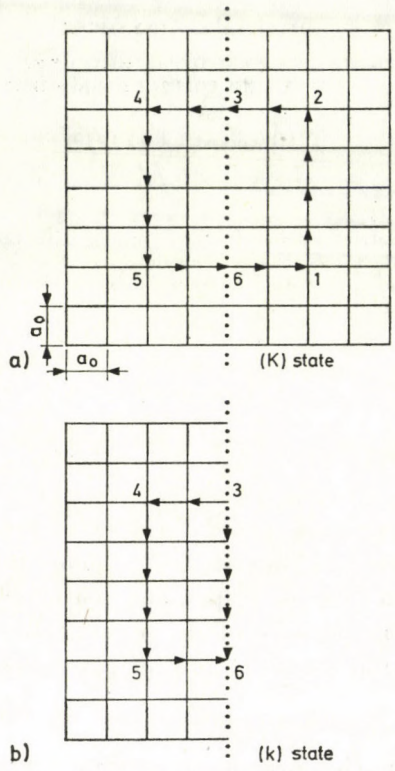

Fig. 1. Burgers circuit associated with a) the interior of a perfect crystal b) the surface of a perfect crystal

the natural state, while upper case Latin letters will be used to denote the initial state. Stoke's theorem may also be used to convert the line integral of Eq. (1) to a surface integral as follows:

$$b^k = \int_s \partial_{[L} A^k_{K]} \, dF^{LK} = \int_s \frac{1}{2} [\partial_L A^k_K - \partial_K A^k_L] \, dF^{LK}. \tag{2}$$

Still another way to write Eq. (2) is in terms of a surface integral referred to the final state which gives

$$b^k = \int_s \frac{1}{2} A^L_l \, A^K_m [\partial_L A^k_K - \partial_K A^k_L] \, dF^{lm} . \tag{3}$$

or more compactly as

$$b^k = \int_S \Omega_{lm}^{\cdot\cdot k}\, dF^{lm}, \tag{4}$$

where $\Omega_{lm}^{\cdot\cdot k}$ is termed the object of anholonomity and defined as

$$\Omega_{lm}^{\cdot\cdot k} = A_l^L\, A_m^K\, \partial_{[L} A_{K]}^k\,. \tag{5}$$

We see then that the distortion tensor appears in all of the expressions for b^k and thus plays a prime role in the theory of defects. It will therefore now be examined in greater detail.

In the case of the cut or torn crystal shown in Fig. 1b, which contains a free surface, the distortion tensor may be written as

$$A_K^k = \delta_K^k\, H(-\underset{K}{x^1})\,, \tag{6}$$

where δ_K^k is the Kronecker delta, while $H(-x^1)$ is the Heaviside function defined by

$$H(-\underset{K}{x^1}) = \begin{cases} 0 & \text{if} \quad x^1 > 0\,, \\ 1 & \text{if} \quad x^1 < 0\,, \end{cases} \tag{7}$$

and where $\underset{K}{x^1}$ is the distance measured along the unit vector $\underset{K}{e^1}$ of the local coordinate system located at the position of the potential interface of the crystal shown in Fig. 1a. Now according to Eqs. (1) and (6)

$$\underset{k}{b^1} = A_1^1\, \underset{5-1}{\Delta x^1} + A_2^1\, \underset{1-2}{\Delta x^2} + A_1^1\, \underset{2-4}{\Delta x^1} + A_2^1\, \underset{4-5}{\Delta x^2}, \tag{8a}$$

where $\underset{5-1}{\Delta x^1}$ etc. are the distances 5-1 etc. shown in Fig. 1a. Since $A_2^1 = 0$ and since $\underset{5-1}{\Delta x^1} = -\underset{2-4}{\Delta x^1}$ it follows that

$$b_k^1 = 0\,. \tag{8b}$$

On the other hand

$$\underset{k}{b^2} = A_1^2\, \underset{5-1}{\Delta x^1} + A_2^2\, \underset{1-2}{\Delta x^2} + A_1^2\, \underset{2-4}{\Delta x^1} + A_2^2\, \underset{4-5}{\Delta x^2}. \tag{9a}$$

Since A_2^2 is equal to zero along the line 1—2 in Fig. 1a, the second term in the above equation vanishes. Thus, only the last term remains which is

$$\underset{k}{b^2} = -4a_0\,. \tag{9b}$$

This is simply the distance 3—6 shown by the dotted arrows in Fig. 1b, since a_0 is defined as the unit cell dimensions of the simple cubic lattice. It is to be emphasized here that $\underset{k}{b^2}$ is not a measure of dislocation content, but rather a measure of the amount of newly created surface. The ramifications of this concept will be met with later.

In order to see what the closure failure of Fig. 1b means in terms of Eq. (2) it is a simple matter to show that $\underset{k}{b^1} = 0$ since from the equation

$$\underset{k}{b^1} = \int_S \left[\frac{1}{2} \partial_1 A_2^1 \underset{K}{dF^{12}} - \frac{1}{2} \partial_1 A_2^1 \underset{K}{dF^{21}} \right] = 0 \tag{10}$$

in view of the fact that $A_2^1 = 0$. However

$$\underset{k}{b^2} = \int_S \left[\frac{1}{2} \partial_1 A_2^2 \underset{K}{dF^{12}} - \frac{1}{2} \partial_1 A_2^2 \underset{K}{dF^{21}} \right] \tag{11a}$$

and since

$$\underset{K}{dF^{12}} = -\underset{K}{dF^{21}} \tag{11b}$$

and using Eq. (6)

$$\underset{k}{b^2} = \int_S \partial_1 H(-\underset{K}{x^1}) \underset{K}{dF^{12}} . \tag{11c}$$

However, since (5)

$$\partial_1 H = (-\underset{K}{x^1}) = -\delta (\underset{K}{x^1}) , \tag{11d}$$

where $(\delta \underset{K}{x^1})$ is the Dirac delta function defined as zero for $\underset{K}{x^1} \neq 0$, and which possesses the following property

$$\int_{-\infty}^{+\infty} \delta (\underset{K}{x^1}) \underset{K}{dx^1} = 1 . \tag{11e}$$

Eq. (11c) reduces to

$$\underset{k}{b^2} = \int \underset{K}{dx^2} = -4a_0 , \tag{11f}$$

which is identical to that given by Eq. (9b). We have thus established the consistency of our analysis.

Still more insight into the nature of the Burgers circuit of Fig. 1b can be obtained by analyzing it with respect to Eq. (4). In particular, from Eq. (5) we may write

$$\underset{k}{\Omega_{12}^{\cdot\cdot 2}} = \frac{1}{2} A_1^1 A_2^2 \partial_1 A_2^2 - \frac{1}{2} A_1^2 A_2^1 \partial_1 A_2^2 . \tag{12}$$

The inverse distortions A_l^K can be obtained from the following relationship

$$A_K^k A_l^K = \delta_l^k \tag{13}$$

and since from the relation

$$dx^K = A_k^K dx^k \tag{14}$$

it is apparent that A_k^K need be defined only within the (k) state, we can write

$$A_k^K = \delta_k^K . \tag{15}$$

This, together with Eq. (6) enables us to write Eq. (12) as

$$\underset{k}{\Omega_{12}^{\cdot\cdot 2}} = -\frac{1}{2}\,\delta\,(\underset{k}{x^1}) \tag{16a}$$

and similarly

$$\underset{k}{\Omega_{21}^{\cdot\cdot 2}} = +\frac{1}{2}\,\delta\,(\underset{k}{x^1}) \tag{16b}$$

which when substituted into Eq. (4) gives

$$\underset{k}{b^2} = -4a_0 \tag{17}$$

which is again identical to the values obtained by the previous two methods which led to Eqs. (9b) and (11f). It is a simple matter to show that only the components of the anholonomic object given by $\underset{k}{\Omega_{12}^{\cdot\cdot 2}}$ and $\underset{k}{\Omega_{21}^{\cdot\cdot 2}}$ are non-zero for the surface shown in Fig. (1b). Even in this case, however, it vanishes everywhere except at the surface. Thus, the anholonomic object measures the amount of free surface, associated with a given Burgers circuit. Since there are no dislocations associated with the state shown in Fig. 1b, the torsion tensor $S_{lm}^{\cdot\cdot k} = 0$ (4).

Burgers circuits associated with more complex surfaces

In order to gain some perspective with respect to the more complex distortions to be considered shortly, let us first consider the elastically strained state of Fig. 2a which can be obtained from the following distortion:

$$A_K^{\varkappa} = \begin{pmatrix} 1 & 0 & 0 \\ -\tan\theta/2 & 1 & 0 \\ 0 & 0 & 1 \end{pmatrix} \tag{18}$$

while from the relation

$$A_K^{\varkappa}\, A_{\lambda}^K = \delta_{\lambda}^{\varkappa} \tag{19}$$

we obtain the inverse distortion

$$A_{\varkappa}^K = \begin{pmatrix} 1 & 0 & 0 \\ \tan\theta/2 & 1 & 0 \\ 0 & 0 & 1 \end{pmatrix}. \tag{20}$$

The elastic distortions will be denoted by Greek letters. It also follows that these distortions connect both the base vectors, as well as the components according to

$$e_\varkappa = A_\varkappa^K e_K \tag{21a}$$

and

$$dx^\varkappa = A_K^\varkappa \, dx^K . \tag{21b}$$

We can now write, similar to Eq. (1)

$$b^\varkappa = \oint A_K^\varkappa \, dx^K . \tag{22}$$

Next, there are two ways to express the Burgers circuits associated with the $(\varkappa)$ state. In the first case, we may write

$$A_K^\varkappa = \delta_K^\varkappa . \tag{23}$$

This has the effect of keeping the components associated with the (K) state of Fig. 1a identical in value to those of the $(\varkappa)$ state shown in Fig. 2a. This process is termed dragging [6] and obviously leads to $b^\varkappa = 0$. On the other

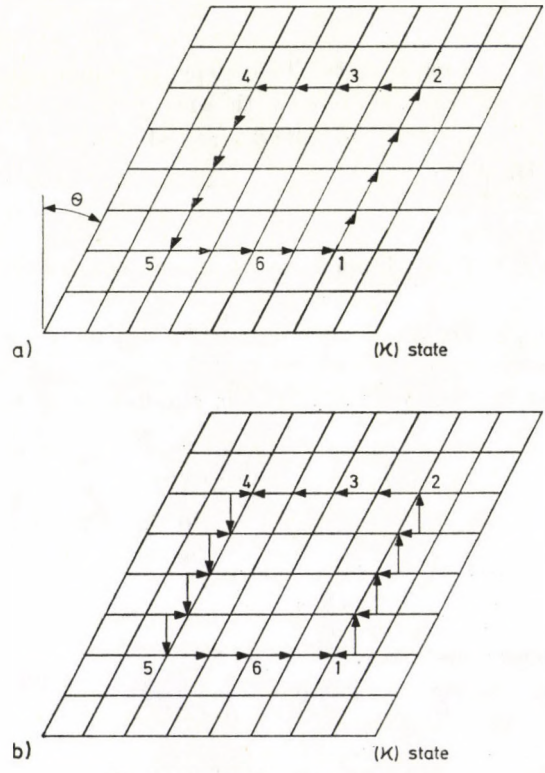

Fig. 2. Elastically distorted state

hand, $b^{\varkappa}$ may be computed by employing Eq. (18), together with Eq. (22). This leads to the Burgers circuit shown in Fig. 2b, where again $b^{\varkappa} = 0$. Another way of viewing this elastic distortion is in terms of either $\Omega_{\lambda\mu}^{\cdot\cdot\varkappa}$ and $S_{\lambda\mu}^{\cdot\cdot\varkappa}$. In particular, since the distortion tensor is constant, their spatial derivatives vanish, and accordingly so do the anholonomic object and torsion.

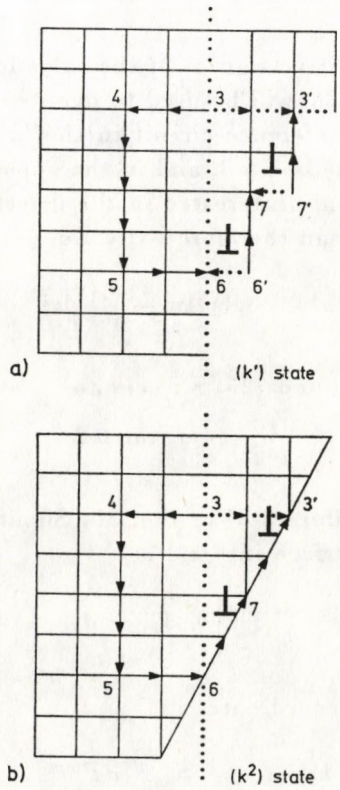

Fig. 3. Dislocated states associated with a free surface

Let us now envisage a process in which a triangular-shaped piece of material is added to the rightmost face of Fig. 1b so as to generate the states shown in Fig. 3. In particular, the (k^1) state Fig. 3a is step-shaped, while the (k^2) state of Fig. 3b is smooth. These same configurations could also have been generated by a plastic deformation of the (K) state in Fig. 1a. Considering first the (k^2) state, it is seen, that the Burgers circuit 5-6-7-3′-3-4-5 contains the closure failure 3-3′. This closure failure is due to dislocations, as indicated by the standard edge dislocation symbols. We may treat this closure failure more quantitatively by writing a distortion tensor

$$A_k^{k^2} = \delta_k^{k^2} H(-\underset{k^2}{x^1}) \tag{24}$$

similar to Eq. (6), where

$$\underset{k^2}{x^1} = \underset{k}{x^1} - \underset{k}{x^2} \tan \theta/2 \,. \tag{25}$$

In order to obtain the correct closure failure associated with the (k^2) state, we must now write

$$\underset{d}{b^{k^2}} = - \oint A_k^{k^2} \, dx^k \,, \tag{26}$$

which, except for the negative sign, is of the same form as Eq. (1) The additional subscript d in Eq. (26) will be used to denote dislocations. Also important to note, is that the reference circuit in the (k) state must now involve four solid arrows along the line 6-3, and in the opposite sense to those shown in Fig. 1b, since we are only interested in the defect content with respect to this particular state. We can therefore write Eq. (26) as

$$\underset{k^2,d}{b^1} = -A_1^1 \underset{5-6}{\Delta x^1_5} - A_2^1 \underset{6-3}{\Delta x^2} - A_1^1 \underset{3-4}{\Delta x^1} - A_2^1 \underset{4-5}{\Delta x^2} \,, \tag{27a}$$

which in view of Eq. (24) and (25) reduces to

$$\underset{k^2,d}{b^1} = 4 \, a_0 \tan \theta/2 \tag{27b}$$

and is just the closure failure 3-3′ in Fig. 3b. Similar to Eq. (2) we can also write $\underset{d}{b^{k^2}}$ in terms of a surface integral as

$$\underset{d}{b^{k^2}} = - \int_s \frac{1}{2} \left[\partial_l \, A_k^{k^2} - \partial_k \, A_{l^2}^k \right] dF^{lk} \tag{28}$$

or in terms of (k^2) state coordinates as

$$\underset{d}{b^{k^2}} = - \int_s S_{l^2 m^2}^{\cdot\cdot k^2} \, dF^{l^2 m^2} \,, \tag{29a}$$

where $S_{l^2 m^2}^{\cdot\cdot k^2}$ is the torsion tensor defined as

$$S_{l^2 m^2}^{\cdot\cdot k^2} = A_{l^2}^l \, A_{m^2}^m \, \partial_{[l} \, A_{m]}^{k^2} \tag{29b}$$

and is thus of the same form as that given by the anholonomic object of Eq. (5). However, both are basically different in that the torsion tensor measures the dislocation content of a crystal, whereas the anholonomic object is related to the creation of free surfaces. Thus $S_{l^2 m^2}^{\cdot\cdot k^2} = 0$, since no additional free surface is created in generating the (k^2) state from the (k) state. Eq. (28) can now be used to write

$$\underset{k^2,d}{b^1} = - \int_s \left[\frac{1}{2} \partial_2 \, A_1^1 \, dF^{21} - \frac{1}{2} \partial_2 A_1^1 \, dF^{12} \right] , \tag{30}$$

where with the help of Eq. (24) and (25) we see that

$$\partial_2 A_1^1 = \frac{\partial A_1^1}{\partial x^1}\underset{k^2}{} \frac{\partial x^1}{\partial x^2}\underset{k^2}{} = \underset{k^2}{\delta(x^1)} \tan \theta/2 \,, \tag{31}$$

which when substituted into Eq. (30) gives

$$\underset{k^2,\, d}{b^1} = 4a_0 \tan \theta/2 \,, \tag{32}$$

which is identical to that given by Eq. (27b) obtained by the line integral method. The torsion tensor can also be found from Eq. (30) to be

$$\underset{k^2}{S_{12}^{\cdot\cdot 1}} = -\underset{k^2}{S_{21}^{\cdot\cdot 1}} = -\frac{1}{2}\underset{k^2}{\delta(x^1)} \tan \theta/2 \,, \tag{33}$$

which when used in conjunction with Eq. (29a) also leads to the same result as that given by Eq. (32). It should also be pointed out that in obtaining Eq. (32) use was made of the fact that

$$\underset{k}{\delta(x^1)} = \underset{k^2}{\delta(x^1)} \tag{34}$$

which follows readily from Eq. (25) and a relation of the type given by Eq. (31).

We have proceeded to a point where we are now in a position to consider the still more complex (k^1) state illustrated in Fig. 3a. As in the case of the (k^2) state we can again write

$$\underset{d}{b^{k^1}} = -\oint A_k^{k^1}\, dx^k \tag{35}$$

or alternately

$$\underset{d}{b^{k^1}} = -\int_S S_{l^1 m^1}^{\cdot\cdot\cdot k^1}\, dF^{l^1 m^1} \,, \tag{36}$$

where $S_{l^1 m^1}^{\cdot\cdot\cdot k^1} = S_{l^2 m^2}^{\cdot\cdot\cdot k^2}$ and $\underset{d}{b^{k^1}} = \underset{d}{b^{k^2}}$. In addition to the dislocation content, the (k^1) state also has associated with it a contribution from the newly created surface steps indicated by the dotted arrows 7′-7 and 6′-6 in Fig. 3a. This particular closure failure can be represented by

$$b^{k^1} = \oint A_k^{k^1}\, dx^k \tag{37}$$

or alternately as

$$b^{k^1} = \int_S S_{l^1 m^1}^{\cdot\cdot\cdot k^1}\, dF^{l^1 m^1} \,, \tag{38}$$

where

$$S_{l^1 m^1}^{\cdot\cdot\cdot k^1} = A_{l^1}^{l} A_{m^1}^{m} \partial_{[l} A_{m]}^{k^1} \,. \tag{39}$$

It is a simple matter to show that

$$\Omega_{l\dot{1}m^1}^{\quad\dot{.}\dot{.}k^1} = S_{l\dot{1}m^1}^{\quad\dot{.}\dot{.}k^1} = S_{l^2m^2}^{\quad\dot{.}\dot{.}k^2}, \tag{40}$$

so that $b^{k^1} = -\overset{d}{b}{}^{k^1}$. More generally, we could also have written the total closure failure associated with Burgers circuit in Fig. 3a as

$$b^{k^1} = -\int_s [S_{l\dot{1}m^1}^{\quad\dot{.}\dot{.}k^1} - \Omega_{l\dot{1}m^1}^{\quad\dot{.}\dot{.}k^1}]\, dF^{l^1m^1} = 0\,. \tag{41}$$

Thus, for the (k^1) state, the torsion tensor just balances the anholonomic object.

There is still deeper mathematical significance associated with the (k) and (k^1) states, both of which possess an anholonomic object. In particular, if the rotations $\partial_{[m}\overset{L}{e}_{l]}$ or $\partial_{[m^1}\overset{l}{e}_{l^1]}$ do not vanish at every point, then the coordinate system is anholonomic (6). In fact, the following equations

$$\partial_{[m}\overset{L}{e}_{l]} = 0 \tag{42a}$$

and

$$\partial_{[m^1}\overset{l}{e}_{l^1]} = 0 \tag{42b}$$

are the integrability conditions of the systems

$$\partial_m \overset{L}{x} = \overset{L}{e}_m \tag{43a}$$

and

$$\partial_{m^1} \overset{l}{x} = \overset{l}{e}_{m^1}\,. \tag{43b}$$

Since the base vectors can be related to one another through equations of the type

$$\overset{L}{e}_l = A_l^K\, \overset{L}{e}_K \tag{44a}$$

and

$$\overset{l}{e}_{l^1} = A_{l^1}^k\, \overset{l}{e}_k\,, \tag{44b}$$

we can write

$$\overset{L}{e}_l = A_L^K\, \overset{L}{e}_K \overset{*}{=} A_l^k\, \delta_K^L = A_l^L \tag{45a}$$

and

$$\overset{l}{e}_{l^1} = A_{l^1}^k\, \overset{l}{e}_k \overset{*}{=} A_{l^1}^k\, \delta_k^l = A_{l^1}^l\,, \tag{45b}$$

where the symbol $\overset{*}{=}$ indicates that we have chosen the base vectors with respect to a given coordinate system, while $\overset{L}{e}_K$ and $\overset{l}{e}_k$ are unity when $L = K$ and $l = k$. Eq. (45) now allow us to write the integrability conditions of Eq. (42) as

$$\partial_{[m}\overset{L}{e}_{l]} \overset{*}{=} \partial_{[m}A_{l]}^L \neq 0 \tag{46a}$$

and

$$\partial_{[m^1}\overset{k}{e}_{l^1]} \overset{*}{=} \partial_{[m^1}A_{l^1]}^l \neq 0\,. \tag{46b}$$

On the other hand, for the (k^2) state of Fig. 3b

$$\partial_{[m^2} \overset{l}{e}_{l^2]} \overset{*}{=} \partial_{[m^2} A^l_{l^2]} = 0 \,. \tag{47}$$

The above equations become somewhat more clear when we write out the components as

$$\frac{1}{2} \partial_1 A^1_2 - \frac{1}{2} \partial_2 A^1_1 \tag{48a}$$

and

$$\frac{1}{2} \partial_1 A^2_2 - \frac{1}{2} \partial_2 A^2_1 . \tag{48b}$$

It follows that whereas the relations vanish on the planar surface 6-7-3′ in Fig. 3b, Eq. (48a) becomes finite on the stepped surface of Fig. (3a). In particular, whereas the first term in this equation vanishes, the second becomes a Dirac delta function. Thus, keeping the face planar in Fig. (3b) has precluded the introduction of an anholonomic object.

Some further tensor quantities associated with surfaces

The torsion tensor can now be used to obtain the dislocation density as can be seen by writing Eq. (29) in differential form as follows [7]:

$$db^{k^2} = -S_{l^2 m^2}{}^{k^2} \, dF^{l^2 m^2} = -S_{l^2 m^2}{}^{k^2} \, \varepsilon^{n^2 l^2 m^2} \, dF_{n^2} = \alpha^{n^2 k^2} \, dF_{n^2} \,, \tag{49}$$

where $\alpha^{n^2 k^2}$ is defined as the dislocation density given by

$$\alpha^{n^2 k^2} = -\varepsilon^{n^2 l^2 m^2} \, S_{l^2 m^2}{}^{k^2} \tag{50}$$

and where $\varepsilon^{n^2 l^2 m^2}$ is the permutation tensor defined by

$$\varepsilon^{n^2 l^2 m^2} = e^{n^2 l^2 m^2} / \sqrt{g} \,, \tag{51}$$

while $e^{n^2 l^2 m^2}$ is the permutation symbol and g is the determinant of the metric tensor $g_{k^2 l^2}$. The indices n^2 and k^2 in $\alpha^{n^2 k^2}$ refer to the line direction and Burgers vector component respectively of the dislocations. Thus, for the configuration in Fig. 3b, we may write

$$\underset{k}{\alpha^{31}} = -2 S_{i\underset{2}{}}{}^{1} = \underset{k^2}{\delta(x^1)} \tan \theta/2 \,, \tag{52a}$$

where Eq. (33) has been utilized. Now upon integration, the above equation becomes

$$\underset{k^2}{\alpha^{31}} = \int_{-\infty}^{+\infty} \underset{k^2}{\delta(x^1)} \, dx^1 \tan \theta/2 = \tan \theta/2 \,. \tag{52b}$$

In terms of Fig. 3b, this result simply refers to the length 3-3′ divided by 6-3. In those cases where only an anholonomic object is present we can write, similar to Eq. (50) [8]

$$\alpha^{nk} = \varepsilon^{nlm}\, \Omega_{lm}^{\cdot\cdot k}\,. \tag{53}$$

For the configuration shown in Fig. 1b, the above equation becomes

$$\underset{k}{\alpha^{32}} = 2\underset{k}{\Omega_{12}^{\cdot\cdot 2}} = -\underset{k}{\delta(x^1)}\,, \tag{54a}$$

where Eq. (16) have been utilized. Upon integration, the above relation simply reduces to

$$\underset{k}{\alpha^{31}} = -1\,, \tag{54b}$$

which in terms of Fig. 1b is the distance 3-6 divided by 6-3. Finally, for the (k^1) state

$$\alpha^{n^1k^1} = -\varepsilon^{n^1l^1m^1}[S_{l^1m^1}^{\cdot\cdot k^1} - \Omega_{l^1m^1}^{\cdot\cdot k^1}] = 0 \tag{55}$$

as expected, since the torsion tensor and anholonomic object just cancel one another. However, Eq. (55) could be written in terms of either $S_{l^1m^1}^{\cdot\cdot k^1}$ or $\Omega_{l^1m^1}^{\cdot\cdot k^1}$ to find the respective dislocation and surface densities. It is also important to note here that it is the equality of the torsion tensor and the anholonomic object in anholonomic coordinates that has enabled ZORAWSKI [8] to develop an eloquent theory of defects based on $\Omega_{l^1m^1}^{\cdot\cdot k^1}$ rather than $S_{l^1m^1}^{\cdot\cdot k^1}$.

Another important tensor quantity is the Riemann—Christoffel curvature tensor which may be written as follows [6] :

$$R_{lm0}^{\cdot\cdot k} = \partial_l \Gamma_{m0}^k - \partial_m \Gamma_{l0}^k + \Gamma_{lp}^k \Gamma_{m0}^p - \Gamma_{mp}^k \Gamma_{l0}^p, \tag{56}$$

where the Γ_{lm}^k are given by [8]

$$\Gamma_{lm}^k = \begin{Bmatrix} k \\ lm \end{Bmatrix} - \Omega_{lm}^{\cdot\cdot k} + g_{l0} g^{kn} \Omega_{mn}^{\cdot\cdot 0} - g_{m0} g^{kn} \Omega_{nl}^{\cdot\cdot 0} \tag{57}$$

and where $\begin{Bmatrix} k \\ lm \end{Bmatrix}$ are Christoffel symbols of the second kind defined by

$$\begin{Bmatrix} k \\ lm \end{Bmatrix} = \frac{1}{2} g^{k0} (\partial_l g_m + \partial_{m0} g_{l0} - \partial_0 g_{lm}\,. \tag{58}$$

The metric tensor can be written as

$$g_{lm} = e_l \cdot e_m = A_l^K A_m^K = \underset{k}{\delta_l^m H^2(-x^1)}\,, \tag{59}$$

while

$$g^{lm} = \underset{k}{\delta_l^m H^2(-x^1)} \tag{60}$$

so that from Eq. (58), the non-vanishing components of $\left\{ \begin{matrix} k \\ lm \end{matrix} \right\}$ become

$$\left\{ \begin{matrix} 1 \\ 11 \end{matrix} \right\}_k = \left\{ \begin{matrix} 2 \\ 12 \end{matrix} \right\}_k = - \left\{ \begin{matrix} 1 \\ 22 \end{matrix} \right\}_k = \underset{k}{\delta}(x^1) \,. \tag{61}$$

Utilizing Eq. (16), Eq. (57) gives the following non-zero components of Γ^k_{lm}

$$\underset{k}{\Gamma^1_{11}} = \underset{k}{\Gamma^2_{12}} = \underset{k}{\delta}(x^1) \,, \tag{62a}$$

$$\underset{k}{\Gamma^1_{22}} = - \underset{k}{\delta}(x^1) \tag{62b}$$

and

$$\underset{k}{\Gamma^2_{22}} = \left\{ \begin{matrix} 2 \\ 21 \end{matrix} \right\}_k - 2 \underset{k}{\Omega^{\cdot\cdot 2}_{21}} = 0 \,. \tag{62c}$$

Now in a two-dimensional space, the curvature tensor $R^{\cdot\cdot\cdot k}_{lm0}$ becomes $R^{\cdot\cdot\cdot k}_{120}$, where the remaining indices are 1 or 2. It therefore follows from Eq. (56) and (62) that $R^{\cdot\cdot\cdot k}_{lm0} = 0$. Similar results can be obtained for the remaining states discussed earlier. This is an important finding and means that the integrability conditions associated with Γ^k_{lm} are satisfied [9]. Physically, this means that the parallel displacement of any vector from one point to another is independent of path. This is certainly true for all of the Burgers circuits considered thus far. The results given by Eq. (62) are also interesting in connection with the following relation [3, 6]:

$$dC^k = - \Gamma^k_{lm} C^m \, dx^l \,, \tag{63}$$

which says that the parallel transport of a vector C^m over a given distance dx^l gives rise to a change in this vector by dC^k. For example, when $\underset{k}{\Gamma^2_{12}}$ is used in conjunction with Eq. (63) we find that dC^2 becomes equal to $-C^2$ as a test vector C^2 is displaced parallel along the x^1 direction and across the free surface. In other words, the test vector C^2 is contracted to zero at the free surface, as it should be. It is possible under some conditions to have $\Gamma^k_{lm} = 0$. States in which this occurs are said to possess distant or teleparallelism [6]. This will occur either when both $\Omega^{\cdot\cdot k}_{lm}$ and $S^{\cdot\cdot k}_{lm}$ vanish or in the case where both are present $\Omega^{\cdot\cdot k}_{lm} = S^{\cdot\cdot k}_{lm}$. In both cases we must also have $\left\{ \begin{matrix} k \\ lm \end{matrix} \right\} = 0$.

Summary and conclusions

It has been shown that well-defined Burgers circuits can be associated with free surfaces in both deformed and undeformed crystals and that a closure failure is associated with such surfaces. In addition, such free surfaces have associated with them well-defined tensor quantities such as distortion, torsion, anholonomic object, etc.

Acknowledgements

The present effort was carried out at the Institut für Theoretische und Angewandte Physik der Universität Stuttgart in The Federal Republic of Germany in conjuction with a Senior U. S. Scientist Award presented to the author by The Alexander von Humboldt Stiftung in connection with a one-year sabbatical leave. Financial support for the present study was also provided in part by the United States Energy Research and Development Administration under Contract No. AT-(40-1)-3935. The author is indebted to Professor KRÖNER for his kind assistance during the course of this investigation.

REFERENCES

1. M. J. MARCINKOWSKI and K. SADANANDA, Acta Crystallographica, **A31**, 280, 1975.
2. M. J. MARCINKOWSKI, K. SADANANDA and W. H. CULLEN, Jr., Acta Crystallographica, **A31**, 292, 1975.
3. E. KRÖNER, Archive for Rational Mechanics and Analysis, **4**, 273, 1959.
4. K. KONDO, Memoirs of the Unifying Study of the Basic Problems in Engineering Sciences by Means of Geometry, Gakuyutsu Bunken Fukyu-kai, Tokyo, 1955.
5. R. DE WIT, Journal of Research of the National Bureau of Standards -A. Physics and Chemistry, **77A**, 607, 1973.
6. J. A. SCHOUTEN, "Ricci-Calculus", Springer-Verlag, Berlin, 1954.
7. E. KRÖNER, Kontinuumstheorie der Versetzungen und Eigenspannungen, Springer-Verlag, Berlin, 1958.
8. M. ZORAWSKI, Théorie Mathématique des Dislocations, Dunod, Paris, 1967.
9. E. SCHRÖDINGER, Space-Time Structure, Cambridge at The University Press, 1954.

Acta Physica Academiae Scientiarum Hungaricae, Tomus 46 (4), pp. 277—297 (1979)

PHYSICAL ASPECTS OF MATTER ACCRETION ON STARS

By

L. BARONI

ISTITUTO DI FISICA, UNIVERSITA DI BOLOGNA, BOLOGNA, ITALY

P. L. FORTINI

ISTITUTO DI ASTRONOMIA, BOLOGNA AND ISTITUTO DI FISICA, UNIVERSITA DI FERRARA, FERRARA, ITALY

C. GUALDI and G. CALLEGARI

ISTITUTO DI FISICA, UNIVERSITA DI FERRARA, FERRARA, ITALY

(Received 17. V. 1979)

The present status of the theory of matter accretion on stars is reviewed. The paper deals mainly with thermodynamics and hydrodynamics of accreting gas in the absence of a magnetic field. Particular emphasis is put on the main problems which are still unresolved.

Introduction

The physical problems in the theory of matter accretion on the stellar objects are reviewed. As it is well known, such theory has been recently used to explain X-ray emission by galactic binary systems.

In this paper we limit ourselves to the general physical features of accretion and therefore we do not take into account the particular problems connected with neutron stars and black-holes. We hope to give an account of this aspect of the theory in a forthcoming paper.

Section 1 deals with the early theories proposed by EDDINGTON, HOYLE and LYTTLETON in connection with star energy source and terrestrial climatic variations.

In Sections 2 and 3 we deal with the thermodynamics of falling matter, while the role of radiation pressure will be taken into account in Section 4. In Sections 5 and 6 we shall treat in detail the accretion on to objects moving through the ambient gas at a supersonic speed. Section 7 is concerned with BONDI's theory of subsonic accretion and Section 8 gives finally a review on the general hydrodynamical problem.

§ 1. Early accretion theories

The idea that matter withdrawn from interstellar gas by the gravitational force of a star can supply energy to the star itself by deposition of its kinetic energy onto the surface, can be traced back to EDDINGTON [7]. The hope was to explain the origin of stellar energy, as thermonuclear reactions were not

known at that time. Neglecting the interaction of atoms among themselves and taking into account the constancy of energy and angular momentum with respect to the star centre, one finds that particles having a distance from the centre less than

$$R_0 = \left(\frac{2GMR}{v^2}\right)^{1/2} \tag{1}$$

must necessarily fall on the surface.

In the above formula G is the Newtonian gravitational constant, M and R are the mass and radius of the star, respectively, and v is the velocity of the star relative to the gas cloud. In fact if we call v' the velocity of a particle grazing the stellar surface, we have clearly:

$$R_0 \, v = Rv' ,$$

$$v'^2 - v^2 = \frac{2GM}{R} ,$$

and therefore

$$\left(\frac{R_0}{R}\right)^2 = 1 + \frac{2GM}{Rv^2} .$$

As in cases of interest, $2GM/Rv^2 \gg 1$, one has at once formula (1). The rate of accreted mass is:

$$\frac{dM}{dt} = \pi R_0^2 q v = \frac{2\pi GMRq}{v} , \tag{2}$$

where ϱ is the mass density of the cloud.

One easily sees that for a normal (i.e. not collapsed) star and a number density of the gas ~ 1 atom/cm^3, this process cannot supply the required energy by many orders of magnitude.

About after ten years, HOYLE and LYTTLETON [9] proposed a theory of accretion in which the effects of collisions among particles in the cloud were taken into account.

The purpose of their paper was to explain the earth climatic changes during Geological Eras due to a variation in the solar luminosity when the sun enters a cosmic cloud in its motion around the galactic centre.

With reference to Fig. 1, the gas flows from left to right with collisions taking place in A, to the right of the sun S' as its gravitational attraction causes two opposite fluxes of particles to collide. The effect of such collisions is to destroy the particle angular momentum about the sun. If, after collision, the radial component of the velocity is less than the escape velocity at A, the particles fall on to the sun surface; therefore the accretion radius R_A can be calculated by requiring that in A, radial velocity is equal to parabolic

velocity. This interpretation of facts, though quite rough, gives the right answer anyway: a more rigorous treatment has been given by BONDI and HOYLE [2] (see further on § 5). A gas element is subject to hyperbolic motion around the sun, i.e.:

$$\frac{P}{r} = 1 + e \cos \theta \,,$$

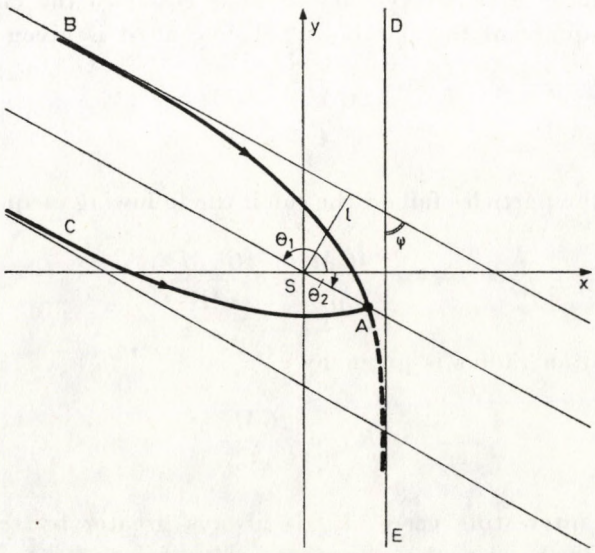

Fig. 1

where p and e are respectively the orbit parameter and eccentricity. The direction parallel to the initial assymptote is given by $r \to \infty$, that is:

$$e \cos \theta_1 + 1 = 0$$

and, as $\theta_1 - \theta_2 = \pi$, also:

$$e \cos \theta_2 + 1 = 0,$$
$$e \sin \theta_2 = (e^2 - 1)^{1/2},$$

from which follows:

$$SA = \frac{p}{2} \,.$$

Taking time derivative of the trajectory equation, one gets the radial component of the velocity:

$$\dot{r} = \frac{e}{p} r^2 \dot{\theta} \sin \theta = \frac{eh}{p} \sin \theta \,,$$

since

$$r^2 \dot{\theta} = h = \sqrt{GMp} = vl .$$

Therefore

$$|r_B| = e\,|\sin\theta_1|\frac{h}{p} = e\sin\theta_2\frac{h}{p} = |\dot{r}_A|. \tag{3}$$

This means that the radial velocity at A is equal to the cloud velocity at infinity. The square of the parabolic velocity at A is given by

$$\frac{2GM}{SA} = \frac{4GM}{p}$$

and therefore the particles fall on the sun if the following inequality is satisfied

$$v^2 < \frac{4GM}{p} = \frac{4G^2 M^2}{v^2 l^2} ,$$

thus the accretion radius is given by

$$R_A = \frac{2GM}{v^2} ,$$

In physically interesting cases, R_A is always greater by several orders of magnitude than R_0, i.e. the accretion radius for non interacting particles (see formula (1)). The rate of matter accretion is now

$$\frac{dM}{dt} = \pi R_A^2 \varrho v = \frac{4\pi G^2 M^2 \varrho}{v^3} . \tag{4}$$

(HOYLE and LYTTLETON [10], HOYLE and LYTTLETON [11]).

Since the velocity of escape at the surface of the sun is very large, i.e. $6.2 \cdot 10^7$ cm/sec, one can assume that all the particles reaching the surface of the sun arrive with the escape velocity which, as one can easily see, corresponds to a kinetic energy $\sim 9 \cdot 10^{-9}$ ergs per hydrogen atom. Now the ionization energy of the hydrogen atom is about $4 \cdot 10^{-11}$ ergs, hence it can be concluded that the particle cannot get rid of any appreciable portion of its energy by ionization processes before reaching the sun: therefore the kinetic energy of the falling particles has the net effect to increase the sun's radiation, as the extra energy gained in this way must be reemitted.

The energy brought to the sun per second is easily obtained by (4) and turns out to be

$$4 \cdot 10^{68} \frac{\varrho}{v^3} \text{ erg/sec} .$$

We see that the increase in sun's radiation depends on the density of the cloud and on the velocity of the sun relative to it, being directly proportional to the first factor and inversely proportional to the cube of the latter factor. Thus slight changes in these factors bring about considerable ranges of variation in the solar radiation, and, for plausible values of ϱ and v, it may be caused to change from 0.1 to 1000% according to the density and velocity of the cloud.

According to the authors, if the increase in the solar luminosity is moderate ($<10\%$), we shall have on the earth an increase in the precipitation of snow (because of the enhanced evaporation) in those regions normally within the snow line and therefore the onset of an Ice Epoch.

If on the other hand the solar luminosity is increased by a factor greater than 2, a hot and humid climate will ensue even in polar regions: in this way the peculiarities of the carboniferous Epoch can be explained.

One easily sees that, assuming a constant density $\sim 10^{-18}$ gr/cm^3 of the cosmic clouds, the above figures can be obtained for a relative velocity of ~ 20 km/sec and 2 km/sec, respectively.

§ 2. Critical temperature of the accreting gas

The physical problems involved in accretion onto normal stars have been investigated for the first time by HOYLE and LYTTLETON [12]. Let us consider a radial flux of matter with a temperature T' toward a star of Mass M. Because of the continuity equation for a stationary flux ($\dot{M}$ = constant through a spherical surface of radius r) one gets:

$$\varrho = \frac{\dot{M}}{4\pi r^2 v}.$$

For free falling gas, $v = \sqrt{2GM/r}$ and therefore

$$\varrho = \frac{\dot{M}}{4\pi\sqrt{2GM}} r^{-3/2}. \tag{5}$$

Our assumption of a radial stationary flux requires that the gravitational force (which acts inwards) on a volume element dV, i.e. $GM\varrho dV/r^2$, is greater than the pressure gradient (which acts outwards) due to the density gradient. The latter is given by $R\varrho T' dV/r$, where R is the perfect gas constant and T' the gas temperature. As the gravitational force goes as $r^{-7/2}$ and the pressure gradient as $r^{-5/2}$, the latter is equal to the former for r sufficiently great and this for any temperature T'. The accretion can take place only if this value of r (which will be called r_T or thermal radius) is greater than the accretion radius (formula (3)).

From the above consideration, one sees that a critical temperature must exist above which $r_T < R_A$. For the sun, with $v = 20$ km/sec, such a temperature turns out to be $\sim 16\,000$ °K.

As is well known, the gas temperature of a cloud in which no high surface temperature star is present, cannot be greater than 10^4 °K, because of recombination effects. Therefore the problem of critical temperature for stars of 1 $M_\odot$ has no particular difficulty.

On the contrary one encounters some difficulties for massive stars, like $V-$Puppis stars, with masses $\sim 20\ M_\odot$, surface temperatures $T \sim 20\,000$ °K and relative velocity with respect to the cloud of about 5 km/sec. For such stars the critical temperature is of several thousands degrees: it is thereforevital to see if the cosmic cloud can emit radiation by processes other than inverse photoelectric effect. One easily sees that free-free transitions are ineffective. In fact the cross-section for the emission of 1 e.v photon at a temperature $\sim 10^4$ °K is $\sim 10^{-25}$ cm^2, while the cross section for the capture of an electron by a proton is $\sim 5 \cdot 10^{-21}$ cm^2: it turns out therefore that an electron is captured before it can emit by free-free transitions an appreciable fraction of its energy.

A more effective process is however infrared emission by hydrogen molecules, which will be considered in the next section.

§ 3. Cooling mechanism for the falling gas

Let us consider a hydrogen plasma (protons, electrons and H_2, H_2^+ molecules) lighted by a source at a temperature T. Every ionization contributes kT to the thermal energy of the gas. Calling ϱ the cloud density, X the fraction by weight of ionized matter, m_H the proton mass, u the mean velocity of electrons, and σ the cross section for recombination of H_2^+ or H^+ with the electron at the cloud temperature T', the number of electrons per c.c. is $X\varrho/m_H$ and the number of recombinations per c.c. per second is:

$$X^2 \left(\frac{\varrho}{m_H}\right)^2 \mu\sigma\,.$$

At equilibrium the ionizations per second must be equal to the recombinations per second and therefore the thermal energy given by electrons to molecules per c.c. and per second is:

$$XY \left(\frac{\varrho}{m_H}\right)^2 \mu\sigma'\, kT'\,,$$

where Y is the fraction by weight of molecules and $\sigma' \sim 2 \cdot 10^{-18}$ cm^2 is the

cross section for equipartition of energy between electrons and molecules. On equating these two formulae and remembering that

$$\sigma \sim \frac{4 \cdot 10^{-27}}{T'}$$

(STUCKELBERG—MORSE [16]), we get:

$$T' = \sqrt{40T\frac{X}{Y}} .$$

From this one sees that, unless $\frac{X}{Y}$ is very large, T' is small compared with T.

Let us now investigate whether the energy acquired by a molecule in one excitation act can be radiated away before the molecule undergoes a second excitation. As the electric dipole moment of a hydrogen molecule in the ground state vanishes, one has to do with forbidden transitions whose probability is less than the probability of allowed transitions by a factor of 10^8. Assuming a mean life of 10^{-6} sec for an allowed transition, the mean life of a forbidden one is therefore 10^2 sec.

The time elapsed between two successive excitations is given by $1/\sigma n_e v$ where $\sigma \sim 10^{-18}$ cm^2 is the excitation. For a gas with an electron number density $n_e = 10^3$ cm^{-3} and $v \sim 5 \cdot 10^7$ cm sec^{-1}, one gets a time $\sim 10^7$ sec: this means that the molecule can give away its excitation energy before a second process can take place.

Another process which can give energy to the gas is the angular momentum destruction induced by molecular collisions of the falling matter. The number of collisions to which a molecule is subject over a distance equal to the accretion radius is given by

$$\frac{2GM}{v^2} \sigma n_H ,$$

where $\sigma \sim 10^{-16}$ cm^2 is the geometrical collision cross section and $n_H = 10^3$ hydrogen atoms per c.c. For a star mass $M = 5\ M_\odot$ and $v = 5$ km/sec, this number is $\sim 10^3$ and therefore sufficient to ensure equipartition among molecular states. The characteristic time of accretion is $\sim GM/v^3$, which is $\gg 10^2$ sec: therefore the energy gained in this way is radiated away. Let us now investigate whether an appreciable number of molecular hydrogen can exist at a distance comparable with accretion radius, particularly near massive stars which emit a substantial amount of ionizing radiation. First of all the material sufficiently near the star is completely ionized and in this domain its tempera-

ture is the star surface temperature. Assuming radial accretion, the number of recombinations per c.c. per sec at a distance x from the star is

$$v(T)\sigma(T)\frac{\varrho^2(x)}{m_H^2},$$

where $v(T)$ is the velocity of electrons and $\sigma(T)$ is the recombination cross section. Remembering that $\varrho(x) = \varrho(r)\,(r/x)^{3/2}$the total number of recombination within a sphere of radius r is:

$$\frac{v(T)\sigma(T)}{m_H^2}\int_R^r 4\pi x^2 e^2(x)\,dx = \frac{4\pi}{m_H^2}v(T)\;\sigma(T)\varrho^2(r)r^3\log\frac{r}{R},$$

where R is the radius of the star.

As ionizations and recombinations per second must be equal and as about one half of the ionizing photons can be given by recombinations themselves and the energy required for a single ionization process is $\sim 2.5\cdot 10^{-11}$ erg, the star must supply an amount of energy

$$2\pi v(T)\sigma(T)\frac{\varrho^2(r)}{m_H^2}r^3\log\frac{r}{R}\cdot 2.5\cdot 10^{-11}\ \text{erg/sec}$$

in order to produce a number of ionizations about equal to one half recombinations. Assuming that the star radiates as a black-body and calling ε the amount of radiation with an energy greater than $2.5\cdot 10^{-11}$ erg, one must have:

$$\varepsilon = 2\pi v(T)\,\sigma(T)\frac{\varrho^2(r)}{m_H^2}r^3\log\frac{r}{R}\cdot 2.5\cdot 10^{-11}.$$

This equation allows one to calculate the radius r of the sphere within which matter is completely ionized (Strömgren's radius). In the case of V-Puppis $E\sim 10^{35}$ erg/sec, $R\sim 5\cdot 10^{11}$ cm, and therefore $r = 5\cdot 10^{16}$ cm, which is greater than $R_A\sim 10^{16}$ cm (and this always in the envisaged case of $\sim 10^3$ atoms cm^{-3}). Outside the Strömgren's sphere, only a small fraction of the material can be ionized. In fact the number of ionizing quanta at a distance $x > r$ goes down with an exponential law of the kind $e^{(r-x)/\tau}$, where τ is the ionization mean free path.

So, in order that an accretion process can take place onto stars like V-Puppis, the gas density must be greater than 10^3 atoms cm^{-3}.

§ 4. Effects of radiation pressure

In order to evaluate the effect of radiation pressure it is first of all necessary to calculate the mean life of atomic levels for the absorption of a quantum of radiation. This will be achieved through the estimate of the number of atoms, within a distance r from the star, which are excited by a quantum of energy $\hbar\omega_0$, where ω_0 is the frequency of the line. The probability that a quantum of energy between $h\omega$ and $\hbar\,(\omega + d\omega)$ is absorbed before it reaches a distance r, is approximately given by

$$\frac{\pi}{2} w_{ab}\, \gamma \frac{Nrc^2}{\omega_0^2(\omega - \omega_0)^2}$$

(HEITLER [8] p. 186, eq. (16)), where N is the number density of hydrogen atoms and therefore Nr is the number of atoms contained in a cylinder of unitary cross section and height r, w_{ab} is the transition probability for spontaneous emission between the states a and b, $\gamma = 2/3\; r_0\; \omega_0^2/c$ is the natural width of the line and $r_0 = 2.8{-}10^{-13}$ cm the classical radius of the electron (HEITLER [8], p. 35, formula (6)).

As $\gamma \sim w_{ab}$ (HEITLER [8], p. 184, formula (12)), one has:

$$\frac{\pi}{2} \gamma w_{ab} \sim 6 \cdot 10^{18}$$

for $\omega_0 \sim 2 \cdot 10^{16}$ rad/sec corresponding to the energy required for a transition from the ground state to the first excited level in a hydrogen atom ($\sim$10 eV). The quantum can be considered completely absorbed for a value of ω given by

$$6 \cdot 10^{18} \frac{Nrc^2}{\omega_0^2(w - \omega_0)^3} = 1$$

i.e.:

$$|\omega - \omega_0| \sim \sqrt[3]{10^7\, Nr}\,.$$

The radiation emitted in this frequency interval is completely absorbed before it can reach a distance r.

If $u(\omega)$ is the black body radiation energy density, for a temperature 20 000 °K, $u(\omega_0) \sim 5 \cdot 10^{-14}$ erg/cm^3 Hz. Thus the required emission of absorbed radiation is approximately given by

$$4\pi R^2\, c\mu(\omega_0)\, 2\, |\omega - \omega_0| \sim 10^2\, R^2\, (Nr)^{1/2}\,,$$

where R is the radius of the sphere.

As one erg corresponds to about $5 \cdot 10^{10}$ quanta, the number of atoms excited per second is $5 \cdot 10^{12} R^2(Nr)^{1/2}$. As the total number of atoms within a sphere of radius r is $4/3\ \pi N r^3$, the fraction of atoms excited per second within such a sphere is of the order of $10^2 R^2 N^{-1/2} r^{-5/2}$, and therefore the mean life of the first excited level of hydrogen atom at a distance $r = 5 \cdot 10^{16}$ cm and with a density $N = 10^4$ cm^{-3} and a stellar radius $R = 5 \cdot 10^{11}$ cm, turns out to be:

$$10^{-12} R^{-2} N^{1/2} r^{5/2} \sim 10^9 \text{ sec} .$$

The exciting quantum has approximatively $5 \cdot 10^{-22}$ momentum units and therefore every atom gets in the mean about $5 \cdot 10^{-31}$ momentum units per second.

The gravitational force exerted by a star of mass $M \sim 20\ M_\odot$ on a hydrogen atom at a distance $\sim 5 \cdot 10^{16}$ cm is $\sim 10^{-30}$ dyne, so that the absorption of this line contributes 1/6 the total pressure necessary to sustain the atom against gravity.

It follows that none of the transitions $1s \rightarrow np$ can sustain hydrogen atoms because of the probability decrease with increasing n (CONDON and SHORTLEY, [3]).

If matter density is sufficiently high, line excitations cannot sustain atoms against gravity at the capture radius and matter moves therefore towards the star surface, as required by accretion theory.

On the other hand, the effect of radiation pressure on ionized matter is quite negligible. In fact, in this case, it is entirely due to the interaction of photons with free electrons (Thomson scattering) with a cross section $\sigma_T = 6.65 \cdot 10^{-25}$ cm^2.

The pair electron-proton is subjected to two forces:

1) the radiation pressure force acting on the electron and pointing outwards, which is given by

$$\frac{L}{4\pi r^2 c} \sigma_T ,$$

where L is the star luminosity, r the distance of the pair from the star.

2) The gravitational force acting on the proton and pointing inwards, i.e.

$$\frac{GMm_H}{r^2} .$$

At equilibrium one gets:

$$L_E = \frac{4\pi GMm_H c}{\sigma_T} = 1.2 \cdot 10^{38} \frac{M}{M_\odot} \text{ erg/sec} . \qquad (6)$$

This value of the luminosity is called the Eddington limit: for $L > L_E$ matter is "blown away" by radiation pressure.

For a 20 $M_\odot$ star, $L_E = 2.4 \cdot 10^{39}$ erg·sec^{-1}. As the effective luminosity is $\sim 10^{37}$ erg/sec, radiation pressure is entirely negligible.

§ 5. Supersonic accretion in the case of interacting particles

We have seen above that accretion can be treated in two extreme approximations: one is to consider non interacting gas particles, in which case the accretion radius is given by (1), the other is to consider interacting particles: the latter case leads to the accretion radius given by (3) and this applies when the mean free path of a particle is much less than R_A. A more rigorous treatment than the one given in Section 1 has been given by BONDI and HOYLE [2] for the case of non interacting as well as of interacting particles.

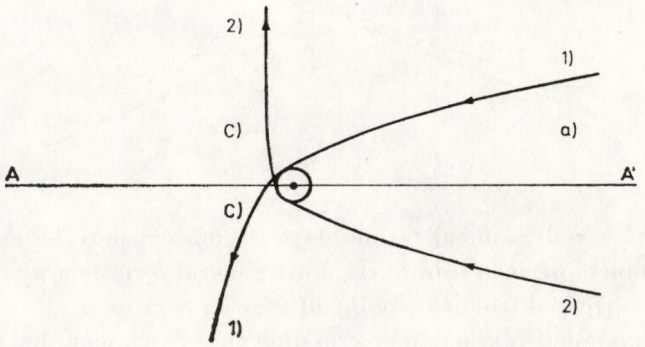

Fig. 2

Let us consider first the case of non interacting particles. With reference to Fig. 2, trajectories 1 and 2 represent the paths of particles grazing the star surface which is represented by the circle. These trajectories divide the space into three regions: a), b) and c). All particles moving in region a) hit the stellar surface. In region b) there is but one trajectory through a given point. In c) however there are two trajectories through a given point, apart from the points of the accretion axis, where there is an infinite number because of cylindrical symmetry. If we now consider the case of interacting particles with a low gas temperature (cf. § 3), there is no change in the properties of regions a) and b): in fact particles cannot collide as only one trajectory goes through each point. This is not true for region c), where particles collide even if their temperature is low: these collisions tend to prevent two fluxes of particles from passing through each point not on the axis. In fact it is clear that the two stream region cannot have dimensions much greater than the mean free path of the particles and therefore this region

shall have dimensions much less than R_A (formula (3)). As a consequence the mechanism of accretion is determined by the four regions a), b), c1) and c2) shown in Fig. 3.

Region c1) is a two stream region with a thickness of the order of the mean free path and regions a), b) and c2) are all single stream. For a very high density of the cloud, region c1) becomes a surface of discontinuity. In c2) the pressure is very high as the density is great. This pressure causes a force on region c1) directed outwards which balance the momentum transverse component of matter coming in from b).

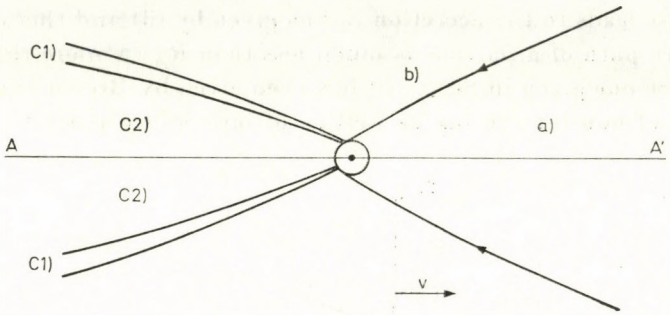

Fig. 3

Using a hydrodynamical terminology region c1) may be called a shock wave. The problem of accretion in its most general form is a hydrodynamical one and will be treated from this point of view in Section 8.

The behaviour of a particle crossing the shock can be qualitatively described in this way: the gas loses the component of the velocity perpendicular to the shock wave front, while the parallel component, i.e. the one directed radially, is left unchanged. With reference to Fig. 1, if the particle impact parameter is greater than R_A (cf. formula (3)), the radial velocity is greater than the parabolic velocity and the gas goes to infinity, while if the impact parameter is less than R_A, the gas falls on to the star after crossing the shock wave front.

This result, strictly rigorous in case of Fig. 1, where it was assumed that collisions took place only on the axis, is still true also in the more general case of a shock, provided the Mach cone is narrow enough, i.e. for relative velocities V much greater than the sound velocity a; the opening θ of such a cone is given by

$$\sin \theta = \frac{a}{V} .$$

From these considerations one already sees the importance of sound speed in accretion problems.

§ 6. Braking force

A very important dynamical effect is the braking force produced by the cloud on the star. This force is due to the particles changing their momenta, via the interaction with the gravitational field of the star. This process has been investigated for the first time by BONDI and HOYLE [2] and by DODD and MCCREA [5—6].

Let us consider first the case of non interacting particles. With references to Fig. 1 we call ψ the angle between asymptotes of the hyperbolic trajectory of a particle coming from B whose impact parameter is l. The particle comes in from infinity and goes to infinity, in the direction of the asymptote DE, thereby changing only the velocity direction (not modulus !), through an angle ψ. From standard formulae of celestial mechanics (OGORODNIKOV, [14]) one has:

$$\operatorname{tg}\frac{\psi}{2}=\frac{GM}{lV^2},$$

where M is the mass of the star and V the relative velocity between star and particle.

The vectorial change in the velocity is given in modulus by $2V\sin\psi/2$ and makes an angle $\pi+\psi/2$ with the arrival direction. The component of $\Delta\vec{V}$ along axis SA is therefore $|\Delta\vec{V}|=2V\sin^2\psi/2$. On expressing $\sin^2\psi/2$ by $\operatorname{tg}\psi/2$ one gets:

$$|\Delta\vec{V}|=\frac{2V}{1+\left(\dfrac{lV^2}{GM}\right)^2}\cdot$$

Consider now a ring of radius l, thickness dl centered on SA and area $2\pi l\,dl$. The total mass which crosses this area per unit time is $\varrho V\,2\pi l\,dl$, where ϱ is the cloud density. These particles act on the star with a force:

$$dF=\varrho\Delta V V 2\pi l dl$$

from which we get the total force:

$$F=4\pi V^2 e\int_0^{l_1}\frac{ldl}{1+\dfrac{l^2V^4}{G^2M^2}}=2\pi\varrho\frac{G^2M^2}{V^2}\ln\left(1+\frac{l_1^2V^4}{G^2M^2}\right),$$

where l_1 is the extension of the cloud. This force is not negligible if

$$\frac{l_1^2V^4}{G^2M^2}\gg 1$$

i.e. when the linear dimensions of the cloud are much greater than the accretion radius $\sim GM/V^2$. This means that the braking effect is essentially due to the particles far away and not to those falling on the star.

One important consequence of this fact is that the same expression for the force is valid also in the case of interacting particles.

As accretion increases when relative velocity decreases (cf. formula (3)), Mc CREA [6] has investigated the problem if the braking of stars by interstellar gas in the galaxy is responsible for the exceedingly great luminosity of some of them and SALPETER [15] has examined whether the emission of quasars can be explained in terms of the braking of massive objects by diffuse matter.

§ 7. Hydrodynamics of accretion in the case of subsonic relative velocity of stars and clouds

Let us now consider the case where the relative velocity between the star and the cloud is equal or less than the sound velocity in the cloud. This problem has been investigated by BONDI [1] in the hydrodynamical approximation. See also ZEL'DOVICH and NOVIKOV [17], p. 435. A star of mass M is at rest in an infinitely extended gas cloud with a density ϱ_∞ and pressure p_∞. The motion of the gas is stationary and spherically symmetric. We shall neglect the increase of the star mass, so that the field of force is constant. The gas can be characterized by its adiabatic index γ, density ϱ, pressure p and sound velocity:

$$a = \left(\frac{\gamma p}{\varrho}\right)^{1/2}.$$

The phenomenon obeys the following equations:

1) Continuity equation:

$$4\pi r^2 \varrho v = A \text{ (constant)}, \tag{7}$$

where r is the radial coordinate, v the velocity of the gas directed toward the star and A is a constant which represents the accretion rate in gram per second.

2) Bernoulli equation:

$$\frac{v^2}{2} + \int_{p_\infty}^{p} \frac{dp}{\varrho} - \frac{GM}{r} = \text{const} = 0\,.$$

The integration constant is zero because of boundary conditions at infinity.

3) Adiabatic equation:

$$\frac{p}{p_\infty} = \left(\frac{\varrho}{\varrho_\infty}\right)^\gamma . \tag{8}$$

By means of (8), the Bernoulli equation takes the form:

$$\frac{v^2}{2} + \frac{\gamma}{\gamma - 1}\frac{p_\infty}{\varrho_\infty}\left[\left(\frac{p}{\varrho_\infty}\right)^{\gamma-1} - 1\right] = \frac{GM}{r} . \tag{9}$$

Eqs. (8) and (9) are valid in case no heat exchange takes place between two neighbouring fluid elements. We can however take account of heat exchange by suitably modifying γ, which in any case must always lie between 1 and 5/3.

The adiabatic index is in general defined as:

$$\gamma = \left(\frac{\partial \log p}{\partial \log \varrho}\right)_{S = \text{const.}} ,$$

where S is the entropy per gram given by

$$S = -\frac{\mathcal{R}}{\mu}\ln\left(\frac{\varrho}{m\mu}\right) + \frac{3}{2}\frac{\mathcal{R}}{\mu}\ln kT + \text{constant.}$$

Here $\mathcal{R} = 8.31 \cdot 10^7$ erg/°K · gr is the perfect gas constant, $K = 1.38 \cdot 10^-$ erg/°K is the Boltzmann constant with $\mathcal{R} = N_0 K$ and $N_0 = 6.023 \cdot 10^{23}$ gr^{-1} is Avogadro's number (inverse of proton mass); μ is the molecular weight defined, for a neutral gas, as the number of nucleons in a nucleus. For a neutral gas the number of particles per c.c. n is given by $n = \frac{\pi}{\mu m_H}$. The perfect gas equation is:

$$p = nkT = \frac{\varrho}{\mu m_H}kT = \frac{\varrho}{\mu}(N_0 k)T = \frac{\varrho \mathcal{R} T}{\mu} .$$

If the gas is completely ionized the number of particles per c.c. n is given by the number of nuclei per c.c., i.e. $\frac{\varrho}{\mu m_H}$ plus the number of electrons $z\frac{\varrho}{\mu m_H}$, i.e.:

$$n = \frac{1+z}{\mu}\frac{\varrho}{m_H} .$$

In this way to a completely ionized gas can be attributed a molecular weight

$$\mu' = \frac{\mu}{1+z} ,$$

where μ is the molecular weight for the neutral gas.

So for neutral hydrogen and helium one has respectively: $\mu = 1$ and $\mu = 4$; for the same gases when completely ionized, $\mu' = 1/2$ and $\mu' = 4/3$, respectively. When the gas is either completely ionized or neutral, γ can be calculated by the above formulae getting:

$$\ln p = \text{const} + \frac{5}{3} \log \varrho,$$

from which

$$\gamma = \frac{5}{3}.$$

In general however the ionization state of a gas depends on pressure and density, i.e. γ is a function of p and ϱ bounded between 1 and 5/3. (Cf. ZEL'DOVICH and NOVIKOV [17] p. 213).

As during accretion the physical conditions of the gas are variable, one can expect a variation of γ too.

These configurations are particularly important for accretion onto compact objects, while for normal stars, γ can be considered fairly well constant. Eqs. (7) and (9) can be put in a dimensional form by introducing the sound speed at infinity:

$$a_\infty^2 = \gamma \frac{p_\infty}{\varrho_\infty}$$

and putting:

$$r = x \frac{GM}{a_\infty^2}, \quad v = y a_\infty, \quad \varrho = z \varrho_\infty$$

the continuity equation takes the form:

$$x^2 y z = \lambda, \tag{10}$$

where λ is given by:

$$A = \frac{4\pi\lambda (GM)^2 \varrho_\infty}{a_\infty^3}. \tag{11}$$

The Bernoulli equation has the form:

$$\frac{1}{2} y^2 + \frac{z^{\gamma-1} - 1}{\gamma - 1} = \frac{1}{x}. \tag{12}$$

To solve (10) and (11), let us put

$$u = y z^{-\frac{\gamma-1}{2}}, \tag{13}$$

where u is the ratio of the local velocity of the gas v to the local sound speed $\left(\frac{\gamma p}{\varrho}\right)^{1/2}$ In fact going over to original variables

$$u = \frac{v}{a_\infty}\left(\frac{\varrho}{p_\infty}\right)^{-\frac{\gamma-1}{2}}.$$

But

$$a = \left(\frac{\gamma p}{\varrho}\right)^{1/2} = \left(\frac{\gamma p_\infty}{\varrho_\infty}\right)^{1/2}\left(\frac{\varrho_H}{p_\infty}\cdot\frac{p}{\varrho}\right)^{1/2}$$

and therefore, because (8):

$$a = a_\infty\left[\frac{\varrho_\infty}{\varrho}\left(\frac{\varrho}{\varrho_\infty}\right)^{\gamma}\right]^{1/2} = a_\infty\left(\frac{\varrho}{\varrho_\infty}\right)^{\frac{\gamma-1}{2}}$$

so that

$$u = \frac{v}{a}.$$

From (13) and (10), we get:

$$y = u^{\frac{2}{\gamma+1}}\left(\frac{\lambda}{x^2}\right)^{\frac{\gamma-1}{\gamma+1}},\quad z = \left(\frac{\lambda}{x^2 u}\right)^{\frac{2}{\gamma+1}}$$

and (12) becomes:

$$u^{\frac{4}{\gamma+1}}\left(\frac{1}{2}+\frac{1}{\gamma-1}\frac{1}{u^2}\right) = \lambda^{-2\frac{\gamma-1}{\gamma+1}}\left[\frac{x^{\frac{\gamma-1}{\gamma+1}}}{\gamma-1}+x^{-\frac{5-3\gamma}{\gamma+1}}\right]. \tag{14}$$

The right and left hand side of this equation are separately the sum of a positive and a negative power of their variables, and therefore each of them has a minimum. The left hand side minimum occurs when $u = 1$ and is given by $\frac{1}{2}\frac{\gamma+1}{\gamma-1}$. The x dependent part of the right hand side has a minimum when $x = \frac{1}{4}(5-3\gamma)$, the value of which is

$$\frac{1}{4}\frac{\gamma+1}{\gamma-1}\left[\frac{1}{4}(5-3\gamma)\right]^{-\frac{5-3\gamma}{\gamma+1}}. \tag{15}$$

On substitution of these values in (14) one gets the results that λ cannot be greater than

$$\lambda_c = \left(\frac{1}{2}\right)^{\frac{\gamma+1}{2(\gamma-1)}}\left(\frac{5-3\gamma}{4}\right)^{-\frac{5-3\gamma}{2(\gamma-1)}}. \tag{16}$$

Therefore the accretion rate cannot be greater than

$$A_c = \frac{4\pi\,\lambda c\,(GM)^2\,\varrho_\infty}{a_\infty^3}. \tag{17}$$

A_c takes on values between 1.12 (for $\gamma = 1$) and 0.75 (for $\gamma = 5/3$). This means that if $\lambda > \lambda_c$, the problem has no solution and accretion cannot take place. A simple graphical discussion (see ZEL'DOVICH and NOVIKOV [17], p. 436) shows that if $\lambda > \lambda_c$, the velocity of the gas is everywhere less than the speed of sound (subsonic accretion everywhere). If $\lambda > \lambda_c$, there exists a distance above which the velocity of the gas is less than the sound speed and beneath which it is greater (supersonic accretion).

In this case, as for $x = 1/4(5 - 3\gamma)$, $u = 1$, i.e. $v = a$, the radius at which transition to supersonic accretion takes place is

$$r_s = \frac{5 - 3\gamma}{4} \frac{GM}{a_\infty^2} .$$

At this radius $y = \left(\frac{2}{5-3\gamma}\right)^{1/2}$ and so:

$$v_s = a_s = a_\infty \left(\frac{2}{5-3\gamma}\right)^{1/2} .$$

As $z = \left(\frac{2}{5-3\gamma}\right)^{\frac{1}{\gamma-2}}$, we get for the density:

$$\varrho_s = \varrho_\infty \left(\frac{2}{5-3\gamma}\right)^{\frac{1}{\gamma-1}},$$

Only supersonic accretion an can give energy to the star, while the subsonic case can be considered as a settling of the gas on the stellar atmosphere, the latter case is possible if pressure, near the star surface is sufficiently high.

To ensure supersonic accretion, the existence of r_s is not sufficient, but it is also necessary that phenomena taking place in stellar atmosphere do not perturb the gas conditions at a distance r_s.

From the barometric formula, one can evaluate the height of the atmosphere:

$$H = \frac{N_0 kTR^2}{GM\mu} .$$

The above condition is therefore

$$H + R < r_s .$$

If now $r_s \gg R$, supersonic accretion is certainly possible for $H \ll R$ and this entails:

$$T \ll 10^7 \left(\frac{M}{M_\odot}\right)\left(\frac{R_\odot}{R}\right) .$$

Condition $r_s \gg R$ is definitely verified, for a realistic state of gas at infinity, i.e. $T \leq 10^4$ °K, even for stars with a radius substantially greater then R_0. A fortiori this condition holds for collapsed stars.

We have therefore a vast class of stars for which accretion is supersonic and therefore can be a source of energy.

In computations, λ_c can be considered of unity order, so that from (17) we get

$$A = \frac{dM}{dt} = \frac{4\pi G^2 M^2 \varrho_\infty}{a_\infty^3} \tag{18}$$

If a star moves with respect to intersteller gas at a speed less than the speed of sound, accretion is essentially dominated by sound velocity, while for supersonic relative velocity (cf. formula (4)) it is dominated by the star velocity.

The hydrodynamical problem in the case of arbitrary relative velocity has not yet been solved. We have only BONDI's conjecture (BONDI [1]) that accretion rate is given by

$$A = \frac{4\pi (GM)^2 \varrho_\infty}{(v^2 + a_\infty^2)^{3/2}}, \tag{19}$$

which admits, as limiting cases, formulae (4) and (18). BONDI's conjecture has not been confirmed, not invalidated: there is only a partial confirmation by DODD [4]. In any case, formula (19) agrees with one's intuition and certainly gives the correct order of magnitude.

In order to make up one's mind which of the theories exposed so far is to be applied to real cases, one must first of all check whether the body has a subsonic or supersonic velocity with respect to the gas.

If the velocity is subsonic, one can apply (approximately) the theory discussed in this section (body at rest), if on the contrary one has to do with supersonic velocity one must apply the theory of Section 1.

In the cases so far examined, i.e. those relative to stars, the geometrical radius of a body turns out to be always many orders of magnitude less than the various accretion radii considered; in the case of galaxies or of clusters of galaxies the geometrical radius and accretion radius are comparable.

§ 8. The general hydrodynamical problem

The general hydrodynamical problem, i.e. the solution of hydrodynamical time dependent equations at various Mach's number, has been studied for the first time by HUNT [13] though in an incomplete form. The procedure consists in integrating the time dependent equations of fluid dynamics, from

a given initial time up to the time when a stationary solution is reached. The fundamental equations are:

$$\frac{\partial \varrho}{\partial t} + \frac{1}{r^2}\frac{\partial}{\partial r}(r^2 m) + \frac{1}{r\sin\theta}\frac{\partial}{\partial \theta}(n\sin\theta) = 0$$

(conservation of mass per unit volume),

$$\frac{\partial m}{\partial t} + \frac{1}{r^2}\frac{\partial}{\partial r}\left[r^2\left(p + \frac{m^2}{\varrho}\right)\right] + \frac{1}{r\sin\theta}\frac{\partial}{\partial \theta}\left(\frac{mn}{\varrho}\sin\theta\right) =$$

$$= -\frac{\varrho}{r^2} + \frac{v_\theta n}{r} + \frac{2p}{r}$$

(conservation of radial momentum per unit volume),

$$\frac{\partial n}{\partial t} + \frac{1}{r^2}\frac{\partial}{\partial r}\left(\frac{r^2 mn}{\varrho}\right) + \frac{1}{r\sin\theta}\frac{\partial}{\partial \theta}\left[\left(p + \frac{n^2}{\varrho}\right)\sin\theta\right] = -\frac{v_\theta m}{r} + \frac{p}{r}\cot\theta$$

(conservation of transverse momentum per unit volume),

$$\frac{\partial E}{\partial t} + \frac{1}{r^2}\frac{\partial}{\partial r}\left[r^2(E+p)\frac{m}{\varrho}\right] + \frac{1}{r\sin\theta}\frac{\partial}{\partial \theta}\left[(E+p)\frac{n}{\varrho}\sin\theta\right] = -\frac{m}{r^2}$$

(conservation of total energy per unit volume),

$$p = (\gamma - 1)\left(E - \frac{1}{2}\frac{m^2 + n^2}{\varrho}\right)$$

(equation of state).

The solution found by HUNT by numerical integration of the above equations are not general, because:

a) the mass M of the star is taken as a constant.
b) The braking forces of Section 6 are neglected.
c) The cooling of the gas is not taken into account.
d) Only $\gamma = 5/3$ is considered.

While assumption from a) to c) are well justified in many cases of physical interest, assumption d) is a severe restriction to the generality of the solution (the author is fully aware of this limitation).

HUNT's results (for Mach's numbers 0.6; 1.4; 2.4) confirm the result obtained in preceding sections. In particular:

1) for subsonic relative velocities one has practically spherical symmetric accretion and therefore BONDI's theory for a body at rest can be applied.

2) In the case of supersonic relative velocities there appears a shock front, which, for increasing Mach's number, approaches the body and shrinks downstream to the axis of accretion (HOYLE—LYTTLETON—BONDI's theory).

§ 9. Conclusions

The physical theory of accretion, as it appears from the above considerations turns out to be in a fairly satisfactory state. In fact one can confidently use the laws discussed in the preceding sections to get reliable order of magnitude estimates. It appears also that the main features were already clear by the mid fifties and no substantial progress has been made since then. There remains however a set of important problems still to be solved or deepened.

1) A thorough investigation of the general hydrodynamical problem with varying γ and any star velocity is still lacking. This problem is crucial for the theory of accretion onto collapsed stars in binary systems where the velocities are highly supersonic. HUNT's solution, which takes into account Mach's numbers up to 2.4 is clearly inadequate. It would be very interesting also a proof of BONDI's conjecture (19).

2) Due to the great difficulties of the magneto-hydrodynamical equations, the influence of a magnetic field on accretion has not yet been satisfactorily investigated. What one can find in the literature is only a host of partial results which, though very important, are not yet systematically arranged in a general framework. This state of affairs is particularly relevant for accretion onto neutron stars and black-holes, in connection with the theory of galactic X-ray sources. We hope to give a survey of these partial results in a forthcoming paper.

REFERENCES

1. H. BONDI, Mont. Not. R. Astron. Soc., **112,** 195, 1952.
2. H. BONDI and F. HOYLE, Mont. Not. R. Astron. Soc., **104,** 273, 1944.
3. E. V. CONDON and G. M. SHORTLEY, The Theory of Atomic Spectra, Cambridge, p. 136, 1964.
4. K. N. DODD, Proc. Cambr. Philos. Soc., **49,** 486, 1953.
5. K. N. DODD, and W. H. MC CREA, Mont. Not. R. Astron. Soc., **112,** 205, 1951.
6. K. N. DODD and W. H. MC CREA, Mont. Not. R. Astron. Soc. **113,** 162, 1953.
7. A. S. EDDINGTON, The Internal Constitution of the Stars, Cambridge Univ. Press, 1926.
8. W. HEITLER, Quantum Theory of Radiation Oxford, 1936.
9. F. HOYLE and R. A. LYTTLETON, Proc. Cambr. Phil. Soc., **35,** 405, 1939.
10. F. HOYLE and R. A. LYTTLETON, Proc. Cambr. Phil. Soc., **35,** 592, 1939.
11. F. HOYLE and R. A. LYTTLETON, Proc. Cambr. Phil. Soc., **36,** 325, 1940.
12. F. HOYLE and R. A. LYTTLETON, Proc. Cambr. Phil. Soc., **36,** 424, 1940.
13. R. HUNT, Mont. Not. R. Astron. Soc., **154,** 141, 1971.
14. K. K. OGORODNIKOV, Dynamics of Stellar Systems. Pergamon, p. 122, 1965.
15. E. SALPETER, Astrophys. J., **140,** 796, 1964.
16. E. G. G. STUCKELBERG and P. M. MORSE, Phys. Rev., **36,** 16, 1930.
17. YA. B. ZEL'DOVICH and I. D. NOVIKOV, Relativistic Astrophysics, Vol. 1, Chicago Press, 1971.

Acta Physica Academiae Scientiarum Hungaricae, Tomus 46 (4), pp. 299—308 (1979)

ON THE PROPAGATION OF SONIC WAVES IN A DISSOCIATING GAS

By

V. D. SHARMA and RADHE SHYAM

APPLIED MATHEMATICS SECTION, INSTITUTE OF TECHNOLOGY, BANARAS HINDU UNIVERSITY
VARANASI 221005, INDIA

(Received in revised form 17. V. 1979)

The effects of non-equilibrium dissociation and that of wave front curvature on the propagation of sonic waves and their consequent formation into shock waves are examined. Special attention is paid to waves of plane, cylindrical and spherical geometry propagating into regions of weak equilibrium or strong equilibrium. It is found that a state of strong equilibrium has a stabilizing influence in that not all compression waves will grow into shock waves. Further, it is interesting to note that in a weak equilibrium state, all compression waves, no matter how weak initially, always end up into a shock whereas all expansion waves decay but not completely unlike the situation that occurs in a strong equilibrium state.

1. Introduction

The growth and decay behaviour of sonic waves, following the analysis of THOMAS [2], has been investigated by several workers [1—7] in a variety of material media. Calling a state with a zero reaction rate and a non-zero affinity a weak equilibrium state, and one with both of these quantities zero a strong equilibrium state, BOWEN [8] has investigated the influence of these thermodynamical states on the propagation of plane acceleration waves in a mixture of chemically reacting elastic materials. In this paper, using the singular surface theory due to THOMAS [9, 10], we have investigated the growth and decay behaviour of sonic waves propagating into regions of strong and weak equilibrium of an ideal dissociating gas. It is found that in a strong equilibrium state there exists a critical value of the initial discontinuity such that all compression waves whose initial discontinuity is less than this critical value damp to zero and waves with initial discontinuity greater than this critical value grow without bound in a finite time. For the case of weak equilibrium state, it is found that all compression waves grow into a shock after a finite time whereas all expansion waves decay and ultimately take a stable wave form. It is found that the geometry of the wave front affects the growth properties indirectly in that the critical value of the initial discontinuity depends on the initial curvatures of the wave front. The critical values of the initial discontinuity for cylindrical and spherical waves for which the respective waves never completely decay are found to be larger in magnitude than the corresponding value for plane waves. The specific source of non-equilibrium

effects considered here is the dissociation recombination reaction in a symmetrical diatomic gas; the present method can, however, be employed to vibrational excitation, ionization etc. Here we have considered the useful approximation of the ideal dissociating gas due to LIGHTHILL [13]. The species that make up the gas mixture are assumed to behave individually as thermally perfect gases. The temperature range is taken from 2500 °K to 4500 °K. In this temperature range, the contribution of energy from electronic excitation and ionization are both assumed negligible. The radiation heat loss from the mixture and the molecular transport effects leading to viscosity, diffusion and heat conduction are also neglected.

2. Basic equations

The equations governing the three-dimensional unsteady motion of an ideal dissociating gas are [14]

$$\frac{\partial \varrho}{\partial t} + u_i \varrho_{,i} + \varrho u_{i,i} = 0 , \tag{1}$$

$$\varrho \frac{\partial u_i}{\partial t} + \varrho u_j u_{i,j} + p_{,i} = 0 , \tag{2}$$

$$\varrho \left(\frac{\partial h}{\partial t} + u_i h_{,i} \right) = \frac{\partial p}{\partial t} + u_i p_{,i} \tag{3}$$

$$\frac{\partial \alpha}{\partial t} + u_i \alpha_{,i} = W , \tag{4}$$

where the summation convention on repeated indices is employed, and a comma followed by an index denotes the partial derivative with respect to a space variable. The range of Latin indices is taken to be 1, 2, 3. The symbols appearing in (1)—(4) are as follows: ϱ is the density; p is the pressure; u_i are the gas velocity components; h is the specific enthalpy; α is the mass fraction of the reactant species, which takes part in the simple reversible reaction

$$A_2 = X \rightleftharpoons A + A + X . \tag{5}$$

(The species X can be either the diatomic molecular species A_2 or the atomic species A) and W is the rate of progress of reaction (5), namely

$$W = \tau^{-1}\{K(1 - \alpha) - \alpha^2\} . \tag{6}$$

The quantities τ and K are the forward-reaction time,

$$\tau^{-1} = 4\varrho^2 k_r(1 + \alpha)/m^2 \tag{7}$$

and the equilibrium constant,

$$K = \frac{\varrho_d}{\varrho} \exp\left(-T_d/T\right), \tag{8}$$

respectively. The quantities k_r, m, ϱ_d and T_d appearing in (7) and (8) are respectively the recombination rate coefficient, the molecular weight of A_2, the characteristic density for dissociation and the characteristic temperature for dissociation. In the temperature range 2500 °K $\sim$ 4500 °K, the variation in these quantities is very small and hence they will be treated as constants.

The thermal and caloric equations of state for the gas mixture are [13]

$$p = \varrho(1 + \alpha)\, RT\,, \tag{9}$$

$$h = \{(4 + \alpha)\, T + \alpha T_d\}\, R\,, \tag{10}$$

where R is the gas constant for A_2.

Eq. (3) with the help of (1), (2), (4) and (6—10) is conveniently transformed into

$$\frac{\partial p}{\partial t} + u_i p_{,i} + \varrho a_f^2 u_{i,i} + \varrho a_f^2 \sigma W = 0\,, \tag{11}$$

where a_f is the frozen sound speed given by $a_f^2 = \dfrac{\Gamma p}{\varrho}$; Γ being the ratio of frozen specific heats given by $\Gamma = (4 + \alpha)/3$, and σ is a function of local thermodynamic properties given by

$$\sigma = \frac{1}{3\Gamma}\left\{(T_d/T) - (\Gamma - 1)^{-1}\right\}.$$

3. Kinematics of moving singular surfaces

In this Section, appropriate kinematics to describe the motion of a weak discontinuity surface is outlined. We shall assume that the reader has some familiarity with the kinematics of moving singular surfaces [9, 10]. We consider a moving singular surface Σ given by $f(x_i, t) = 0$, and that we denote by n_i the unit normal vector $f_{,i}/|\mathrm{grad}\, f|$ and by $G = -\dfrac{\partial f}{\partial t}\Big/|\mathrm{grad}\, f|$ the normal speed of advance of Σ. For definiteness, we require that the description of the surface Σ is such that G is always positive. This means that the normal n_i always points in the direction of propagation of Σ. The jump in any quantity across Σ is denoted by $[Z] = Z_1 - Z_0$, where Z_0 denotes the value of Z immediately ahead of the wave front, and Z_1 is the value of Z immediately behind it. If, across Σ, the function Z is continuous, while its first and second order partial

derivatives with respect to x_i and t suffer jump discontinuities then it can be shown that [9, 10]

$$[Z,_i] = Bn_i\,; \quad \left[\frac{\partial Z}{\partial t}\right] = -GB\,, \tag{12, 13}$$

$$[Z,_{ij}] = \bar{B}n_i n_j + g^{\alpha\beta} B,_\alpha (n_i x_{j,\beta} + n_j x_{i,\beta}) - Bg^{\alpha\beta} g^{\gamma\delta} b_{\alpha\gamma} x_{i,\beta} x_{j,\delta}\,, \tag{14}$$

$$\left[\frac{\partial^2 Z}{\partial x_i\, \partial t}\right] = \left(-G\bar{B} + \frac{\delta B}{\delta t}\right) n_i - g^{\alpha\beta}(GB),_\alpha x_{i\beta}\,, \tag{15}$$

where $\beta = [Z,_i]\, n_i$, $\bar{B} = [Z,_{ij}]\, n_i n_j$ and $\dfrac{\delta(\ )}{\delta t}$ represent the rate of change of ( ) as seen by an observer fixed on Σ. A comma followed by a Greek index say (α) denotes partial derivatives with respect to the surface coordinate y^α. The range of Greek indices is 1, 2. Quantities $g^{\alpha\beta}$ and $b_{\alpha\beta}$ are the contravariant and covariant components of the first and second fundamental tensors of Σ respectively. We also recall the following relations which we shall be using in our further analysis

$$n_{i,\alpha} = -g^{\beta\nu} b_{\beta\alpha} x_{i,\gamma}\,; \quad 2\Omega = g^{\alpha\beta} b_{\alpha\beta} \text{ and } \frac{\delta n_i}{\delta t} = -g^{\alpha\beta} G,_\alpha x_{i,\beta}, \tag{16, 17, 18}$$

where Ω is the mean curvature of Σ.

4. Derivation of the growth equation

A moving singularity surface Σ, across which the flow parameters are continuous but which is such that at least some of the first partial derivatives of these flow parameters suffer jump discontinuities at the surface, is called a weak discontinuity or a sonic wave. It follows from Section 2, that the quantities p, ϱ, α, u_i, a_f, τ, W and σ are continuous across Σ and they will have their subscript 0 values at the wave front. Assuming the state ahead of Σ to be uniform, it is shown in [1] that either $G - u_{n0} = \pm a_{f_0}$ or $G - u_{n0} = 0$, where $u_{n0} = u_{i0}\, n_i$ is the component of fluid velocity normal to the wave front Σ. The case $G - u_{n0} = 0$ which corresponds to a material surface is discarded as uninteresting, and we assume without loss of generality that

$$G = u_{n_0} + a_{f_0}\,. \tag{19}$$

When the medium ahead of the wave is uniform and at rest, it follows from (19) that the wave front Σ propagates through the medium with the frozen sound speed. As a result of which the successive positions of the wave front Σ at different instants form a family of parallel surfaces with straight lines

as their orthogonal trajectories [11]. Thus given the wave surface at $t = 0$, say Σ_0, the position of the surface at any time $t > 0$ can be determined by measuring the distance traversed by the wave front along the normals to Σ_0. In the rest of the paper, we shall be concerned with the situation when the medium ahead of Σ is uniform and at rest. Then, on evaluating equations (1), (2) and (4) across Σ and using (12),(13) and (19), we get

$$\zeta = \frac{\varrho_0 \lambda}{a_{f_0}} = \xi / a_{f_0}^2, \quad \lambda_i = \lambda n_i, \quad \eta = 0, \tag{20, 21, 22}$$

where

$$\lambda_i = [u_{i,j}]\, n_j, \quad \xi = [p,_i]\, n_i\,, \quad \zeta = [\varrho,_i]\, n_i$$

and $\eta = [\alpha,_i] n_i$ are the quantities defined over Σ.

If we differentiate (2) and (11) with respect to x_k, take jumps across Σ, and multiply the resulting equations by n_k, we find, on using the relations (12)—(22), that

$$\varrho_0 \frac{\delta \lambda}{\delta t} = -(\bar{\xi} - \varrho_0 a_{f_0} \bar{\lambda})\,, \tag{23}$$

$$\frac{\delta \xi}{\delta t} = a_{f_0}(\xi - \varrho_0 a_{f_0} \bar{\lambda}) - 2(\Lambda_0 - a_{f_0} \Omega)\xi - \frac{(\Gamma_0 + 1)}{\varrho_0 a_{f_0}} \xi^2, \tag{24}$$

where

$$\bar{\lambda} = [u_{i,jk}]\, n_i n_j n_k, \quad \bar{\zeta} = [p,_{ij}]\, n_i n_j$$

and

$$\Lambda_0 = \frac{1}{2}\left\{3\Gamma_0(\Gamma_0 - 1)\sigma_0^2\left(W_0 + \frac{\alpha_0^2}{\tau_0}\right) + \frac{W_0}{3\Gamma_0}(3\Gamma_0 \sigma_0 - 1)\right\}.$$

Eqs. (23) and (24) can be combined to yield

$$\frac{\delta \zeta}{\delta t} + (\Lambda_0 - a_{f_0} \Omega)\,\zeta + \frac{(\Gamma_0 + 1)\, a_{f_0}}{2\varrho_0} \zeta^2 = 0\,, \tag{25}$$

where use has been made of (20).

Eq. (25) is the required growth equation for the discontinuity ζ which we have been seeking. In view of the relations (20), Eq. (25) yields a differential equation for λ and one for ξ. Thus, Eq. (25) is sufficient to predict the growth or decay of a discontinuity associated with the wave surface Σ. For a family of parallel surfaces, propagating with constant velocity, the mean curvature Ω has the representation [12]

$$\Omega = \frac{\Omega_0 - K_0 a_{f_0} t}{1 - 2\Omega_0 a_{f_0} t + K_0 a_{f_0}^2 t^2}\,, \tag{26}$$

where Ω_0 and K_0 are respectively the mean and Gaussian curvatures of Σ_0. Substituting for Ω in (25) and integrating, we get

$$\zeta = \frac{\zeta_0(1 - 2\Omega_0 a_{f_0} t + K_0 a_{f_0}^2 t^2)^{-\frac{1}{2}} \exp(-\Lambda_0 t)}{1 + \frac{(\Gamma_0 + 1)}{2\varrho_0} a_{f_0} \zeta_0 \int_0^t \{(1 - 2\Omega_0 a_{f_0} \hat{t} + K_0 a_{f_0}^2 \hat{t}^2)^{-\frac{1}{2}} \exp(-\Lambda_0 \hat{t})\} d\hat{t}}, \quad (27)$$

where ζ_0 is the value of ζ at the wave front at $t = 0$.

It is clear from (27) that the temporal behaviour of the density gradient at the wave head will depend critically on the sign of Λ_0. Following BOWEN [8], it follows that for a state of strong equilibrium Λ_0 is non-negative whereas for a weak equilibrium state Λ_0 may be positive or negative. To make the exact result (27) more accessible, we discuss the following three cases of plane, cylindrical and spherical waves.

5. Discussion

Case (i): Plane waves

For a plane wave front $\Omega_0 = K_0 = 0$, the Eq. (27) reduces to the form

$$\zeta = \frac{\zeta_0 \exp(-\Lambda_0 t)}{1 + \frac{\zeta_0}{\zeta_c}\{1 - \exp(-\Lambda_0 t)\}}, \quad (28)$$

where

$$\zeta_c = 2\varrho_0 \Lambda_0/(\Gamma_0 + 1) a_{f_0}$$

Eq. (28) shows that if $\zeta_0 > 0$ (i.e. an expansion wave front) and $\Lambda_0 > 0$ then the denominator of (28) remains positive and $\zeta \to 0$ as $t \to \infty$, the wave damps out. Also if $\zeta_0 < 0$ (i.e. a compression wave front) and if it has the magnitude less than ζ_c then the denominator of (28) remains positive and $\zeta \to 0$ as $t \to \infty$, i.e. a compression wave decays and damps out ultimately. Further, if ζ_0 is negative and has a magnitude equal to ζ_c, then $\zeta = \zeta_0$ and the wave propagates without any growth or decay. But if ζ_0 is negative and has a magnitude greater than ζ_c then $|\zeta| \to \infty$ for a finite t^* given by

$$t^* = \frac{1}{\Lambda_0}\left\{\log\left(1 - \frac{\zeta_c}{\zeta_0}\right)^{-1}\right\}. \quad (29)$$

Thus at a finite time t^* the density gradient at the wave front becomes infinite and this signifies the appearance of a shock wave. Thus we find that ζ_c is a critical value of the initial discontinuity in the sense that all compression waves

with initial discontinuity less than this value attenuate while all compression waves with initial discontinuity greater than this value grow into a shock wave after a finite time. It is evident from the expressions of ζ_c and t^* that they are increasing functions of Λ_0, i.e. the dissociation effects are to increase the shock formation time.

For $\Lambda_0 < 0$ (which can only occur in weak equilibrium state) it follows from (28) that if $\zeta_0 > 0$ then $\zeta \to |\zeta_c|$ as $t \to \infty$, i.e. all expansion waves decay and ultimately take a stable wave form. This interesting feature of expansion waves does not appear in the former case in which all expansion waves decay and damp out ultimately. But if $\zeta_0 < 0$ and $\Lambda_0 < 0$ then we have the criterion

$$\bar{t} = \frac{1}{|\Lambda_0|} \log \left(1 + \frac{|\zeta_c|}{|\zeta_0|}\right), \tag{30}$$

for the shock formation at a finite time. Thus, in this case we find that a discontinuity, no matter how small, associated with a compression wave always grows into a shock. It is also evident from (30) that the weak equilibrium state causes the compression wave to steepen more swiftly than it does in an inert atmosphere (in which $\Lambda_0 = 0$).

Case (ii): Spherical waves

If the wave front Σ at time $t = 0$ is a sphere of radius R_0, then at any time $t > 0$, Σ is a sphere of radius $R = R_0 + a_{f_0} t$. For such a wave $\Omega_0 = -\dfrac{1}{R_0}$ and $K_0 = \dfrac{1}{R_0^2}$ and thus the Eq. (27) reduces to

$$\zeta = \frac{\zeta_0 (R_0/R) \exp\{-\Lambda_0 (R - R_0)/a_{f_0}\}}{1 + \dfrac{(\Gamma_0 + 1)}{2\varrho_0} \zeta_0 R_0 \exp(\Lambda_0 R_0/a_{f_0}) E_i(\Lambda_0 R_0/a_{f_0}) \left\{1 - \dfrac{E_i(\Lambda_0 R/a_{f_0})}{E_i(\Lambda_0 R_0/a_{f_0})}\right\}}, \tag{31}$$

where $E_i(x) = \int_x^\infty t^{-1} e^{-t} dt$ is a tabulated function known as exponential integral function. For $\Lambda_0 > 0$, the term in the curly bracket in the denominator of (31) increases monotonically from 0 to 1 as R increases from R_0 to ∞. Hence in this case also there exists a critical value of initial discontinuity $\hat{\zeta}_c$, the magnitude of which is given by

$$|\hat{\zeta}_c| = \frac{2\varrho_0 \exp(-\Lambda_0 R_0/a_{f_0})}{(\Gamma_0 + 1) R_0 E_i(\Lambda_0 R_0/a_{f_0})} \tag{32}$$

such that if $\zeta_0 < 0$ and has a magnitude less than $|\hat{\zeta}_c|$ then the denominator of (31) remains positive and finite and thus $\zeta \to 0$ as $R \to \infty$, the compression

wave decays and damps out ultimately. Further, if $\zeta_0 < 0$ and has a magnitude equal to $|\hat{\zeta}_c|$, then $|\zeta| \to \zeta_c$ as $R \to \infty$. i.e. the wave does not completely decay and ultimately takes a stable wave form. But if $\zeta_0 < 0$ and has a magnitude greater than $|\hat{\zeta}_c|$, then we have the criterion

$$E_i(\Lambda_0 \hat{R}/a_{f_0}) = \left(1 - \frac{|\hat{\zeta}_c|}{|\zeta_0|}\right) E_i(\Lambda_0 R_0/a_{f_0}) \tag{33}$$

for the shock formation at a finite $R = \hat{R} = R_0 + a_{f_0}\hat{t}$. From the inequality $E_i(x) < e^{-x}/x$, it follows that $|\hat{\zeta}_c|$ (critical value of the discontinuity for the spherical wave) is greater than the corresponding value for a plane wave.

From the expression (32), it follows that $\frac{\partial|\hat{\zeta}_c|}{\partial \Lambda_0} > 0$ which means that the critical value of the initial discontinuity increases with Λ_0. Also $\frac{\partial|\hat{\zeta}_c|}{\partial R_0} < 0$ which implies that the initial curvature has a stabilizing effect on the tendency of the wave surface Σ to grow into a shock in the sense that an increase in the value of the initial curvature causes an increase in the critical amplitude. Further, it is also evident from (33) that $\frac{\partial \hat{t}}{\partial \Lambda_0} > 0$ which means that an increase in Λ_0 will cause the shock formation time $\hat{t}$ to increase, i.e. the non-equilibrium dissociation effects are to increase the shock formation time $\hat{t}$. On the other hand, if the wave is expansion ($\zeta_0 > 0$), then $\zeta \to 0$ as $R \to \infty$, the wave decays and damps out ultimately.

For $\Lambda_0 < 0$, the denominator of (31) reduces to

$$1 + \frac{(\Gamma_0 + 1)}{2\varrho_0} \zeta_0 R_0 \exp(\Lambda_0 R_0/a_{f_0}) \int_{-\Lambda_0 R_0/a_{f_0}}^{-\Lambda_0 R/a_{f_0}} x^{-1} e^x \, dx \,. \tag{34}$$

When $\zeta_0 > 0$, the denominator (34) remains positive and tends to infinity as $R \to \infty$. This happens because of the diverging nature of the integral involved therein. Also, numerator of (31), for $\Lambda_0 < 0$, tends to infinity as $R \to \infty$. Hence, by making use of L'Hospital's rule, we obtain that $\zeta \to |\zeta_c|$ (critical value for a plane wave) as $R \to \infty$. Also, (34) shows that if $\zeta_0 < 0$ then we have the criterion

$$\int_{-\Lambda_0 R_0/a_{f_0}}^{-\Lambda_0 \bar{R} a_{f_0}} x^{-1} e^x \, dx = \frac{2\varrho_0 \exp(-\Lambda_0 R_0/a_{f_0})}{|\zeta_0|(\Gamma_0 + 1)R_0}$$

for the shock formation at a finite $R = \bar{R}$.

Case (iii): Cylindrical waves

In this case also the growth and decay phenomenon is very much similar to those of plane and spherical waves. If the diverging wave front Σ at $t = 0$ is a cylinder of radius R_0, then at any time $t > 0$, Σ is a cylinder of radius $R = R_0 + a_{f_0} t$. For such a wave $\Omega_0 = -\dfrac{1}{2R_0}$ and $K_0 = 0$ and thus Eq. (27) assumes the form

$$\zeta = \frac{\zeta_0 (R_0/R)^{1/2} \exp\{-\Lambda_0 (R - R_0)/a_{f_0}\}}{1 + \dfrac{(\Gamma_0+1)}{2\varrho_0} \zeta_0 \exp(\Lambda_0 R_0/a_{f_0}) \left(\dfrac{\pi R_0}{\Lambda_0 a_{f_0}}\right)^{1/2} \operatorname{erfc}(\Lambda_0 R_0/a_{f_0})^{1/2}} \times \tag{35}$$

$$\times \left\{1 - \frac{\operatorname{erfc}(\Lambda_0 R/a_{f_0})^{1/2}}{\operatorname{erfc}(\Lambda_0 R_0/a_{f_0})^{1/2}}\right\}$$

where $\operatorname{erfc}(x) = \dfrac{2}{\sqrt{\pi}} \displaystyle\int_x^\infty e^{-t^2} dt$ is the complementary error function. For $\Lambda_0 > 0$, if $\zeta_0 > 0$ then ζ remains positive for all $R > R_0$ and monotonically approaches zero as $R \to \infty$. Also if $\zeta_0 < 0$ and has a magnitude less than $|\tilde{\zeta}_c|$, where

$$|\tilde{\zeta}_c| = \left(\frac{\Lambda_0 a_{f_0}}{\pi R_0}\right)^{1/2} \frac{2\varrho_0 \exp(-\Lambda_0 R_0/a_{f_0})}{(\Gamma_0+1) \operatorname{erfc}(\Lambda_0 R_0/a_{f_0})^{1/2}} \tag{36}$$

then $\zeta \to 0$ as $R \to \infty$, the wave damps out. Further, if $\zeta_0 < 0$ and has a magnitude equal to $|\tilde{\zeta}_c|$ then the wave decays and $\zeta \to |\zeta_c|$ (critical value for a plane wave) as $R \to \infty$, i.e. the wave ultimately takes a stable wave form. From the inequality $\operatorname{erfc}(x) < e^{-x^2}/x\sqrt{\pi}$, it follows immediately that $|\tilde{\zeta}_c|$ (for cylindrical wave) is greater than the corresponding critical value for a plane wave. But if $\zeta_0 < 0$ and has a magnitude greater than $|\tilde{\zeta}_c|$ then we have the criterion

$$\operatorname{erfc}\left(\frac{\Lambda_0 \tilde{R}}{a_{f_0}}\right)^{1/2} = \left(1 - \frac{|\tilde{\zeta}_c|}{|\zeta_0|}\right) \operatorname{erfc}\left(\frac{\Lambda_0 R_0}{a_{f_0}}\right)^{1/2}. \tag{37}$$

for the shock formation at a finite $R = \tilde{R}$. However, if $\zeta_0 > 0$ and $\Lambda_0 > 0$ then (35) shows that $\zeta \to 0$ as $R \to \infty$, the wave damps out. It is evident from (36) and (37) that the dissociation effects are to increase the shock formation time.

For $\Lambda_0 < 0$, the growth and decay phenomenon is again similar to those of plane and spherical waves, i.e. if $\zeta_0 > 0$ the $\zeta \to |\zeta_0|$ (critical value for a plane wave) as $R \to \infty$. But if $\zeta_0 < 0$, then we have the criterion

$$\int_{(-\Lambda_0 R_0/a_{f_0})^{1/2}}^{(-\Lambda_0 R^*/a_{f_0})^{1/2}} \exp(x^2)\, dx = \left(\frac{R_0 a_{f_0}}{|\Lambda_0|}\right)^{-1/2} \frac{\varrho_0 \exp(-\Lambda_0 R_0/a_{f_0})}{(\Gamma_0 + 1)|\zeta_0|}$$

for the shock formation at a finite distance $R = R^*$.

REFERENCES

1. R. Ram and M. Gaur, Acta Phys. Hung., **40**, 85, 1976.
2. T. Y. Thomas, J. Math. Mech., **6**, 455, 1957.
3. C. N. Kaul, Proc. Ind. Theo. Appl. Mech. Cong., **5**, 81, 1959.
4. C. N. Kaul, Int. J. Engng. Sci., **13**, 641, 1965.
5. C. N. Kaul, J. Math. Analysis Applic., **25**, No. 2, 425, 1969.
6. S. Srinivasan and R. Ram, ZAMP, **26**, 307, 1975.
7. R. S. Singh and R. Ram, Acta Physica Polonica A**52**, 201, 1977.
8. R. M. Bowen, Arch. Ratl. Mech. Anal., **33**, 169, 1969.
9. T. Y. Thomas, J. Math. Mech., **6**, 311, 1957.
10. T. Y. Thomas, Int. J. Engng. Sci. **4**, 207, 1966.
11. T. Y. Thomas, Concepts from Tensor Analysis and Differential Geometry, Academic Press, 1961.
12. E. P. Lane, Metric Differential Geometry of Curves and Surfaces, Univ. Chicago Press, 1940.
13. M. J. Lighthill, J. Fluid Mech., **2**, 1, 1957.
14. T. Y. Li and S. J. Hsia, Studies on Dissociating Gasdynamics Pt. I. On the Linearized Dissociating Gasdynamics, Tech. Rep. AE 6501, Univ. of Cincinnati, Ohio, July 1965.

Acta Physica Academiae Scientiarum Hungaricae, Tomus 46 (4), pp. 309—317 (1979)

SELF-SIMILAR MAGNETOGASDYNAMIC PROBLEMS WITH RADIATIVE HEAT TRANSFER

By

B. G. VERMA and J. B. SINGH

DEPARTMENT OF MATHEMATICS, UNIVERSITY OF GORAKHPUR, GORAKHPUR (U.P.) INDIA

(Received 24. V. 1979)

In the self-similar piston problems, relating to plane, cylindrical or spherical piston, the effects of transverse magnetic field have been studied. It has been observed that on account of the magnetic field the range between the shock front and the piston increases. The effect of magnetic field increases towards the piston and is more pronounced near it than at the shock front. There is very slow change in the flow velocity. While the radiation affects the pressure more than the other flow variables, the flux falls steeply behind the shock front. Also, there is a rapid fall in values of pressure and temperature behind the shock. A comparison between the results obtained with and without radiation in the presence of magnetic field has been illustrated through figures.

1. Introduction

WANG [1] considered the piston problem with thermal radiation for one dimensional unsteady shock using the similarity method of SEDOV [2]. HELLIWELL [3] took a more general case of the piston problem with radiation heat transfer for general opacity and transparent limit and NICASTRO [4] considered the similarity analysis of the radiative gasdynamic equations with spherical symmetry without considering the magnetic field.

Our aim in the present paper is to study the effect of azimuthal (transverse) magnetic field in the case of self similar piston problem with thermal radiation as treated by HELLIWELL [3] for a plane, cylindrical or spherical piston. As in ELLIOT [5] we have assumed the radiation parameters to be independent of the magnetic field. The effect of magnetic field is prominent on the piston surface.

We have taken a differential approximation for the equations of radiative transfer in a gray gas and made certain simplifying assumptions to make the discussion less complicated. These assumptions include a perfect gray gas in local thermodynamic equilibrium, transparent shock, cool piston neither an emitter nor a reflector, negligible radiation pressure and energy. The radiative effects are presumed frequency independent and ambient gas ahead of the shock wave is cool and shock wave itself is transparent to radiation.

We have calculated the results with and without radiation in transverse magnetic field by Runge—Kutta numerical method for the particular value

of γ, α and β in the transparent limit for a spherical shock wave. The calculation can also be done for general opacity in the presence of a magnetic field by the above method which is given in detail in the section 'results and discussion' taking different values of γ and β. A comparison between the magnetic field effects with and without radiation has been made for the spherical piston case through the Figures 1—6.

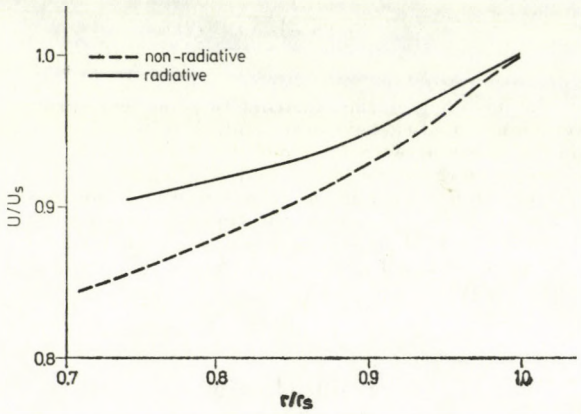

Fig. 1. Velocity distribution

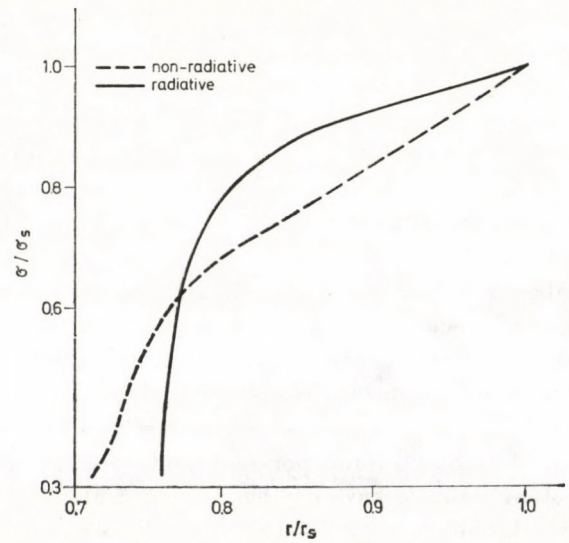

Fig. 2. Density distribution

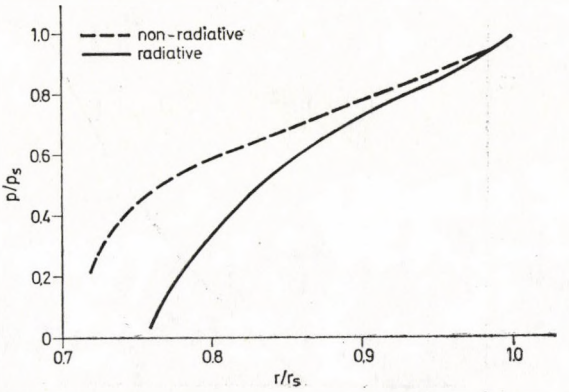

Fig. 3. Pressure distribution

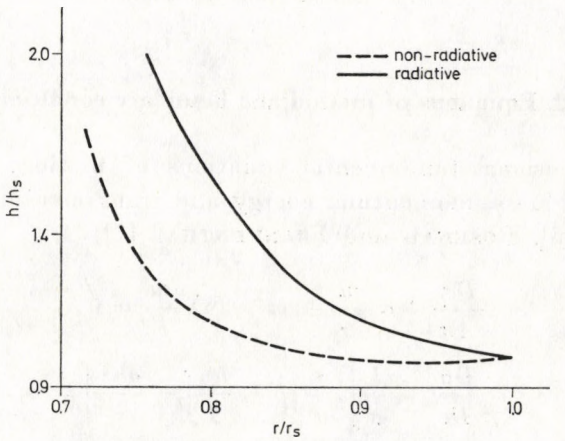

Fig. 4. Magnetic field distribution

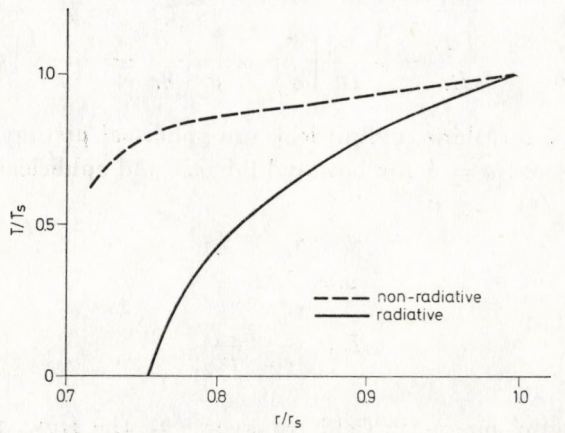

Fig. 5. Temperature distribution

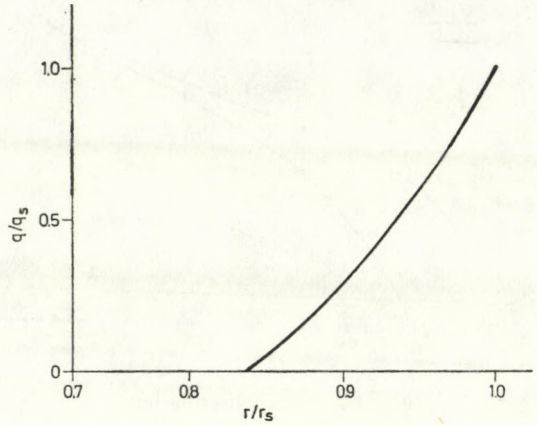

Fig. 6. Radiative flux distribution

2. Equations of motion and boundary conditions

One dimensional fundamental equations of motion, taking inviscid perfect gas, for mass, momentum, energy and transverse megnetic field are (cf. SUMMERS [6], ROSENAU and FRANKENTHAL [7])

$$\frac{D\sigma}{Dt} + \sigma \frac{\partial u}{\partial r} + (\nu - 1)\frac{\sigma u}{r} = 0\,, \tag{2.1}$$

$$\frac{Du}{Dt} + \frac{1}{\sigma}\left[\frac{\partial}{\partial r}\left(p + \frac{h^2}{2}\right) + \frac{ah^2}{r}\right] = 0\,, \tag{2.2}$$

$$\frac{Dh}{Dt} + h\frac{\partial u}{\partial r} + \frac{ahu}{r} = 0\,, \tag{2.3}$$

$$\frac{DE}{Dt} + p\frac{D}{Dt}\left(\frac{1}{\sigma}\right) + \frac{1}{\sigma}\left(\frac{\partial}{\partial r} + \frac{\nu - 1}{r}\right)q = 0\,, \tag{2.4}$$

where $\nu = 1, 2, 3$ for plane, cylindrical and spherical pistons respectively and $a = 0$ for plane and $a = 1$ for both cylindrical and spherical cases.

$$q = q_- - q_+\,, \tag{2.5}$$

$$p = \Gamma\sigma T\,, \tag{2.6}$$

$$E = \frac{p}{(\gamma - 1)\sigma}\,. \tag{2.7}$$

Here h is the magnetic field transverse to the flow, p the pressure σ the density, u the velocity, γ the specific heat ratio, E the specific internal

energy, t the time and r is the single spatial co-ordinate being either axial in flows with planar geometry or radial in cylindrically and spherically symmetric flows. In addition, q denotes the magnitude of the flux of thermal radiation along the co-ordinate direction, $q_{\mp}$ are its forward and backward components, respectively.

Finally, the equations under differential approximation for the variation in the radiative flux components may be written, following HELLIWELL [3], as follows: *general opacity*

$$\left(\frac{\partial}{\partial r} + \frac{\nu - 1}{r}\right)(q_- - q_+) = 4\pi kB - 2k(q_- + q_+)\,, \tag{2.8}$$

$$\frac{\partial}{\partial r}(q_- + q_+) = -\frac{3}{2}k(q_- - q_+)\,; \tag{2.9}$$

transparent limit

$$\frac{\partial}{\partial r}q + \frac{\nu - 1}{r}q = 4\pi kB\,, \tag{2.10}$$

where B denotes Planck's radiation function and is given by $B = \varrho T^4/\pi$, ϱ is Stefan's constant and k is the local volumetric absorption coefficient.

We assume in the present analysis the simple relation (involving solely the density and temperature) of the form

$$k = K\sigma^{\alpha} T^{\beta}\,. \tag{2.11}$$

The piston speed is taken as

$$U = U_0 t^n \quad (n > -1). \tag{2.12}$$

The density and magnetic field distribution laws are

$$\sigma = \sigma_1 = \sigma_0 r^{-w_1} \quad (w > 0) \tag{2.13}$$

and

$$h = h_1 = h_0 r^{-w_1} \quad (w_1 > 0)\,, \tag{2.14}$$

where n, w and w_1 are arbitrary constants. A shock wave running ahead of the piston in a self-similar flow pattern must be strong in order that the ambient pressure ahead may be neglected compared with that behind the shock.

We assume the piston to be cool and black and gas ahead of the shock wave to be also cool so that it does emit radiative energy. Thus no radiative flux passes into the gas behind the shock wave from upstream.

The jump conditions, to those of strong shock which is transparent, are

$$u_2 = 2c/(\gamma + 1), \tag{2.15}$$

$$\sigma_2 = [(\gamma + 1)/(\gamma - 1)]\sigma_1, \tag{2.16}$$

$$p_2 = [2/(\gamma + 1)]\sigma_1 c^2, \tag{2.17}$$

$$h_2 = [(\gamma + 1)/(\gamma - 1)]h_1, \tag{2.18}$$

where c is the shock speed and the suffixes 1 and 2 denote conditions upstream and downstream, respectively. Thus for the region of disturbed gas between the piston and precursor shock wave (2.13)—(2.18) together with

$$q_+ = 0 \tag{2.19}$$

provide the boundary conditions just behind the shock, while (2.12) with

$$q_- = 0 \tag{2.20}$$

give the corresponding conditions at the piston face.

As WANG [1] determined for the plane case in the formulation of self-similar piston problem

$$w = \frac{5}{5\alpha + 2\beta}, \tag{2.21}$$

$$n = \frac{-w}{w + 5}, \tag{2.22}$$

and to make the magnetic field nondimensional, we choose

$$2w_1 = w. \tag{2.23}$$

3. Similarity considerations and solutions

A dimensionless similarity variable, λ, can be defined as

$$\lambda = \left(\frac{\delta\lambda_p}{U_0}\right) rt^{-\delta}, \tag{3.1}$$

where $\delta = n + 1$ and the parameter λ_p is inserted so that immediately behind the shock wave one may choose $\lambda = 1$. The position of the piston face is given by $\lambda = \lambda_p$. Then the field variables of the flow pattern in terms of dimensionless functions of λ, are

$$u = \frac{rV(\lambda)}{t}, \tag{3.2}$$

$$\sigma = \frac{\sigma_0 R(\lambda)}{r^w}, \tag{3.3}$$

$$p = \frac{\sigma_0 P(\lambda)}{r^{w-2} t^2}, \tag{3.4}$$

$$h = \frac{\sigma_0^{1/2} H(\lambda)}{r^{\frac{w-1}{2}} t}, \tag{3.5}$$

$$q = \frac{\sigma_0 Q_+(\lambda)}{r^{w-3} t^3}. \tag{3.6}$$

It is also convenient to define a dimensionless acoustic speed and Alfvén speed in terms of the variables Z and X, respectively, where

$$\frac{\gamma p}{\sigma} = \frac{\gamma P}{R}\left(\frac{r}{t}\right)^2 = Z\left(\frac{r}{t}\right)^2, \tag{3.7}$$

$$\frac{h^2}{\sigma} = \frac{H^2}{R}\left(\frac{r}{t}\right)^2 = X\left(\frac{r}{t}\right)^2. \tag{3.8}$$

With these new variables the governing equations and associated boundary conditions for a gas of general opacity are,

$$\frac{\lambda}{R}\frac{Rd}{d\lambda} = \frac{\begin{array}{c}[2\gamma V(\delta - V)\{(\delta - V)(\nu - w) + V - 1\} - 2ZV(w-2) - \\ - (2Z+\gamma X)\{(w-2)(\delta - V)+2\}+2\gamma\{ZwV+aX(\delta - V)\}+ \\ + (2a - 2\nu + w + 4)\gamma XV + 2\gamma f]\end{array}}{2\gamma(\delta - V)\{(\delta - V)^2 - (X + Z)\}}, \tag{3.9}$$

$$\lambda\frac{dV}{d\lambda} = (\delta - V)\frac{\lambda}{R}\frac{dR}{d\lambda} - (\nu - w)V, \tag{3.10}$$

$$\lambda\frac{dZ}{d\lambda} = Z(\gamma - 1)\frac{\lambda}{R}\frac{dR}{d\lambda} + \frac{2Z(V-1) + (\gamma - 1)wZV + \gamma f}{(\delta - V)}, \tag{3.11}$$

$$\lambda\frac{dX}{d\lambda} = X\frac{\lambda}{R}\frac{dR}{d\lambda} + \frac{(2a - 2\nu + w + 4)XV - 2X}{(\delta - V)}. \tag{3.12}$$

To the other two equations for Q_- and Q_+ we use the similarity transformations in equations (2.8) and (2.9) and get

$$\begin{aligned} 2\lambda\frac{dQ_-}{d\lambda} &= \left\{(2w - \nu - 5) - \frac{7}{4}K_2\lambda^{\frac{2\beta}{\delta}}Z^\beta R^\alpha\right\}Q_- + \\ &+ \left\{(\nu - 1) - \frac{1}{4}K_2\lambda^{\frac{2\beta}{\delta}}Z^\beta R^\alpha\right\}Q_+ + K_1\lambda^{\left(\frac{2\beta+5}{\delta}\right)}Z^{\beta+4}R^\alpha, \end{aligned} \tag{3.13}$$

$$2\lambda \frac{dQ_+}{d\lambda} = \left\{(\nu - 1) + \frac{1}{4} K_2 \lambda^{\frac{2\beta}{\delta}} Z^\beta R^\alpha\right\} Q_- + \left\{(2w - \nu - 5) + \right.$$
$$\left. + \frac{7}{4} K_2 \lambda^{\frac{2\beta}{\delta}} Z^\beta R^\alpha\right\} Q_+ - K_1 \lambda^{\left(\frac{2\beta+5}{\delta}\right)} Z^{\beta+4} R^\alpha, \tag{3.14}$$

where

$$f = f(Z, R, Q_-, Q_+, \lambda) = \tag{3.15}$$
$$= (\gamma - 1) Z^\beta R^{\alpha-1} \lambda^{\frac{2\beta}{\delta}} \{K_1 Z^4 \lambda^{5/\delta} - K_2(Q_- + Q_+)\},$$
$$K_1 = \frac{4K\varrho\sigma_0^{\alpha-1}}{(\gamma\Gamma)^{\beta+4}} \left(\frac{U_0}{\delta\lambda_p}\right)^{\left(\frac{2\beta+5}{\delta}\right)},$$
$$K_2 = \frac{2K\sigma_0^\alpha}{(\gamma\Gamma)^\beta} \left(\frac{U_0}{\delta\lambda_p}\right)^{\frac{2\beta}{\delta}},$$

subject to the boundary conditions

$$V = \frac{2\delta}{\gamma + 1}, \tag{3.16}$$

$$R = \frac{\gamma + 1}{\gamma - 1}, \tag{3.17}$$

$$Z = \frac{2\gamma(\gamma - 1)\delta^2}{(\gamma + 1)^2}, \tag{3.18}$$

$$X = M_A^{-2}\delta^2 \frac{\gamma + 1}{\gamma - 1}, \tag{3.19}$$

$$Q_\pm = 0 \quad \text{at} \quad \lambda = 1, \tag{3.20}$$

$$V = \delta, \; Q_- = 0 \text{ at } \lambda = \lambda_p. \tag{3.21}$$

In the transparent limit, by putting $K_2 = 0$ in the general set, we get appropriate equations. The equations for V, R, Z and X then become independent of the radiative flux components Q_+, and may be solved separately. The variation of Q with λ is then obtained, following HELLIWELL [3], as

$$Q = \int_{\lambda_p}^{\lambda} \left(\frac{\eta}{\lambda}\right)^{2+\nu-w} g(\eta) \frac{d\eta}{\eta} - \int_\lambda^1 \left(\frac{\eta}{\lambda}\right)^{2+\nu-w} g(\eta) \frac{d\eta}{\eta} + \tag{3.22}$$
$$+ \left(\frac{1 - \lambda_p^{\nu-1}}{1 + \lambda_p^{\nu-1}}\right) \int_{\lambda_p}^1 \left(\frac{\eta}{\lambda}\right)^{2+\nu-w} g(\eta) \frac{d\eta}{\eta},$$

where

$$g(\eta) = \frac{1}{2} K_1 Z^{\beta+4} R^\alpha \eta^{\left(\frac{2\beta+5}{\delta}\right)}$$

and Z, R are regarded as functions of η.

From (3.1)—(3.6), the relationships between the similarity solution and the physical variables are

$$\frac{U}{U_s} = \frac{(\gamma+1)\,V\lambda}{2\delta}, \tag{3.23}$$

$$\frac{\sigma}{\sigma_s} = \frac{\gamma-1}{\gamma+1} R\lambda^{-w}, \tag{3.24}$$

$$\frac{p}{p_s} = \frac{(\gamma+1)\,ZR\lambda^{2-w}}{2\gamma\delta^2}, \tag{3.25}$$

$$\frac{h}{h_s} = \frac{M_A(\gamma-1)(RX)^{1/2}}{\delta(\gamma+1)}\,\lambda^{\frac{2-w}{2}}, \tag{3.26}$$

$$\frac{T}{T_s} = \frac{(\gamma+1)^2 Z\lambda^2}{2\gamma(\gamma-1)\delta^2}, \tag{3.27}$$

$$\frac{q}{q_s} = \frac{(Q_- - Q_+)}{Q_{s-}}\,\lambda^{3-w}, \tag{3.28}$$

where $\lambda = r/r_s$ and the suffix s denotes values just behind the shock front.

Acknowlegdements

One of the authors (J. B. S.) is thankful to Dr. J. P. VISHWAKARMA for useful discussions. The assistance from U. G. C. in the form of a teacher fellowship is also gratefully acknowledged by J. B. S.

REFERENCES

1. K. C. WANG, J. Fluid Mech., **20**, 447, 1964.
2. L. I. SEDOV, Similarity and dimensional methods in mechanics, Academic Press, 1959.
3. J. B. HELLIWELL, J. Fluid Mech., **37**, 497, 1969.
4. J. R. A. J. NICASTRO, Physics of Fluids, **13**, 2000, 1970.
5. L. A. ELLIOT, Proc. Roy. Soc. A., **258**, 287, 1960.
6. D. SUMMERS, Astron. and Astrophysics, **45**, 151, 1975.
7. P. ROSENAU and S. FRANKENTHAL, Phys. of Fluids, **19**, 1889, 1976.

Acta Physica Academiae Scientiarum Hungaricae, Tomus 46 (4), pp. 319—331 (1979)

EFFECTS OF MASS TRANSFER ON STEADY HYDROMAGNETIC FREE CONVECTIVE FLOW OF AN INCOMPRESSIBLE VISCOUS FLUID PAST AN INFINITE VERTICAL POROUS WALL

By

G. A. GEORGANTOPOULOS

DEPARTMENT OF MECHANICS, UNIVERSITY OF PATRAS, PATRAS, GREECE

(Received 24. V. 1979)

An analysis of the mass transfer effects on the hydromagnetic free — convective flow of an electrically conducting, incompressible viscous fluid, past an infinite, non-conducting, porous, vertical wall with constant suction, has been carried out, in presence of a transverse magnetic field. The induced magnetic field is taken into consideration and the terms representing the viscous dissipative heat and the Joule heating are included in the energy equation. Approximate solutions to coupled non-linear equations governing the flow are obtained, when the magnetic Prandtl number is unity and the magnetic parameter $M < 1$. Expressions are given for the velocity, the induced magnetic field, the temperature, the skin friction, the electric current density and the rate of heat transfer in terms of the Nusselt number. The variations of the above quantities are presented graphically, and the paper is concluded with a quantitative discussion.

1. Introduction

It is known that flows arising from differences in concentration or material constitution alone and in conjunction with temperature differences have great significance not only for their own interest but also for the applications to geophysics, aeronautics and engineering. There are many interesting aspect of such flows, so in recent years analytical solutions to such problems of flow have been presented by many authors. SPARROW et al [4] have presented an analytical study of the effects of buoyancy in a binary boundary layer into which a foreign gas is injected through a porous surface. SOUNDALGEKAR [3] has studied the effects of mass transfer on steady free convective flow of a dissipative, incompressible fluid past an infinite vertical porous wall, with constant suction. Recently, HALDAVNEKAR and SOUNDALGEKAR [1] have carried out an analysis of the mass transfer effects on the steady free convective flow of an incompressible electrically conducting, viscous fluid past an infinite porous plate with constant suction and transverse magnetic field. In this study the magnetic Reynolds number of the flow is taken to be small enough so that the induced magnetic field can be neglected. Also the viscous dissipative heat in the equation of energy is assumed to be negligible as compared to Joule dissipative heat.

Hence, in the present analysis we study the effects of the mass-transfer on the steady free convective flow, of an electrically conducting, incompressible, viscous fluid, past an infinite vertical non-conducting porous wall with constant suction, in the presence of a uniform transverse magnetic field. The induced magnetic field is not assumed negligible and the terms, which represent the viscous dissipative heat and the Joule dissipative heat remain in the equation of energy. Approximate solutions to a coupled non-linear system of equations governing the flow are derived when the magnetic Prandtl number is unity, and expressions are obtained for the velocity field, the induced magnetic field, the temperature field, the skin friction, the rate of heat transfer, in terms of the Nusselt number and for the electrical current density. Finally, all the above quantities are shown graphically, followed by a discussion.

2. Mathematical analysis

We assume as the coordinate origin 0, an arbitrary point on an infinite vertical porous wall, which is taken to be an electrical insulator. The x'-axis is chosen along the vertical wall in the upward direction and the y'-axis is chosen normal to it. The electrostatic system of units has been used throughout, and we assume that, in the present analysis, all the physical variables are function of the space coordinate y only. Also the applied magnetic field is uniform and perpendicular to the wall, so that in the region considered, $H = H(H_x, H_y, 0)$. Under these assumptions, the steady free convective flow on an electrically conducting, viscous incompressible fluid is governed by the following set of equations

$$v' \frac{\partial u'}{\partial y'} = \nu \frac{\partial^2 u'}{\partial y'^2} + g\beta(T'_w - T'_\infty) + g\beta^*(C' - C'_\infty) + \frac{\mu_0}{\varrho} + H_y \frac{\partial H_x}{\partial y'}, \tag{1}$$

$$v' \frac{\partial H_x}{\partial y'} = H_y \frac{\partial u'}{\partial y'} + \frac{1}{\sigma\mu_0} \frac{\partial^2 H_x}{\partial y'^2}, \tag{2}$$

$$v' \frac{\partial T'}{\partial y'} = \frac{k}{\varrho c_p} \frac{\partial^2 T'}{\partial y'^2} + \frac{\nu}{c_p} \left(\frac{\partial u'}{\partial y'}\right)^2 + \frac{1}{\sigma\varrho c_p} \left(\frac{\partial H_x}{\partial y'}\right)^2, \tag{3}$$

$$v' \frac{\partial C'}{\partial y'} = D \frac{\partial^2 C'}{\partial y'^2}, \tag{4}$$

$$\frac{\partial v'}{\partial y'} = 0, \tag{5}$$

where all the above physical quantities have their usual meaning, except C' which is known as the species concentration, D is the molecular diffusivity and

β^* is the volume coefficient of expansion with concentration. The second and the third terms on the right hand side of Eq. (3) signify, respectively,the heat generated by friction (or viscous dissipative heat) and the Joule heating.

The boundary conditions for the velocity field, for the temperature field and for the species concentration are:

$$\begin{aligned} y = 0; \quad & u' = 0, \quad T' = T'_w, \quad C' = C'_w, \\ y \to \infty: \quad & u' \to 0, \quad T' \to T'_\infty \quad C' \to C'_\infty . \end{aligned} \tag{6}$$

The appropriate boundary conditions on H_x are (for detailed discussion see PANDE [2]):

$$\begin{aligned} y = 0: \quad & H_x = 0 , \; H_y = H_0 , \\ y \to \infty: \quad & H_x \to 0, \quad H_y \to H_0. \end{aligned} \tag{7}$$

From Maxwell's equations the components of electrical current density are given by

$$j_x = 0, \quad j_y = 0$$

and (8)

$$j_z = - \left(\frac{\partial H_x}{\partial y'} \right) ;$$

and the divergence equation for the magnetic field gives

$$H_y = \text{constant} = H_0, \tag{9}$$

where H_0 is the externally applied transverse magnetic field.

Integration of (5) gives

$$v' = -v_0 , \tag{10}$$

where v_0 is the constant suction velocity. The negative sign in (10) indicated that the suction velocity is directed towards the wall.

We now define the following non-dimensional parameters:

$$u = \frac{u'}{v_0}, \quad y = \frac{y' v_0}{\nu}, \quad \theta = \frac{T' - T'_\infty}{T'_w - T'_\infty},$$

$$C = \frac{C' - C'_\infty}{C'_w - C'_\infty}, \quad H = \left(\frac{\mu_0}{\varrho} \right)^{1/2} \frac{H_x}{v_0},$$

$$G_r = \frac{\nu g \, \beta (T'_w - T'_\infty)}{v_0^3} \text{ (the Grashof number)},$$

$$G_c = \frac{\nu g \beta^* (C'_w - C'_\infty)}{v_0^3} \text{ (the modified Grashof number)} ,$$

$$P_m = \sigma\nu\mu_0 \qquad \text{(the magnetic Prandtl number)},$$

$$P = \frac{\varrho\nu c_p}{k} \qquad \text{(the Prandtl number)},$$

$$E = \frac{v_0^2}{c_p(T'_w - T'_\infty)} \qquad \text{(the Eckert number)},$$

$$S_c = \frac{\nu}{D} \qquad \text{(the Schmidt number)},$$

$$M = \left(\frac{\mu_0}{\varrho}\right)^{1/2} \frac{H_0}{v_0} \qquad \text{(the magnetic field parameter)}. \tag{11}$$

With the help of Eqs. (9) and (10) and of the non-dimensional quantities (11) the Eqs. (1), (2), (3) and (4) reduce to:

$$\frac{\partial^2 u}{\partial y^2} + \frac{\partial u}{\partial y} = -G_r\theta - G_c C - M\frac{\partial H}{\partial y}, \tag{12}$$

$$\frac{1}{P_m}\frac{\partial^2 H}{\partial y^2} + \frac{\partial H}{\partial y} + M\frac{\partial u}{\partial y} = 0, \tag{13}$$

$$\frac{\partial^2 \theta}{\partial y^2} + P\frac{\partial \theta}{\partial y} = PE\left(\frac{\partial u}{\partial y}\right)^2 - \frac{PE}{P_m}\left(\frac{\partial H}{\partial y}\right)^2, \tag{14}$$

$$\frac{\partial^2 C}{\partial y^2} + S_c\frac{\partial C}{\partial y} = 0, \tag{15}$$

and the boundary conditions (6) and (7) in the non-dimensional form become:

$$\begin{aligned} &y = 0: \quad u = 0, \quad \theta = 1, \quad C = 1, \quad H = 0, \\ &y \to 0: \quad u \to 0, \quad \theta \to 0, \quad C \to 0, \quad H \to 0. \end{aligned} \tag{16}$$

Eqs. (12)—(15) are coupled non-linear differential equations and to solve we follow the power series solution method. As the fluid is incompressible and the suction velocity is small the Eckert number E is also small ($\ll 1$). Hence, we expand u, H, θ and C in powers of E and neglect terms of order E^2 and higher.

Thus, we have

$$\begin{aligned} u &= u_0 + Eu_1, \\ \theta &= \theta_0 + E\theta_1, \\ H &= H_0 + EH_1, \\ C &= C_0 + EC_1. \end{aligned} \tag{17}$$

On substituting (17) into Eqs. (12)—(15), equating the coefficient of E and neglecting terms in E^2 and higher order, we get

$$u_0'' + u_0' = -G_r\theta_0 - G_c C_0 - MH_0', \tag{18}$$

$$u_1'' + u_1' = -G_r\theta_1 - G_c C_1 - MH_1', \tag{19}$$

$$\frac{1}{P_m} H_0'' + H_0' + Mu_0' = 0, \tag{20}$$

$$\frac{1}{P_m} H_1'' + H_1' + Mu_1' = 0, \tag{21}$$

$$\theta_0'' + P'\theta = 0, \tag{22}$$

$$\theta_1'' + P\theta_1' = Pu_0'^2 - \frac{P}{P_m} H_0'^2, \tag{23}$$

$$C_0'' + S_c C_0' = 0, \tag{24}$$

$$C_1'' + S_c C_1' = 0, \tag{25}$$

where the dashes indicate derivatives with respect to y.

The corresponding boundary conditions are:

$$\begin{aligned} &y = 0\colon u_0 = 0,\ u_1 = 0,\ \theta_0 = 1,\ \theta_1 = 0,\ C_0 = 1,\ C_1 = 0,\ H_0 = 0,\ H_1 = 0,\\ &y \to 0\colon u_0 \to 0,\ u_1 \to 0,\ \theta_0 \to 0,\ \theta_1 \to 0,\ C_0 \to 0,\ C_1 \to 0,\ H_0 \to 0,\ H_1 \to 0. \end{aligned} \tag{26}$$

Solving Eqs. (18)—(25) under the boundary conditions (26), when the magnetic Prandtl number $P_m = 1$ and substituting the solutions obtained in (17) we have

$$\begin{aligned} u(y) = {} & A_1(e^{-\alpha y} - e^{-Py}) + A_2(e^{-\alpha y} - e^{-Scy}) + A_3(e^{-\beta y} - e^{-Py}) + \\ & + A_4(e^{-\beta y} - e^{-Scy}) + \frac{E}{2}(\Gamma_7 e^{-\alpha y} + \Delta_8 e^{-\beta y} - (B_6 + \Gamma_0) e^{-Py} + \\ & + (B_7 + \Gamma_8) e^{-2\alpha y} + (B_8 + \Gamma_9) e^{-2Py} - (B_9 + \Delta_1) e^{-(\alpha+P)y} + \\ & + (\Gamma_1 + \Delta_2) e^{-2Scy} - (\Gamma_2 + \Delta_3) e^{-(\alpha+S_c)y} + (\Gamma_3 + \Delta_4) e^{-2\beta y} - \\ & - (\Gamma_4 + \Delta_5) e^{-(\beta+P)y} - (\Gamma_5 + \Delta_6) e^{-(\beta+S_c)y} + (\Gamma_6 + \Delta_7) e^{-(P+S_c)y}), \end{aligned} \tag{27}$$

$$\begin{aligned} H(y) = {} & A_1(e^{-\alpha y} - e^{-Py}) + A_2(e^{-\alpha y} - e^{-Scy}) - A_3(e^{-\beta y} - e^{-Py}) - \\ & - A_4(e^{-\beta y} - e^{-Scy}) + \frac{E}{2}(\Gamma_7 e^{-\alpha y} - \Delta_8 e^{-\beta y} + (\Gamma_0 - B_6) e^{-Py} + \\ & + (B_7 - \Gamma_8 e^{-2\alpha y} + (B_8 - \Gamma_9) e^{-2Py} + (\Delta_1 - B_9) e^{-(\alpha+P)} + \\ & + (\Gamma_1 - \Delta_2) e^{-2Scy} + (\Delta_3 - \Gamma_2) e^{-(\alpha+S_c)y} + (\Gamma_3 - \Delta_4) e^{-2\beta y} + \\ & + (\Delta_5 - \Gamma_4) e^{-(\beta+P)y} + (\Delta_6 - \Gamma_5) e^{-(\beta+S_c)y} + (\Gamma_6 - \Delta_7) e^{-(P+S_c)y}), \end{aligned} \tag{28}$$

$$\theta(y) = e^{-Py} + E(B_5 e^{-Py} - A_5 e^{-2\alpha y} - A_6 e^{-2Py} + A_7 e^{-(\alpha-P)y} - A_8 e^{-2Scy} + \\ + A_9 e^{-(\alpha+S_c)y} - B_1 e^{-2\beta y} + B_2 e^{-(\beta+P)y} + B_3 e^{-(\beta+S_c)y} - B_4 e^{-(P+S_c)y}) \quad (29)$$

and

$$C = e^{-Scy}, \quad (30)$$

where

$$a = 1 + M, \ \beta = 1 - M, \ A_1 = \frac{G_r}{2P(P-\alpha)}, \ A_2 = \frac{G_c}{2S_c(S_c-\alpha)},$$

$$A_3 = \frac{G_r}{2P(P-\beta)}, \ A_4 = \frac{G_c}{2S_c(S_c-\beta)}, \ A_5 = \frac{\alpha P(A_1+A_2)^2}{2\alpha - P},$$

$$A_6 = P(A_1^2 + A_3^2), \ A_7 = \frac{4A_1P^2(A_1+A_2)}{(\alpha+P)}, \ A_8 = \frac{S_cP(A_1^2+A_4^2)}{2S_c-P},$$

$$A_9 = \frac{4\alpha A_2 S_c P(A_1+A_2)}{(\alpha+S_c)(\alpha+S_c-P)}, \ B_1 = \frac{\beta P(A_3+A_4)^2}{2\beta - P},$$

$$B_2 = \frac{4P^2A_3(A_3+A_4)}{\beta+P}, \quad B_3 = \frac{4\beta P S_c A_4(A_3+A_4)}{(\beta+S_c)(\beta+S_c-P)},$$

$$B_4 = \frac{4P^2(A_1A_2+A_3A_4)}{P+S_c}, \ B_5 = A_5+A_6-A_7+A_8-A_9+B_1-B_2-B_3+B_4$$

$$B_6 = \frac{B_5G_r}{P(P-\alpha)}, \ B_7 = \frac{G_rA_5}{2\alpha^2}, \ B_8 = \frac{G_rA_6}{2P(2P-\alpha)},$$

$$B_9 = \frac{G_rA_7}{P(P+\alpha)}, \ \Gamma_1 = \frac{G_rA_8}{2S_c(2S_c-\alpha)}, \ \Gamma_2 = \frac{G_rA_9}{S_c(S_c+\alpha)},$$

$$\Gamma_3 = \frac{G_rB_1}{2\beta(2\beta-\alpha)}, \ \Gamma_4 = \frac{G_rB_2}{(\beta+P)(\beta+P-\alpha)}, \ \Gamma_5 = \frac{G_rB_3}{(\beta+S_c)(\beta+S_c-\alpha)},$$

$$\Gamma_6 = \frac{G_rB_4}{(P+S_c)(P+S_c-\alpha)}, \ \Gamma_7 = B_6-B_7-B_8+B_9-\Gamma_1+\Gamma_2-\Gamma_3+\Gamma_4+\Gamma_5-\Gamma_6,$$

$$\Gamma_0 = \frac{B_5G_r}{P(P-\beta)}, \ \Gamma_8 = \frac{A_5G_r}{2\alpha(2\alpha-\beta)}, \ \Gamma_9 = \frac{A_6G_r}{2P(2P-\beta)},$$

$$\Delta_1 = \frac{A_7G_r}{(\alpha+P)(\alpha+P-\beta)}, \ \Delta_2 = \frac{A_8G_r}{2S_c(2S_c-\beta)}, \ \Delta_3 = \frac{A_9G_r}{(\alpha+S_c)(\alpha+S_c-\beta)},$$

$$\Delta_4 = \frac{B_1G_r}{2\beta^2}, \ \Delta_5 = \frac{B_2G_r}{\beta(\beta+P)}, \ \Delta_6 = \frac{B_3G_r}{S_c(S_c+\beta)}, \quad (31)$$

$$\Delta_7 = \frac{B_4G_r}{(P+S_c)(P+S_c-\beta)} \quad \Delta_8 = \Gamma_0-\Gamma_8-\Gamma_9+\Delta_1-\Delta_2+\Delta_3-\Delta_4+\Delta_5+\Delta_6-\Delta_7.$$

Using the expressions (27), (28) and (29) the skin friction τ, the electric current density, Z, and the rate of heat transfer, expressed in terms of the Nusselt number Nu, in the nondimensional terms, are given respectively, by

$$\tau = \frac{\tau_w \nu}{v_0^2} = \left(\frac{\partial u}{\partial y}\right)_{y=0}$$

$$= A_1(P-\alpha) + A_2(S_c-\alpha) + A_3(P-\beta) + A_4(S_c-\beta) +$$

$$+ \frac{E}{2}(-\alpha\Gamma_7 - \beta\Delta_8 + P(B_6+\Gamma_0) - 2\alpha(B_7+\Gamma_8) -$$

$$- 2P(B_8+\Gamma_9) + (\alpha+P)(B_9+\Delta_1) - 2S_c(\Gamma_1+\Delta_2) +$$

$$+ (\alpha+S_c)(\Gamma_2+\Delta_3) - 2\beta(\Gamma_3+\Delta_4) + (\beta+P)(\Gamma_4+\Delta_5) +$$

$$+ (\beta+S_c)(\Gamma_5+\Delta_6) - (P+S_c)(\Gamma_6+\Delta_7)), \tag{32}$$

$$Z = \frac{j_z \nu}{v_0^2}\left(\frac{\mu_0}{\varrho}\right)^{1/2} = -\left(\frac{\partial H}{\partial y}\right) =$$

$$= -A_1(Pe^{-Py} - \alpha e^{-\alpha y}) - A_2(S_c e^{-S_c y} - \alpha e^{-\alpha y}) +$$

$$+ A_3(Pe^{-Py} - \beta e^{-\beta y}) + A_4(S_c e^{-S_c y} - \beta e^{-\beta y}) -$$

$$- \frac{E}{2}(\beta\Delta_8 e^{-\beta y} - \alpha\Gamma_7 e^{-\alpha y} - P(\Gamma_0 - B_6)\, e^{-Py} -$$

$$- 2\alpha(B_7 - \Gamma_8)e^{-2\alpha y} - 2P(B_8 - \Gamma_9)\, e^{-2Py} -$$

$$- (\alpha+P)(\Delta_1 - B_9)\, e^{-(\alpha+P)y} - 2S_c(\Gamma_1 - \Delta_2)\, e^{-2S_c y} -$$

$$- (\alpha+S_c)(\Delta_3 - \Gamma_2)\, e^{-(\alpha+S_c)y} - 2\beta(\Gamma_3 - \Delta_4)\, e^{-2\beta y} -$$

$$- (\beta+P)(\Delta_5 - \Gamma_4)\, e^{-(\beta+P)y} - (\beta+S_c)(\Delta_6 - \Gamma_5)\, e^{-(\beta+S_c)y} -$$

$$- (P+S_c)(\Gamma_6 - \Delta_7)\, e^{-(P+S_c)y}) \tag{33}$$

and

$$Nu = \frac{q'\nu}{k(T'_w - T'_\infty)\, v_0} = -\left(\frac{\partial\theta}{\partial y}\right)_{y=0} = -P + E(P(-B_2 + B_4 -$$

$$- B_5 + 2A_6 - A_7) + \alpha(2A_5 - A_7 - A_9) + \beta(2B_1 - B_2 - B_3) +$$

$$+ S_c(2A_8 - A_9 - B_3 + B_4)). \tag{34}$$

3. Discussion

This paper is concerned with the study of the effects of mass transfer on the hydromagnetic free-convection flow past an infinite vertical porous wall with constant suction. The results are displayed in Figs. (1)—(8), respectively, for the dimensionless forms of the velocity, the induced magnetic

fields, the skin friction, the electric current density and the Nusselt number. The variations of the temperature field are given in Table I for different values of the magnetic parameter M. In order to be realistic, the values of the Schmidt number S_c, are chosen to be 0.22, 0.60 and 0.75 which correspond to hydrogen, water-vapour and oxygen, respectively, at approximately 25 °C and 1 atmosphere, when for the Prandtl number P we get the value $P = 0.71$, corresponding in the air. The values of all the other parameters are chosen arbitrarily.

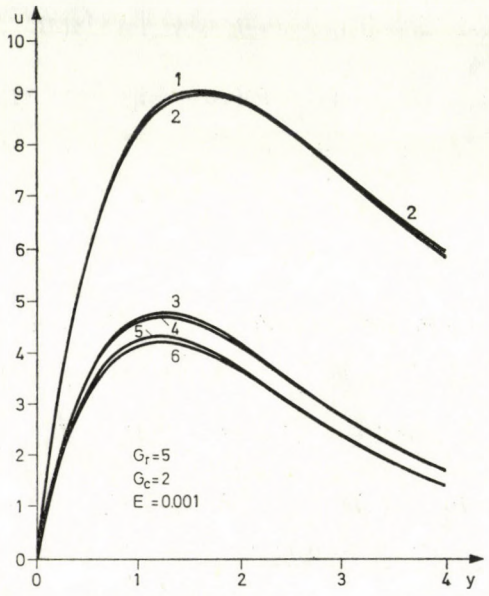

Fig. 1. The velocity profiles u for $P = 0.71$

The variation of the velocity field for different values of S_c and M are shown in Fig. 1. From this Figure we see that the velocity is greater in the case of the hydrogen ($S_c = 0.22$) than in the case of the oxygen ($S_c = 0.75$). Also we remark that as magnetic parameter M increases the velocity decreases for all the values of the Schmidt number S_c, which quantitatively agrees with the expectations since the magnetic field exerts a retarding force on the flow. In Fig. 2 the velocity profiles are shown for constant G_c and M and for different values of S_c, G_r, and E. It is known that the Eckert number E may be interpreted as the addition of heat due to viscous dissipation while the Grashof number G_r as the addition of heat due to free-convection currents. Thus the case when $(T'_w - T'_\infty) > 0$ or $G > 0$ with $E > 0$ corresponds to the external cooling of the wall, while the case when $(T'_w - T'_\infty) < 0$ or $G < 0$ with $E < 0$ corresponds to the external heating of the wall. From Fig. 2 we observe that, in the case $G < 0$ with $E < 0$, for large values of Schmidt number S_c, the velocity is negative and decreases as E increases. Thus the

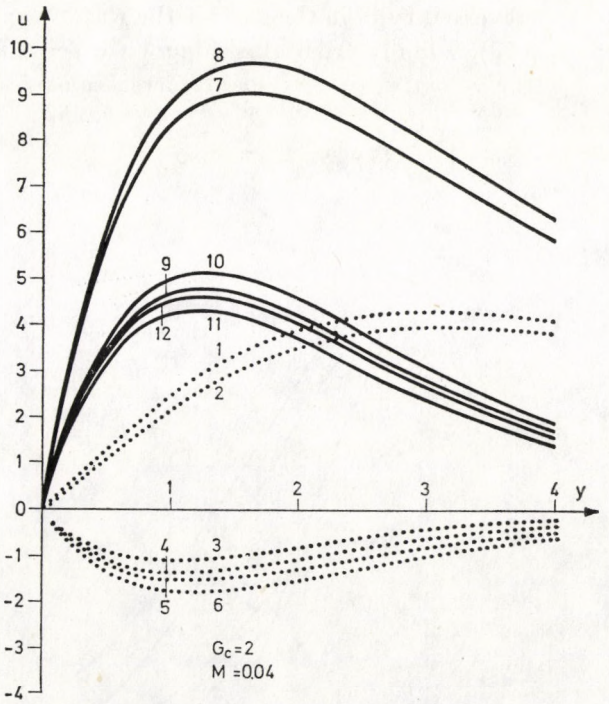

Fig. 2. The velocity profiles u for $P = 0.71$

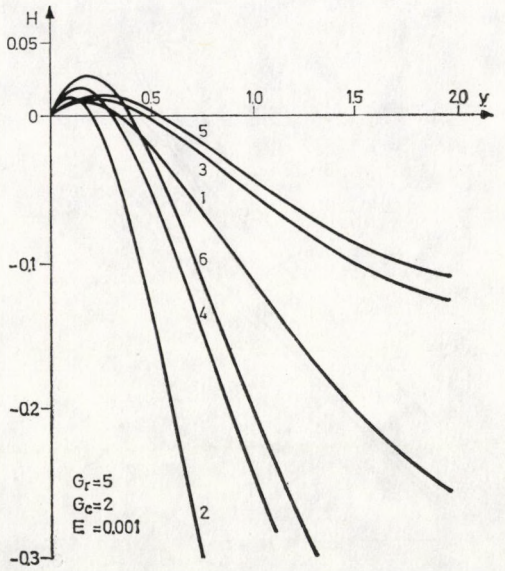

Fig. 3. The induced magnetic field H for $P = 0.71$

velocity profile is of reversed type in the case of the water vapour ($S_c = 0.60$) and oxygen ($S_c = 0.75$). Finally from this Figure we see that, in the case $G > 0$ with $E > 0$, the velocity is positive and increases as E increases for all values of S_c.

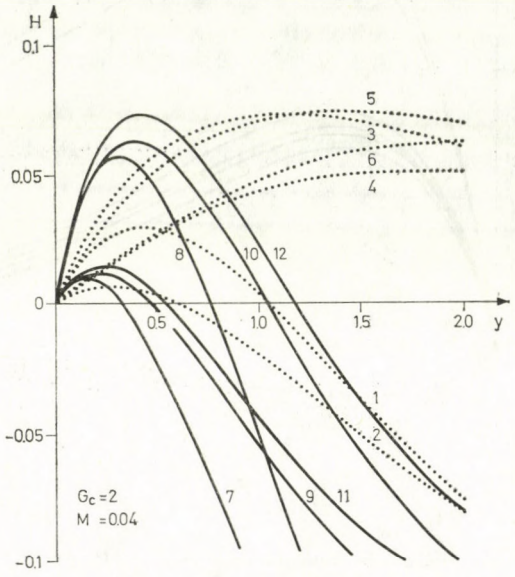

Fig. 4. The induced magnetic field H for $P = 0.71$

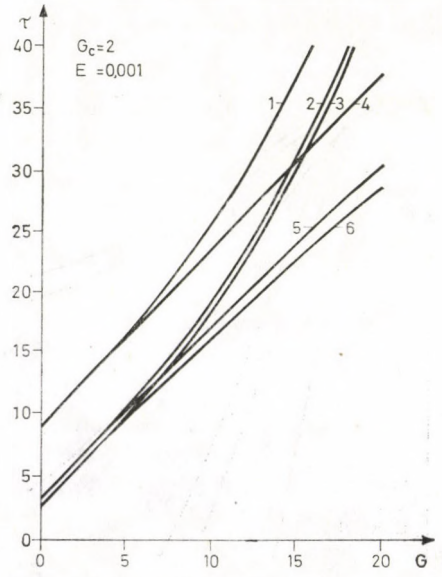

Fig. 5. The variations of the skin friction τ for $P = 0.71$

The variations of the induced magnetic field H are shown in Fig. 3 for different values of S_c and M. From this Figure we see that the induced magnetic field gets positive values near to the wall, while far from the wall it gets negative values, and this means that there is a reverse of the induced magnetic

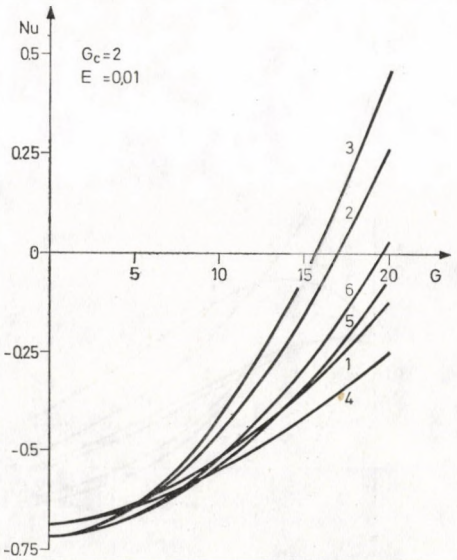

Fig. 6. The variations of the Nusselt number Nu for $P = 0.71$

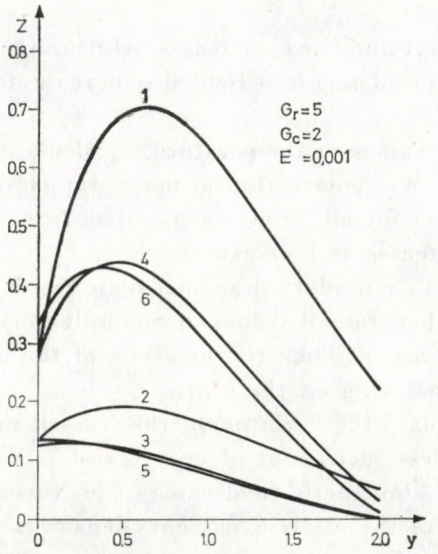

Fig. 7. The electric current density Z for $P = 0.71$

field. Also we remark that as M increases the induced magnetic field also increases for all values of the Schmidt number. In Fig. 4 the variations of induced magnetic field H are shown with y for different values of S_c and E. We observe that, in the case $G < 0$ with $E < 0$, the induced magnetic field

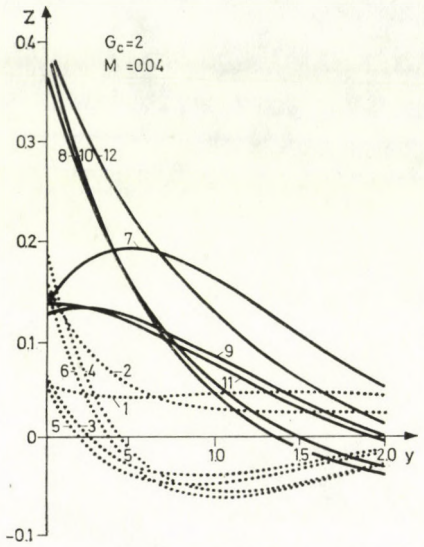

Fig. 8. The electric current density Z for $P = 0.71$

decreases as the Eckert number E increases, while in the case $G > 0$ with $E > 0$ as E increases the induced magnetic field also increases for all values of Schmidt number S_c.

The numerical values of temperature θ, calculated from expression (29) are given in Table I. We remark that as magnetic parameter M increases, the temperature decreases for all values of S_c. Also, from this Table we see that the temperature increases as E increases.

The skin friction τ is plotted against G in Fig. 5 for different values of M and S_c. We see that, for all values of Schmidt number S_c, as M increases the skin friction decreases. Thus the presence of the magnetic field helps in reducing the frictional drag on the wall.

The Fig. 6 displays the variation of the Nusselt number which represent the local dimensionless coefficient of heat transfer. We see that an increase in the strength of the magnetic field causes the Nusselt number to decrease.

The variation of the electric current density Z is shown in Figs. 7 and 8. From the Fig. 7 we see that as magnetic parameter M increases the

Table I

The variation of the temperature θ profiles for $P = 0.71$

	$G_r = 5$		$G_c = 2$		$E = 0.001$	
	$S_c = 0.22$		$S_c = 0.60$		$S_c = 0.75$	
y	$M = 0.04$	$M = 0.15$	$M = 0.04$	$M = 0.15$	$M = 0.04$	$M = 0.15$
0.0	1.000000	1.000000	1.000000	1.000000	1.000000	1.000000
0.2	0.769644	0.767742	0.768657	0.763513	0.769126	0.763703
0.4	0.587249	0.584201	0.587289	0.580236	0.587218	0.580162
0.6	0.447354	0.443656	0.447592	0.440307	0.446990	0.439841
0.8	0.341264	0.337269	0.340715	0.334003	0.339324	0.333193
1.0	0.260985	0.256952	0.259137	0.253331	0.257399	0.252294
	$G_r = -5$		$G_c = 2$		$M = 0.04$	
	$S_c = 0.22$		$S_c = 0.60$		$S_c = 0.75$	
y	$E = -0.001$	$E = -0.003$	$E = -0.001$	$E = -0.003$	$E = -0.001$	$E = -0.003$
0.0	1.000000	1.000000	1.000000	1.000000	1.000000	1.000000
0.2	0.747046	0.735604	0.740685	0.716521	0.739263	0.712257
0.4	0.557748	0.539929	0.550220	0.517345	0.549234	0.514386
0.6	0.416179	0.395414	0.409617	0.375730	0.409417	0.375128
0.8	0.310326	0.288775	0.305472	0.274214	0.305904	0.275510
1.0	0.231076	0.210099	0.228137	0.200984	0.228948	0.203416
	$G_r = 5$		$G_c = 2$		$M = 0.14$	
	$S_c = 0.22$		$S_c = 0.60$		$S_c = 0.75$	
y	$E = 0.001$	$E = 0.003$	$E = 0.001$	$E = 0.003$	$E = 0.001$	$E = 0.003$
0.0	1.000000	1.000000	1.000000	1.000000	1.000000	1.000000
0.2	0.769644	0.803400	0.768657	0.800437	0.769126	0.801846
0.4	0.587249	0.628433	0.587289	0.628553	0.587218	0.628338
0.6	0.447354	0.488940	0.447593	0.489658	0.446790	0.487247
0.8	0.341264	0.381591	0.340715	0.379942	0.339324	0.375771
1.0	0.260985	0.299528	0.259137	0.293984	0.257399	0.288769

electric current also increases for all values of S_c. Finally from Fig. 8 we see that the electric current density increases as the Eckert number E increases.

REFERENCES

1. D. D. Haldavnekar and V. M. Soundalgekar, Acta Phys. Hung., **43**, 243, 1977.
2. G. C. Pande, Ph. D. Thesis, University of Lucknow, India, 1971.
3. V. M. Soundalgekar, Proc. Indian Acad. Sci., **84A**, No. 5, 194, 1976.
4. E. M. Sparrow, W. J. Minkowycz and E. R. G. Eckert, Trans. ASME, Journal of Heat Transfer, **86**, Sec. C. 508, 1964.

Acta Physica Academiae Scientiarum Hungaricae, Tomus 46 (4), pp. 333—340 (1979)

DEPENDENCE ON THE GEOMETRY AND ON THE BASIS SET OF LOCALIZED ORBITAL ENERGY AND MOMENT CONTRIBUTIONS

I. ENERGY QUANTITIES

By

E. KAPUY, C. KOZMUTZA, ZS. OZORÓCZY and J. PIPEK

QUANTUM THEORY GROUP, PHYSICAL INSTITUTE, TECHNICAL UNIVERSITY OF BUDAPEST, BUDAPEST

(Received 31. V. 1979)

In a series of papers we investigate the localized orbital contributions at the molecular experimental and theoretical equilibrium geometries using various basis sets. The present study deals with some energy quantities obtained from localized charge densities: the kinetic, the (effective) potential and the selfinteraction energies are discussed. Several regularities were found for the systems considered, namely the molecules HF, H_2O, NH_3 and CH_4, respectively.

1. Introduction

As the simplest antisymmetric wavefunction of a closed-shell system, a single determinant of one-particle functions is invariant under any unitary transformation [1], the tranformations could be chosen to obtain new orbitals localized as much as possible [2]. Several localization procedures have been published as well as many advantages of using localized orbitals have been pointed out recently [3—7]. In a series of papers we also investigated various properties of localized charge densities for some ten- and eighteen-electron systems [8—11].

It is known that in any quantum-chemical calculation the problem arises which type of basis set and which geometry data are to be used for the study of the given molecular system. As to the choice of a suitable basis set, there are usually the computer time and/or size which make a limit for the number of basis functions. It has been pointed out, e.g., that at least one *d* function on the oxygen is necessary to take for the molecule H_2O in order to obtain an acceptable value for the total energy as well as for the electric moments (more details on basis set dependence see in [12—14]). An exhaustive analysis of the effect of basis set variation on the localized charge distribution of H_2O has also been done [1]. From the results it follows that in the presence of polarization functions (at least one *d*-type on the oxygen) the energy contributions as well as the electric moment components provide regular differences for bond and lone pair localized orbitals. The change of energy contributions parallels with that of total energy and similarly the first and second order moment components (localized moments) with that of the corresponding total molecular

values [10]. These results confirm — together with those obtained for the transferable property [11] — that the localized orbital energy contributions and the localized moments are suitable for characterizing even larger molecules.

It is interesting to investigate how the choice of geometry data influence the values for the localized orbital energy and moment contributions. The molecules are often investigated at their experimental equilibrium geometry (if available). In many cases — for simplicity — standard [15] or model [8] preferable. for the determination of harmonic force constants which geometry geometrical values are taken for the calculations. It is known that there are not too many differences between the total molecular properties whether calculated at the experimental or theoretical (or nearby) geometries. In spite of this, many authors argue (see, e.g., [16] and reference therein), which geometry data are preferable for the determination of harmonic force constants. In this paper we summarize our results obtained for HF, H_2O and NH_3 core, bond and lone pair localized orbitals and those obtained for CH_4 core and bond pair localized orbitals. We investigated the localized charge densities at the molecular experimental and calculated equilibrium geometries by the use of different basis sets.

2. Total energies and total kinetic energies

For a systematic study a suitable basis set is necessary. Various basis sets were chosen for the molecule H_2O in order to investigate it at the experimental and the calculated equilibrium geometry. The results are given in Table I the values suggest that the so-called 6-31G/d basis set seems to be the more convenient as the total energy is quite acceptable (the *p*-type polarization functions on hydrogens do not give large contributions to the total energy) and also the virial coefficient is one of the best. The detailed description of the basis sets considered are given in the corresponding papers: STO-3G [17], 4-31G [18], 6-31G [19] while 6-31G/d and 6-31G/d+p [20]. In order to investigate similar results as well, for a comparison the values obtained by the so-called DUNNING' basis sets are also given [12]. From the values one can see that the resulting total energy by basis 6-31G/d is better than any of (sp/s) type but worse than, e.g., DUNNING's contracted Gaussians of [4s3pld/2s]. The calculations, however, are rather effective, as pointed out in [18—20] with basis sets of split-valence types. Therefore we made our geometry dependence study by the use of basis 6-31G/d. For a comparison the corresponding values which we obtained by using 6-31G basis are also given. All calculations were performed on a CDC 3300 computer (Hungarian Academy of Sciences, Budapest).

The experimental geometry data were taken as those used in an earlier work [7]. The theoretically obtained values for basis 6-31G were as given in

Table I

Total energies calculated for H_2O (in hartree)

		Total energy	Total kinetic energy
STO-3G	Exp	−74.96381	74.53346
	Calc	−74.96543	74.46618
4-31G	Exp	−75.90847	75.87753
	Calc	−75.90987	75.89167
6-31G	Exp	−75.98480	75.91439
	Calc	−75.98628	75.93238
6-31G/d	Exp	−76.01205	75.76360
	Calc	−76.01231	75.80832
6-31G/d+p	Exp	−76.02318	75.74601
	Calc	−76.02365	75.80347
[4s3p/2s]	Exp	−76.00209	—
[4s3p1d/2s]	Exp	−76.02882	—
[4s3p1d/2s1p]	Exp	−76.04172	75.98016
	Calc	−76.04209	76.02276

Table II

Total energies calculated using basis 6-31G and 6-31G/d (in hartree)

		Basis 6-31G	
		Total energy	Total kinetic energy
HF	Exp	−99.98341	100.06277
	Calc	−99.98343	100.05384
H_2O	Exp	−75.98480	75.91439
	Calc	−75.98628	75.93238
NH_3	Exp	−56.16146	56.12776
	Calc	−56.16632	56.18475
CH_4	Exp	−40.18035	40.17622
	Calc	−40.18060	40.24605
		Basis 6-31G/d	
		Total energy	Total kinetic energy
HF	Exp	−100.00326	99.84123
	Calc	−100.00333	99.85858
H_2O	Exp	−76.01205	75.76360
	Calc	−76.01231	75.80832
NH_3	Exp	−56.18513	56.01449
	Calc	−56.18536	56.06068
CH_4	Exp	−40.19585	40.10471
	Calc	−40.19602	40.14709

[19], except for HF, where the $R = 1.7403$ a.u. was calculated (not given in the above reference). As to basis set 6-31G/d — even they have already been calculated [21] — we also were looking for the theoretical equilibrium geometries. This was necessary because in the calculations (as reported in [21]), an average value of 0.8 was used for the exponent of *d*-type functions, while we performed the calculations by using optimized exponents for each compound (values taken from [20]). The calculated equilibrium geometry data (only slightly different from those given in [21], are the following:

HF	$R = 1.7183$ a.u.	
H_2O	$R = 1.7876$ a.u.,	$\alpha = 105.51°$
NH_3	$R = 1.8943$ a.u.,	$\alpha = 107.13°$
CH_4	$R = 2.0512$ a.u.	(tetr.)

The results obtained for these molecules are given in Table II. The total energies are rather different obtained by basis 6-31G at the experimental and the calculated equilibrium: the largest difference was found for NH_3 ($\approx$0.005 a.u.), that for H_2O is about 0.0015 a.u. while for HF and CH is less than 0.0003 a.u. The case is not the same for the total kinetic energies: the larger differences were found for CH_4 and NH_3. As to the results obtained by basis set 6-31G/d, they are rather close to each other at the experimental and the theoretical equilibrium, but only for the total energy. The kinetic energy result depends strongly on the geometry: the differences obtained at experimental and the calculated equilibrium are about 0.04—0.05 a.u., except for HF (less than 0.02 a.u.). The total energies and total kinetic energies obtained for these molecules suggest, that the inclusion of *d*-type function on the heavy atom is important. Although the use of a basis (sp/s) type may be sufficient for some cases, the geometry should then be chosen very carefully.

3. Energy contributions of core orbitals

Several quantities can be used for characterizing localized orbital densities (see, e.g., [7—9, 22]). In the present paper we investigate four quantities as energy contributions obtained from the individual localized orbitals. There are three different types of localized charge distributions for the systems considered: core, bond and lone pair orbitals. The energy contributions studied are the following: the kinetic, the potential, the self-interaction, and the so-called effective potential energy quantities. First the core orbitals are investigated.

The values obtained are given in Table III. In order to avoid the superfluous enlargement of the paper the results obtained only by basis 6-31G/d

Table III

Energy contributions from core localized orbitals using basis 6-31G/d (in hartree)

		Kinetic energy	Potential energy
HF	Exp	39.3595	−79.9215
	Calc	39.3585	−79.9255
H_2O	Exp	30.6572	−63.4006
	Calc	30.6536	−63.4108
NH_3	Exp	23.0578	−48.8815
	Calc	23.0555	−48.8940
CH_4	Exp	16.5918	−36.3665
	Calc	16.5933	−36.3813
		Self-interaction	**Effective potential**
HF	Exp	5.48787	−65.1388
	Calc	5.48780	−65.1378
H_2O	Exp	4.84412	−50.8877
	Calc	4.84384	−50.8820
NH_3	Exp	4.20048	−38.3918
	Calc	4.20024	−38.3860
CH_4	Exp	3.56153	−27.6859
	Calc	3.56160	−27.6829

are presented. The kinetic energy contributions do not differ much whether obtained at the experimental or at the calculated equilibrium geometry. (They differ less from each other than the corresponding total kinetic energy values for all compounds studied). As the potential energy contributions do not involve the whole ("effective") potential energy for a given localized orbital, we calculated the effective ones for each type of localized orbital densities by the following equation:

$$V^i_{\text{eff}} = V_i + \sum_i \left(2\langle ii|jj\rangle - \langle ij|ij\rangle\right),$$

where V_i = potential energy contribution of the i-th localized orbital, the expression in parentheses represents the interaction energy between the i-th and j-th localized orbital and so V^i_{eff} is the resulting effective potential energy contribution for the given i-th orbital. Both V_i and V^i_{eff} are given in Table III for the core orbitals. The results suggest that as the V^i_{eff} potentials show smaller differences between the experimental and the calculated equilibrium geometries, these contributions may be used as transferable quantities (similarly to the kinetic ones [23]) in a study of related large molecules.

The self-interaction energy contributions do not change much either as going from the experimental to the calculated equilibrium position of nuclei. It is remarkable that the signs of these changes parallel with those found for the kinetic energy contributions (see Table III). It generally holds that all deviations calculated for the core orbitals between the experimental and the theoretically determined equilibrium geometries are rather small, smaller than 0.05% in any cases.

4. Energy contributions obtained for bond and lone pair orbitals

The quantities discussed for core orbitals are given also for the bond orbitals: they are given in Table IV. The most remarkable results show that all quantities are larger at the calculated than at the experimental geometries. This may certainly be due to the shorter bond length at the theoretically

Table IV

Energy contributions from bond pair localized orbitals using basis 6-31G/d_A^-(in hartree)

		Self-interaction	Effective potential
HF	Exp	2.20646	−10.4503
	Calc	2.21469	−10.4828
H_2O	Exp	1.62373	−8.65182
	Calc	1.63501	−8.70041
NH_3	Exp	1.19079	−7.16050
	Calc	1.19847	−7.19583
CH_4	Exp	0.86508	−5.87136
	Calc	0.87018	−5.89695
		Kinetic energy	**Potential energy**
HF	Exp	0.91894	−3.31001
	Calc	0.92292	−3.32581
H_2O	Exp	0.83325	−2.57031
	Calc	0.83907	−2.59100
NH_3	Exp	0.75750	−2.00023
	Calc	0.76160	−2.01317
CH_4	Exp	0.68737	−1.53839
	Calc	0.69001	−1.54592

obtained total energy minima. As it is well known the shorter the bond distance the larger the nuclear potential, so the electron density becomes also more compact [24]. This fact is reflected even in the energy contributions obtained for bond pair localized orbitals.

As to the values of energy contributions resulting for lone pair orbitals (HF, H_2O and NH_3), similar conclusion could be found for the kinetic energy contributions. The self-interactions, however, are always larger at the experimental than at the calculated equilibrium geometry of nuclei (see Table V). The effective potential values do not change in the same direction for the studied systems. The general conclusion can be made that there are the kinetic energy terms which reflect the most suitably (i.e. for all of different types of localized orbitals) the increasing electron density as going from the experimental to the calculated equilibrium geometries. This result may well be used if the total energy of related larger systems is constructed by the use of the kinetic energy contributions of localized orbitals determined at the calculated equilibrium geometry of a small molecule.

5. Conclusion

Several energy quantities have been discussed using the localized decomposition of the total charge distribution for some small molecules. It can be seen that the kinetic, the self-interaction and the effective potential energy contributions characterize suitably the main differences for the various types of localized orbitals. There is an interesting question, however, to be further analyzed. It is a longstanding goal in the study of localized charge densities, to be able to determine whether a bond or a lone pair distribution is "larger" or "greater" in a given system [25]. There are the self-interaction energy con-

Table V

Energy contributions from lone pair localized orbitals using basis 6-31G/d (in hartree)

		Self-interaction	Effective potential
HF	Exp	2.78488	−11.6279
	Calc	2.78536	−11.6310
H_2O	Exp	1.98861	−9.34880
	Calc	1.99026	−9.35482
NH_3	Exp	1.37712	−7.43426
	Calc	1.37946	−7.43999
		Kinetic energy	**Potential energy**
HF	Exp	1.03012	−3.77782
	Calc	1.02991	−3.77834
H_2O	Exp	0.87860	−2.76981
	Calc	0.87753	−2.76867
NH_3	Exp	0.73644	−1.97108
	Calc	0.73485	−1.96911

tributions which could be related to the "extent" of an individual charge density. As one can see from the results (Table IV and Table V), there are the lone pair orbital self-interaction energies which are larger than the bond pair ones by about 10% (for HF) and 5% $H(_2O)$, but the opposite relation holds (bond pairs are larger than the lone pair one) for molecule NH_3 (approx. by 3 %). These results affirm that there is no reason to expect a larger extent for a bond or a lone pair localized charge distribution. These quantities do not depend only on the enlargement of the basis set but also, e.g., on the number of different types of localized orbitals (i.e. on the system) as well. It can also be noted that the effective potential energy contributions do show similar regularities for the studied molecules.

In the next paper of this series other types of energy quantities will be discussed: the interaction energy contributions between the localized orbitals. After that paper an analysis of the first and second order electric moments of localized charge distributions will follow. It is planned to publish a study on the geometry and basis set dependence of the localized moment characteristics as well.

REFERENCES

1. V. Fock, Z. Physik **61,** 126, 1930.
2. C. A. Coulson, Trans. Faraday Soc. **38,** 433, 1942.
3. J. M. Foster and S. F. Boys, Rev. Mod. Phys., **32,** 300, 1960.
4. C. Edmiston and K. Ruedenberg, Rev. Mod. Phys., **35,** 457, 1963.
5. W. England, L. S. Salmon and K. Ruedenberg, Topics in Current Chemistry, Vol. 23, Springer Verlag, Berlin, 1971.
6. W. von Niessen: J. Chem. Phys. **56,** 4290 (1972.
7. W. England, M. S. Gordon and K. Ruedenberg, Theoret. Chim. Acta (Berlin) **37,** 177, 1975.
8. R. Daudel, M. E. Stephens, E. Kapuy and C. Kozmutza, Chem. Phys. Letters, **40,** 194, 1976.
9. E. Kapuy, C. Kozmutza and M. E. Stephens, Theoret. Chim. Acta (Berlin) **43,** 175, 1976.
10. E. Kapuy, Zs. Ozoróczy and C. Kozmutza, Acta Phys. Hung., **41,** 125, 1976.
    M. E. Stephens, E. Kapuy and C. Kozmutza, Theoret. Chim. Acta (Berlin) **45,** 111, 1977.
11. E. Kapuy, C. Kozmutza, R. Daudel and M. E. Stephens, Theoret. Chim. Acta, (Berlin) **50,** 31, 1978.
    E. Kapuy, C. Kozmutza, R. Daudel and M. E. Stephens, Theoret. Chim. Acta (Berlin), **53,** 147, 1979.
12. T. H. Dunning, J. Chem. Phys., **53,** 2823, 1970.
    T. H. Dunning, J. Chem. Phys., **55,** 3958, 1971.
13. B. J. Rosenberg and I. Shavitt, J. Chem. Phys., **63,** 2162, 1975.
14. B. J. Rosenberg, W. C. Ermler and I. Shavitt, J. Chem. Phys., **65,** 4072, 1976.
15. J. A. Pople and M. Gordon, J. Am. Chem. Soc., **89,** 4253, 1967.
16. P. Pulay, Mol. Phys., **17,** 197, 1969.
17. R. Ditchfield, W. J. Hehre and J. A. Pople, J. Chem. Phys., **52,** 5001, 1970.
18. R. Ditchfield, W. J. Hehre and J. A. Pople, J. Chem. Phys., **54,** 724, 1971.
19. W. J. Hehre, R. Ditchfield and J. A. Pople, J. Chem. Phys., **56,** 2257, 1972.
20. P. C. Hariharan and J. A. Pople, Theoret. Chim. Acta (Berlin) **28,** 213, 1973.
21. P. C. Hariharan and J. A. Pople, Mol. Phys., **27,** 209, 1974.
22. E. Kapuy, C. Kozmutza and Zs. Ozoróczy, Periodica Polytechnica, **21,** 177, 1977.
23. E. Kapuy and C. Kozmutza, in Research Work of the Techn. Univ. of Budapest, p. 9. 1977,
24. E. Kapuy and F. Török, Quantum Theory of Atoms and Molecules, Akadémiai Kiadó. Budapest, 1975 (in Hungarian).
25. M. A. Robb, W. J. Haines and I. G. Csizmadia, J. Am. Chem. Soc., **95,** 42, 1973.

RECENSIONES

J. U. KELLER:

Technische Thermodynamik in Beispielen, Teil 1, Grundlagen

Walter de Gruyter, Berlin, New York, 1979, pp. 307

This is the first volume of a handbook for technical thermodynamics taught nowadays at German Universities. Its aim set is to be helpful to students interested in the various fields of technical sciences where thermodynamics is an indispensable discipline as, for instance, classical engineering, different fields of technology, physical engineering, physical chemistry, chemical technology and so on. With this book the author's main goal is to help the students to overcome certain difficulties encountered in the case of applications of the laws, fundamental relations and basic concepts of thermodynamics for given, relatively simple tasks and problems.

In the first part of this volume of KELLER's work seventy well selected examples are discussed through detailed calculations and complete solutions. These examples refer to the zeroth, first and second laws of classical thermodynamics, further some of them belong to the domain of thermodynamics of multiphase systems. On the other hand, the second part of this volume is devoted to a short, concise but very careful and clear presentation and definition of the most fundamental and relevant concepts and notions of thermodynamics. The treatment of this part clearly presents that thermodynamics is not a technical discipline but rather an important field of classical physics, i.e. a fundamental science for a high number of applied sciences.

The material contained in the book has been written and arranged in such a manner that university students and even lecturers can equally profit from it. Consequently, the book published in the "de Gruyter Lehrbuch" series will be certainly very useful to everybody interested in the applications of classical thermodynamics. The neat printing and very fine edition of the book is the merit of the Publisher.

I. GYARMATI

A. Z. PATASHINSKII and V. L. POKROVSKII:

Fluctuation Theory of Phase Transitions

Translated and edited by P. J. Shepherd, Pergamon Press, Oxford, New York, Toronto, Sydney, Frankfurt, 1979, pp. 321

Statistical physics can explain various properties of condensed matter and predict diverse phenomena in metals, alloys, insulators, semiconductors, liquid helium and so on. In certain cases the theories treat successfully the properties of condensed matter as sets of an ideal gas of excitations. However, regarding the problem of phase transitions (critical phenomena) fluctuations grow in a system as its critical point is approached. In these cases the fluctuations interact with each other so intensively that it is no longer possible to describe them as an ideal gas.

It is well known that some years ago a new model of critical phenomena based on the hypothesis of scaling the fluctuations was proposed to describe the strong interactions of fluctuations and the predictions of this theory agree well with certain kinds of experiments.

The purpose of the excellent book of the famous Russian authors, members of the so-called Landau school, is to give an account of the physical ideas of the scaling model and to review some of its special applications in the study of various properties of systems close to

phase transitions. The book is not an exhaustive monograph of the theory of phase transitions, although the English edition is a corrected and enlarged version of the original Russian. Of course, as Landau's works have played an important role in the development of the theory of second order phase transitions the book begins with the summary of the Landau theory. The subsequent chapters are devoted to the treatments of the thermodynamics of strongly fluctuating systems, some applications of scaling hypothesis, dynamical phenomena in the critical region, the approximate calculation of critical indices, the microscopic theory of phase transitions, the theory of renormalization group, etc.

Undoubtedly, the book will give an invaluable aid to researchers of the field of solid state physics and can be very useful to university lecturers and young scientists, too.

I. GYARMATI

Printed in Hungary

A kiadásért felel az Akadémiai Kiadó igazgatója. Műszaki szerkesztő: Botyánszky Pál

A kézirat a kiadóba érkezett: 1979 VI. 28. A kézirat nyomdába érkezett: 1979. VII. 5. — Terjedelem: 11 (A/5) ív, 26 ábra

80.7297 Akadémiai Nyomda, Budapest — Felelős vezető: Bernát György

NOTES TO CONTRIBUTORS

I. PAPERS will be considered for publication in Acta Physica Hungarica, only if they have not previously been published or submitted for publication elsewhere. They may be written in English, French, German or Russian.

Papers should be submitted to

Prof. I. Kovács, Editor
Department of Atomic Physics, Technical University
1521 Budapest, Budafoki út 8, Hungary

Papers may be either articles with abstracts or short communications. Both should be as concise as possible, articles in general not exceeding 25 typed pages, short communications 8 typed pages.

II. MANUSCRIPTS

1. Papers should be submitted in five copies.

2. The text of papers must be of high stylistic standard, requiring minor corrections only.

3. Manuscripts should be typed in double spacing on good quality paper, with generous margins.

4. The name of the author(s) and of the institutes where the work was carried out should appear on the first page of the manuscript.

5. Particular care should be taken with mathematical expressions. The following should be clearly distinguished, e.g. by underlining in different colours: special founts (italics, script, bold type, Greek, Gothic, etc.); capital and small letters; subscripts and superscripts, e.g. x^2, x_3; small l and 1; zero and capital O; in expressions written by hand: e and l, n and u, v and v, etc.

6. References should be numbered serially and listed at the end of the paper in the following form: J. Ise and W. D. Fretter, Phys. Rev., *76*, 933, 1949.

For books, please give the initials and family name of the author(s), title, name of publisher, place and year of publication, e.g.: J. C. Slater, Quantum Theory of Atomic Structures, I. McGraw-Hill Book Company, Inc., New York, 1960.

References should be given in the text in the following forms: Heisenberg [5] or [5].

7. Captions to illustrations should be listed on a separate sheet, not inserted in the text.

III. ILLUSTRATIONS AND TABLES

1. Each paper should be accompanied by five sets of illustrations, one of which must be ready for the blockmaker. The other sets attached to the copies of the manuscript may be rough drawings in pencil or photocopies.

2. Illustrations must not be inserted in the text.

3. All illustrations should be identified in blue pencil by the author's name, abbreviated title of the paper and figure number.

4. Tables should be typed on separate pages and have captions describing their content. Clear wording of column heads is advisable. Tables should be numbered in Roman numerals. (I, II, III, etc.).

IV. MANUSCRIPTS not in conformity with the above Notes will immediately be returned to authors for revision. The date of receipt to be shown on the paper will in such cases be that of the receipt of the revised manuscript.

Reviews of the Hungarian Academy of Sciences are obtainable at the following addresses:

AUSTRALIA
C.B.D. LIBRARY AND SUBSCRIPTION SERVICE, Box 4886, G.P.O., *Sydney N.S.W. 2001*
COSMOS BOOKSHOP, 145 Acland Street, *St. Kilda (Melbourne), Victoria 3182*

AUSTRIA
GLOBUS, Höchstädtplatz 3, *1200 Wien XX*

BELGIUM
OFFICE INTERNATIONAL DE LIBRAIRIE, 30 Avenue Marnix, *1050 Bruxelles*
LIBRAIRIE DU MONDE ENTIER, 162 Rue du Midi, *1000 Bruxelles*

BULGARIA
HEMUS, Bulvar Ruszki 6, *Sofia*

CANADA
PANNONIA BOOKS, P.O. Box 1017, Postal Station "B", *Toronto, Ontario M5T 2T8*

CHINA
CNPICOR, Periodical Department, P.O. Box 50, *Peking*

CZECHOSLOVAKIA
MAD'ARSKÁ KULTURA, Národní třida 22, *115 66 Praha*
PNS DOVOZ TISKU, Vinohradská 46, *Praha 2*
PNS DOVOZ TLAČE, *Bratislava 2*

DENMARK
EJNAR MUNKSGAARD, Norregade 6, *1165 Copenhagen*

FINLAND
AKATEEMINEN KIRJAKAUPPA, P.O. Box 128, *SF-00101 Helsinki 10*

FRANCE
EUROPERIODIQUES S. A., 31 Avenue de Versailles, *78170 La Celle St.-Cloud*
LIBRAIRIE LAVOISIER, 11 rue Lavoisier, *75008 Paris*
OFFICE INTERNATIONAL DE DOCUMENTATION ET LIBRAIRIE, 48 rue Gay-Lussac, *75240 Paris Cedex 05*

GERMAN DEMOCRATIC REPUBLIC
HAUS DER UNGARISCHEN KULTUR, Karl-Liebknecht-Strasse 9, *DDR-102 Berlin*
DEUTSCHE POST ZEITUNGSVERTRIEBSAMT, Strasse der Pariser Kommüne 3—4, *DDR-104 Berlin*

GERMAN FEDERAL REPUBLIC
KUNST UND WISSEN ERICH BIEBER, Postfach 46, *7000 Stuttgart 1*

GREAT BRITAIN
BLACKWELL'S PERIODICALS DIVISION, Hythe Bridge Street, *Oxford OX1 2ET*
BUMPUS, HALDANE AND MAXWELL LTD., Cowper Works, *Olney*, Bucks *MK46 4BN*
COLLET'S HOLDINGS LTD., Denington Estate, *Wellingborough*, Northants *NN8 2QT*
W.M. DAWSON AND SONS LTD., Cannon House *Folkestone, Kent CT19 5EE*
H. K. LEWIS AND CO., 136 Gower Street, *London WC1E 6BS*

GREECE
KOSTARAKIS BROTHERS, International Booksellers, 2 Hippokratous Street, *Athens-143*

HOLLAND
MEULENHOFF-BRUNA B.V., Beulingstraat 2, *Amsterdam*
MARTINUS NIJHOFF B.V., Lange Voorhout 9—11, *Den Haag*
SWETS SUBSCRIPTION SERVICE, 347b Heereweg, *Lisse*

INDIA
ALLIED PUBLISHING PRIVATE LTD., 13/14 Asaf Ali Road, *New Delhi 110001*
150 B-6 Mount Road, *Madras 600002*
INTERNATIONAL BOOK HOUSE PVT. LTD., Madame Cama Road, *Bombay 400039*
THE STATE TRADING CORPORATION OF INDIA LTS, Books Import Division, Chandralok, 36 Janpath, *New Delhi 110001*

ITALY
EUGENIO CARLUCCI, P.O. Box 252, *70100 Bari*
INTERSCIENTIA, Via Mazzé 28, *10149 Torino*
LIBRERIA COMMISSIONARIA SANSONI, Via Lamarmora 45, *50121 Firenze*
SANTO VANASIA, Via M. Macchi 58, *20124 Milano*
D. E. A., Via Lima 28, *00198 Roma*

JAPAN
KINOKUNIYA BOOK-STORE CO. LTD., 17-7 Shinjuku-ku 3 chome, Shinjuku-ku, *Tokyo 160-91*
MARUZEN COMPANY LTD., Book Department, P.O. Box 5050 Tokyo International, *Tokyo 100-31*
NAUKA LTD. IMPORT DEPARTMENT, 2-30-19 Minami Ikebukuro, Toshima-ku, *Tokyo 171*

KOREA
CHULPANMUL, *Phenjan*

NORWAY
TANUM-CAMMERMEYER, Karl Johansgatan 41—43, *1000 Oslo*

POLAND
WĘGIERSKI INSTYTUT KULTURY, Marszałkowska 80, *Warszawa*
CKP I W ul. Towarowa 28 *00-958 Warsaw*

ROUMANIA
D. E. P., *Bucureşti*
ROMLIBRI, Str. Biserica Amzei 7, *Bucureşti*

SOVIET UNION
SOJUZPETCHATJ — IMPORT, *Moscow*
and the post offices in each town
MEZHDUNARODNAYA KNIGA, *Moscow G-200*

SPAIN
DIAZ DE SANTOS, Lagasca 95, *Madrid 6*

SWEDEN
ALMQVIST AND WIKSELL, Gamla Brogatan 26, *101 20 Stockholm*
GUMPERTS UNIVERSITETSBOKHANDEL AB, Box 346, *401 25 Göteborg 1*

SWITZERLAND
KARGER LIBRI AG, Petersgraben 31, *4011 Basel*

USA
EBSCO SUBSCRIPTION SERVICES, P.O. Box 1943, *Birmingham, Alabama 35201*
F. W. FAXON COMPANY, INC., 15 Southwest Park, *Westwood, Mass. 02090*
THE MOORE-COTTRELL SUBSCRIPTION AGENCIES, *North Cohocton, N. Y. 14868*
READ-MORE PUBLICATIONS, INC., 140 Cedar Street, *New York, N. Y. 10006*
STECHERT-MACMILLAN, INC., 7250 Westfield Avenue, *Pennsauken* N. J. 08110

VIETNAM
YXUNHASABA, 32, Hai Ba Trung, *Hanoi*

YUGOSLAVIA
JUGOSLAVENSKA KNJIGA, Terazije 27, *Beograd*
FORUM, Vojvode Mišiča 1, *21000 Novi Sad*

Index: 26.022
Acta Phys. Hung. Tom. 46. No. 4. Budapest, 20. XII. 1979 HU-ISSN 0001-6705